

AD-A176 673

(12)

AD

AD-E401-609

SPECIAL PUBLICATION ARLCD-SP-84001

Explosions
STRUCTURES TO RESIST THE EFFECTS OF ACCIDENTAL EXPLOSIVES
VOLUME II, BLAST, FRAGMENT, AND SHOCK LOADS

HENRY AYVAZIAN
MICHAEL DEDE
NORVAL DOBBS
AMMANN & WHITNEY

MARK WHITNEY
PATRICIA BOWLES
WILFRED BAKER

SOUTHWEST RESEARCH INSTITUTE

JOSEPH P. CALTAGIRONE
PROJECT ENGINEER
ARDEC

DTIC
ELECTE
FEB 11 1987
S D

UTIC FILE COPY

DECEMBER 1986



US ARMY
ARMAMENT
MUNITIONS &
CHEMICAL COMMAND

ARMAMENT RDE CENTER

U. S. ARMY ARMAMENT RESEARCH, DEVELOPMENT AND ENGINEERING CENTER

ARMAMENT ENGINEERING DIRECTORATE

DOVER, NEW JERSEY

APPROVED FOR PUBLIC RELEASE; DISTRIBUTION UNLIMITED.

Best Available Copy

87 2 10 057

UNCLASSIFIED

SECURITY CLASSIFICATION OF THIS PAGE (When Data Entered)

| REPORT DOCUMENTATION PAGE | | READ INSTRUCTIONS BEFORE COMPLETING FORM |
|---|-------------------------------------|--|
| 1. REPORT NUMBER Special Publication ARLCD-SP-84001 | 2. GOVT ACCESSION NO. AD-A176673 | 3. RECIPIENT'S CATALOG NUMBER |
| 4. TITLE (and Subtitle) STRUCTURES TO RESIST THE EFFECTS OF ACCIDENTAL EXPLOSIONS. VOLUME II, BLAST, FRAGMENT, AND SHOCK LOADS | | 5. TYPE OF REPORT & PERIOD COVERED Special Publication Jan 84 - Oct 86 |
| 7. AUTHOR(s) Henry Ayvazyan, Michael Dede, Norval Dobbs Ammann & Whitney; Mark Whitney, Patricia Bowles, Wilfred Baker, Southwest Research Institute; Joseph P. Calzagirone, Project Engineer, ARDEC | | 6. PERFORMING ORG. REPORT NUMBER |
| 9. PERFORMING ORGANIZATION NAME AND ADDRESS Ammann and Whitney 96 Morton Street New York, New York 10014 | | 8. CONTRACT OR GRANT NUMBER(s) DAAK10-82-C-0112 |
| 11. CONTROLLING OFFICE NAME AND ADDRESS ARDEC, IMD STINFO Div (SMCAR-MSI) Dover, NJ 07801-5001 | | 10. PROGRAM ELEMENT, PROJECT, TASK AREA & WORK UNIT NUMBERS |
| 14. MONITORING AGENCY NAME & ADDRESS (if different from Controlling Office) ARDEC, AED Energetic Systems Process Div (SMCAR-AES-M) Dover, NJ 07801-5001 | | 12. REPORT DATE December 1986 |
| | | 13. NUMBER OF PAGES 505 |
| | | 15. SECURITY CLASS. (of this report) Unclassified |
| | | 15a. DECLASSIFICATION/DOWNGRADING SCHEDULE |
| 16. DISTRIBUTION STATEMENT (of this Report) Approved for public release; distribution unlimited. | | |
| 17. DISTRIBUTION STATEMENT (of the abstract entered in Block 20, if different from Report) | | |
| 18. SUPPLEMENTARY NOTES This report is Volume II of six volumes which will eventually be published as a tri-service design manual and was sponsored by the Department of Defense Explosives Safety Board. Sections of this volume were prepared by Southwest Research Institute, San Antonio, TX under a subcontract. | | |
| 19. KEY WORDS (Continue on reverse side if necessary and identify by block number) Blast effects Blast pressures Fragment velocity Weapons effects Impulse Protective structures Fragments TNT explosions Air blast Primary fragments Shock loads Surface burst Secondary fragments Ground shock Impulse equivalency (cont) | | |
| 20. ABSTRACT (Continue on reverse side if necessary and identify by block number) This report details design procedures for structures which are subjected to the effects of accidental explosions. The procedures cover the determination of the blast environment and structural design. This volume contains procedures for determining the effects from unconfined and confined explosions (shock, gas, and leakage pressures), including multiple explosions, frangibility, TNT equivalency, external blast loads on structures with and without openings, and the pressure buildup in structures. Another section deals with primary fragments (fragment velocity, distribution of fragments, impact) (cont) | | |

DD FORM 1 JAN 73 1473

EDITION OF 1 NOV 65 IS OBSOLETE

UNCLASSIFIED

SECURITY CLASSIFICATION OF THIS PAGE (When Data Entered)

UNCLASSIFIED

SECURITY CLASSIFICATION OF THIS PAGE(When Data Entered)

19. KEY WORDS (cont)

| | |
|---------------------|-------------------|
| Blast loads | Structure motion |
| Shock pressure | Gas pressures |
| Frangibility | Leakage pressures |
| Vented explosions | |
| Confined explosions | |
| Shock spectra | |
| Fragment impact | |

20. ABSTRACT (cont)

effects) and secondary fragments (velocity, trajectory). The last section on shock loads contains procedures for determining ground shock and air shock effects, structure motions, and shock response spectra. An appendix is included with appropriate example problems and solutions.

UNCLASSIFIED

SECURITY CLASSIFICATION OF THIS PAGE(When Data Entered)

TABLE OF CONTENTS

PAGE

INTRODUCTION

| | | |
|-----|------------------|---|
| 2-1 | Purpose | 1 |
| 2-2 | Objective | 1 |
| 2-3 | Background | 1 |
| 2-4 | Scope of Manual | 2 |
| 2-5 | Format of Manual | 3 |

VOLUME CONTENTS

| | | |
|-----|---------|---|
| 2-6 | General | 4 |
|-----|---------|---|

EXPLOSION EFFECTS

| | | |
|-----|-----------------------------|---|
| 2-7 | Effects of Explosive Output | 4 |
|-----|-----------------------------|---|

BLAST LOADS

| | | |
|----------|------------------------------|-----|
| 2-8 | Blast Phenomena | 5 |
| 2-8.1 | General | 5 |
| 2-8.2 | Explosive Materials | 5 |
| 2-9 | TNT Equivalency | 6 |
| 2-10 | Blast-Loading Categories | 7 |
| 2-10.1 | Unconfined Explosion | 7 |
| 2-10.1.1 | Free Air Burst Explosion | 7 |
| 2-10.1.2 | Air Burst Explosion | 7 |
| 2-10.1.3 | Surface Burst Explosion | 7 |
| 2-10.2 | Confined Explosion | 11 |
| 2-10.2.1 | Fully Vented Explosion | 11 |
| 2-10.2.2 | Partially Confined Explosion | 11 |
| 2-10.2.3 | Fully Confined Explosion | 11 |
| 2-11 | Blast Loading Protection | 11 |
| 2-12 | Blast-Wave Phenomena | 12 |
| 2-13 | Unconfined Explosions | 15 |
| 2-13.1 | Free-Air Burst | 15 |
| 2-13.2 | Air Burst | 17 |
| 2-13.3 | Surface Burst | 28 |
| 2-13.4 | Multiple Explosions | 29 |
| 2-14 | Confined Explosion | 75 |
| 2-14.1 | Effects of Confinement | 75 |
| 2-14.2 | Shock Pressures | 78 |
| 2-14.2.1 | Blast Loads | 78 |
| 2-14.2.2 | Frangibility | 182 |
| 2-14.2.3 | TNT Equivalency | 183 |
| 2-14.2.4 | Multiple Explosions | 185 |

| |
|-------------------------------------|
| <input checked="" type="checkbox"/> |
| <input type="checkbox"/> |
| <input type="checkbox"/> |
| ides |
| or |

| | |
|------|---------|
| Dist | Special |
| A-1 | |



| | | |
|---------------------------------|---|-----|
| 2-14.3 | Gas Pressures | 186 |
| 2-14.3.1 | Blast Loads | 186 |
| 2-14.3.2 | Frangibility | 203 |
| 2-14.3.3 | TNT Equivalency | 203 |
| 2-14.3.4 | Multiple Explosions | 205 |
| 2-14.4 | Leakage Pressures | 205 |
| 2-14.4.1 | Introduction | 205 |
| 2-14.4.2 | Fully Vented Three-Wall Cubicles | 206 |
| 2-14.4.3 | Partially Vented Four-Wall Cubicles - Vent Openings in Roof | 208 |
| 2-14.4.4 | Partially Vented Four-Wall Cubicles - Vent Openings in Wall | 209 |
| 2-15 | External Blast Loads on Structure | 209 |
| 2-15.1 | General | 209 |
| 2-15.2 | Forces Acting on Structures | 232 |
| 2-15.3 | Above-Ground Rectangular Structures Without Openings | 234 |
| 2-15.3.1 | General | 234 |
| 2-15.3.2 | Front Wall Loads | 234 |
| 2-15.3.3 | Roof and Side Wall Loads | 239 |
| 2-15.3.4 | Rear Wall Loads | 245 |
| 2-15.3.5 | Multiple Explosions | 246 |
| 2-15.4 | Above-Ground Rectangular Structure With Openings | 246 |
| 2-15.4.1 | General | 246 |
| 2-15.4.2 | Exterior Front Wall Loads | 251 |
| 2-15.4.3 | Interior Front Wall Loads | 253 |
| 2-15.4.4 | Interior Side Wall and Roof Loads | 258 |
| 2-15.4.5 | Interior Back Wall | 284 |
| 2-15.5 | Pressure Buildup in Structures | 285 |
| 2-15.5.1 | General | 285 |
| 2-15.5.2 | Method of Calculation | 285 |
| PRIMARY AND SECONDARY FRAGMENTS | | |
| 2-16 | General | 293 |
| 2-17 | Primary Fragments | 293 |
| 2-17.1 | General | 293 |
| 2-17.2 | Initial Fragment Velocity | 294 |
| 2-17.2.1 | Explosives with Uniform Cylindrical Containers | 294 |
| 2-17.2.2 | Explosives with Non-Uniform Cylindrical Containers | 294 |
| 2-17.2.3 | Explosives with Non- Cylindrical Containers | 296 |
| 2-17.3 | Fragment Mass Distribution | 296 |
| 2-17.3.1 | Explosives with Uniform Cylindrical Containers | 296 |

| | PAGE |
|--|------|
| 2-17.3.2 Explosives with Non-Uniform Cylindrical Containers | 302 |
| 2-17.3.3 Explosives with Non-Cylindrical Containers | 307 |
| 2-17.4 Variation of Fragment Velocity with Distance | 309 |
| 2-17.5 Primary Fragments - Shape, Caliber, Density and Impact Angle | 310 |
| 2-17.5.1 General | 310 |
| 2-17.5.2 Shape of Primary Fragments | 310 |
| 2-17.5.3 Caliber Density | 315 |
| 2-17.5.4 Nose Shape Factor | 315 |
| 2-17.5.5 Impact Angle | 315 |
| 2-18 Secondary Fragments | 315 |
| 2-18.1 General | 315 |
| 2-18.2 Velocity of Unconstrained Secondary Fragments | 316 |
| 2-18.3 Velocity of Constrained Secondary Fragments | 326 |
| 2-19 Fragment Trajectories | 327 |
| SHOCK LOADS | |
| 2-20 Introduction | 331 |
| 2-21 Ground Shock | 332 |
| 2-21.1 Introduction | 332 |
| 2-21.2 Air Blast-Induced Ground Shock | 333 |
| 2-21.3 Direct-Induced Ground Motion | 338 |
| 2-22 Air Shock | 339 |
| 2-22.1 Introduction | 339 |
| 2-22.2 Method of Analysis | 340 |
| 2-23 Structure Motions | 341 |
| 2-23.1 Introduction | 341 |
| 2-23.2 Net Ground Shock | 341 |
| 2-23.3 Maximum Structure Motion | 344 |
| 2-24 Shock Response Spectra | 344 |
| 2-24.1 Introduction | 344 |
| 2-24.2 Definition of Shock Spectra Grid | 344 |
| 2-24.3 Response Spectra | 345 |
| APPENDIX 2A ILLUSTRATIVE EXAMPLES | 349 |
| APPENDIX 2B LIST OF SYMBOLS | 453 |
| 2C BIBLIOGRAPHY | 473 |
| DISTRIBUTION LIST | 485 |

LIST OF FIGURES

| <u>FIGURE</u> | <u>TITLE</u> | <u>PAGE</u> |
|---------------|---|-------------|
| 2-1 | Blast loading categories..... | 10 |
| 2-2 | Free-field pressure-time variation..... | 13 |
| 2-3 | Peak incident pressure versus peak dynamic pressure density of air behind the shock front and particle velocity..... | 14 |
| 2-4 | Free-air burst blast environment..... | 18 |
| 2-5 | Pressure-time variation for a free-air burst..... | 19 |
| 2-6 | Peak incident pressure versus the ratio of normal reflected pressure/incident pressure for a free air burst..... | 20 |
| 2-7 | Positive phase shock wave parameters for a spherical TNT explosion in free air at sea level..... | 21 |
| 2-8 | Negative phase shock wave parameters for a spherical TNT explosion in free air at sea level..... | 22 |
| 2-9 | Variation of reflected pressure as a function of angle of incidence..... | 23 |
| 2-10 | Variation of scaled reflected impulse as a function of angle of incidence..... | 24 |
| 2-11 | Air burst blast environment..... | 25 |
| 2-12 | Pressure-time variation for air burst..... | 26 |
| 2-13 | Scaled height of triple point..... | 27 |
| 2-14 | Surface burst blast environment..... | 30 |
| 2-15 | Positive phase shock wave parameters for a hemispherical TNT explosion on the surface at sea level..... | 31 |
| 2-16 | Negative phase shock wave parameters for a hemispherical TNT explosion on the surface at sea level..... | 32 |
| 2-17 | Explosive shapes..... | 42 |
| 2-18 | Peak positive incident pressure and scaled impulse for an explosion on the surface at sea level..... | 43 |
| 2-19 | Peak positive incident pressure and scaled impulse for an explosion on the surface at sea level..... | 44 |
| 2-20 | Peak positive incident pressure and scaled impulse for an explosion on the surface at sea level..... | 45 |
| 2-21 | Peak positive incident pressure and scaled impulse for an explosion on the surface at sea level..... | 46 |
| 2-22 | Peak positive incident pressure and scaled impulse for an explosion on the surface at sea level..... | 47 |
| 2-23 | Peak positive incident pressure and scaled impulse for an explosion on the surface at sea level..... | 48 |
| 2-24 | Peak positive incident pressure and scaled impulse for an explosion on the surface at sea level..... | 49 |
| 2-25 | Peak positive incident pressure and scaled impulse for an explosion on the surface at sea level..... | 50 |
| 2-26 | Peak positive incident pressure and scaled impulse for an explosion on the surface at sea level..... | 51 |
| 2-27 | Peak positive incident pressure and scaled impulse for an explosion on the surface at sea level..... | 52 |
| 2-28 | Peak positive incident pressure and scaled impulse for an explosion on the surface at sea level..... | 53 |

FIGURETITLEPAGE

| | | |
|------|--|----|
| 2-29 | Peak positive incident pressure and scaled impulse for an explosion on the surface at sea level..... | 54 |
| 2-30 | Peak positive incident pressure and scaled impulse for an explosion on the surface at sea level..... | 55 |
| 2-31 | Peak positive incident pressure and scaled impulse for an explosion on the surface at sea level..... | 56 |
| 2-32 | Peak positive incident pressure and scaled impulse for an explosion on the surface at sea level..... | 57 |
| 2-33 | Peak positive incident pressure and scaled impulse for an explosion on the surface at sea level..... | 58 |
| 2-34 | Peak positive incident pressure and scaled impulse for an explosion on the surface at sea level..... | 59 |
| 2-35 | Peak positive incident pressure and scaled impulse for an explosion on the surface at sea level..... | 60 |
| 2-36 | Peak positive incident pressure and scaled impulse for an explosion on the surface at sea level..... | 61 |
| 2-37 | Peak positive incident pressure and scaled impulse for an explosion on the surface at sea level..... | 62 |
| 2-38 | Peak positive incident pressure and scaled impulse for an explosion on the surface at sea level..... | 63 |
| 2-39 | Peak positive incident pressure and scaled impulse for an explosion on the surface at sea level..... | 64 |
| 2-40 | Peak positive incident pressure and scaled impulse for an explosion on the surface at sea level..... | 65 |
| 2-41 | Peak positive incident pressure and scaled impulse for an explosion on the surface at sea level..... | 66 |
| 2-42 | Peak positive incident pressure and scaled impulse for an explosion on the surface at sea level..... | 67 |
| 2-43 | Peak positive incident pressure and scaled impulse for an explosion on the surface at sea level..... | 68 |
| 2-44 | Peak positive incident pressure and scaled impulse for an explosion on the surface at sea level..... | 69 |
| 2-45 | Peak positive incident pressure and scaled impulse for an explosion on the surface at sea level..... | 70 |
| 2-46 | Peak positive incident pressure and scaled impulse for an explosion on the surface at sea level..... | 71 |
| 2-47 | Peak positive incident pressure and scaled impulse for an explosion on the surface at sea level..... | 72 |
| 2-48 | Peak positive incident pressure and scaled impulse for an explosion on the surface at sea level..... | 73 |
| 2-49 | Peak positive incident pressure and scaled impulse for an explosion on the surface at sea level..... | 74 |
| 2-50 | Confined explosion structures..... | 76 |
| 2-51 | Barrier and cubicle configurations and parameters..... | 80 |
| 2-52 | Average peak reflected pressure ($N = 1$, $P/L = 0.10$, $h/H = 0.10$)..... | 84 |
| 2-53 | Average peak reflected pressure ($N = 1$, $P/L = 0.25$ and 0.75 , $h/H = 0.10$)..... | 85 |
| 2-54 | Average peak reflected pressure ($N = 1$, $P/L = 0.50$, $h/H = 0.10$)..... | 86 |
| 2-55 | Average peak reflected pressure ($N = 1$, $P/L = 0.10$, $h/H = 0.25$)..... | 87 |

| <u>FIGURE</u> | <u>TITLE</u> | <u>PAGE</u> |
|---------------|--|-------------|
| 2-56 | Average peak reflected pressure (N = 1, P/L = 0.25 and 0.75, h/H = 0.25)..... | 88 |
| 2-57 | Average peak reflected pressure (N = 1, P/L = 0.50 h/H = 0.25)..... | 89 |
| 2-58 | Average peak reflected pressure (N = 1, P/L = 0.10, h/H = 0.50) | 90 |
| 2-59 | Average peak reflected pressure (N = 1, P/L = 0.25 and 0.75, h/H = 0.50)..... | 91 |
| 2-60 | Average peak reflected pressure (N = 1, P/L = 0.50, h/H = 0.50)..... | 92 |
| 2-61 | Average peak reflected pressure (N = 1, P/L = 0.10, h/H = 0.75)..... | 93 |
| 2-62 | Average peak reflected pressure (N = 1, P/L = 0.25 and 0.75, h/H = 0.75)..... | 94 |
| 2-63 | Average peak reflected pressure (N = 1, P/L = 0.50, h/H = 0.75)..... | 95 |
| 2-64 | Average peak reflected pressure (N = 2, P/L = 0.10, h/H = 0.10)..... | 96 |
| 2-65 | Average peak reflected pressure (N = 2, P/L = 0.25, h/H = 0.10)..... | 97 |
| 2-66 | Average peak reflected pressure (N = 2, P/L = 0.50, h/H = 0.10)..... | 98 |
| 2-67 | Average peak reflected pressure (N = 2, P/L = 0.75, h/H = 0.10)..... | 99 |
| 2-68 | Average peak reflected pressure (N = 2, P/L = 0.10, h/H = 0.25)..... | 100 |
| 2-69 | Average peak reflected pressure (N = 2, P/L = 0.25, h/H = 0.25)..... | 101 |
| 2-70 | Average peak reflected pressure (N = 2, P/L = 0.50, h/H = 0.25)..... | 102 |
| 2-71 | Average peak reflected pressure (N = 2, P/L = 0.75, h/H = 0.25)..... | 103 |
| 2-72 | Average peak reflected pressure (N = 2, P/L = 0.10, h/H = 0.50)..... | 104 |
| 2-73 | Average peak reflected pressure (N = 2, P/L = 0.25, h/H = 0.50)..... | 105 |
| 2-74 | Average peak reflected pressure (N = 2, P/L = 0.50, h/H = 0.50)..... | 106 |
| 2-75 | Average peak reflected pressure (N = 2, P/L = 0.75, h/H = 0.50)..... | 107 |
| 2-76 | Average peak reflected pressure (N = 2, P/L = 0.10, h/H = 0.75)..... | 108 |
| 2-77 | Average peak reflected pressure (N = 2, P/L = 0.25, h/H = 0.75)..... | 109 |
| 2-78 | Average peak reflected pressure (N = 2, P/L = 0.50, h/H = 0.75)..... | 110 |
| 2-79 | Average peak reflected pressure (N = 2, P/L = 0.75, h/H = 0.75)..... | 111 |
| 2-80 | Average peak reflected pressure (N = 3, P/L = 0.10, h/H = 0.10)..... | 112 |
| 2-81 | Average peak reflected pressure (N = 3, P/L = 0.25 and 0.75, h/H = 0.10)..... | 113 |

| | | |
|-------|---|-----|
| 2-82 | Average peak reflected pressure (N = 3, P/L = 0.50, h/H = 0.10)..... | 114 |
| 2-83 | Average peak reflected pressure (N = 3, P/L = 0.10, h/H = 0.25)..... | 115 |
| 2-84 | Average peak reflected pressure (N = 3, P/L = 0.25 and 0.75, h/H = 0.25)..... | 116 |
| 2-85 | Average peak reflected pressure (N = 3, P/L = 0.50, h/H = 0.25)..... | 117 |
| 2-86 | Average peak reflected pressure (N = 3, P/L = 0.10, h/H = 0.50)..... | 118 |
| 2-87 | Average peak reflected pressure (N = 3, P/L = 0.25 and 0.75, h/H = 0.50)..... | 119 |
| 2-88 | Average peak reflected pressure (N = 3, P/L = 0.50, h/H = 0.50)..... | 120 |
| 2-89 | Average peak reflected pressure (N = 3, P/L = 0.10, h/H = 0.75)..... | 121 |
| 2-90 | Average peak reflected pressure (N = 3, P/L = 0.25 and 0.75, h/H = 0.75)..... | 122 |
| 2-91 | Average peak reflected pressure (N = 3, P/L = 0.50, h/H = 0.75)..... | 123 |
| 2-92 | Average peak reflected pressure (N = 4, P/L = 0.10, h/H = 0.10)..... | 124 |
| 2-93 | Average peak reflected pressure (N = 4, P/L = 0.25 and 0.75, h/H = 0.10)..... | 125 |
| 2-94 | Average peak reflected pressure (N = 4, P/L = 0.50, h/H = 0.10)..... | 126 |
| 2-95 | Average peak reflected pressure (N = 4, P/L = 0.10, h/H = 0.25 and 0.75)..... | 127 |
| 2-96 | Average peak reflected pressure (N = 4, P/L = 0.25 and 0.75, h/H = 0.25 and 0.75)..... | 128 |
| 2-97 | Average peak reflected pressure (N = 4, P/L = 0.50, h/H = 0.25 and 0.75)..... | 129 |
| 2-98 | Average peak reflected pressure (N = 4, P/L = 0.10, h/H = 0.50)..... | 130 |
| 2-99 | Average peak reflected pressure (N = 4, P/L = 0.25 and 0.75, h/H = 0.50)..... | 131 |
| 2-100 | Average peak reflected pressure (N = 4, P/L = 0.50, h/H = 0.50)..... | 132 |
| 2-101 | Scaled average unit reflected impulse (N = 1, P/L = 0.10, h/H = 0.10)..... | 133 |
| 2-102 | Scaled average unit reflected impulse (N = 1, P/L = 0.25 and 0.75, h/H = 0.10)..... | 134 |
| 2-103 | Scaled average unit reflected impulse (N = 1, P/L = 0.50, h/H = 0.10)..... | 135 |
| 2-104 | Scaled average unit reflected impulse (N = 1, P/L = 0.10, h/H = 0.25)..... | 136 |
| 2-105 | Scaled average unit reflected impulse (N = 1, P/L = 0.25 and 0.75, h/H = 0.25)..... | 137 |
| 2-106 | Scaled average unit reflected impulse (N = 1, P/L = 0.50, h/H = 0.25)..... | 138 |
| 2-107 | Scaled average unit reflected impulse (N = 1, P/L = 0.10, h/H = 0.50)..... | 139 |

| | | |
|-------|--|-----|
| 2-108 | Scaled average unit reflected impulse ($N = 1$, $P/L = 0.25$ and 0.75 , $h/H = 0.50$)..... | 140 |
| 2-109 | Scaled average unit reflected impulse ($N = 1$, $P/L = 0.50$, $h/H = 0.50$)..... | 141 |
| 2-110 | Scaled average unit reflected impulse ($N = 1$, $P/L = 0.10$, $h/H = 0.75$)..... | 142 |
| 2-111 | Scaled average unit reflected impulse ($N = 1$, $P/L = 0.25$ and 0.75 , $h/H = 0.75$)..... | 143 |
| 2-112 | Scaled average unit reflected impulse ($N = 1$, $P/L = 0.50$, $h/H = 0.75$)..... | 144 |
| 2-113 | Scaled average unit reflected impulse ($N = 2$, $P/L = 0.10$, $h/H = 0.10$)..... | 145 |
| 2-114 | Scaled average unit reflected impulse ($N = 2$, $P/L = 0.25$, $h/H = 0.10$)..... | 146 |
| 2-115 | Scaled average unit reflected impulse ($N = 2$, $P/L = 0.50$, $h/H = 0.10$)..... | 147 |
| 2-116 | Scaled average unit reflected impulse ($N = 2$, $P/L = 0.75$, $h/H = 0.10$)..... | 148 |
| 2-117 | Scaled average unit reflected impulse ($N = 2$, $P/L = 0.10$, $h/H = 0.25$)..... | 149 |
| 2-118 | Scaled average unit reflected impulse ($N = 2$, $P/L = 0.25$, $h/H = 0.25$)..... | 150 |
| 2-119 | Scaled average unit reflected impulse ($N = 2$, $P/L = 0.50$, $h/H = 0.25$)..... | 151 |
| 2-120 | Scaled average unit reflected impulse ($N = 2$, $P/L = 0.75$, $h/H = 0.25$)..... | 152 |
| 2-121 | Scaled average unit reflected impulse ($N = 2$, $P/L = 0.10$, $h/H = 0.50$)..... | 153 |
| 2-122 | Scaled average unit reflected impulse ($N = 2$, $P/L = 0.25$, $h/H = 0.50$)..... | 154 |
| 2-123 | Scaled average unit reflected impulse ($N = 2$, $P/L = 0.50$, $h/H = 0.50$)..... | 155 |
| 2-124 | Scaled average unit reflected impulse ($N = 2$, $P/L = 0.75$, $h/H = 0.50$)..... | 156 |
| 2-125 | Scaled average unit reflected impulse ($N = 2$, $P/L = 0.10$, $h/H = 0.75$)..... | 157 |
| 2-126 | Scaled average unit reflected impulse ($N = 2$, $P/L = 0.25$, $h/H = 0.75$)..... | 158 |
| 2-127 | Scaled average unit reflected impulse ($N = 2$, $P/L = 0.50$, $h/H = 0.75$)..... | 159 |
| 2-128 | Scaled average unit reflected impulse ($N = 2$, $P/L = 0.75$, $h/H = 0.75$)..... | 160 |
| 2-129 | Scaled average unit reflected impulse ($N = 3$, $P/L = 0.10$, $h/H = 0.10$)..... | 161 |
| 2-130 | Scaled average unit reflected impulse ($N = 3$, $P/L = 0.25$ and 0.75 , $h/H = 0.10$)..... | 162 |
| 2-131 | Scaled average unit reflected impulse ($N = 3$, $P/L = 0.50$, $h/H = 0.10$)..... | 163 |
| 2-132 | Scaled average unit reflected impulse ($N = 3$, $P/L = 0.10$, $h/H = 0.25$)..... | 164 |
| 2-133 | Scaled average unit reflected impulse ($N = 3$, $P/L = 0.25$ and 0.75 , $h/H = 0.25$)..... | 165 |

| | | |
|-------|---|-----|
| 2-134 | Scaled average unit reflected impulse ($N = 3$, $P/L = 0.50$, $h/H = 0.25$)..... | 166 |
| 2-135 | Scaled average unit reflected impulse ($N = 3$, $P/L = 0.10$, $h/H = 0.50$)..... | 167 |
| 2-136 | Scaled average unit reflected impulse ($N = 3$, $P/L = 0.25$ and 0.75 , $h/H = 0.50$)..... | 168 |
| 2-137 | Scaled average unit reflected impulse ($N = 3$, $P/L = 0.50$, $h/H = 0.50$)..... | 169 |
| 2-138 | Scaled average unit reflected impulse ($N = 3$, $P/L = 0.10$, $h/H = 0.75$)..... | 170 |
| 2-139 | Scaled average unit reflected impulse ($N = 3$, $P/L = 0.25$ and 0.75 , $h/H = 0.75$)..... | 171 |
| 2-140 | Scaled average unit reflected impulse ($N = 3$, $P/L = 0.50$, $h/H = 0.75$)..... | 172 |
| 2-141 | Scaled average unit reflected impulse ($N = 4$, $P/L = 0.10$, $h/H = 0.10$)..... | 173 |
| 2-142 | Scaled average unit reflected impulse ($N = 4$, $P/L = 0.25$ and 0.75 , $h/H = 0.10$)..... | 174 |
| 2-143 | Scaled average unit reflected impulse ($N = 4$, $P/L = 0.50$, $h/H = 0.10$)..... | 175 |
| 2-144 | Scaled average unit reflected impulse ($N = 4$, $P/L = 0.10$, $h/H = 0.25$ and 0.75)..... | 176 |
| 2-145 | Scaled average unit reflected impulse ($N = 4$, $P/L = 0.25$ and 0.75 , $h/H = 0.25$ and 0.75)..... | 177 |
| 2-146 | Scaled average unit reflected impulse ($N = 4$, $P/L = 0.50$, $h/H = 0.25$ and 0.75)..... | 178 |
| 2-147 | Scaled average unit reflected impulse ($N = 4$, $P/L = 0.10$, $h/H = 0.50$)..... | 179 |
| 2-148 | Scaled average unit reflected impulse ($N = 4$, $P/L = 0.25$ and 0.75 , $h/H = 0.50$)..... | 180 |
| 2-149 | Scaled average unit reflected impulse ($N = 4$, $P/L = 0.50$, $h/H = 0.50$)..... | 181 |
| 2-150 | Reflection factor for shock loads on frangible elements..... | 184 |
| 2-151 | Pressure-time variation for a partially vented explosion..... | 187 |
| 2-152 | Peak gas pressure produced by a TNT detonation in a partially contained chamber..... | 188 |
| 2-153 | Scaled gas impulse ($W/V_f = 0.002$, $i_r/W^{1/3} = 20$)..... | 189 |
| 2-154 | Scaled gas impulse ($W/V_f = 0.002$, $i_r/W^{1/3} = 100$)..... | 190 |
| 2-155 | Scaled gas impulse ($W/V_f = 0.002$, $i_r/W^{1/3} = 600$)..... | 191 |
| 2-156 | Scaled gas impulse ($W/V_f = 0.015$, $i_r/W^{1/3} = 20$)..... | 192 |
| 2-157 | Scaled gas impulse ($W/V_f = 0.015$, $i_r/W^{1/3} = 100$)..... | 193 |
| 2-158 | Scaled gas impulse ($W/V_f = 0.015$, $i_r/W^{1/3} = 600$)..... | 194 |
| 2-159 | Scaled gas impulse ($W/V_f = 0.15$, $i_r/W^{1/3} = 20$)..... | 195 |
| 2-160 | Scaled gas impulse ($W/V_f = 0.15$, $i_r/W^{1/3} = 100$)..... | 196 |
| 2-161 | Scaled gas impulse ($W/V_f = 0.15$, $i_r/W^{1/3} = 600$)..... | 197 |

| <u>FIGURE</u> | <u>TITLE</u> | <u>PAGE</u> |
|---------------|--|-------------|
| 2-162 | Scaled gas impulse ($W/V_f = 1.0$, $1_r/W^{1/3} = 100$)..... | 198 |
| 2-163 | Scaled gas impulse ($W/V_f = 1.0$, $1_r/W^{1/3} = 600$)..... | 199 |
| 2-164 | Scaled gas impulse ($W/V_f = 1.0$, $1_r/W^{1/3} = 2000$)..... | 200 |
| 2-165 | Combined shock and gas pressures..... | 202 |
| 2-166 | TNT conversion factor for charges..... | 204 |
| 2-167 | Fully vented three-wall cubicles and direction of blast wave propagation..... | 207 |
| 2-168 | Envelope curves for peak positive pressure outside three-wall cubicles without a roof..... | 210 |
| 2-169 | Envelope curves for peak positive pressure outside three-wall cubicles with a roof..... | 211 |
| 2-170 | Envelope curves for maximum peak pressure outside three-wall cubicles..... | 212 |
| 2-171 | Scaled peak positive impulse out the open front of cubic three-wall cubicle without a roof..... | 213 |
| 2-172 | Scaled peak positive impulse out the open front of rectangular three-wall cubicle without a roof..... | 214 |
| 2-173 | Scaled peak positive impulse behind sidewall of cubic three-wall cubicle without a roof..... | 215 |
| 2-174 | Scaled peak positive impulse behind sidewall of rectangular three-wall cubicle without a roof..... | 216 |
| 2-175 | Scaled peak positive impulse behind backwall of cubic three-wall cubicle without a roof..... | 217 |
| 2-176 | Scaled peak positive impulse behind backwall of rectangular three-wall cubicle without a roof..... | 218 |
| 2-177 | Scaled peak positive impulse out the open front of cubic three-wall cubicle with a roof..... | 219 |
| 2-178 | Scaled peak positive impulse out the open front of rectangular three-wall cubicle with a roof..... | 220 |
| 2-179 | Scaled peak positive impulse behind sidewall of cubic three-wall cubicle with a roof..... | 221 |
| 2-180 | Scaled peak positive impulse behind sidewall of rectangular three-wall cubicle with a roof..... | 222 |
| 2-181 | Scaled peak positive impulse behind backwall of cubic three-wall cubicle with a roof..... | 223 |
| 2-182 | Scaled peak positive impulse behind backwall of rectangular three-wall cubicle with a roof..... | 224 |
| 2-183 | Four wall cubicle vented through its roof..... | 225 |
| 2-184 | Peak positive pressure outside of a four-wall cubicle vented through its roof..... | 226 |
| 2-185 | Scaled positive impulse outside of a four-wall cubicle vented through its roof..... | 227 |
| 2-186 | Four wall cubicle vented through a wall and direction of blast wave propagation..... | 228 |
| 2-187 | Peak positive pressure at the front of a partially vented four-wall cubicle..... | 229 |
| 2-188 | Peak positive pressure at the side of a partially vented four-wall cubicle..... | 230 |

| | | |
|-------|--|-----|
| 2-189 | Peak positive pressure at the back of a partially vented four wall cubicle..... | 231 |
| 2-190 | Idealized pressure-time variation | 233 |
| 2-191 | Front wall loading..... | 235 |
| 2-192 | Velocity of sound in reflected overpressure region versus peak incident overpressure..... | 237 |
| 2-193 | Reflected pressure coefficient versus angle of incidence..... | 238 |
| 2-194 | Reflected scaled impulse versus angle of incidence..... | 240 |
| 2-195 | Roof and side wall loading..... | 241 |
| 2-196 | Peak equivalent uniform roof pressures..... | 242 |
| 2-197 | Scaled rise time of equivalent uniform positive roof pressures..... | 243 |
| 2-198 | Scaled duration of equivalent uniform roof pressures..... | 244 |
| 2-199 | Rear wall loading..... | 247 |
| 2-200 | Idealized structure configuration for interior blast loads..... | 249 |
| 2-201 | Idealized interior blast loads..... | 250 |
| 2-202 | Sub-division of typical front wall with openings..... | 252 |
| 2-203 | Maximum average pressure on interior face of front wall (W/H = 3/4)..... | 254 |
| 2-204 | Maximum average pressure on interior face of front wall (W/H = 3/2)..... | 255 |
| 2-205 | Maximum average pressure on interior face of front wall (W/H = 3)..... | 256 |
| 2-206 | Maximum average pressure on interior face of front wall (W/H = 6)..... | 257 |
| 2-207 | Arrival time, T_1 , for interior front wall blast load (W/H = 3/4 and 3/2)..... | 259 |
| 2-208 | Arrival time, T_1 , for interior front wall blast load (W/H = 3 and 6)..... | 260 |
| 2-209 | Idealized rise time, $T_2 - T_1$, for interior front wall blast load (W/H = 3/4 and 3/2)..... | 261 |
| 2-210 | Idealized rise time, $T_2 - T_1$, for interior front wall blast load (W/H = 3 and 6)..... | 262 |
| 2-211 | Idealized duration, $T_3 - T_1$, for interior front wall blast load (W/H = 3/4 and 3/2)..... | 263 |
| 2-212 | Idealized duration, $T_3 - T_1$, for interior front wall blast load (W/H = 3 and 6)..... | 264 |
| 2-213 | Idealized times T_1 and T_2 for interior side wall blast load..... | 267 |
| 2-214 | Idealized times T_3 and T_4 for interior side wall blast load (L/H = 1, W/H = 3/4)..... | 268 |
| 2-215 | Idealized times T_3 and T_4 for interior side wall blast load (L/H = 1, W/H = 3/2)..... | 269 |
| 2-216 | Idealized times T_3 and T_4 for interior side wall blast load (L/H = 1, W/H = 3)..... | 270 |

| | | |
|-------|---|-----|
| 2-217 | Idealized times T_3 and T_4 for interior side wall blast load ($L/H = 1$, $W/H = 6$)..... | 271 |
| 2-218 | Idealized times T_3 and T_4 for interior side wall blast load ($L/H = 2$, $W/H = 3/4$)..... | 272 |
| 2-219 | Idealized times T_3 and T_4 for interior side wall blast load ($L/H = 2$, $W/H = 3/2$)..... | 273 |
| 2-220 | Idealized times T_3 and T_4 for interior side wall blast load ($L/H = 2$, $W/H = 3$)..... | 274 |
| 2-221 | Idealized times T_3 and T_4 for interior side wall blast load ($L/H = 2$, $W/H = 6$)..... | 275 |
| 2-222 | Idealized times T_3 and T_4 for interior side wall blast load ($L/H = 4$, $W/H = 3/4$)..... | 276 |
| 2-223 | Idealized times T_3 and T_4 for interior side wall blast load ($L/H = 4$, $W/H = 3/2$)..... | 277 |
| 2-224 | Idealized times T_3 and T_4 for interior side wall blast load ($L/H = 4$, $W/H = 3$)..... | 278 |
| 2-225 | Idealized times T_3 and T_4 for interior side wall blast load ($L/H = 4$, $W/H = 6$)..... | 279 |
| 2-226 | Idealized times T_3 and T_4 for interior side wall blast load ($L/H = 8$, $W/H = 3/4$)..... | 280 |
| 2-227 | Idealized times T_3 and T_4 for interior side wall blast load ($L/H = 8$, $W/H = 3/2$)..... | 281 |
| 2-228 | Idealized times T_3 and T_4 for interior side wall blast load ($L/H = 8$, $W/H = 3$)..... | 282 |
| 2-229 | Idealized times T_3 and T_4 for interior side wall blast load ($L/H = 8$, $W/H = 6$)..... | 283 |
| 2-230 | Idealized pressure coefficient for back wall interior blast load ($L/H = 1$ and 2)..... | 287 |
| 2-231 | Idealized pressure coefficient for back wall interior blast load ($L/H = 4$ and 8)..... | 288 |
| 2-232 | Arrival time, T_1 , for interior back wall blast load ($W/H = 3/4$ and $3/2$)..... | 289 |
| 2-233 | Arrival time, T_1 , for interior back wall blast load ($W/H = 3$ and 6)..... | 290 |
| 2-234 | Idealized time $T_2 - T_1$ for interior back wall blast load..... | 291 |
| 2-235 | Leakage pressure coefficient vs. pressure differential..... | 292 |
| 2-236 | Explosive outer casing separated by incompressible fluid..... | 297 |
| 2-237 | Initial velocity of primary fragments for various geometries... | 299 |
| 2-238 | M_A/B versus cylindrical casing geometry..... | 303 |
| 2-239 | Design fragment weight versus design confidence level ($0.3 \leq CL \leq 1$) | 304 |
| 2-240 | Design fragment weight versus design confidence level ($0.986 \leq CL \leq 1$) | 305 |

| | | |
|-------|---|-----|
| 2-241 | $B^2 N_T / W_c$ versus casing geometry..... | 306 |
| 2-242 | Equivalent cylindrical explosive casings..... | 308 |
| 2-243 | Variation of primary fragment velocity with distance..... | 311 |
| 2-244 | Primary fragment shapes..... | 312 |
| 2-245 | Relationship between fragment weight and fragment diameter..... | 313 |
| 2-246 | Interaction of blast wave with an irregular object..... | 317 |
| 2-247 | Idealized pressure-time loading on an irregular fragment..... | 318 |
| 2-248 | Nondimensional object velocity, \bar{V} , as a function of pressure and impulse..... | 320 |
| 2-249 | Target shape factor for unconstrained fragments..... | 323 |
| 2-250 | Specific acquired impulse versus distance..... | 325 |
| 2-251 | Scaled fragment velocities for constrained fragments..... | 328 |
| 2-252 | Fragment range prediction..... | 330 |
| 2-253 | Net ground motions produced by an explosion at the ground surface..... | 334 |
| 2-254 | Typical response shock spectra..... | 346 |

LIST OF TABLES

| <u>Table</u> | <u>Title</u> | <u>Page</u> |
|--------------|---|-------------|
| 2-1 | Heat of Detonation and Heat of Combustion..... | 8 |
| 2-2 | List of Illustrations of Peak Incident Pressure and Impulse Produced by Surface Detonation of Various Explosives..... | 33 |
| 2-3 | List of Illustrations for Average Peak Reflected Pressure and Scaled Average Unit Reflected Impulse..... | 81 |
| 2-4 | List of Illustrations for Interior Side Wall Idealized Times T_3 and T_4 | 284 |
| 2-5 | Specific Weight and Gurney Energy Constant for Various Explosives..... | 295 |
| 2-6 | Initial Velocity of Primary Fragments for Various Geometries.... | 298 |
| 2-7 | Mott Scaling Constants for Mild Steel Casings and Various Explosives..... | 301 |
| 2-8 | Drag Coefficient, C_D , for various shapes..... | 322 |
| 2-9 | Steel Toughness..... | 327 |
| 2-10 | Mass Density for Typical Soils and Rocks..... | 335 |
| 2-11 | Typical Seismic Velocities for Soils and Rocks..... | 336 |
| 2-12 | Coefficient of friction for concrete foundation and underlying soils..... | 343 |

VOLUME 11
BLAST, FRAGMENT AND SHOCK LOADS

INTRODUCTION

2-1 Purpose

The purpose of this six volume manual is to present methods of design for protective construction used in facilities for development, testing, production, maintenance, modification, inspection, disposal and storage of explosive materials.

2-2 Objective

The primary objectives are to establish design procedures and construction techniques whereby propagation of explosion (from one structure or part of a structure to another) or mass detonation can be prevented and protection for personnel and valuable equipment will be provided.

The secondary objectives are:

- (1) Establish the blast load parameters required for design of protective structures;
- (2) Provide methods for calculating the dynamic response of structural elements including reinforced concrete, structural steel, etc.;
- (3) Establish construction details and procedures necessary to afford the required strength to resist the applied blast loads;
- (4) Establish guidelines for siting explosive facilities to obtain maximum cost effectiveness in both the planning and structural arrangements; providing closures, and preventing damage to interior portions of structures due to structural motion, shock, and fragment perforation.

2-3 Background

For the first 60 years of the 20th century, criteria and methods based upon the results of the catastrophic events have been used for the design of explosive facilities. The criteria and methods did not include a detailed or reliable quantitative basis for assessing the degree of protection afforded by the protective facility. In the late 1960's quantitative procedures were set forth in the first edition of the present manual, "Structures to Resist the Effects of Accidental Explosions". This manual was based on extensive research and development programs which permitted a more reliable approach to current and future design requirements. Since the original publication of this manual, more extensive testing and development programs have taken place. This additional research was directed primarily towards materials other than reinforced concrete which was the principal construction material referenced in the initial version of the manual.

Modern methods for the manufacture and storage of explosive materials, which include many exotic chemicals, fuels, propellants, etc., required less space

for a given quantity of explosive material than was previously needed. Such concentration of explosives increases the possibility of the propagation of accidental explosions (one accidental explosion causing the detonation of other explosive materials). It is evident that a requirement for more accurate design techniques has become essential. This manual describes rational design methods to provide the required structural protection.

These design methods account for the close-in effects of a detonation including associated high pressures and nonuniformity of the blast loading on protective structures or barriers as well as intermediate and far-range effects which are involved within the design of structures which are positioned away from the explosion. The dynamic response of structures, constructed of various materials, or combination of materials, can be calculated, and details have been developed to provide the properties necessary to supply the required strength and ductility specified by the design. Development of these procedures has been directed primarily towards analyses of protective structures subjected to the effects of high explosive detonation. However, this approach is general and is applicable to the design of other explosive environments as well as other explosive materials as enumerated above.

The design techniques set forth in this manual are based upon the results of numerous full- and small-scale structural response and explosive effects tests of various materials conducted in conjunction with the development of this manual and/or related projects.

2-4 Scope of Manual

This manual is limited only by variety and range of the assumed design situation. An effort has been made to cover the more probable situations. However, sufficient general information on protective design techniques has been included in order that application of the basic theory can be made to situations other than those which were fully considered.

This manual is generally applicable to the design of protective structures subjected to the effects associated with high explosive detonations. For these design situations, this manual will generally apply for explosive quantities less than 25,000 pounds for close-in effects. However, this manual is also applicable to other situations such as far or intermediate range effects. For these latter cases the design procedures as presented are applicable for explosive quantities in the order of 500,000 pounds which is the maximum quantity of high explosive approved for storage facilities in the Department of Defense manual, "Ammunition and Explosives Safety Standards", DOD 6055.9-STD.

Because the tests conducted so far in connection with this manual have been directed primarily towards the response of structural steel and reinforced concrete elements to blast overpressures, this manual concentrates on design procedures and techniques for these materials. However, this does not imply that concrete and steel are the only useful materials for protective construction. Tests to establish the response of wood, brick blocks, plastics, etc. as well as the blast attenuating and mass effects of soil are contemplated. The results of these tests may require, at a later date, the supplementation of these design methods for these and other materials.

Other manuals are available which enable one to design protective structures against the effects of high explosive or nuclear detonations. The procedures in these manuals will quite often complement this manual and should be consulted for specific applications.

Computer programs, which are consistent with procedures and techniques contained in the manual, have been approved by the appropriate representative of the U.S. Army, the U.S. Navy, the U.S. Air Force and the Department of Defense Explosive Safety Board (DDESB). These programs are available through the following repositories:

1. Department of the Army

Commander and Director
U.S. Army Engineer
Waterways Experiment Station
Post Office Box 631
Vicksburg, Mississippi 39180

Attn: WESKA

2. Department of the Navy

Office-In-Charge
Civil Engineering Laboratory
Naval Battalion Construction Center
Port Hueneme, California 93043

Attn: Code L51

3. Department of the Air Force

Aerospace Structures
Information and Analysis Center
Wright Patterson Air Force Base
Ohio 45433

Attn: AFFDL/FBR

The individual programs are identical at each repository. If any modifications and/or additions to these programs are required, they will be submitted by the organization for review by DDESB and the above services. Upon concurrence of the revisions, the necessary changes will be made and notification of the changes will be made by the individual repositories.

2-5 **Format of Manual**

This manual is subdivided into six specific volumes dealing with various aspects of design. The titles of these volumes are as follows:

| | |
|------------|---|
| Volume I | Introduction |
| Volume II | Blast, Fragment and Shock Loads |
| Volume III | Principles of Dynamic Analysis |
| Volume IV | Reinforced Concrete Design |
| Volume V | Structural Steel Design |
| Volume VI | Special Considerations in Explosive Facility Design |

Appendix A pertinent to a particular volume and containing illustrative examples of explosive effects and structural response problems appears at the end of each volume.

Commonly accepted symbols have been used as much as possible. However, protective design involves many different scientific and engineering fields, and, therefore, no attempt has been made to standardize completely all the symbols used. Each symbol has been defined where it is first introduced, and a list of the symbols, with their definitions and units, is contained in Appendix B of each volume.

VOLUME CONTENTS

2-6 **General**

This volume contains the procedures for determining explosive output and associated structure loadings, fragment effects, as well as, the structural motion effects associated with accidental explosions. These procedures are contained in the following sections: Sections 2-8 through 2-15 deals with the loadings associated with the blast phenomena. This data includes, in addition to the determination of the effects of the explosive output, methods for determining blast loads acting on the exterior of and within structures. Sections 2-16 through 2-19 covers the formation of fragments which can be projected by an explosion and include both primary and secondary fragments effects. Sections 2-20 to 2-24 presents the method for determining the structural motions; including both ground and air shock effects.

EXPLOSION EFFECTS

2-7 **Effects of Explosive Output**

In the design of protective structures to resist the effects of accidental explosions, the principal effects of the explosive output to be considered are blast overpressures (hereafter referred to as blast pressures or pressures), fragments generated by the explosion and the shock loads produced by the shock wave transmitted through the air or ground. Of these three parameters, the blast pressures are usually the governing factor in the determination of the structure response. However, in some situations, fragments and/or shock loads may be just as important as the pressures in determining the configuration of the facility.

Although the quantitative data presented pertains to the blast output of bare TNT spherical or hemispherical charges considered as point source explosions, and other explosives which have been specifically tested. This data can be extended by appropriate means including testing to include other potentially mass-detonating materials (solid, liquid, or gas) of varying shape.

BLAST LOADS

2-8 Blast Phenomena

2-8.1 General

Bare, solid explosives must detonate to produce any explosive effect other than a fire. The term detonation refers to a very rapid and stable chemical reaction which proceeds through the explosive material at a speed, called the detonation velocity, which is supersonic in the unreacted explosive. Detonation velocities range from 22,000 to 28,000 feet per second for most high explosives. The detonation wave rapidly converts the solid or liquid explosive into a very hot, dense, high-pressure gas, and the volume of this gas which had been the explosive material then is the source of strong blast waves in air. Pressures immediately behind the detonation front range from 2,700,000 to 4,900,000 psi. Only about one-third of the total chemical energy available in most high explosives is released in the detonation process. The remaining two-thirds is released more slowly in explosions in air as the detonation products mix with air and burn. This afterburning process has only a slight effect on blast wave properties because it is so much slower than detonation.

The blast effects of an explosion are in the form of a shock wave composed of a high-intensity shock front which expands outward from the surface of the explosive into the surrounding air. As the wave expands, it decays in strength, lengthens in duration and decreases in velocity. This phenomena is caused by spherical divergence as well as by the fact that the chemical reaction is completed, except for some afterburning associated with the hot explosion products mixing with the surrounding atmosphere.

As the wave expands in air, the front impinges on structures located within its path and then the entire structure is engulfed by the shock pressures. The magnitude and distribution of the blast loads on the structure arising from these pressures are a function of the following factors: (1) explosive properties, namely, type of explosive material, energy output (high or low order detonation) and weight of explosive; (2) the location of the detonation relative to the protective structures; and (3) the magnitude and reinforcement of the pressure by its interaction with the ground barrier, or the structure itself. The first of these three factors are discussed in Sections 2-8.2 and 2-9 below and the latter two factors are discussed throughout the remainder of this section.

2-8.2 Explosive Materials

Explosive materials may be classified according to their physical state: solids, liquids, or gases. Solid explosives are primarily high explosives;

however, other materials such as flammable chemicals and propellants may also be classified as potentially explosive materials. Liquid and gaseous explosives encompass a wide variety of substances used in the manufacture of chemicals, fuels, propellants, etc. The blast pressure environment produced will vary not only among the different materials but may also differ for a particular material. Such factors as methods and procedures used in manufacturing, storage, and handling, in addition to specific individual physical and chemical characteristics, may alter the blast effects of an explosive material.

The blast effects of solid materials are best known. This is particularly true for high-explosive materials. The blast pressures, impulses, durations, and other blast effects of an explosion have been well established. These effects are contained in this volume.

Unlike high-explosive materials, other solid, liquid, and gaseous explosive materials will exhibit a variation of their blast pressure output. An explosion of these materials is in many cases incomplete, and only a portion of the total mass of the explosive (effective charge weight) is involved in the detonation process. The remainder of the mass is usually consumed by deflagration resulting in a large amount of the material's chemical energy being dissipated as thermal energy which, in turn, may cause fires or thermal radiation damage.

2-9 TNT Equivalency

The major quantity of blast effects data presented in this manual pertains to the blast pressures output of bare spherical TNT explosive. This data can be extended to include other potentially mass-detonating materials (Class 1.1) by relating the explosive energy of the "effective charge weight" of those materials to that of an equivalent weight of TNT. In addition to the energy output, other factors may affect the equivalency of material compared to TNT. These factors include the material shape (flat, square, round, etc.), the number of explosive items, explosive confinement (casing, containers, etc.), and the pressure range being considered (close-in, intermediate or far ranges). These other factors will be discussed later in this manual.

For blast resistant design, the effects of the energy output on explosive material, of a specific shape, relative to that of TNT, of similar shape, can be expressed as function of the heat of detonation of the various materials as follows:

$$W_E = [H_{EXP}^d / H_{TNT}^d] W_{EXP} \quad 2-1$$

where

W_E = effective charge weight

W_{EXP} = weight of the explosive in question

H_{TNT}^d = heat of detonation of TNT

H_{EXP}^d = heat of detonation of explosive in question

The heat of detonation of some of the more commonly used explosives are listed in Table 2-1.

The above equation for the effective charge weight is related primarily to the blast output associated with the shock effects of unconfined detonations (Section 2-13). The effective charge weight produced by the confinement effects of explosions (Section 2-14) will differ. These differences will be discussed later in this manual.

2-10 Blast-Loading Categories

Blast loads on structures can be divided into two main groups based on the confinement of the explosive charge (unconfined and confined explosions) and further subdivided based on the blast loading produced within the donor structure or acting on acceptor structures. These blast loading categories are illustrated in figure 2-1. Figure 2-1 lists the six (6) blast loading categories possible, namely; free air burst, air burst, surface burst, fully vented explosion, partially vented explosion and fully confined explosion. The five (5) possible pressure loads associated with the blast load categories are also listed. In addition, the location of the explosive charge which would produce these pressure loads are also presented. Lastly, the protective structures subjected to these loads are listed.

The blast load categories and the resulting pressure loads listed in figure 2-1 are qualitatively and, quantitatively defined below and in subsequent sections, respectively.

2-10.1 Unconfined Explosion

2-10.1.1 Free Air Burst Explosion. An explosion, which occurs in free air, produces an initial output whose shock wave propagates away from the center of the detonation, striking the protective structure without intermediate amplification of its wave.

2-10.1.2 Air Burst Explosion. An explosion which is located at a distance from and above the protective structure so that the ground reflections of the initial wave occurs prior to the arrival of the blast wave at the protective structure. As used in this manual, an air burst is limited to an explosion which occurs at two to three times the height of a one or two-story building.

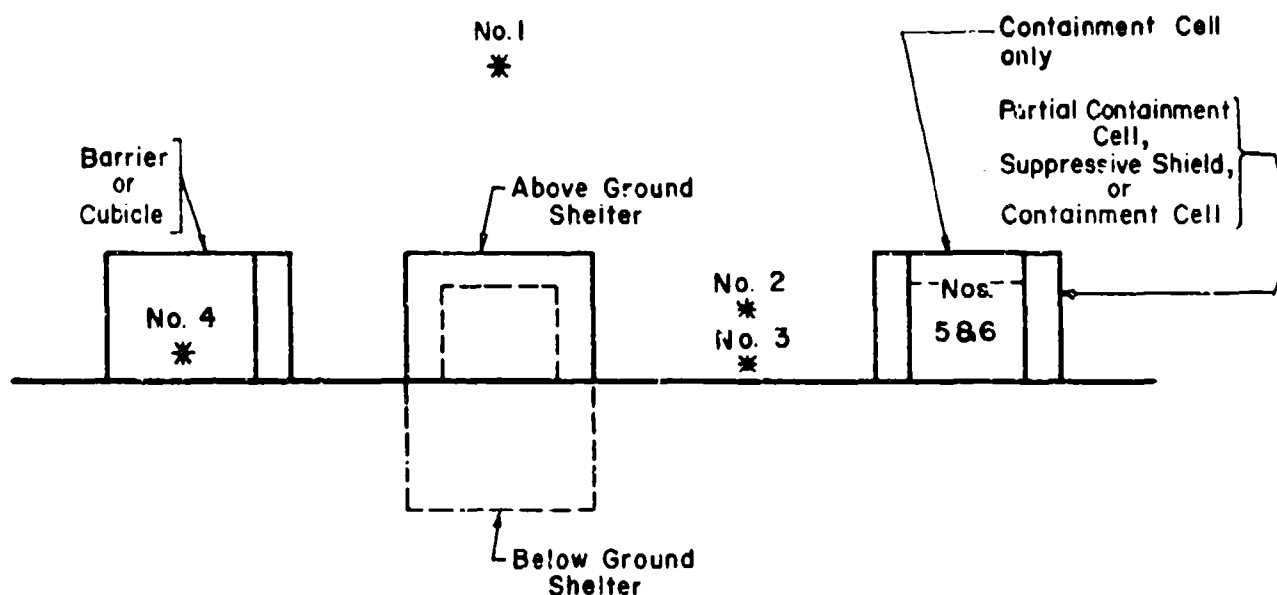
2-10.1.3 Surface-Burst Explosion. A surface burst explosion will occur when the detonation is located close to or on the ground so that the initial shock is amplified at the point of detonation due to the ground reflections.

Table 2-1 Heat of Detonation and Heat of Combustion

| Explosive | | Heat of | Heat of |
|-----------------|------------|-----------------------|-----------------------|
| Name | Symbol | Detonation (ft-lb/lb) | Combustion (ft-lb/lb) |
| Boratol | - | 1.04×10^6 | |
| Boracitol | - | 5.59×10^5 | |
| | BTf | 2.37×10^6 | |
| Composition B | Comp B | 2.15×10^6 | 3.91×10^6 |
| Composition C-4 | Comp C-4 | 2.22×10^6 | |
| Cyclotol 75/25 | - | 2.20×10^6 | 3.68×10^6 |
| | DATB/DATNB | 1.76×10^6 | 4.08×10^6 |
| | DIPAM | 1.89×10^6 | |
| | DNPA | 1.48×10^6 | |
| | EDNP | 1.72×10^6 | |
| | FEFO | 2.03×10^6 | |
| | HMX | 2.27×10^6 | 3.31×10^6 |
| | HNAB | 2.06×10^6 | |
| | HNS | 1.99×10^6 | |
| | LX-01 | 2.41×10^6 | |
| | LX-02-1 | 1.99×10^6 | |
| | LX-04 | 1.99×10^6 | |
| | LX-07 | 2.08×10^6 | |
| | LX-08 | 2.77×10^6 | |
| | LX-09-0 | 2.24×10^6 | |
| | LX-10-0 | 2.17×10^6 | |
| | LX-11 | 1.72×10^6 | |
| | LX-14 | 2.20×10^6 | |
| | NG | 2.22×10^6 | 2.26×10^6 |
| | NQ | 1.49×10^6 | 2.79×10^6 |

Table 2-1 Heat of Detonation and Heat of Combustion (cont.)

| Explosive | | Heat of | Heat of |
|-----------------|----------|-----------------------|-----------------------|
| Name | Symbol | Detonation (ft-lb/lb) | Combustion (ft-lb/lb) |
| Octol 70/30 | - | 2.20×10^6 | 3.81×10^6 |
| | PBX-9007 | 2.18×10^6 | |
| | PBX-9010 | 2.06×10^6 | |
| | PBX-9011 | 2.14×10^6 | |
| | PBX-9205 | 2.04×10^6 | |
| | PBX-9404 | 2.18×10^6 | |
| | PBX-9407 | 2.24×10^6 | 3.31×10^6 |
| | PBX-9501 | 2.22×10^6 | |
| Pentolite 50/50 | - | 2.14×10^6 | |
| | PETN | 2.31×10^6 | 2.70×10^6 |
| | RDX | 2.27×10^6 | 3.20×10^6 |
| | TETRYL | 2.11×10^6 | 4.08×10^6 |
| | TNETB | | 2.34×10^6 |
| | TNT | 1.97×10^6 | 5.05×10^6 |



| BLAST LOADING CATEGORIES | | | |
|--------------------------|-----------------------|--|--|
| CHARGE CONFINEMENT | CATEGORY | PRESSURE LOADS | PROTECTIVE STRUCTURE |
| Unconfined Explosions | 1. Free Air Burst | a. Unreflected | Shelter |
| | 2. Air Burst | b. Reflected | |
| | 3. Surface Burst | b. Reflected | |
| Confined Explosions | 4. Fully Vented | c. Internal Shock d. Leakage | Cubicle |
| | 5. Partially Confined | c. Internal Shock e. Internal Gas d. Leakage | Partial Containment Cell or Suppressive Shield |
| | 6. Fully Confined | c. Internal Shock e. Internal Gas | Full Containment Cell |

Figure 2-1 Blast loading categories

2-10.2 *Confined Explosion*

2-10.2.1 *Fully Vented Explosion.* A fully vented explosion will be produced within or immediately adjacent to a barrier or cubicle type structure with one or more surfaces open to the atmosphere. The initial wave, which is amplified by the nonfrangible portions of the structure, and the products of detonation are totally vented to the atmosphere forming a shock wave (leakage pressures) which propagates away from the structure.

2-10.2.2 *Partially Confined Explosion.* A partially confined explosion will be produced within a barrier or cubicle type structure with limited size openings and/or frangible surfaces. The initial wave, which is amplified by the frangible and nonfrangible portions of the structure, and the products of detonation are vented to the atmosphere after a finite period of time. The confinement of the detonation products, which consist of the accumulation of high temperatures and gaseous products, is associated with a build up of quasi-static pressure (hereafter referred to as gas pressure). This pressure has a long duration in comparison to that of the shock pressure.

2-10.2.3 *Fully Confined Explosions.* Full confinement of an explosion is associated with either total or near total containment of the explosion by a barrier structure. Internal blast loads will consist of unvented shock loads and very long duration gas pressures which are a function of the degree of containment. The magnitude of the leakage pressures will usually be small and will only affect those facilities immediately outside the containment structure.

2-11 *Blast Loading Protection*

Protection of personnel and valuable equipment (acceptor system) will usually involve protective shelters located away from the detonation. Their design may involve one or more of the following blast-loading categories: free-air burst, air burst, surface burst and exterior or leakage pressures from either vented or partially confined explosions. These shelters are usually enclosed buildings located at pressure ranges of a few hundred psi or less. Depending on the shelter design pressures, these structures can be either above, below, or at ground surface. In this manual, primary consideration is given to above ground shelters. However, some consideration is given in Volume VI regarding shelters positioned at other locations. For the third type of pressure loading of figure 2-1 (interior shock pressure), protection is required when the shelter is located immediately adjacent to the explosion. The reflected pressures here may be in the order of thousands of psi, but with pressure durations usually small. The acceptor portion of such an explosive system may include other explosive materials and/or personnel. The structures associated with the fifth pressure-loading type is a containment type building and is usually used to prevent escape of toxic chemicals, radiological and/or biological materials or to limit blast pressures at the exterior to a level consistent with personnel protection.

Of the six categories, those from air bursts are seldom encountered and the free air burst is the least likely to occur. The possibility of such blast

environments exist where potentially explosive materials are stored at heights adjacent to, or away from, protective structures, such as in manufacturing (process or storage tanks, etc.) or missile sites. In the latter, the rocket propellant would be a source of explosive danger to the ground crew and control facilities.

The other four blast-loading categories can occur in most explosive manufacturing and storage facilities. In such installations, transportation of explosive materials between buildings either by rail, vehicle, or in the case of liquid or gases, through piping, is a common occurrence. Also, storage and handling of explosives within buildings are common occurrences.

Although the blast-loading categories can be separated and classified individually, no clear-cut limits differentiate each category. In most explosive facilities, the various blast environments will overlap, and judgement should be used in the application of the following recommendations for determining the blast parameters consistent with the various blast-loading categories.

2-12 Blast-Wave Phenomena

The violent release of energy from a detonation converts the explosive material into a very high pressure gas at very high temperatures. A pressure front associated with the high pressure gas propagates radially into the surrounding atmosphere as a strong shock wave, driven and supported by the hot gases. The shock front, termed the blast wave, is characterized by an almost instantaneous rise from ambient pressure to a peak incident pressure P_{s0} (fig 2-2).

This pressure increase or shock front travels radially from the burst point with a diminishing shock velocity U which is always in excess of the sonic velocity of the medium. Gas molecules behind the front move at lower flow velocities, termed particle velocities u . These latter particle velocities are associated with the dynamic pressures, whose maximum values are denoted q_0 , or the pressures formed by the winds produced by the passage of the shock front. As the shock front expands into increasingly larger volumes of the medium, the peak incident pressures at the fronts decrease and the durations of the pressures increase. Those parameters which vary as the peak incident pressure varies are presented in figure 2-3.

At any point away from the burst, the pressure disturbance has the shape shown in figure 2-2. The shock front arrives at a given location at time t_A and, after the rise to the peak value, P_{s0} the incident pressure decays to the ambient value in time t_0 which is the positive phase duration. This is followed by a negative phase with a duration t_0^- that is usually much longer than the positive phase and characterized by a negative pressure (below ambient pressure) having a maximum value of p_3^- as well as a reversal of the particle flow. The negative phase is usually less important in a design than is the positive phase, and its amplitude P_3

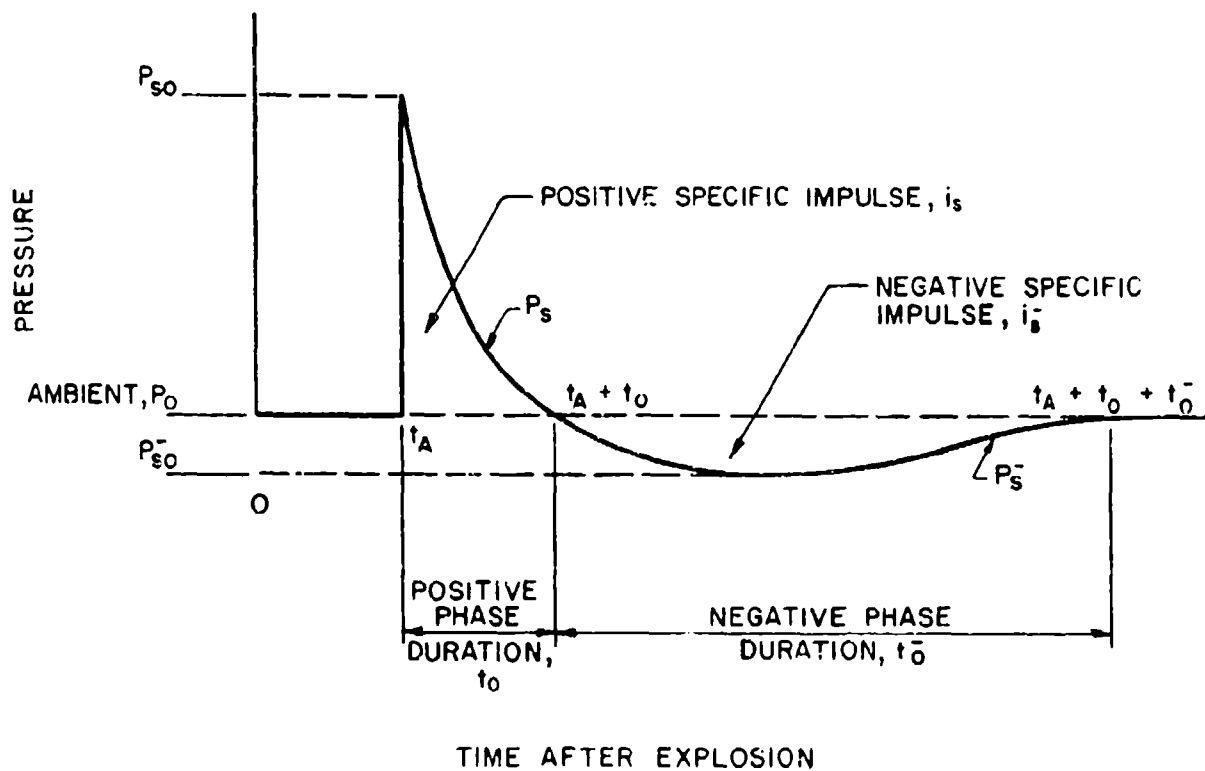


Figure 2-2 Free-field pressure-time variation

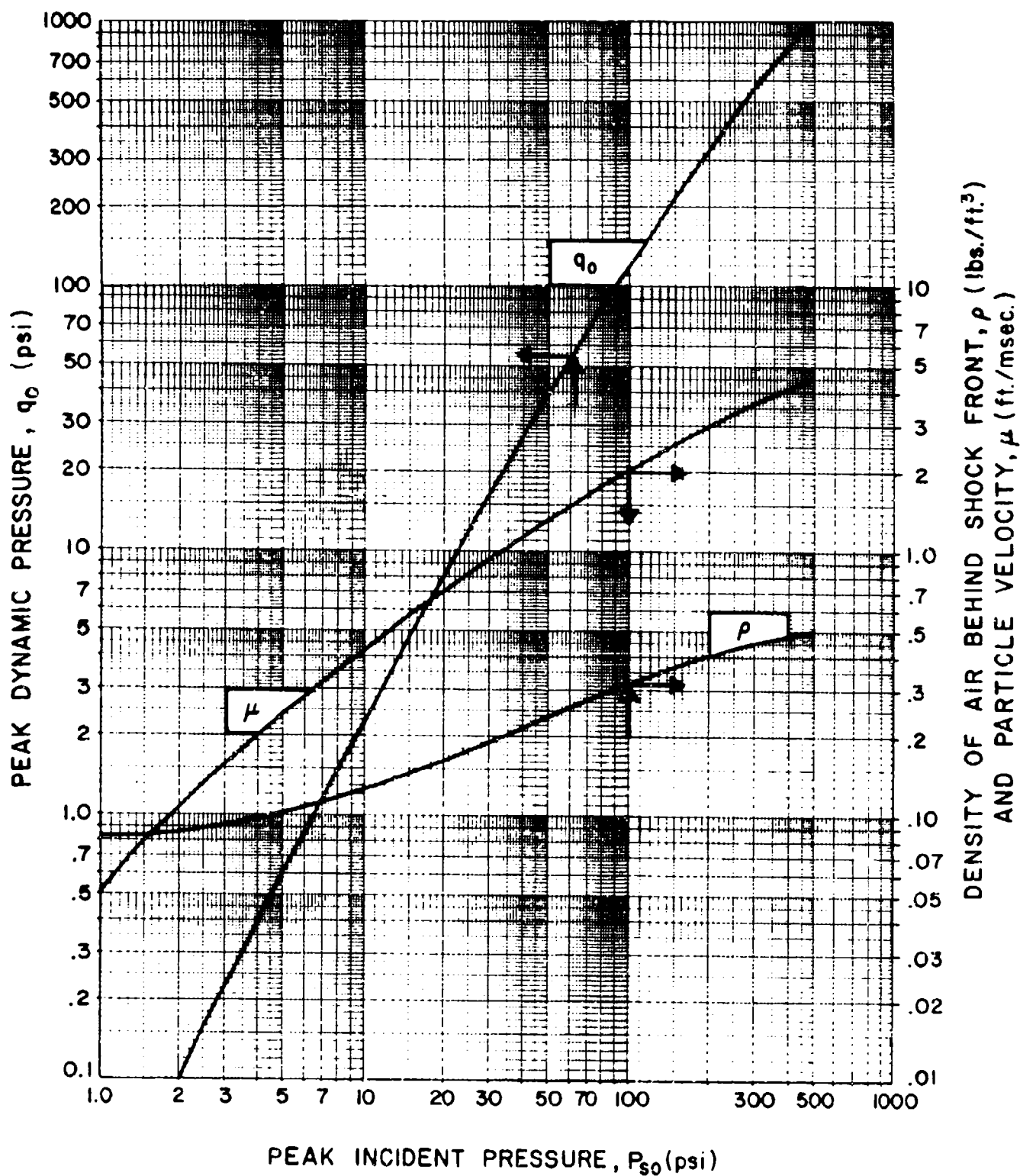


Figure 2-3 Peak incident pressure versus peak dynamic pressure density of air behind the shock front and particle velocity

must, in all cases, be less than ambient atmosphere pressure p_o . The incident impulse density associated with the blast wave is the integrated area under the pressure-time curve and is denoted as i_s for the positive phase and i_s^- for the negative phase.

An additional parameter of the blast wave, the wave length, is sometimes required in the analysis of structures. The positive wave length L_w^+ is that length at a given distance from the detonation which, at a particular instant of time, is experiencing positive pressures. The negative wave length L_w^- is similarly defined for negative pressures.

The above treatment of the blast wave phenomena is general. In subsequent sections of this volume, the magnitude of the various parameters is presented depending upon the category of the detonation as previously described: free air burst, surface burst, exterior or leakage pressures, or interior or high pressure blast loading.

2-13 Unconfined Explosions

2-13.1 Free-Air Burst

When a detonation occurs adjacent to and above a protective structure such that no amplification of the initial shock wave occurs between the explosive source and the protective structure, then the blast loads acting on the structure are free-air blast pressures (fig. 2-4).

As the incident wave moves radially away from the center of the explosion, it will impact with the structure, and, upon impact, the initial wave (pressure and impulse) is reinforced and reflected (fig. 2-5). The reflected pressure pulse of figure 2-5 is typical for infinite plane reflectors.

When the shock wave impinges on a surface oriented so that a line which describes the path of travel of the wave is normal to the surface, then the point of initial contact is said to sustain the maximum (normal reflected) pressure and impulse. Figure 2-6 presents the ratios of the normal reflected pressures to the incident pressures as a function of the incident pressures.

The peak pressure and impulse patterns on the structure vary with distance from a maximum at the normal distance R_A to a minimum (incident pressure) where the plane of the structure's surface is perpendicular to the shock front. The positive phase pressures, impulses, durations and other parameters of this shock environment for a spherical TNT explosions are given in fig. 2-7 versus the scaled distance ($Z = R/W^{1/3}$).

The smallest scaled distance of $0.136 \text{ ft/lb}^{1/3}$ represents the radius of the spherical TNT explosive and, therefore, represents the surface of the explosive. Some parameters have been extrapolated to the charge surface which are shown as dashed portions of the curves. These dashed curves represent an upper limit of scatter in experimental data and variation in

theoretical predictions, giving for design purposes conservative limits for these parameters.

In some blast loading situations, negative blast wave parameters (fig. 2-8) are needed to predict the loading-time function of the blast wave acting on a structure. This is particularly true in flexible type protective structures (usually steel-frame structures) where the overall motion of the structure will be affected by the phasing of the blast loads acting on the various structure surfaces. The effects of the negative phase parameters are usually not important for the design of the more rigid type structures (reinforced concrete).

The curves presented in figures 2-7 and 2-8 which give the blast wave parameters as a function of scaled distance, extend only to a scaled distance $Z = 100 \text{ ft./lb.}^{1/3}$. For most protective structures, or even light structures, damage is relatively superficial beyond this scaled distance, consisting at most of broken windows or deformation of light panels or blow-out walls. But, the curves are also not extended beyond these levels because the blast wave properties start to be seriously affected by atmospheric conditions so that overpressures are very much less or very much more than the "ideal" parameters transmitted through a homogeneous atmosphere.

In the low pressure region, the pressure varies as a function of sound velocity with altitude above the ground surface. At very far distances from an explosion ($Z = 1000 \text{ ft./lb.}^{1/3}$), the peak pressures (really sound pressures at these levels) can be ten times greater or more than ten times less than the ideal pressures for a homogenous atmosphere.

Even with enhancement caused by real atmospheric conditions (also called blast focusing), the pressures are still quite low and structural damage should be superficial. If it is necessary to predict such low levels, one should obtain and study more detailed reports listed in the bibliography.

The variation of the pressure and impulse patterns on the surface of a structure between the maximum and minimum values is a function of the angle of incidence α . This angle is formed by the line which defines the normal distance R_A between the point of detonation and the structure, and line R (slant distance) which defines the path of shock propagation between the center of the explosion and any other point in question on the structure surface (fig. 2-4).

The effects of the angle of incidence on the peak reflected pressure P_{ra} and the reflected impulse i_{ra} are shown in figures 2-9 and 2-10, respectively. The figures are plots of the angle of incidence versus the peak reflected pressure or the reflected impulse as a function of the scaled normal distance between the charge and the surface in question. The usual load condition involves the ground surface and, therefore, this

normal scaled distance is referred to as the scaled height of charge above the ground ($H_c/W^{1/3}$). All other blast parameters are obtained from figures 2-7 and 2-8 for the scaled slant distance $R/W^{1/3}$ to the point in question.

2-13.2 Air Burst

The air burst environment is produced by detonations which occur above the ground surface and at a distance away from the protective structure so that the initial shock wave, propagating away from the explosion, impinges on the ground surface prior to arrival at the structure. As the shock wave continues to propagate outward along the ground surface, a front known as the Mach front (fig. 2-11) is formed by the interaction of the initial wave (incident wave) and the reflected wave. This reflected wave is the result of the reinforcement of the incident wave by the ground surface.

Some variation of the pressures over the height of the Mach front occurs but, for design purposes, this variation can be neglected and the shock considered as a plane wave over the full height of the front. The blast parameters in the Mach front are calculated at the ground surface. The pressure-time variation of the Mach front (a, fig. 2-12) is similar to that of the incident wave except that the magnitude of the blast parameters are somewhat larger.

The height of the Mach front increases as the wave propagates away from the center of the detonation. This increase in height is referred to as the path of the triple point and is formed by the intersection of the initial, reflected, and Mach waves. A protected structure is considered to be subjected to a plane wave (uniform pressure) when the height of the triple point exceeds the height of the structure. The scaled height of the triple point $H_T/W^{1/3}$ versus scaled ground distance Z_G and scaled charge height $H_c/W^{1/3}$ is plotted in figure 2-13.

If the height of the triple point does not extend above the height of the structure, then the magnitude of the applied loads will vary with the height of the point being considered. Above the triple point, the pressure-time variation consists of an interaction of the incident and reflected incident wave pressures resulting in a pressure-time variation (b, fig. 2-12) different from that of the Mach incident wave pressures. The magnitude of pressures above the triple point is smaller than that of the Mach front. In most practical design situations, the location of the detonation will be far enough away from the structure so as not to produce this pressure variation. An exception may exist for multi-story buildings even though these buildings are usually located at very low-pressure ranges where the triple point is high.

In determining the magnitude of the air blast loads acting on the surface of an above-ground protective structure, the peak incident blast pressures in the Mach wave acting on the ground surface immediately before the structure are calculated first. The peak incident pressure P_{ra} is determined for this point from figure 2-9 using the scaled height of charge above the ground $H_c/W^{1/3}$ and the angle of incidence α .

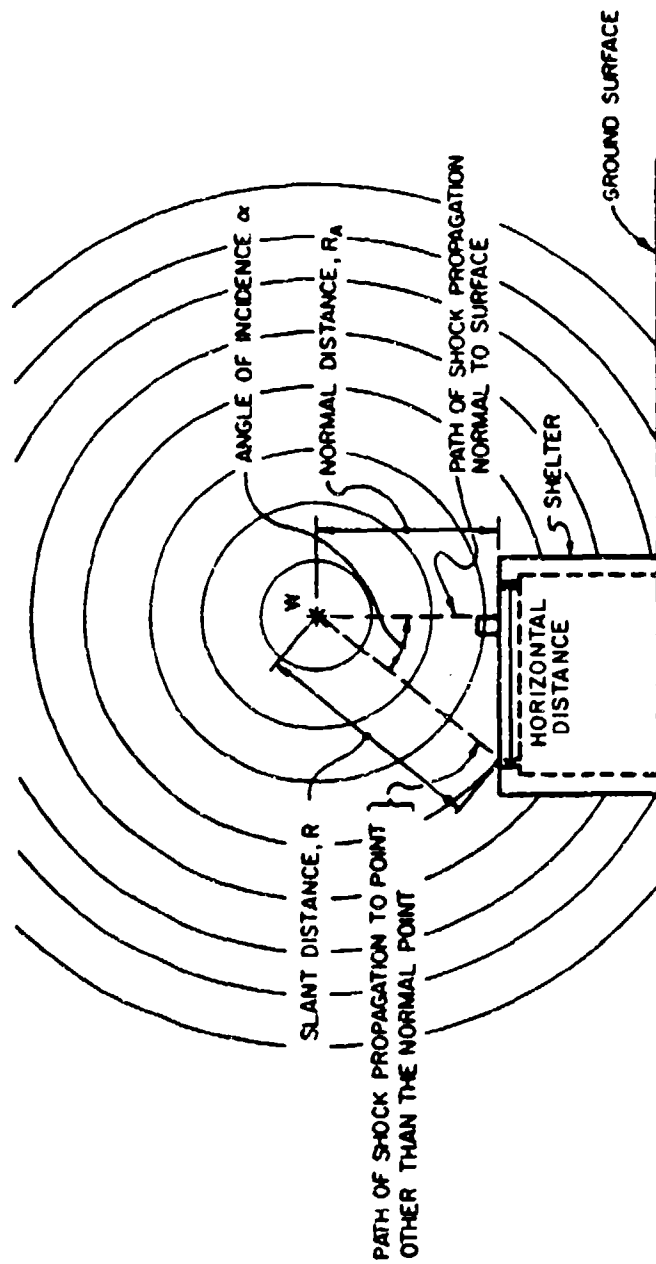


Figure 2-4 Free-air burst blast environment

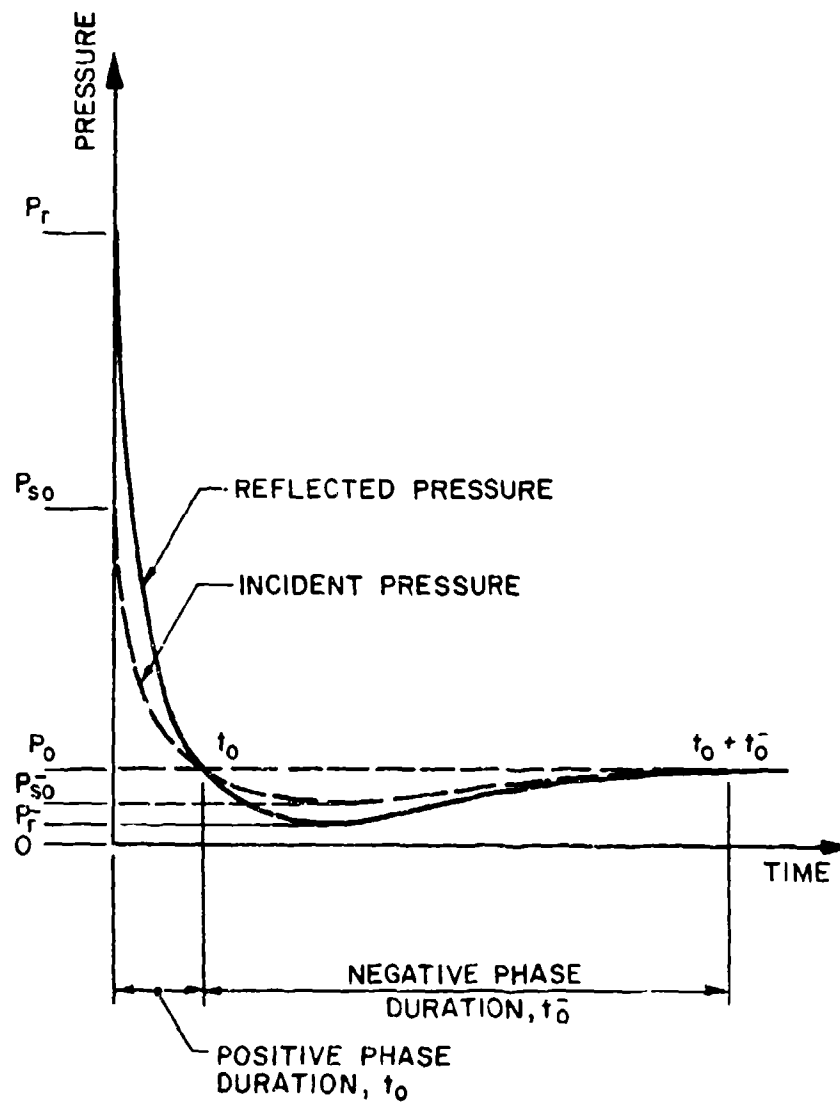


Figure 2-5 Pressure-time variation for a free-air burst

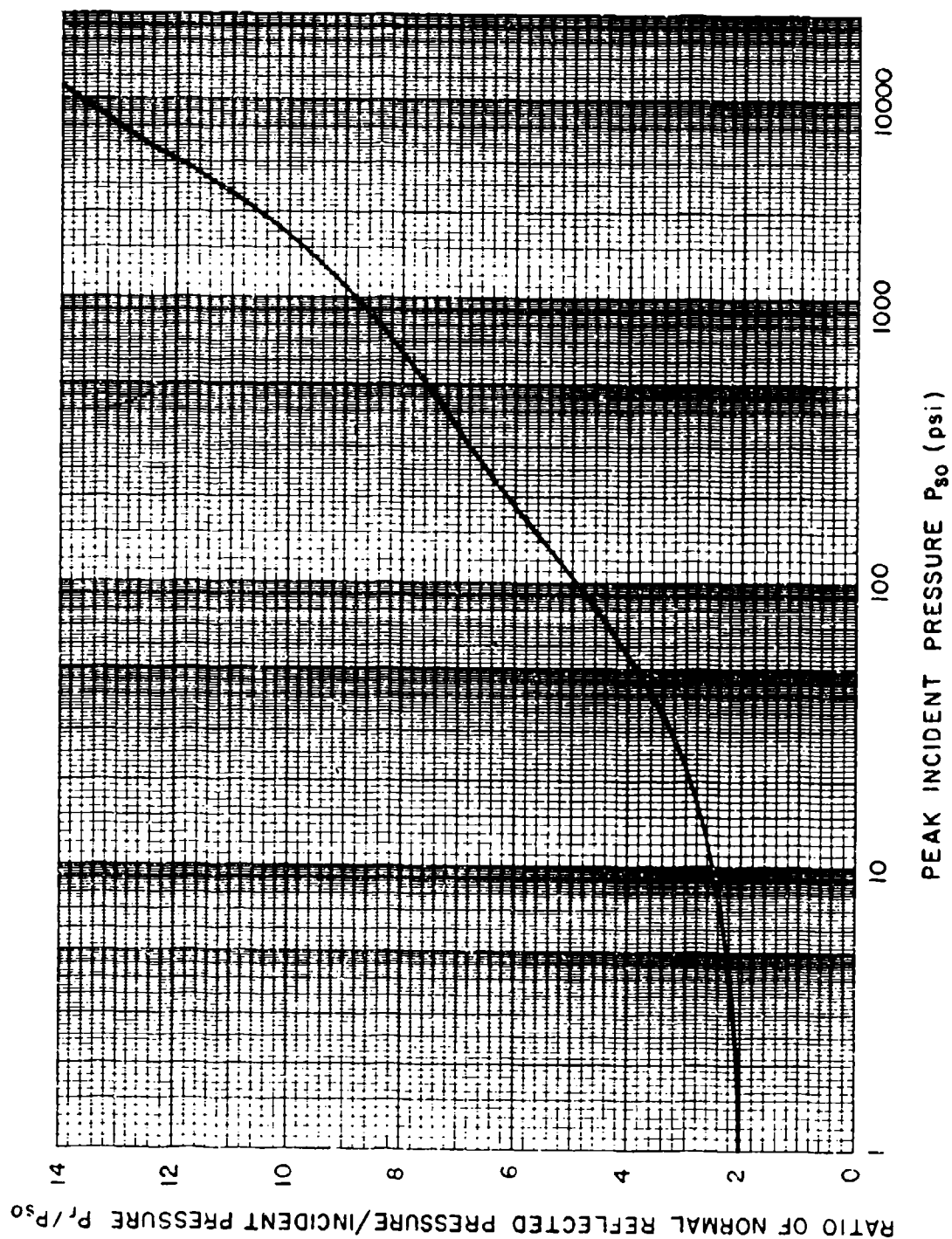
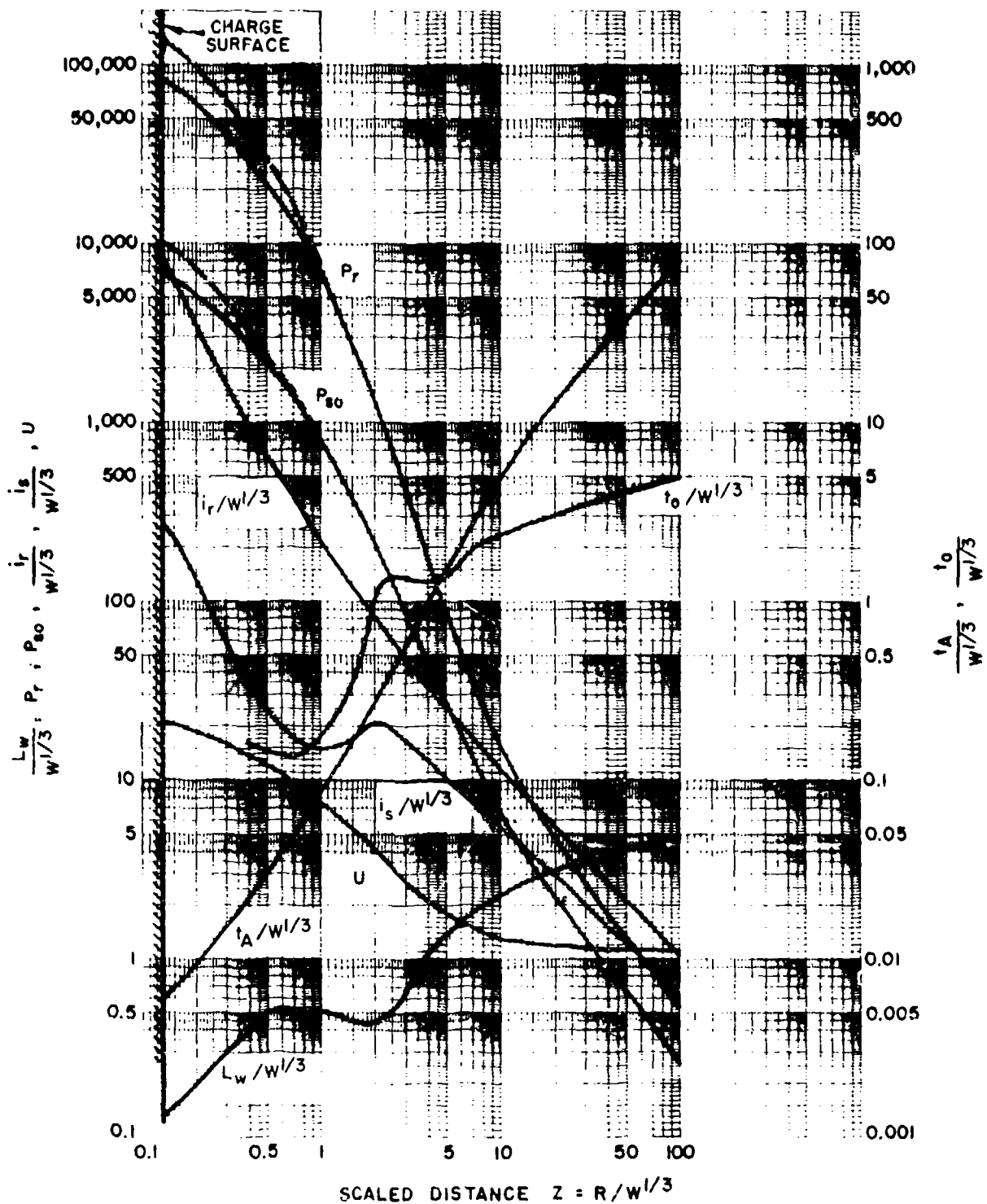
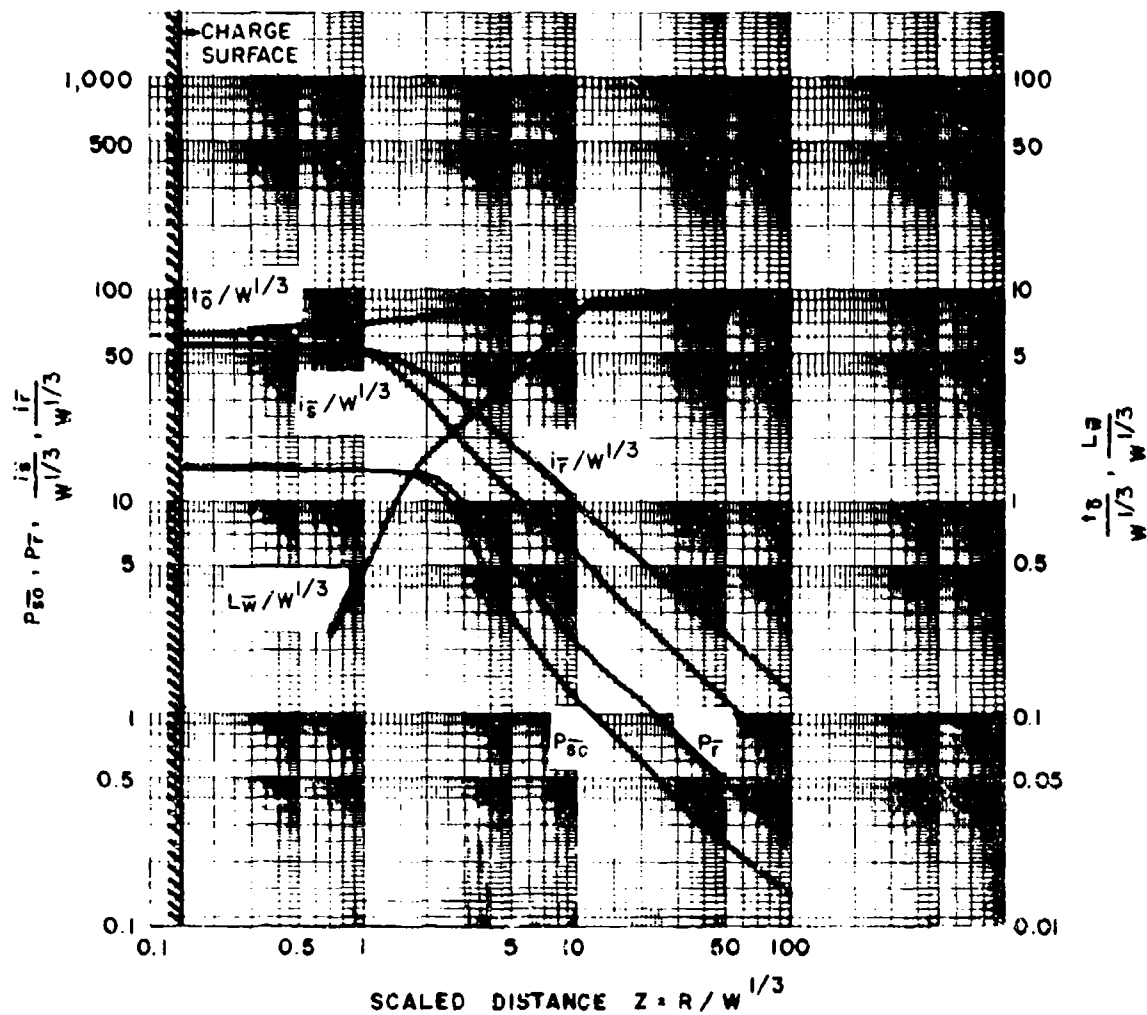


Figure 2-6 Peak incident pressure versus the ratio of normal reflected pressure/ incident pressure for a free air burst



- P_{so} = PEAK POSITIVE INCIDENT PRESSURE, psi
 P_r = PEAK POSITIVE NORMAL REFLECTED PRESSURE, psi
 $i_s/W^{1/3}$ = SCALED UNIT POSITIVE INCIDENT IMPULSE, psi-ms/lb^{1/3}
 $i_r/W^{1/3}$ = SCALED UNIT POSITIVE NORMAL REFLECTED IMPULSE, psi-ms/lb^{1/3}
 $t_A/W^{1/3}$ = SCALED TIME OF ARRIVAL OF BLAST WAVE, ms/lb^{1/3}
 $t_0/W^{1/3}$ = SCALED POSITIVE DURATION OF POSITIVE PHASE, ms/lb^{1/3}
 U = SHOCK FRONT VELOCITY, ft/ms
 W = CHARGE WEIGHT, lbs
 $L_w/W^{1/3}$ = SCALED WAVE LENGTH OF POSITIVE PHASE, ft/lb^{1/3}

Figure 2-7 Positive phase shock wave parameters for a spherical TNT explosion in free air at sea level



- P_{s0} = PEAK NEGATIVE INCIDENT PRESSURE, psi
 P_T = PEAK NEGATIVE NORMAL REFLECTED PRESSURE, psi
 $i_s / W^{1/3}$ = SCALED UNIT NEGATIVE INCIDENT IMPULSE, psi-ms/lb^{1/3}
 $i_T / W^{1/3}$ = SCALED UNIT NEGATIVE NORMAL REFLECTED IMPULSE, psi-ms/lb^{1/3}
 $t_0 / W^{1/3}$ = SCALED DURATION OF NEGATIVE PHASE, ms/lb^{1/3}
 $L_W / W^{1/3}$ = SCALED WAVE LENGTH OF NEGATIVE PHASE, ft/lb^{1/3}

Figure 2-8 Negative phase shock wave parameters for a spherical TNT explosion in free air at sea level

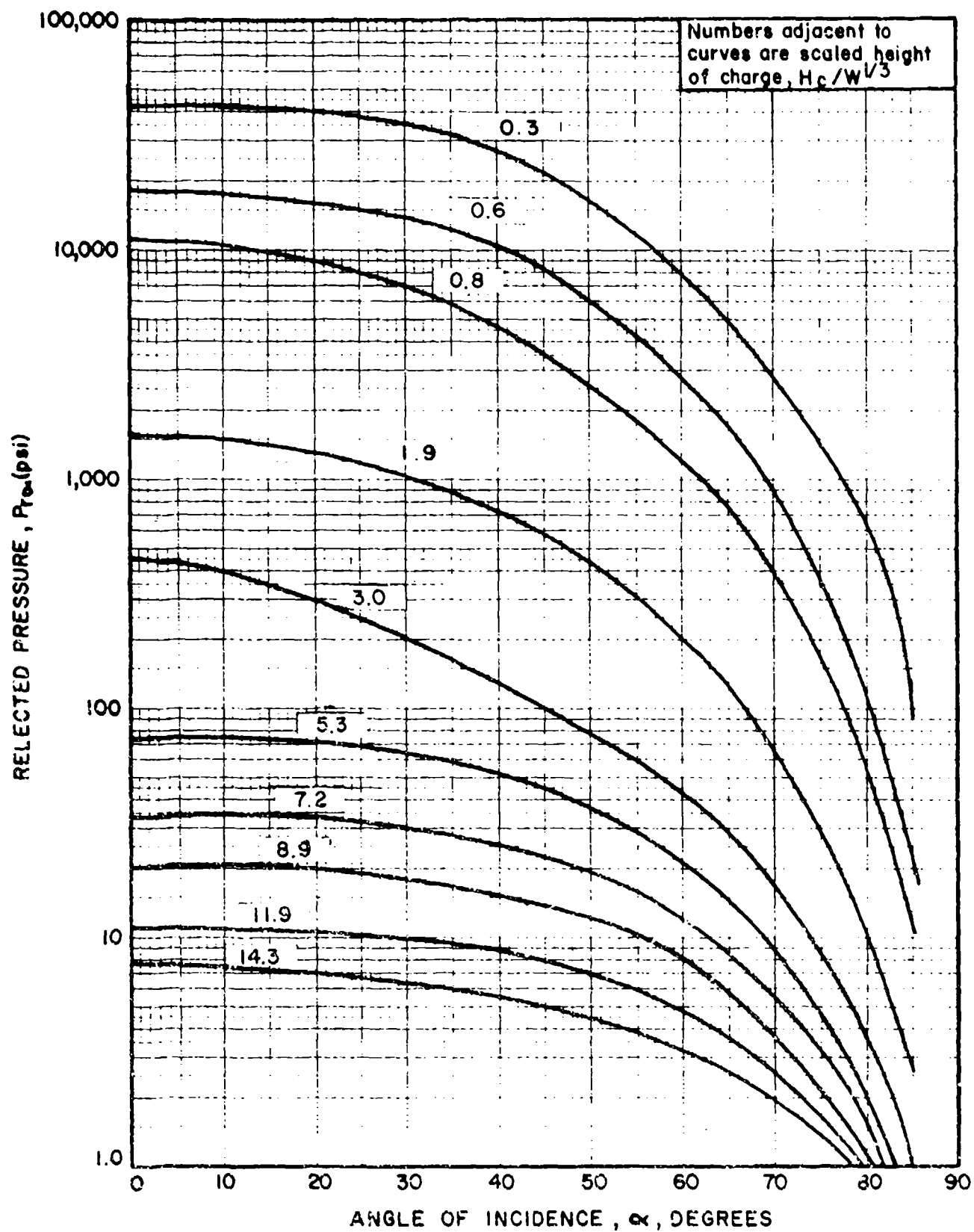


Figure 2-9 Variation of reflected pressure as a function of angle of incidence

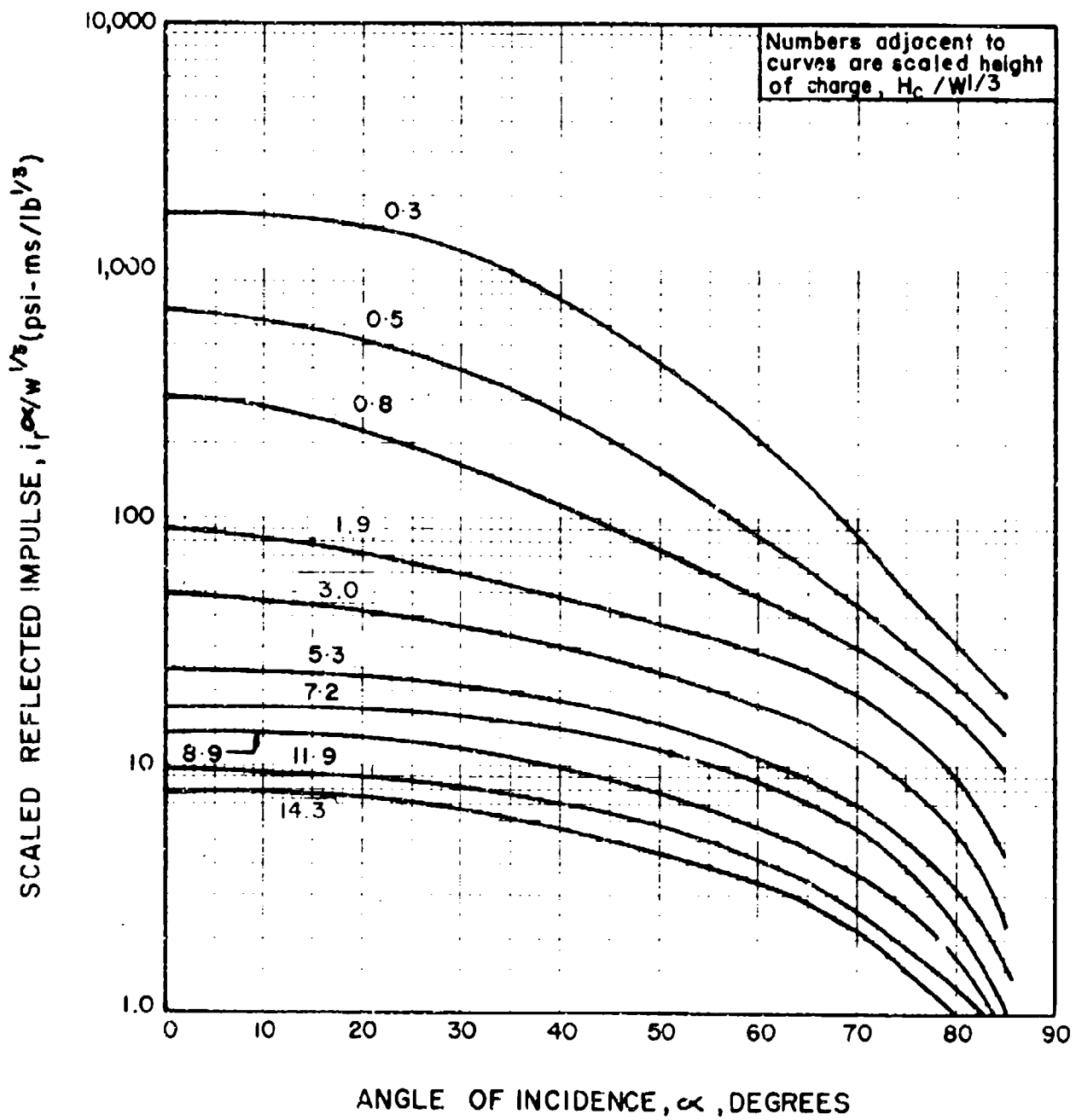


Figure 2-10 Variation of scaled reflected impulse as a function of angle of incidence

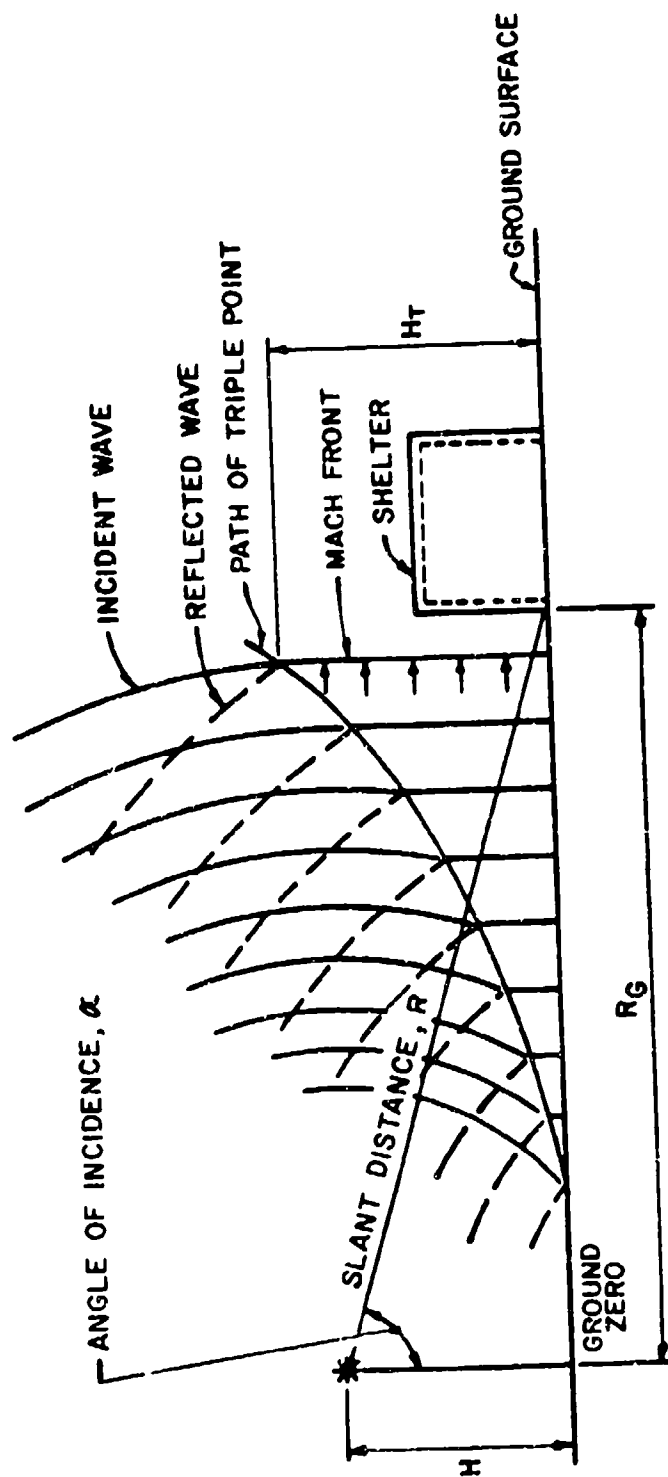
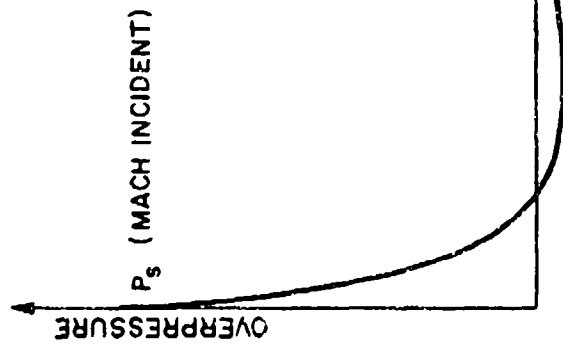
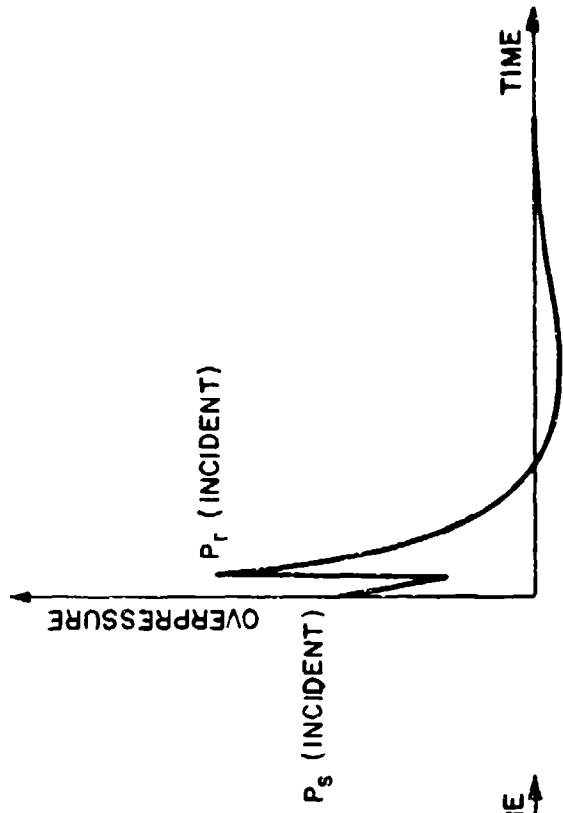


Figure 2-11 Air burst blast environment



(a) MACH FRONT



(b) POINT ABOVE TRIPLE POINT

Figure 2-12 Pressure-time variation for air burst

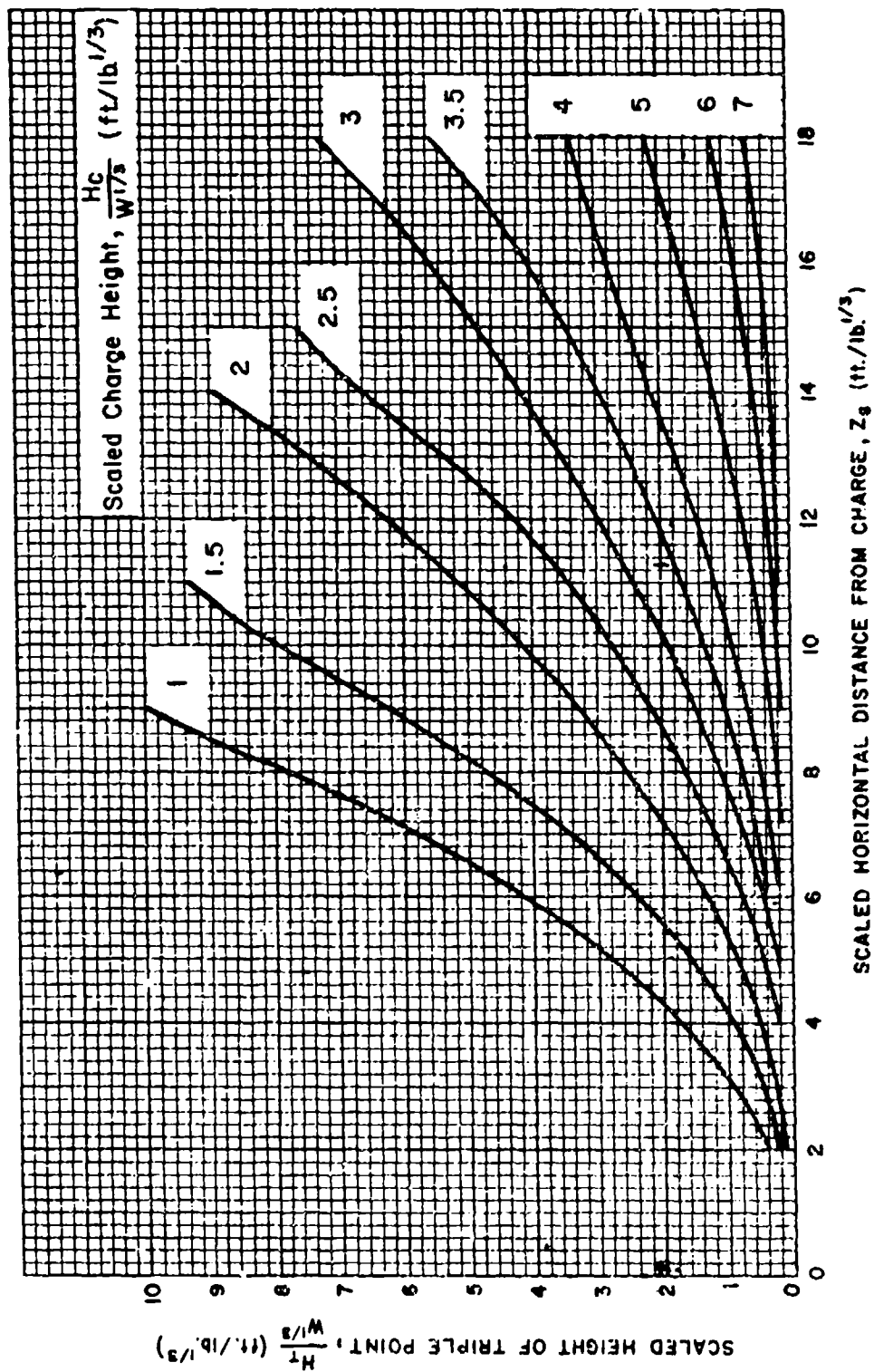


Figure 2-13 Scaled height of triple point

A similar procedure is used with figure 2-10 to determine the impulse i_{ra} of the blast wave acting on the ground surface immediately before the structure. An estimate of the other blast parameters may be obtained from figures 2-7 and 2-8 by setting the values of P_{ra} and i_{ra} equal to the values of the peak incident pressure P_{s0} and incident impulse i_s of the mach wave, respectively. The scaled distances corresponding to P_{s0} and i_s are determined from figure 2-7. The scaled distance corresponding to P_{s0} is used to obtain values of P_r , P_{s0} , $t_A/W^{1/3}$, U , $L_W/W^{1/3}$ and $L_W^-/W^{1/3}$ while the scaled distance corresponding to i_s is used to obtain values of i_r , i_s , t_r , $t_0/W^{1/3}$ and $t_0^-/W^{1/3}$.

2-13.3 Surface Burst

A charge located on or very near the ground surface is considered to be a surface burst. The initial wave of the explosion is reflected and reinforced by the ground surface to produce a reflected wave. Unlike the air burst, the reflected wave merges with the incident wave at the point of detonation to form a single wave, similar in nature to the mach wave of the air burst but essentially hemispherical in shape (fig. 2-14).

The positive phase parameters of the surface burst environment for hemispherical TNT explosions are given in figure 2-15 while the negative phase parameters are given in figure 2-16. A comparison of these parameters with those of free-air explosions (fig. 2-7 and 2-8) indicate that, at a given distance from a detonation of the same weight of explosive, all of the parameters of the surface burst environment are larger than those for the free-air environment.

As for the case of air bursts, protected structures subjected to the explosive output of a surface burst will usually be located in the pressure range where the plane wave (fig. 2-14) concept can be applied. Therefore, for a surface burst, the blast loads acting on structure surface are calculated as described for an air burst except that the incident pressures and other positive phase parameters of the free-field shock environment are obtained from figure 2-15 while theoretical negative phase blast parameters are shown in figure 2-16.

As for the case of an air burst, the curves presented in figures 2-15 and 2-16 which give the blast wave parameters as a function of scaled distance, extend only to a scaled distance $Z = 100 \text{ ft/lb}^{1/3}$ (see section 2-13.1).

Blast parameters for explosives detonated on the ground surface other than hemispherical TNT are listed in table 2-2. These explosives include both uncased and cased high explosives, propellants and propelling charges as well as pyrotechnic mixtures. The various shapes of the explosive materials are given in figure 2-17. The blast parameters for the various explosives are illustrated in figures 2-18 through 2-49. For each

explosive material considered, the peak incident pressure P_{s0} and scaled incident impulse $i_s/W^{1/3}$ is presented as a function of the scaled ground distance $Z_G = R_G/W^{1/3}$ from the point of detonation.

The charge weight W is equal to the actual weight of the explosive material under consideration increased by the required factor of safety (20 percent).

An estimate of the blast parameters other than incident pressure and impulse, may be obtained from figures 2-15 and 2-16. The scaled ground distance corresponding to the incident pressure P_{s0} is used to obtain the values of P_r , P_{s0} , $P_{\bar{r}}$, $t_A/W^{1/3}$, U , $L_W/W^{1/3}$ and $L_{\bar{W}}/W^{1/3}$. In addition, this scaled ground distance $Z_G = R_G/W^{1/3}$ is used to calculate the equivalent TNT design charge weight W for pressure using the actual ground distance R_G . The absolute values of the scaled blast parameters are obtained by multiplying the scaled values by the equivalent TNT design charge weight.

The scaled ground distance corresponding to the incident impulse requires a graphical solution. The point corresponding to the scaled incident impulse and scaled ground distance for the explosive material in question is plotted on figure 2-15. A 45 degree line is drawn through this point. The point where the line intersects the scaled impulse curve corresponds to the scaled impulse and scaled ground distance for the equivalent TNT charge. This scaled ground distance is then used to obtain the values of $i_r/W^{1/3}$, $i_{\bar{s}}/W^{1/3}$, $i_{r/W}^{1/3}$, $t_o/W^{1/3}$ and $t_{o/W}^{1/3}$. In addition, this scaled ground distance and the actual ground distance is used to calculate the equivalent TNT design charge weight for impulse. The absolute values of the scaled blast parameters are obtained by multiplying the scaled values by the equivalent TNT design charge weight.

It may be noted that the above data for explosives other than TNT is limited to surface bursts with container shapes indicated in figure 2-17. This data should not be extrapolated for scaled distances less than those indicated on figures 2-18 through 2-49. In addition, the blast pressure and impulse for propellants and, in particular, the pyrotechnic mixtures were obtained from tests which utilized booster charges to initiate the explosive material. Therefore, the blast parameters for both of these materials should be considered as upper limits.

2-13.4

Multiple Explosions

When two or more explosions of similar material occur several milliseconds apart, the blast wave of the initial explosion will propagate ahead of the waves resulting from the subsequent explosions, with the phasing of the propagation of these latter waves being governed by the initiation time and orientation of the individual explosives. If the time delay between explosions is not too large, the blast waves produced by the subsequent explosions will eventually overtake and merge with that of the initial detonation. The distance from the explosion at which this merger occurs

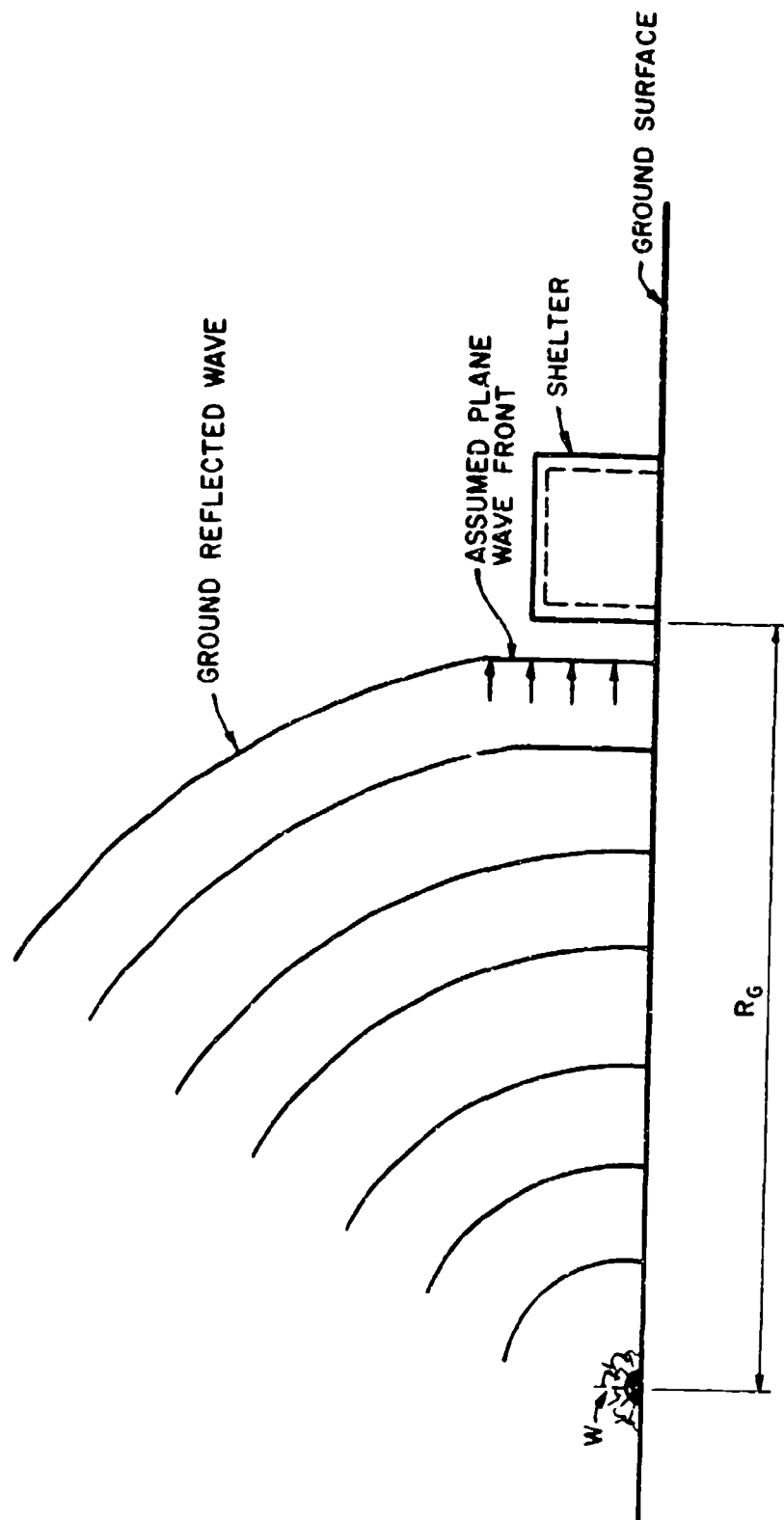
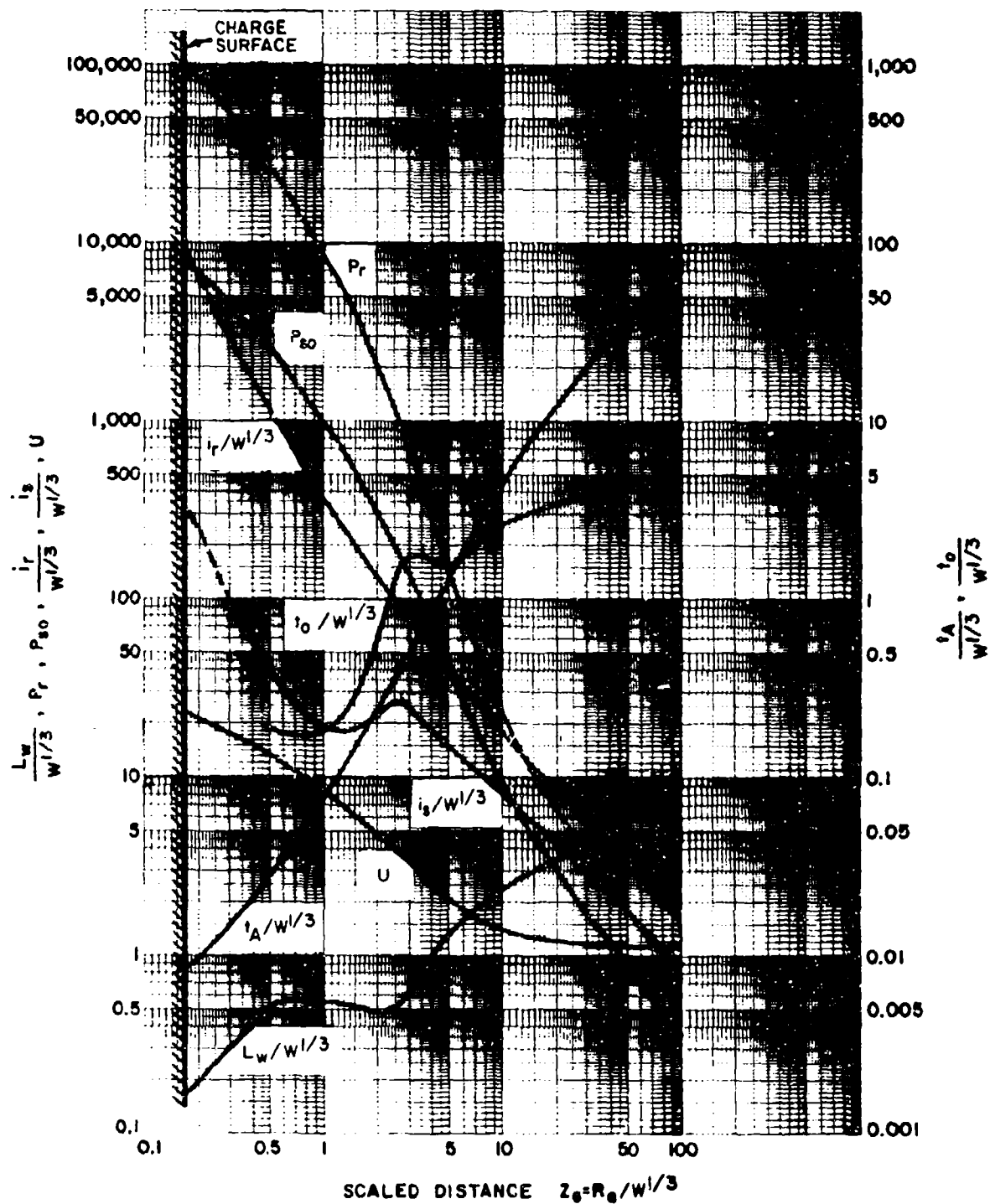
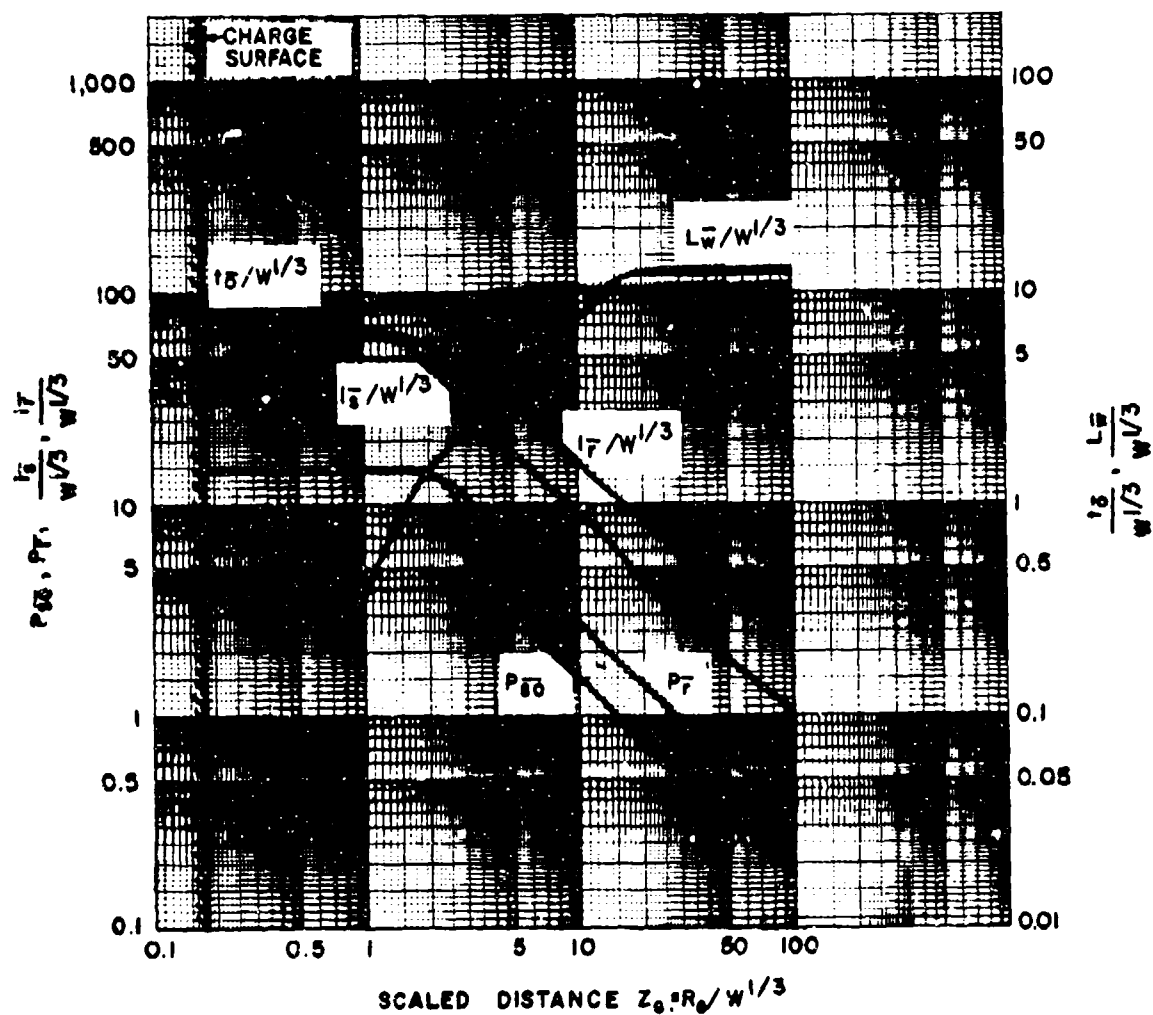


Figure 2-14 Surface burst blast environment



- P_{s0} = PEAK POSITIVE INCIDENT PRESSURE, psi
 P_r = PEAK POSITIVE NORMAL REFLECTED PRESSURE, psi
 $i_s/W^{1/3}$ = SCALED UNIT POSITIVE INCIDENT IMPULSE, psi-ms/lb^{1/3}
 $i_r/W^{1/3}$ = SCALED UNIT POSITIVE NORMAL REFLECTED IMPULSE, psi-ms/lb^{1/3}
 $t_A/W^{1/3}$ = SCALED TIME OF ARRIVAL OF BLAST WAVE, ms/lb^{1/3}
 $t_0/W^{1/3}$ = SCALED POSITIVE DURATION OF POSITIVE PHASE, ms/lb^{1/3}
 U = SHOCK FRONT VELOCITY, ft/ms
 W = CHARGE WEIGHT, lbs
 $L_w/W^{1/3}$ = SCALED WAVE LENGTH OF POSITIVE PHASE, ft/lb^{1/3}

Figure 2-15 Positive phase shock wave parameters for a hemispherical TNT explosion on the surface at sea level



- P_{i0} = PEAK NEGATIVE INCIDENT PRESSURE, psi
 P_{T1} = PEAK NEGATIVE NORMAL REFLECTED PRESSURE, psi
 $i_{i0}/W^{1/3}$ = SCALED UNIT NEGATIVE INCIDENT IMPULSE, psi-ms/lb^{1/3}
 $i_{T1}/W^{1/3}$ = SCALED UNIT NEGATIVE NORMAL REFLECTED IMPULSE, psi-ms/lb^{1/3}
 $L_{i0}/W^{1/3}$ = SCALED DURATION OF NEGATIVE PHASE, ms/lb^{1/3}
 $L_{T1}/W^{1/3}$ = SCALED WAVE LENGTH OF NEGATIVE PHASE, ft/lb^{1/3}

Figure 2-16 Negative phase shock wave parameters for a hemispherical TNT explosion on the surface at sea level

Table 2-2 List of Illustrations of Peak Incident Pressure and
Impulse Produced by Surface Detonation
of Various Explosives

| MATERIAL | FIGURE | DENSITY RANGE | SHAPE | CONFIGURATIONS | | | REMARKS |
|-------------------|--------|---------------|-------|----------------|---------|---------|---|
| | | | | L/H/W | L/L' | W/W' | |
| Composition A-3 | 2-18a | 1.59 to 1.91 | 2-17a | 2.0/1.0/2.5 | - | - | 1) 91% RDX, 9% WAX |
| | | | | 2.4/1.0/2.9 | - | - | 2) Fiberboard shipping containers |
| | | | | 1.8/1.0/2.6 | - | - | |
| Composition A-5 | 2-18b | 1.67 to 1.72 | 2-17a | 2.5/1.0/2.0 | - | - | 1) 98.5% RDX, 1.5 +/- .5% Stearic Acid |
| | 2-18c | 1.67 to 1.72 | 2-17j | - | - | - | 2) Fiberboard shipping containers |
| Composition B | 2-19a | 1.65 | 2-17b | - | - | - | 1) Mixture of RDX and TNT (60/40 percent, respectively) with 1% WAX added |
| | 2-19b | 1.65 | 2-17k | - | - | - | |
| | 2-19c | 1.65 | 2-17j | - | - | - | |
| Composition C-4 | 2-20a | 1.52 to 1.61 | 2-17a | 1.6/1.0/1.3 | - | - | 1) 91% RDX, 9% plasticizer (nonexplosive) |
| | 2-20b | 1.52 to 1.61 | 2-17a | 2.5/1.0/2.0 | - | - | 2) Fiberboard shipping container and M112 extruded demolition blocks (Fig. 2-20a) |
| | | | | 9.0/1.0/9.0 | - | - | 3) Dryer bed configuration (Fig. 2-20b) |
| Guanidine Nitrate | 2-20c | 0.72 | 2-17a | 1.0/1.0/1.0 | - | - | 1) Bulk powder form |
| | | | | | | | 2) Tested in simulated storage bin configurations |
| Cyclotol 70/30 | 2-21a | 1.71 | 2-17a | 2.3/1.0/2.8 | - | - | 1) Type IX, Class A |
| | 2-21b | 1.71 | 2-17c | 2.0/1.0/2.5 | 1.2/1.0 | 2.5/1.0 | 2) Used primarily as a munition filler |
| | | | | 1.0/2.0/2.0 | - | - | 3) Fiberboard shipping containers and hopper |

Table 2-2 List of Illustrations of Peak Incident Pressure and
Impulse Produced by Surface Detonation
of Various Explosives (Continued)

| MATERIAL | FIGURE | DENSITY RANGE | SHAPE | CONFIGURATIONS | | | REMARKS |
|---------------------------------|--------|---------------|-------|----------------|---------|---------|---|
| | | | | L/H/W | L/L' | W/W' | H/D |
| M42 Grenades | 2-21c | - | 2-17d | - | - | - | 1.0/1.0 |
| | | | | | | | 1) Each grenade is filled with .066 lb. of Composition A5 explosive. 2) A plywood tray filled with 64 M42 grenades |
| HMX | 2-22a | 1.87 | 2-17a | 2.0/1.0/3.0 | - | - | - |
| | 2-22b | 1.87 | 2-17j | - | - | - | 1.0/1.2 |
| M483 Projectile Single Round | 2-22c | - | 2-17h | - | - | - | 4.0/1.0 |
| | | | | | | | 1) A single full up M483 was placed vertically with the nose pointed downward |
| Lead Azide | 2-23a | - | 2-17i | - | - | - | - |
| | | | | | | | 1) Wet dextrinated 2) Conductive rubber beaker/bag |
| Lead Styphnate | 2-23b | - | 2-17i | - | - | - | - |
| | 2-23c | - | 2-17m | - | - | - | - |
| LX-14 | 2-24a | - | 2-17a | 2.8/1.0/2.8 | - | - | - |
| | 2-24b | - | 2-17f | - | - | - | 2.0/1.0 |
| | 2-24c | - | 2-17a | 2.2/1.0/2.2 | - | - | - |
| Octol 75/25 | 2-25a | - | 2-17a | 1.2/1.0/1.2 | - | - | - |
| | | | | 2.0/1.0/2.5 | - | - | - |
| | 2-25b | - | 2-17c | 1.0/2.0/2.0 | 1.2/1.0 | 2.5/1.0 | - |
| M718/741 RAAM Projectile | 2-25c | - | 2-17h | - | - | - | 2.0/1.0 |
| | | | | | | | 1) Pallet of eight projectiles |

Table 2-2 List of Illustrations of Peak Incident Pressure and Impulse Produced by Surface Detonation of Various Explosives (Continued)

| MATERIAL | FIGURE | DENSITY RANGE | SHAPE | CONFIGURATIONS | | | W/W' | H/D | REMARKS |
|----------------|--------|---------------|-------|----------------|------|------|------|----------|--|
| | | | | L/H/W | L/L' | L/L' | | | |
| Nitrocellulose | 2-26a | - | 2-17j | - | - | - | - | 1.3/1.0 | 1) Dehydrated nitrocellulose (13.5% nitrogen) MIL-N-244A, Grade C |
| | 2-26b | - | 2-17a | 1.2/1.0/1.2 | - | - | - | - | |
| | 2-26c | - | 2-17a | 64.0/1.0/64.0 | - | - | - | - | 2) Standard shipping containers (Fig. 2-26a, b) 3) Dryerbed (Fig. 2-26c) |
| Nitroglycerine | 2-27a | - | 2-17i | - | - | - | - | 1.0/1.0 | 1) Liquid high explosive in polymethylpentene plastic laboratory beakers |
| PBXC-203 | 2-27b | 1.6+/-0.5 | 2-17j | - | - | - | - | 2.0/1.0 | 1) Granular molding powder |
| | 2-27c | 1.6+/-0.5 | 2-17g | - | - | - | - | 20.0/1.0 | 2) Nominal composition by weight of 91% RDX and 9% ethylenevinyl acetate copolymer (EVA) 3) Cylindrical fiberboard container 4) Single, double and triple extruded rods in varying lengths |
| RDX Slurry | 2-28a | - | 2-17j | - | - | - | - | 3.7/1.0 | 1) Mixture consisted of RDX in a solution of 60% acetic acid, 32% water and 2% nitric acid. |
| | | - | | - | - | - | - | 2.4/1.0 | 2) Encased in polyethylene container |
| RDX 98/2 | 2-28b | - | 2-17a | 1.7/1.0/2.6 | - | - | - | - | 1) High explosive received wet with isopropyl alcohol |
| | 2-28c | - | 2-17j | - | - | - | - | 1.2/1.0 | 2) Plywood orthorhombic Nutsche container |
| | | - | | - | - | - | - | 0.9/1.0 | 3) Fiberboard shipping containers |

Table 2-2 List of Illustrations of Peak Incident Pressure and Impulse Produced by Surface Detonation of Various Explosives (Continued)

| MATERIAL | FIGURE | DENSITY RANGE | SHAPE | CONFIGURATIONS | | | REMARKS |
|--------------------|--------|---------------|-------|----------------|----------|---------|--|
| | | | | L/H/W | L/L' | W/W'' | |
| TNT (Flake) | 2-29a | - | 2-17j | - | - | - | 1) Flake TNT bulk form |
| | 2-29b | - | 2-17a | 1.2/1.0/1.2 | - | - | 2) Fiberboard cylindrical container |
| | 2-29c | - | 2-17c | 1.0/2.4/2.0 | 1.25/1.0 | 2.5/1.0 | 3) Orthorhombic fiberboard container |
| Tetracene | 2-30a | - | 2-17i | - | - | - | 4) Hopper constructed from plywood |
| | | - | | | | | 1) A primary explosive, was detonated in beakers in a dry state and in a wet state in storage bags |
| Nitroguanidine | 2-30b | - | 2-17j | - | - | - | 1) Aluminum storage bin |
| | | - | | | | | 2) Bulk form |
| Benite Propellant | 2-31a | - | 2-17a | 1.4/1.0/1.4 | - | - | 1) 40% nitrocellulose, 44.3% potassium nitrate, 6.3% sulfur, 9.4% charcoal and 0.5% ethyl centralite |
| | 2-31b | - | 2-17a | 1.1/1.0/1.1 | - | - | 2) Container made of wood and fiberboard |
| Black Powder | 2-31c | - | - | 1.0/1.0/1.0 | - | - | 1) Class I, 4 by 8; Class 6, 20 by MIL-P-2238 Grade A1, 4 by 8, Grade A3, 12 by 16; Grade A-3a |
| | | - | | | | | 2) Tested in loose powder form |
| 95-WACO Propellant | 2-32a | - | 2-17j | - | - | - | 3) Storage bins and tote bins boxes were constructed from plywood |
| | 2-32b | - | 2-17a | 1.6/1.0/2.9 | - | - | 1) Multi perforated |
| | 2-32c | - | 2-17e | - | - | - | 2) Tested in cardboard drums (Fig. 2-32a), full-sized metal shipping containers (Fig. 2-32b) and aluminum hoppers (Fig. 2-32c) |

Table 2-2 List of Illustrations of Peak Incident Pressure and
Impulse Produced by Surface Detonation
of Various Explosives (Continued)

| MATERIAL | FIGURE | DENSITY | RANGE | SHAPE | CONFIGURATIONS | | | REMARKS |
|-----------------------|--------|---------|-------|-------|----------------|---------|---------|---|
| | | | | | L/H/W | L/L' | W/H' | H/D |
| DIGL-RP Propellant | 2-33a | - | - | 2-17a | 3.2/1.0/1.5 | - | - | - |
| | | - | - | | 1.9/1.0/3.2 | - | - | - |
| | | - | - | | 1.4/1.0/2.2 | - | - | - |
| | 2-33b | - | - | 2-17j | - | - | - | 1.0/1.0 |
| | 2-33c | - | - | 2-17a | 2.2/1.0/2.7 | - | - | - |
| M1 Propellant | | | | | | | | 1) Composition of nitrocellulose, diethyleneglycol dinitrate, Akantite II Antralite I, magnesium oxide and graphite. |
| | | | | | | | | 2) Plywood containers (15420 and 15422) |
| | | | | | | | | 3) Cylindrical fiberboard container (15421) |
| | 2-34a | - | - | 2-17j | - | - | - | 1) 84.2%, 13.15% N nitrocellulose; |
| | 2-34b | - | - | 2-17j | - | - | - | 9.9% dinitrotoluene; 4.9% dibutyl- |
| | 2-34a | - | - | 2-17c | 3.5/1.0/3.5 | 7.0/1.0 | 7.0/1.0 | phthalate; and 1.0% diphenylamine |
| | 2-34a | - | - | 2-17e | - | - | - | 2) Cylindrical drums, open hopper, closed feed hopper |
| M26 C1 | 2-34b | - | - | 2-17c | 3.4/1.0/3.4 | 9.0/1.0 | 9.0/1.0 | - |
| | 2-34b | - | - | 2-17a | - | - | - | 1.0/1.3 |
| | | | | | | | | 1.0/1.3 |
| | 2-34c | - | - | 2-17j | - | - | - | 1.0/1.5 |
| | 2-35a | - | - | 2-17a | 10.5/1.0/60.0 | - | - | - |
| | 2-35b | - | - | 2-17a | 2.2/1.0/2.2 | - | - | - |
| | 2-35c | - | - | 2-17j | - | - | - | 1.7/1.0 |
| M30 A1 | | | | | | | | 1) Multi perforated propellant |
| | | | | | | | | 2) Cylindrical fiberboard shipping containers, dryer bed configurations constructed from plywood, cylindrical container constructed from stainless steel (Fig. 2-35c) |
| | 2-36a | - | - | 2-17j | - | - | - | 1.5/1.0 |
| | 2-36b | - | - | 2-17j | - | - | - | 1.5/1.0 |
| | 2-36c | - | - | 2-17a | 2.4/1.0/12.0 | - | - | - |
| | 2-37a | - | - | 2-17a | 2.4/1.0/12.0 | - | - | - |
| | | | | | | | | 1) Propellant single perforated and multi perforated |
| | | | | | | | | 2) Cylindrical shipping drums and orthorhombic simulated dryers |

Table 2-2 List of Illustrations of Peak Incident Pressure and
Impulse Produced by Surface Detonation
of Various Explosives (Continued)

| MATERIAL | FIGURE | DENSITY | RANGE | SHAPE | CONFIGURATIONS | | | REMARKS |
|-------------------------------|--------|---------|-------|-------|----------------|---------|---------|--|
| | | | | | L/H/W | L/L' | W/W' | H/D |
| M31 A1E1 | 2-37b | - | - | 2-17a | 3.1/1.0/1.0 | - | - | - |
| | 2-37c | - | - | 2-17a | 3.1/1.0/1.0 | - | - | - |
| | 2-38a | - | - | 2-17a | 3.8/1.0/2.0 | - | - | - |
| | 2-38b | - | - | 2-17a | 3.8/1.0/2.0 | - | - | - |
| M5 Propellant | 2-38c | - | - | 2-17j | - | - | - | 1) Triple-base slotted stick propellant |
| | 2-39a | - | - | 2-17j | - | - | - | 2) Simulated fiberboard carton |
| | 2-39b | - | - | 2-17a | 1.4/1.0/6.8 | - | - | 3) Simulated wooden shipping/storage container |
| | 2-39c | - | - | 2-17a | 1.0/1.7/4.4 | - | - | 4) Short side (L) parallel to shock front, or |
| M6 Propellant | 2-40a | - | - | 2-17j | - | - | - | 5) Long side (W) parallel to shock front |
| | 2-40b | - | - | 2-17e | - | - | - | 1) Single base propellant |
| | 2-40c | - | - | 2-17c | 3.4/1.0/3.4 | 5.8/1.0 | 5.8/1.0 | 2) Shipping drums with 10% moisture |
| | 2-41a | - | - | 2-17g | - | - | - | 3) Carpet rolls cylindrically shaped |
| 2.75 in. Rocket Grain MK 43-1 | 2-41b | - | - | 2-17a | 16.5/1.0/70.0 | - | - | 4) M5 was loaded into charging buckets and conveyor belt configuration |
| | 2-41c | - | - | 2-17j | 3.8/1.0/35.0 | - | - | 1) Multi perforated propellant |
| | 2-41d | - | - | 2-17j | - | - | - | 2) Cylindrical shipping drum |
| | 2-41e | - | - | 2-17j | - | - | - | 3) Closed and open hoppers |
| WC 344 Ball | 2-41f | - | - | 2-17j | - | - | - | 1) M5 Propellant |
| | 2-41g | - | - | 2-17j | - | - | - | 2) Tested in shelves holding one, seven, and nine rocket grains |
| | 2-41h | - | - | 2-17j | - | - | - | 1) Double base propellant |
| | 2-41i | - | - | 2-17j | - | - | - | 2) Dryer bed constructed from plywood |
| | 2-41j | - | - | 2-17j | - | - | - | 3) Cylindrical fiberboard containers |

Table 2-2 List of Illustrations of Peak Incident Pressure and
Impulse Produced by Surface Detonation
of Various Explosives (Continued)

| MATERIAL | FIGURE | DENSITY | RANGE | SHAPE | CONFIGURATIONS | | | W/W* | H/D | REMARKS |
|------------------------------|--------|---------|-------|-------|----------------|------|------|------|----------|--|
| | | | | | L/H/W | L/L' | L/L' | | | |
| XM37 RAP | 2-42a | - | - | 2-17j | - | - | - | - | 1.0/1.3 | 1) Consist of nitrocellulose 50%, nitroglycerine 36.2%, others 13.8% |
| | 2-42b | - | - | 2-17g | - | - | - | - | 9.0/1.0 | 2) Forward and aft grains simulated |
| | 2-42c | - | - | 2-17a | 1.0/1.5/1.0 | - | - | - | - | extruded billet, Ro Con shipping drum |
| | 2-43a | - | - | 2-17j | - | - | - | - | 1.0/1.6 | |
| | 2-43b | - | - | 2-17g | - | - | - | - | 10.0/1.0 | |
| | 2-43c | - | - | 2-17a | 1.2/1.0/1.2 | - | - | - | - | |
| JA-2 (LS460) | 2-44a | - | - | 2-17j | - | - | - | - | 1.0/1.0 | 1) Double base propellant |
| | 2-44b | - | - | 2-17a | 10.0/1.0/10.0 | - | - | - | - | 2) 60% nitrocellulose, 24.6% diethylene glycol dinitrate, 15.4% others |
| | | | | | 5.0/1.0/5.0 | - | - | - | - | 3) Fiberboard cylindrical container |
| | | | | | 2.5/1.0/2.5 | - | - | - | - | 4) Orthorhombic fiberboard container |
| M10 Propellant | 2-44c | - | - | 2-17a | 1.0/2.7/1.5 | - | - | - | - | 1) 98% nitrocellulose (13.5% N), 1% potassium sulfate and 1% diphenyl- amine |
| | 2-45a | - | - | 2-17a | 1.0/1.6/1.1 | - | - | - | - | 2) Single perforated |
| | | | | | 2.1/1.0/1.3 | - | - | - | - | 3) Fiberboard box, metal lined wooden boxes, orthorhombic stainless steel vented container |
| | | | | | 1.5/1.0/1.2 | - | - | - | - | |
| 105mm, M314 A3 Illuminant | 2-45b | - | - | 2-17j | - | - | - | - | 1.0/1.4 | 1) 7.7% Luminac 4116 type A, 56% mag- nesium, 36% sodium nitrate |
| | 2-45c | - | - | 2-17j | - | - | - | - | 1.0/6.0 | 2) Fiberboard shipping drums (Fig. 2-45b) |
| | | | | | | | | | | 3) Simulated steel mixer/mill (Fig. 2-45c) |

Table 2-2 List of Illustrations of Peak Incident Pressure and Impulse Produced by Surface Detonation of Various Explosives (Continued)

| MATERIAL | FIGURE | DENSITY RANGE | SHAPE | CONFIGURATIONS | | | REMARKS |
|--------------------------------|--------|---------------|-------|----------------|------|------|---|
| | | | | L/W/H | L/L' | W/Y' | |
| I559 Igniter Mixture | 2-46a | - | 2-17j | - | - | - | 1) I136 premix (90% strontium nitrate and 10% calcium resinute) and a premix (23.3% lead dioxide and 77.7% magnesium) |
| | 2-46b | - | 2-17j | - | - | - | 2) Rubber and aluminum cylinder configurations (Fig. 2-46a and 2-46b respectively) |
| I560 Subigniter Mixture | 2-46c | - | 2-17j | - | - | - | 1) Magnesium/strontium nitrate/strontium peroxide/polyvinyl chloride 27.5/27.5/30/15% by weight respectively |
| | 2-47a | - | 2-17j | - | - | - | 2) Rubber (Fig. 2-46c) and aluminum (Fig. 2-47a) cylinder configurations |
| R284 Tracer Mixture | 2-47b | - | 2-17j | - | - | - | 1) Strontium nitrate/polyvinyl chloride/(50/100 mesh) magnesium in 53.7/18.1/28.2% by weight, respectively |
| | 2-47c | - | 2-17j | - | - | - | 2) Rubber (Fig. 2-47b) and aluminum (Fig. 2-47c) cylinder configurations |
| M314-A3 First Fire Composition | 2-48a | - | 2-17a | 1.0/1.17/1.0 | - | - | 1) 50% barium nitrate, 5% laminac Type 8, 20% silicon, 15% zirconium hydrate, 10% tetranitro carbazole |
| | 2-48b | - | 2-17j | - | - | - | 2) Cardboard box (Fig. 2-48a) simulated mix/muller (Fig. 2-48b) |

Table 2-2 List of Illustrations of Peak Incident Pressure and
Impulse Produced by Surface Detonation
of Various Explosives (Continued)

| MATERIAL | FIGURE | DENSITY RANGE | SHAPE | CONFIGURATIONS | | | REMARKS |
|------------------------------------|--------|---------------|-------|----------------|------|------|---|
| | | | | L/W/V | L/L' | W/V' | |
| M49A1 Trip Flare Composition | 2-48c | - | 2-17j | - | - | - | 1) Magnesium 36%, sodium nitrate 54%, binder 10% |
| | 2-49a | - | 2-17j | - | - | - | 2) Shipping drum fiberboard (Fig. 48c), simulated steel mixer/muller (Fig. 2-49a) |

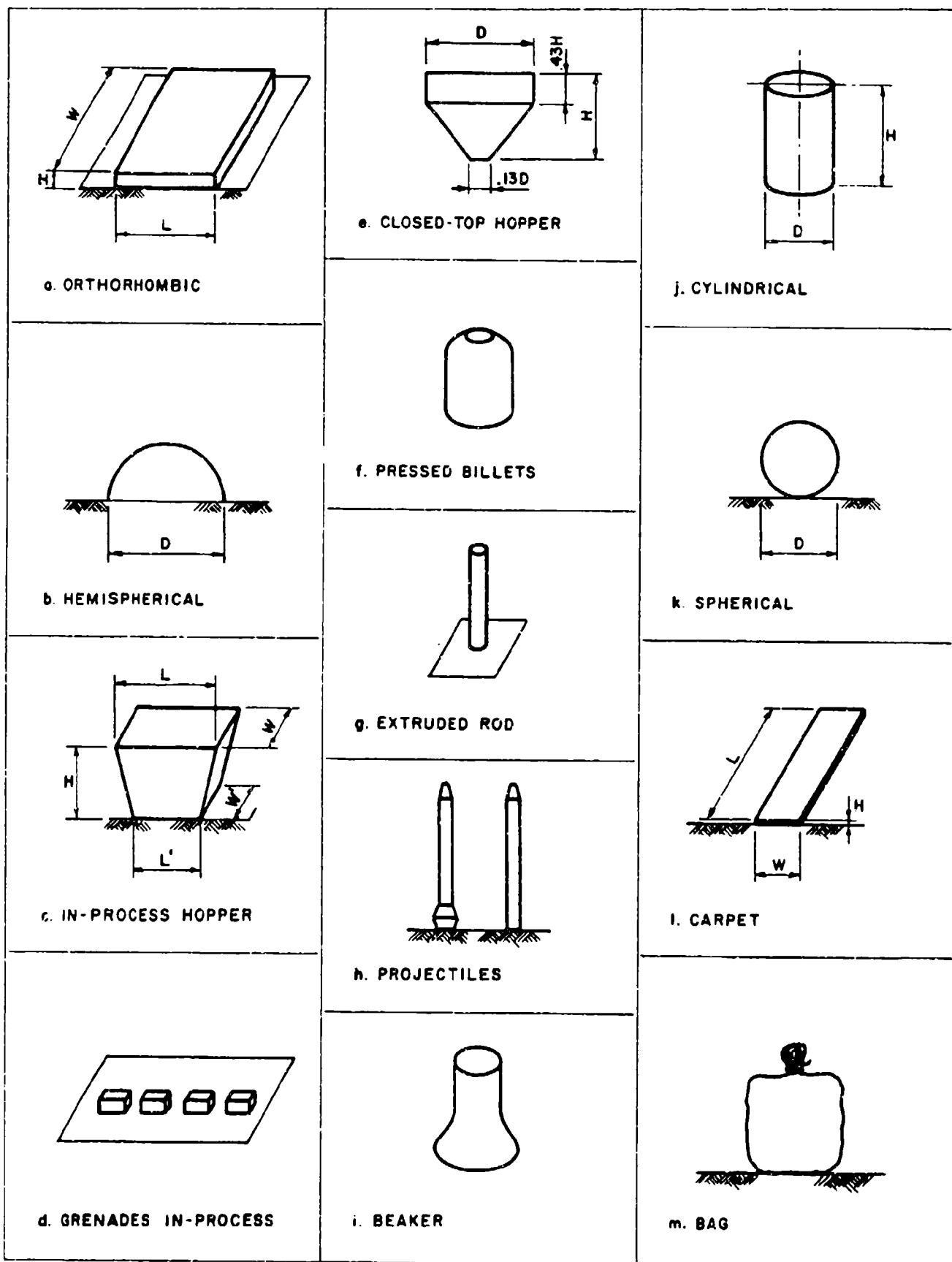


Figure 2-17 Explosive shapes

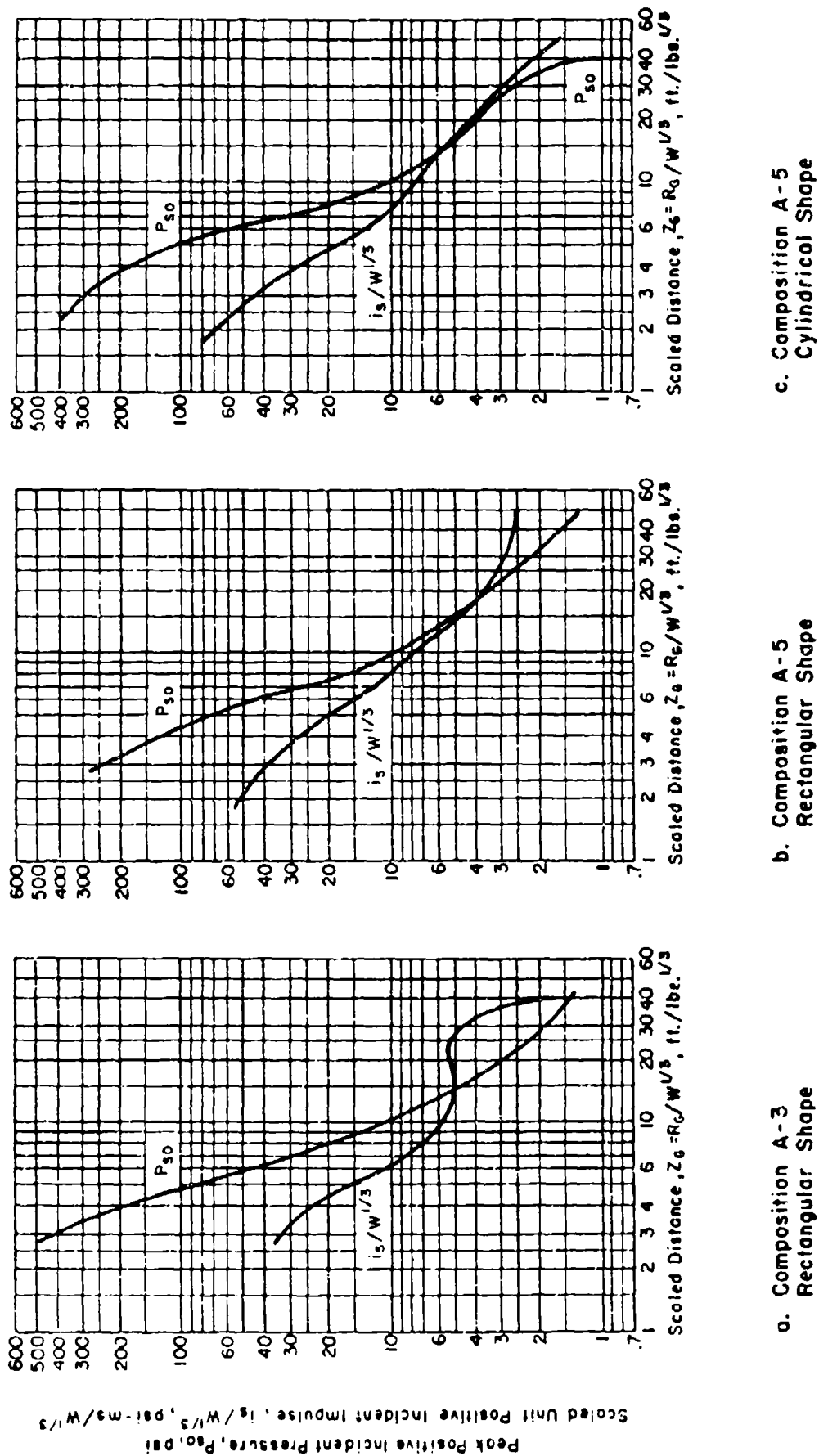
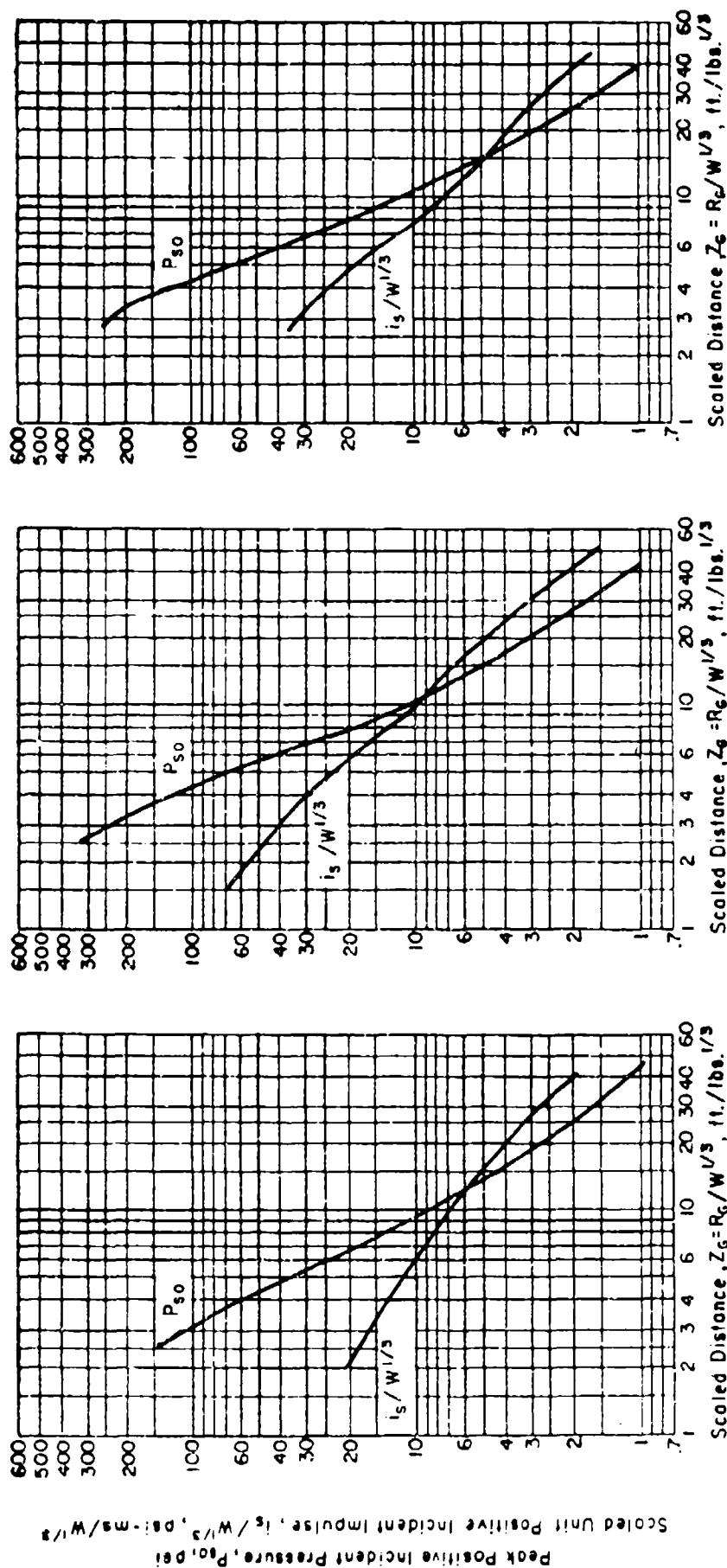


Figure 2-18 Peak positive incident pressure and scaled impulse for an explosion on the surface at sea level



a. Composition B
Hemispherical

b. Composition B
Cast Spherical

c. Composition B
Cylindrical

Figure 2-19 Peak positive incident pressure and scaled impulse for an explosion on the surface at sea level

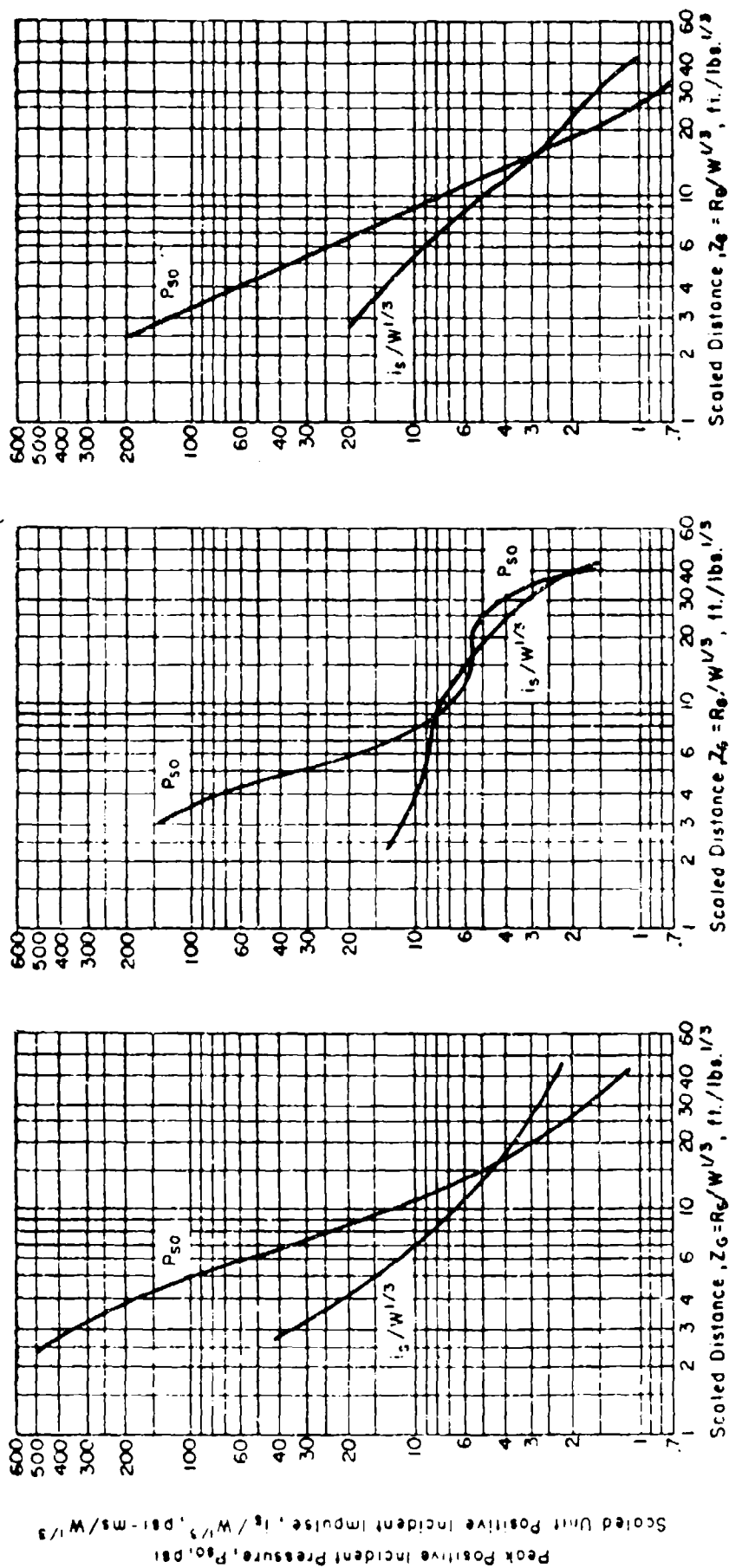
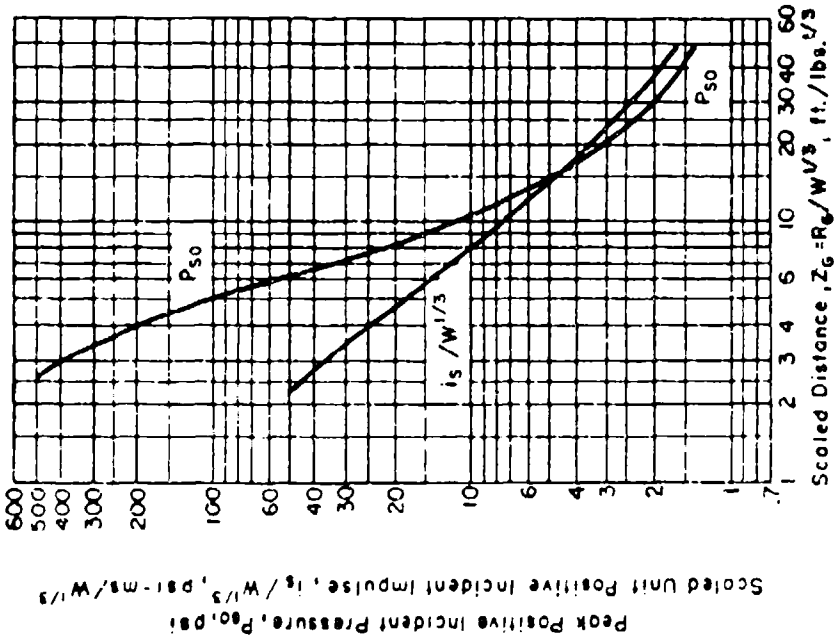
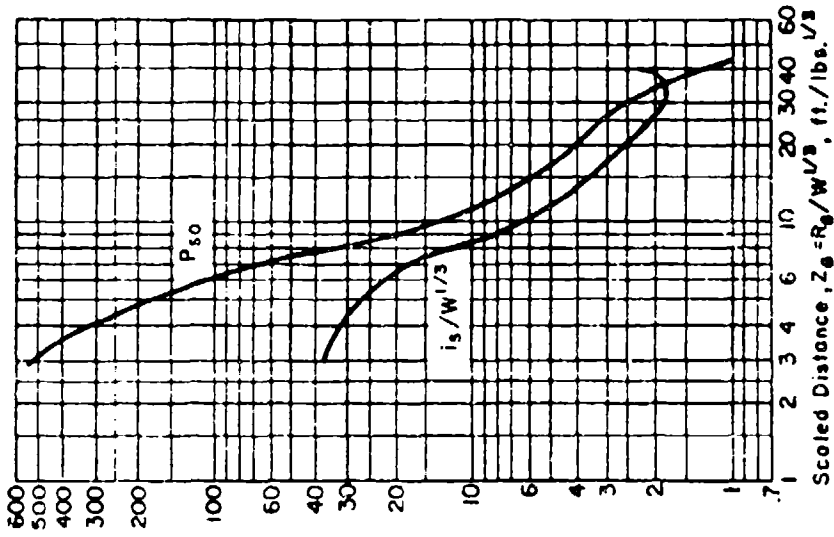


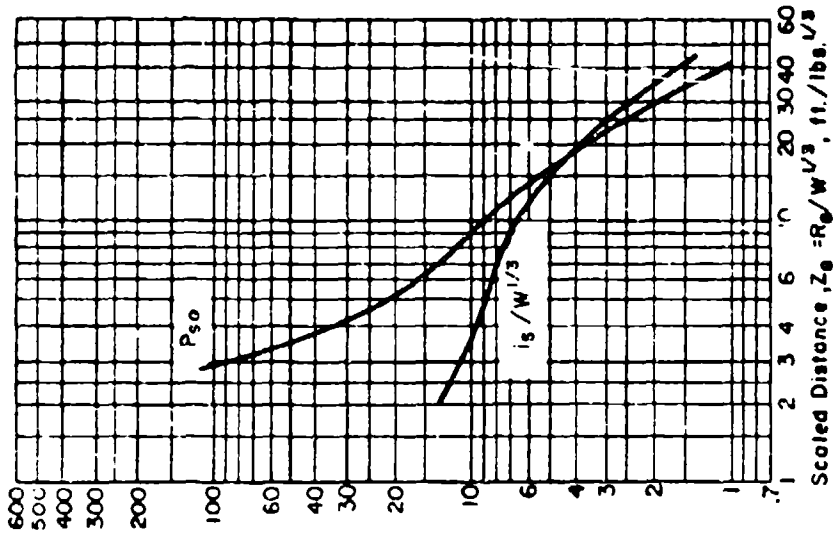
Figure 2-20 Peak positive incident pressure and scaled impulse for an explosion on the surface at sea level



a. Cyclotol 70/30
Orthorhomic

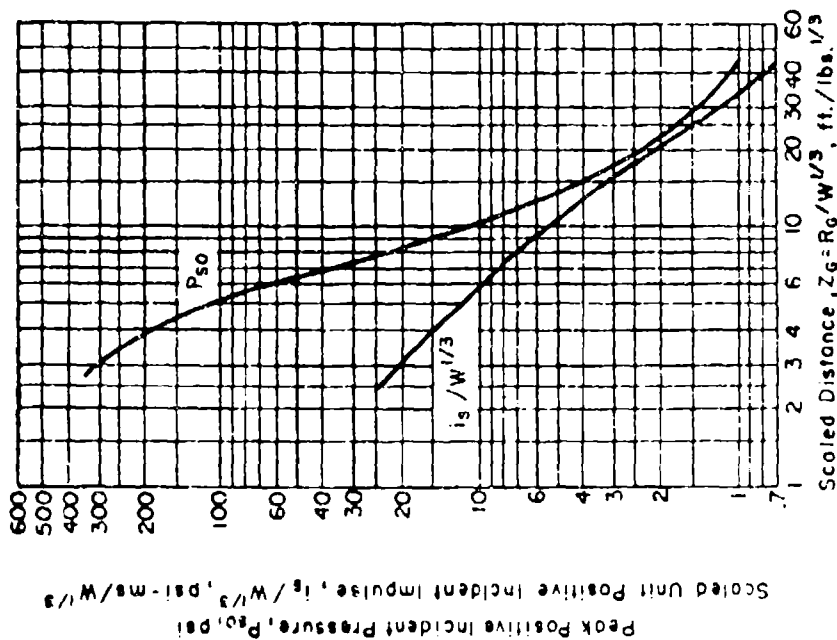


b. Cyclotol 70/30
Hoppers

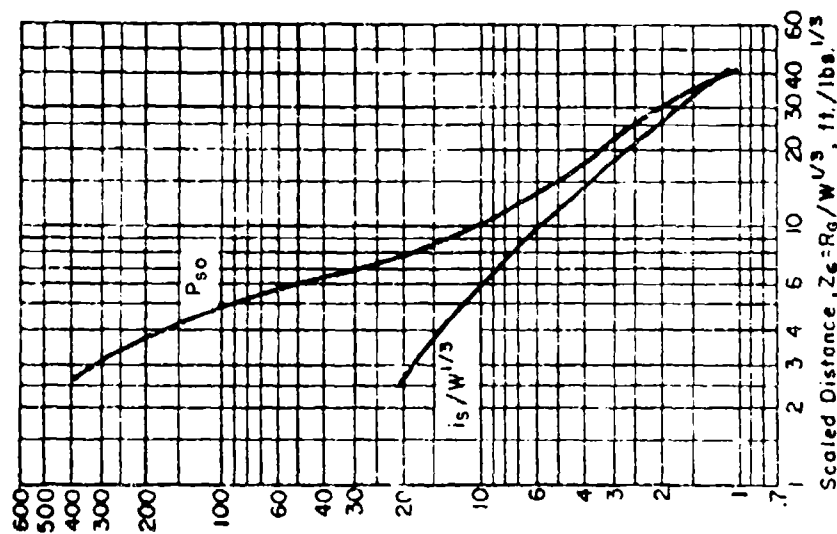


c. 64 M42 Grenades
Tray of 64

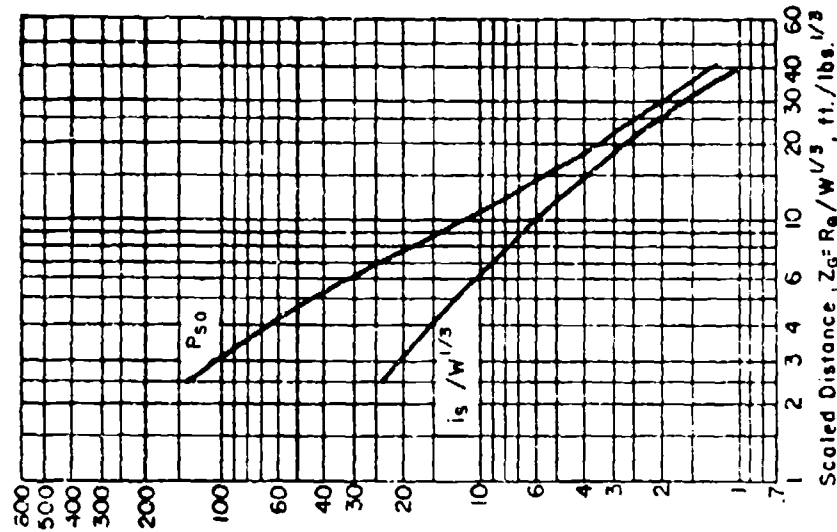
Figure 2-21 Peak positive incident pressure and scaled impulse for an explosion on the surface at sea level



a. HMX
Orthorhombic



b. HMX
Cylindrical



c. M483 155mm ICM Projectile
Single Round

Figure 2-22 Peak positive incident pressure and scaled impulse for an explosion on the surface at sea level

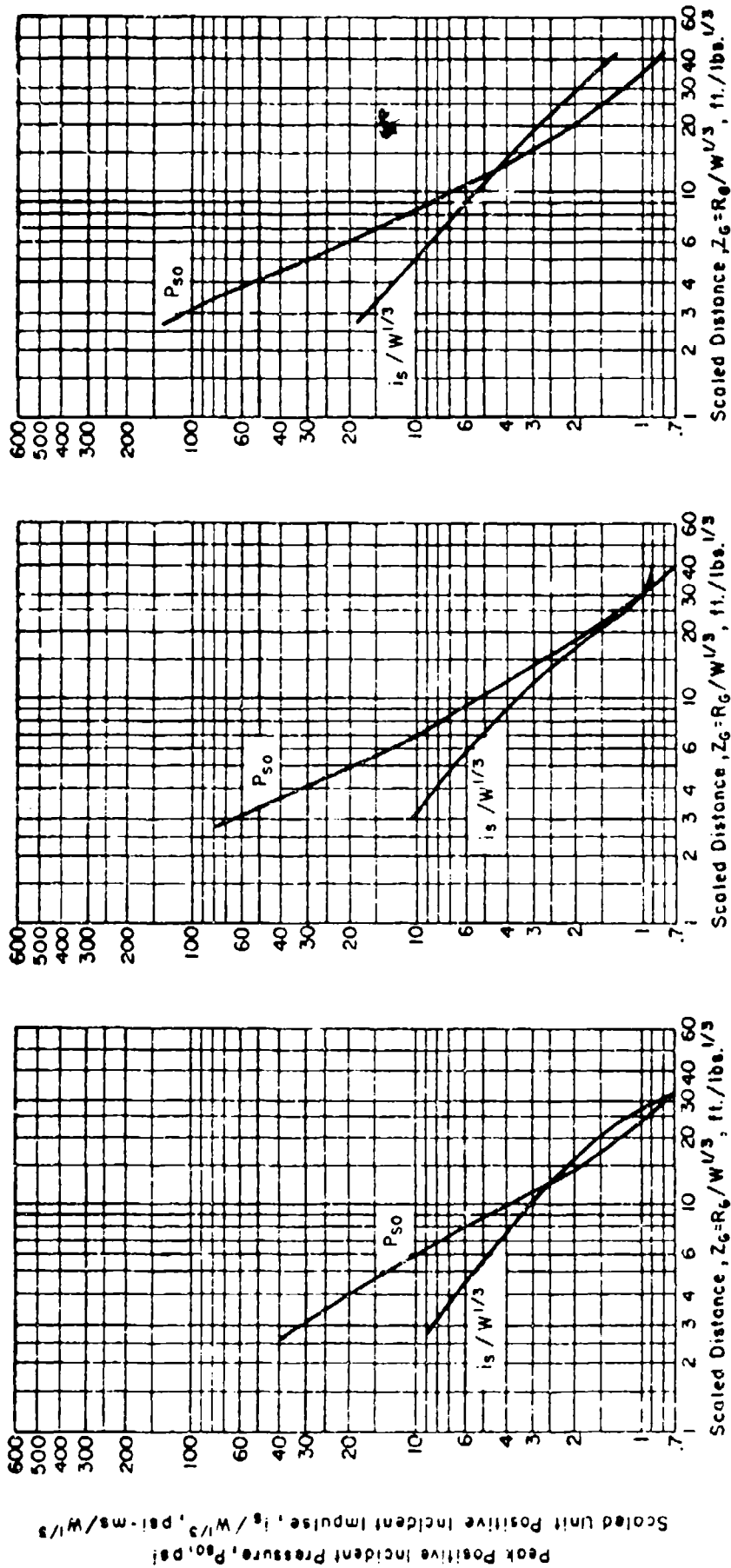
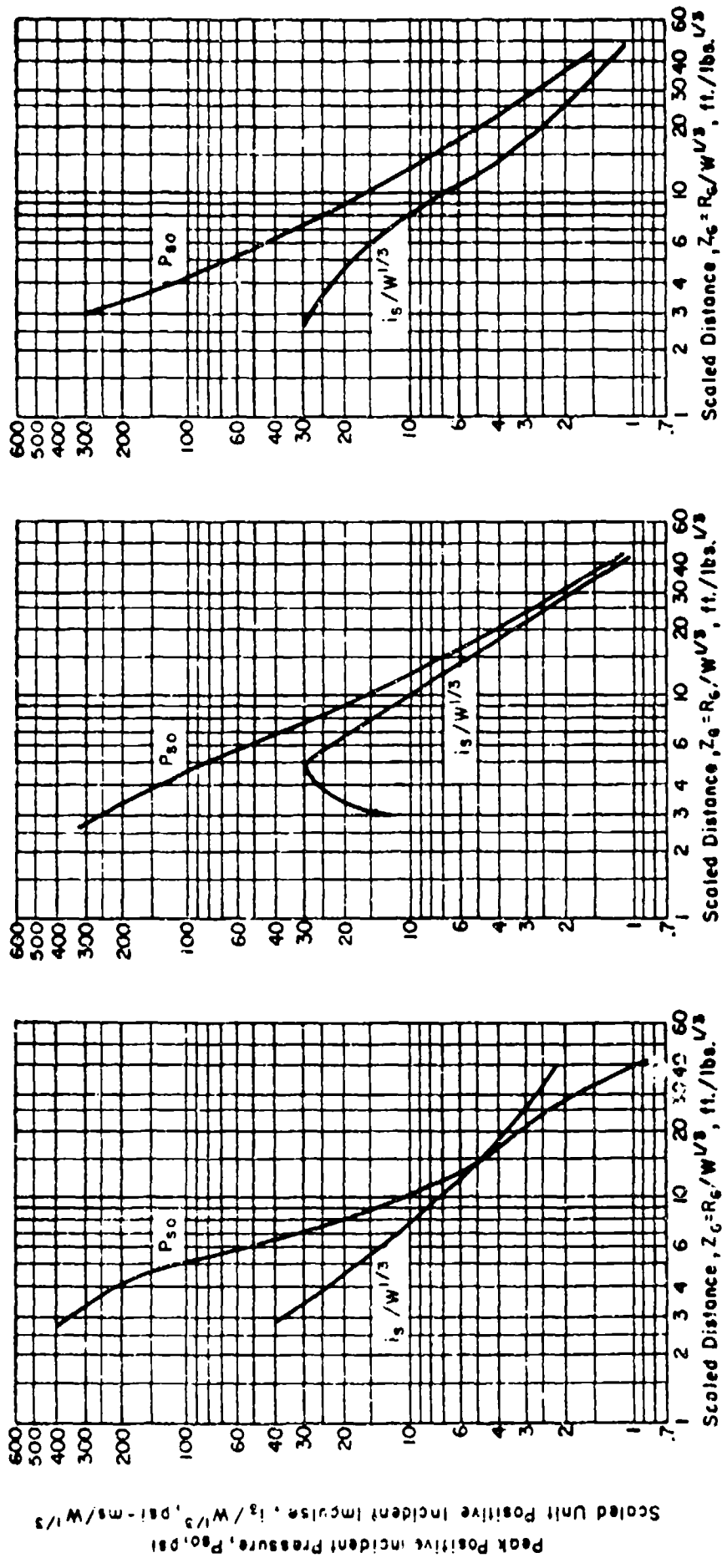


Figure 2-23 Peak positive incident pressure and scaled impulse for an explosion on the surface at sea level

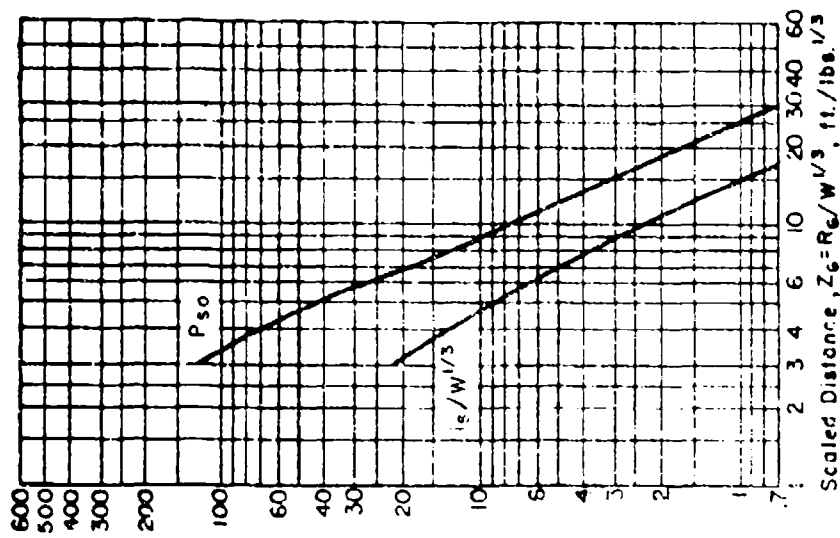


a. LX-14
Orthorhombic

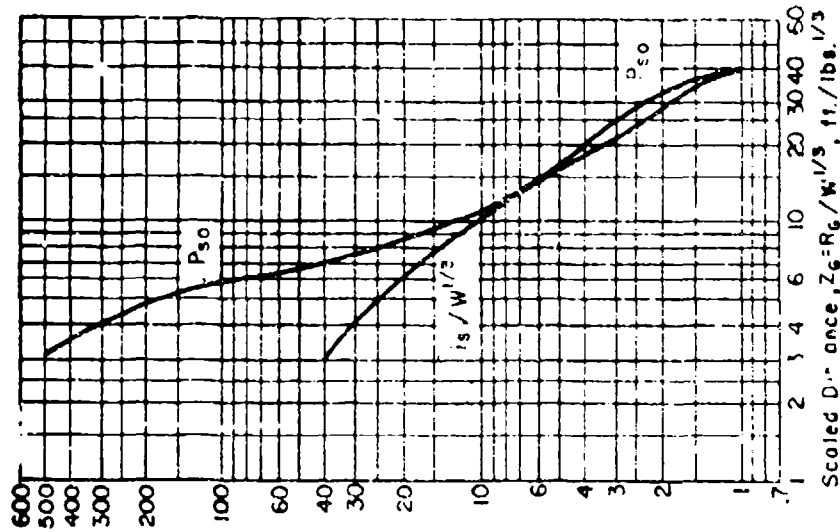
b. LX-14
Pressed billets

c. LX-14
Orthorhombic

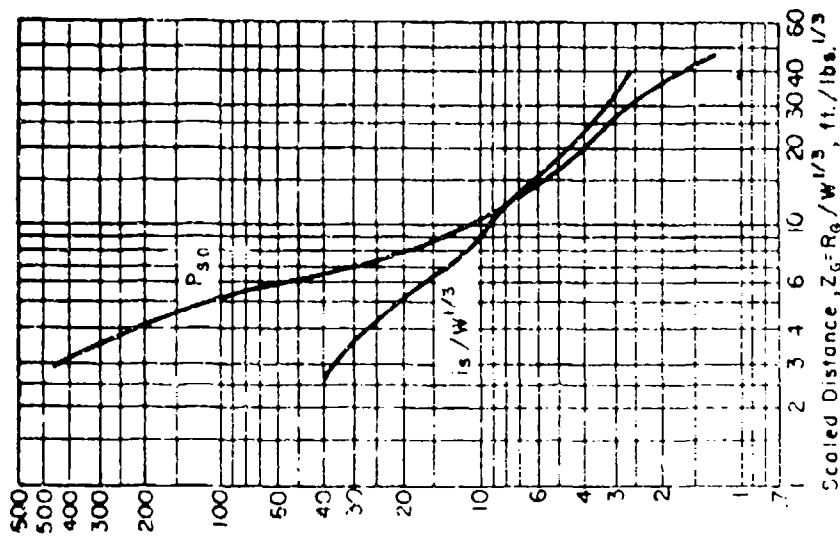
Figure 2-24 Peak positive incident pressure and scaled impulse for an explosion on the surface at sea level



a. Octol 75/25
Orthorhombic

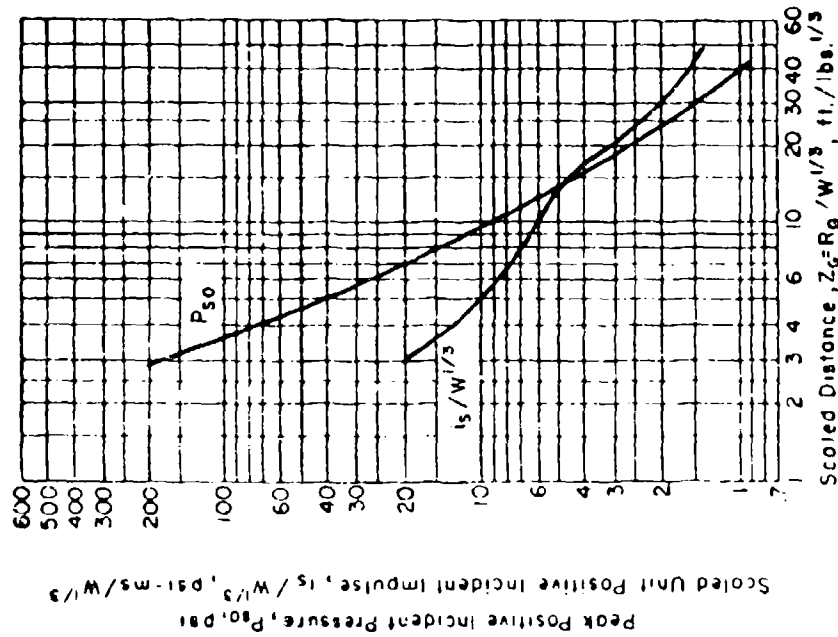


b. Octol 75/25
Hopper

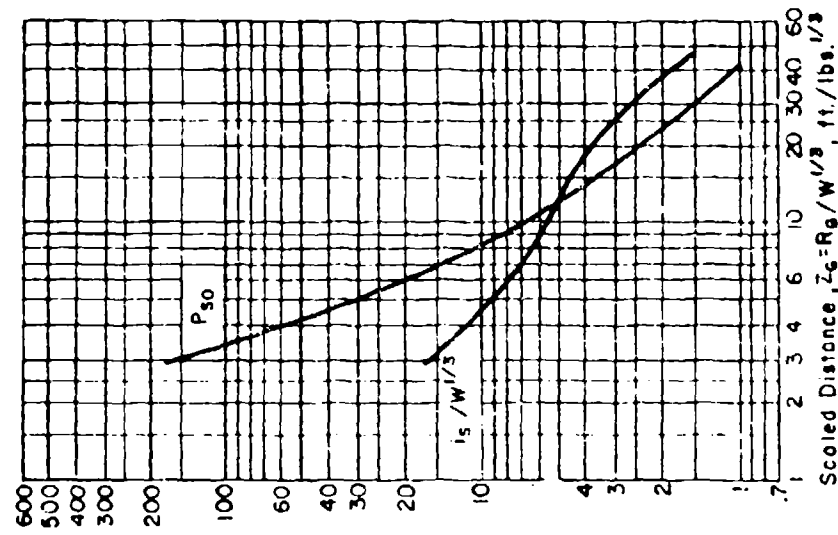


c. M718/741 RAAM
Pallet of eight rounds

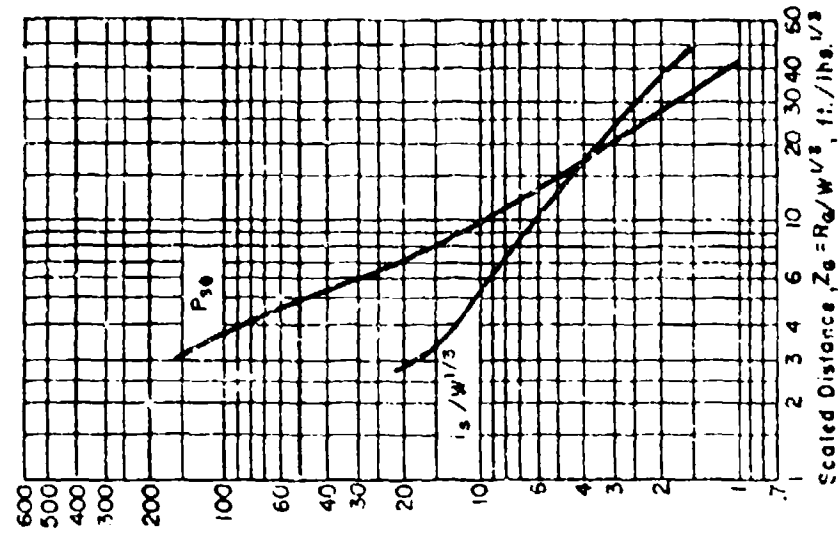
Figure 2-25 Peak positive incident pressure and scaled impulse for an explosion on the surface at sea level



a. Nitrocellulose
Cylindrical

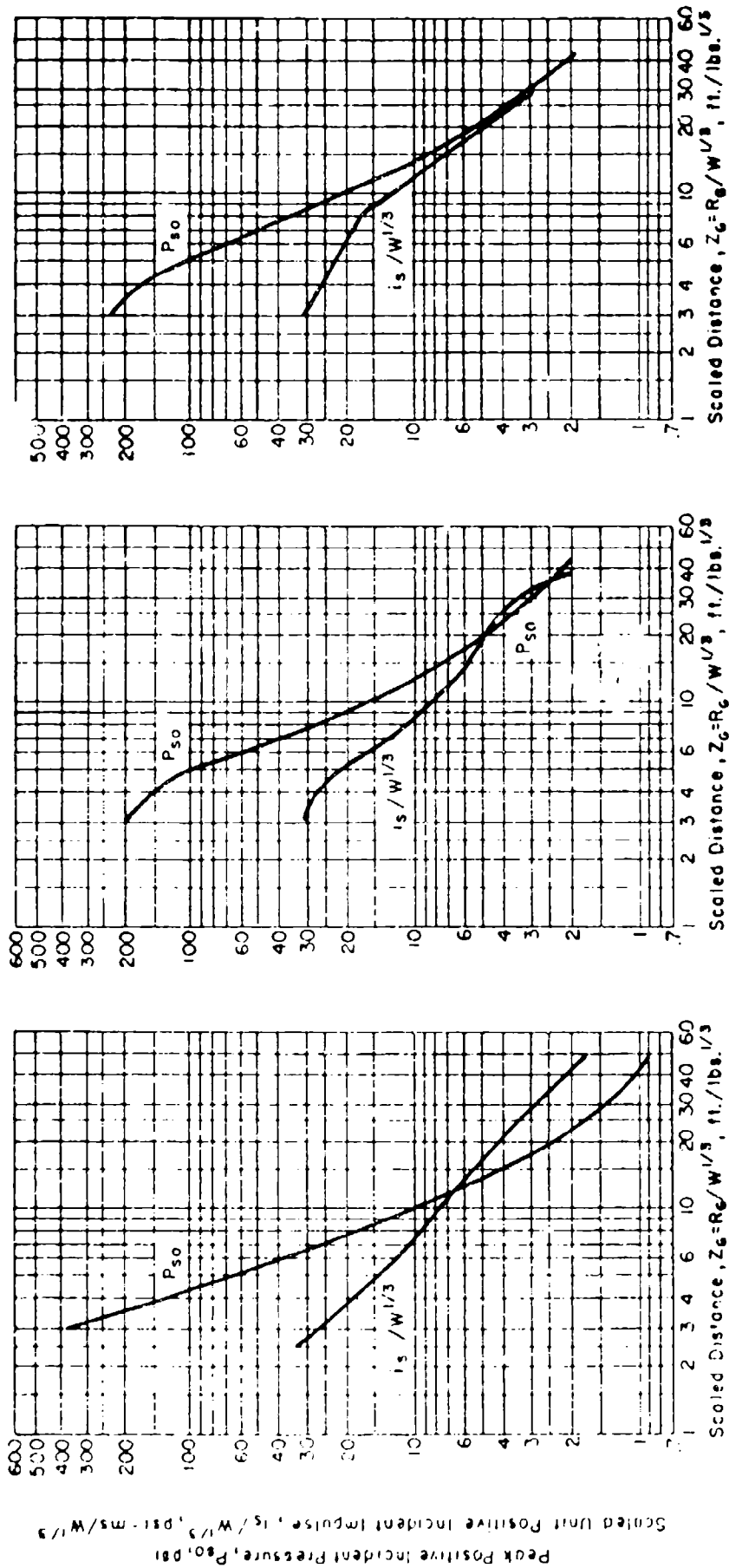


b. Nitrocellulose
Dryer bed



c. Nitrocellulose
Orthorhombic

Figure 2-26 Peak positive incident pressure and scaled impulse for an explosion on the surface at sea level

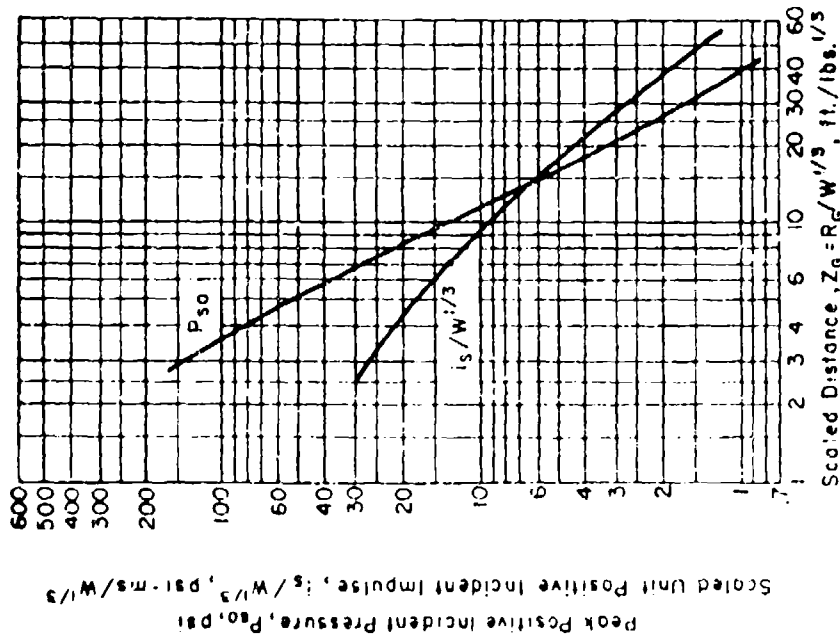


a. Nitroglycerine
Cylindrical

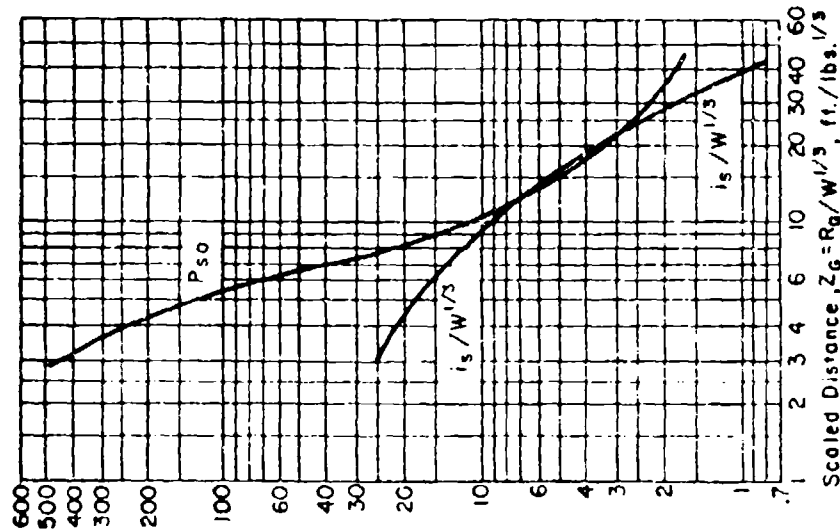
b. PBXC-203
Cylindrical

c. PBXC-203
Extruded rod

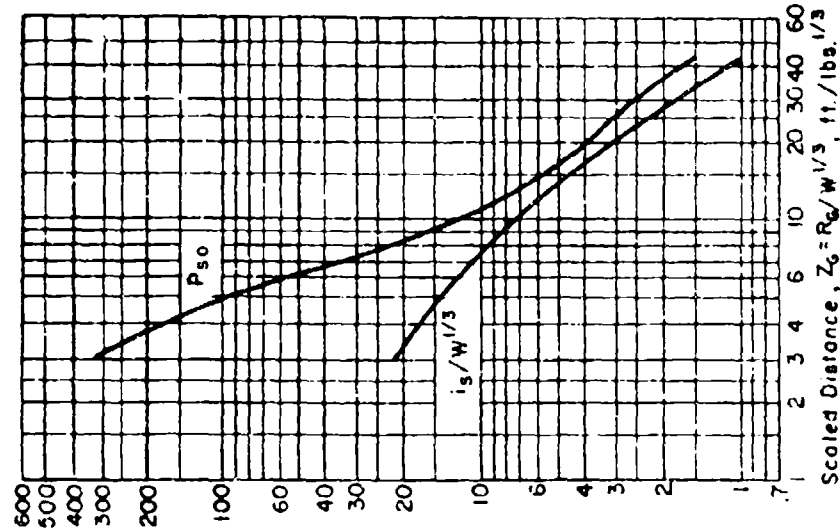
Figure 2-27 Peak positive incident pressure and scaled impulse for an explosion on the surface at sea level



a. RDX Slurry
Cylindrical

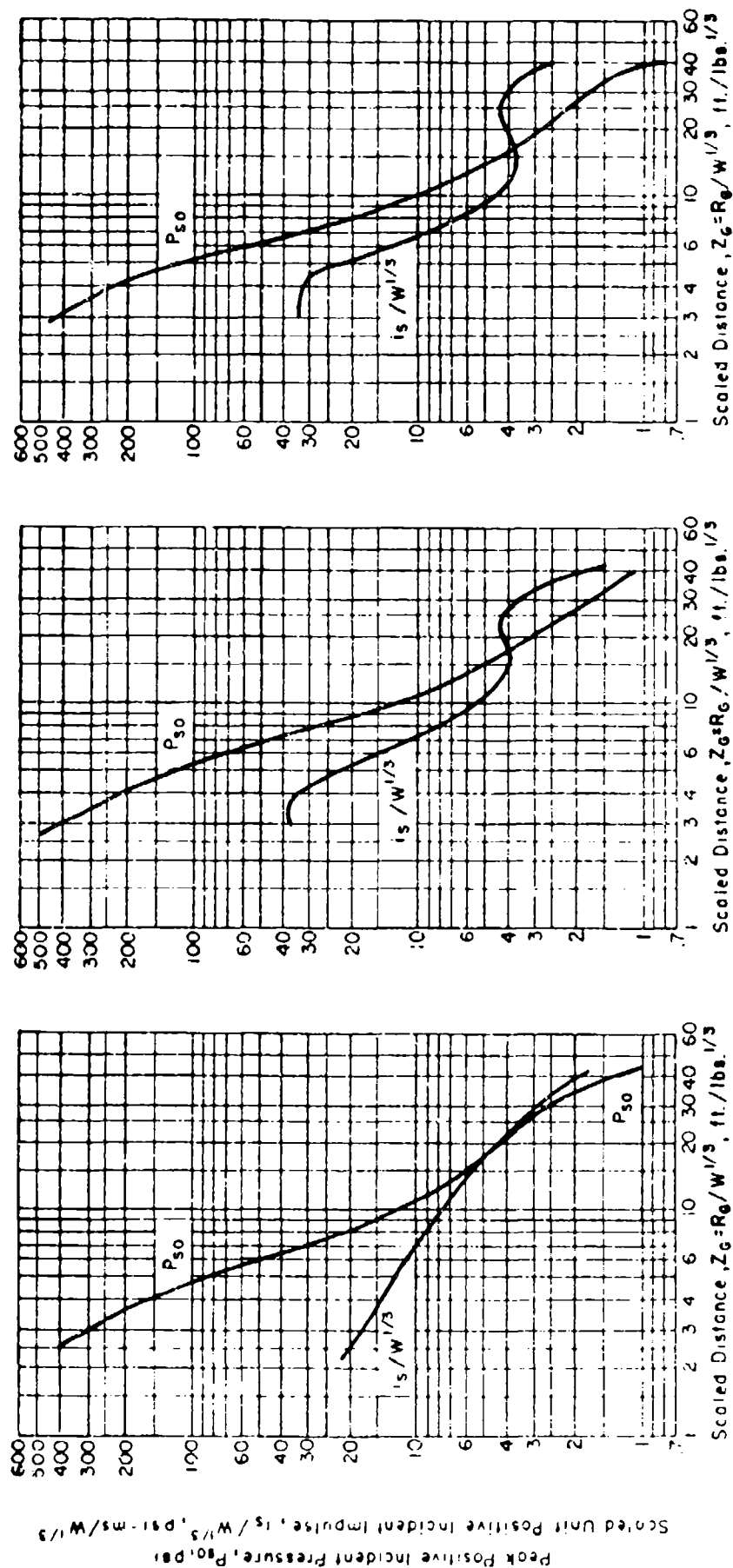


b. RDX 98/2
Orthorhombic



c. RDX 98/2
Cylindrical

Figure 2-26 Peak positive incident pressure and scaled impulse for an explosion on the surface at sea level



a. TNT
Cylindrical

b. TNT
Orthorhombic

c. TNT
Hepper

Figure 2-29 Peak positive incident pressure and scaled impulse for an explosion on the surface at sea level

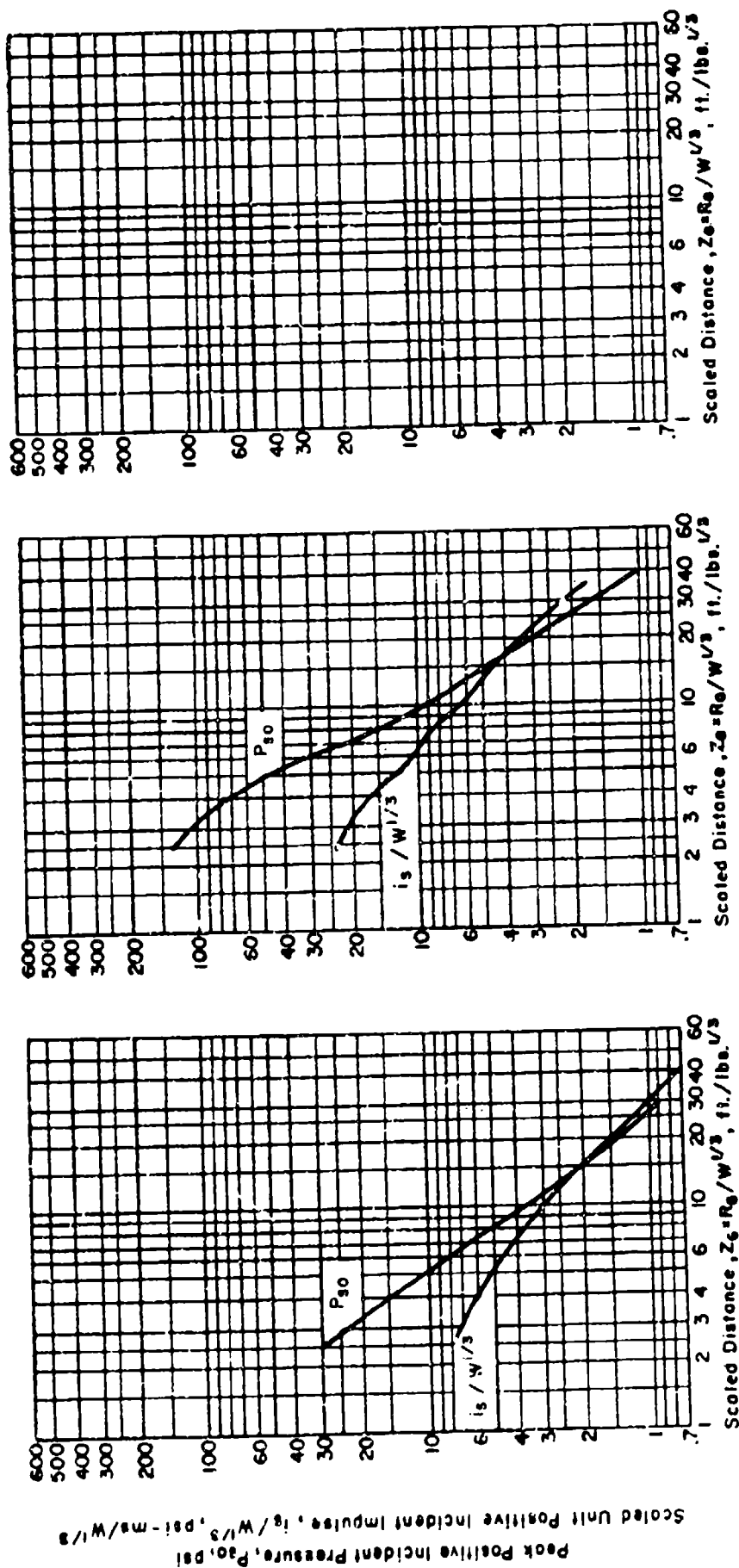
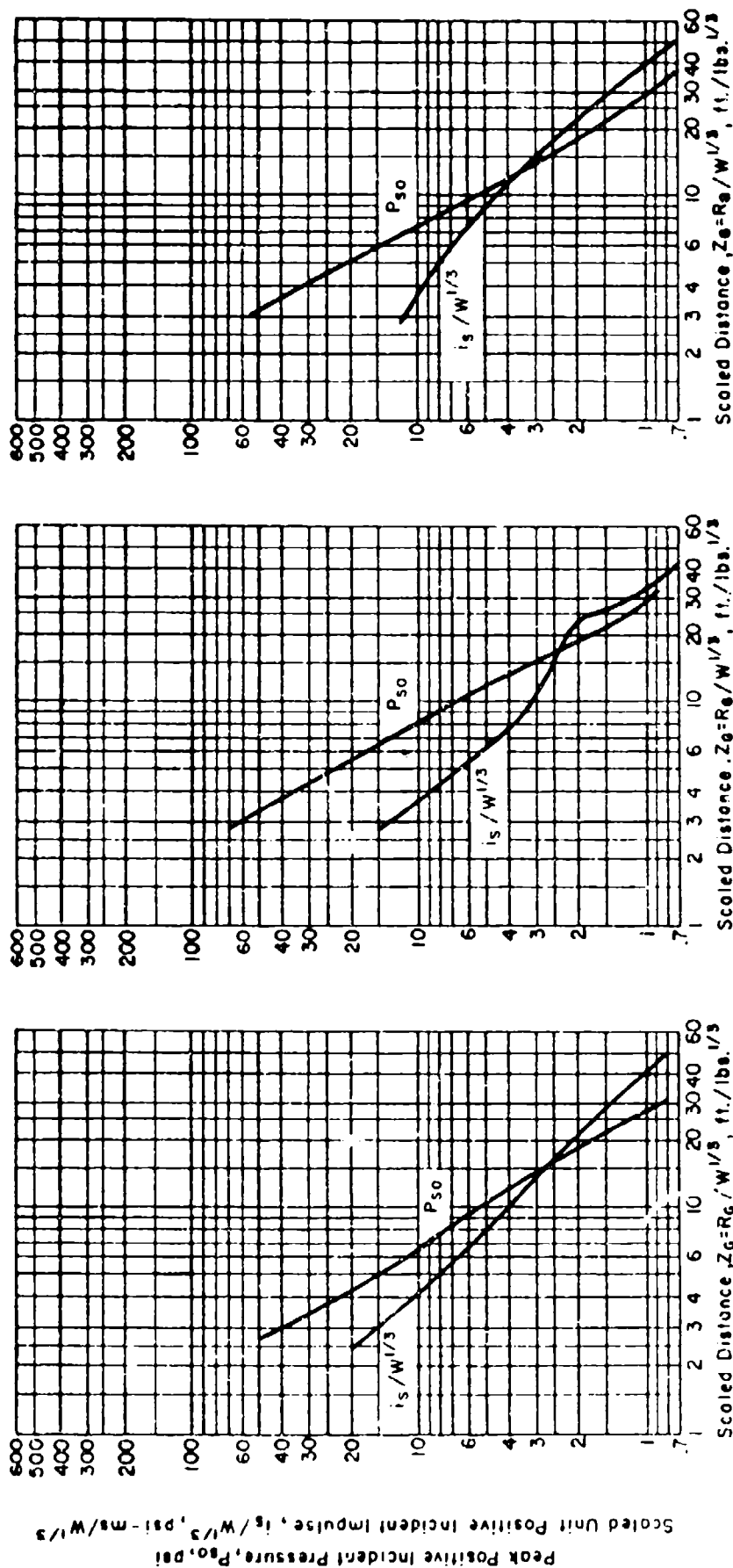


Figure 2-30 Peak positive incident pressure and scaled impulse for an explosion on the surface at sea level

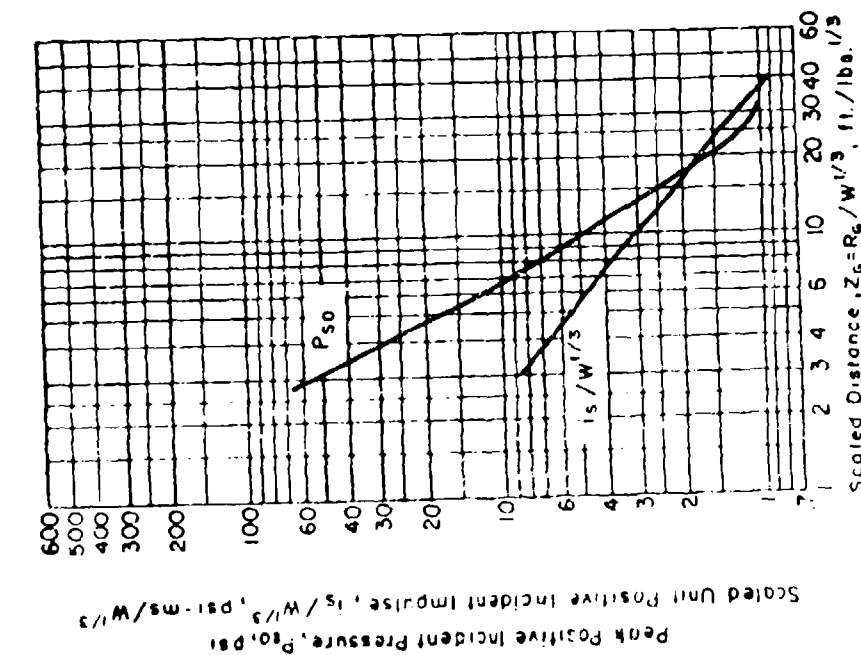


c. Black Powder

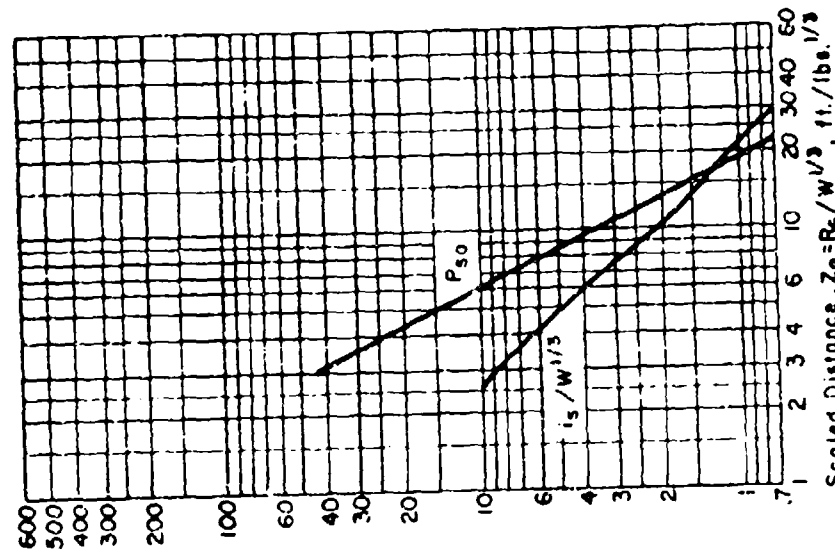
b. Benite Propellant
Orthorhombic

a. Benite Propellant
Orthorhombic

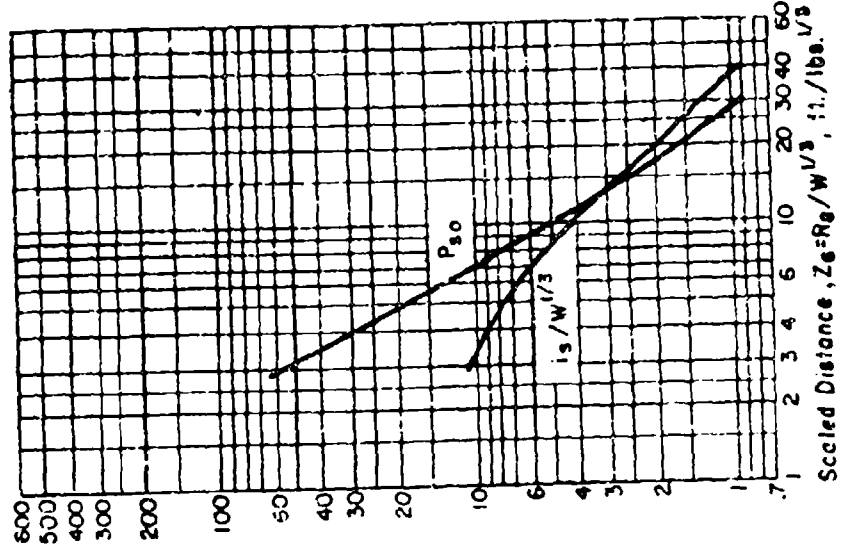
Figure 2-31 Peak positive incident pressure and scaled impulse for an explosion on the surface at sea level



a. BS-NACO Propellant
Cylindrical

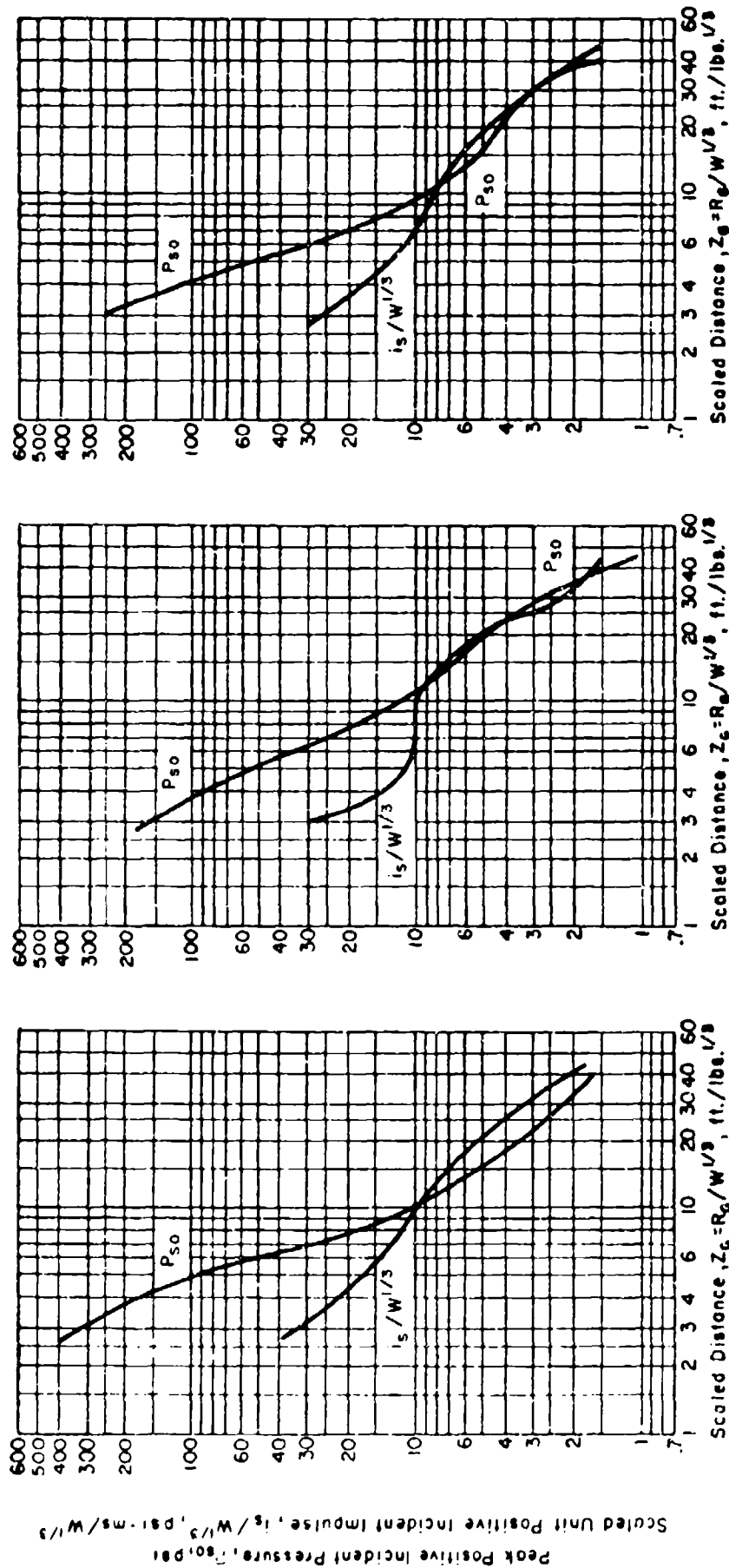


b. BS-NACO Propellant
Orthorhombic



c. BS-NACO Propellant
Hoppers

Figure 2-32 Peak positive incident pressure and scaled impulse for an explosion on the surface at sea level

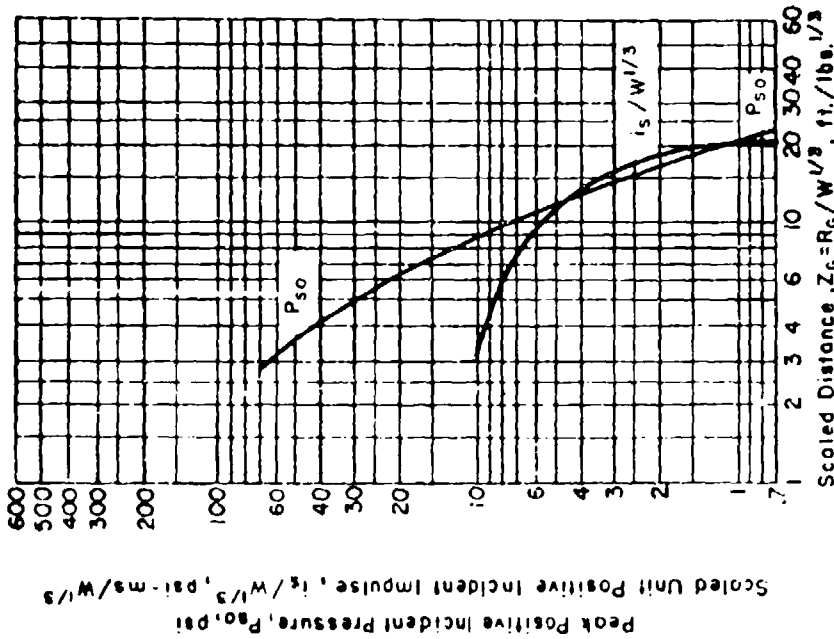


a. DIGL - RP I5420 Propellant
Orthorhombic

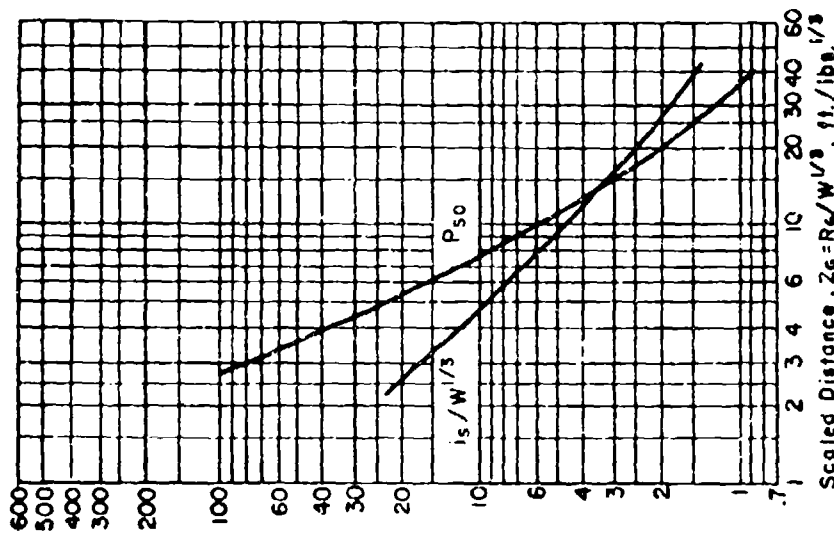
b. DIGL - RP I5421 Propellant
Cylindrical

c. DIGL - RP I5422 Propellant
Orthorhombic

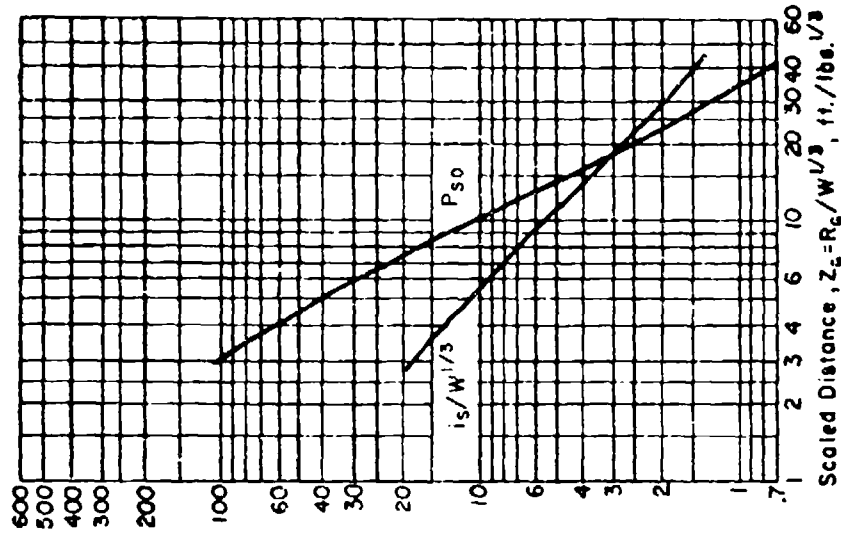
Figure 2-33 Peak positive incident pressure and scaled impulse for an explosion on the surface at sea level



a. M1 Propellant
(Single perforated)

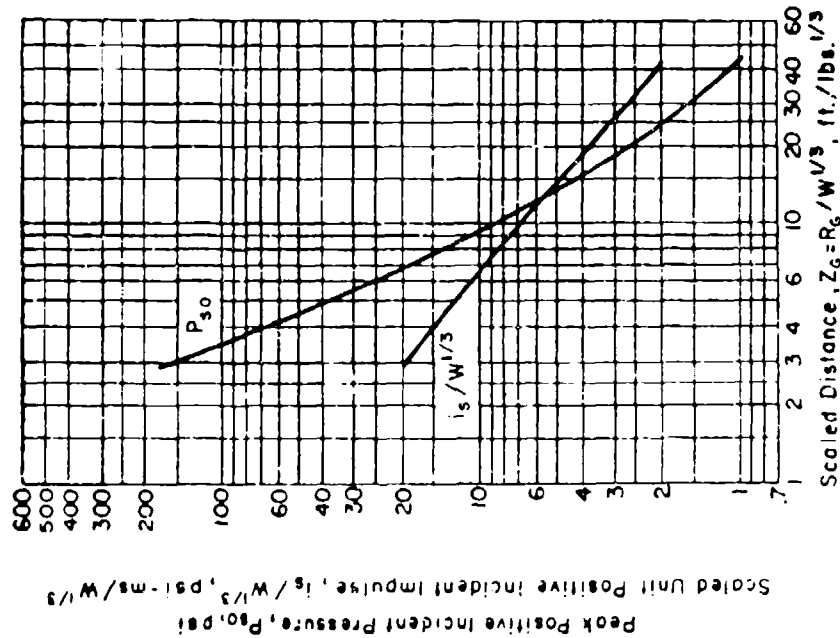


b. M1 Propellant
(Multi-perforated)

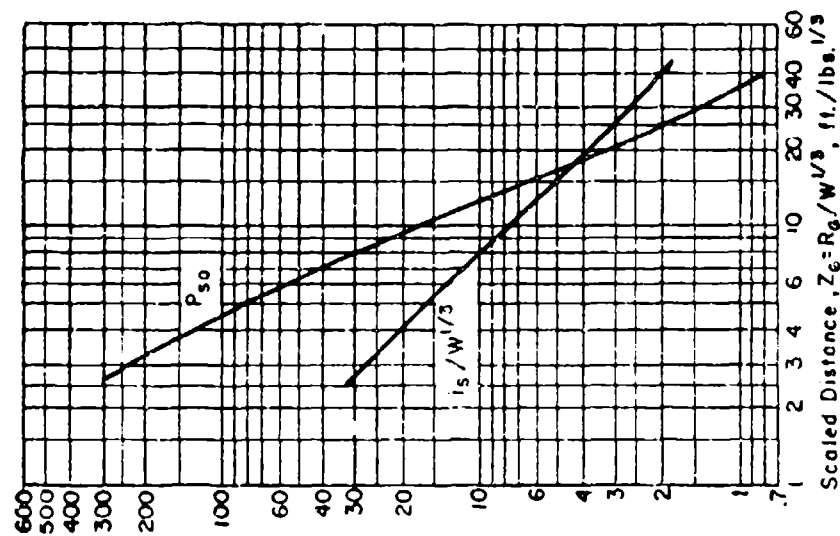


c. M26 E1 Propellant
(Multi-perforated)
Blender barrel

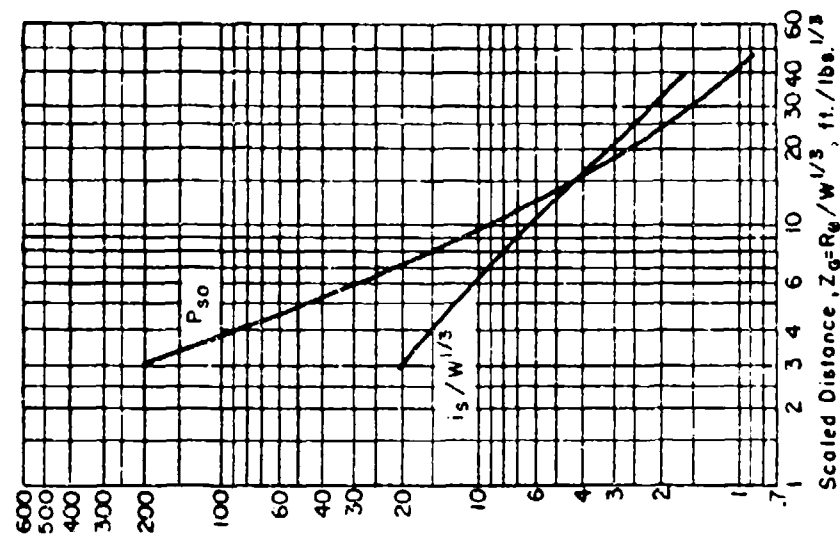
Figure 2-34 Peak positive incident pressure and scaled impulse for an explosion on the surface at sea level



a. M26E1 Propellant
(Multi-perforated)
Orthorhombic dryer bed

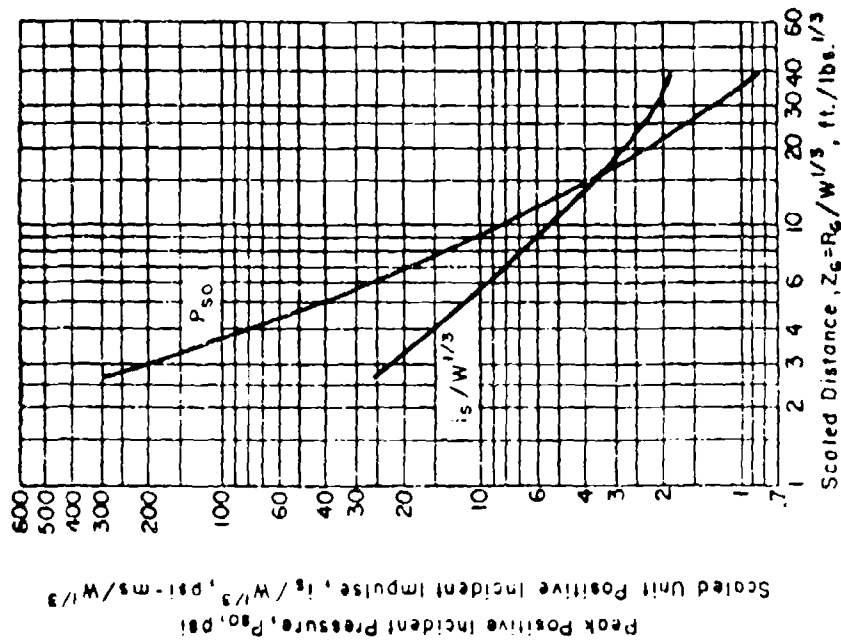


b. M26E1 Propellant
(Multi-perforated)
Orthorhombic drop buggy

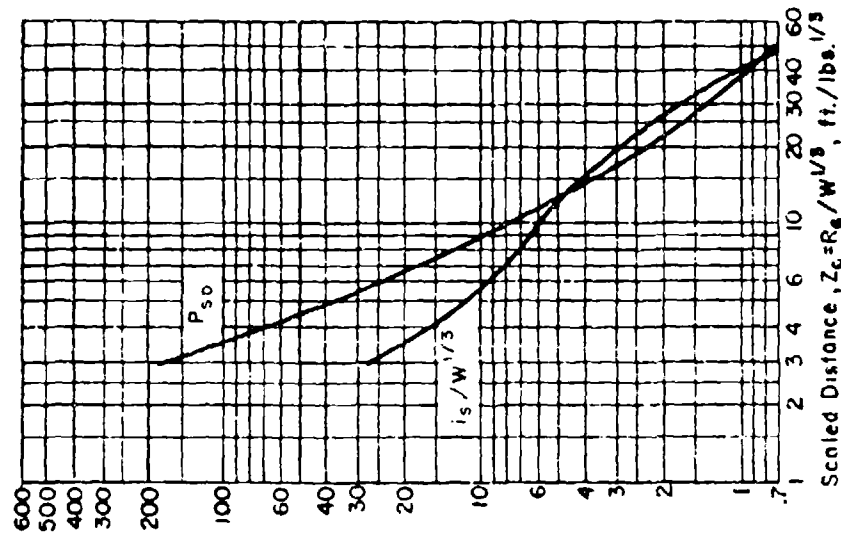


c. M26E1 Propellant
(Multi-perforated)
Cylindrical

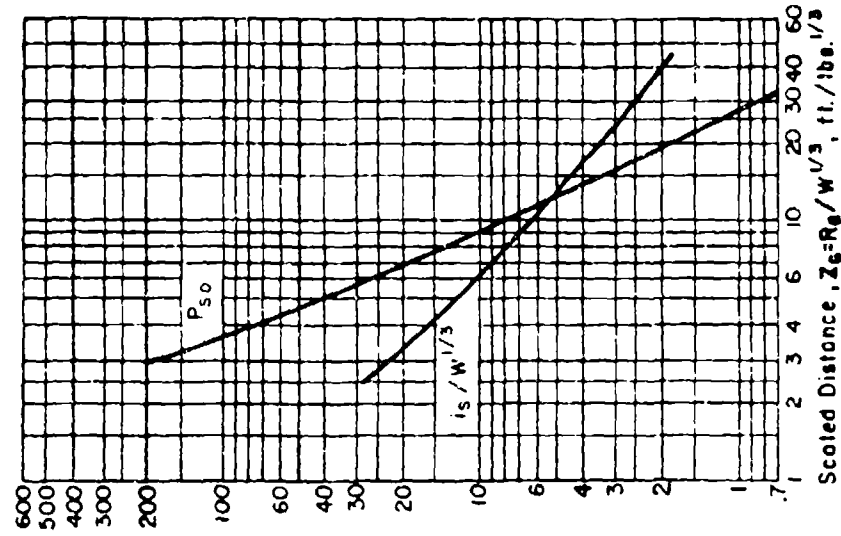
Figure 2-35 Peak positive incident pressure and scaled impulse for an explosion on the surface at sea level



a. M30 Al Propellant
(Single perforated)
Cylindrical

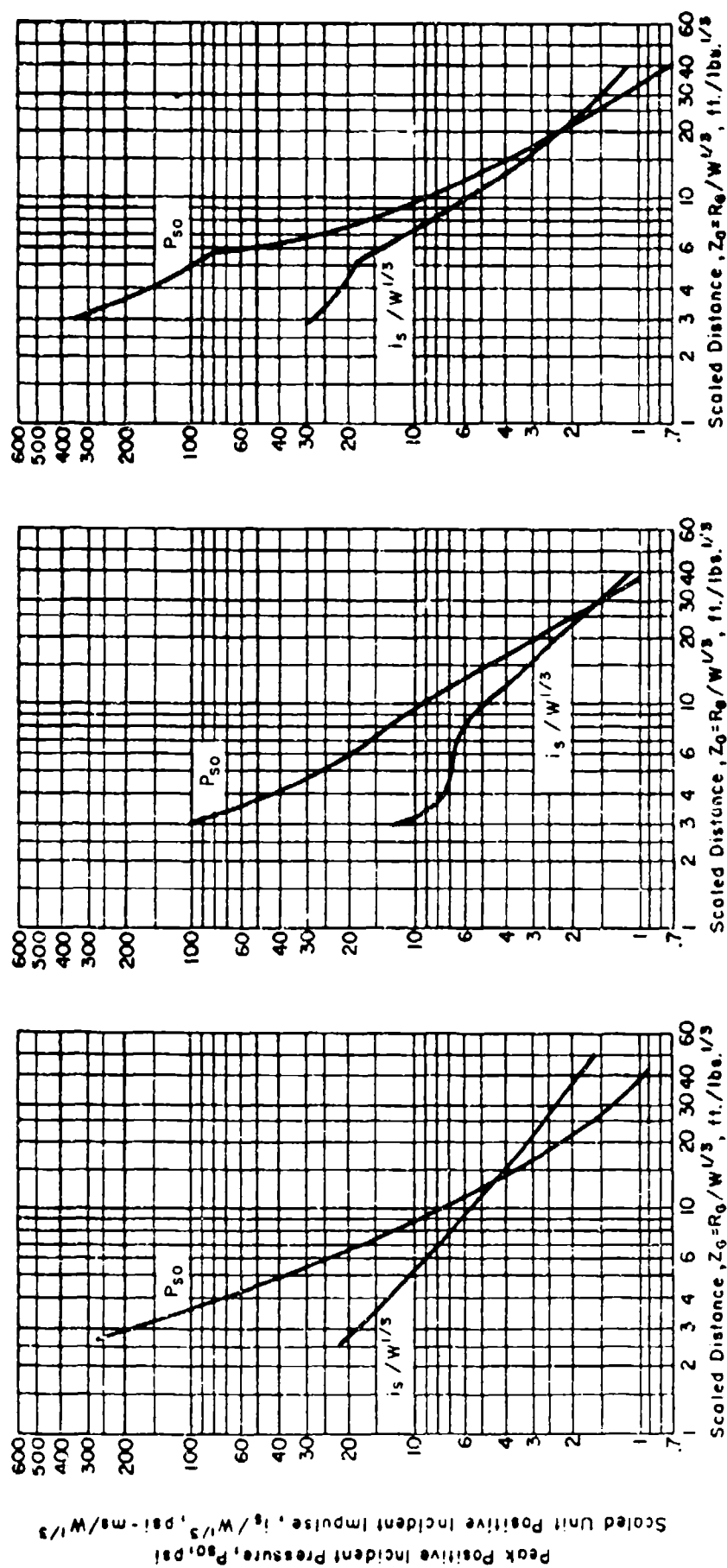


b. M30 Al Propellant
(Multi-perforated)
Cylindrical



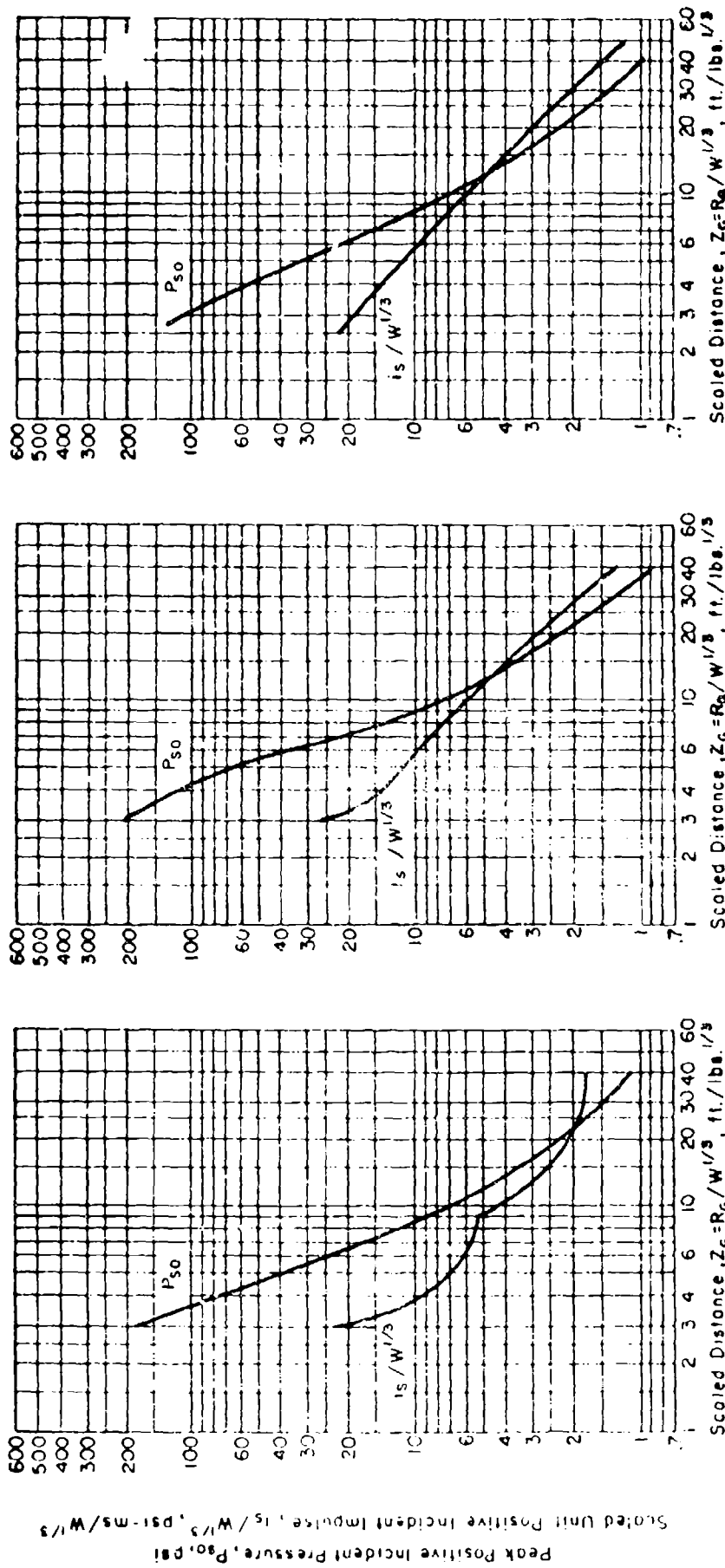
c. M30 Al Propellant
(Single perforated)
Orthorhombic dryer bed

Figure 2-36 Peak positive incident pressure and scaled impulse for an explosion on the surface at sea level



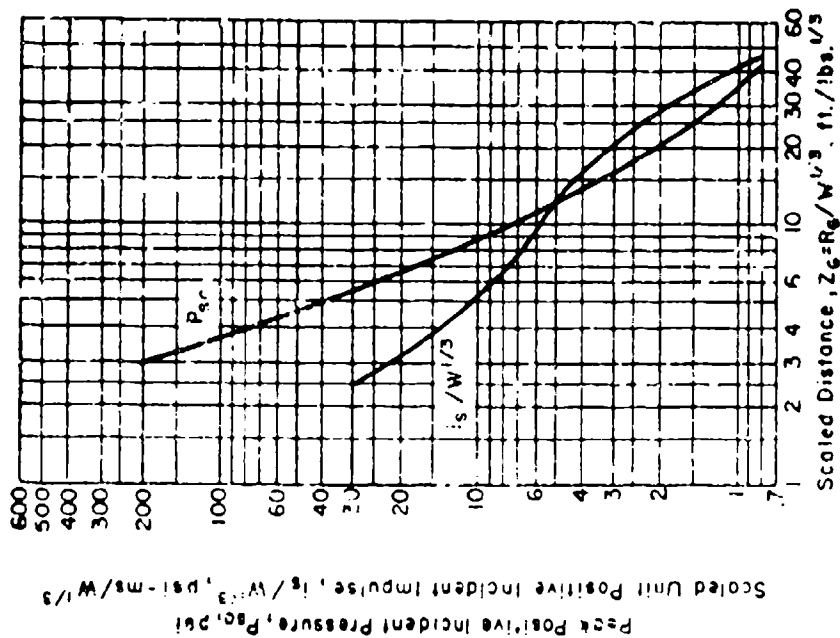
- a. M30 Al Propellant (Multi-perforated) Orthorhombic dryer-bed
- b. M31 Al E1 Slotted Stick Propellant Orthorhombic (Short Side)
- c. M31 Al E1 Slotted Stick Propellant Orthorhombic (Long Side)

Figure 2-37 Peak positive incident pressure and scaled impulse for an explosion on the surface at sea level

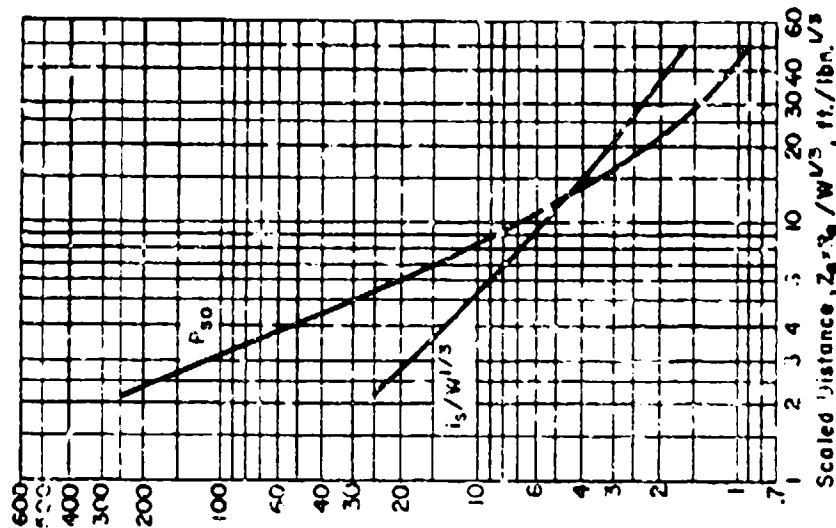


- a. M31A1E1 Slotted Stick Propellant Orthorhombic (Short Side)
- b. M31A1E1 Slotted Stick Propellant Orthorhombic (Long Side)
- c. N5 Propellant Shipping containers

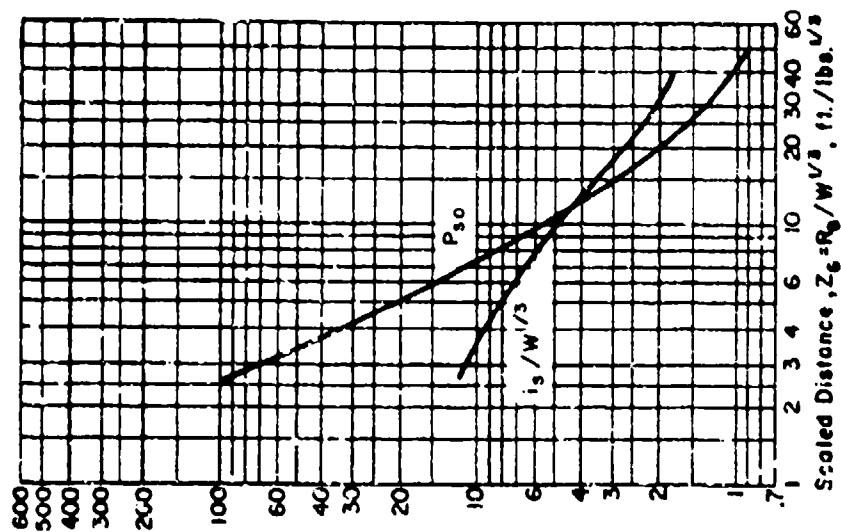
Figure 2-38 Peak positive incident pressure and scaled impulse for an explosion on the surface at sea level



a. N5 Propellant
Carpet rolls

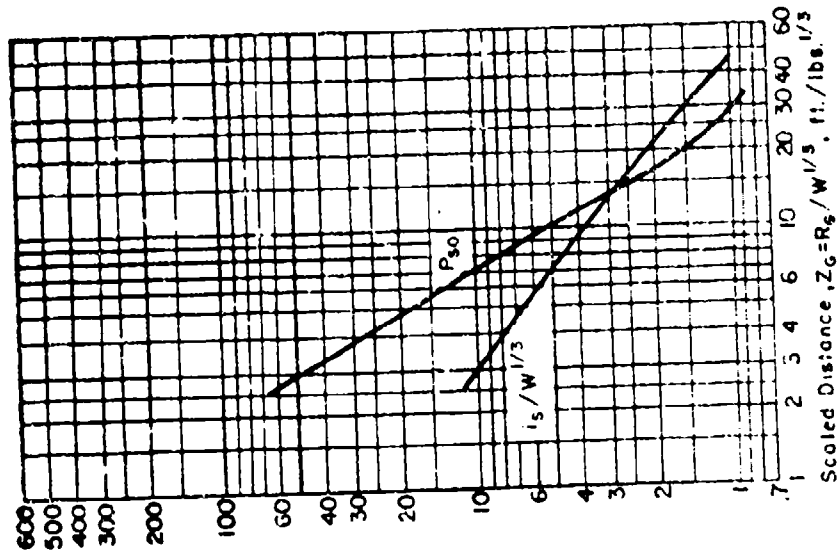


b. N5 Propellant
Charge buckets

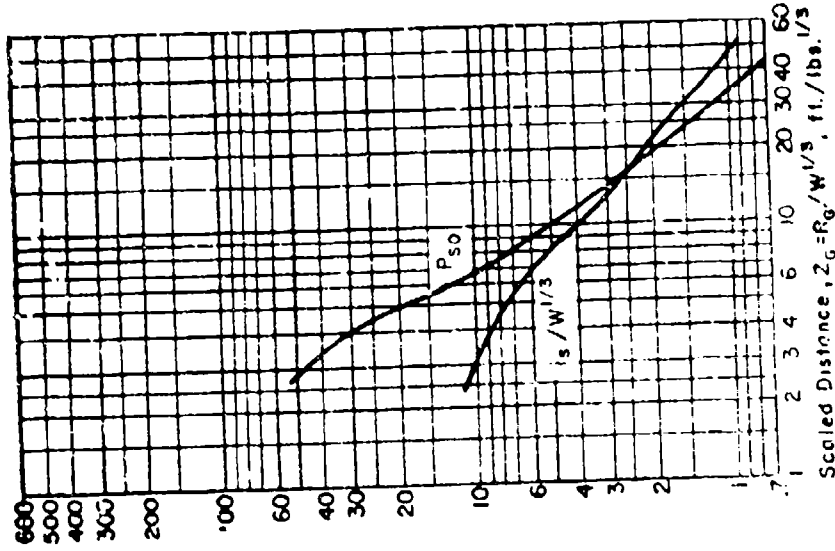


c. N5 Propellant
Conveyor belt configuration

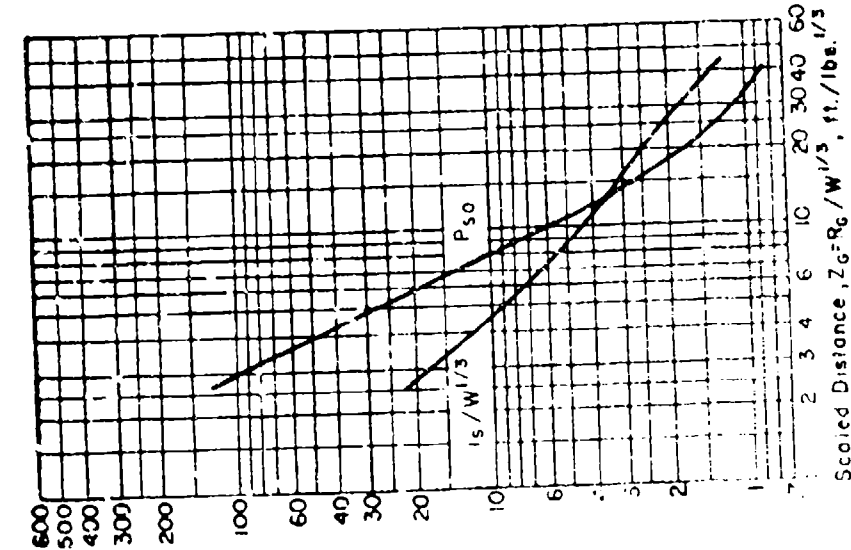
Figure 2-39 Peak positive incident pressure and scaled impulse for an explosion on the surface at sea level



a. M6 Propellant
Shipping drums

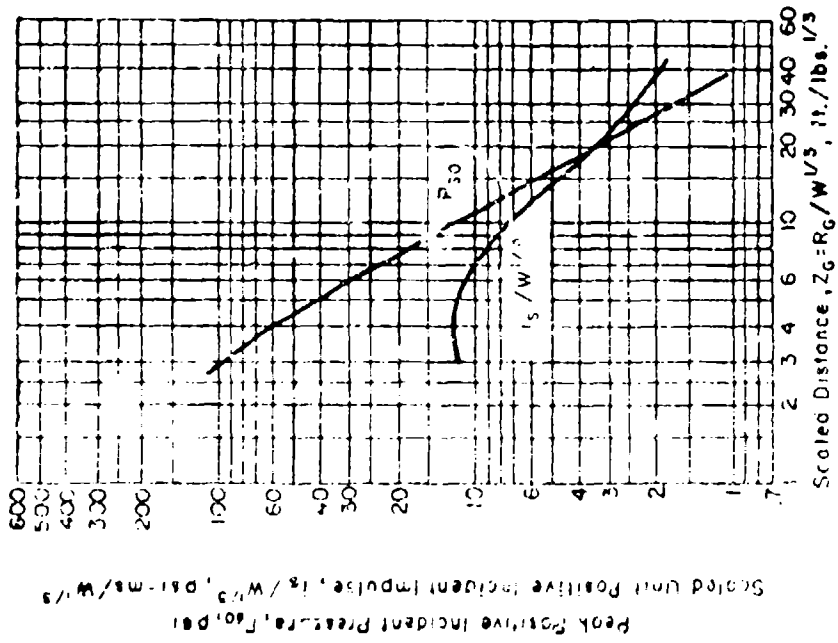


b. M6 Propellant
Closed hopper

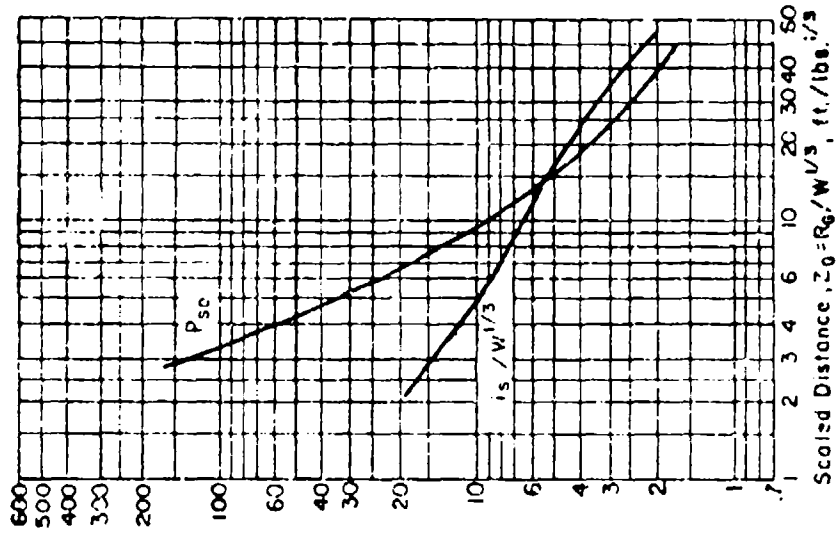


c. M6 Propellant
Open hopper

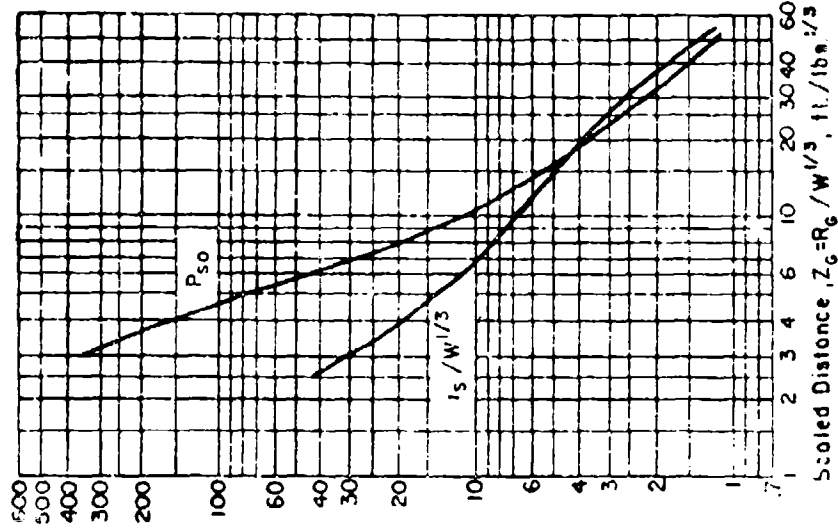
Figure 2-40 Peak positive incident pressure and scaled impulse for an explosion on the surface at sea level



a. 2.75 in. Rocket Grain
MK 43-1

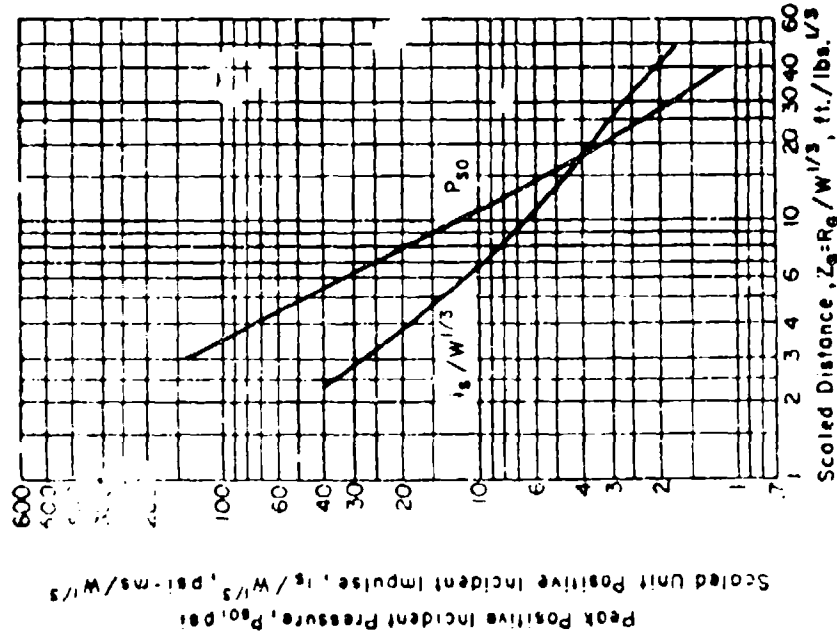


b. WC844 Ball Powder
Orthorhombic

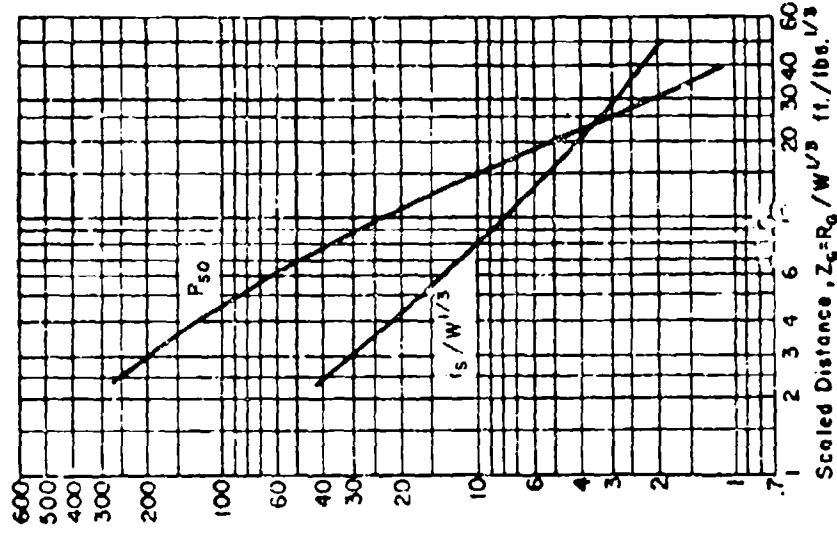


c. WC844 Ball Powder
Cylindrical

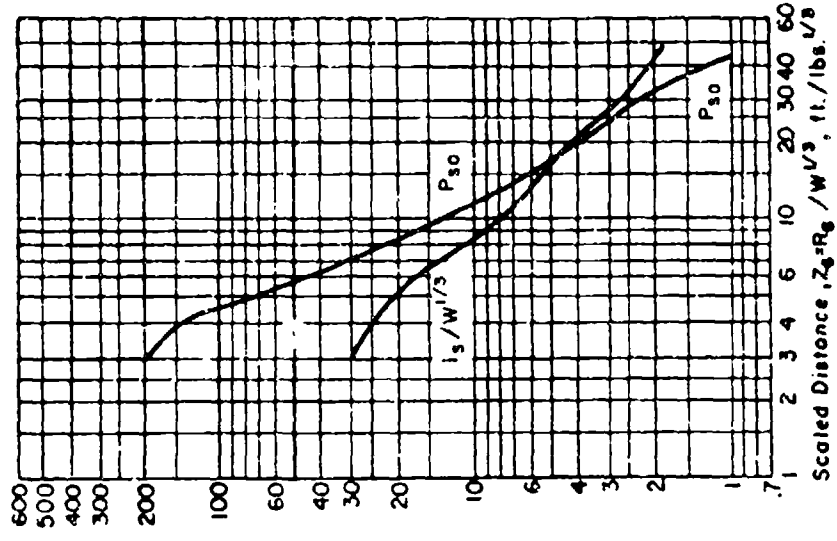
Figure 2-41 Peak positive incident pressure and scaled impulse for an explosion on the surface at sea level



a. XM37 RAP Propellant
(Single forward grain)

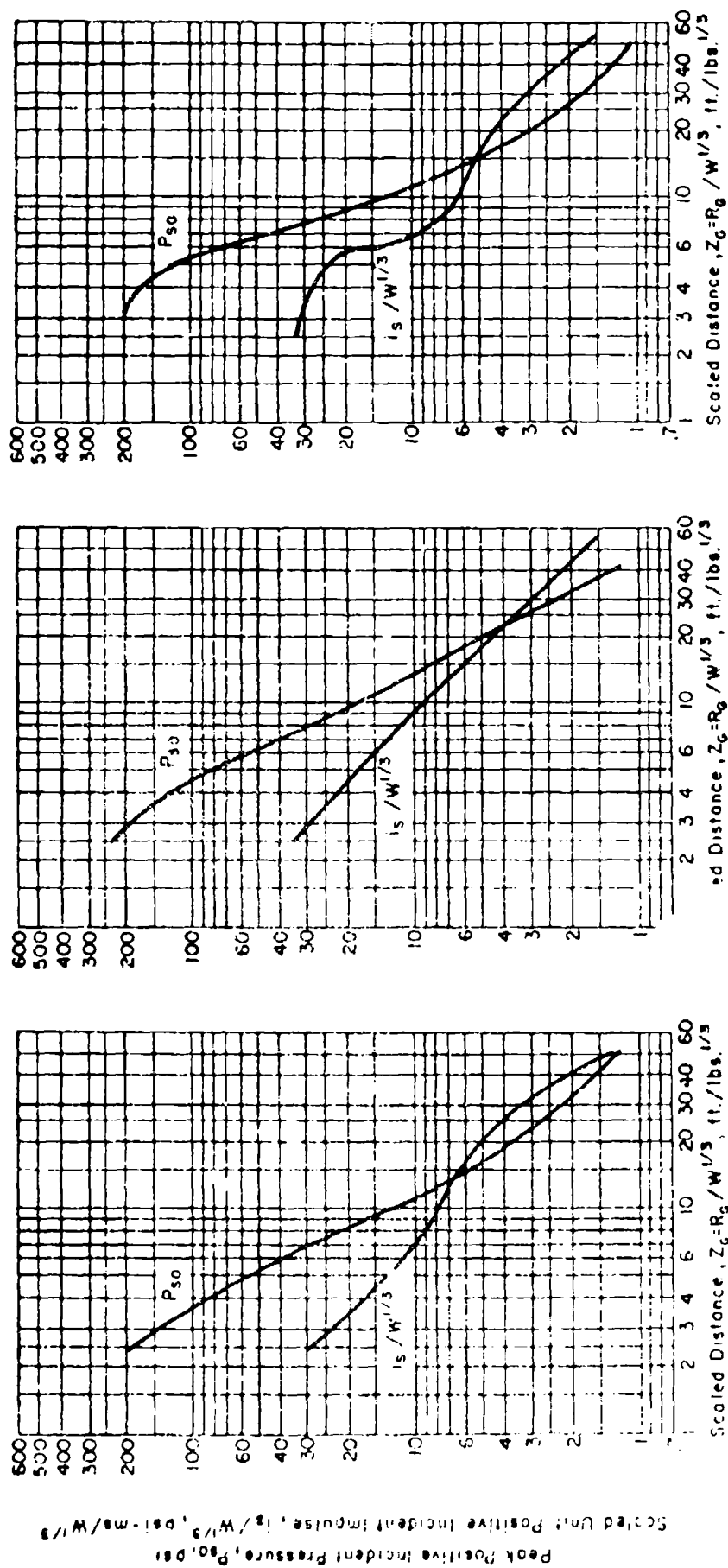


b. XM37 RAP Propellant
(Forward grains)
Extruded billet



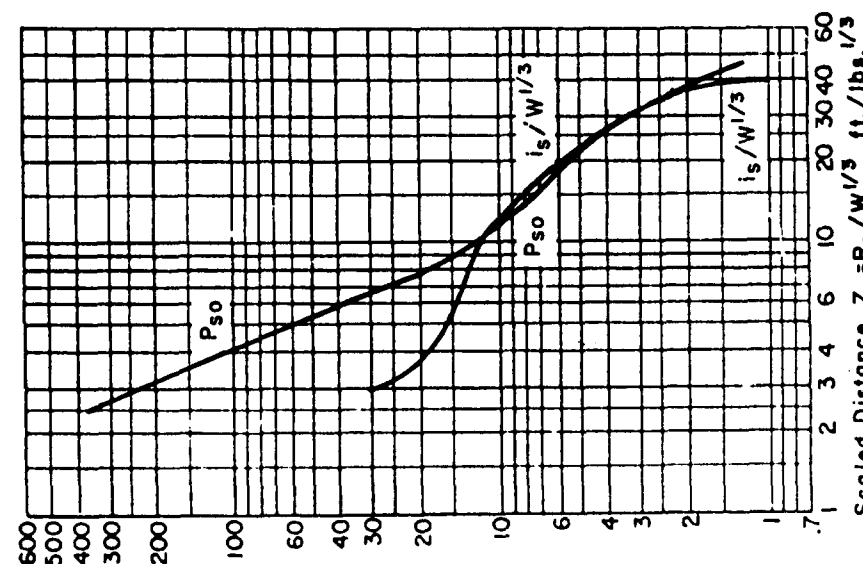
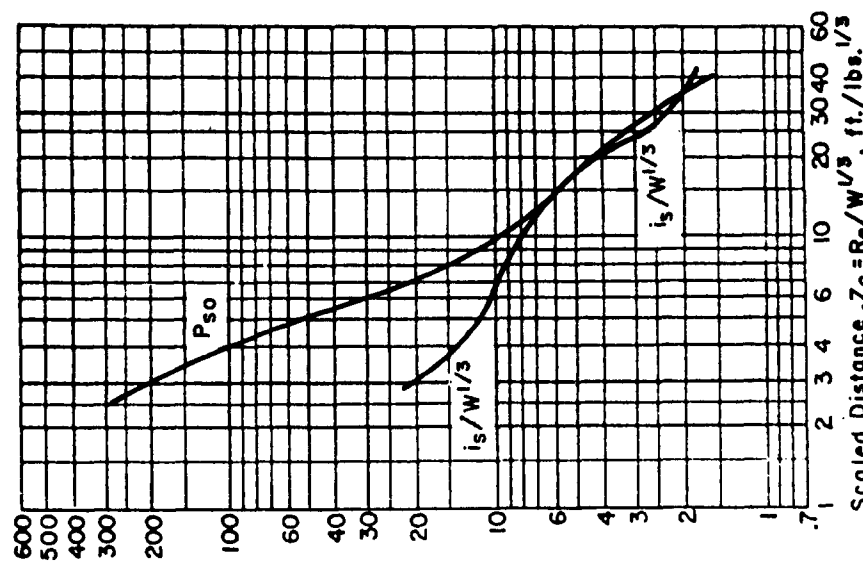
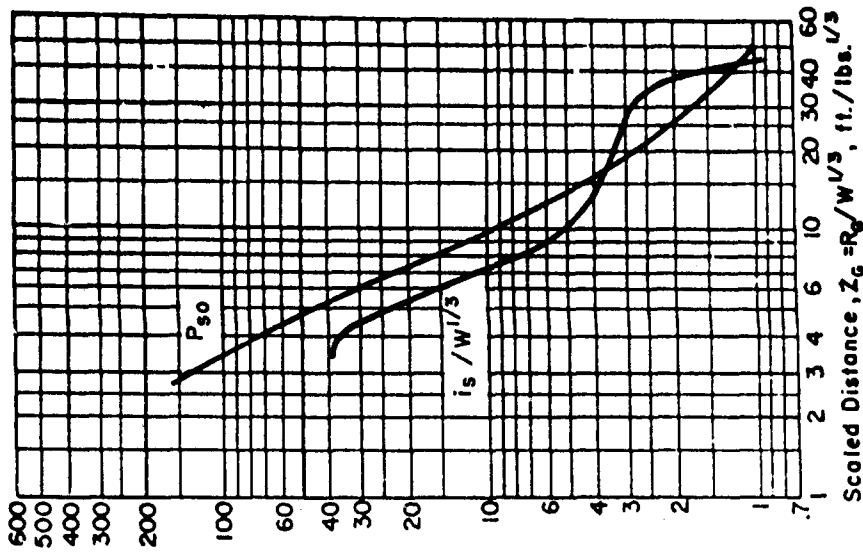
c. XM37 RAP Propellant
(Forward grains)
Ro Con shipping containers

Figure 2-42 Peak positive incident pressure and scaled impulse for an explosion on the surface at sea level



- a. XM37 RAP Propellant (Single aft grain)
- b. XM37 RAP Propellant (Aft grain) Extruded billets
- c. XM37 RAP Propellant (Aft grains) Ro Con shipping containers

Figure 2-43 Peak positive incident pressure and scaled impulse for an explosion on the surface at sea level

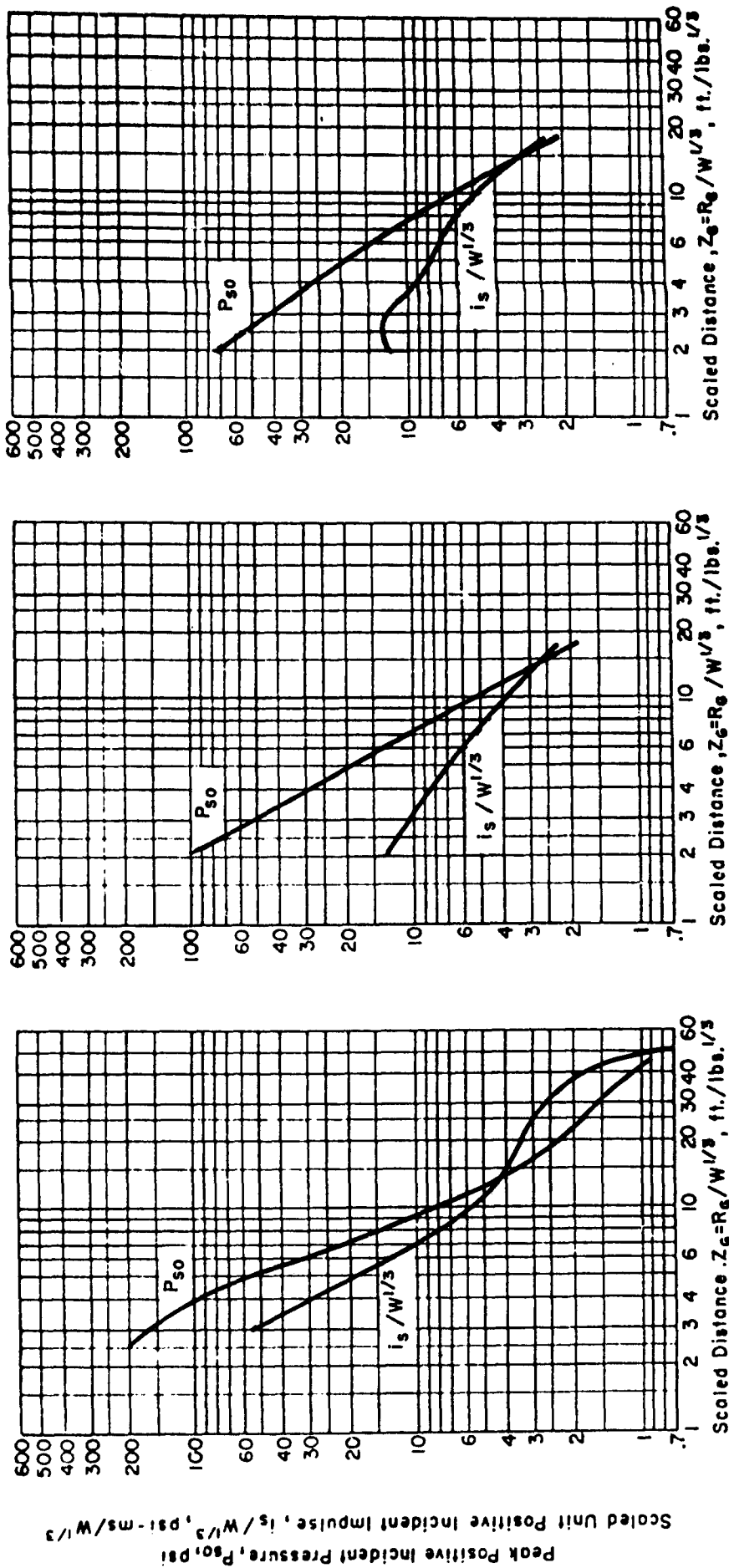


a. JA-2 (L5460) Propellant
Cylindrical

b. JA-2 (L5460) Propellant
Orthorhombic

c. MIO Propellant
Orthorhombic
($H/W > 1$)

Figure 2-44 Peak positive incident pressure and scaled impulse for an explosion on the surface at sea level

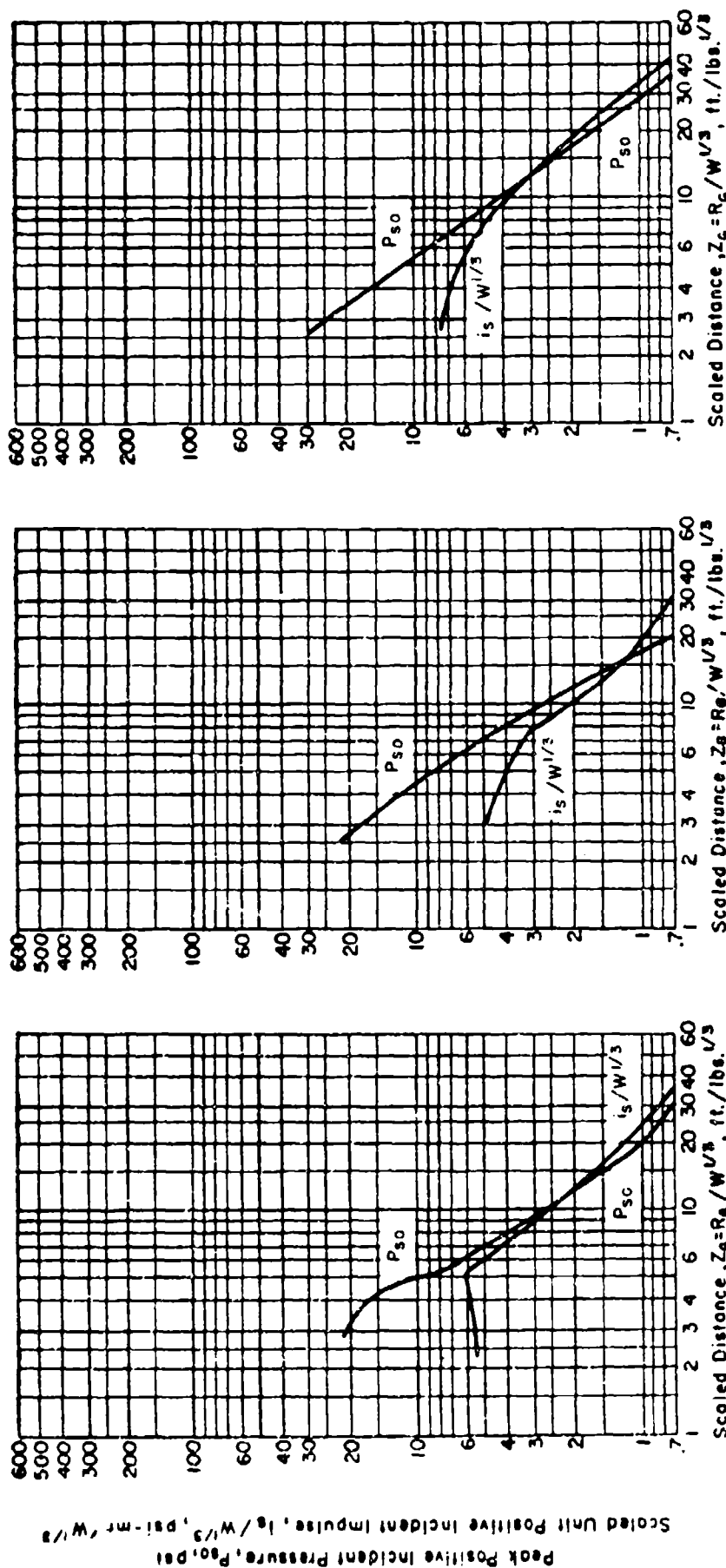


u. M10 Propellant
Orthorhombic
($H/W < 1$)

b. 105mm M314-A3
Illuminated Composition
(Cylindrical)

c. 105mm M314-A3
Illuminated Composition
(Cylindrical)

Figure 2-45 Peak positive incident pressure and scaled impulse for an explosion on the surface at sea level

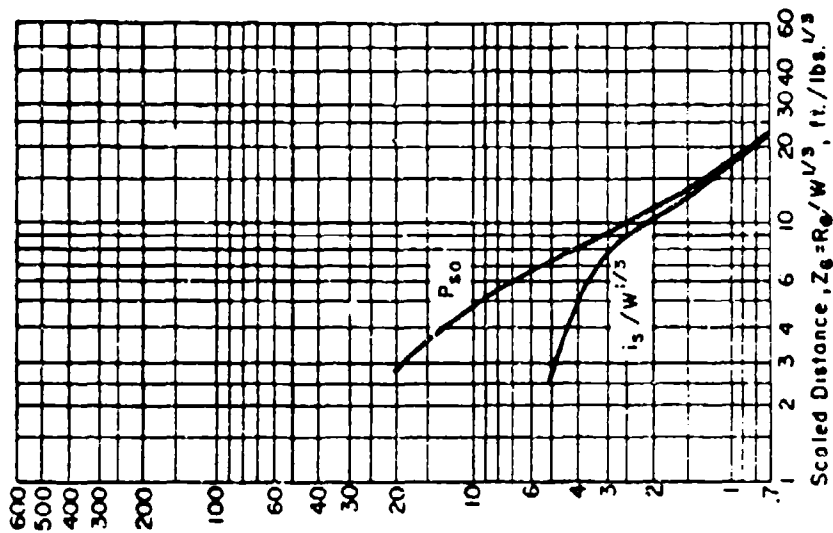


a. 1559 Igniter Mixture Cylinder

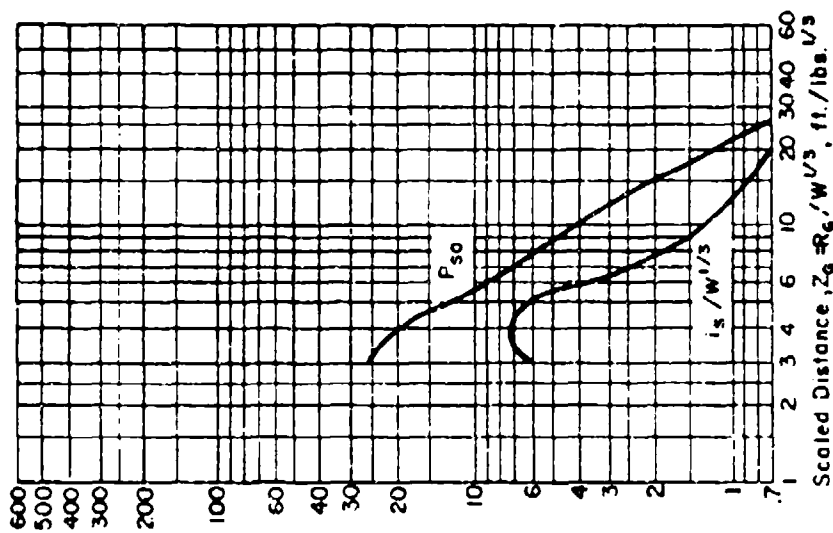
b. 1559 Igniter Mixture Cylinder

c. 1560 Subigniter Mixture Cylinder

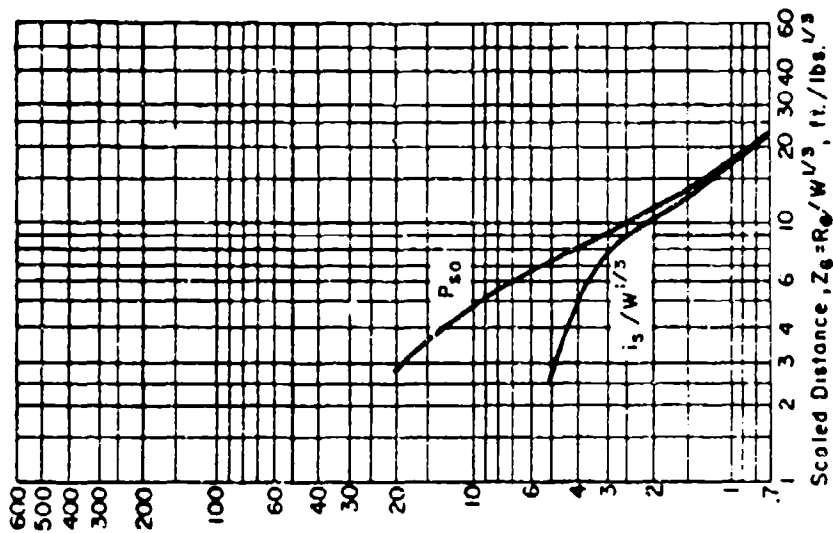
Figure 2-46 Peak positive incident pressure and scaled impulse for an explosion on the surface at sea level



a. I560 Subigniter Mixture
Cylinder

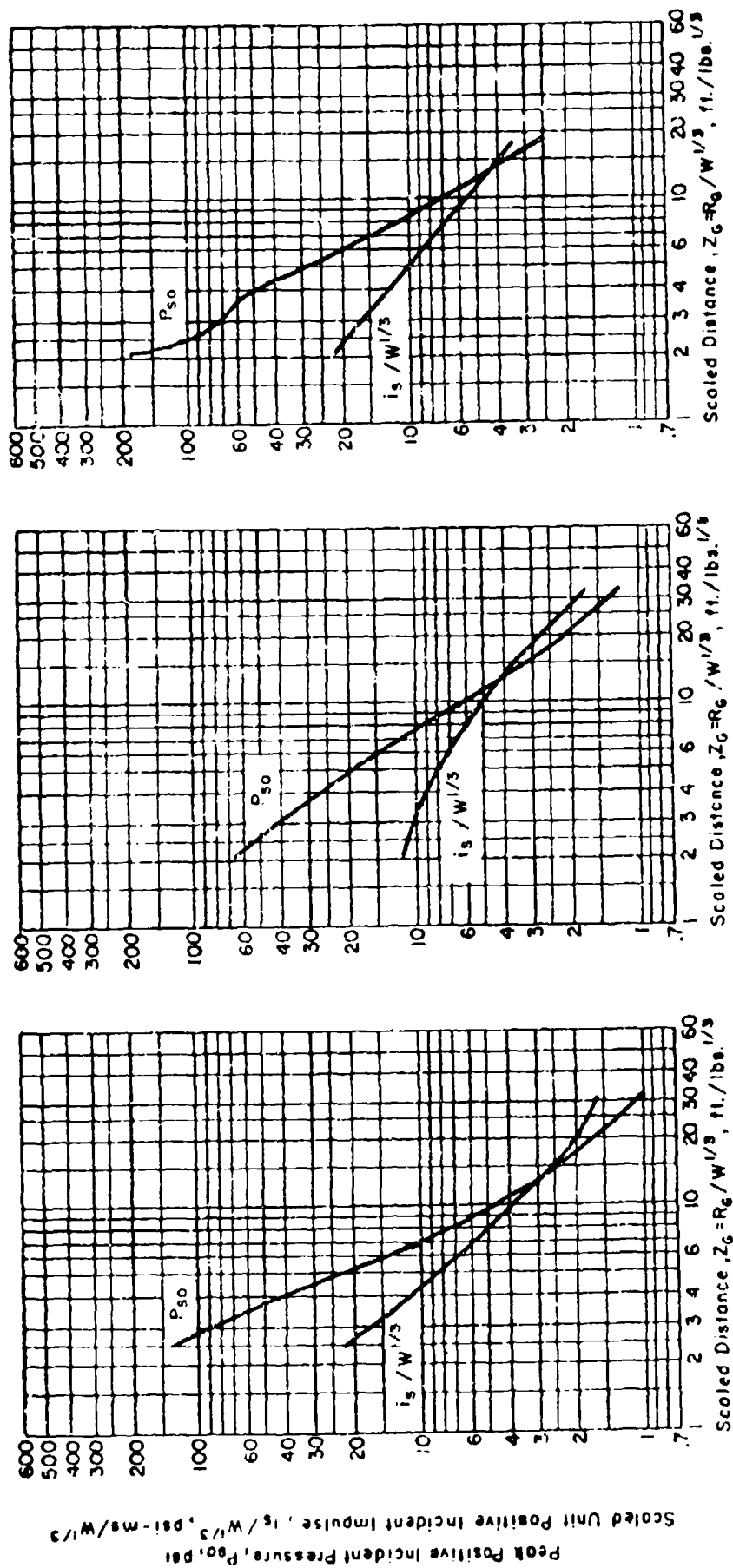


b. R284 Tracer Mixture
Cylinder



c. R284 Tracer Mixture
Cylinder

Figure 2-47 Peak positive incident pressure and scaled impulse for an explosion on the surface at sea level

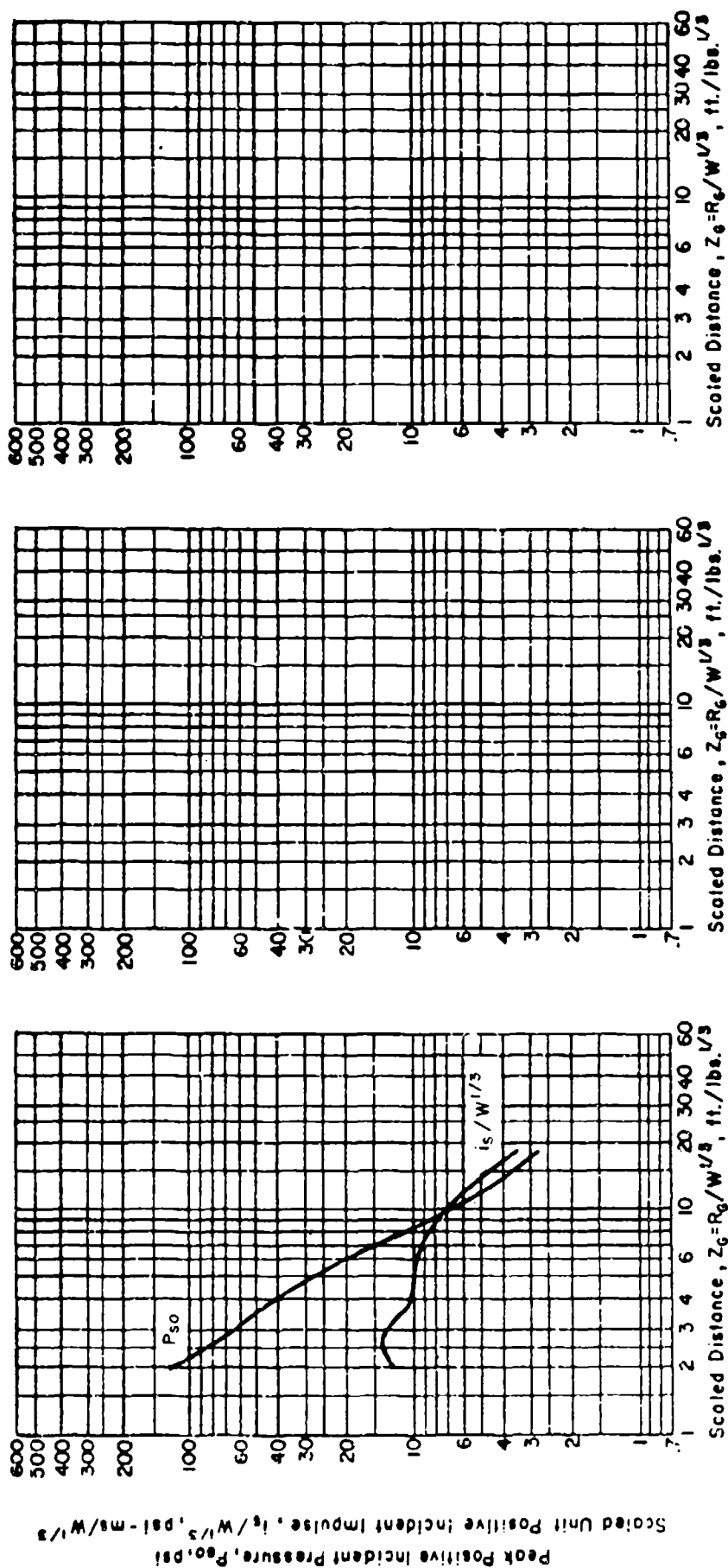


c. M49-A1 Trip Flare Composition
Cylinder

b. M314-A3 First Fire Composition
Cylinder

a. M314-A3 First Fire Composition
Orthorhombic

Figure 2-48 Peak positive incident pressure and scaled impulse for an explosion on the surface at sea level



a. M49-AI Trip Flare Composition
Cylindrical

b.

c.

Figure 2-49 Peak positive incident pressure and scaled impulse for an explosion on the surface at sea level

will depend on: (1) the magnitude of the individual explosions, (2) the time delays between the initiation of the explosions, (3) the separation distances between and orientation of the explosives, and (4) obstructions between the explosives themselves and other obstructions between the explosives and other parts of the facility (buildings, walls, barricades, terrain, etc.) which will distort, hinder, and generally interfere with wave propagation.

The pressure-time relationships associated with the wave propagation will depend upon the interaction of the individual waves themselves. After all the waves have merged, the pressures associated with the common or merged wave will have a pressure-time relationship which is similar to that produced by a single explosion (fig. 2-12). However, at closer distances to the explosion, the pressure-time relationship will be more closely represented by a pressure-time curve with multiple peak pressures (similar to that occurring above the triple point (fig. 2-12)). The multiple peak pressures represent the interaction as the various waves reach the point in question. At distances even closer to the explosion, the time history of the pressures acting on the ground surface may consist of a series of completely separate blast loads. This loading condition is a result of the arrival of the subsequent blast waves at a particular point during or after the occurrence of the negative phase pressures produced by the initial wave at that point.

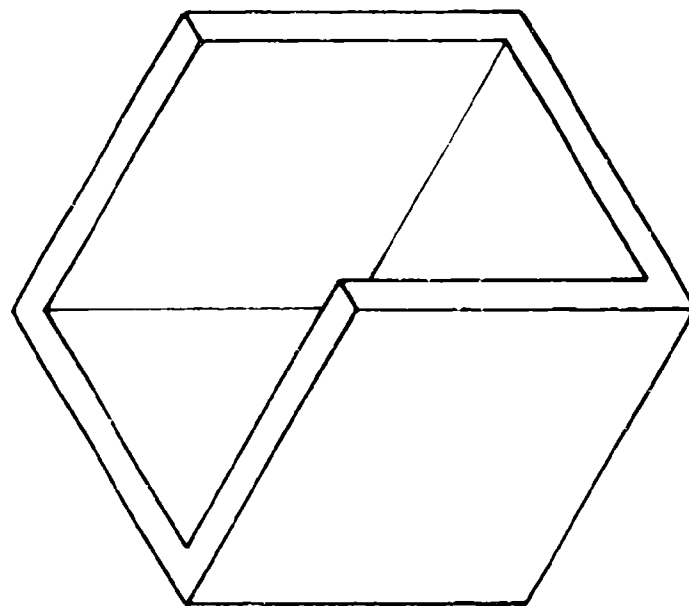
The latter pressure-time relationship is probably most likely to occur at high pressures close to the explosions while the multiple peak pressure pulse is normally associated with low pressures at far distances. However, in many instances, the multiple peak pressure pulse will occur at high pressures, in particular where the individual explosives are positioned close together, e.g., in a cubicle or other storage facility.

2-14 Confined Explosions

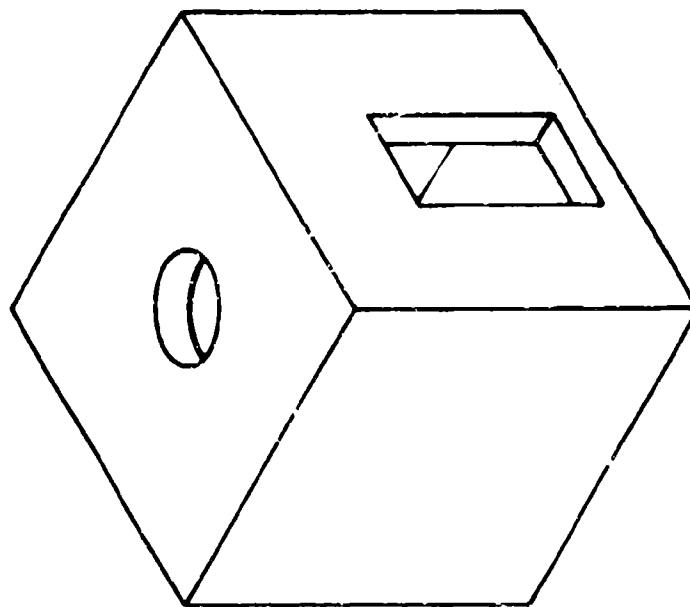
2-14.1 Effects of Confinement

When an explosion occurs within a structure, the peak pressures associated with the initial shock front (free-air pressures) will be extremely high and, in turn, will be amplified by their reflections within the structure. In addition, and depending upon the degree of confinement, the effects of the high temperatures and accumulation of gaseous products produced by the chemical process involved in the explosion will exert additional pressures and increase the load duration within the structure. The combined effects of these pressures may eventually destroy the structure unless the structure is designed to sustain the effects of the internal pressures. Provisions for venting of these pressures will reduce their magnitude as well as their duration.

The use of cubicle-type structures (fig. 2-50a) or other similar barriers, with one or more surfaces either sufficiently frangible or open to the atmosphere will provide some degree of venting depending on the opening size. This type of structure will permit the blast wave from an internal explosion to spill over onto the surrounding ground surface, thereby, significantly reducing the magnitude and duration of the internal pressures. The exterior pressures are quite often referred to as "leakage" pressures while the pressures reflected and reinforced within the structure are termed interior "shock pressures". The pressures associated with the accumulation of the gaseous products and temperature rise are identified as "gas" pressures. For the



a. Cubicle Structure



b. Enclosed Structure with Openings

Figure 2-50 Confined explosion structures

design of most fully vented cubicle type structures, the effects of the gas pressure may be neglected.

Detonation in an enclosed structure with relatively small openings (fig. 2-50b) is associated with both shock and gas pressures whose magnitudes are a maximum. The duration of the gas pressure and, therefore, the impulse of the gas pressure is a function of the size of the opening. It should be noted that the onset of the gas pressure does not necessarily coincide with the onset of the shock pressure. Further, it takes a finite length of time after the onset for the gas pressure to reach its maximum value. However, these times are very small and, for design purposes of most confined structures, they may be treated as instantaneous.

The term "frangible" pertains to those elements of a protective structure which fail and whose strength and mass are such as to reduce the amplification of the shock pressures and the confinement of the explosive gases. To reduce the amplification of the shock pressures, frangible elements must fail so as to relieve quickly the interior pressures acting on those surfaces and minimize their reflection to the nonfrangible elements of the structure. Blast tests of glass panels have shown that a true frangible material does not exist and that some reflection of the initial blast pressures may be expected from very weak and light elements. Further, the buildup of gas pressures is a function of the ratio of the weight of the charge to the volume of the confining structure and the venting area. As stated, this pressure buildup will not begin until sometime after the onset of the shock pressures. Therefore, an element which is not considered frangible for the shock pressure may be frangible for gas pressures.

In addition to being dependent upon the physical properties of an element, frangibility will also be a function of the magnitude of the applied blast loads and, therefore, a function of the quantity of explosive being contained and the distance from the frangible element. Although frangibility is imperfectly understood and difficult to measure, in general, it can be assumed that if a closure's resistance to outward motion is equal to or less than 25 pounds per square foot of surface area, the resistance can be neglected since the time to reach failure is practically zero. In this case, frangibility can be stated solely in terms of the weight (inertial force) of the vent area closure. For resistances greater than 25 psf, the evaluation of frangibility must include the effects of resistance in addition to the weight of an element. The combined effects of the inertial force and the resistance can be accounted for by performing a dynamic analysis and determining the time to reach failure. However, if the blast pressure is very large in comparison to the resistance of the element, the effects of the resistance can be neglected without introducing significant errors. Therefore, it is advantageous to use vent closures that are light and inherently weak and/or weakly supported; such as, corrugated metal decking supported on steel joists, metal panels for walls, plexiglass or thin fiberglass panels supported by wood or lightweight steel frames or gypsum board panels.

In the following paragraphs of this section, a simple cantilever barrier as well as cubicle-type and containment type structures will be discussed. The cubicles are assumed to have one or more surfaces which are open or frangible while the containment structures are either totally enclosed or have small

size openings. The effects of the inertia of frangible elements of these structures will be discussed in subsequent sections.

2-14.2 Shock Pressures

2-14.2.1 Blast Loadings. When an explosion occurs within a cubicle or containment-type structure, the peak pressures as well as the impulse associated with the shock front will be extremely high and will be amplified by the confining structure. Because of the close-in effects of the explosion and the reinforcement of blast pressures due to the reflections within the structure, the distribution of the shock loads on any one surface will be non-uniform with the structural surface closest to the explosion subjected to the maximum load.

An approximate method for the calculation of the internal shock pressures has been developed using theoretical procedures based on semi-empirical blast data and on the results of response tests on slabs. The calculated average shock pressures have been compared with those obtained from the results of tests of a scale-model steel cubicle and have shown good agreement for a wide range of cubicle configurations. This method consists of the determination of the peak pressures and impulses acting at various points of each interior surface and then integrating to obtain the total shock load. In order to simplify the calculation of the response of a protective structure wall to these applied loads, the peak pressures and total impulses are assumed to be uniformly distributed on the surface. The peak average pressure and total average impulse is given for any wall surface. The actual distribution of the blast loads is highly irregular due to the multiple reflections and time phasing and results in localized high shear stresses in the element. The use of the average blast loads when designing is predicated on the ability of the element to transfer these localized loads to regions of lower stress. Reinforced concrete with properly designed shear reinforcement and steel plates exhibit this characteristic.

The parameters which are necessary to determine the average shock loads are the structure's configuration and size, charge weight, and charge location. Figure 2-51 shows many possible simple barriers, cubicle configurations and containment type structures and the definition of the various parameters pertaining to each. Surfaces depicted are not frangible for determining the shock loadings. The effects of frangibility will be discussed later.

Because of the wide range of required parameters, the procedure for the determination of the shock loads was programmed for solutions on a digital computer. The results of these calculations are presented in figures 2-52 through 2-100 for the average peak reflected pressures p_r and figures 2-101 through 2-149 for the average scaled unit impulse $i_p/w^{1/3}$. These shock loads are presented as a function of the parameters defining the configurations presented in figure 2-51. Each illustration is for a particular combination of values of h/H , l/L and the number N of reflecting surfaces adjacent to the surface for which the shock loads are being calculated. The wall (if any) parallel and opposite to the surface in question has been found to have a neg-

ligible contribution to the shock loads for the range of parameters used and was therefore not considered.

The general procedure for use of the above illustrations is as follows:

1. From figure 2-51, select the particular surface of the structure which conforms to the protective structure given and note the number, N, of adjacent reflecting surfaces as indicated in parenthesis,
2. Determine the values of the parameters indicated for the selected surface of the structure in Item 1 above and calculate the following quantities:

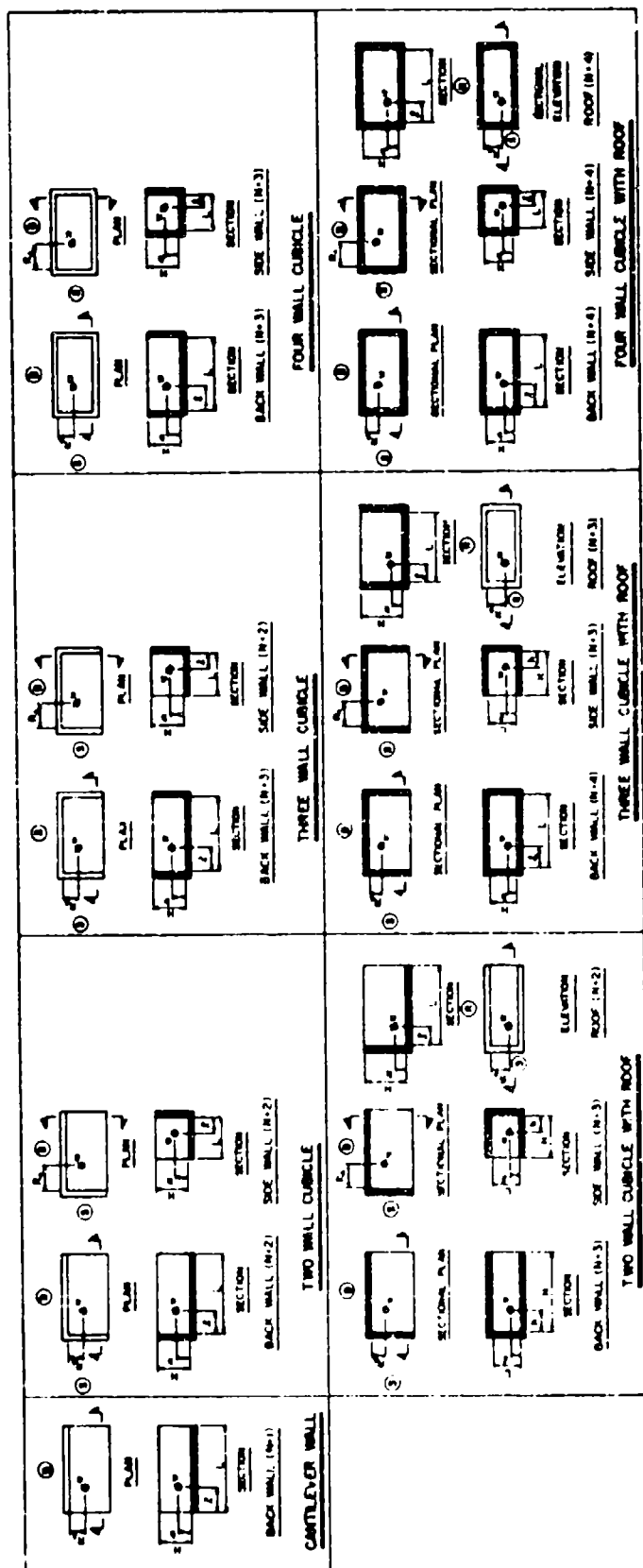
$$\frac{h}{H}, \frac{l}{L}, \frac{L}{H}, \frac{L}{R_A}, \text{ and } Z_A = R_A/W^{1/3}, \text{ and}$$

3. Refer to Table 2-3 for the proper peak reflected pressure and impulse charts conforming to the number of adjacent reflected surfaces and the values of l/L and h/H of Item 2 above, and enter the charts to determine the values of p_r and $i_r/W^{1/3}$,

In most cases, the above procedure will require interpolation for one or more of the parameters which define a given situation, in order to obtain the correct average reflected pressure and average reflected impulse. Examples of this interpolation procedure are given in the Appendix 2A.

Because of the limitations in the range of the test data and the limited number of values of the parameters given in the above shock load charts, extrapolation of the data given in figures 2-52 through 2-149 may be required for some of the parameters involved. On the other hand, the limiting values as given in the charts for other parameters will not require extrapolation. The values of the average shock loads corresponding to the values of the parameters which exceed their limiting values (as defined by the charts), will be approximately equal to those corresponding to the limiting values. The following are recommended procedures which will be applicable in most cases for either extrapolation, or establishing the limits of impulse loads corresponding to values of the various parameter which exceed the limits of the charts:

1. To extrapolate beyond the limiting values of Z_A , plot a curve of values of p_r versus Z_A for constant values of L/R_A , L/H , h/H and l/L . Extrapolate curve to include the value of p_r corresponding to the value of Z_A required. Repeat similarly for value of $i_r/W^{1/3}$.



Notes:

1. B denotes Back Wall, S denotes Side Wall and R denotes Roof.
2. Numbers in parentheses indicate number, N, of reflecting surfaces adjacent to surface in question.
3. h is always measured to the nearest reflecting surface.
4. ℓ is always measured to the nearest reflecting surface except for the cantilever wall where it is measured to the nearest free edge.
5. For values of average peak pressures for barrier and cubicle arrangements shown, see Figures 2-52 to 2-100.
6. For respective scaled average reflected impulses, see Figures 2-101 to 2-149. For reference list of above Figures for particular values of required parameters in Note 6, see Figure 2-3.

Required parameters: N , ℓ/L , h/H , L/R_A , $2_A \approx R_A/W^{1/3}$

Figure 2-51 Barrier and cubicle configurations and parameters

Table 2-3 List of Illustrations for Average Peak Reflected Pressure and
Scaled Average Unit Reflected Impulse

| h/H | L/L | Average Peak Reflected Pressure | | | | Scaled Average Unit Reflected Impulse | | | |
|------|------|-------------------------------------|------|-------|-------|---------------------------------------|-------|-------|-------|
| | | No. of Adjacent Reflecting Surfaces | | | | No. of Adjacent Reflecting Surfaces | | | |
| | | One | Two | Three | Four | One | Two | Three | Four |
| 0.10 | 0.10 | 2-52 | 2-64 | 2-80 | 2-92 | 2-101 | 2-113 | 2-129 | 2-141 |
| | 0.25 | 2-53 | 2-65 | 2-81 | 2-93 | 2-102 | 2-114 | 2-130 | 2-142 |
| | 0.50 | 2-54 | 2-66 | 2-82 | 2-94 | 2-103 | 2-115 | 2-131 | 2-143 |
| | 0.75 | 2-55 | 2-67 | 2-83 | 2-95 | 2-104 | 2-116 | 2-132 | 2-144 |
| 0.25 | 0.10 | 2-55 | 2-68 | 2-83 | 2-95 | 2-104 | 2-117 | 2-132 | 2-144 |
| | 0.25 | 2-56 | 2-69 | 2-84 | 2-96 | 2-105 | 2-118 | 2-133 | 2-145 |
| | 0.50 | 2-57 | 2-70 | 2-85 | 2-97 | 2-106 | 2-119 | 2-134 | 2-146 |
| | 0.75 | 2-56 | 2-71 | 2-84 | 2-96 | 2-105 | 2-120 | 2-133 | 2-145 |
| 0.50 | 0.10 | 2-58 | 2-72 | 2-86 | 2-98 | 2-107 | 2-121 | 2-135 | 2-147 |
| | 0.25 | 2-59 | 2-73 | 2-87 | 2-99 | 2-108 | 2-122 | 2-136 | 2-148 |
| | 0.50 | 2-60 | 2-74 | 2-88 | 2-100 | 2-109 | 2-123 | 2-137 | 2-149 |
| | 0.75 | 2-59 | 2-75 | 2-87 | 2-99 | 2-108 | 2-124 | 2-136 | 2-148 |
| 0.75 | 0.10 | 2-61 | 2-76 | 2-89 | 2-95 | 2-110 | 2-125 | 2-138 | 2-144 |
| | 0.25 | 2-62 | 2-77 | 2-90 | 2-96 | 2-111 | 2-126 | 2-139 | 2-145 |
| | 0.50 | 2-63 | 2-78 | 2-91 | 2-97 | 2-112 | 2-127 | 2-140 | 2-146 |
| | 0.75 | 2-62 | 2-79 | 2-90 | 2-96 | 2-111 | 2-128 | 2-139 | 2-145 |

2. To extrapolate beyond the limiting values of L/R_A , extrapolate the given curve of p_r versus L/R_A for constant values of Z_A , L/H , h/H and l/L to include the value of p_r corresponding to the value of L/R_A required. Repeat this extrapolation for value of $i_r/W^{1/3}$,
3. Values of p_r and $i_r/W^{1/3}$ corresponding to values of L/H greater than 5 shall be taken as equal to those corresponding to $L/H = 6$ for actual values of Z_A , h/H , and l/L but with a fictitious value of L/R_A in which R_A is the actual value and L is a fictitious value equal to $5H$,
4. Values of p_r and $i_r/W^{1/3}$ corresponding to values of l/L less than 0.10 and greater than 0.75 shall be taken as equal to those corresponding to $l/L = 0.10$ and 0.75 , respectively, and
5. Values of p_r and $i_r/W^{1/3}$ corresponding to values of h/H less than 0.10 and greater than 0.75 shall be taken as equal to those corresponding to $h/H = 0.10$ and 0.75 , respectively.

A computer program is available which executes the interpolation procedure using numerical tables equivalent to figure 2-52 through 2-149. Availability of this program is listed in Section 2-4.

A protective element subjected to high intensity shock pressures may be designed for the impulse rather than the pressure pulse only if the duration of the applied pressure acting on the element is short in comparison to its response time. However, if the time to reach maximum displacement is equal to or less than three times the load duration, then the pressure pulse should be used for these cases. The actual pressure-time relationship resulting from a pressure distribution on the element is highly irregular due to the multiple reflections and time phasing. For these cases, the pressure-time relationship may be approximated by a fictitious peak triangular pressure pulse. The average peak reflected pressure of the pulse is obtained from figures 2-52 through 2-100 and the average impulse from Figure 2-101 through 2-149 and a fictitious duration is established as a function of the reflected pressure p_r and impulse i_r acting on the element.

$$t_o = \frac{2i_r}{p_r}$$

2-2

The above solution for the average shock load does not account for increased blast effects produced by contact charges. Therefore, if the values of the average shock loads given in figures 2-52 through 2-149 are to be applicable, a separation distance between the element and explosive must be maintained. This separation is measured between the surface of the element and the surface

of either the actual charge or the spherical equivalent, whichever results in the larger normal distance between the element's surface and the center of the explosive (the radius of a spherical TNT charge is $r = 0.136 W^{1/3}$). For the purposes of design, the following separation distances are recommended for various charge weights:

| Weight of Explosive (lbs) | Separation Distance |
|---------------------------|---------------------|
| up to 500 | 1.0 |
| 501 to 1,000 | 1.5 |
| 1,001 to 2,000 | 2.0 |
| 2,001 to 3,000 | 2.5 |
| above 3,000 | 3.0 |

The above separation distances do not apply to floor slabs or other similar structural elements placed on grade. However, a separation distance of at least one foot should be maintained to minimize the size of craters associated with contact explosions.

It should be noted that these separation distances do not necessarily conform to those specified by other government regulations; their use in a particular design must be approved by the cognizant military construction agency.

Average shock loads over entire wall or roof slabs were discussed above. An approximate method may be used to calculate shock loads over surfaces other than an entire wall. These surfaces might include a blast door, panel, column, or other such items found inside any shaped structure.

The method assumes a fictitious strip centered in front of the charge having a width equal to the normal distance R_A and a height equal to that of the structure. This is the maximum representative area that may be considered. Average shock loads can be determined on entire area or any surface falling within the boundaries of the representative area.

The procedure for determining the shock loads consists of partitioning the surface under consideration into subareas. These subareas do not need to be the same size. The angle of incidence to the center of each subarea is calculated. The reflected pressure and scaled impulse are determined for each subarea using Figures 2-9 and 2-10 respectively. A weighted average with respect to area is taken for both pressure and scaled impulse.

Both the pressure and the impulse are multiplied by a factor of 1.75 to account for secondary shocks. Idealized duration is calculated using Equation 2-2.

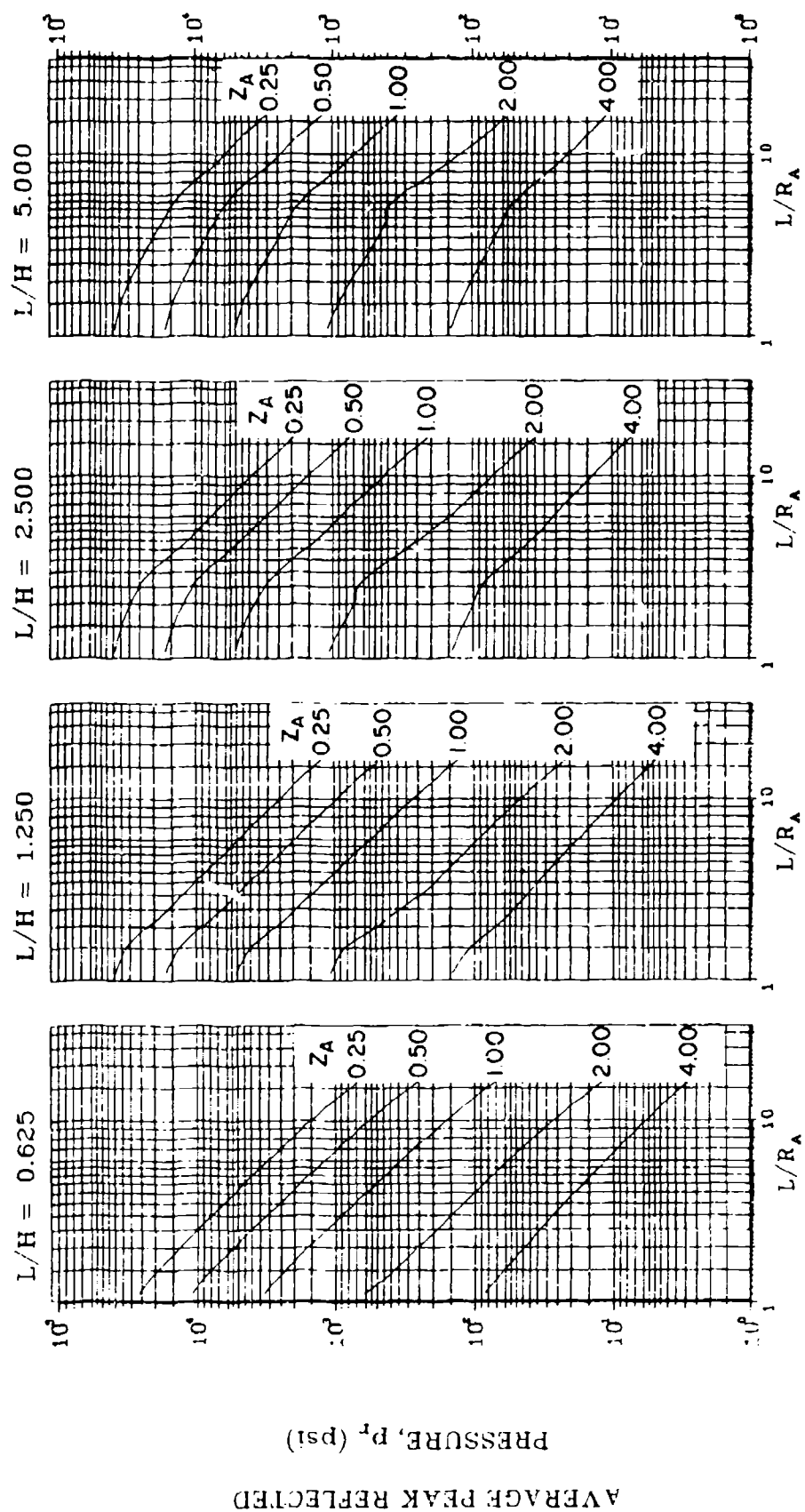


Figure 2-52 Average peak reflected pressure ($N = 1$, $L/H = 0.10$, $h/H = 0.10$)

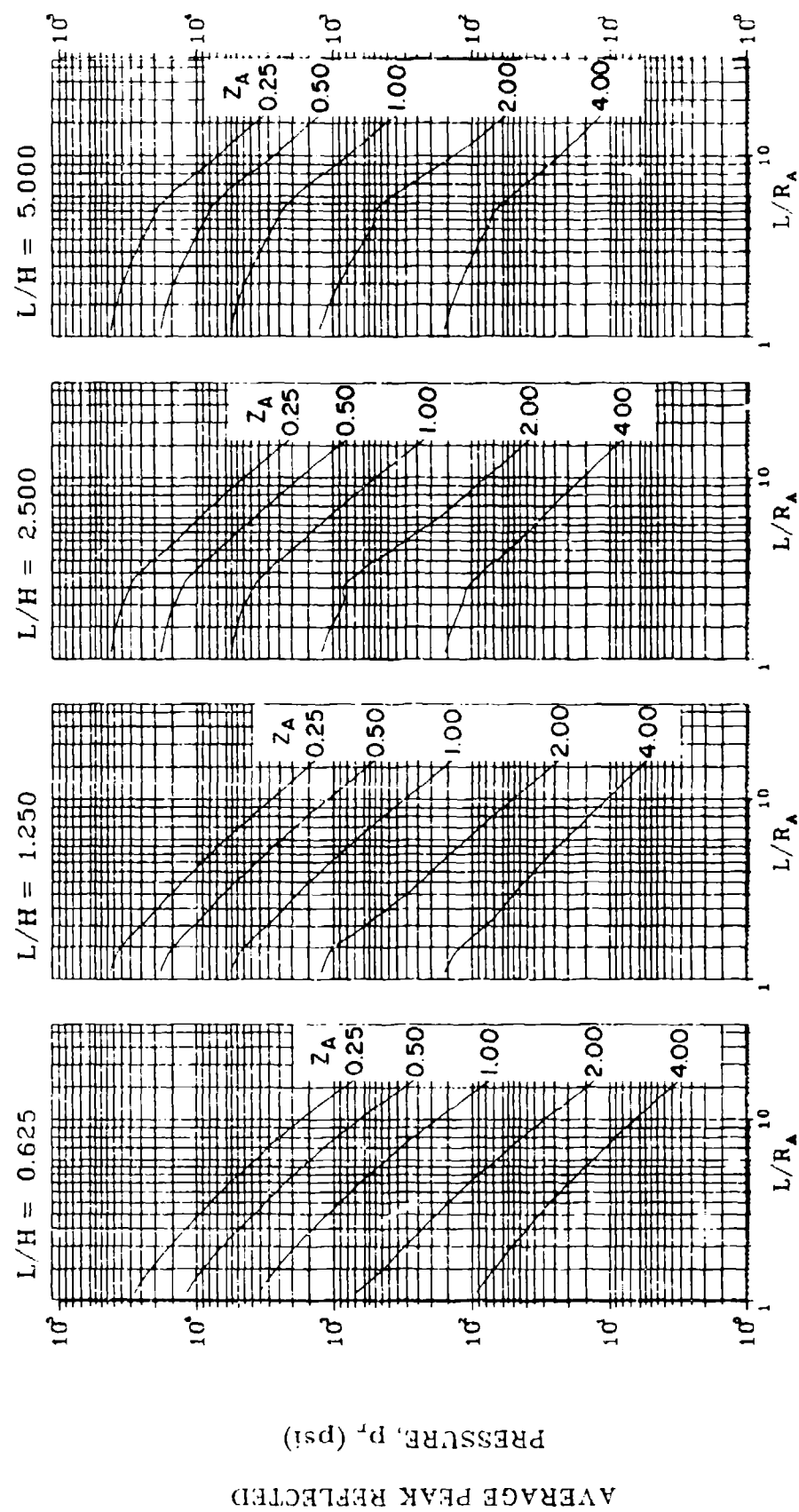


Figure 2-53 Average peak reflected pressure ($N = 1$, $L/H = 0.25$ and 0.75 , $h/H = 0.10$)

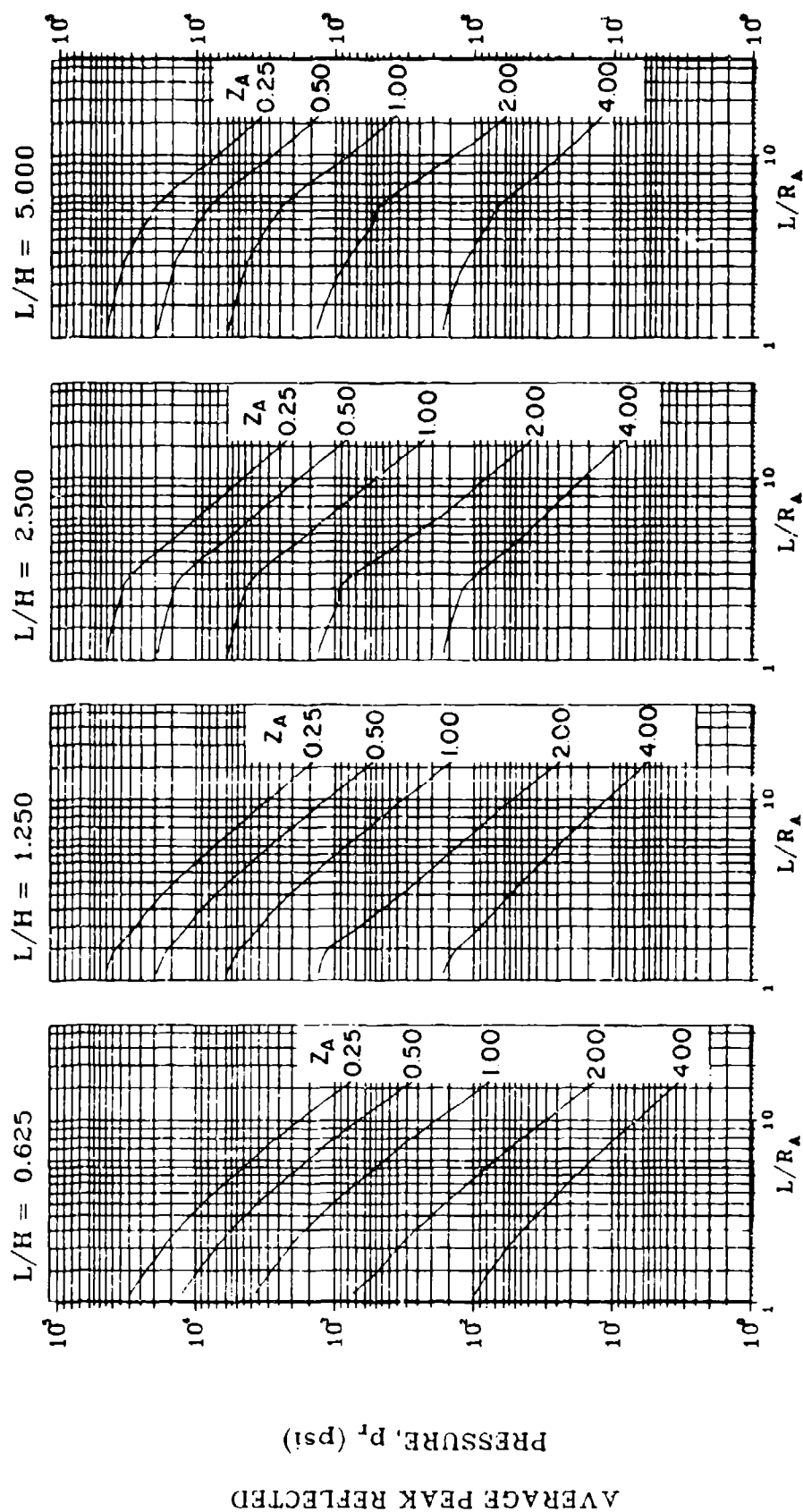


Figure 2-54 Average peak reflected pressure ($N = 1$, $h/H = 0.10$)

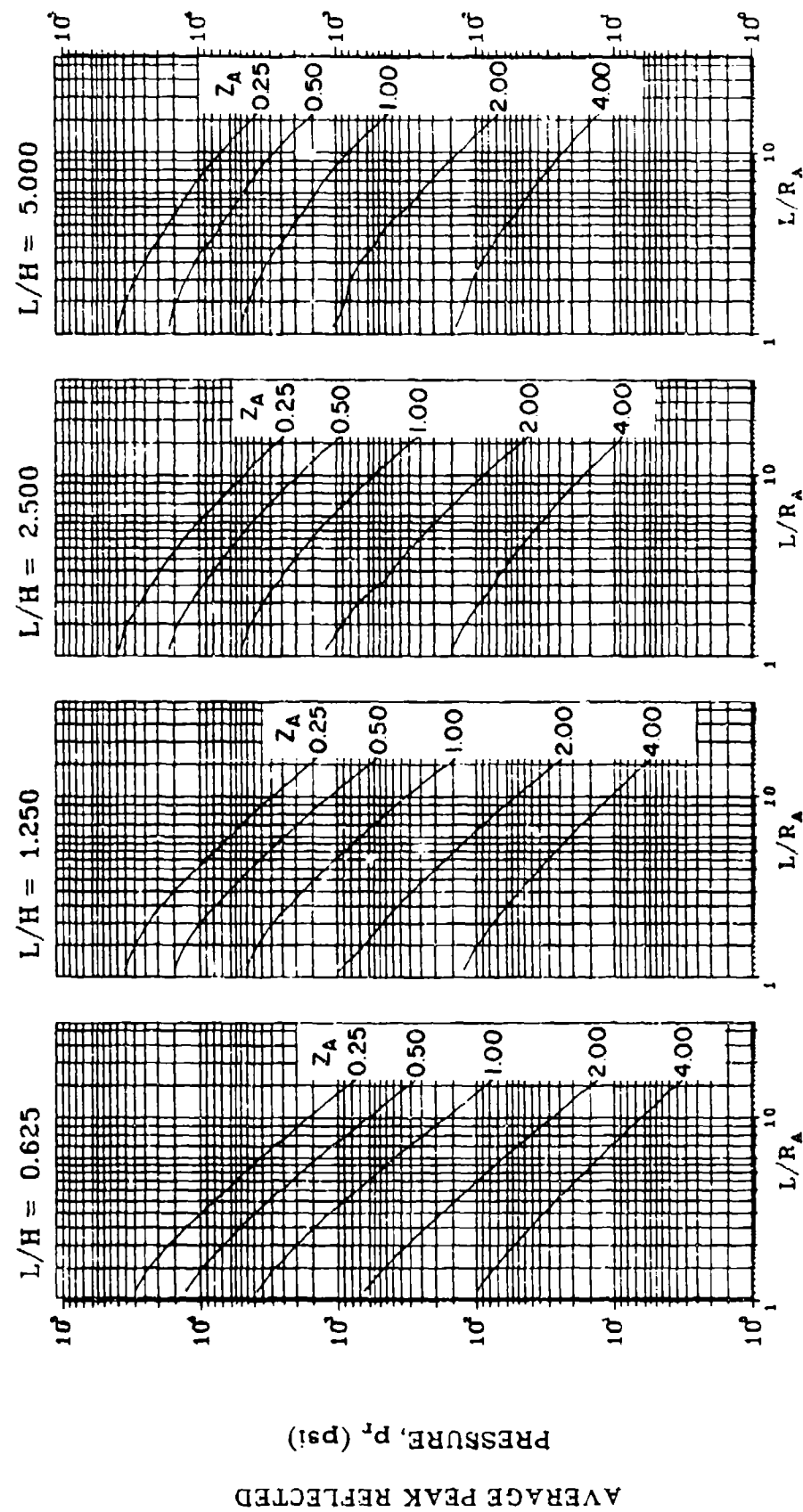


Figure 2-55 Average peak reflected pressure ($N = 1$, $h/H = 0.25$)

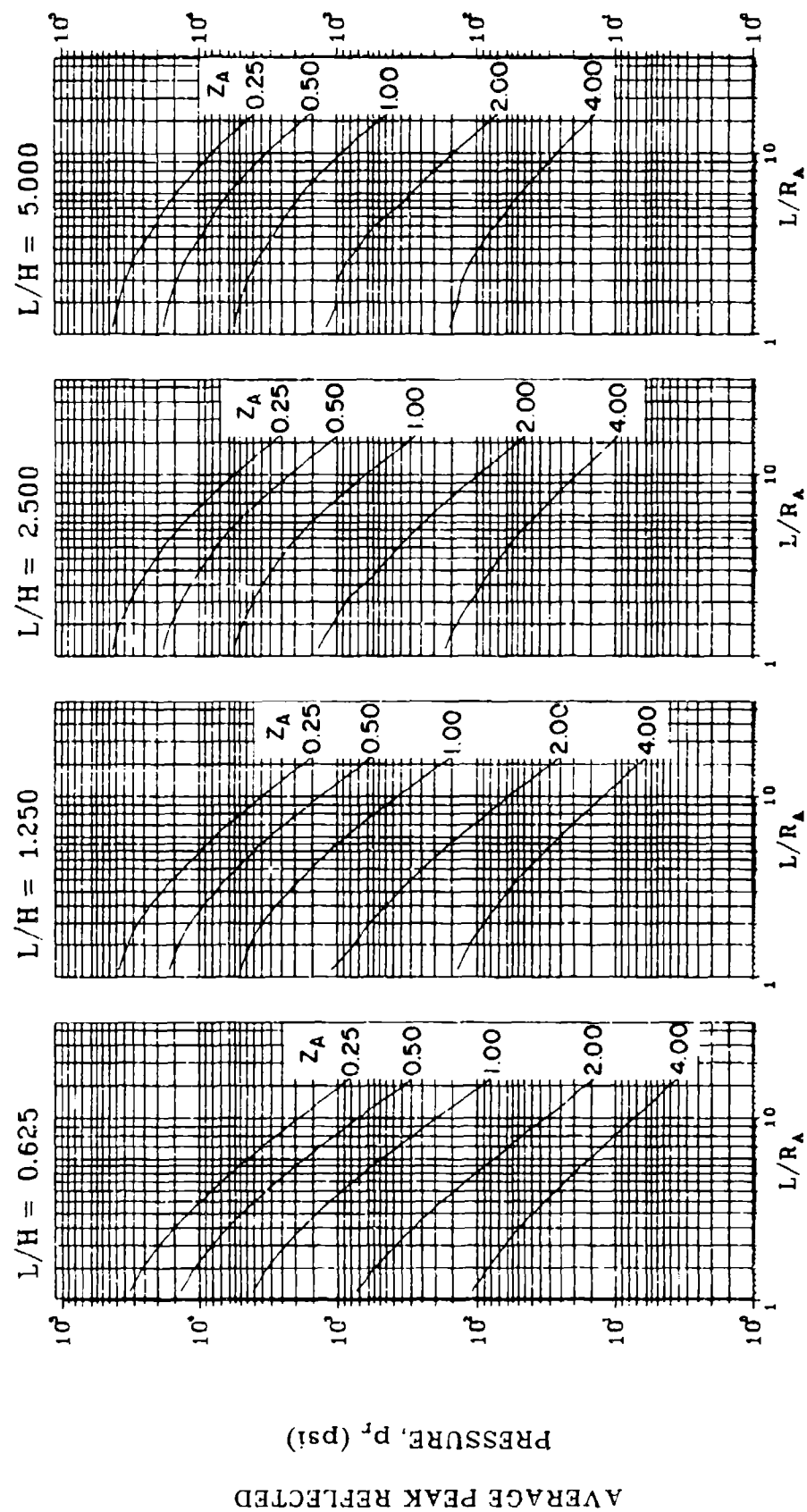


Figure 2-56 Average peak reflected pressure
($N = 1$, $L/L = 0.25$ and 0.75 , $h/H = 0.25$)

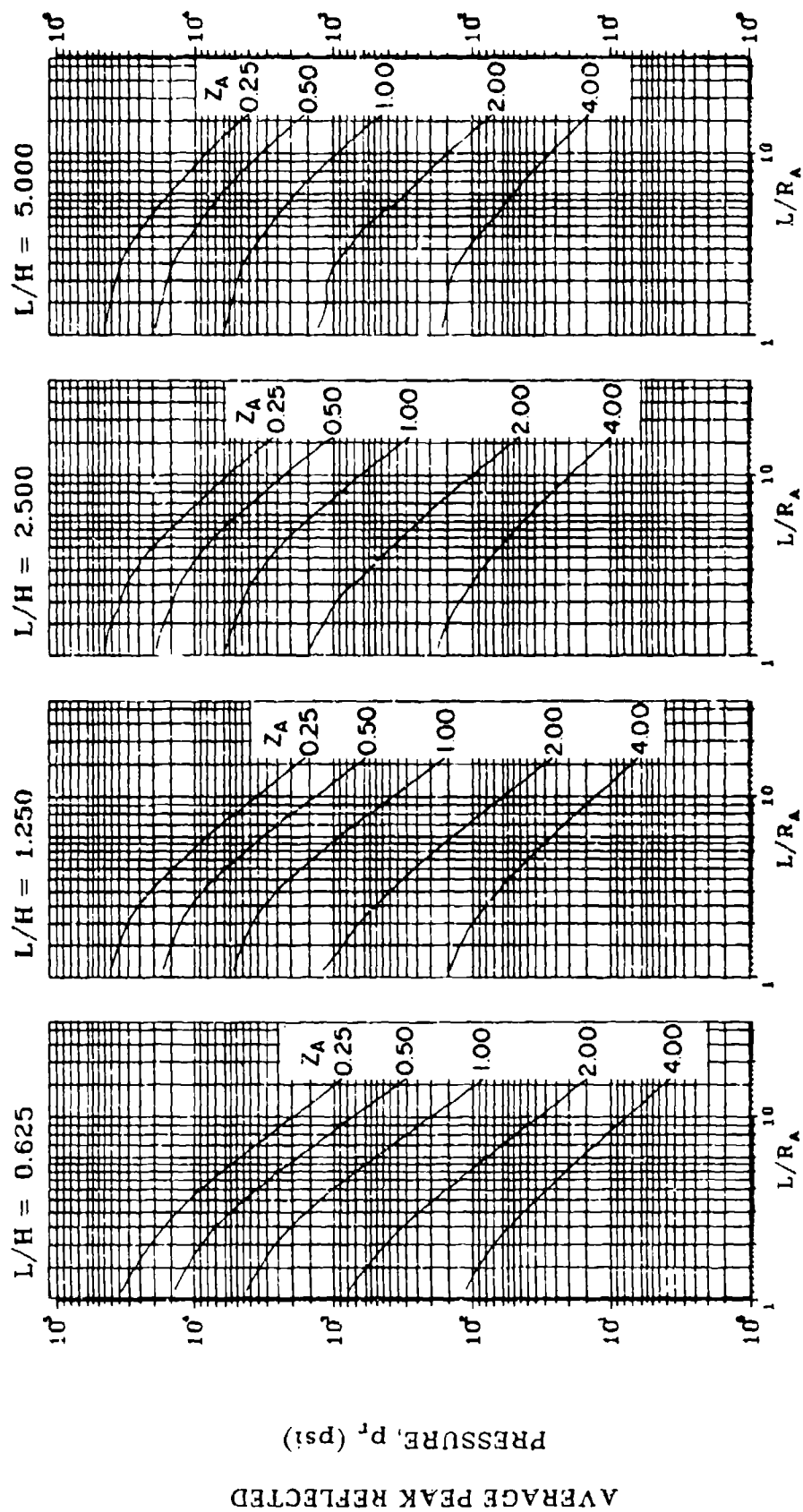


Figure 2-57 Average peak reflected pressure ($N = 1$, $\ell/L = 0.50$, $h/H = 0.25$)

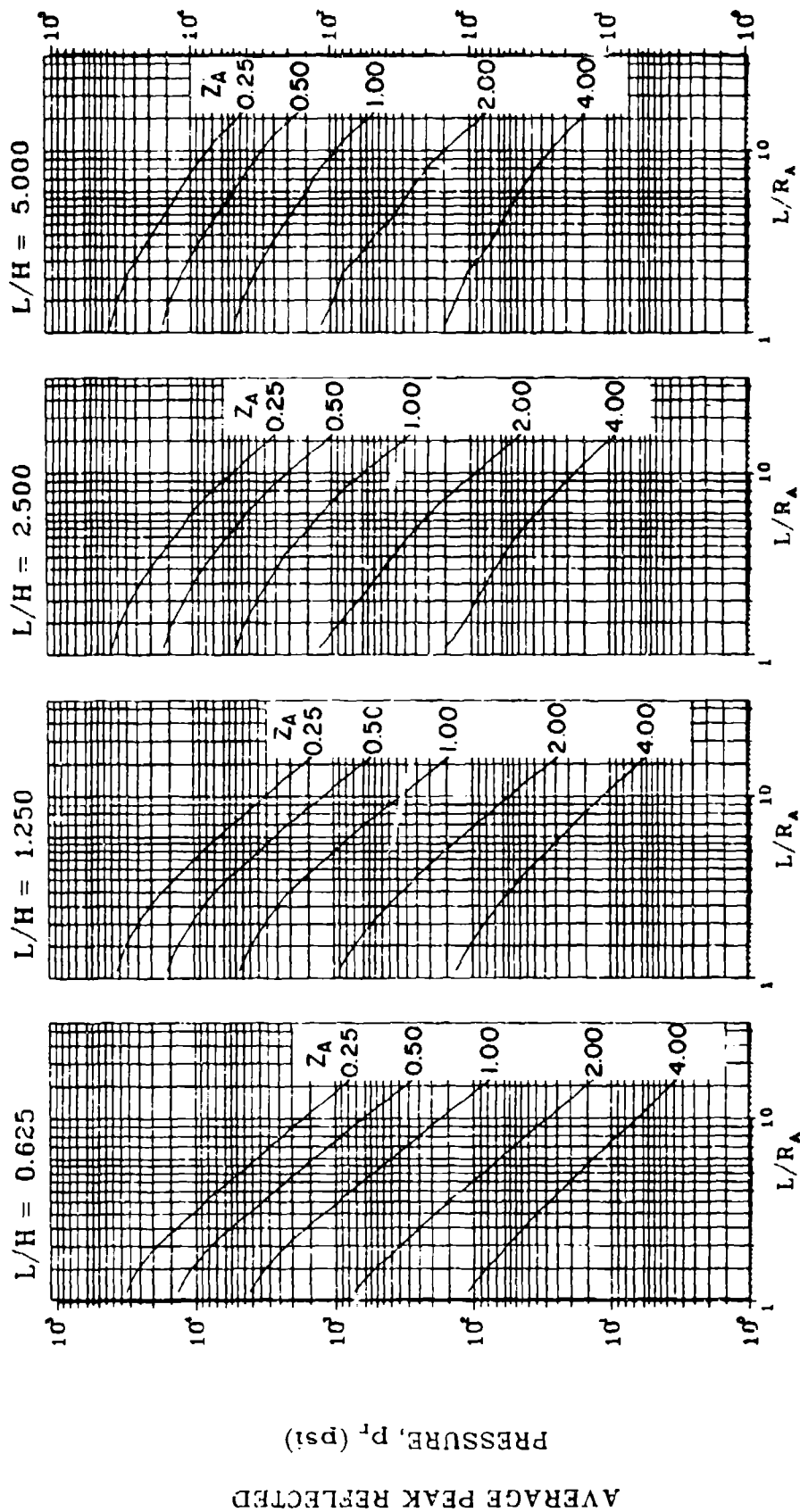


Figure 2-58 Average peak reflected pressure ($N = 1$, $L/L = 0.10$, $h/H = 0.50$)

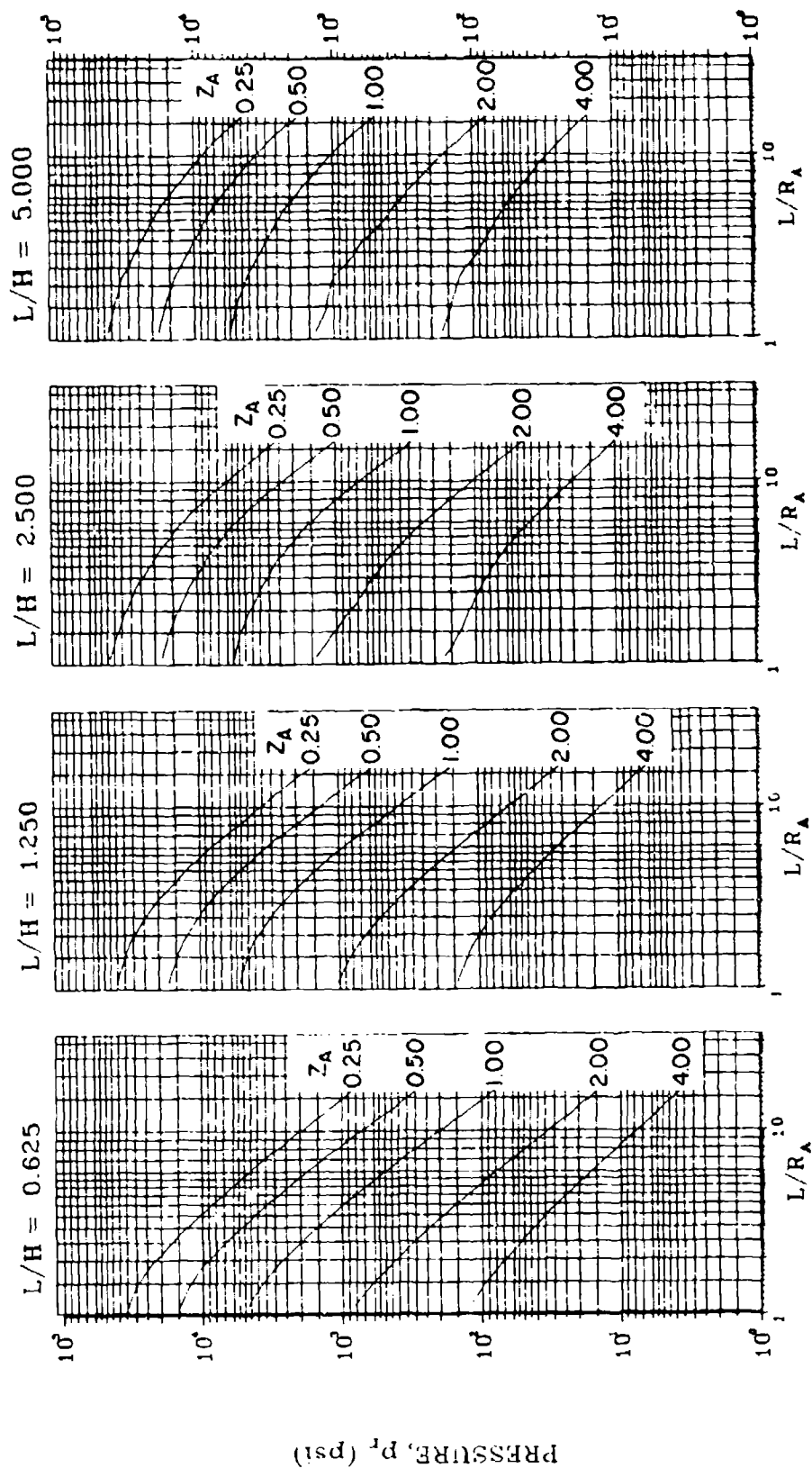


Figure 2-59 Average peak reflected pressure ($N = 1$, $\rho/L = 0.25$ and 0.75 , $h/H = 0.50$)

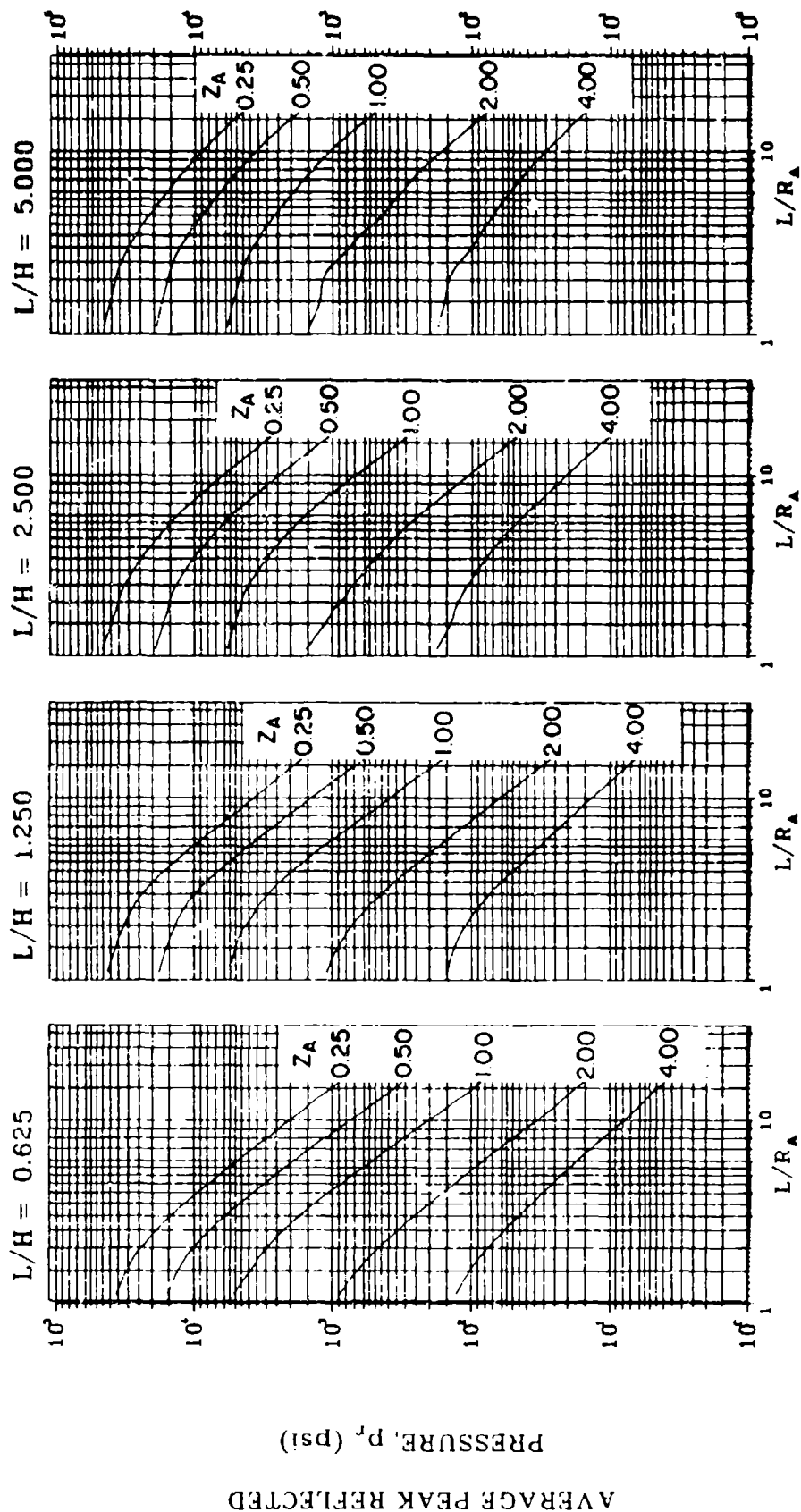


Figure 2-60 Average peak reflected pressure ($N = 1$, $\rho/L = 0.50$, $h/H = 0.50$)

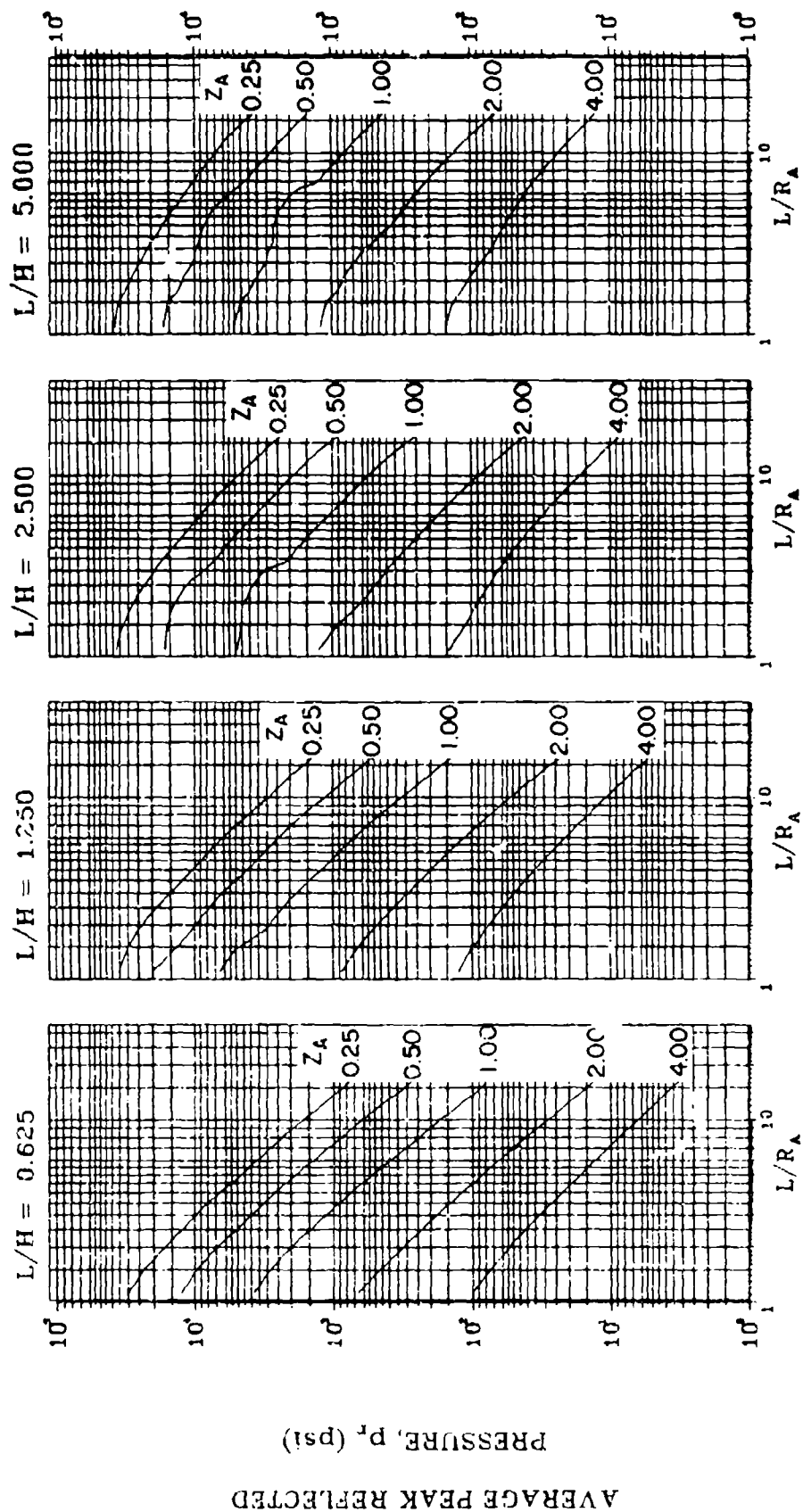


Figure 2-61 Average peak reflected pressure ($N = 1$, $\ell/L = 0.10$, $h/H = 0.75$)

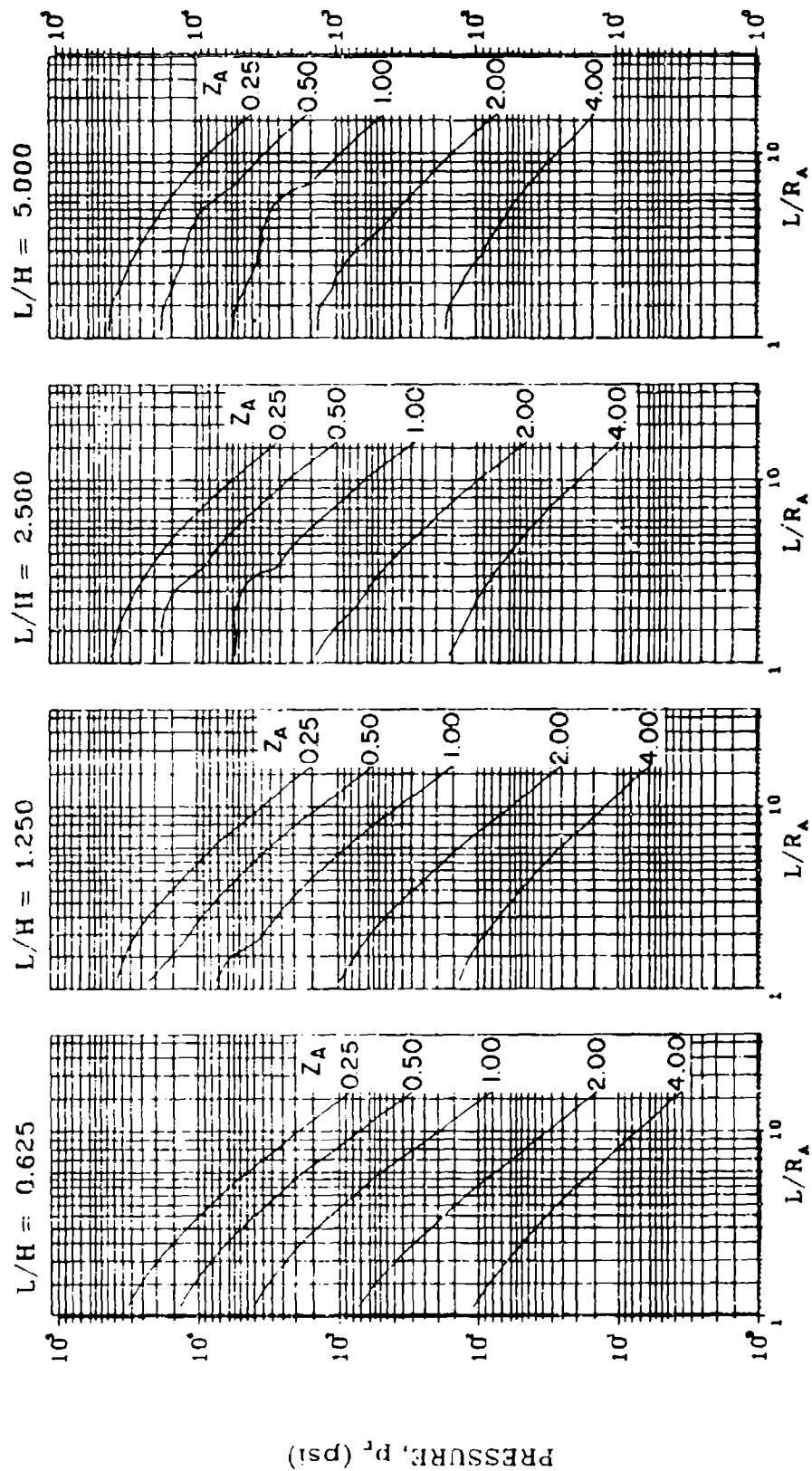


Figure 2-62 Average peak reflected pressure ($N = 1$, $\ell/L = 0.25$ and 0.75 , $h/H = 0.75$)

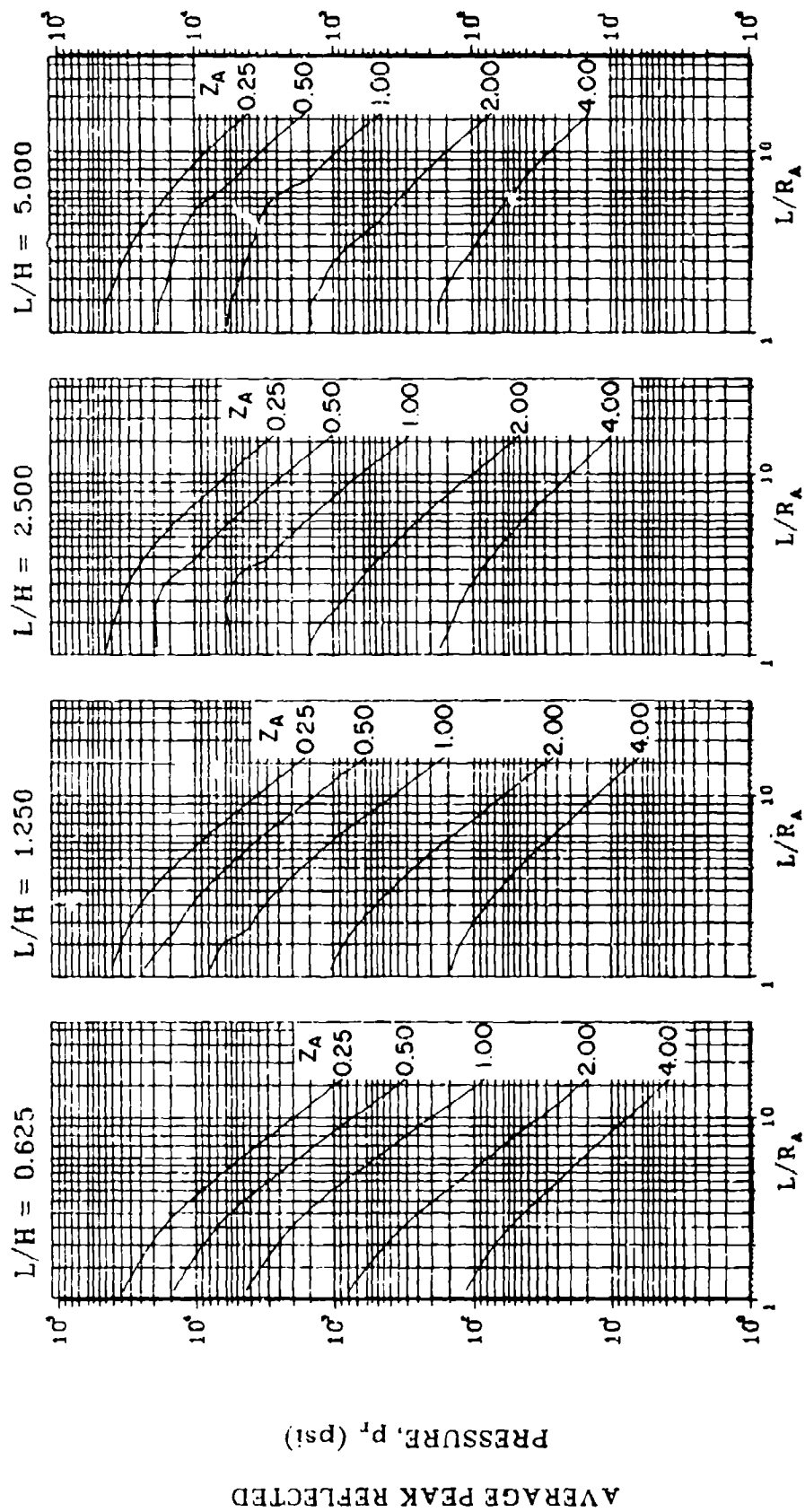


Figure 2-63 Average peak reflected pressure ($N = 1$, $\ell/L = 0.50$, $h/H = 0.75$)

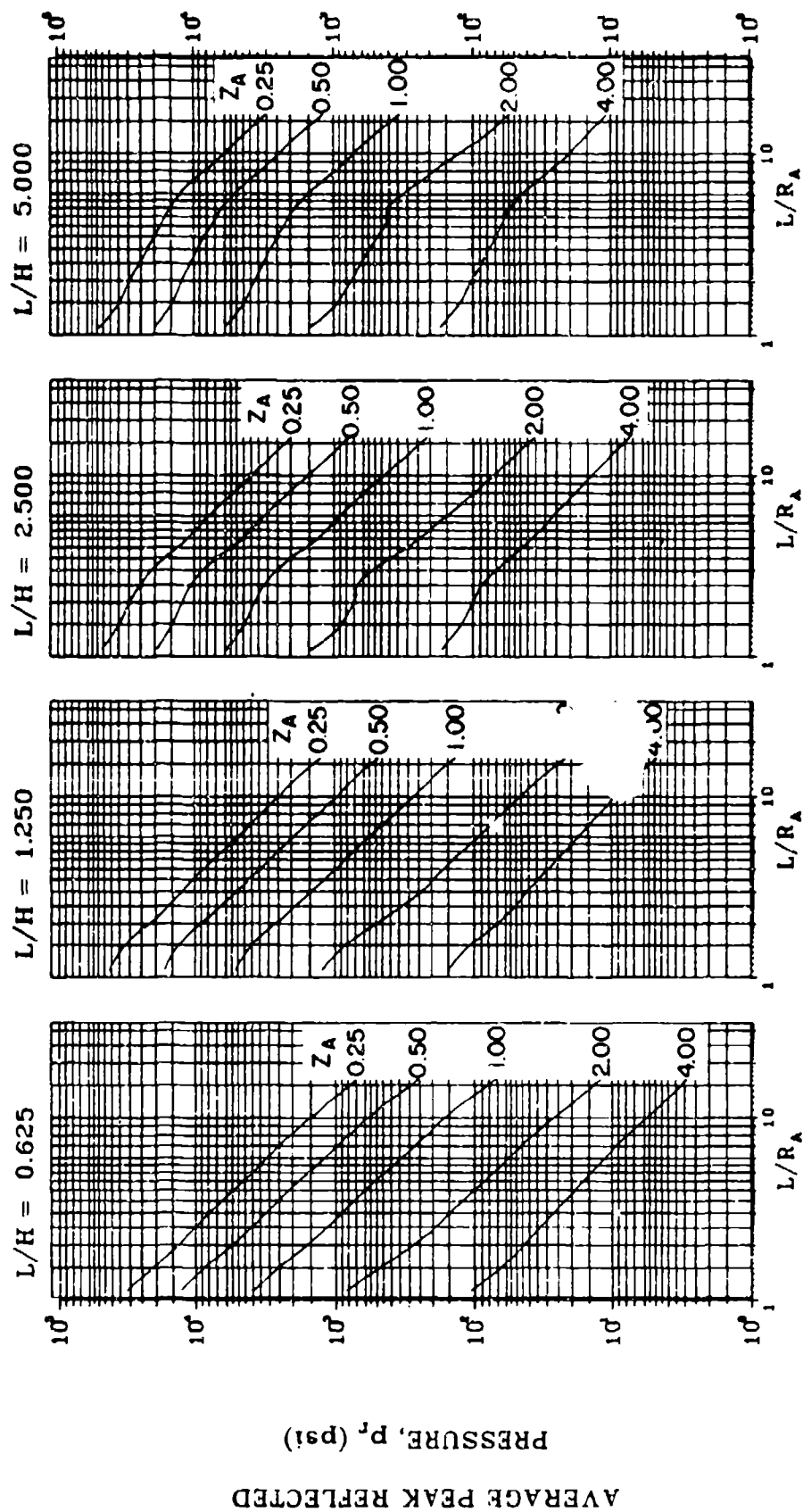


Figure 2-64 Average peak reflected pressure ($N = 2$, $\rho/L = 0.10$, $h/H = 0.10$)

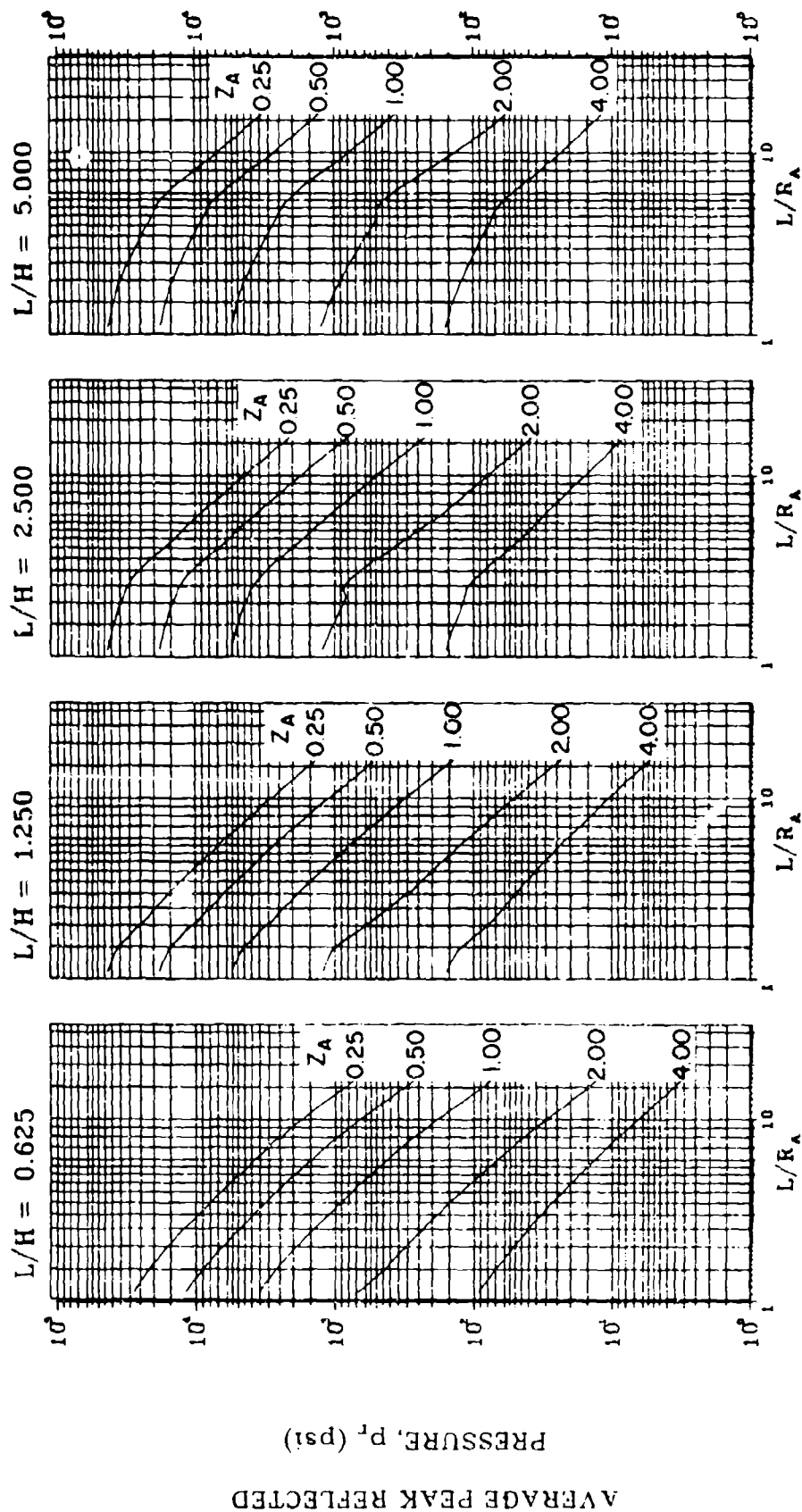


Figure 2-65 Average peak reflected pressure ($N = 2$, $\ell/L = 0.25$, $h/H = 0.10$)

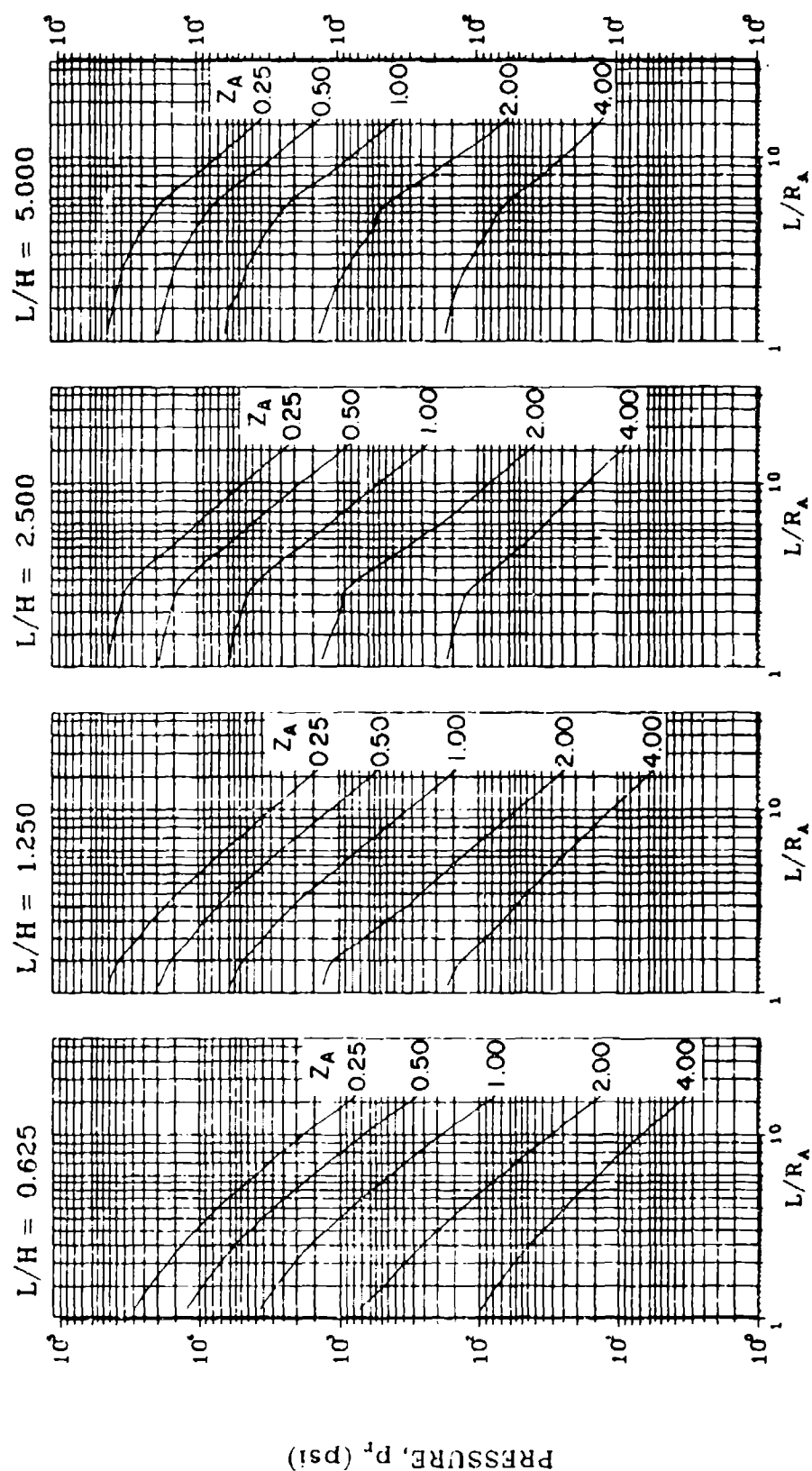


Figure 2-66 Average peak reflected pressure ($N = 2$, $\ell/l = 0.50$, $h/H = 0.10$)

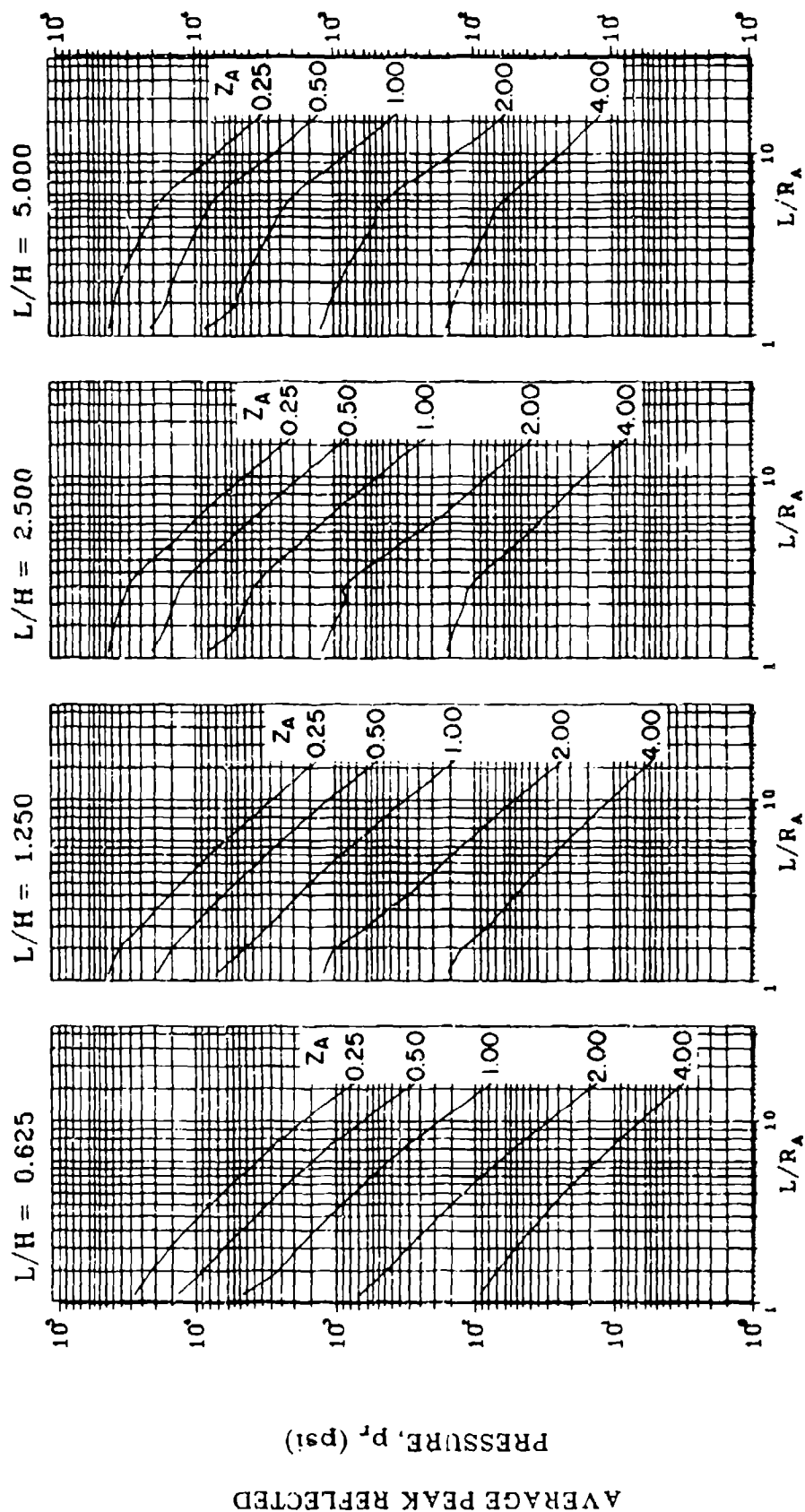


Figure 2-67 Average peak reflected pressure ($N = 2$, $\ell/L = 0.75$, $h/H = 0.10$)

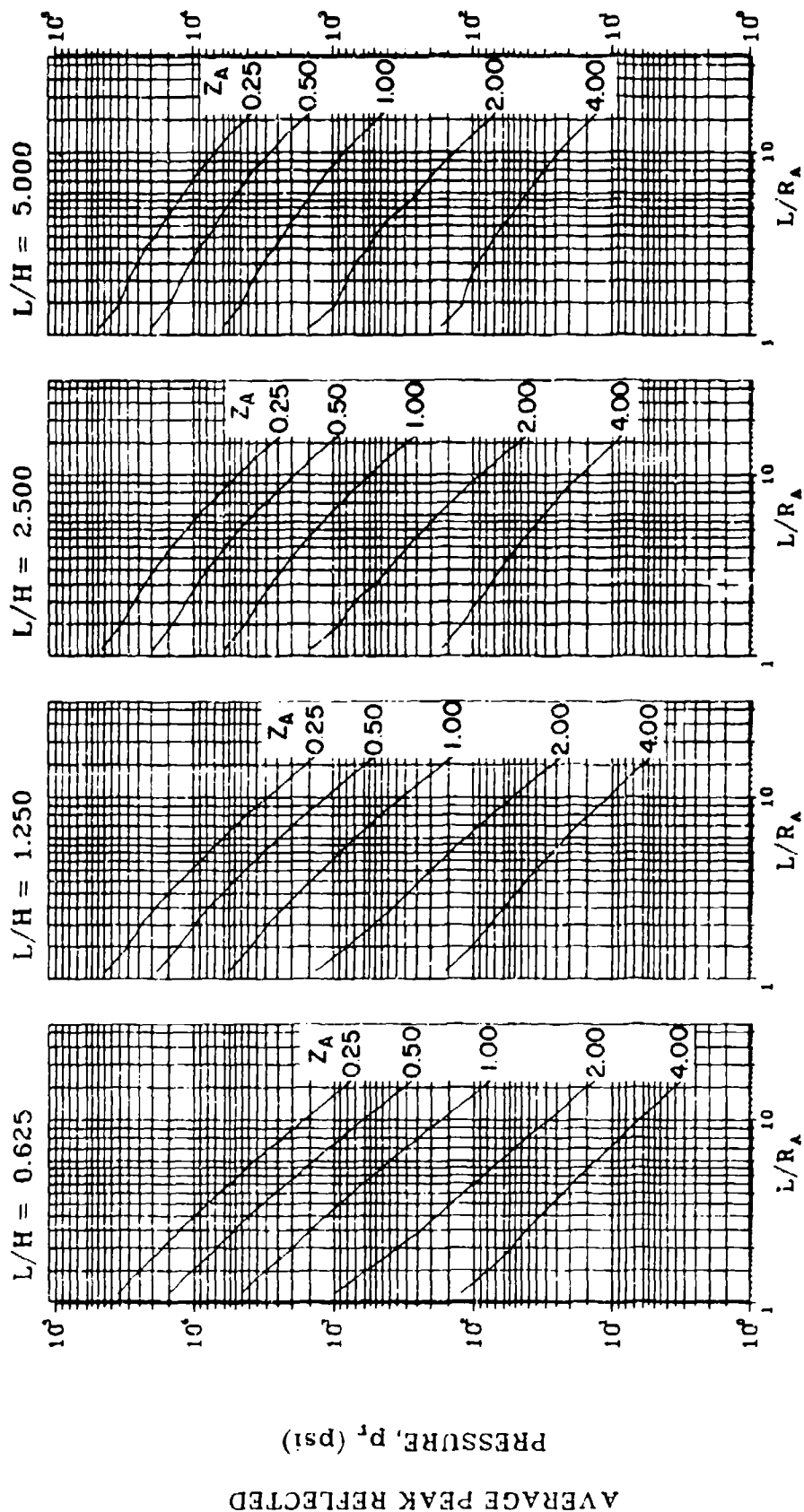


Figure 2-68 Average peak reflected pressure ($N = 2$, $\ell/L = 0.10$, $h/H = 0.25$)

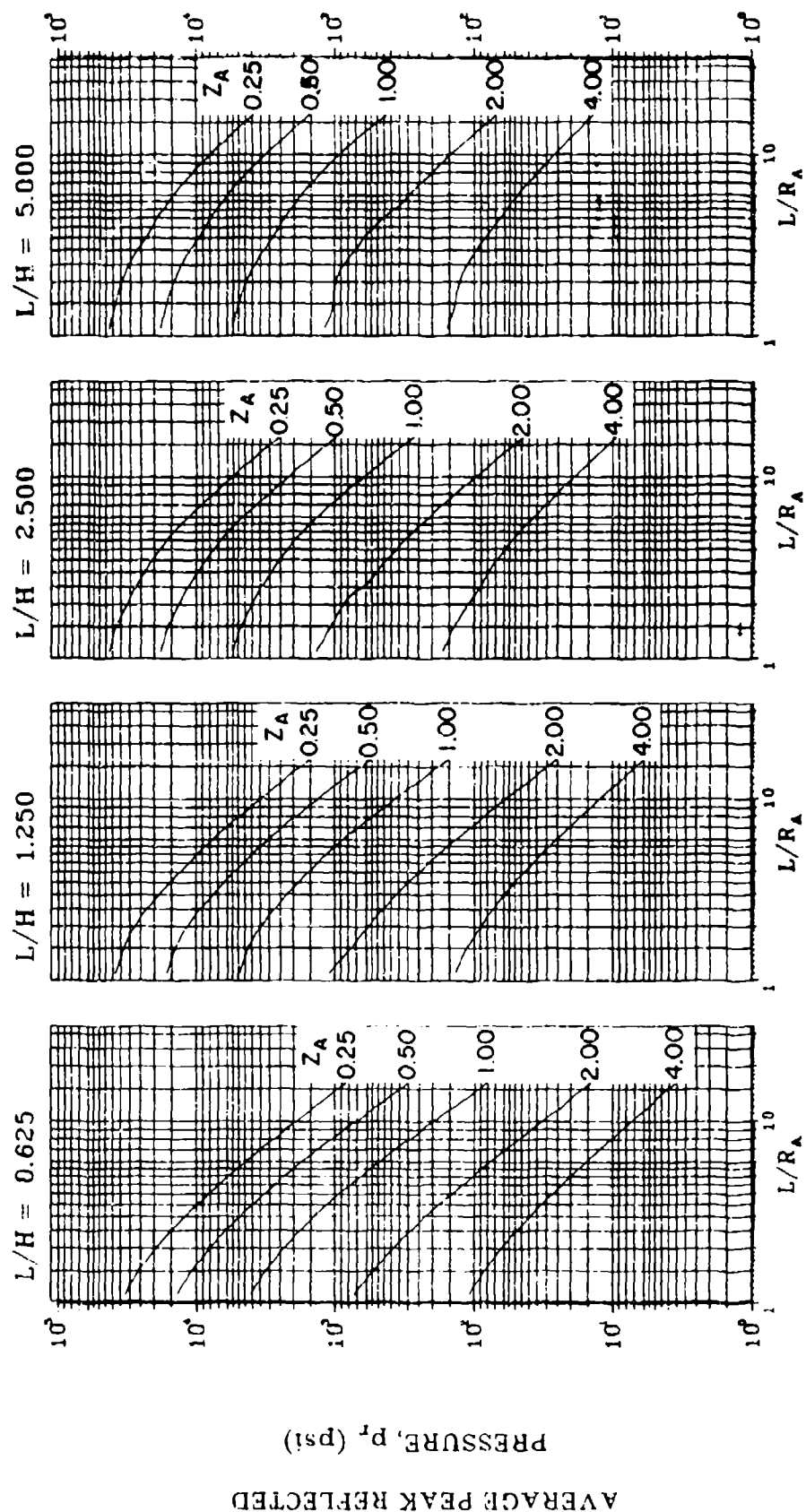
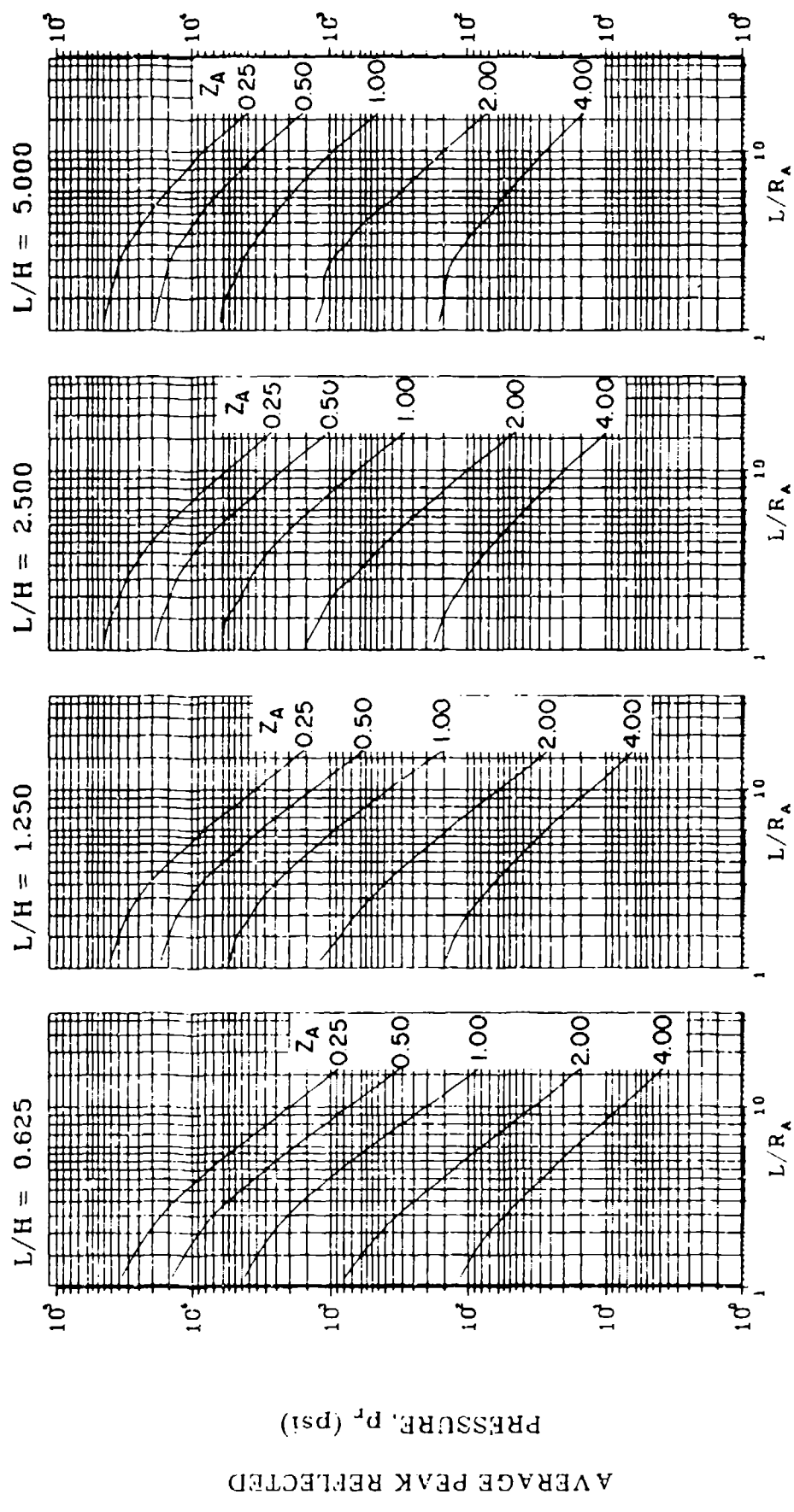


Figure 2-69 Average peak reflected pressure ($N = 2$, $\ell/L = 0.25$, $h/H = 0.25$)



AVERAGE PEAK REFLECTED PRESSURE, p_r (psi)

Figure 2-70 Average peak reflected pressure ($N = 2$, $\ell/l = 0.50$, $h/H = 0.25$)

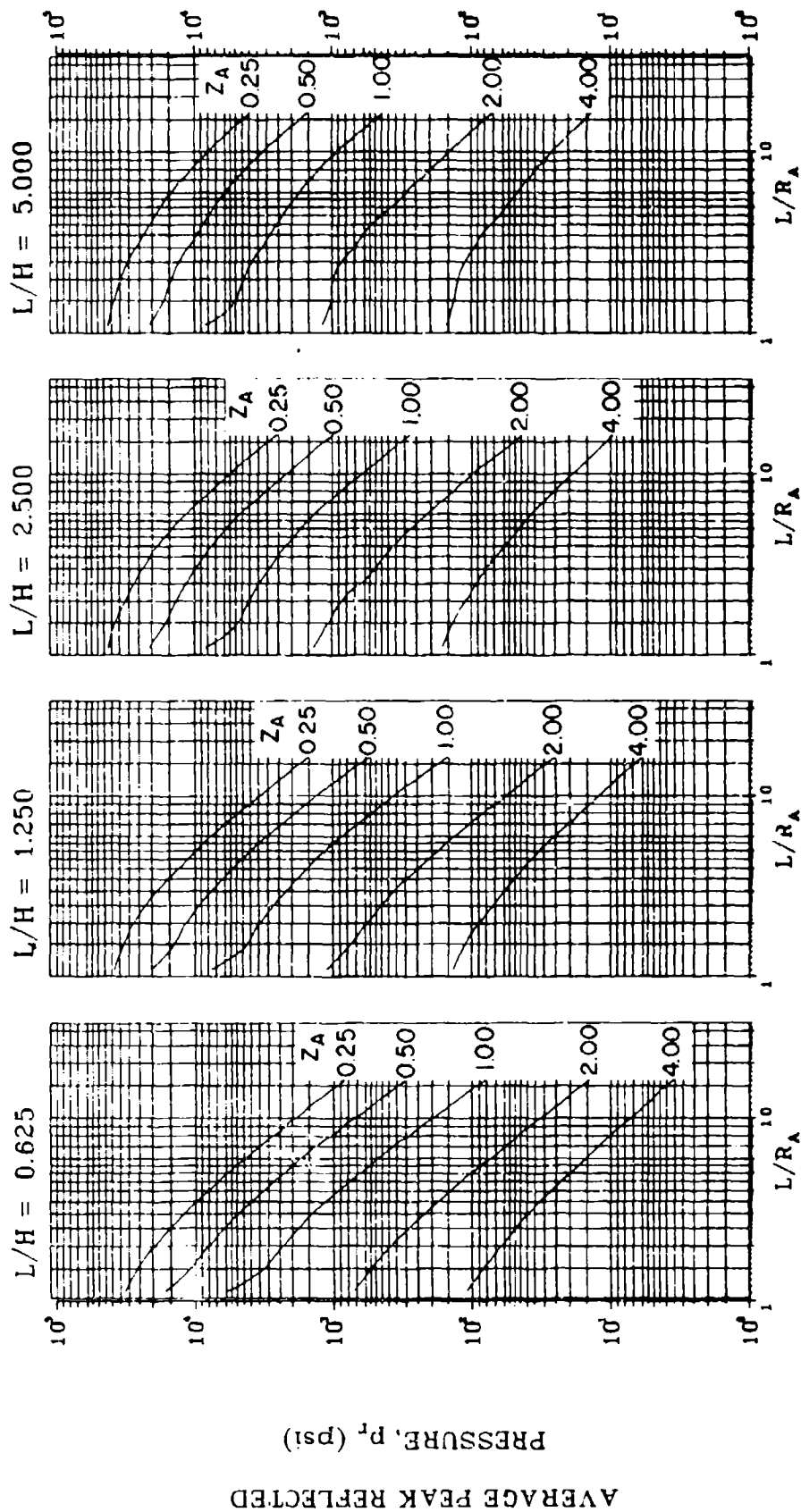


Figure 2-71 Average peak reflected pressure ($N = 2$, $\ell/L = 0.75$, $h/H = 0.25$)

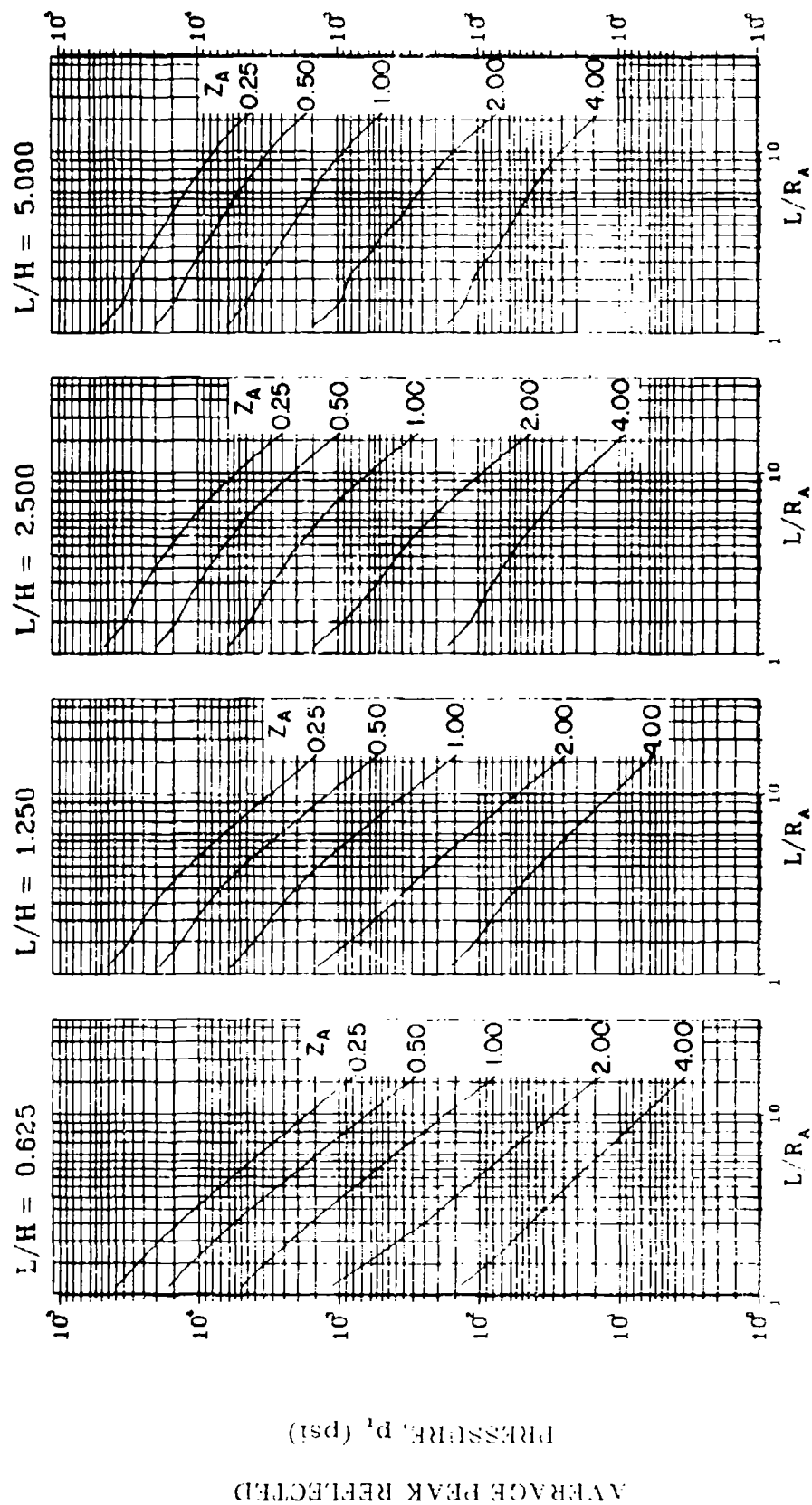


Figure 2-72 Average peak reflected pressure ($N = 2$, $\ell/L = 0.10$, $h/H = 0.50$)

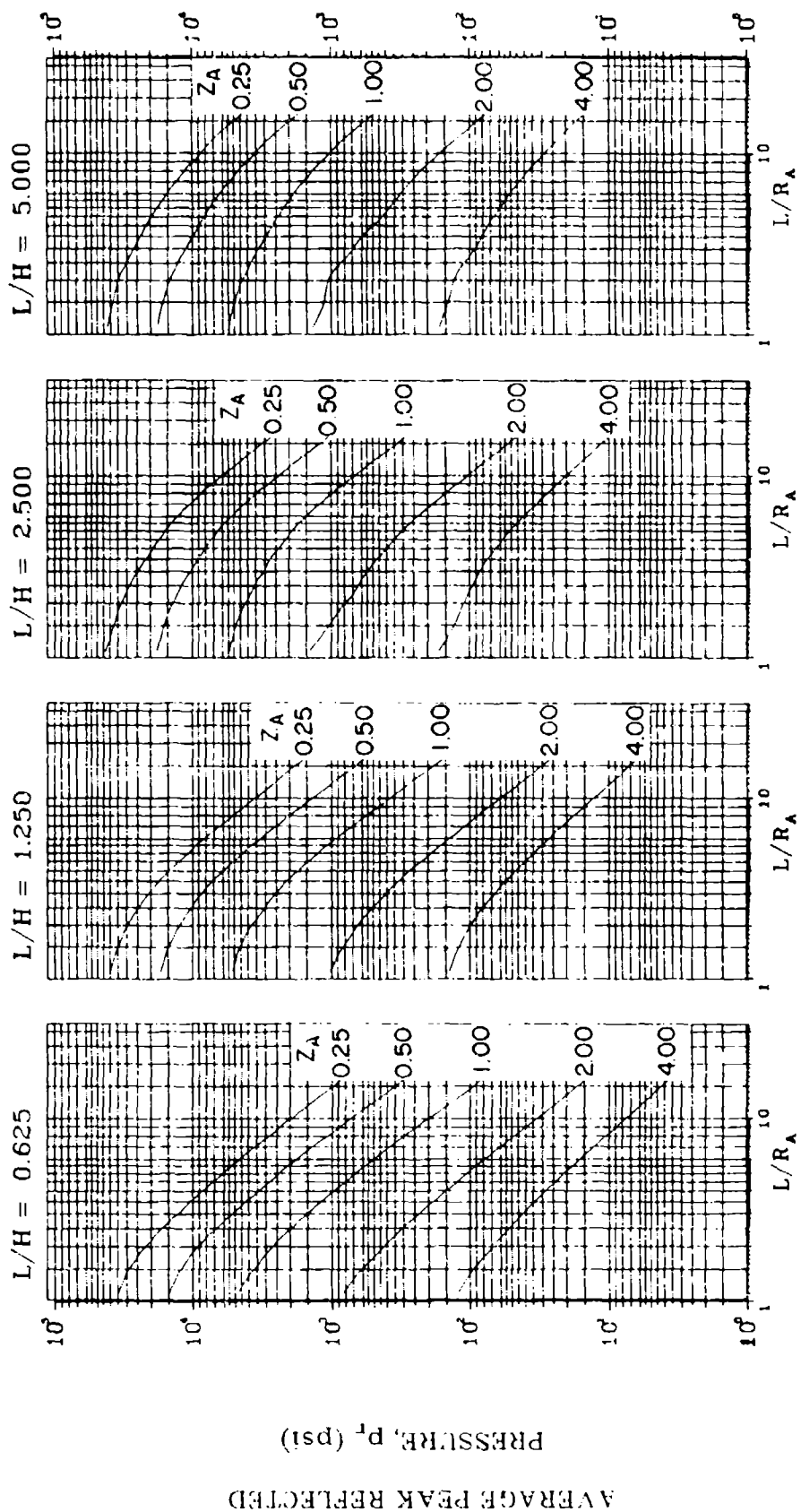


Figure 2-73 Average peak reflected pressure ($N = 2$, $\ell/L = 0.25$, $h/H = 0.50$)

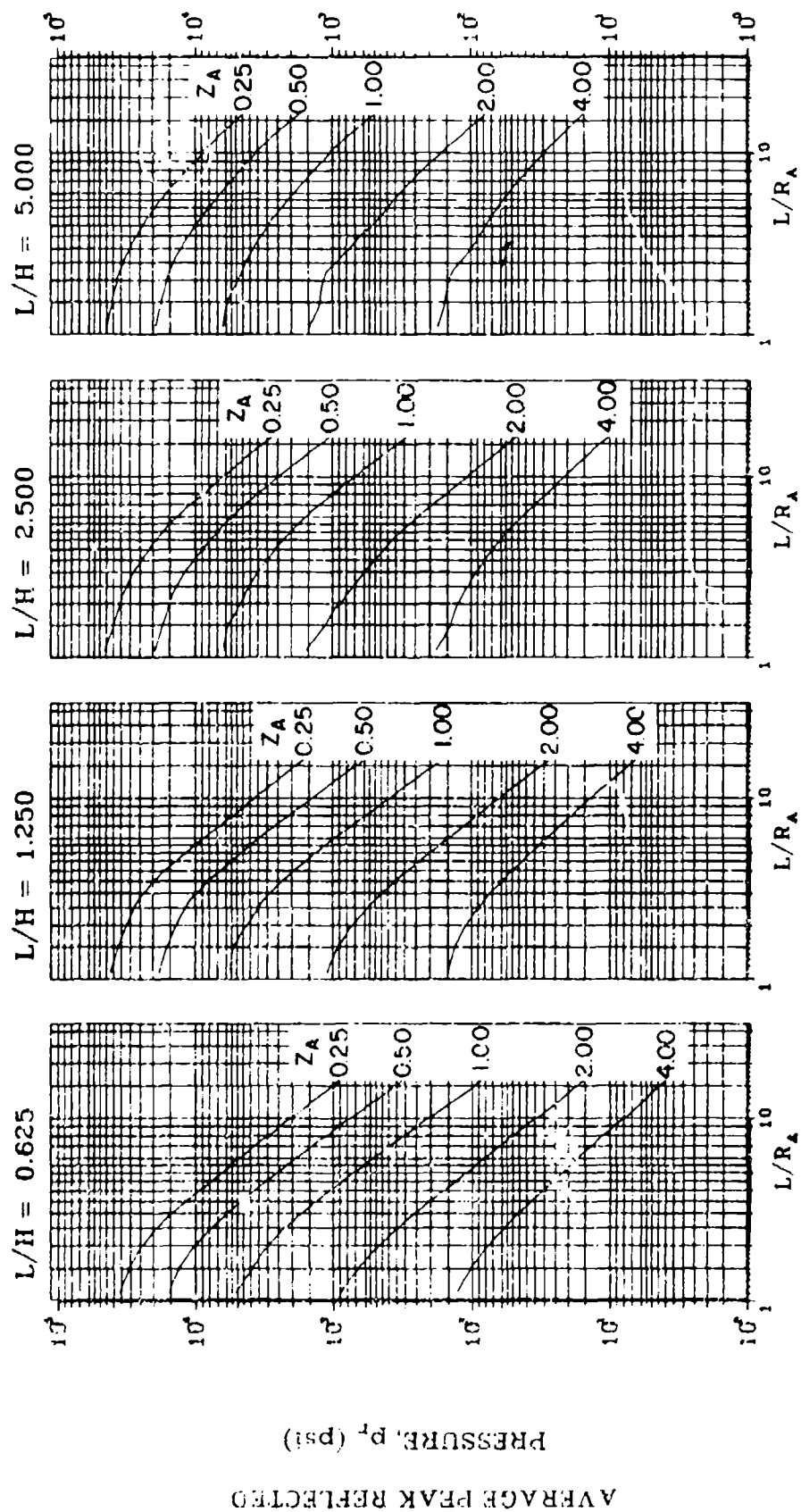


Figure 2-74 Average peak reflected pressure ($N = 2$, $q/L = 0.50$, $h/H = 0.50$)

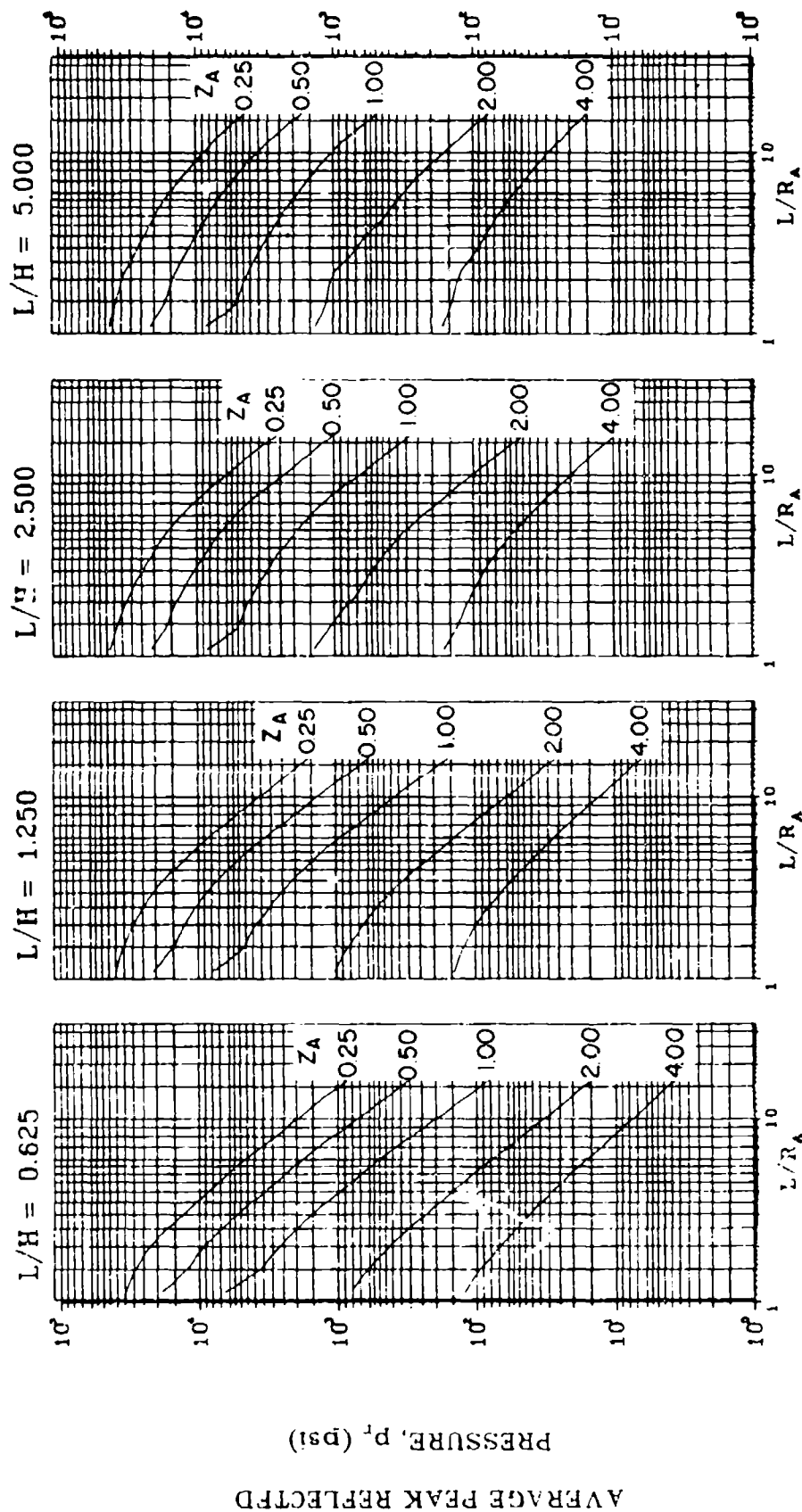


Figure 2-75 Average peak reflected pressure ($N = 2$, $\ell/L = 0.75$, $h/H = 0.50$)

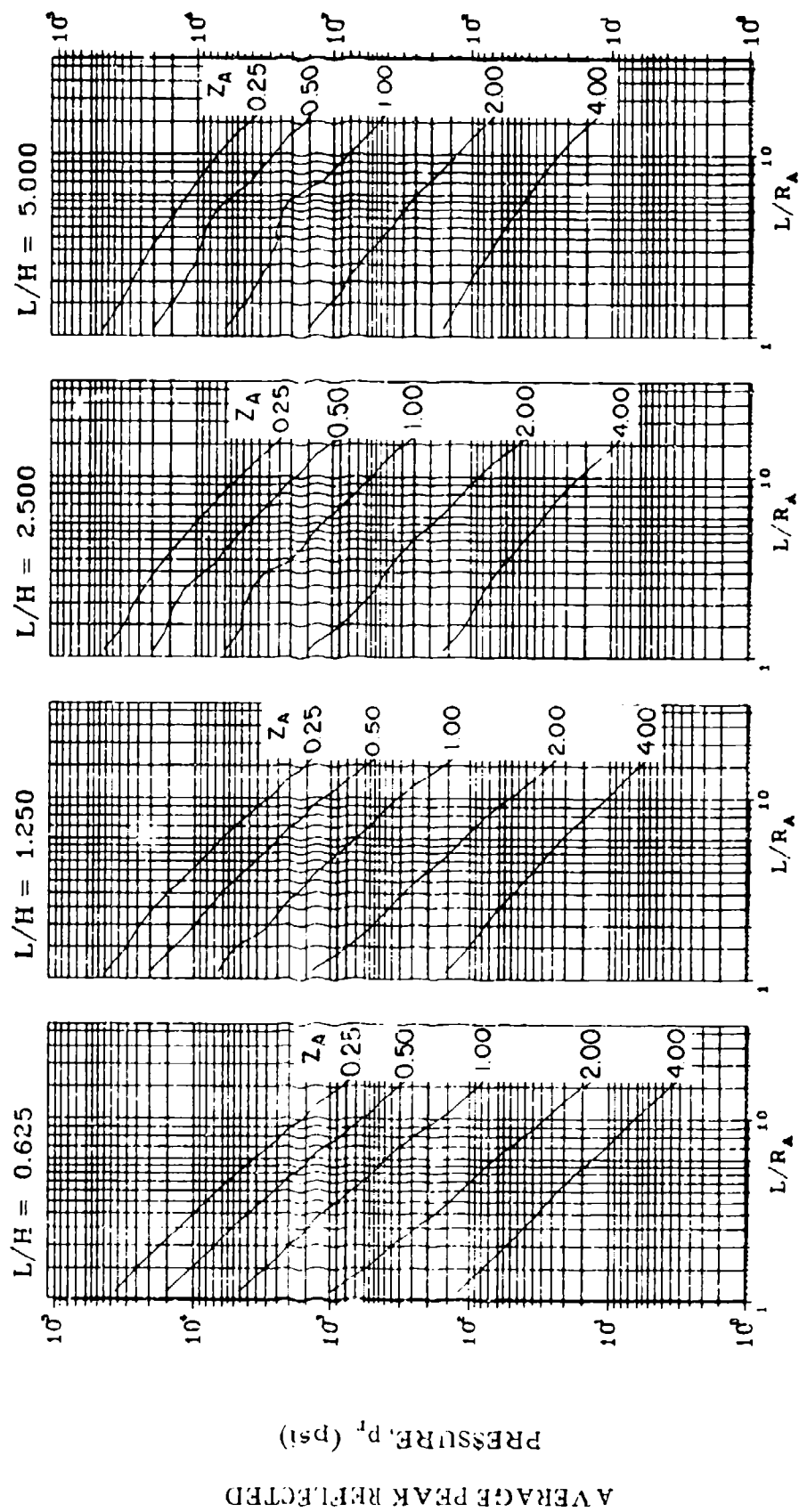


Figure 2-76 Average peak reflected pressure ($N = 2$, $l/L = 0.10$, $h/H = 0.75$)

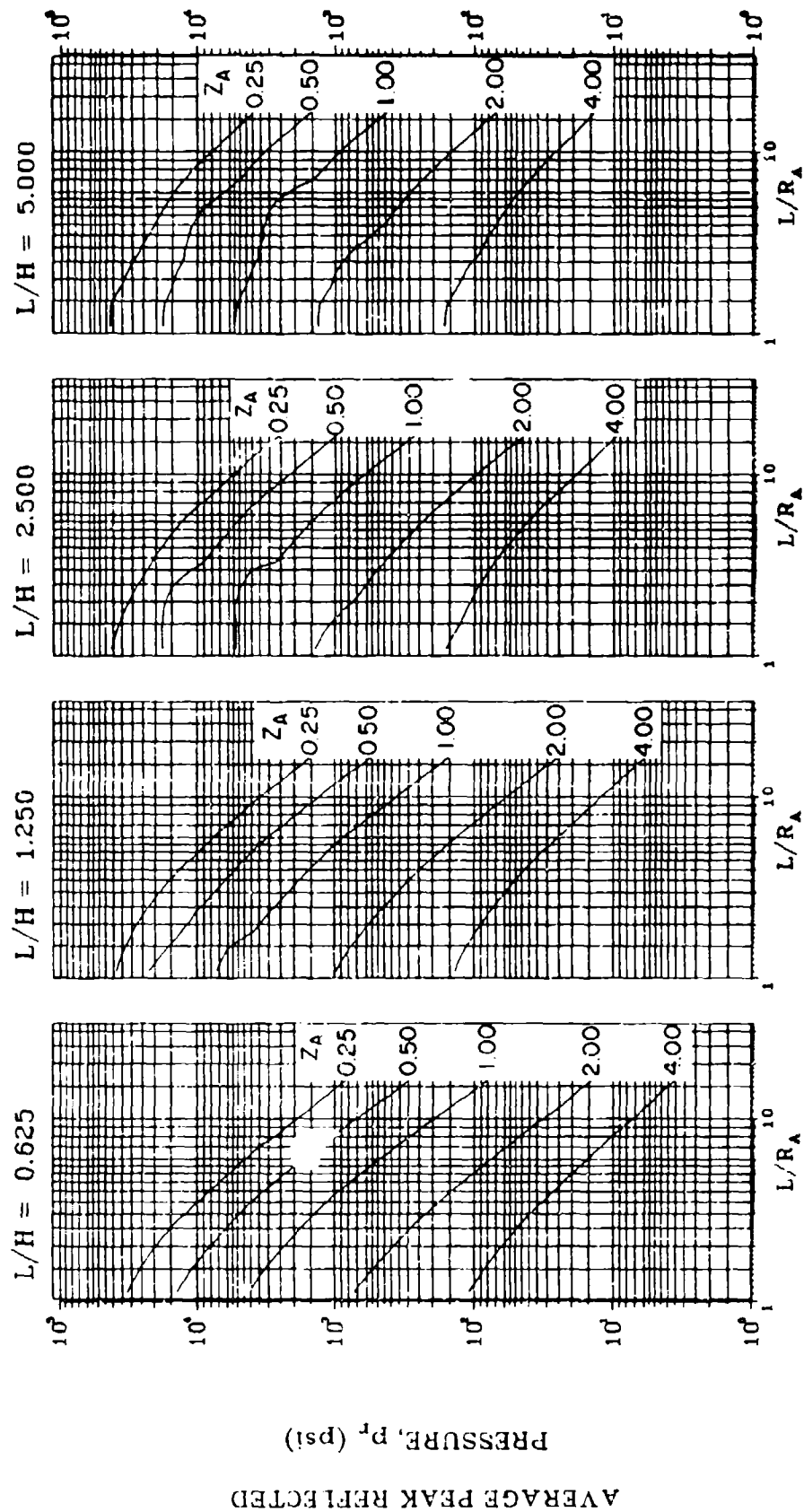


Figure 2-77 Average peak reflected pressure ($N = 2$, $\ell/L = 0.25$, $h/H = 0.75$)

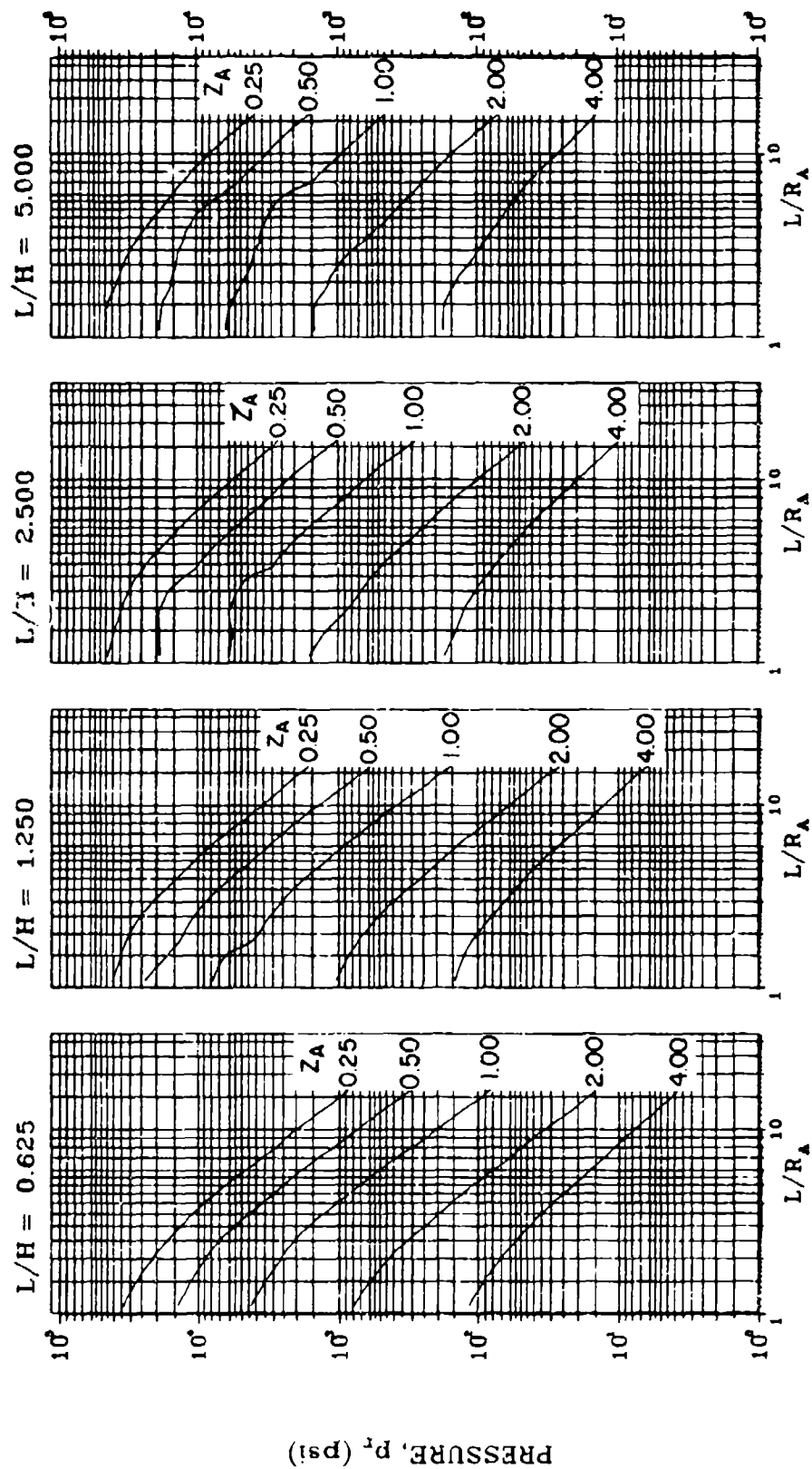


Figure 2-78 Average peak reflected pressure ($N = 2$, $\ell/L = 0.50$, $h/H = 0.75$)

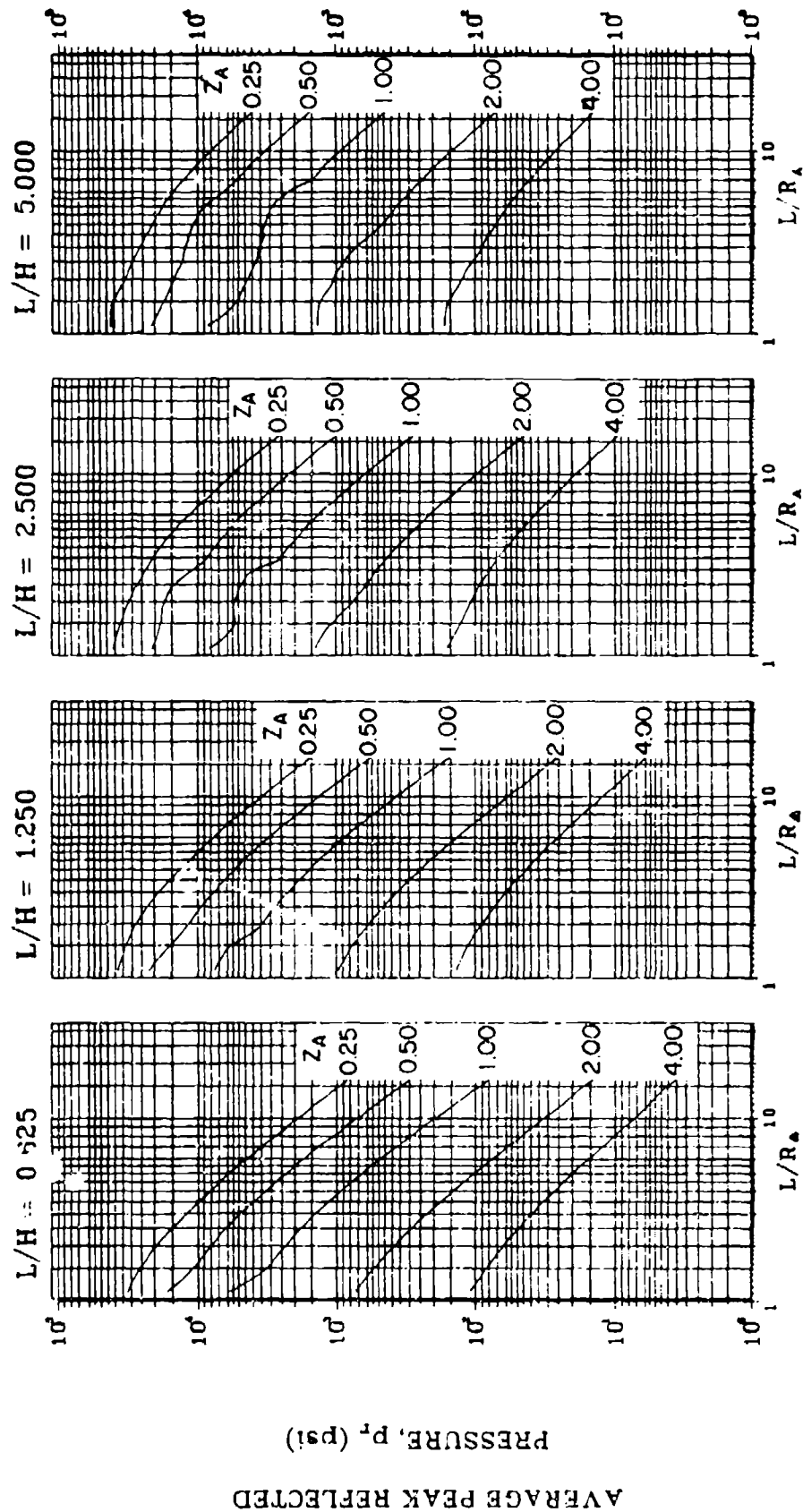


Figure 2-79 Average peak reflected pressure ($N = 2$, $L/L = 0.75$, $h/H = 0.75$)

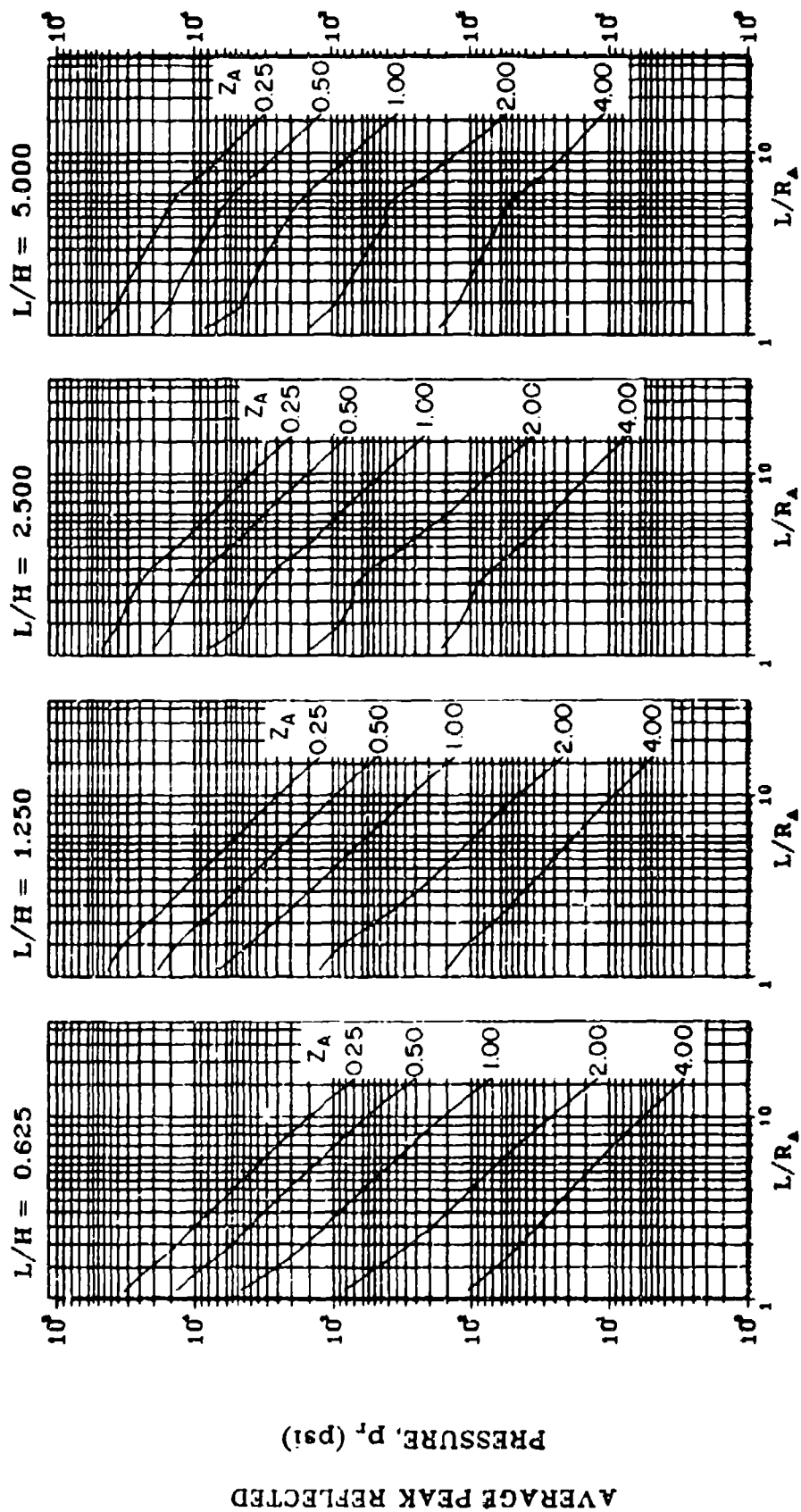


Figure 2-80 Average peak reflected pressure ($N = 3$, $\ell/L = 0.10$, $h/H = 0.10$)

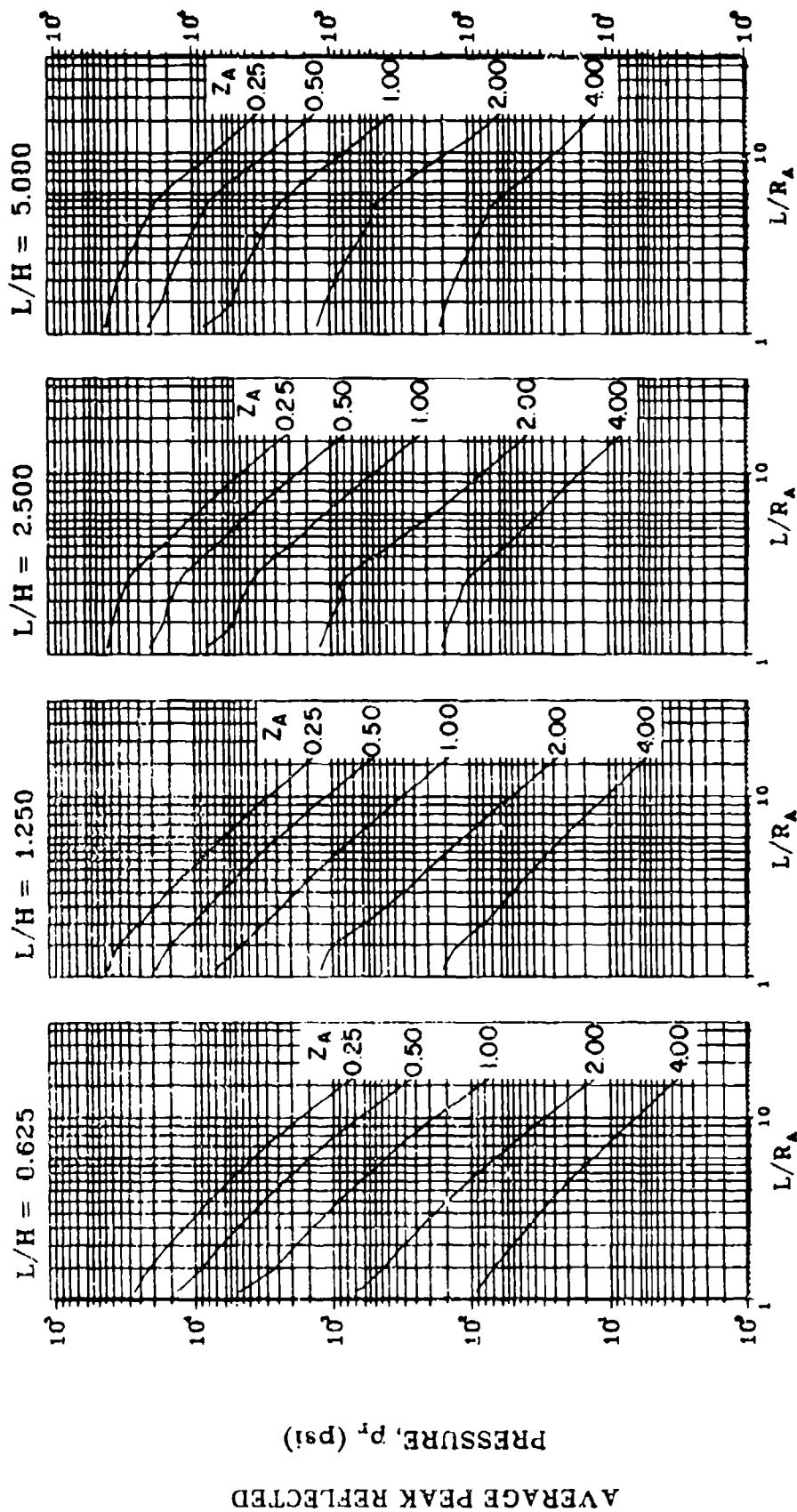


Figure 2-81 Average peak reflected pressure ($N = 3$, $\lambda/L = 0.25$ and 0.75 , $h/H = 0.10$)

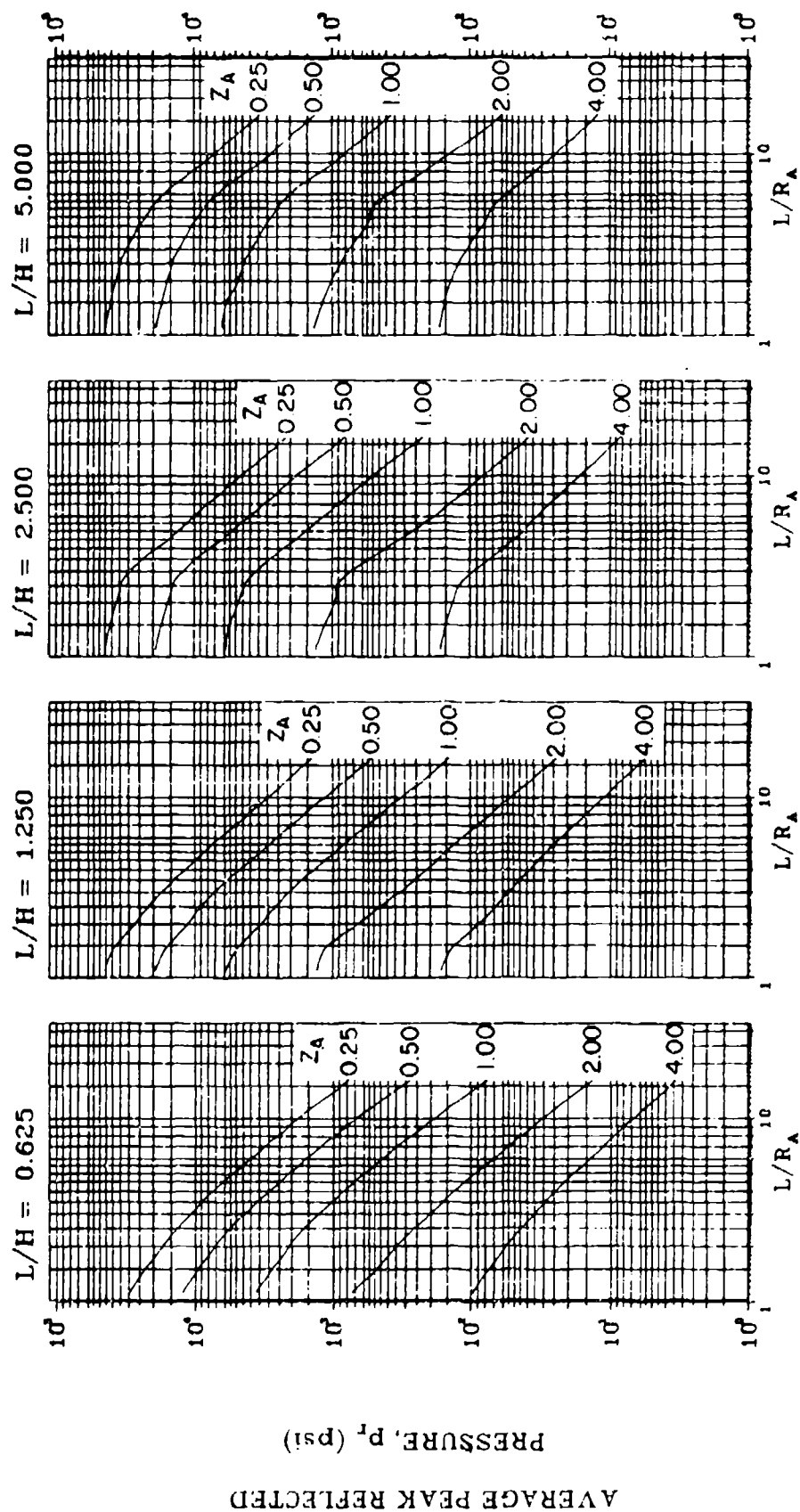


Figure 2-82 Average peak reflected pressure ($N = 3$, $\zeta/L = 0.50$, $h/H = 0.10$)

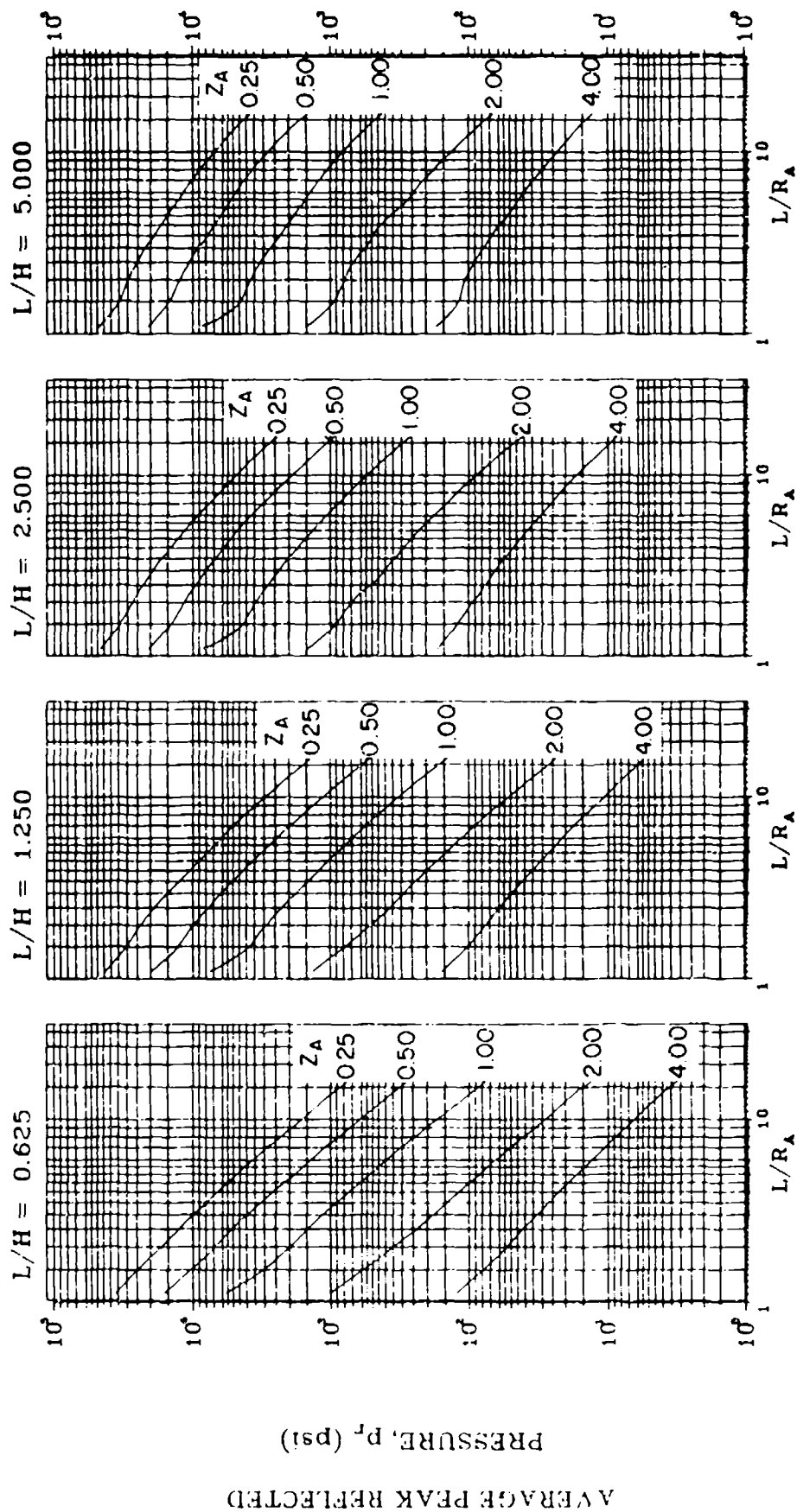


Figure 2-83 Average peak reflected pressure ($N = 3$, $\ell/L = 0.10$, $h/H = 0.25$)

AVERAGE PEAK REFLECTED
PRESSURE, p_r (psi)

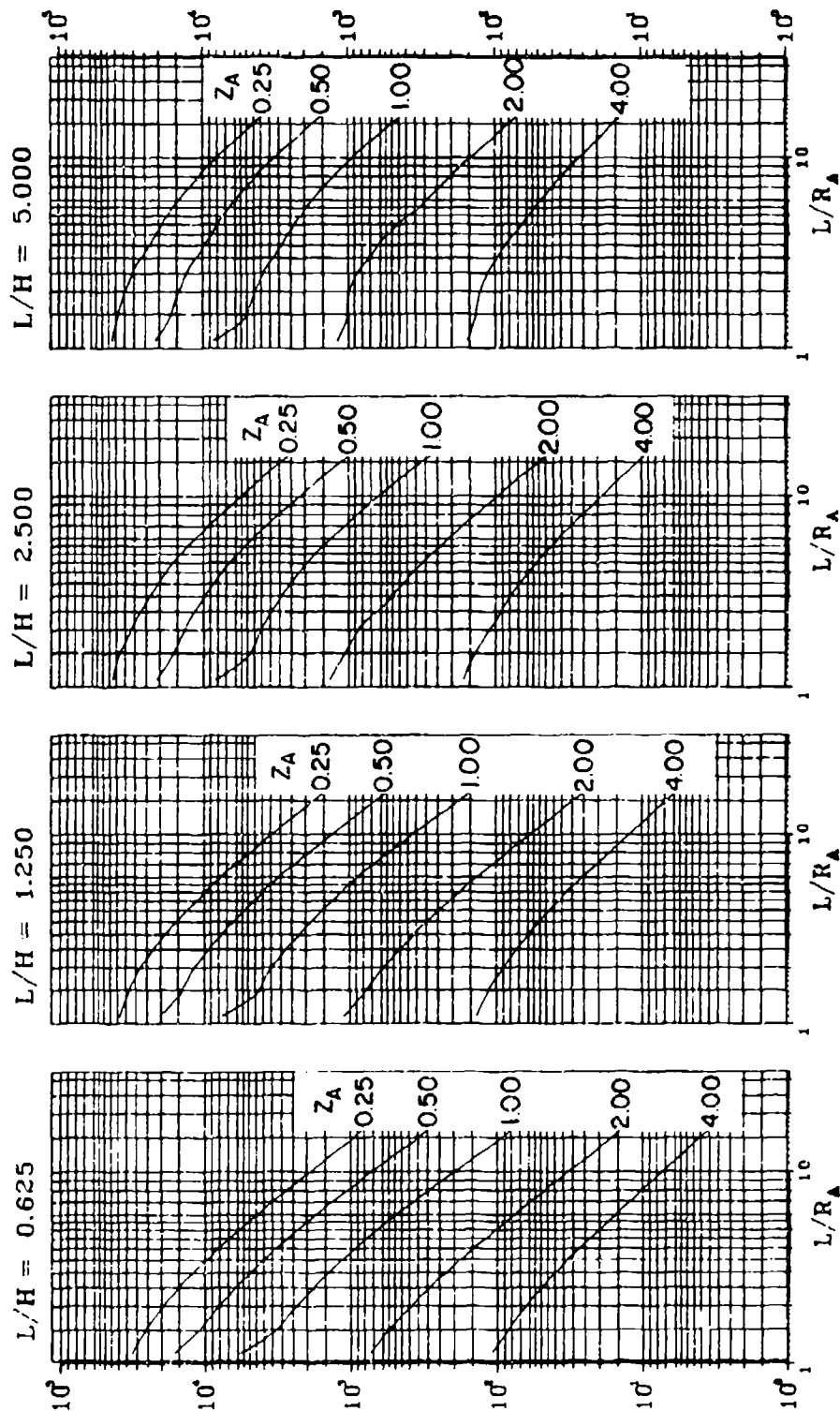


Figure 2-84 Average peak reflected pressure ($N = 3$, $\ell/L = 0.25$ and 0.75 , $h/H = 0.25$)

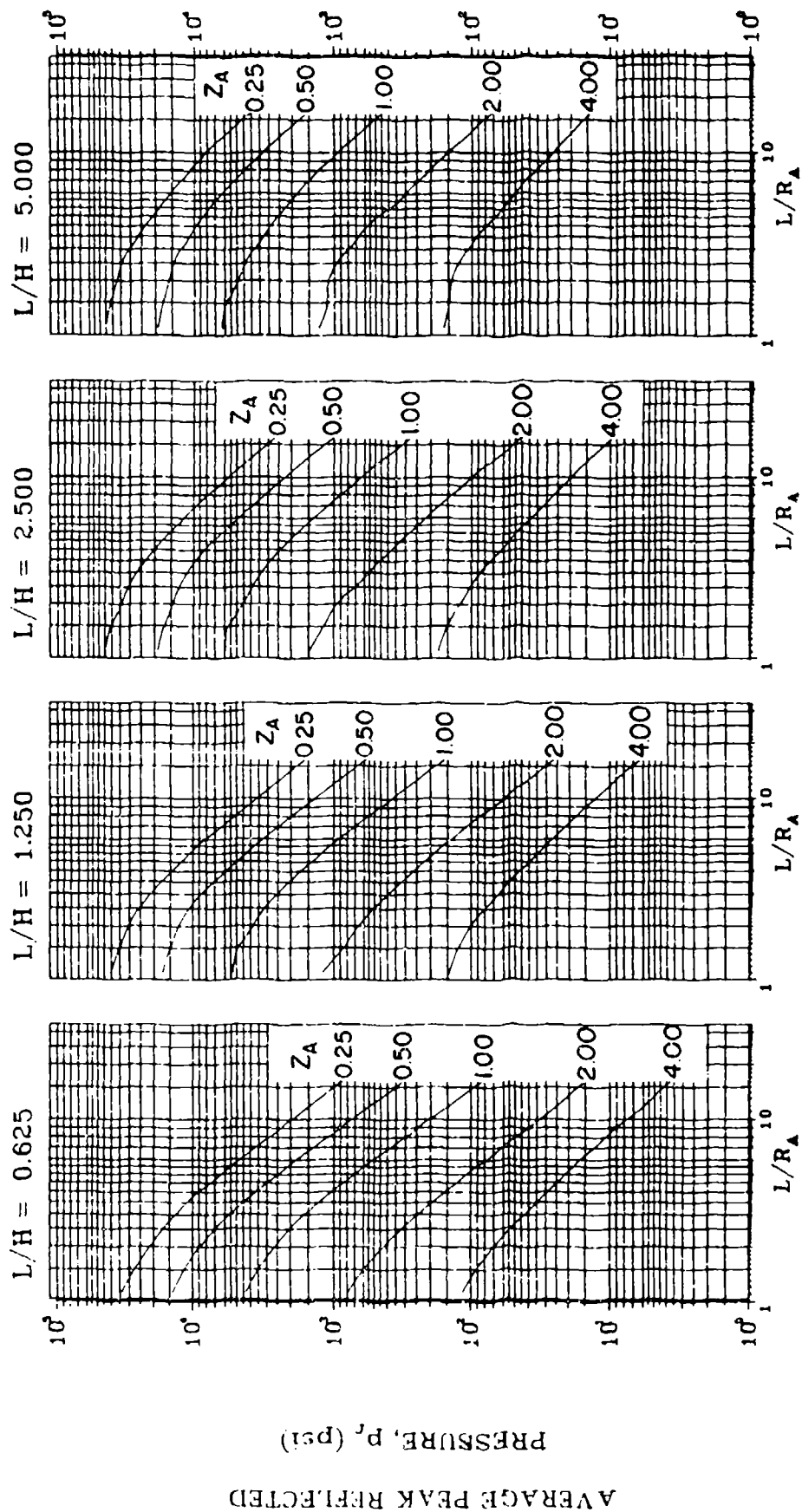


Figure 2-85 Average peak reflected pressure ($N = 3$, $\ell/L = 0.50$, $h/H = 0.25$)

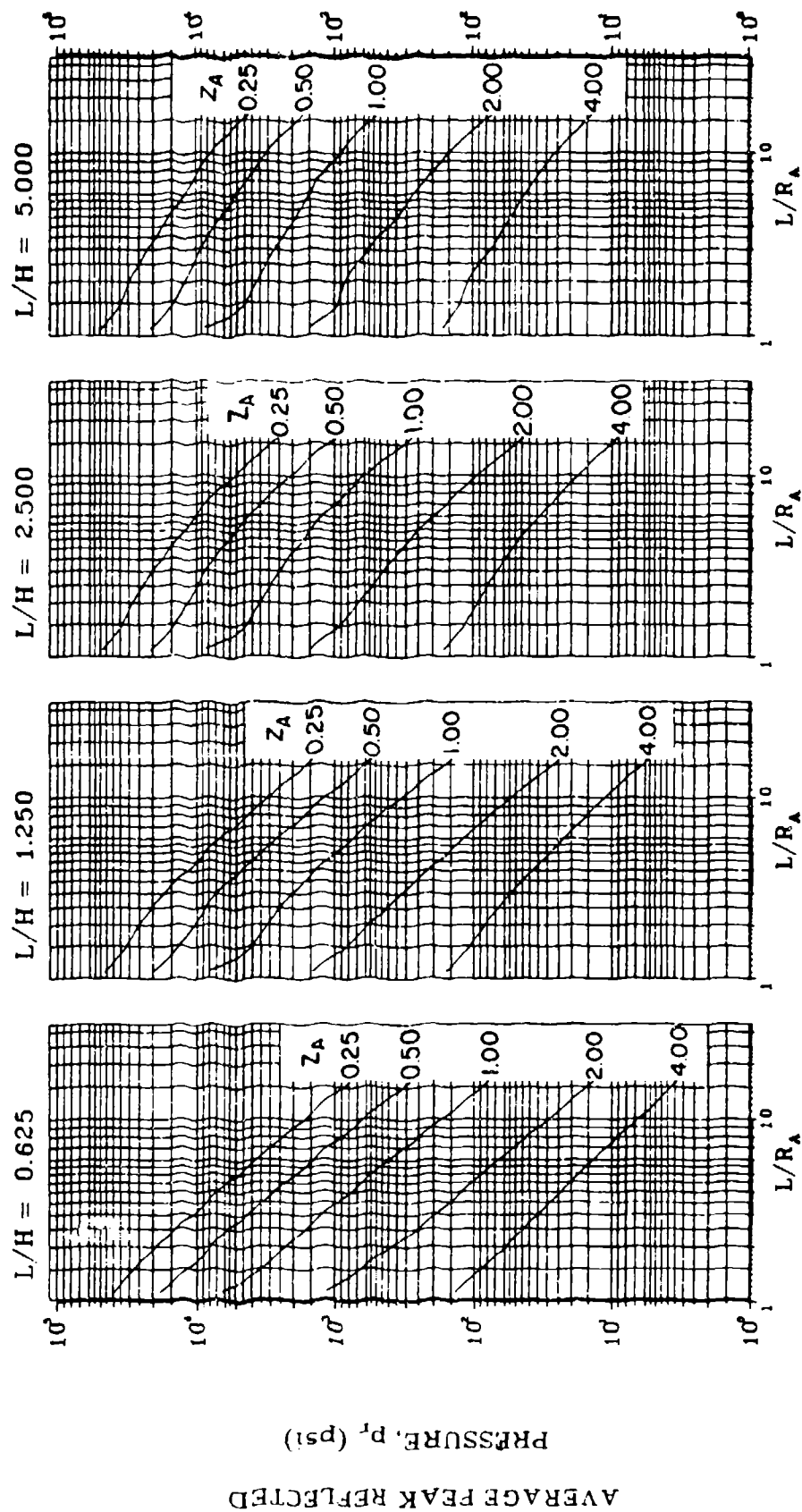


Figure 2-86 Average peak reflected pressure ($N = 3$, $\ell/L = 0.10$, $h/H = 0.50$)

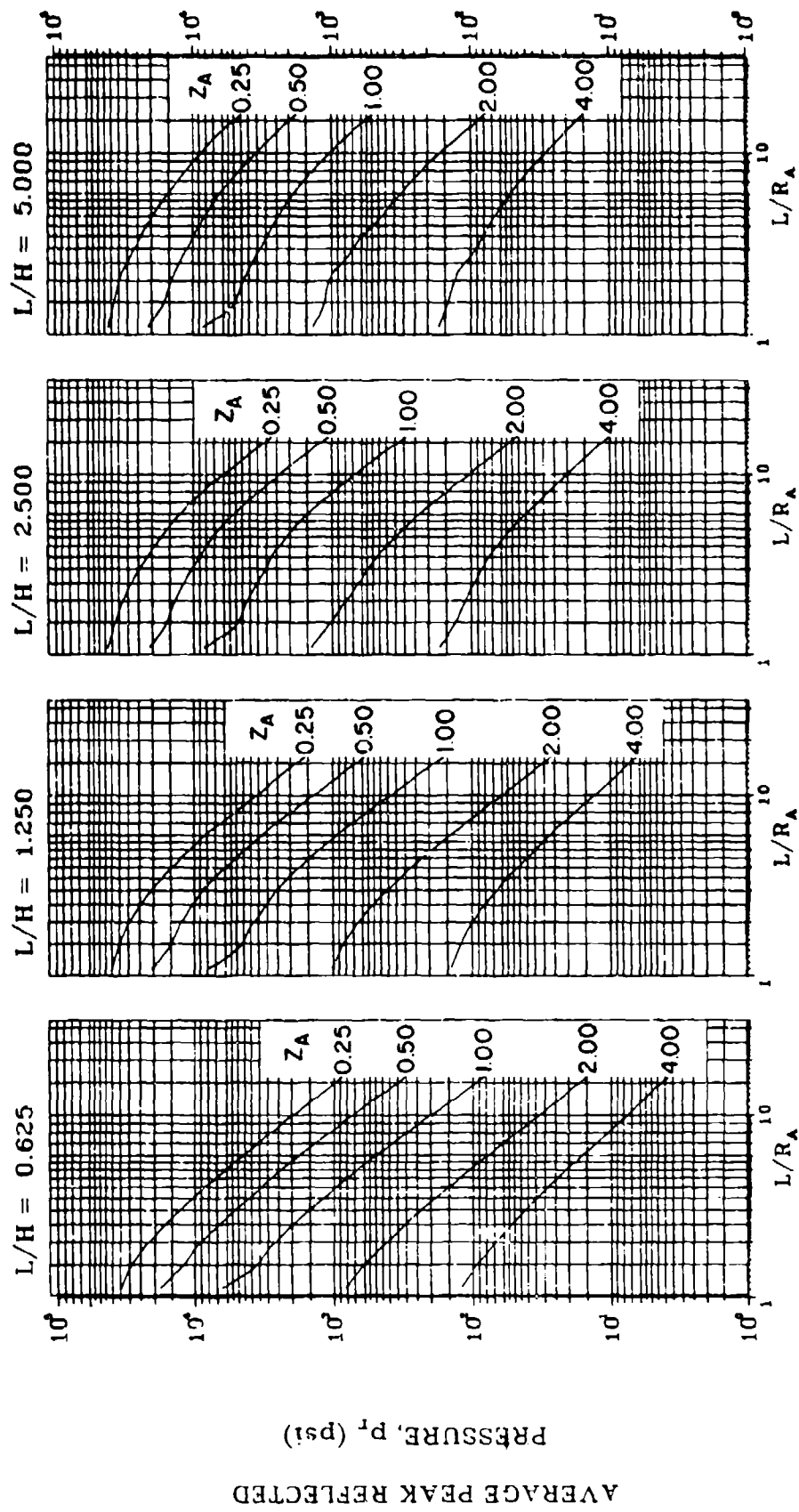


Figure 2-87 Average peak reflected pressure ($N = 3$, $\ell/L = 0.25$ and 0.75 , $h/H = 0.50$)

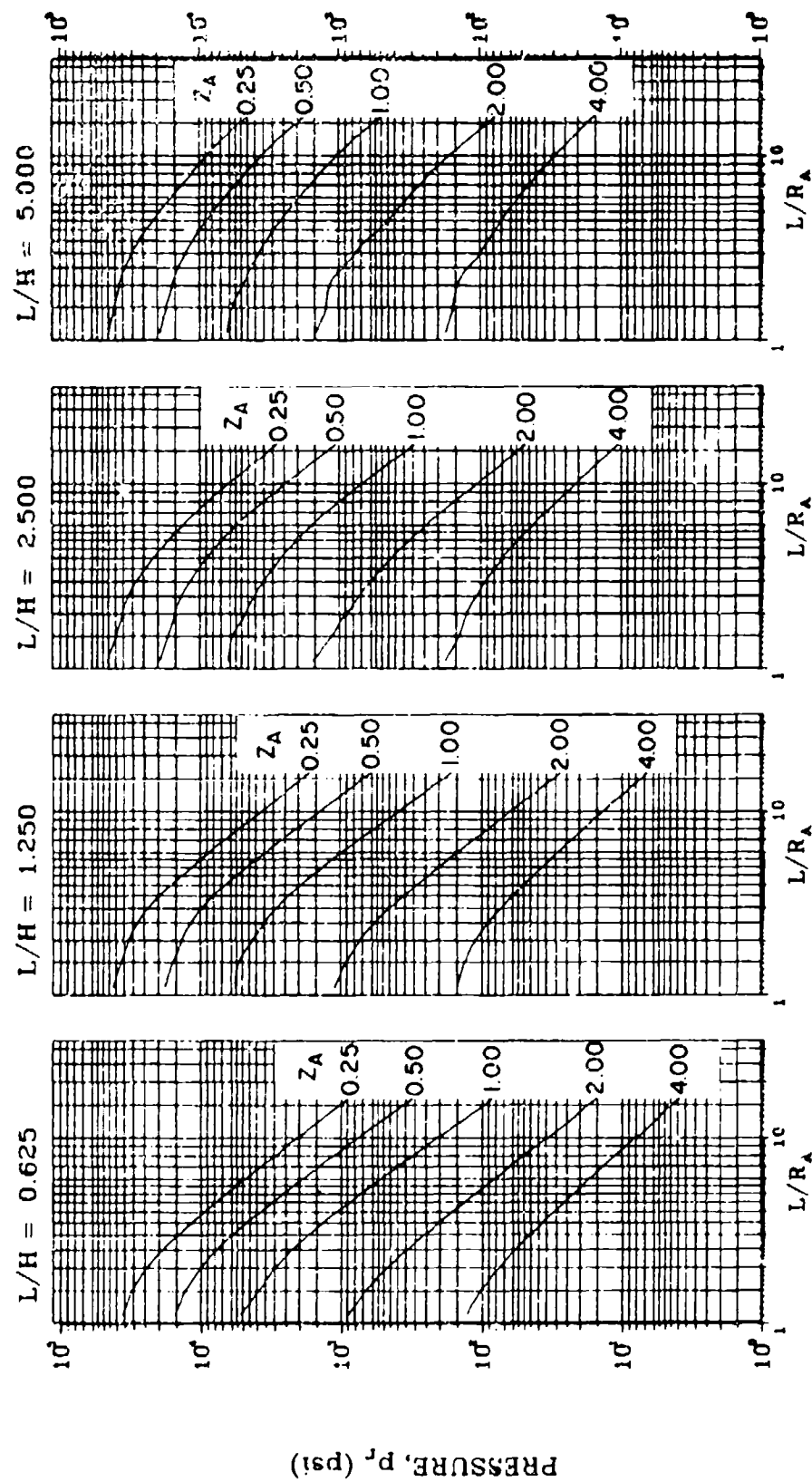


Figure 2-88 Average peak reflected pressure ($N = 3$, $\ell/L = 0.50$, $h/H = 0.50$)

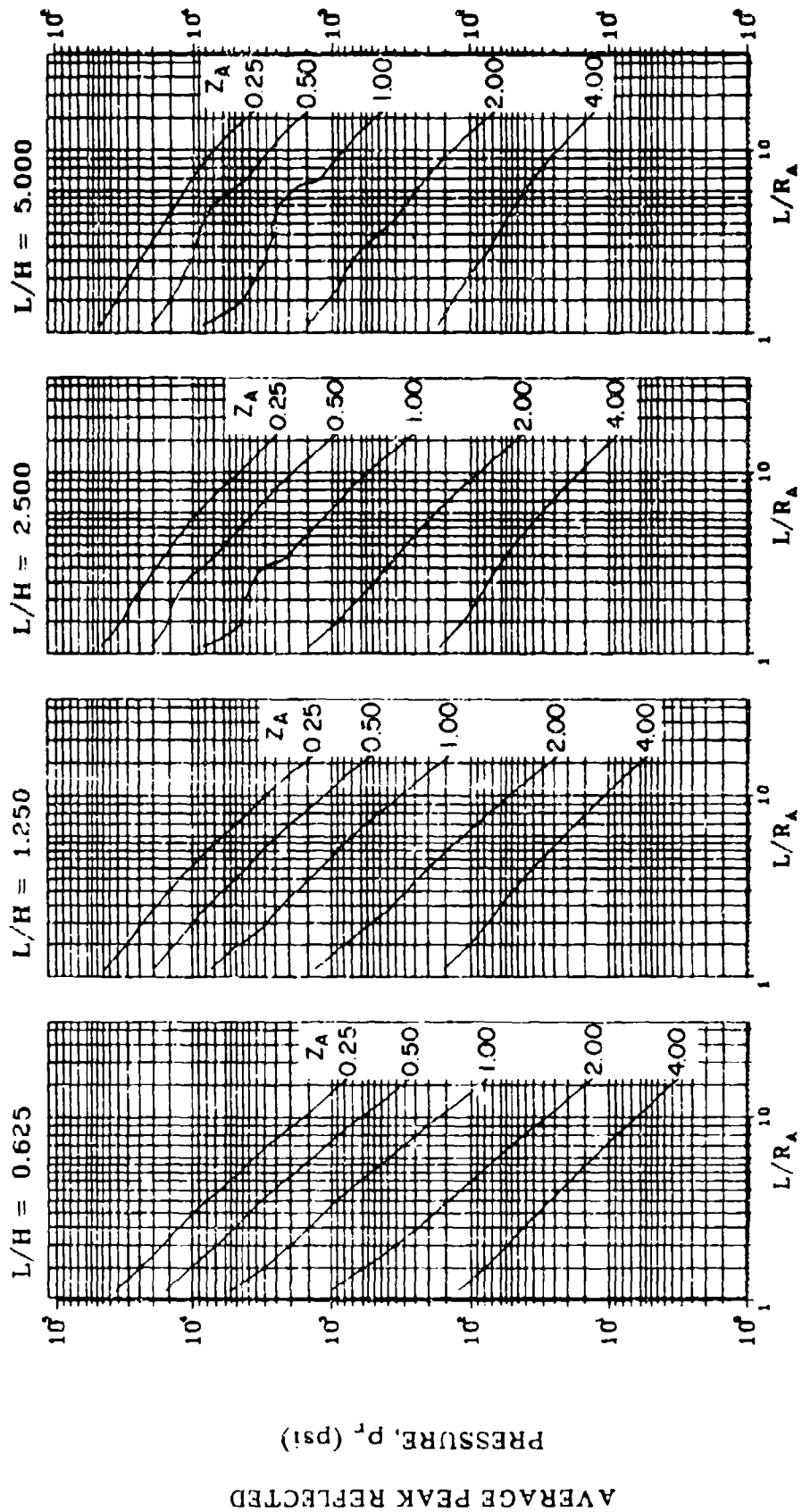


Figure 2-89 Average peak reflected pressure ($N = 3$, $\ell/L = 0.10$, $h/H = 0.75$)

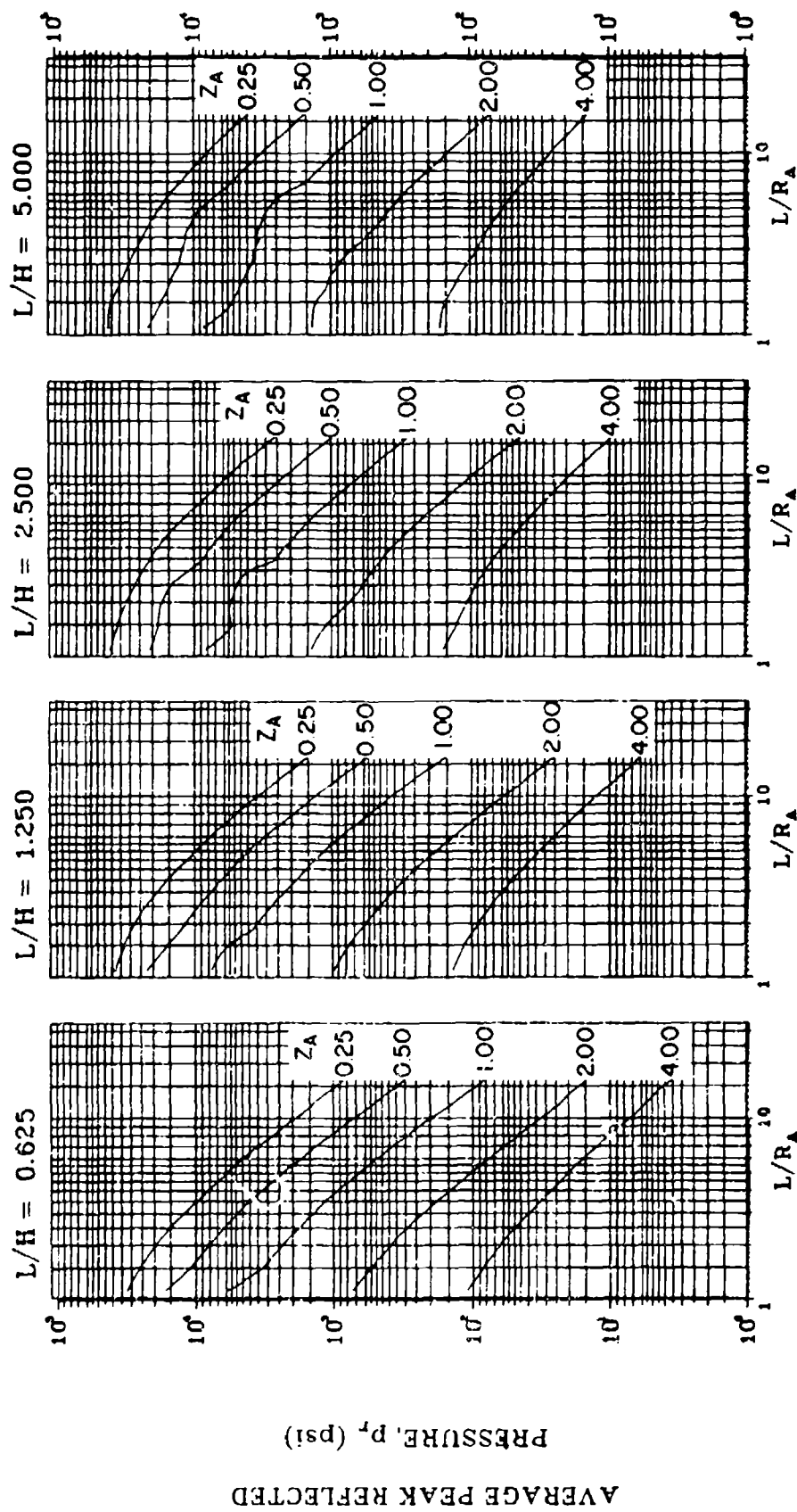


Figure 2-90 Average peak reflected pressure ($N = 3$, $\lambda/L = 0.25$ and 0.75 , $h/H = 0.75$)

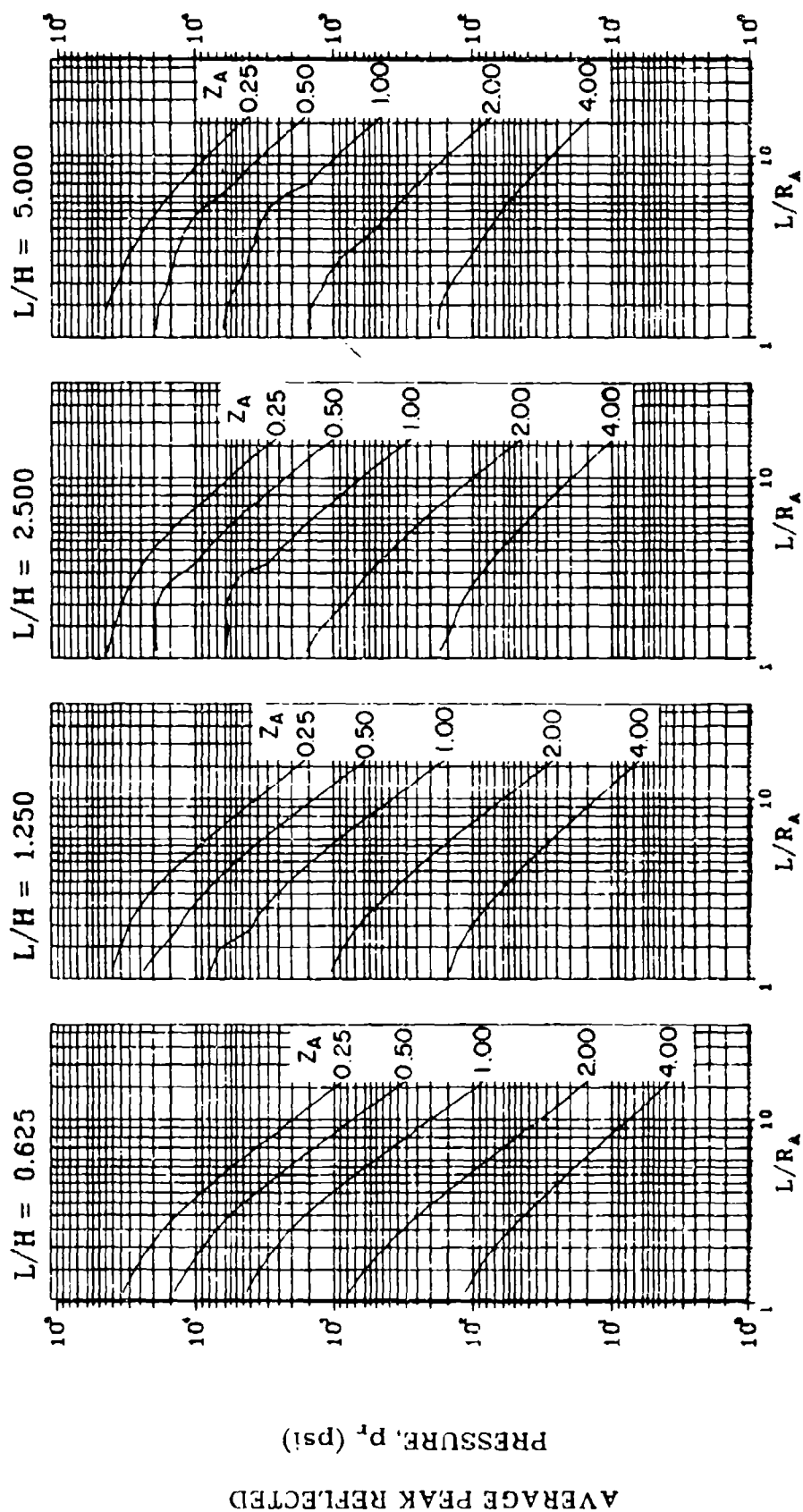


Figure 2-91 Average peak reflected pressure ($N = 3$, $l/L = 0.50$, $h/H = 0.75$)

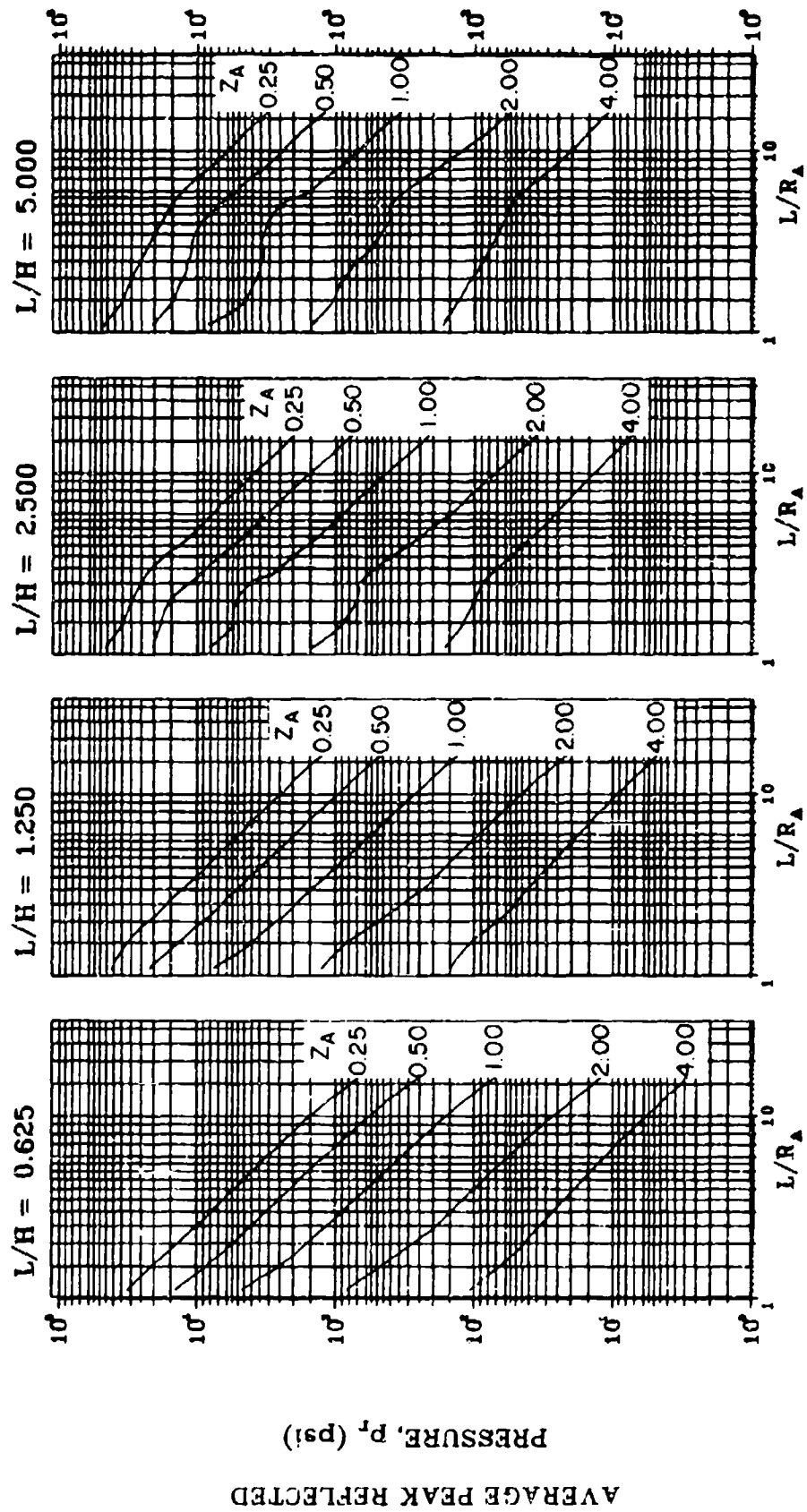


Figure 2-92 Average peak reflected pressure ($N = 4$, $l/L \approx 0.10$, $h/H = 0.10$)

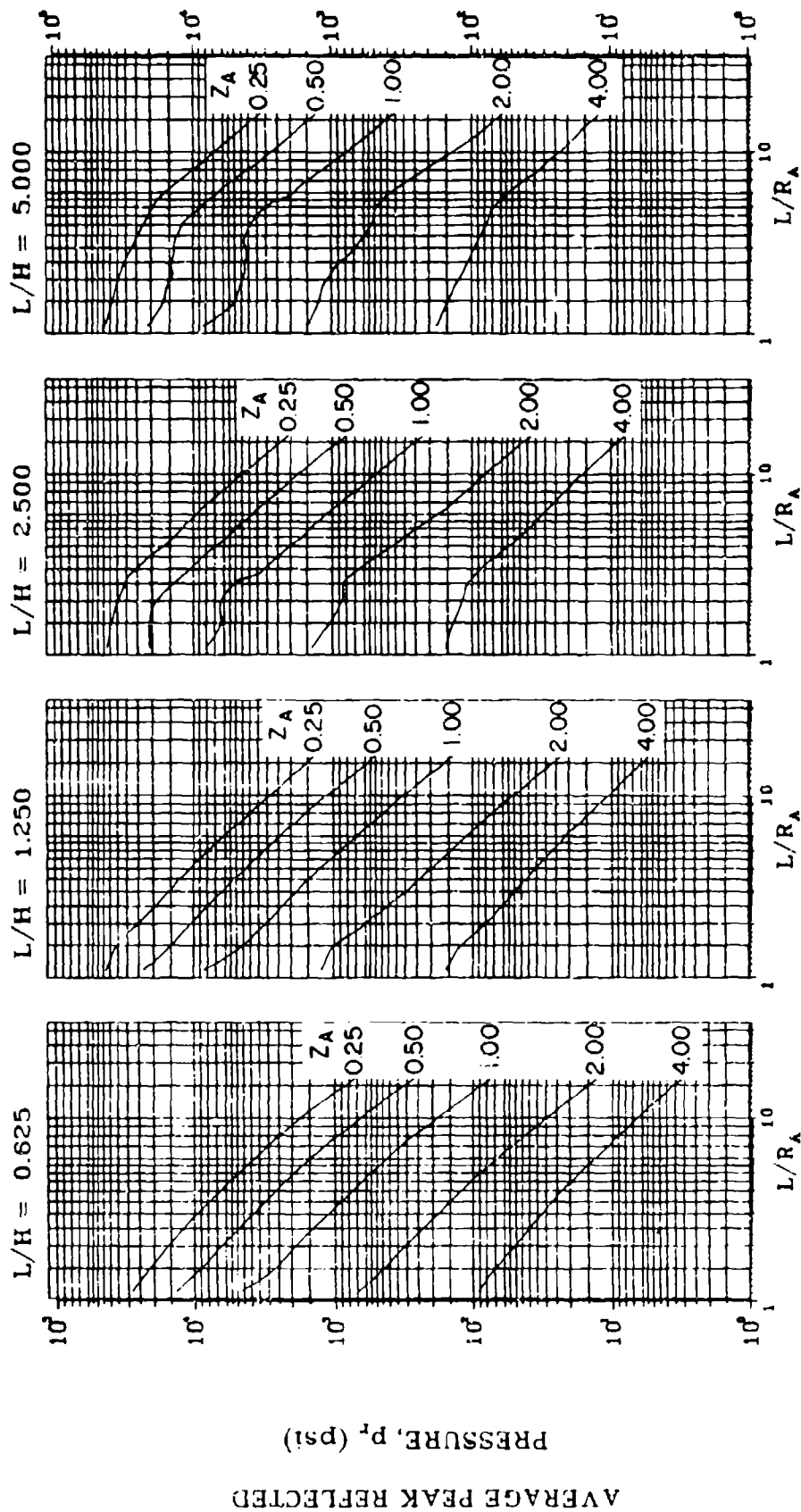


Figure 2-93 Average peak reflected pressure ($N = 4$, $\ell/L = 0.25$ and 0.75 , $h/H = 0.10$)

AVERAGE PEAK REFLECTED
PRESSURE, p_r (psi)

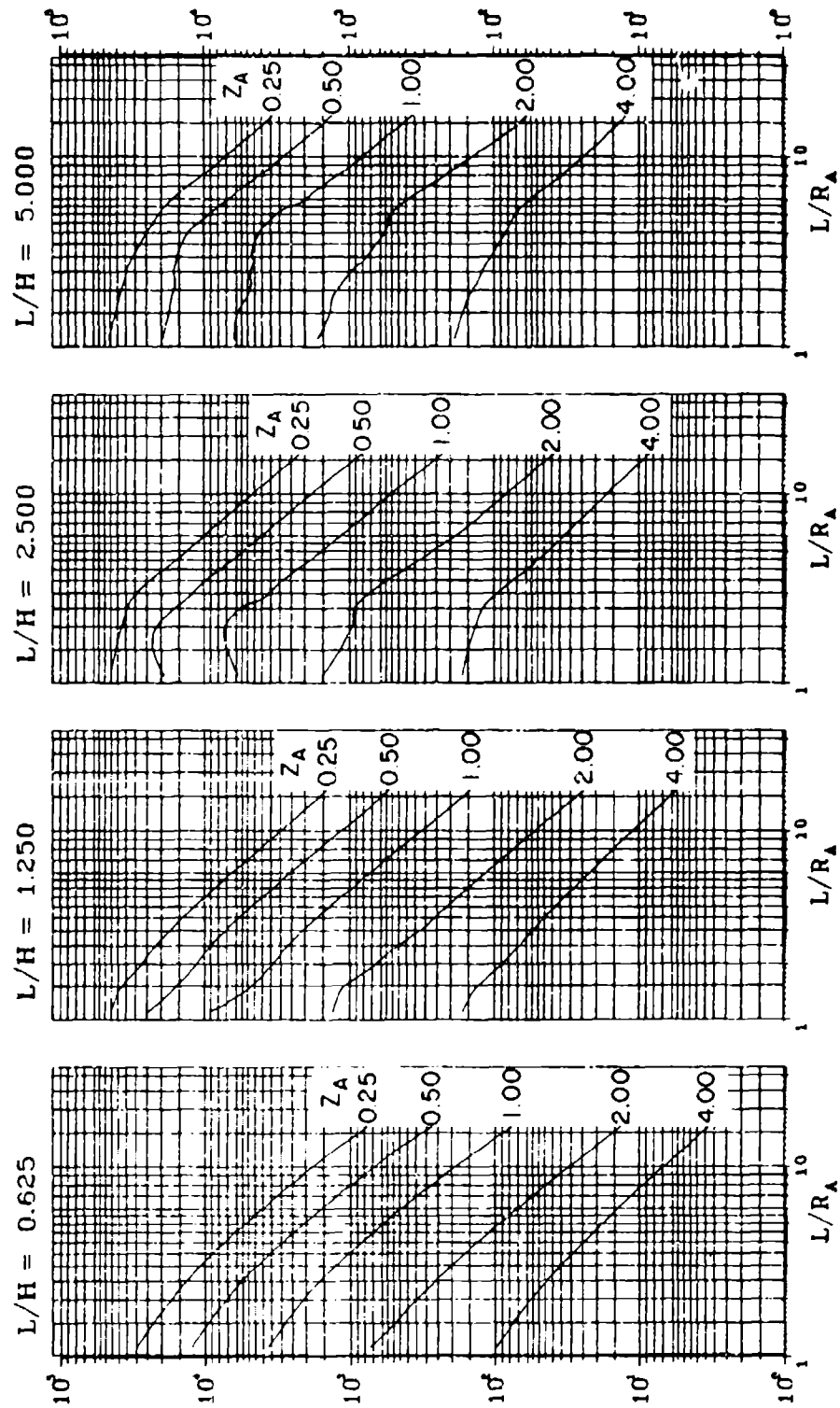


Figure 2-94 Average peak reflected pressure ($N = 4$, $\ell/L = 0.50$, $h/H = 0.10$)

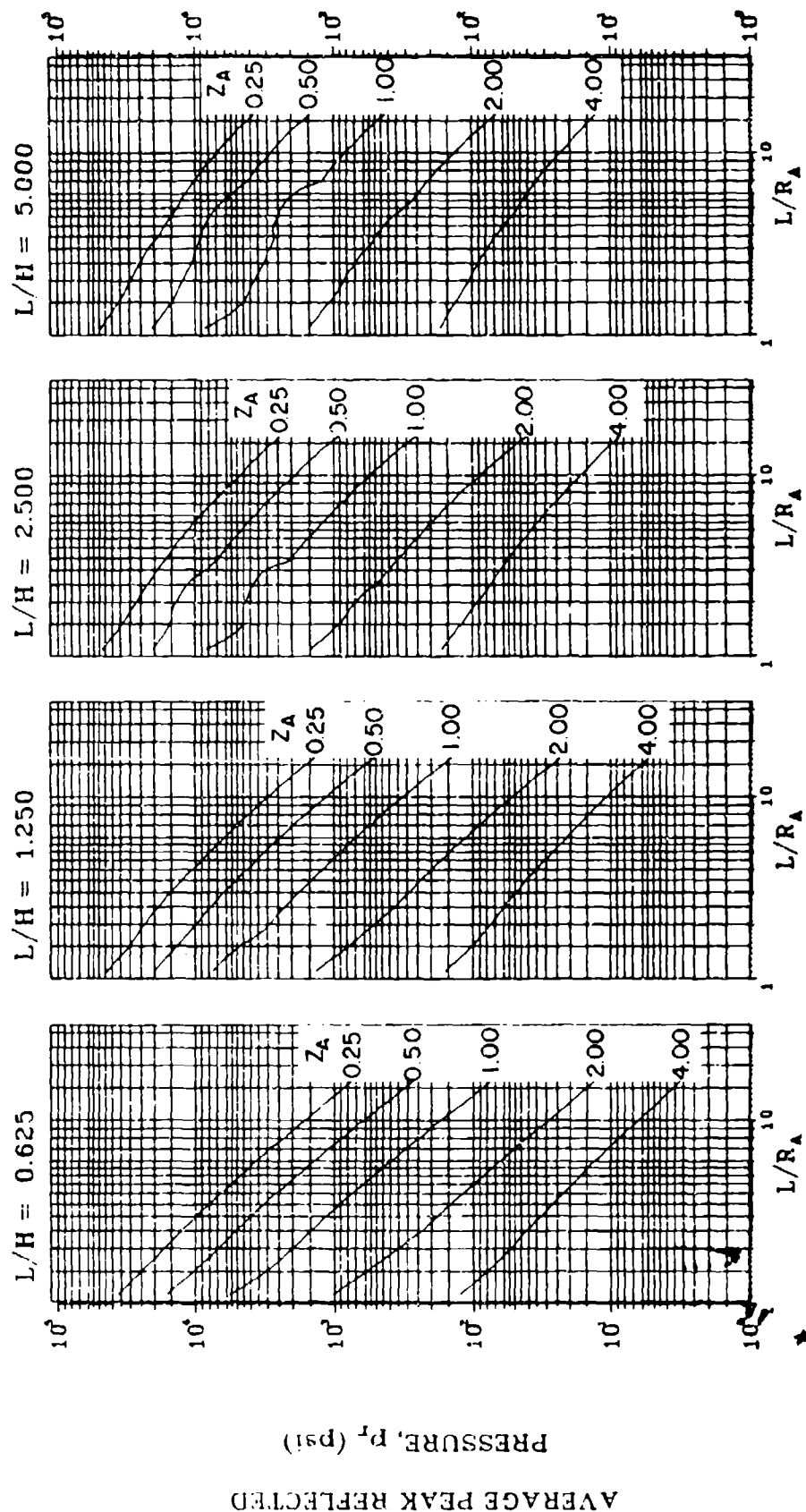


Figure 2-95 Average peak reflected pressure ($N = 4$, $\ell/L = 0.10$, $h/H = 0.25$ and 0.75)

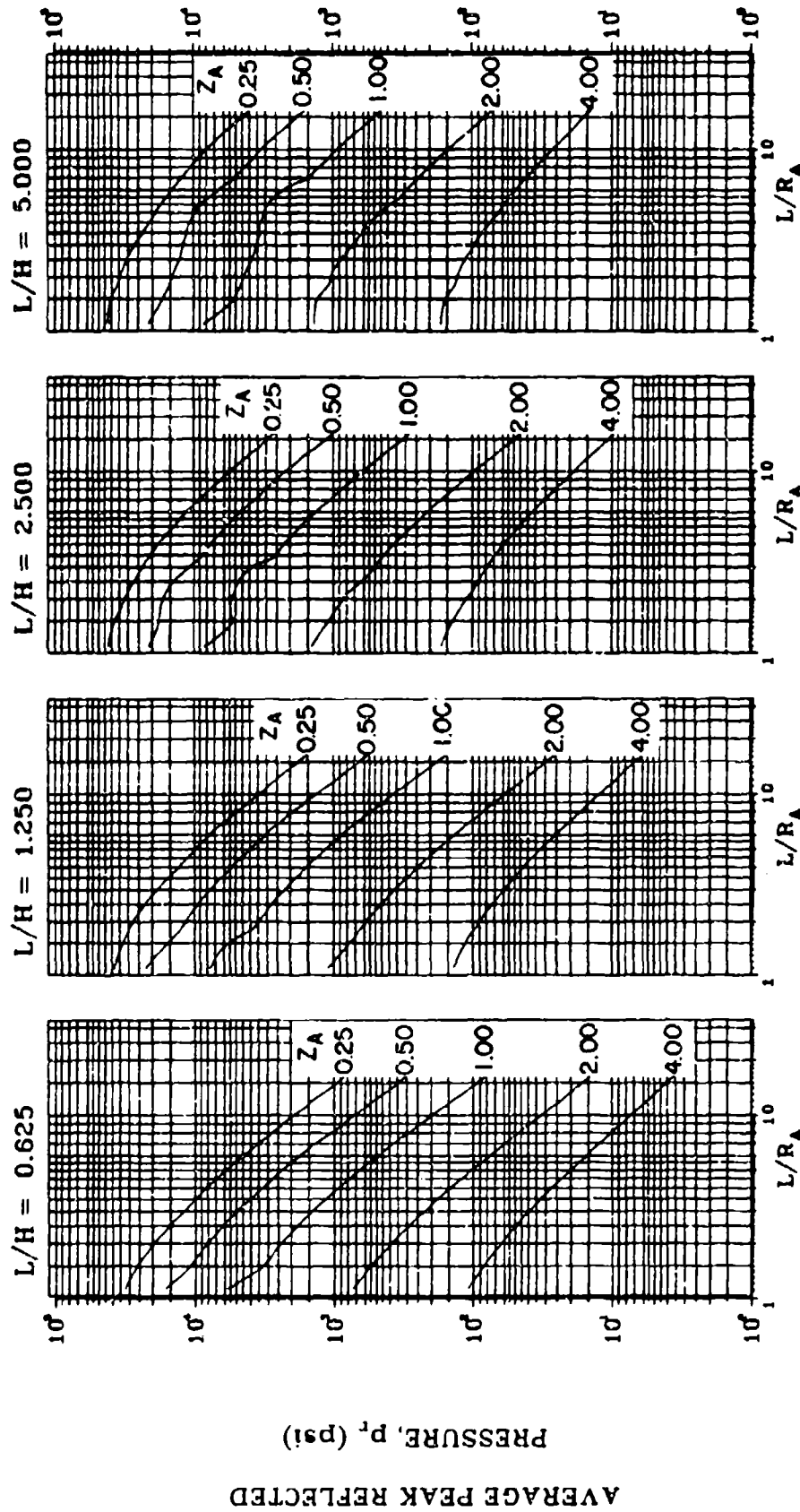


Figure 2-96 Average peak reflected pressure ($N = 4$, $\ell/L = 0.25$ and 0.75 , $h/H = 0.25$ and 0.75)

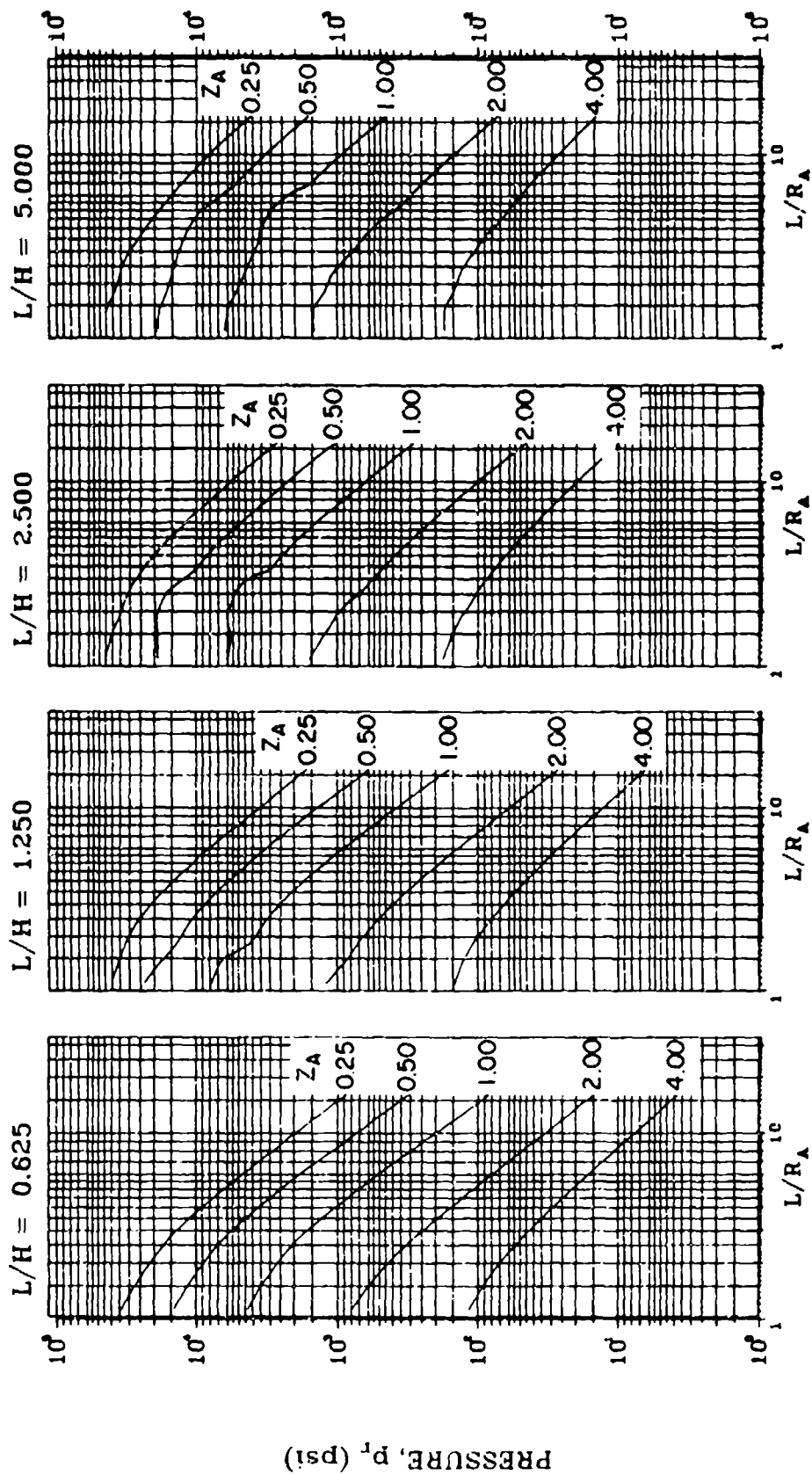


Figure 2-97 Average peak reflected pressure ($N = 4$, $z/L = 0.50$, $h/H = 0.25$ and 0.75)

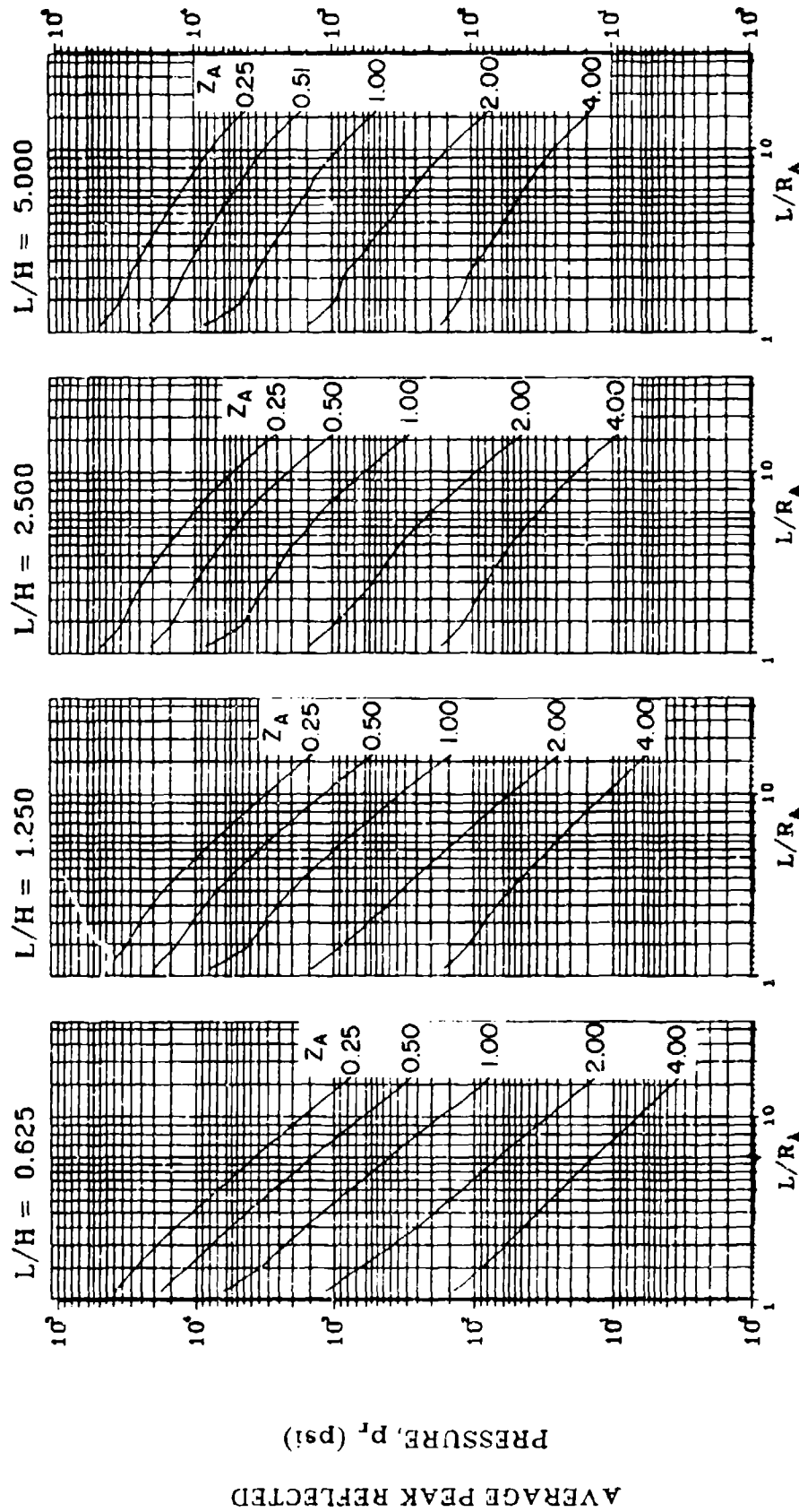


Figure 2-98 Average peak reflected pressure ($N = 4$, $\ell/L = 0.10$, $h/H = 0.50$)

AVERAGE PEAK REFLECTED
PRESSURE, p_r (psi)

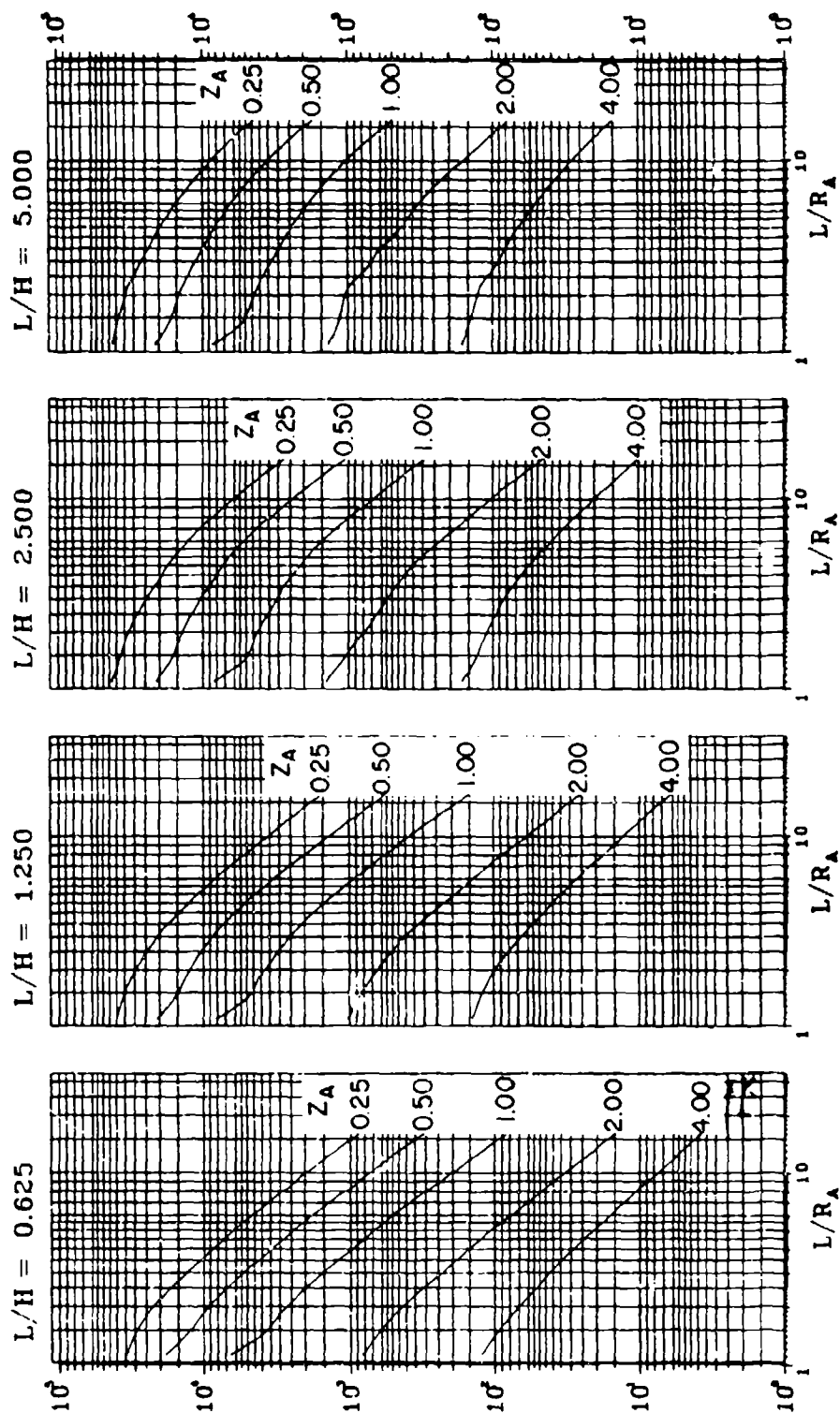


Figure 2-99 Average peak reflected pressure
($N = 4$, $L/L = 0.25$ and 0.75 , $h/H = 0.50$)

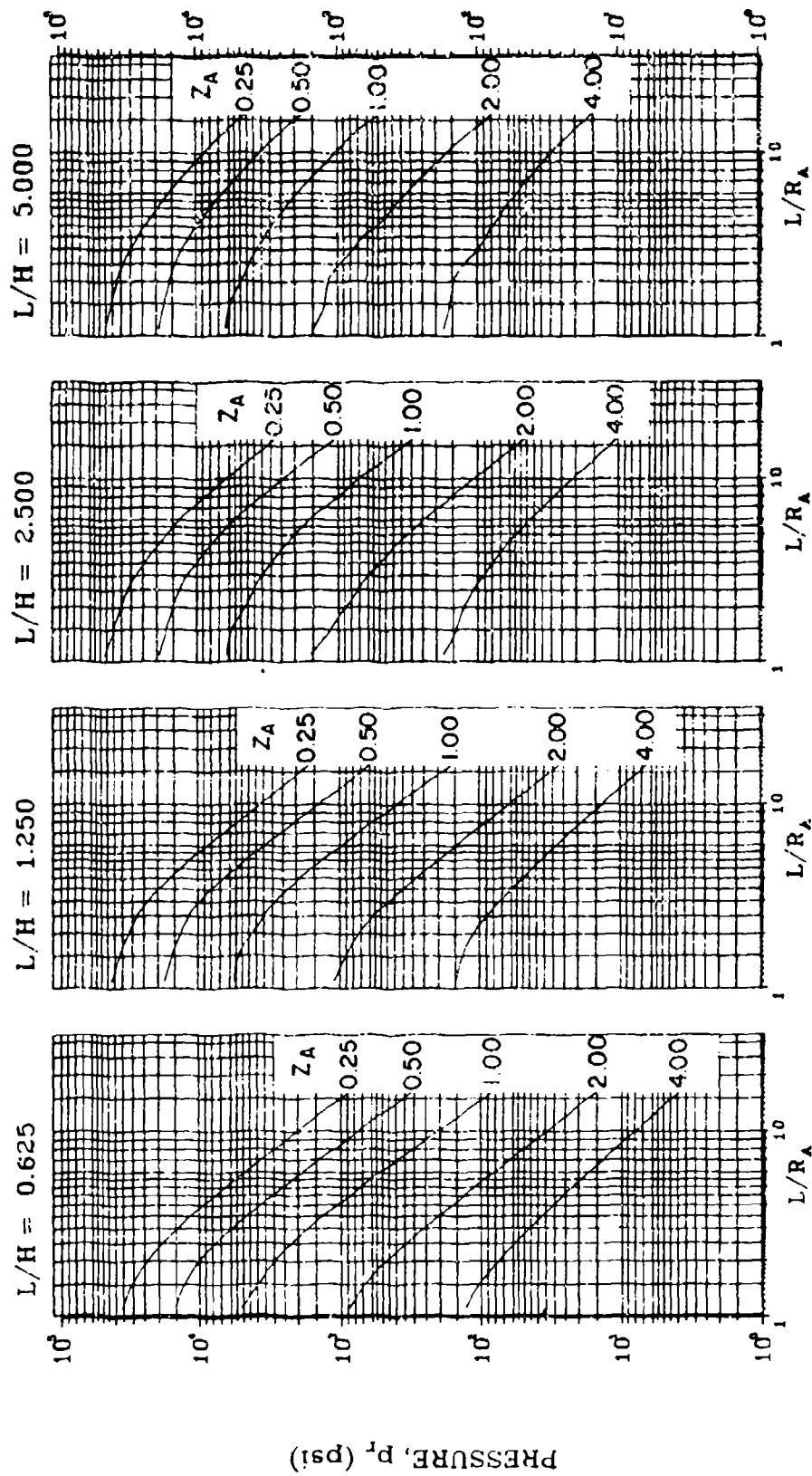


Figure 2-100 Average peak reflected pressure ($N = 4$, $\ell/L = 0.50$, $h/H = 0.50$)

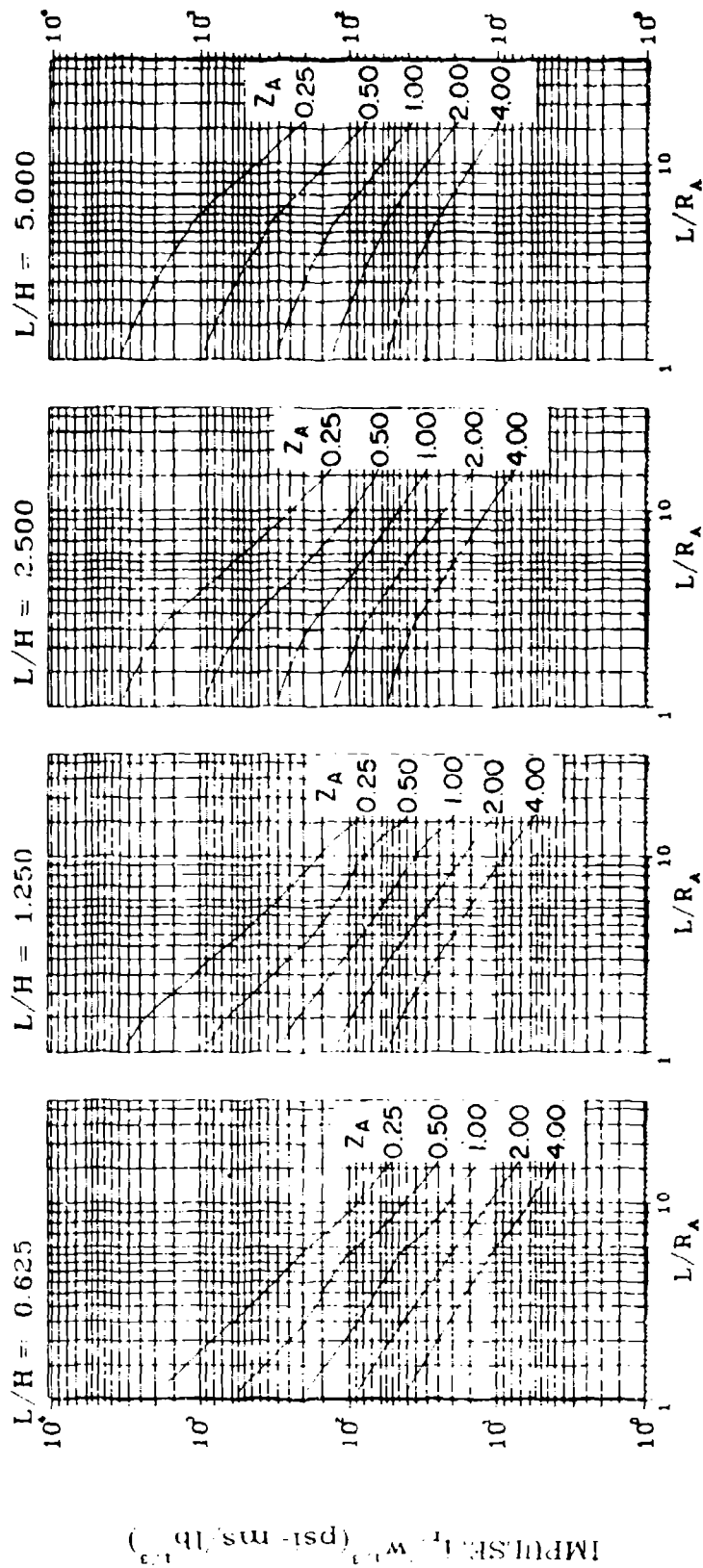


Figure 2-101 Scaled average unit reflected impulse
($N = 1$, $\ell/L = 0.10$, $h/H = 0.10$)

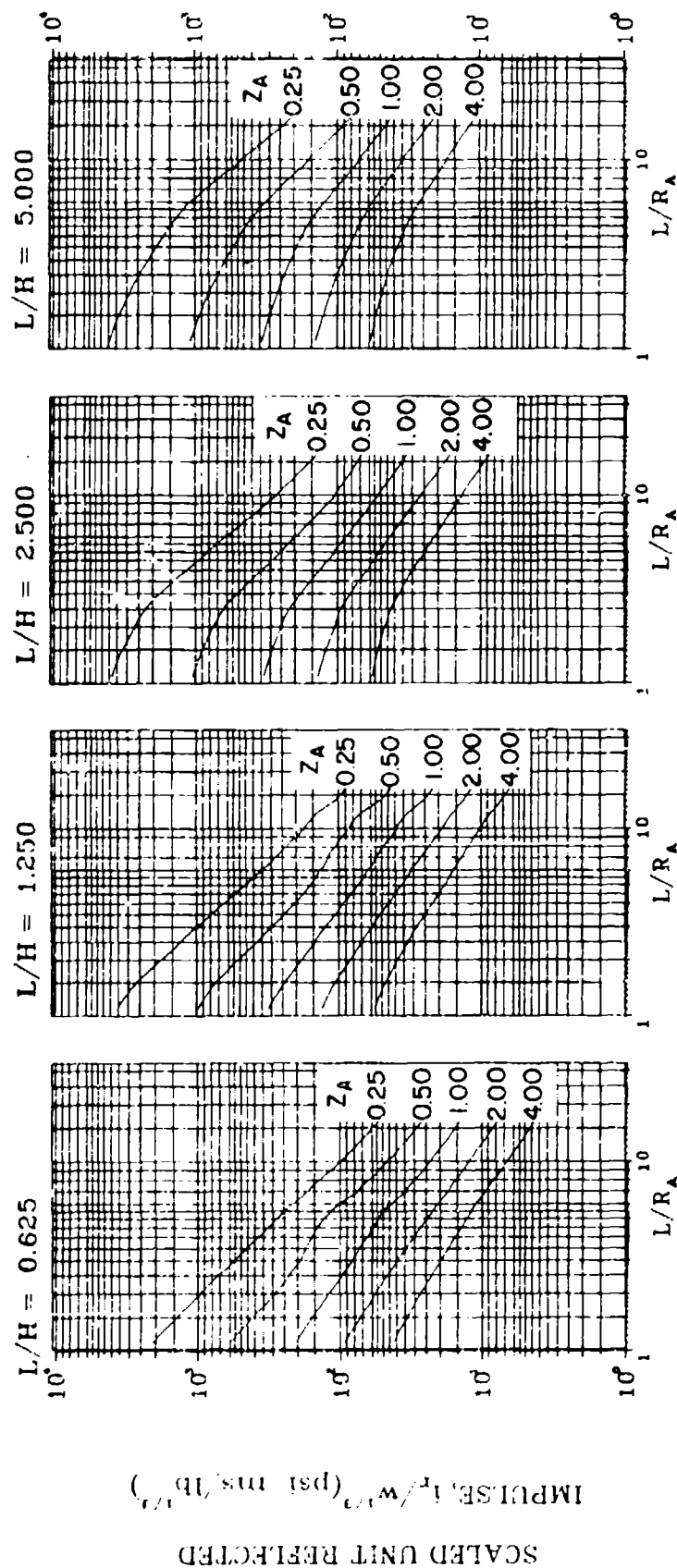


Figure 2-102 Scaled average unit reflected impulse
($N = 1$, $\ell/L = 0.25$ and 0.75 , $h/H = 0.10$)

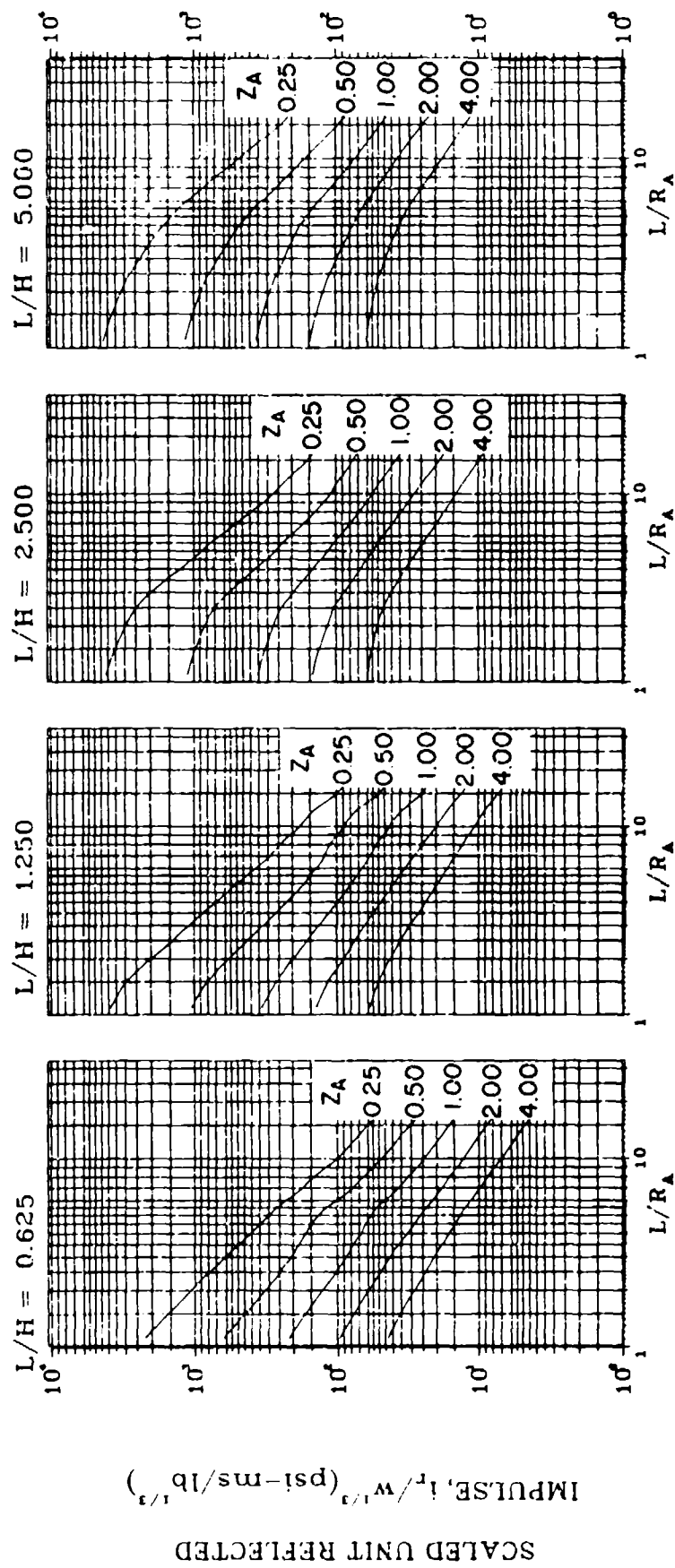


Figure 2-103 Scaled average unit reflected impulse
($N = 1, \ell/L = 0.50, h/H = 0.10$)

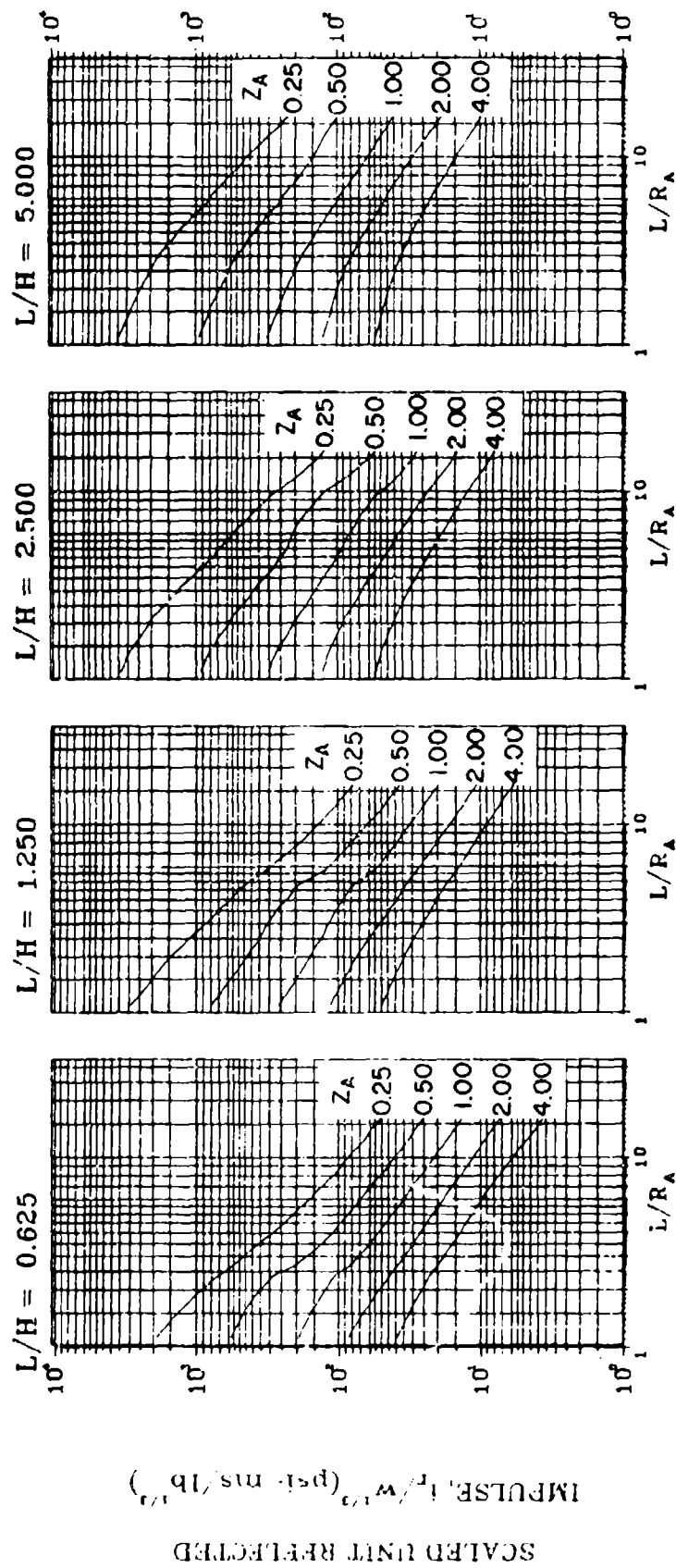


Figure 2-104 Scaled average unit reflected impulse
 $(N = 1, \ell/L = 0.10, h/H = 0.25)$

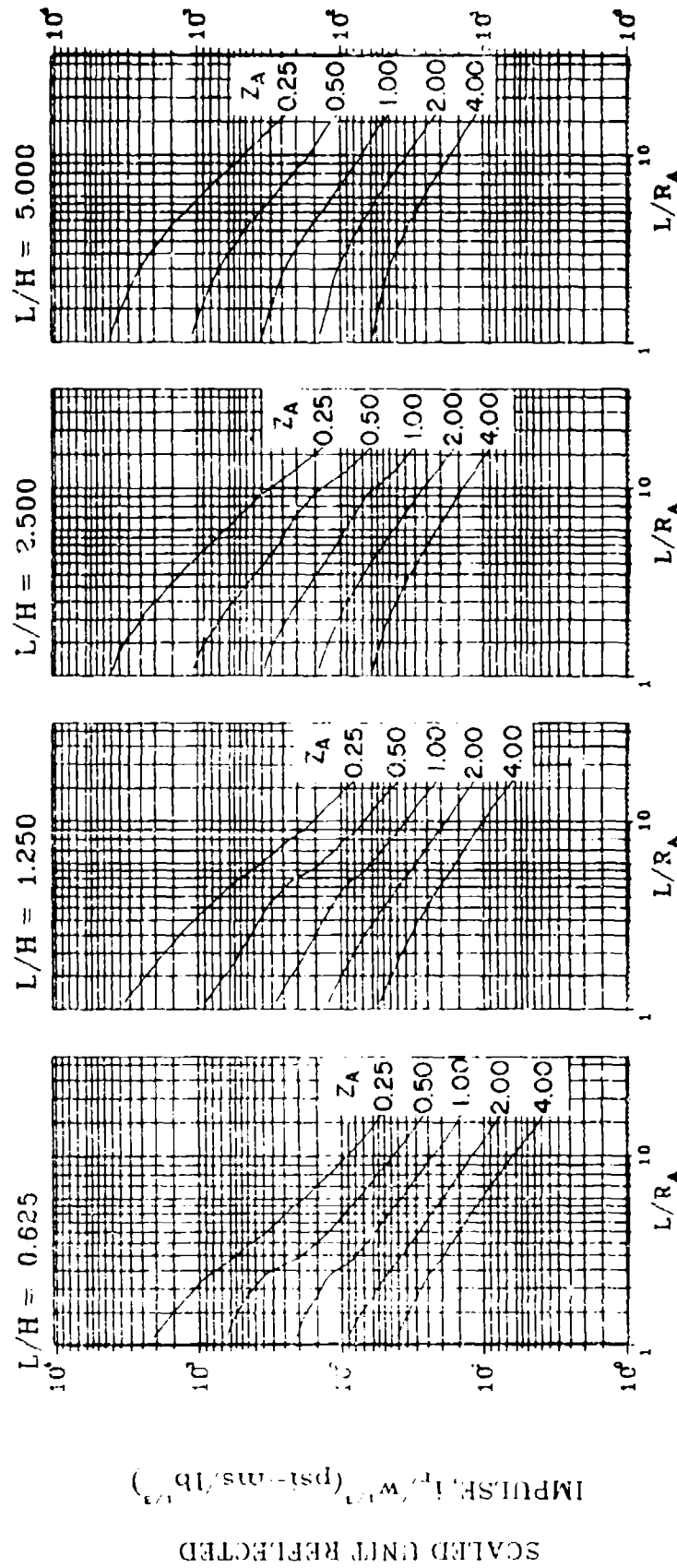


Figure 2-105 Scaled average unit reflected impulse
($N = 1$, $l/L = 0.25$ and 0.75 , $h/H = 0.25$)

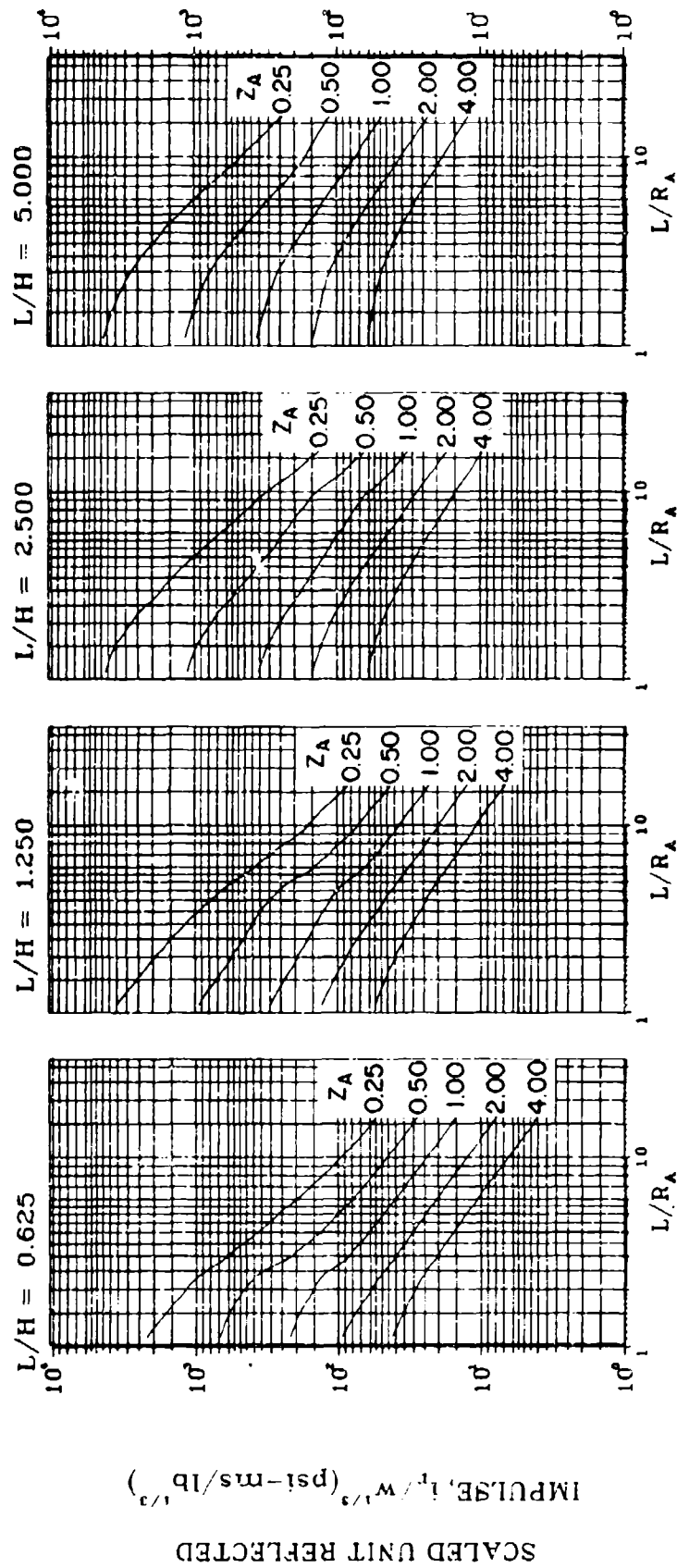


Figure 2-106 Scaled average unit reflected impulse
($N = 1, \ell/L = 0.50, h/H = 0.25$)

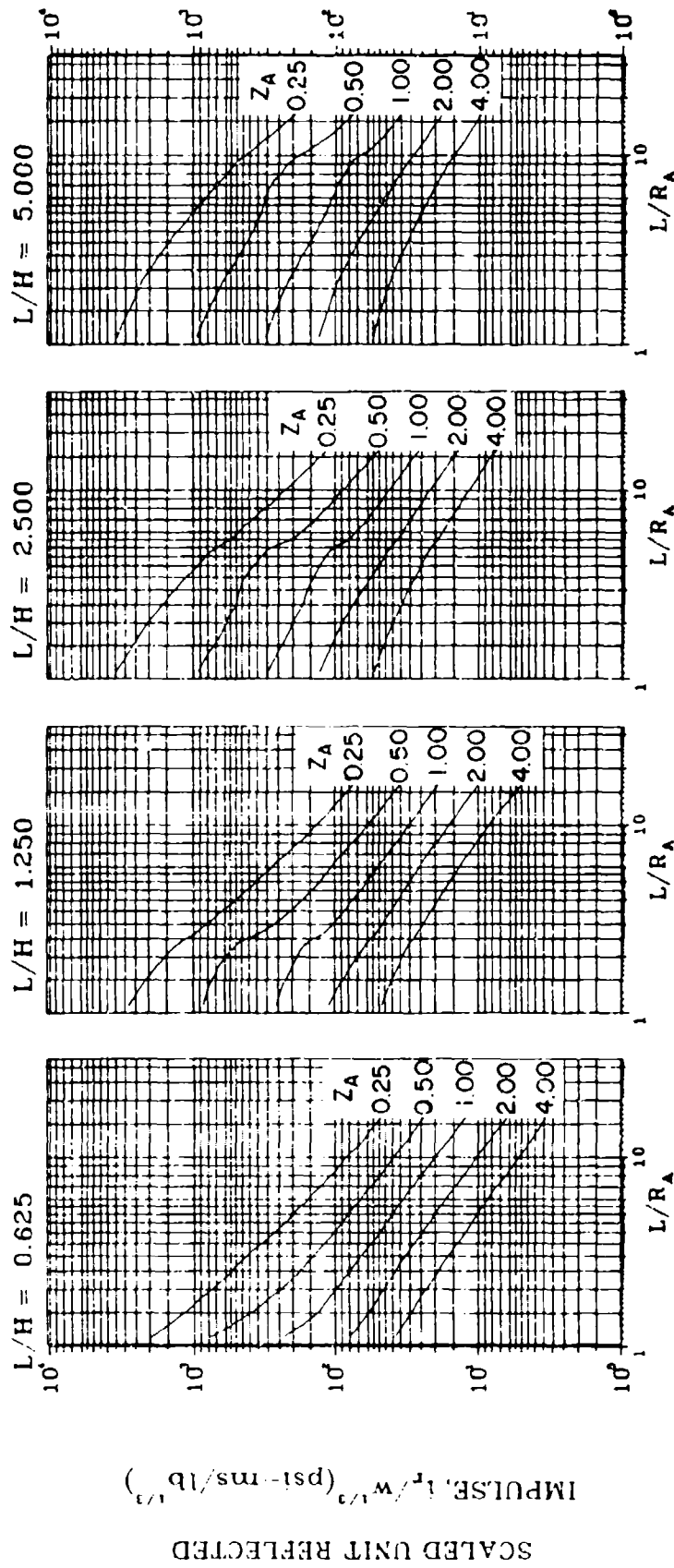


Figure 2-107 Scaled average unit reflected impulse
($N = 1$, $Q/L = 0.10$, $h/H = 0.50$)

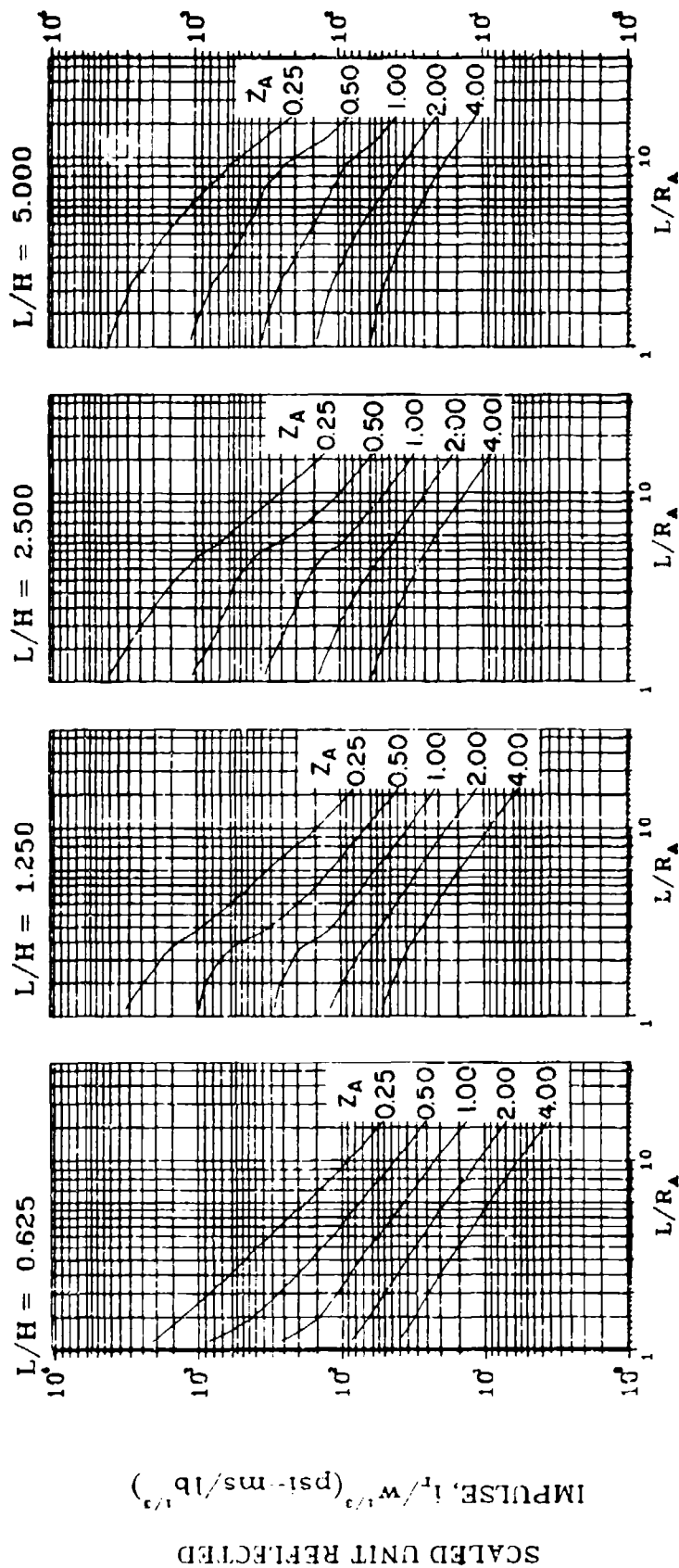


Figure 2-108 Scaled average unit reflected impulse
($N = 1$, $\ell/L = 0.25$ and 0.75 , $h/H = 0.50$)

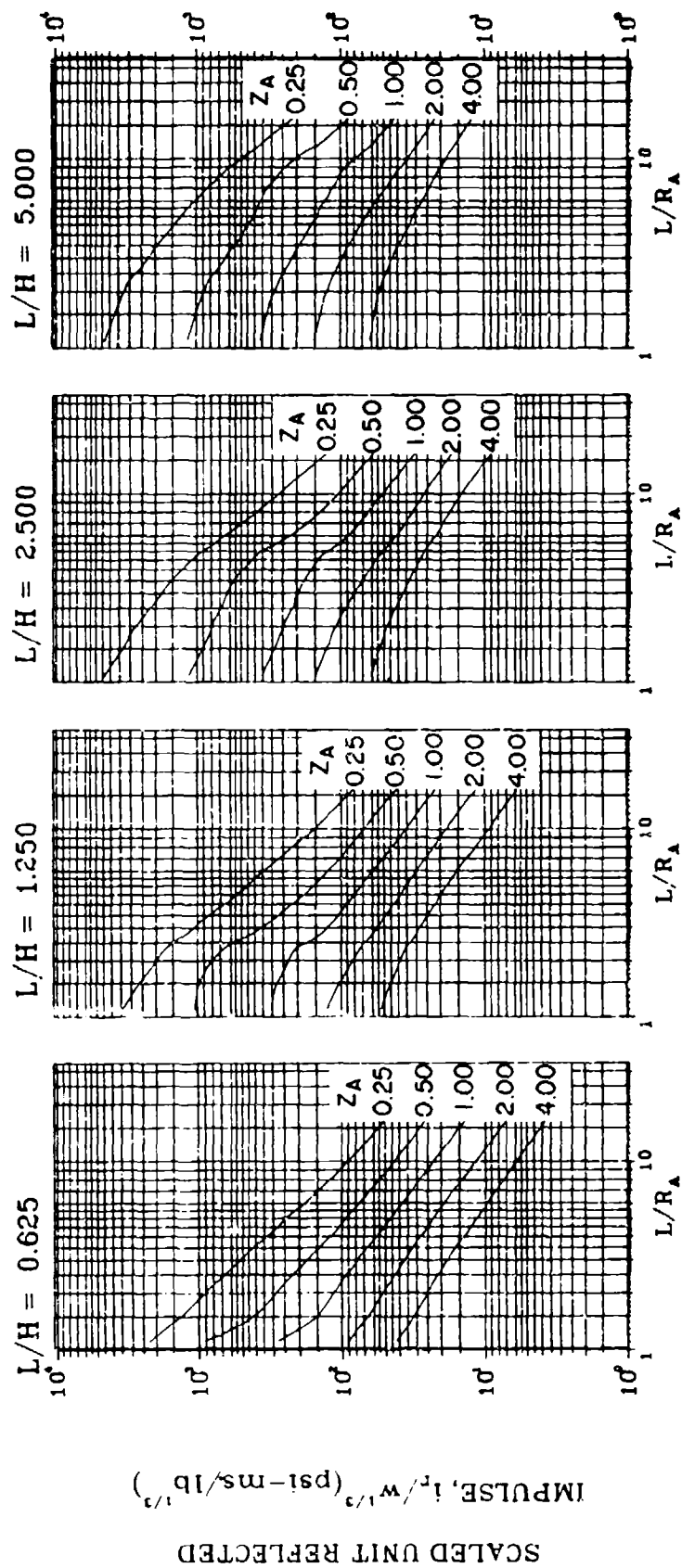


Figure 2-109 Scaled average unit reflected impulse
($N = 1$, $\ell/L = 0.50$, $h/H = 0.50$)

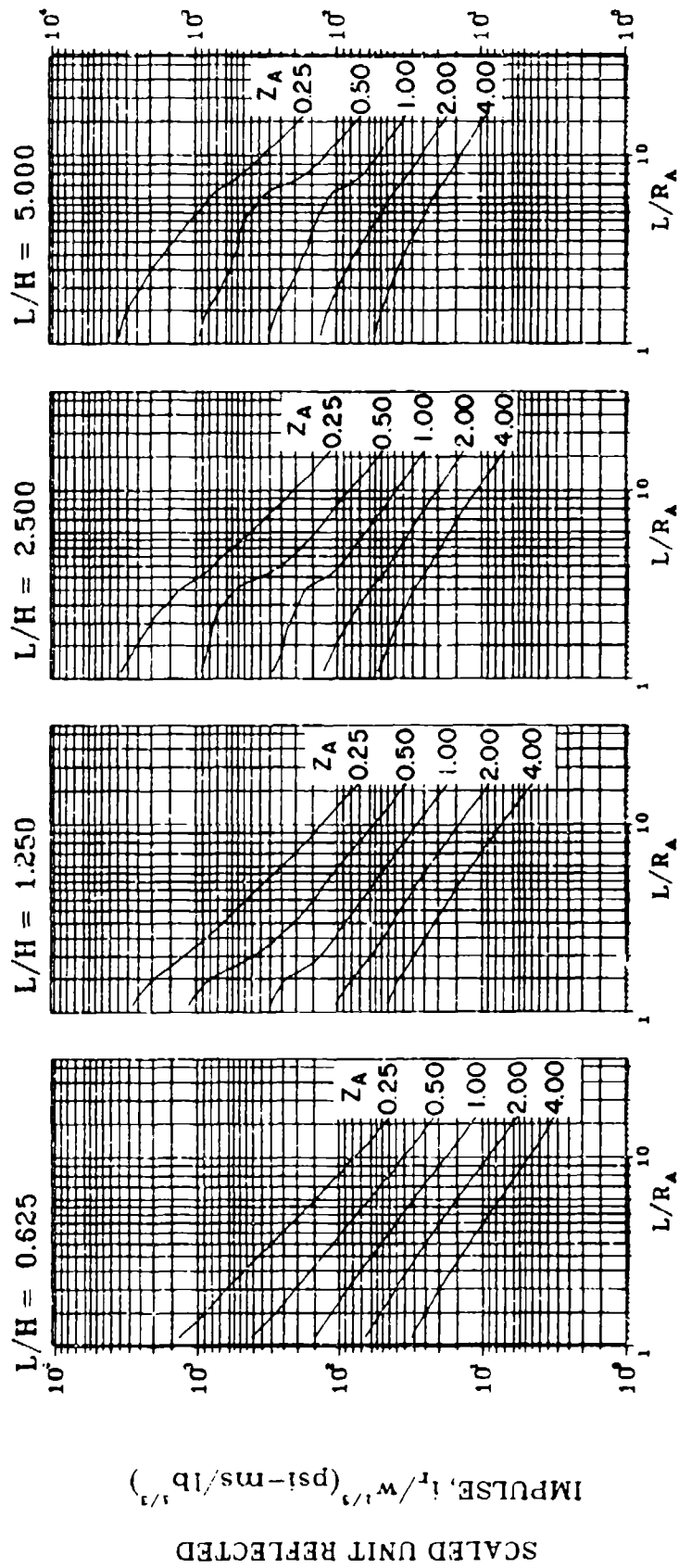


Figure 2-110 Scaled average unit reflected impulse
($N = 1$, $\ell/L = 0.10$, $h/H = 0.75$)

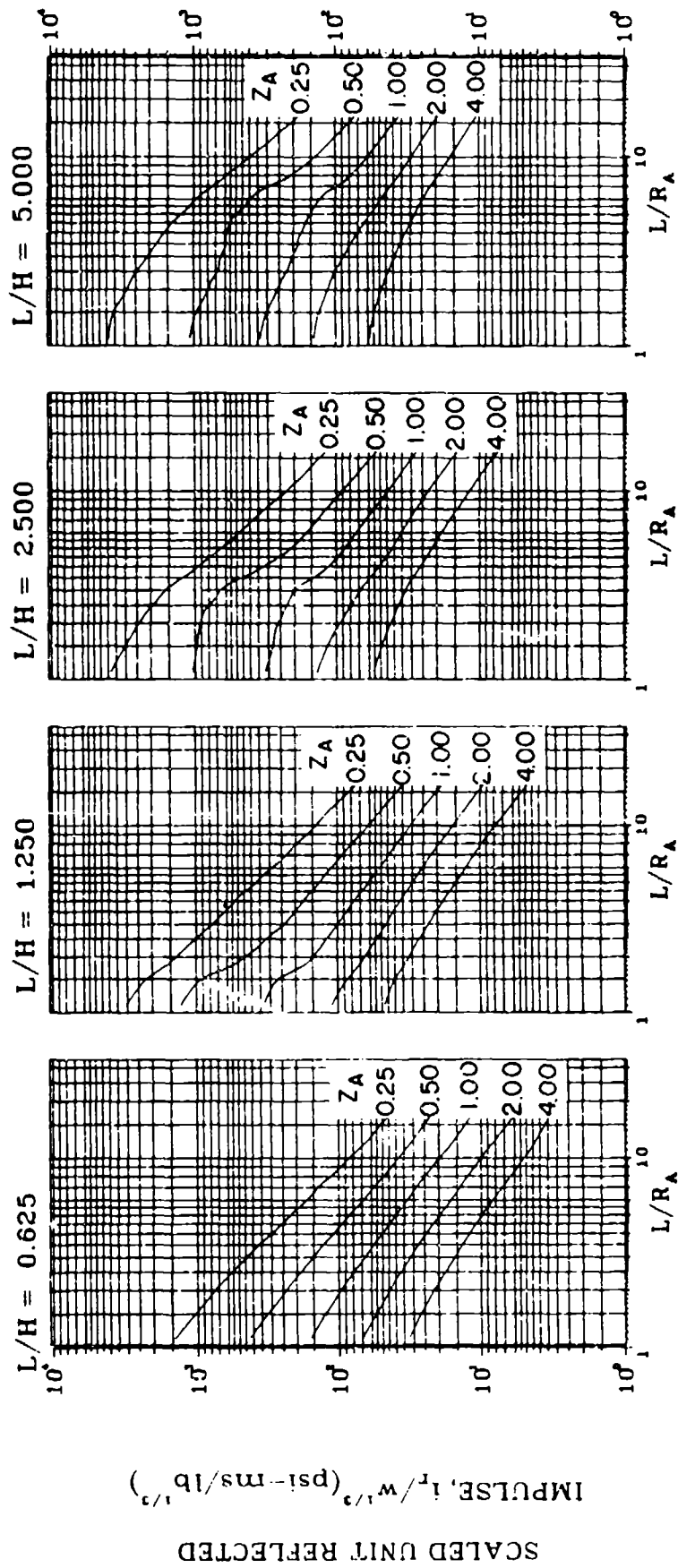


Figure 2-111 Scaled average unit reflected impulse
($N = 1$, $\ell/L = 0.25$ and 0.75 , $h/H = 0.75$)

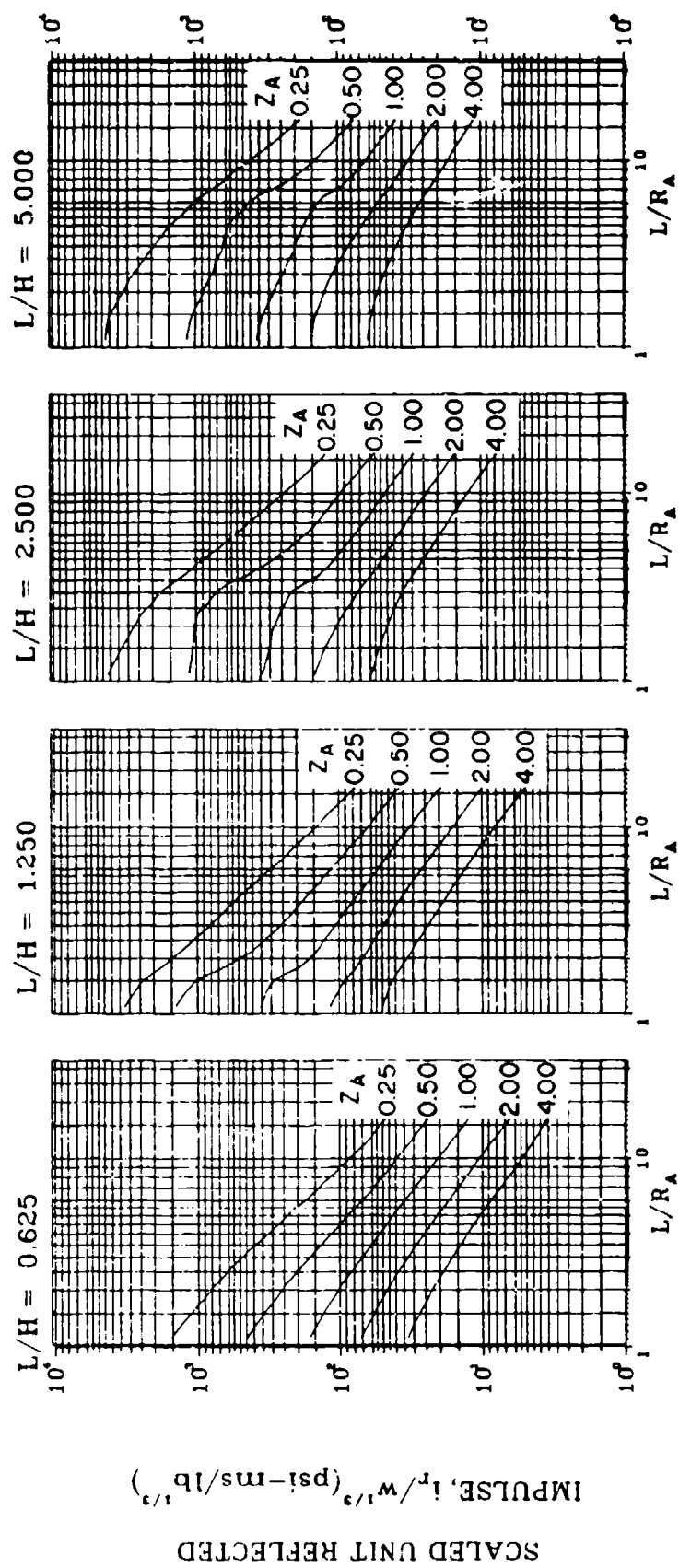


Figure 2-112 Scaled average unit reflected impulse
($N = 1$, $\ell/L = 0.50$, $h/H = 0.75$)

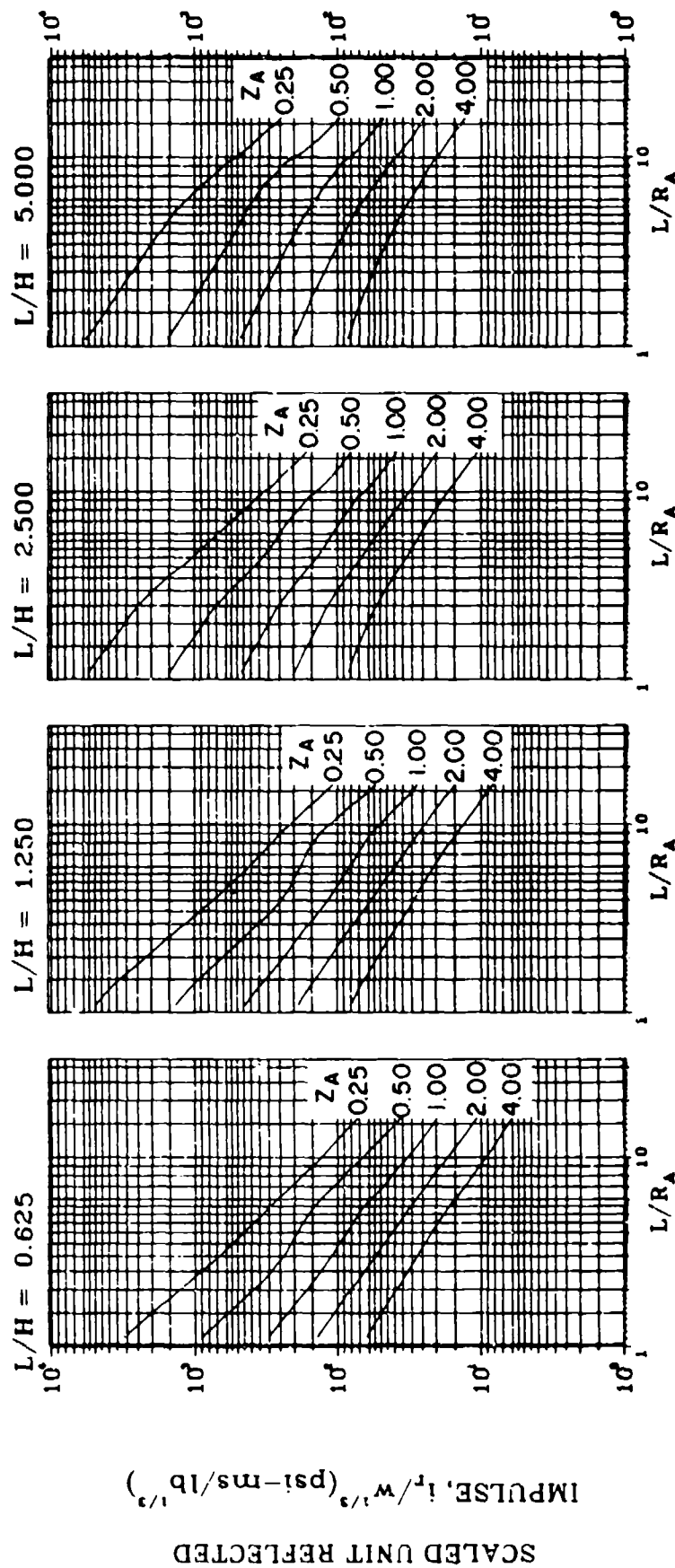


Figure 2-113 Scaled average unit reflected impulse
($N = 2$, $\ell/L = 0.10$, $h/H = 0.10$)

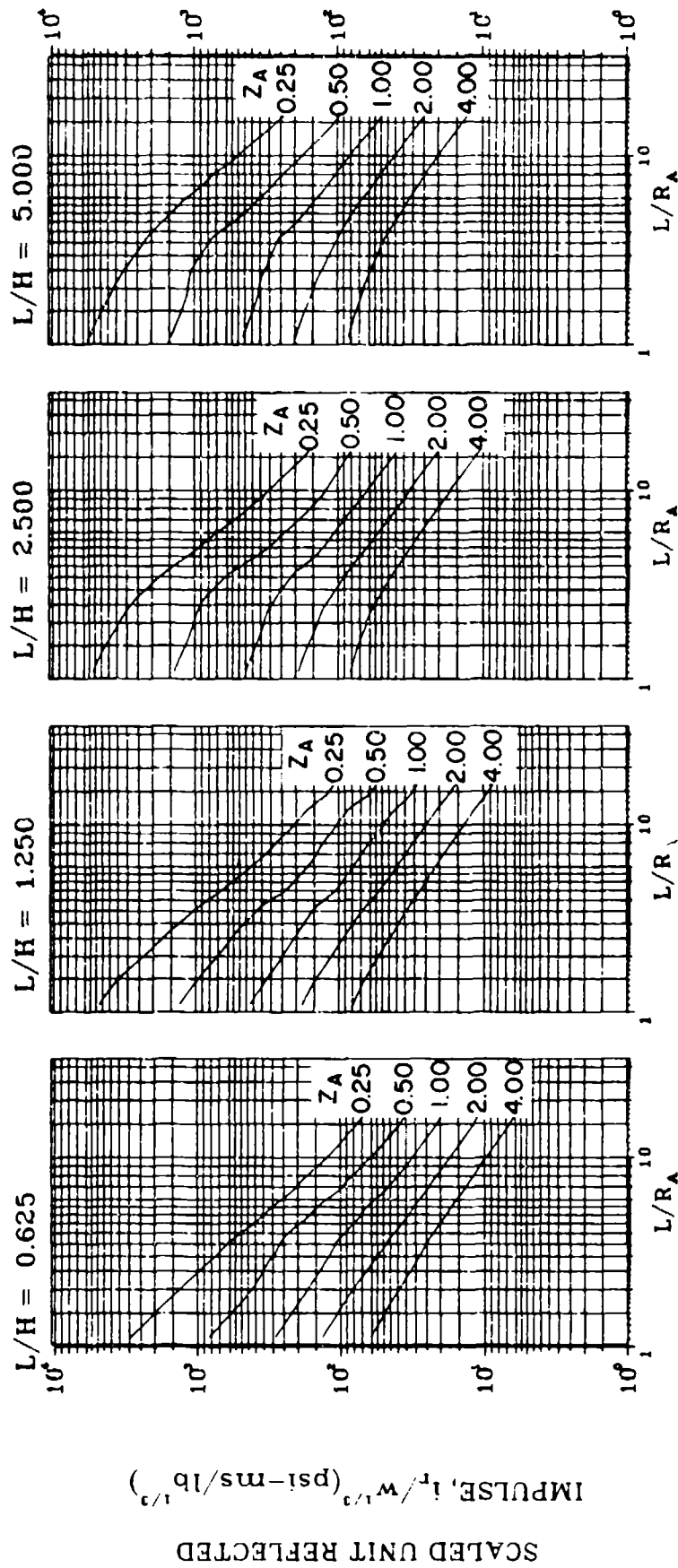


Figure 2-114 Scaled average unit reflected impulse
($N = 2$, $\ell/L = 0.25$, $h/H = 0.10$)

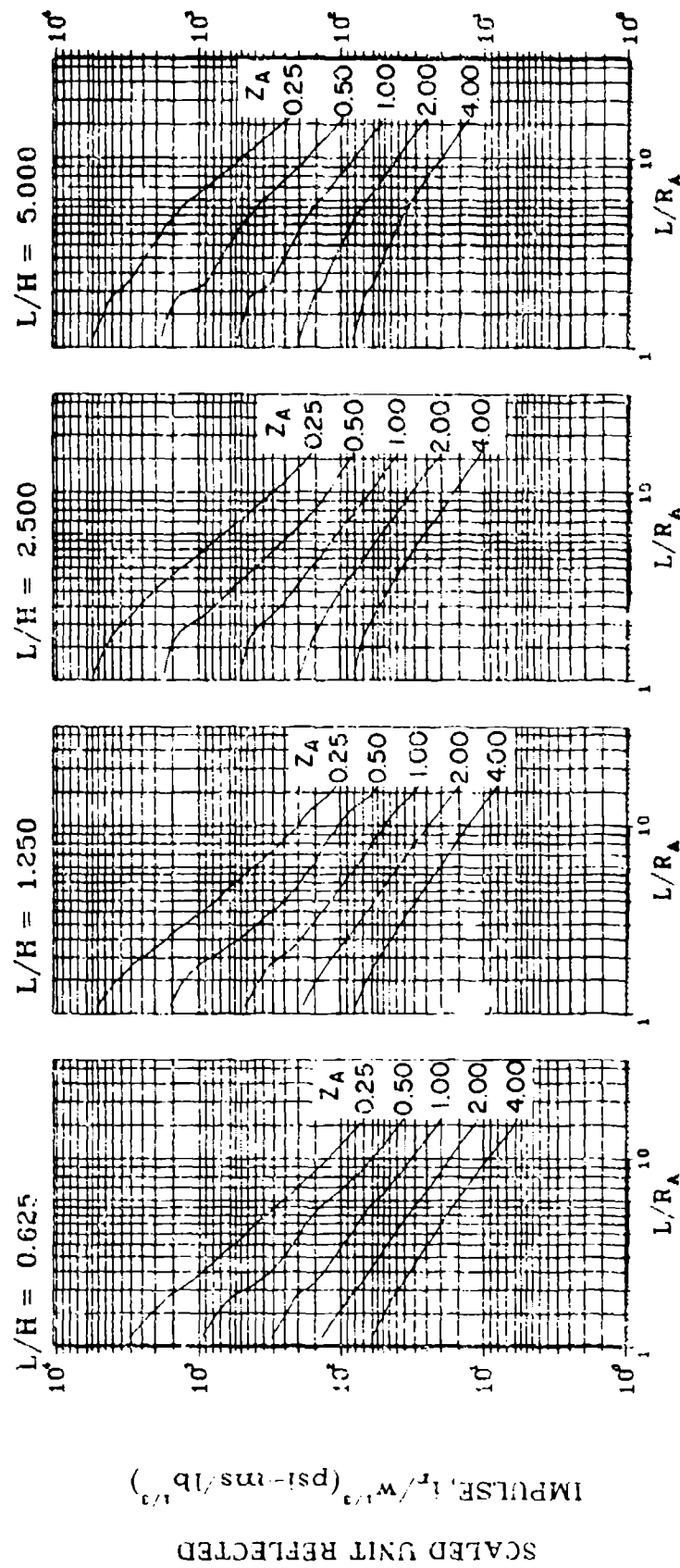


Figure 2-115 Scaled average unit reflected impulse
($N = 2$, $\ell/L = 0.50$, $h/h = 0.10$)

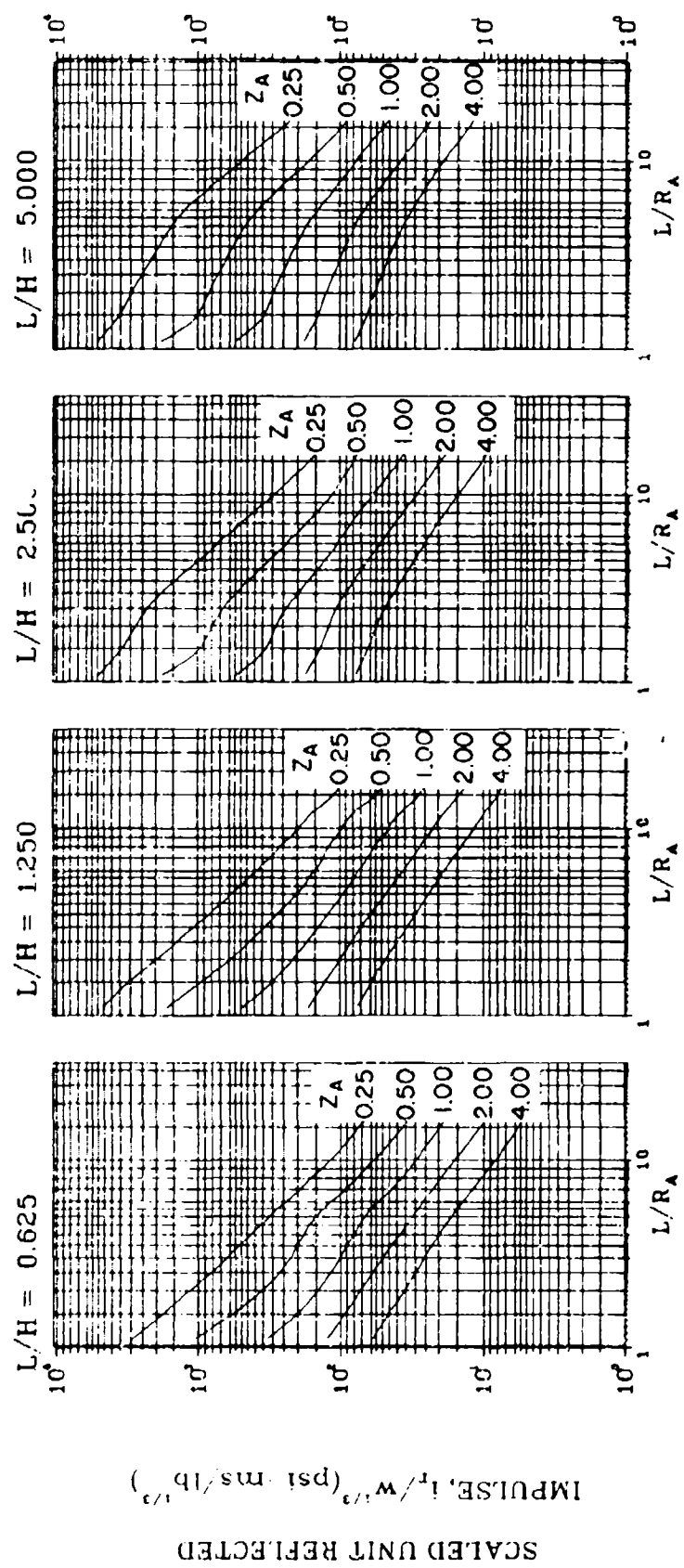


Figure 2-116 Scaled average unit reflected impulse
($N = 2$, $\ell/L = 0.75$, $h/H = 0.10$)

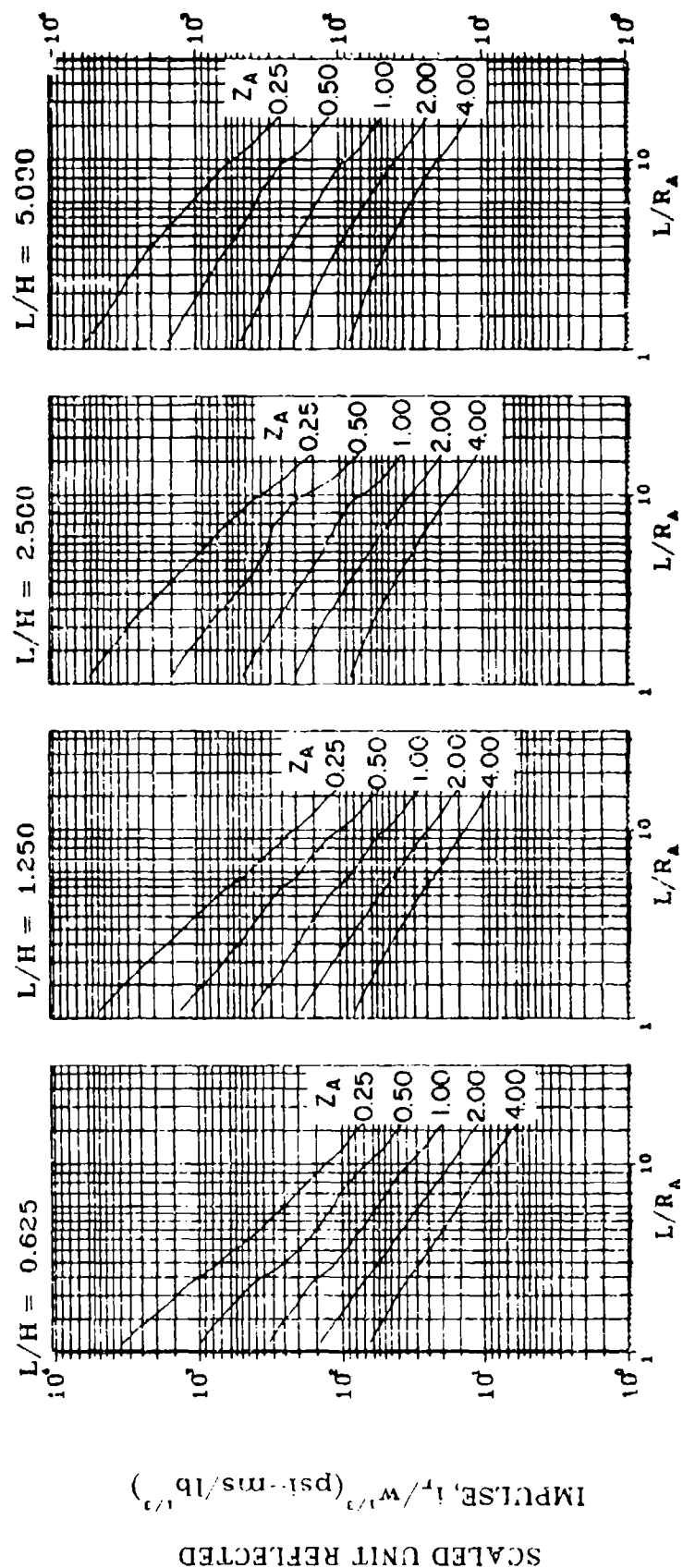


Figure 2-117 Scaled average unit reflected impulse
($N = 2$, $\psi/L = 0.10$, $h/H = 0.25$)

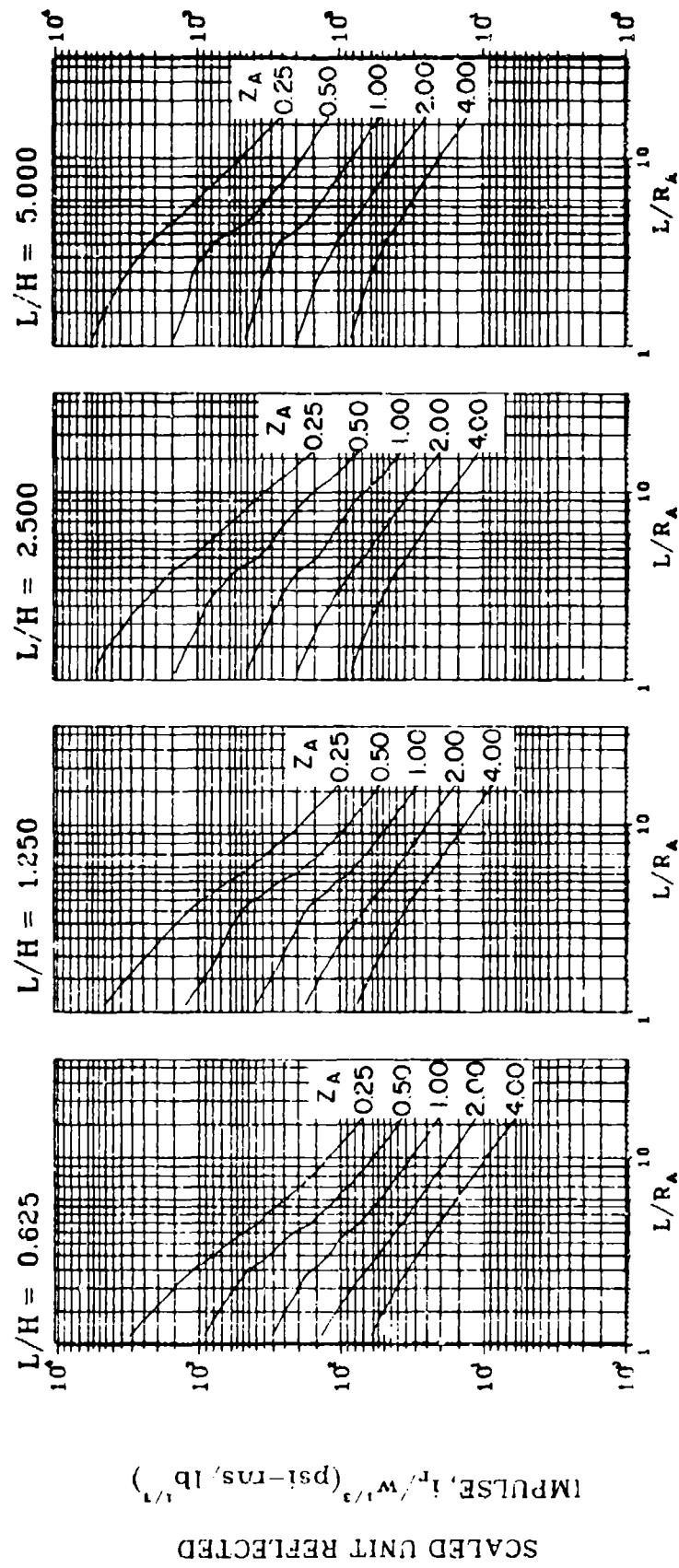


Figure 2-118 Scaled average unit reflected impulse
($N = 2$, $\ell/L = 0.25$, $h/H = 0.25$)

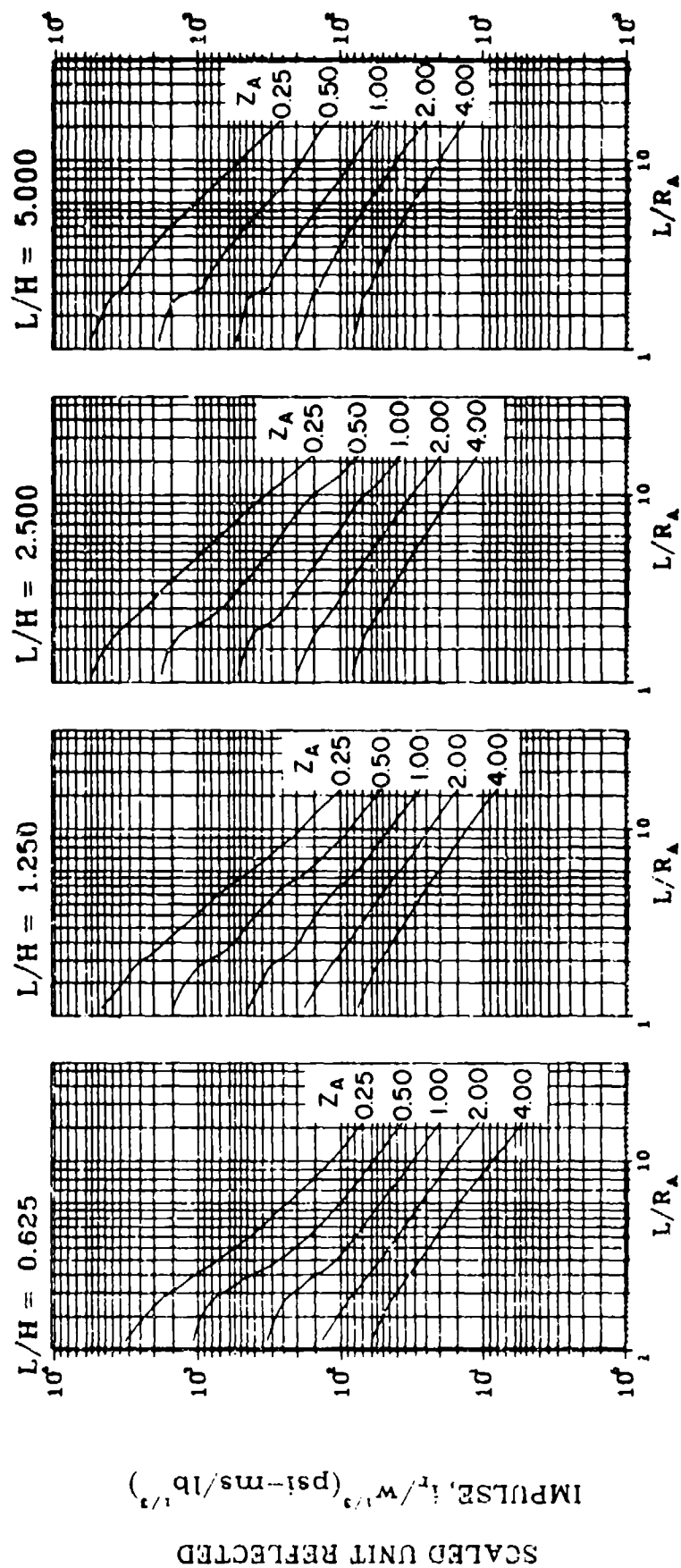


Figure 2-119 Scaled average unit reflected impulse
($N \approx 2$, $L/L \approx 0.50$, $h/H = 0.25$)

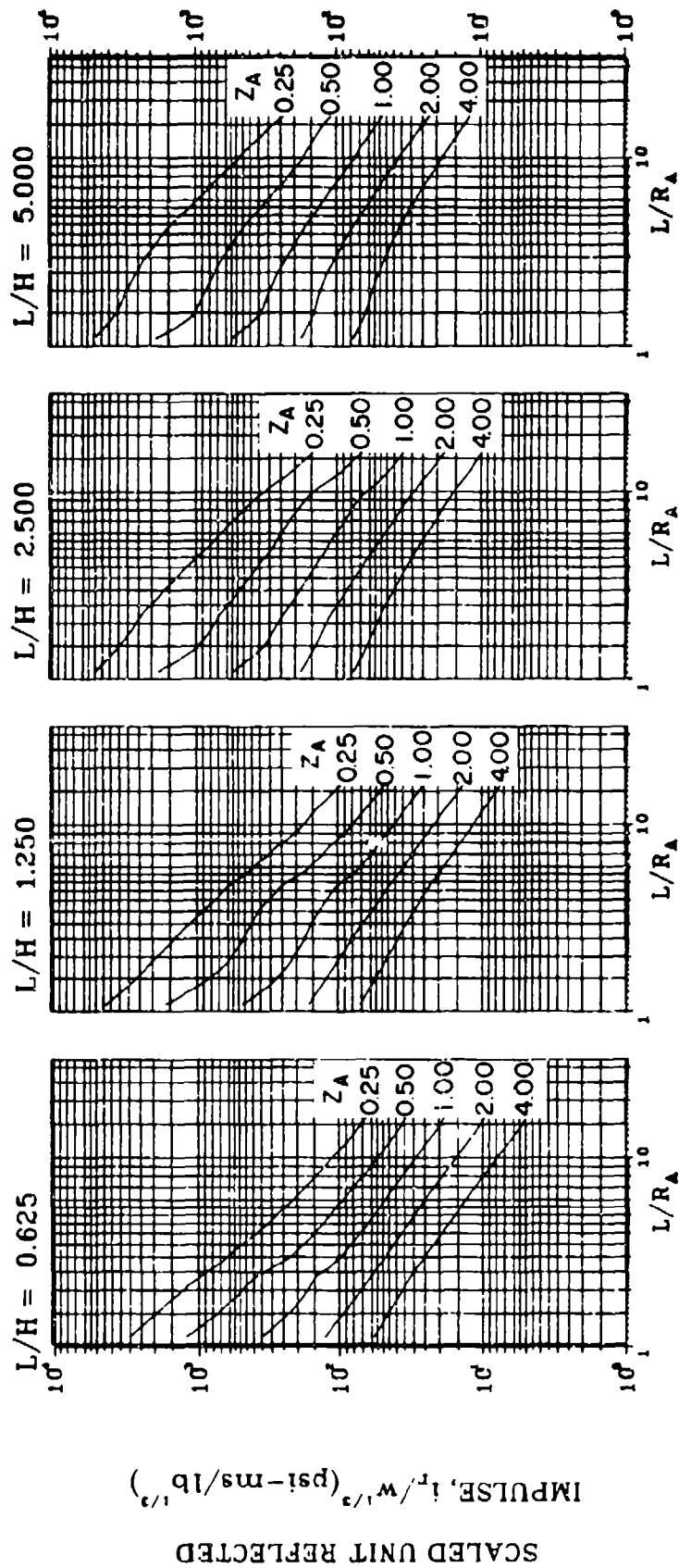


Figure 2-120 Scaled average unit reflected impulse
($N = 2$, $l/L = 0.75$, $h/H = 0.25$)

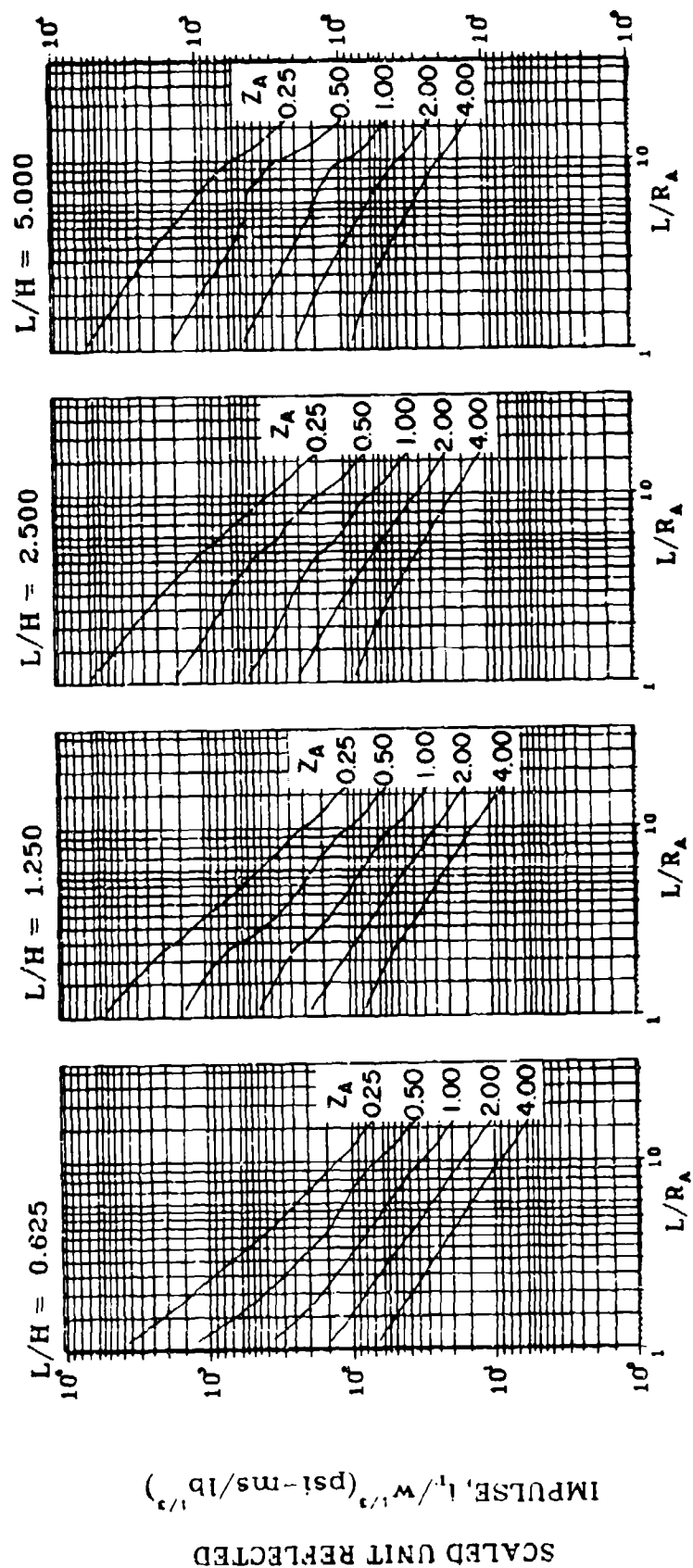


Figure 2-121 Scaled average unit reflected impulse
($N = 2$, $\ell/L = 0.10$, $h/H = 0.50$)

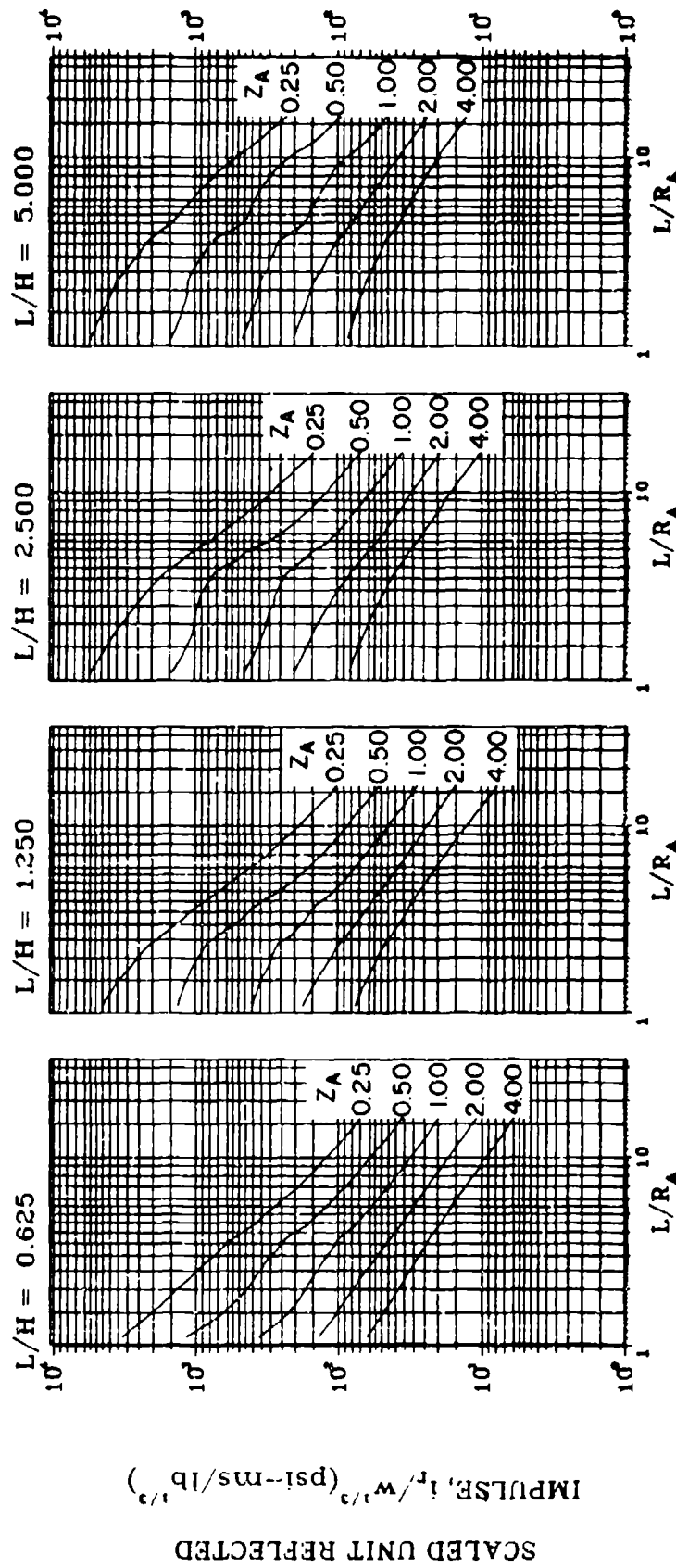


Figure 2-122 Scaled average unit reflected impulse
($N = 2$, $\xi/L = 0.25$, $h/H = 0.50$)

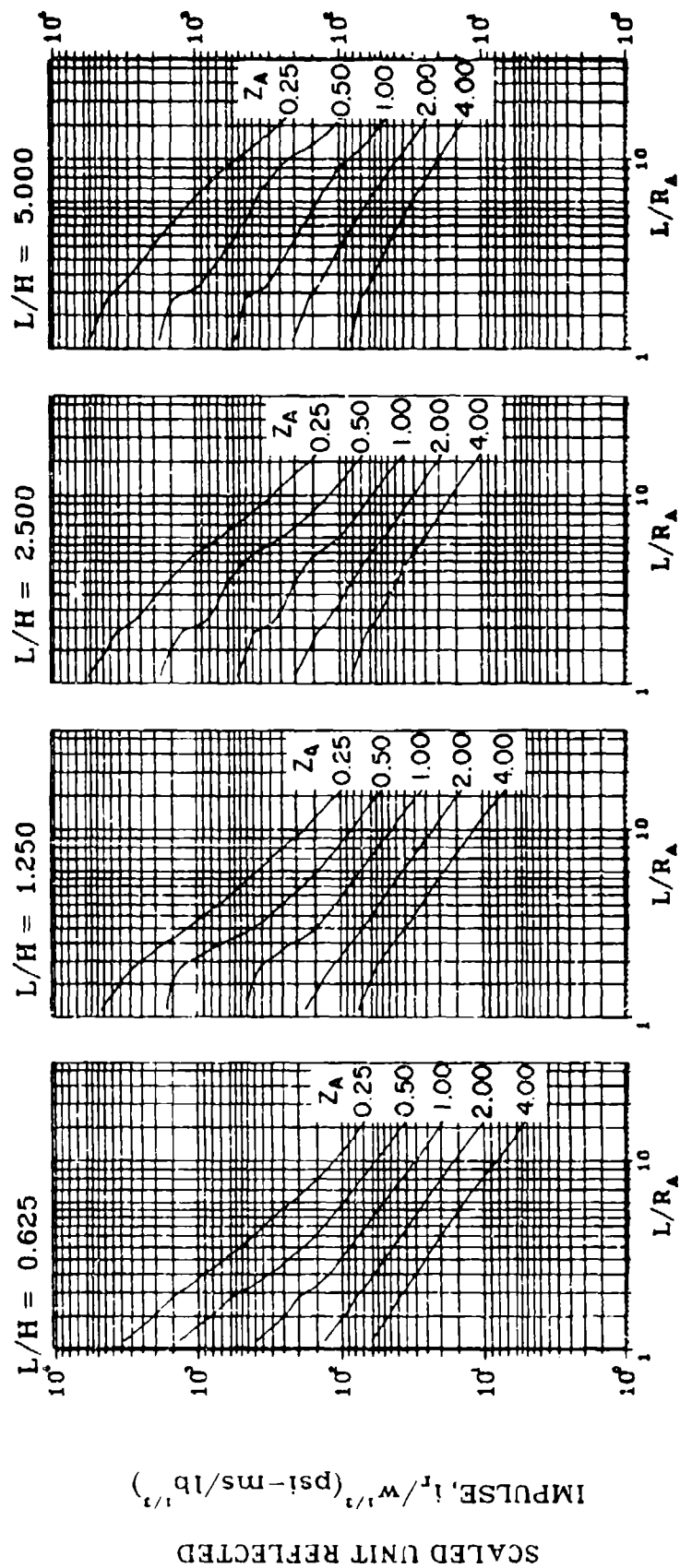


Figure 2-123 Scaled average unit reflected impulse
($N = 2$, $Q/L = 0.50$, $h/H = 0.50$)

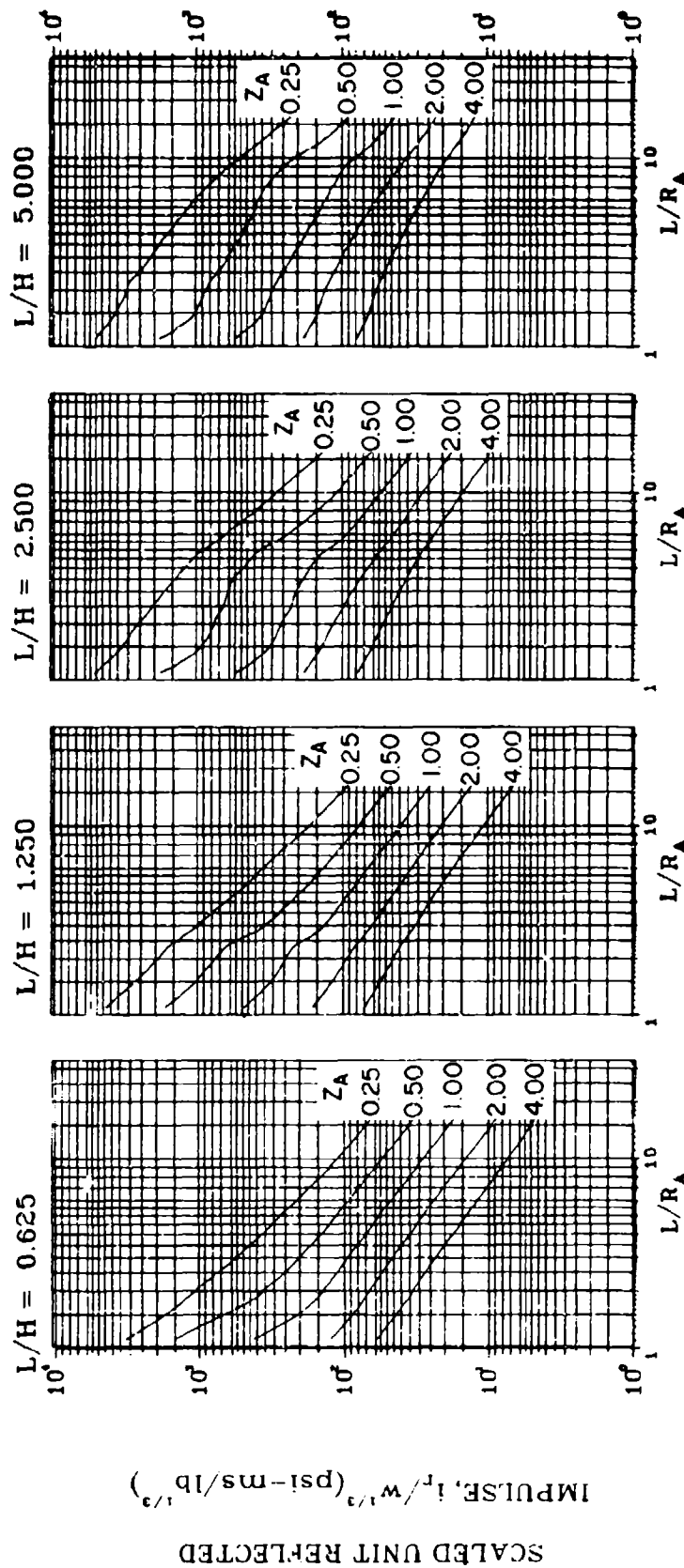


Figure 2-124 Scaled average unit reflected impulse
($N = 2$, $l/L = 0.75$, $h/H = 0.50$)

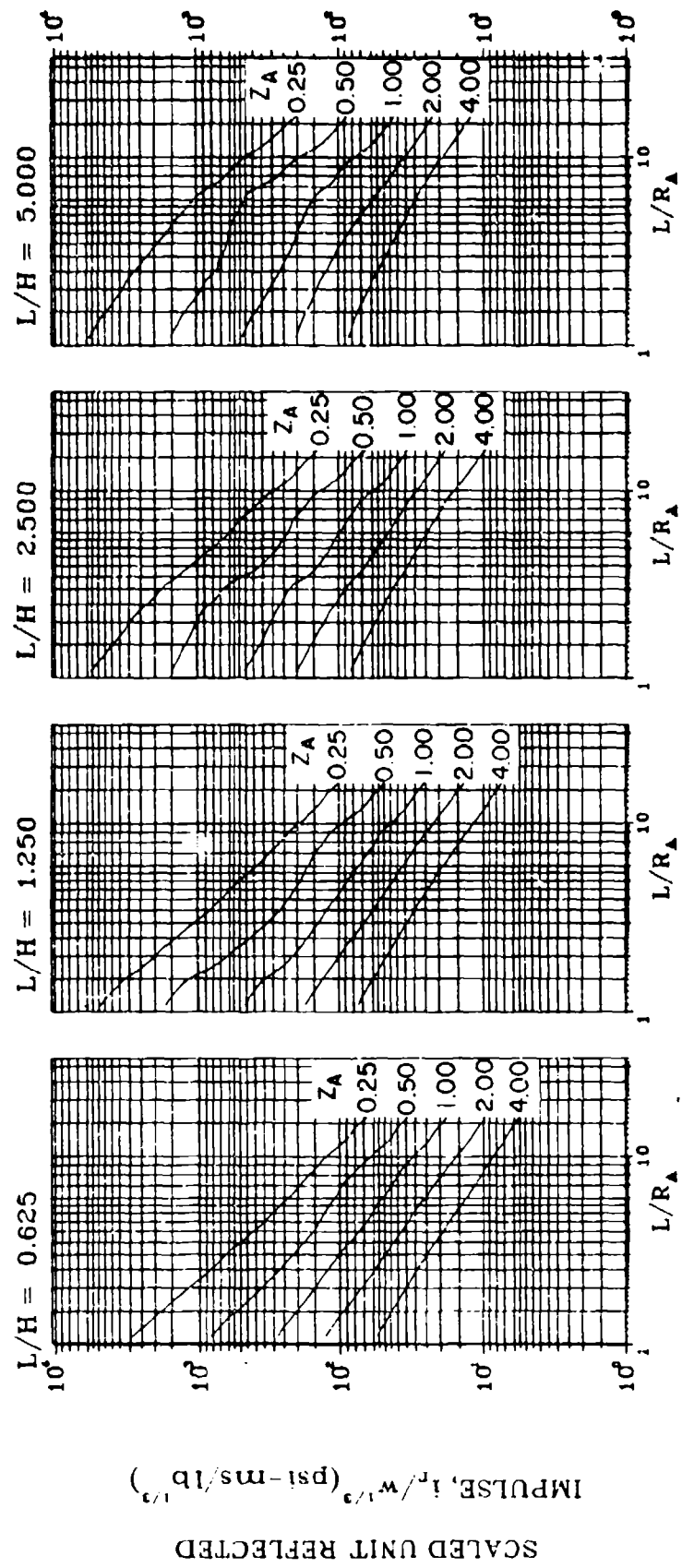


Figure 2-125 Scaled average unit reflected impulse
($N = 2$, $l/L = 0.10$, $h/H = 0.75$)

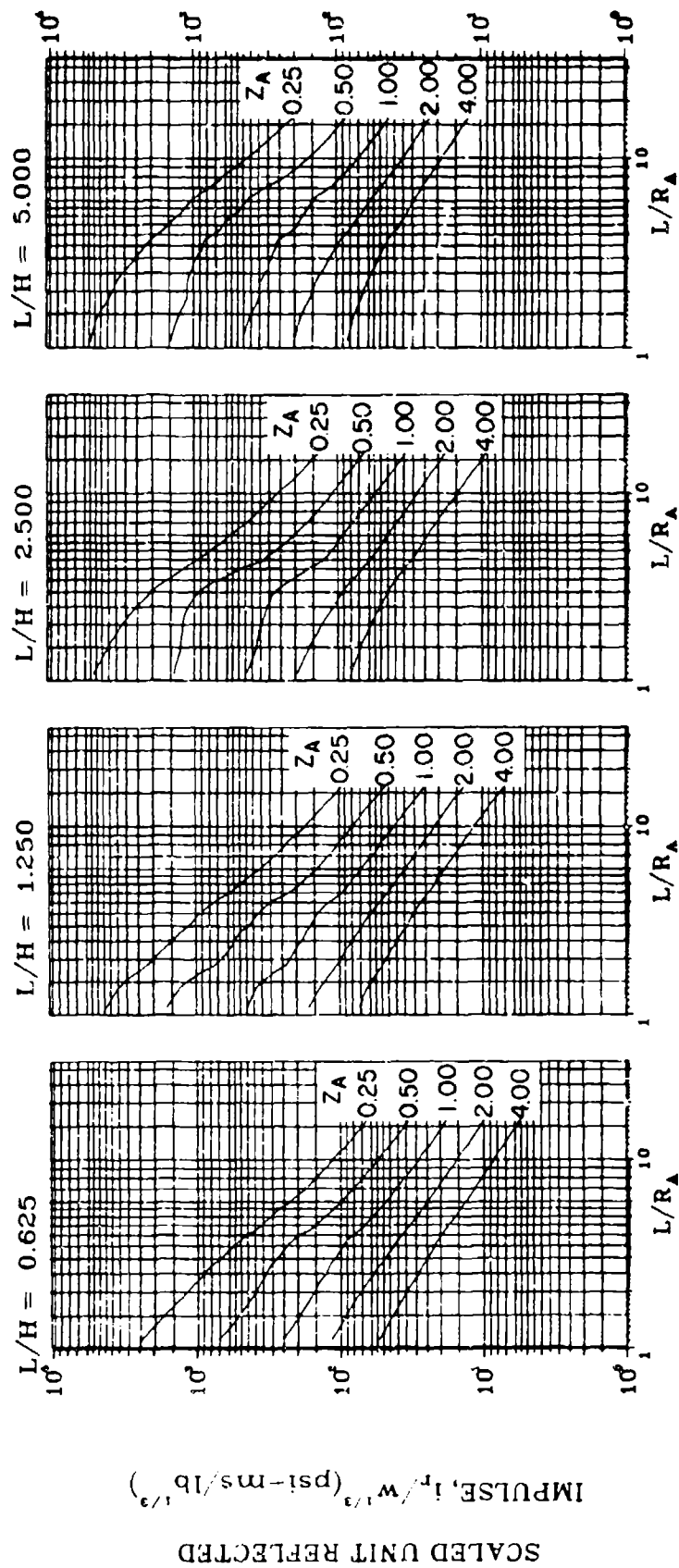


Figure 2-126 Scaled average unit reflected impulse
($N = 2$, $\ell/L = 0.25$, $h/H = 0.75$)

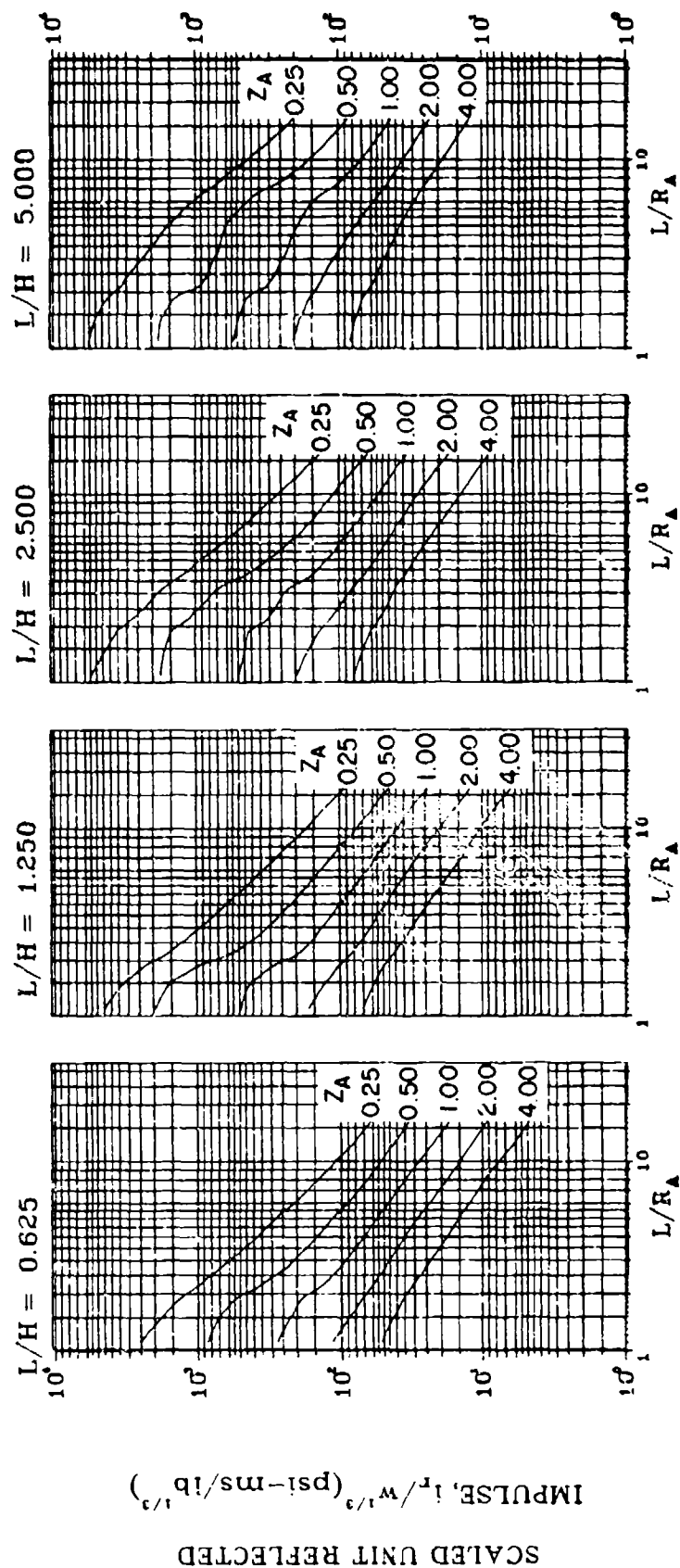


Figure 2-127 Scaled average unit reflected impulse
($N = 2$, $\ell/L = 0.50$, $h/H = 0.75$)

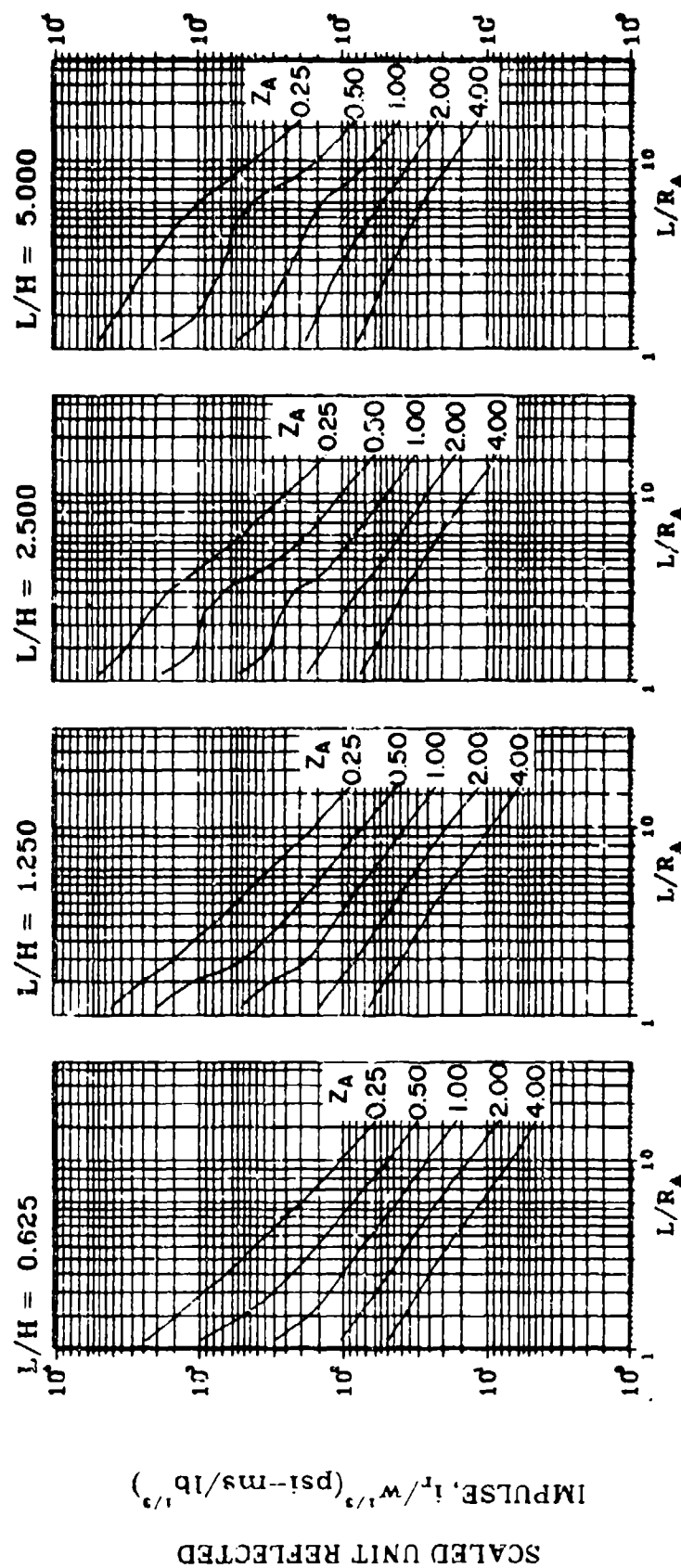


Figure 2-128 Scaled average unit reflected impulse
($N = 2$, $\ell/L = 0.75$, $h/H = 0.75$)

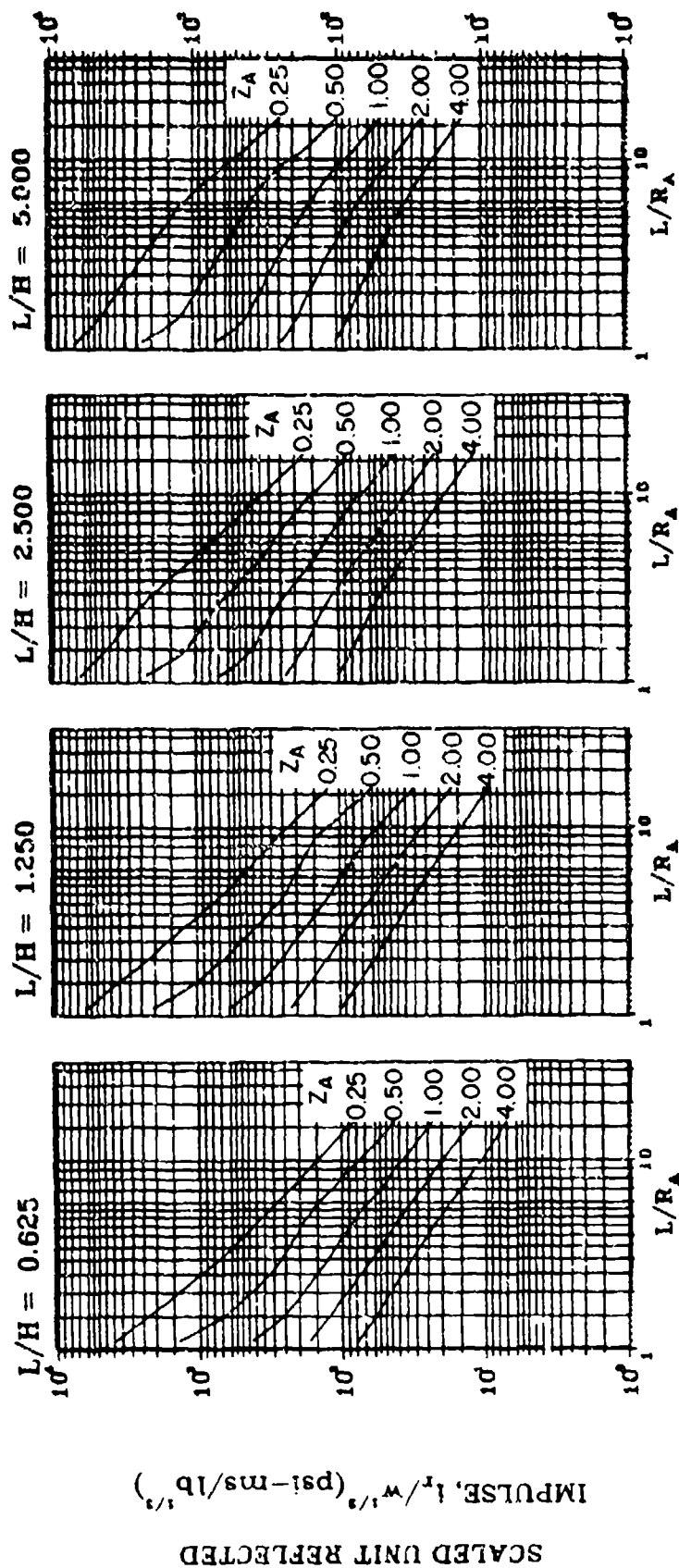


Figure 2-129 Scaled average unit reflected impulse
($N = 3$, $\ell/L = 0.10$, $h/H = 0.10$)

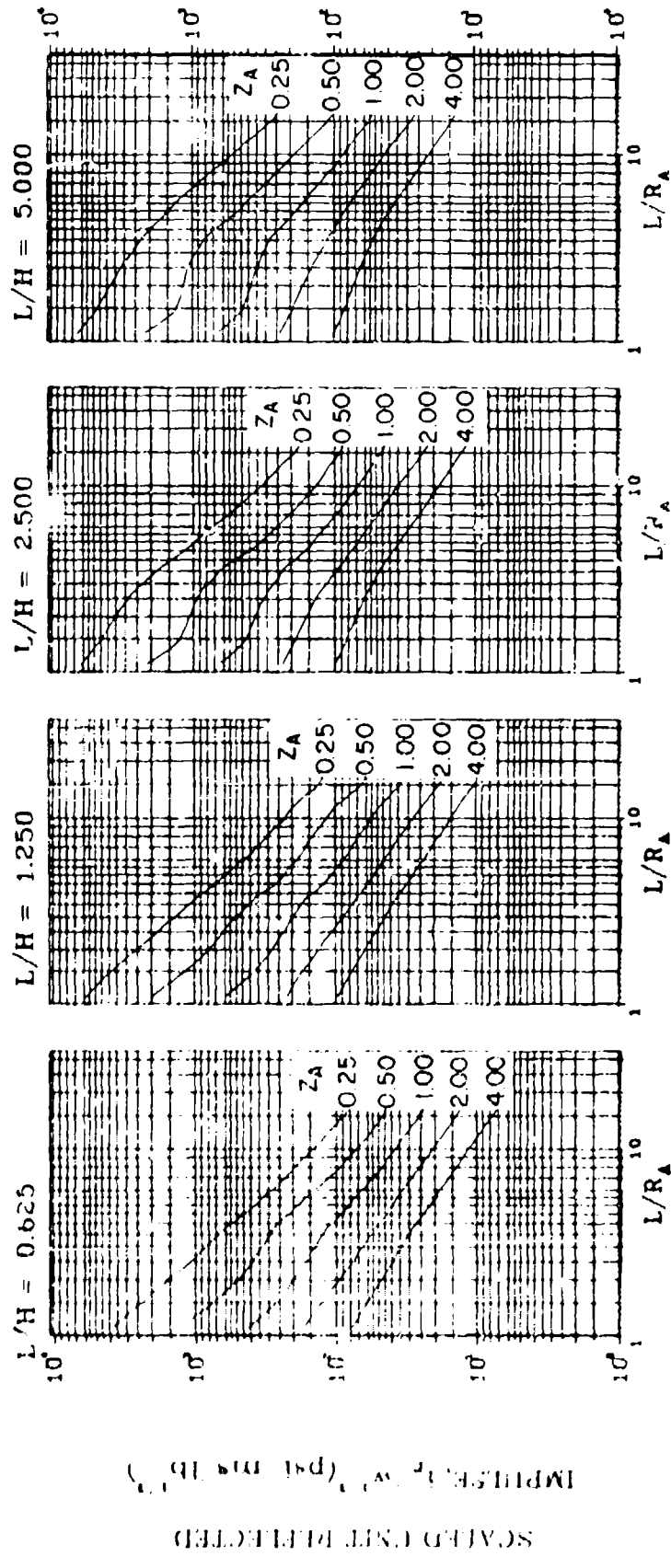


Figure 2-130 Scaled average unit reflected impulse
($N = 3$, $L/L = 0.25$ and 0.75 , $h/h = 0.10$)

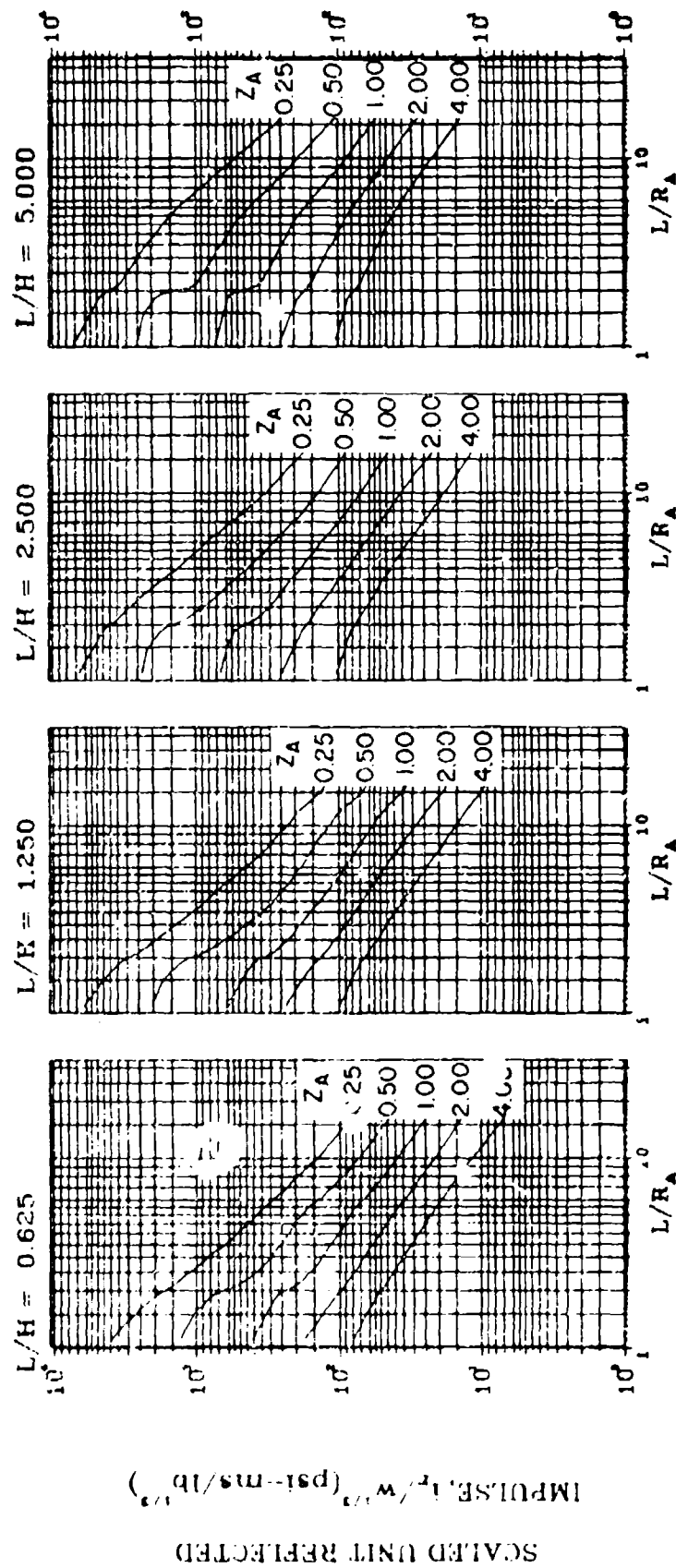


Figure 2-131 Scaled average unit reflected impulse
($N = 3$, $L/L = 0.50$, $h/H = 0.10$)

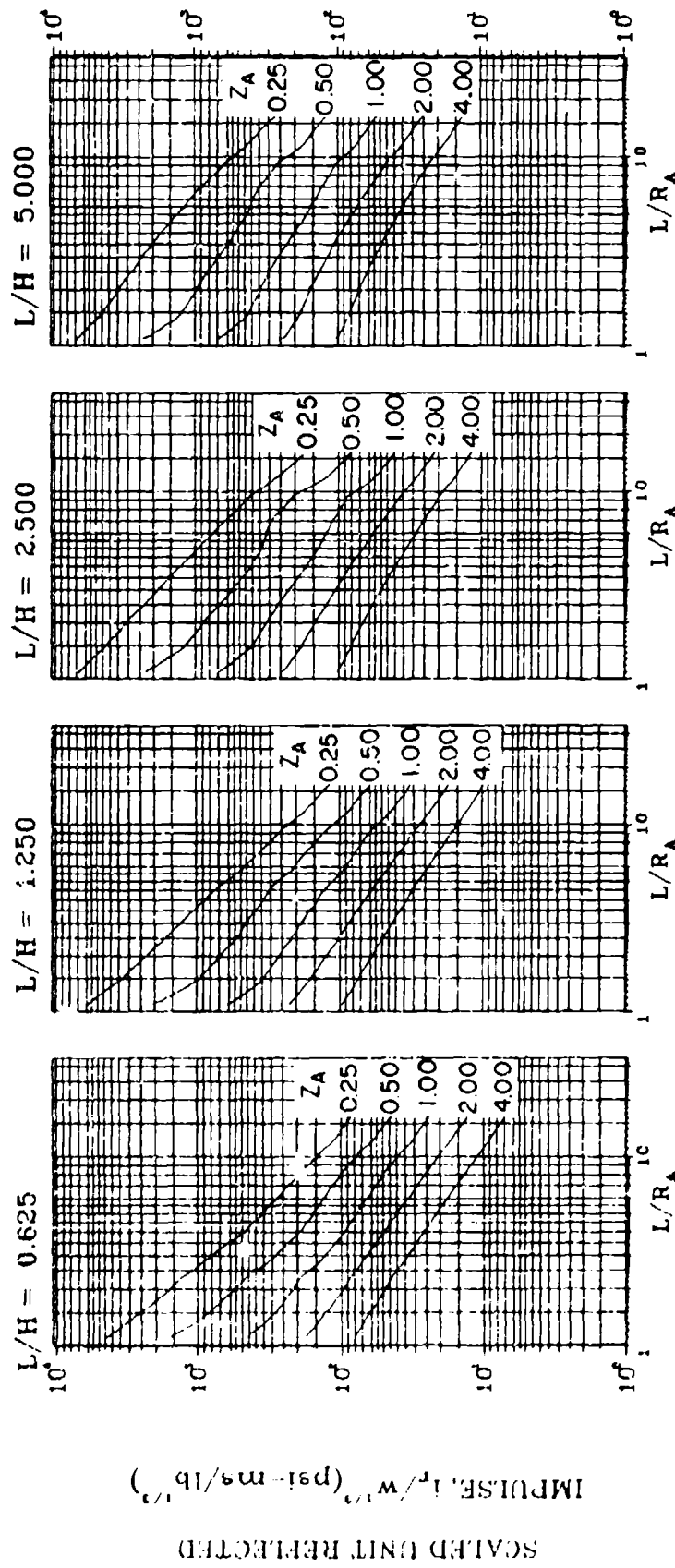


Figure 2-132 Scaled average unit reflected impulse
($\eta = 3$, $L/L = 0.10$, $h/H = 0.25$)

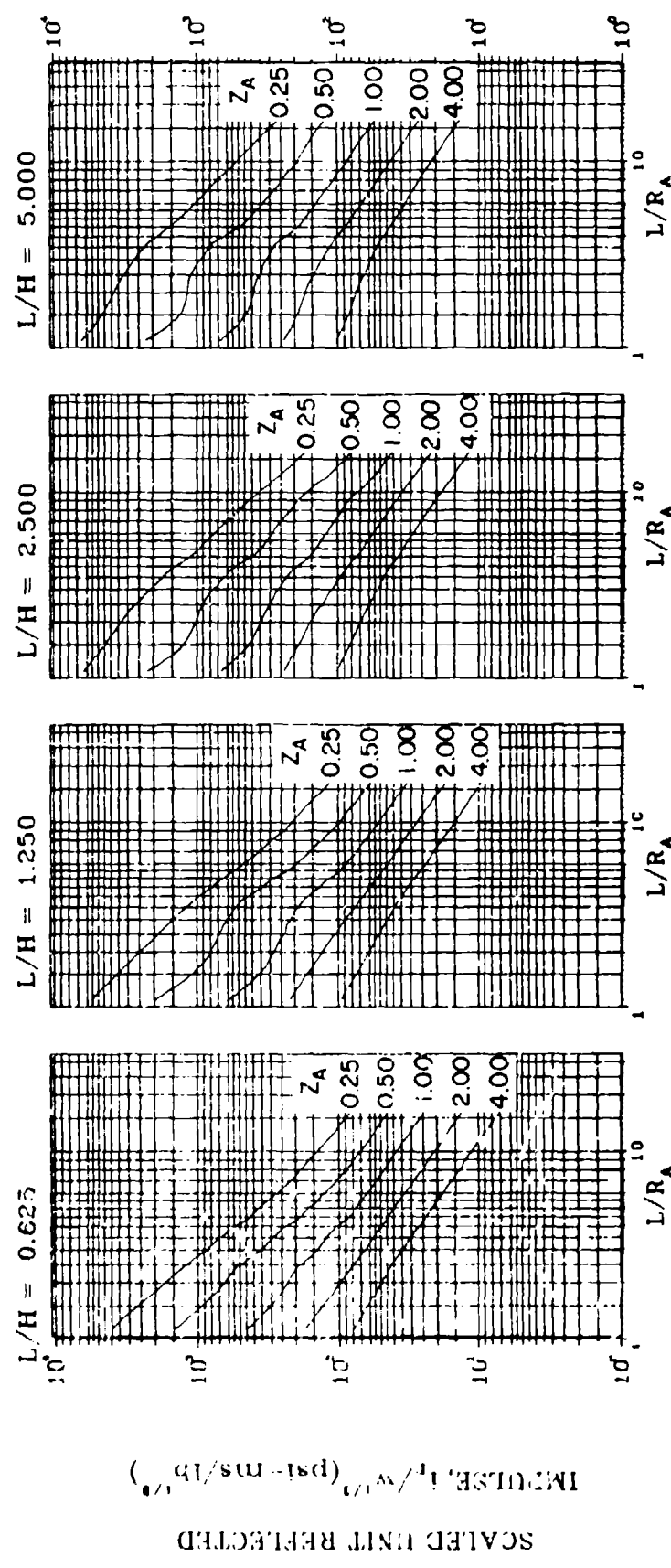


Figure 2-133 Scaled average unit reflected impulse
($N = 3$, $L/L = 0.25$ and 0.75 , $h/H = 0.25$)

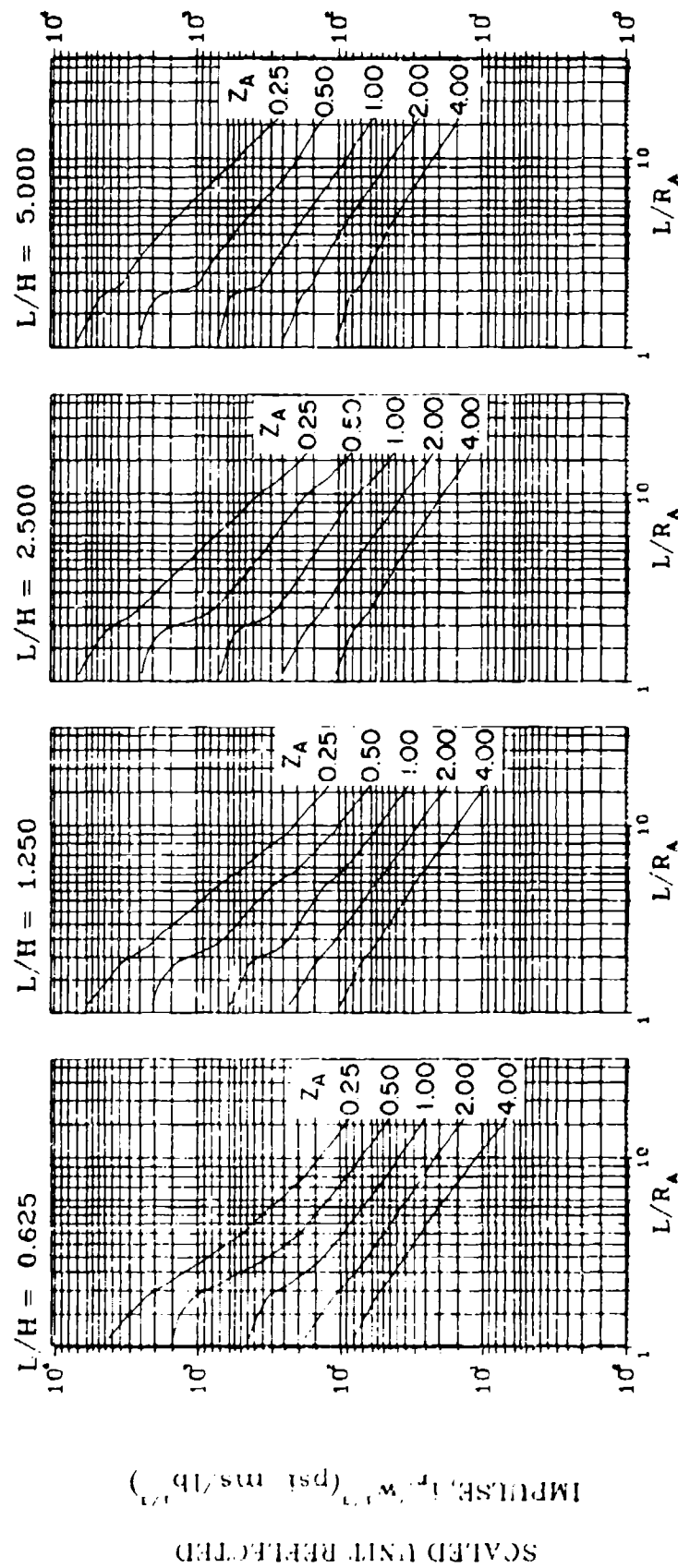


Figure 2-134 Scaled average unit reflected impulse
($N = 3$, $\ell/L = 0.50$, $h/H = 0.25$)

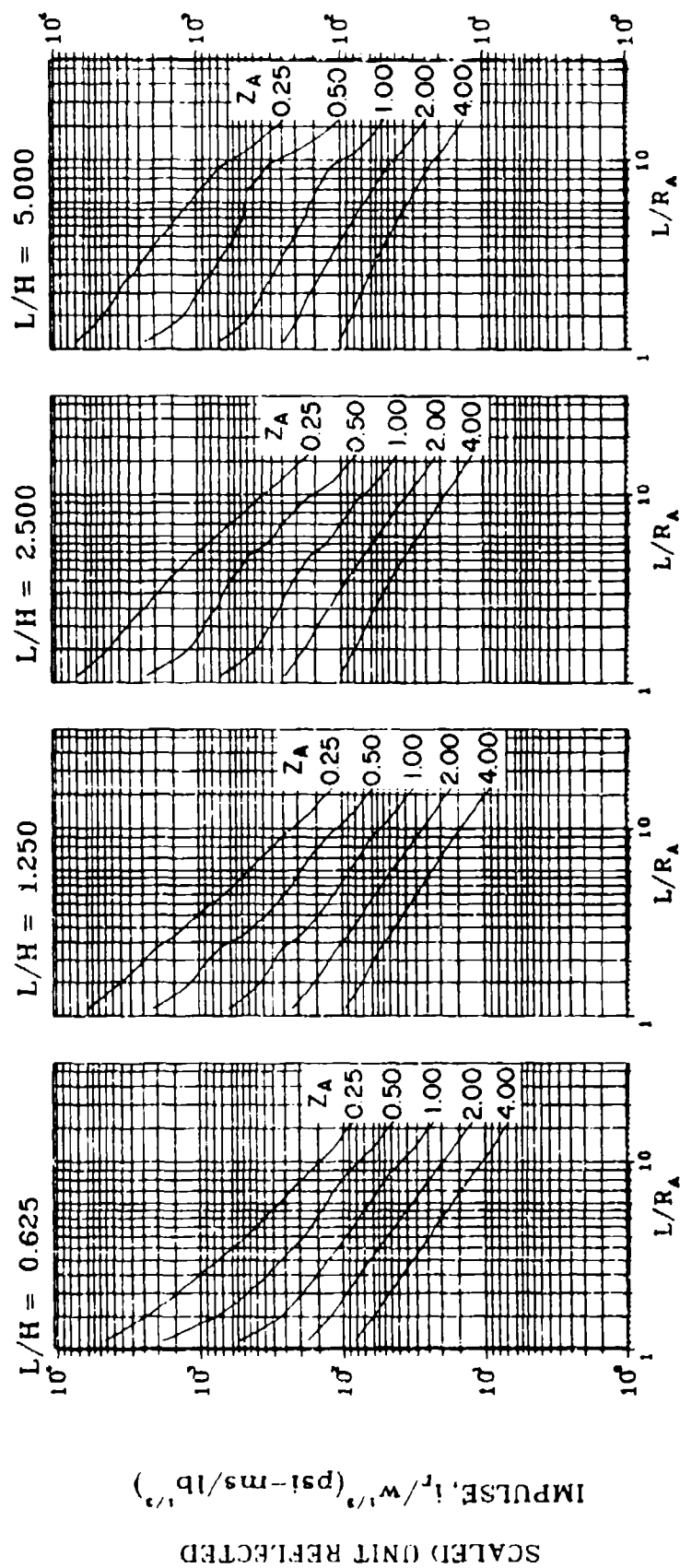


Figure 2-135 Scaled average unit reflected impulse
($N = 3$, $q/L = 0.10$, $h/H = 0.50$)

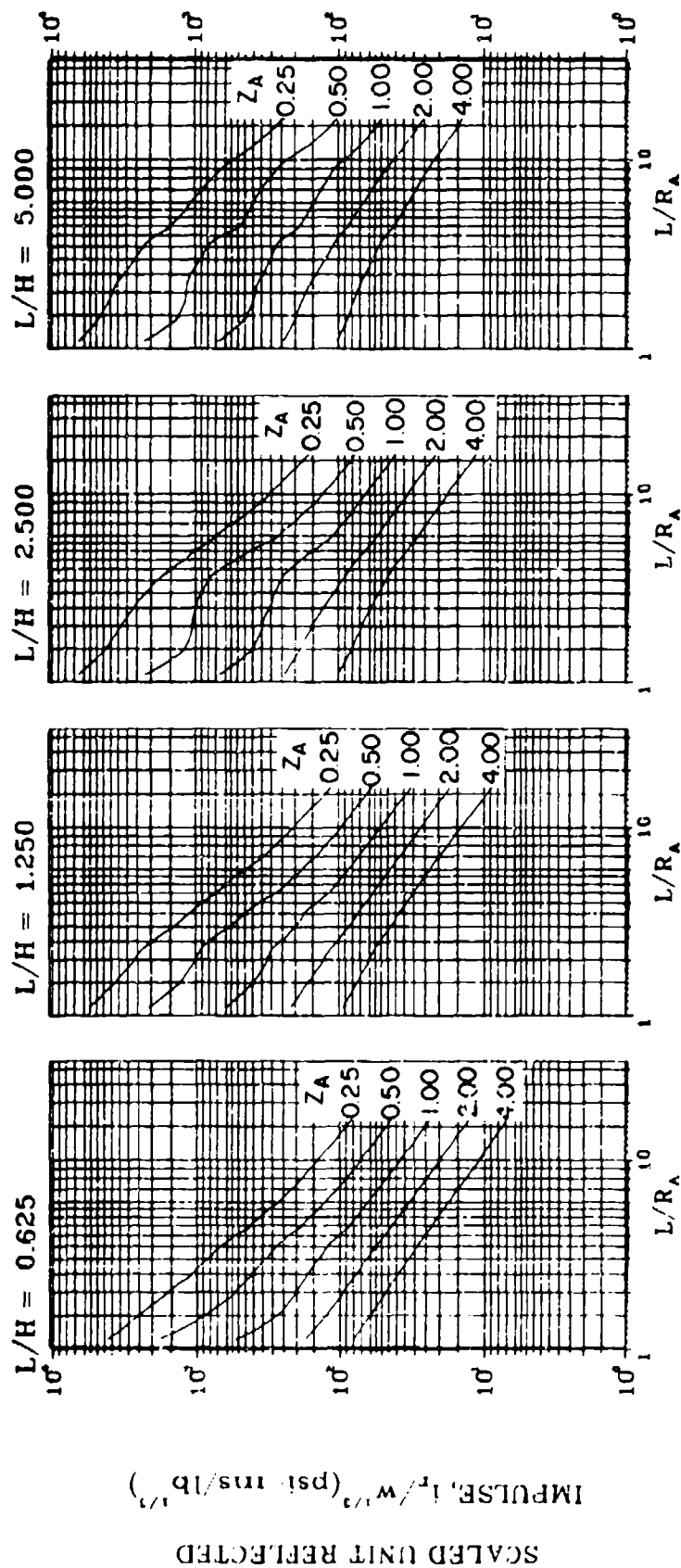


Figure 2-136 Scaled average unit reflected impulse
($N = 3$, $\ell/L = 0.25$ and 0.75 , $\bar{n}/H = 0.50$)

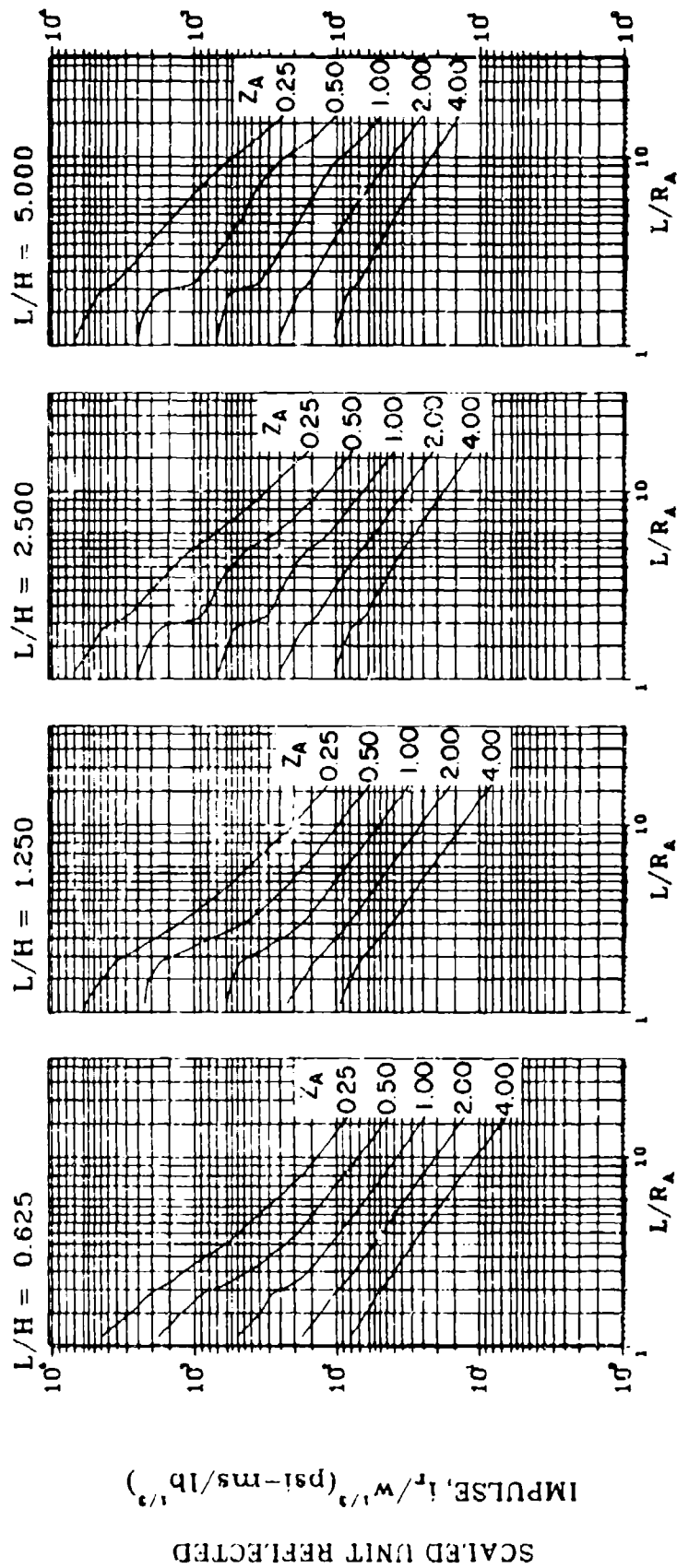


Figure 2-137 Scaled average unit reflected impulse
($N = 3$, $\ell/L = 0.50$, $h/H = 0.50$)

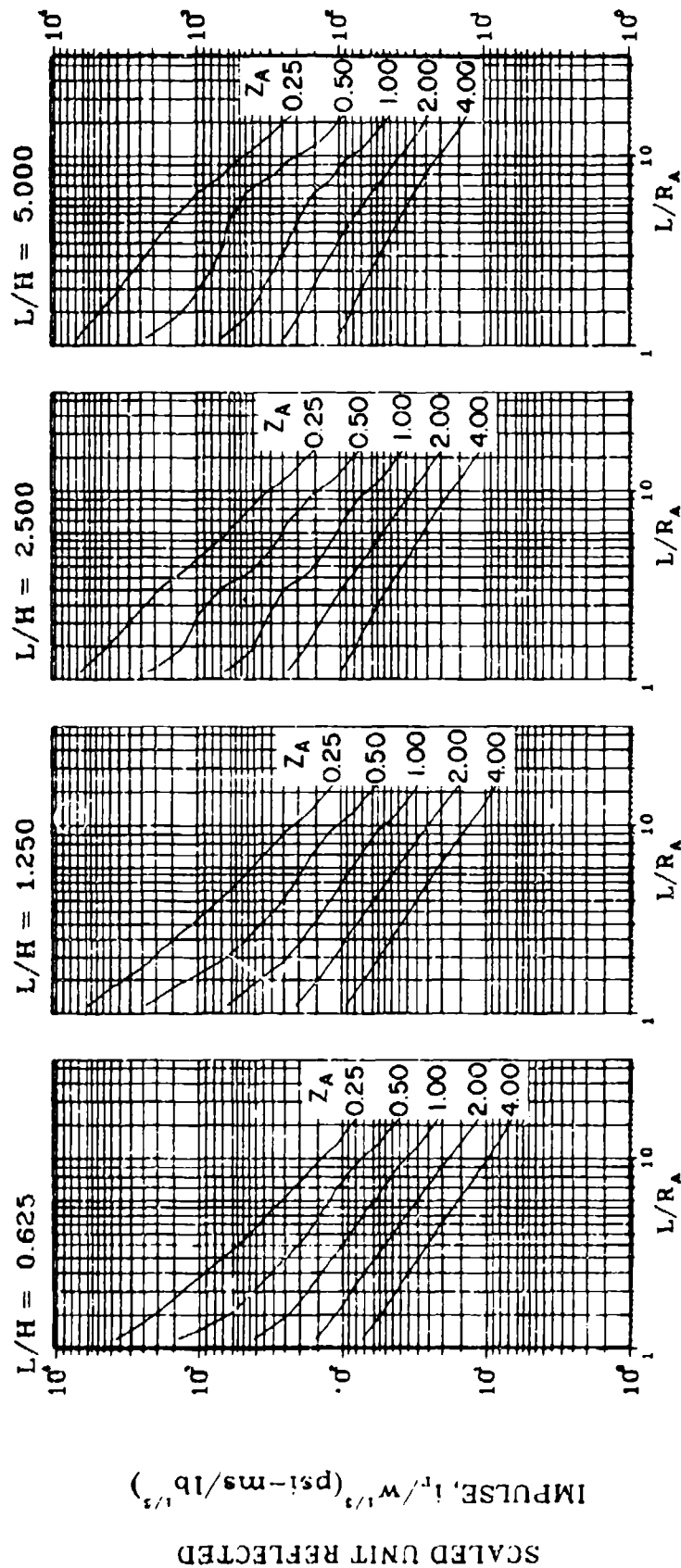


Figure 2-138 Scaled average unit reflected impulse
($N = 3$, $\ell/L = 0.10$, $h/H = 0.75$)

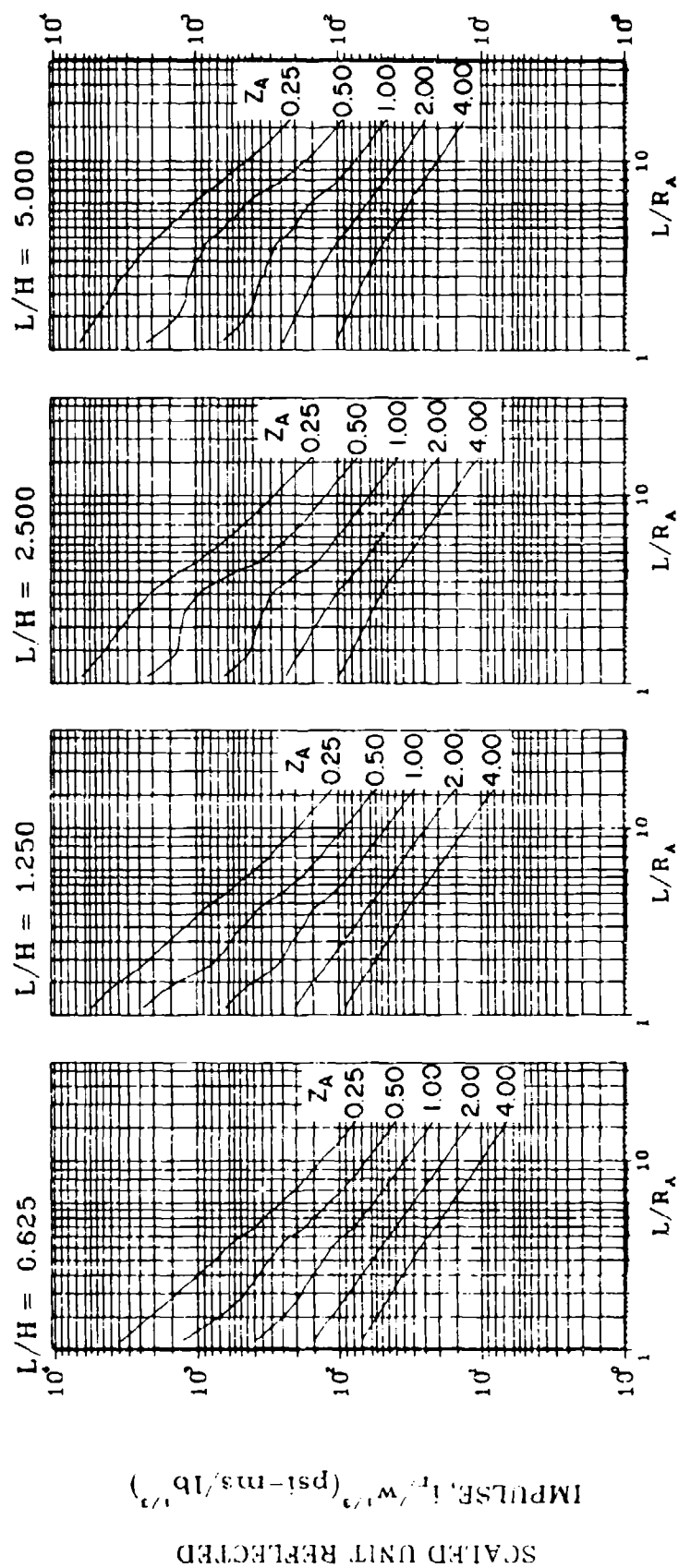


Figure 2-139 Scaled average unit reflected impulse
($N = 3$, $L/L = 0.25$ and 0.75 , $h/H = 0.75$)

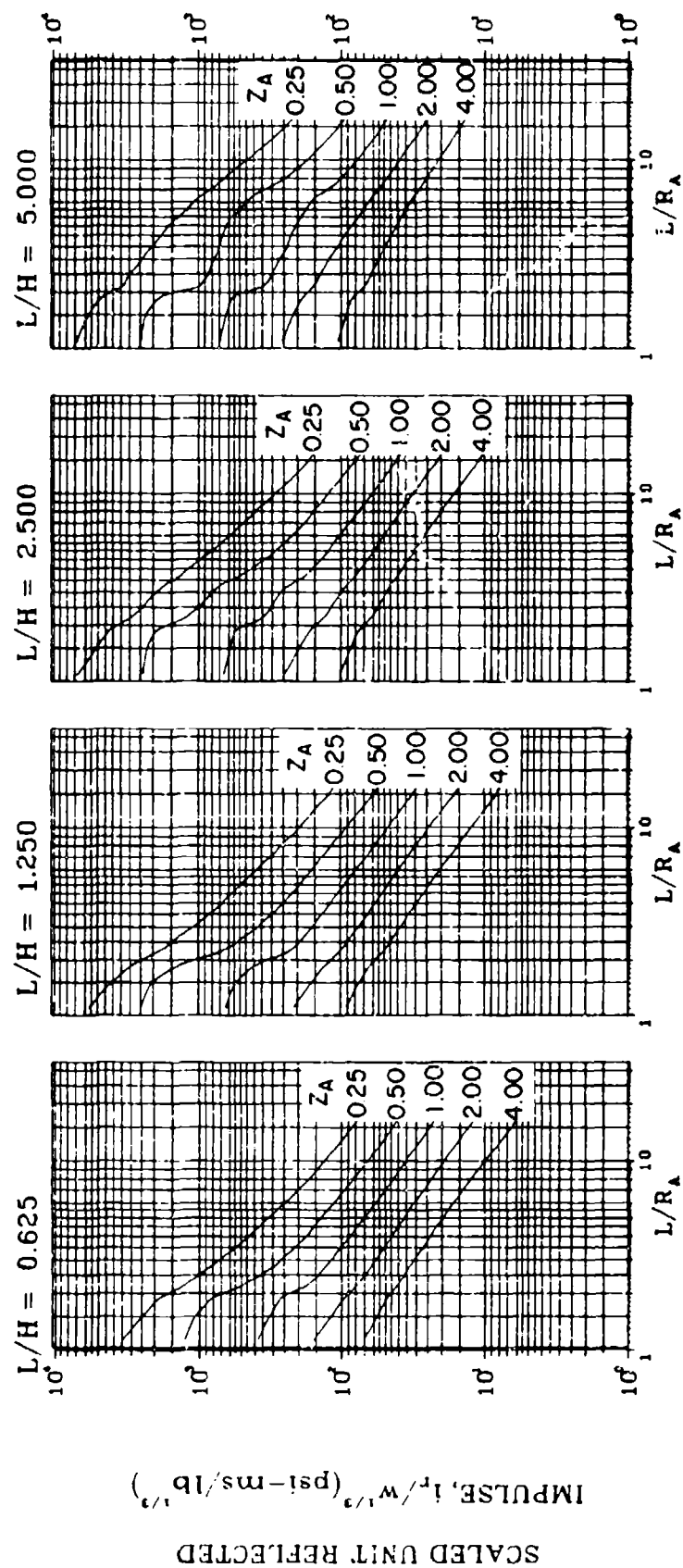


Figure 2-140 Scaled average unit reflected impulse
($N = 3$, $L/L = 0.50$, $h/H = 0.75$)

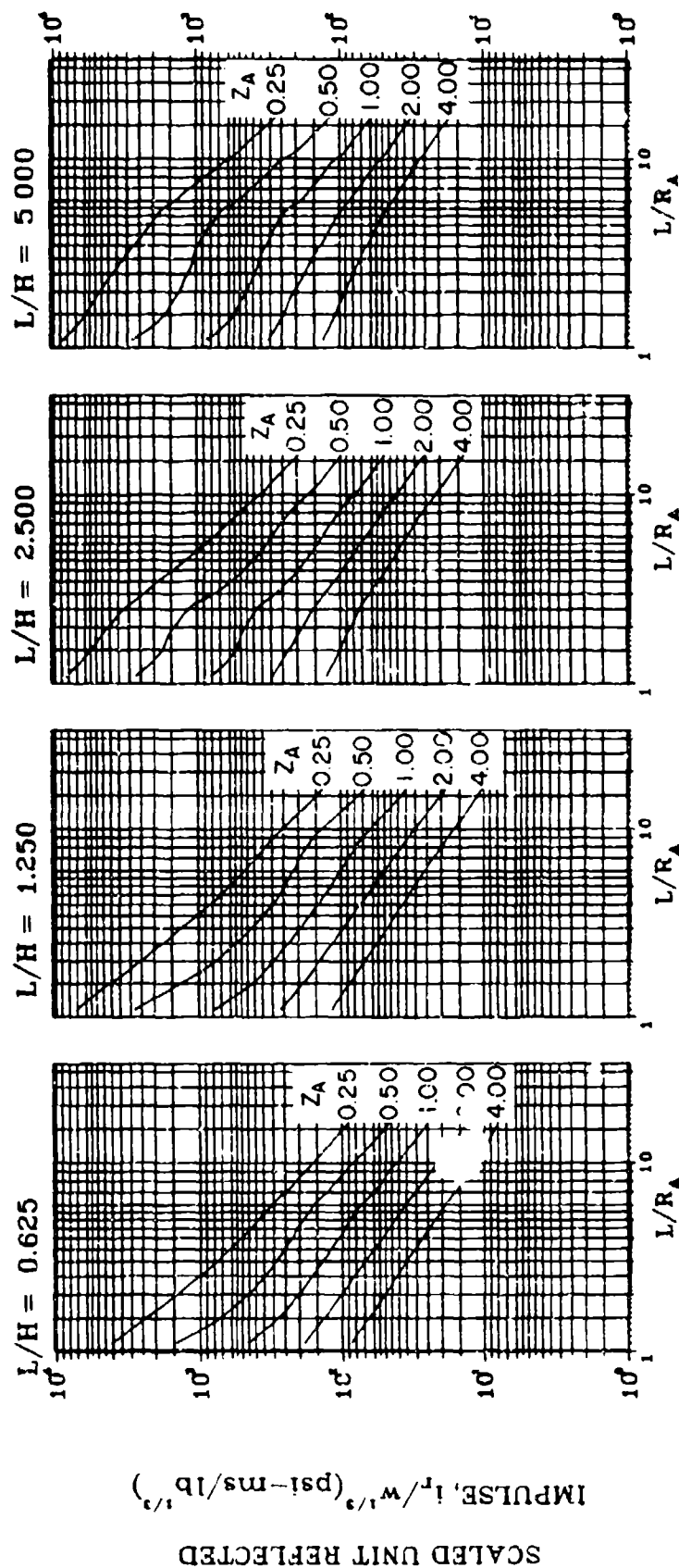


Figure 2-141 Scaled average unit reflected impulse
($N = 4$, $\ell/L = 0.10$, $h/H = 0.10$)

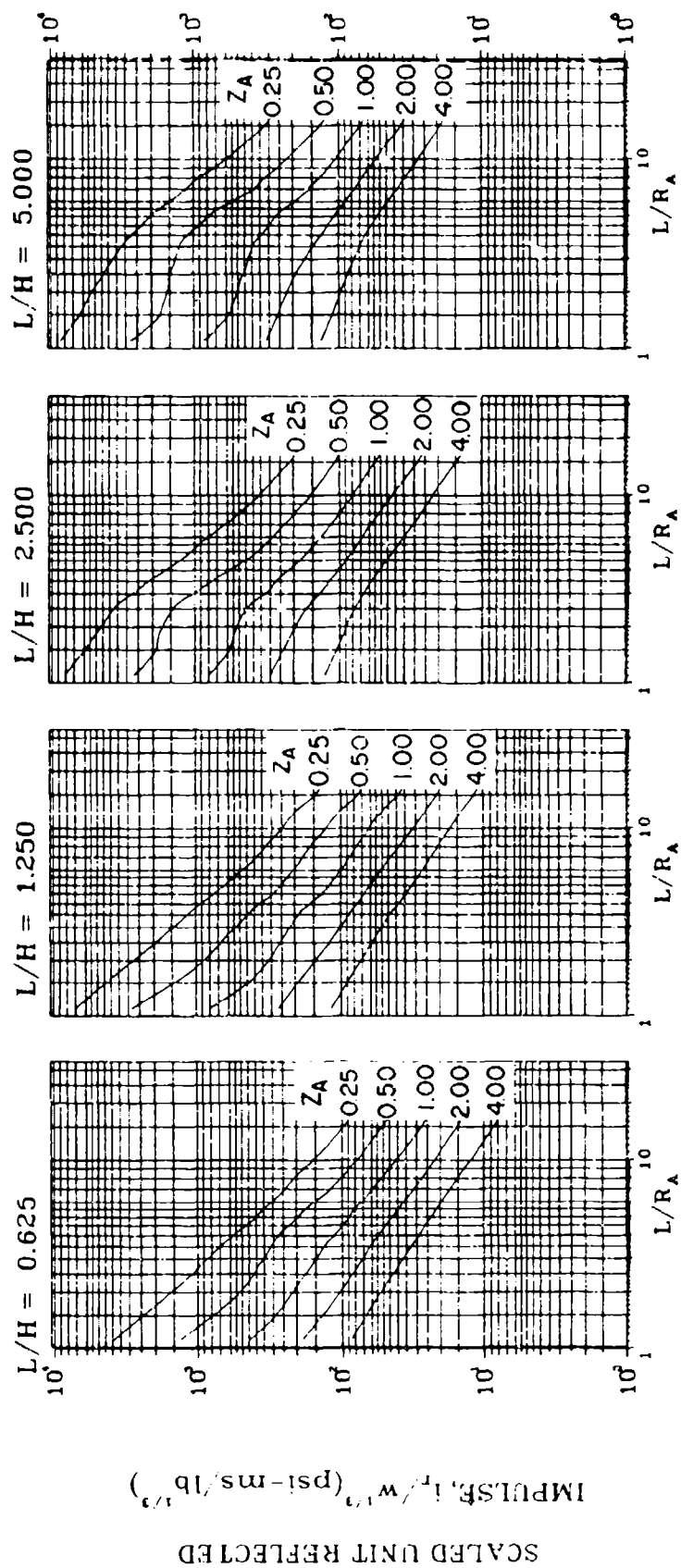


Figure 2-142 Scaled average unit reflected impulse
($N = 4$, $\ell/L = 0.25$ and 0.75 , $h/H = 0.10$)

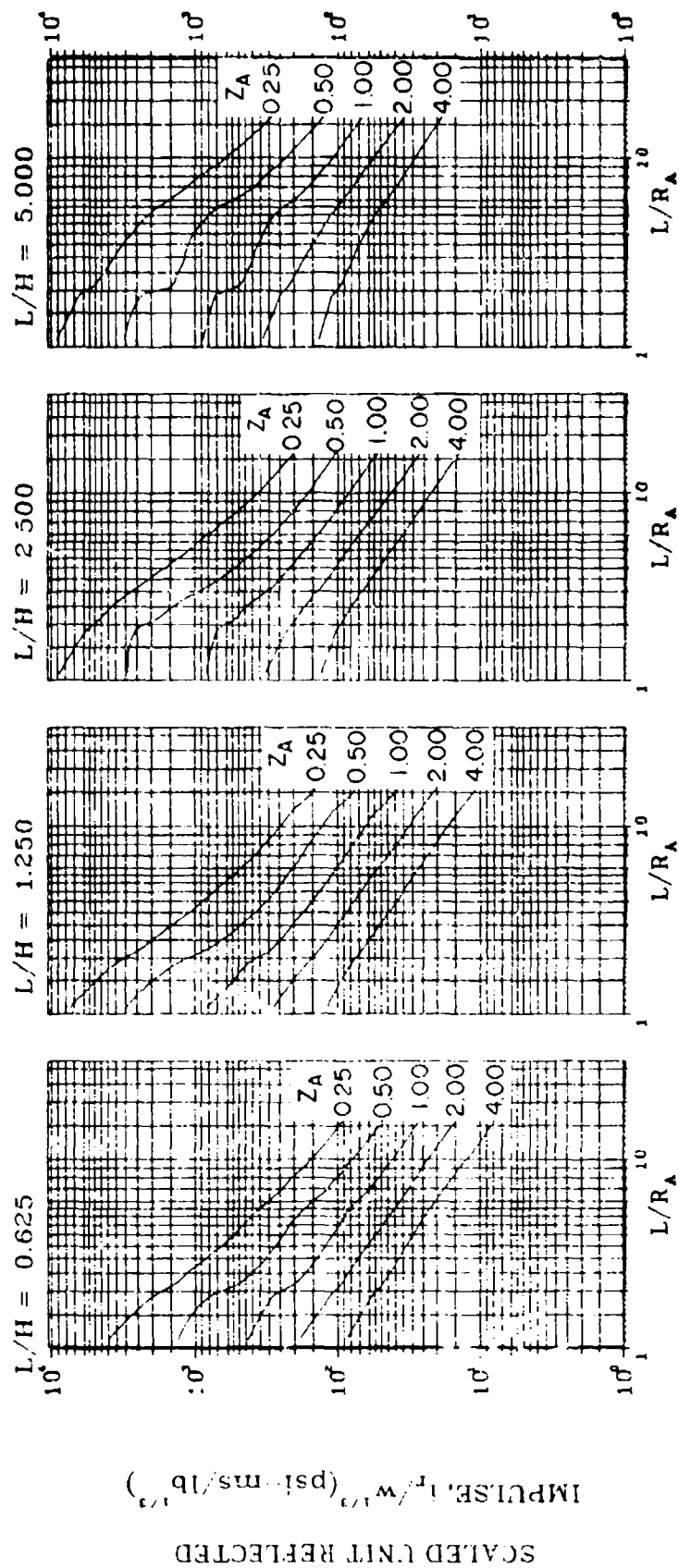


Figure 2-143 Scaled average unit reflected impulse
($N = 4$, $\ell/L = 0.50$, $h/H = 0.10$)

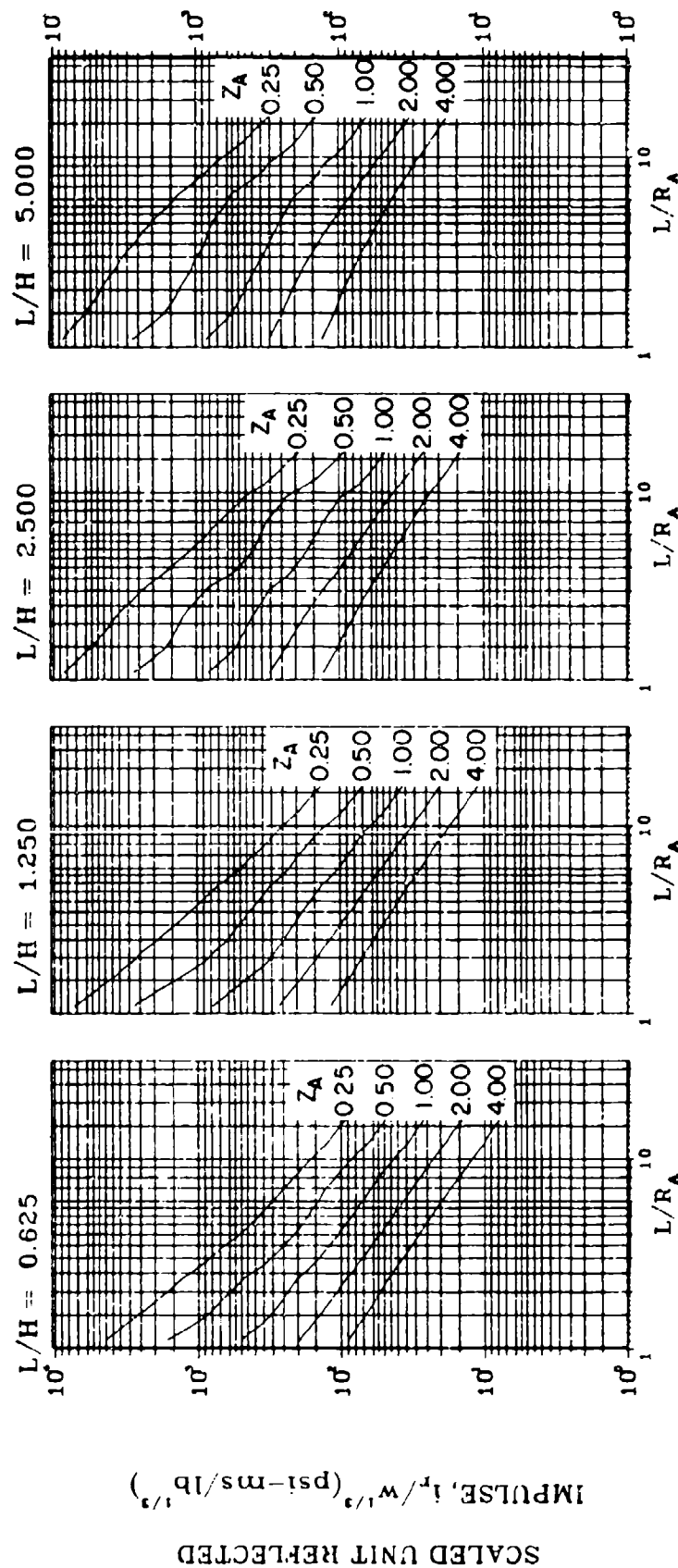


Figure 2-144 Scaled average unit reflected impulse
($N = 4$, $\ell/L = 0.10$, $h/H = 0.25$ and 0.75)

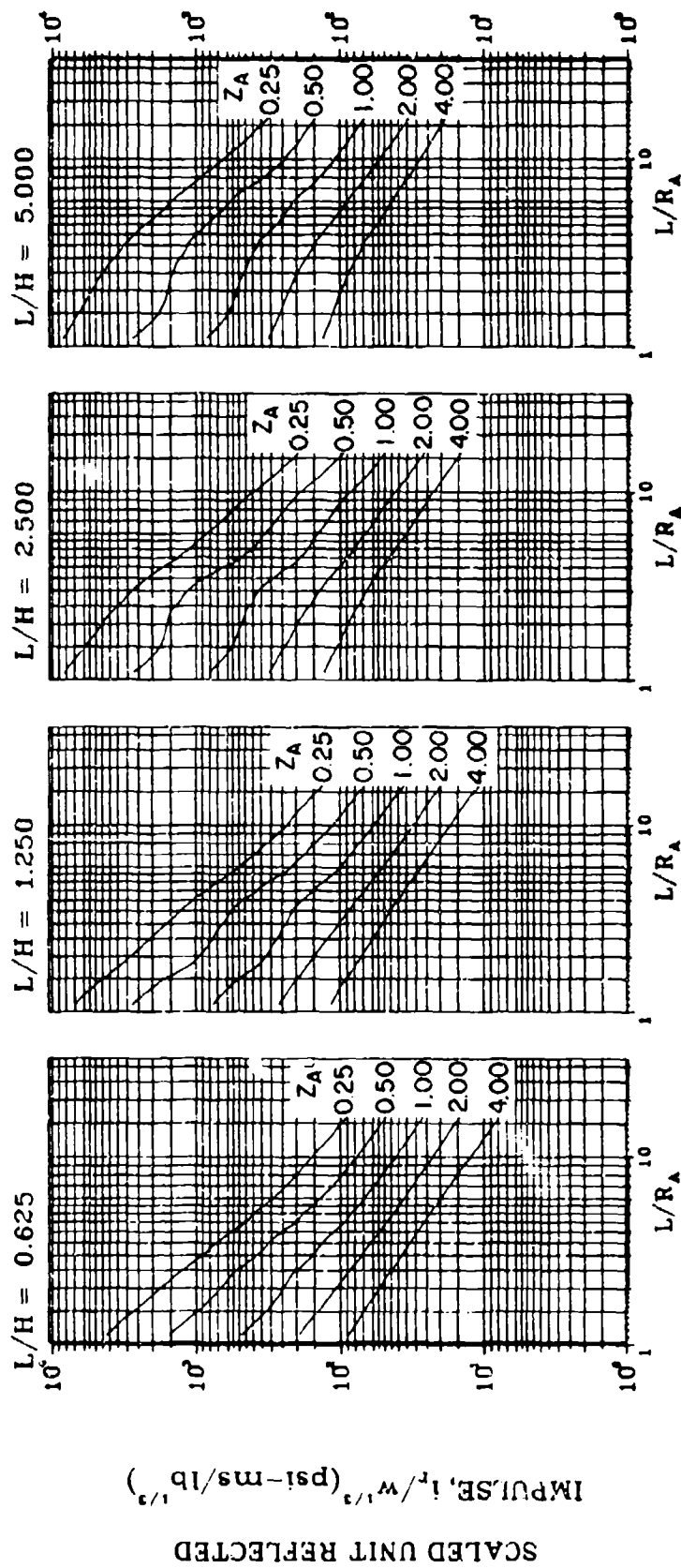


Figure 2-145 Scaled average unit reflected impulse
($N = 4$, $L/L = 0.25$ and 0.75 , $h/H = 0.25$ and 0.75)

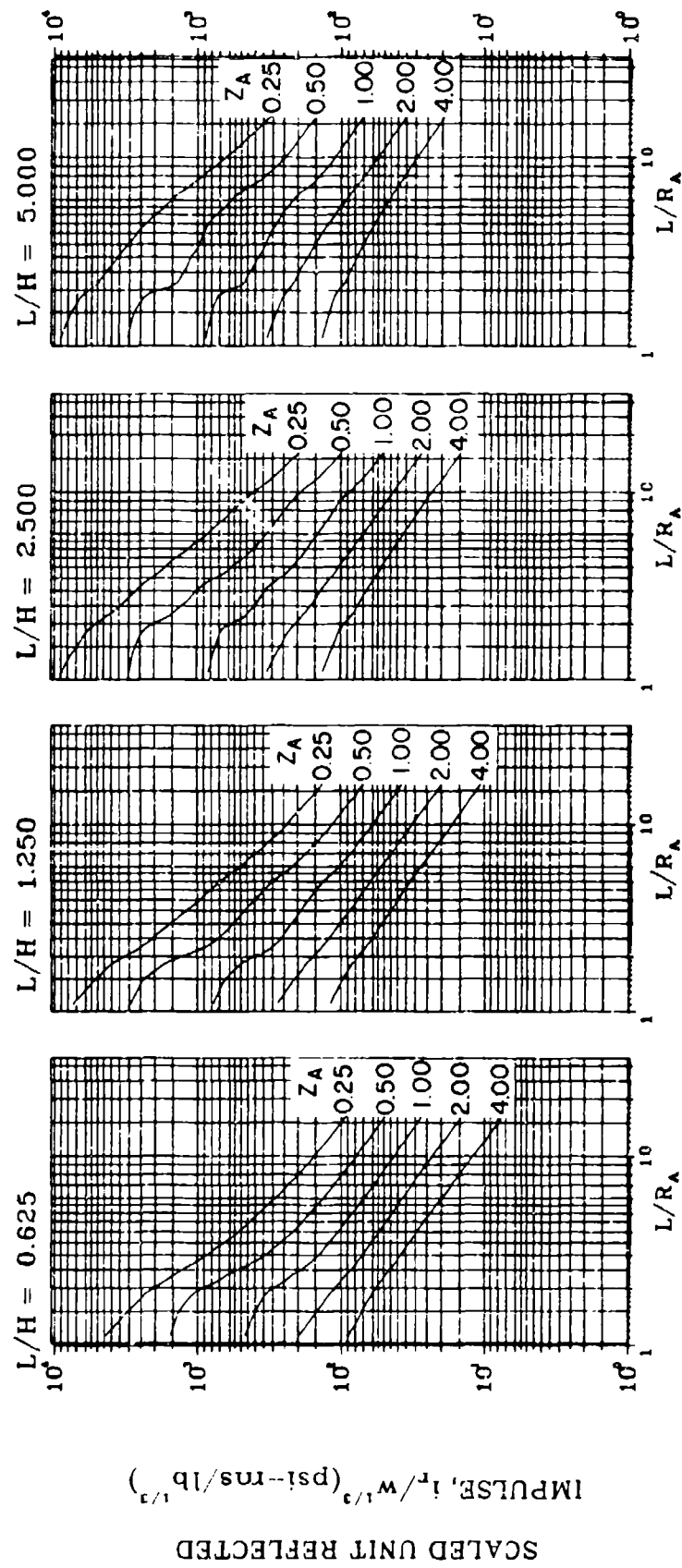


Figure 2-146 Scaled average unit reflected impulse
($N = 4$, $z/L = 0.50$, $h/H = 0.25$ and 0.75)

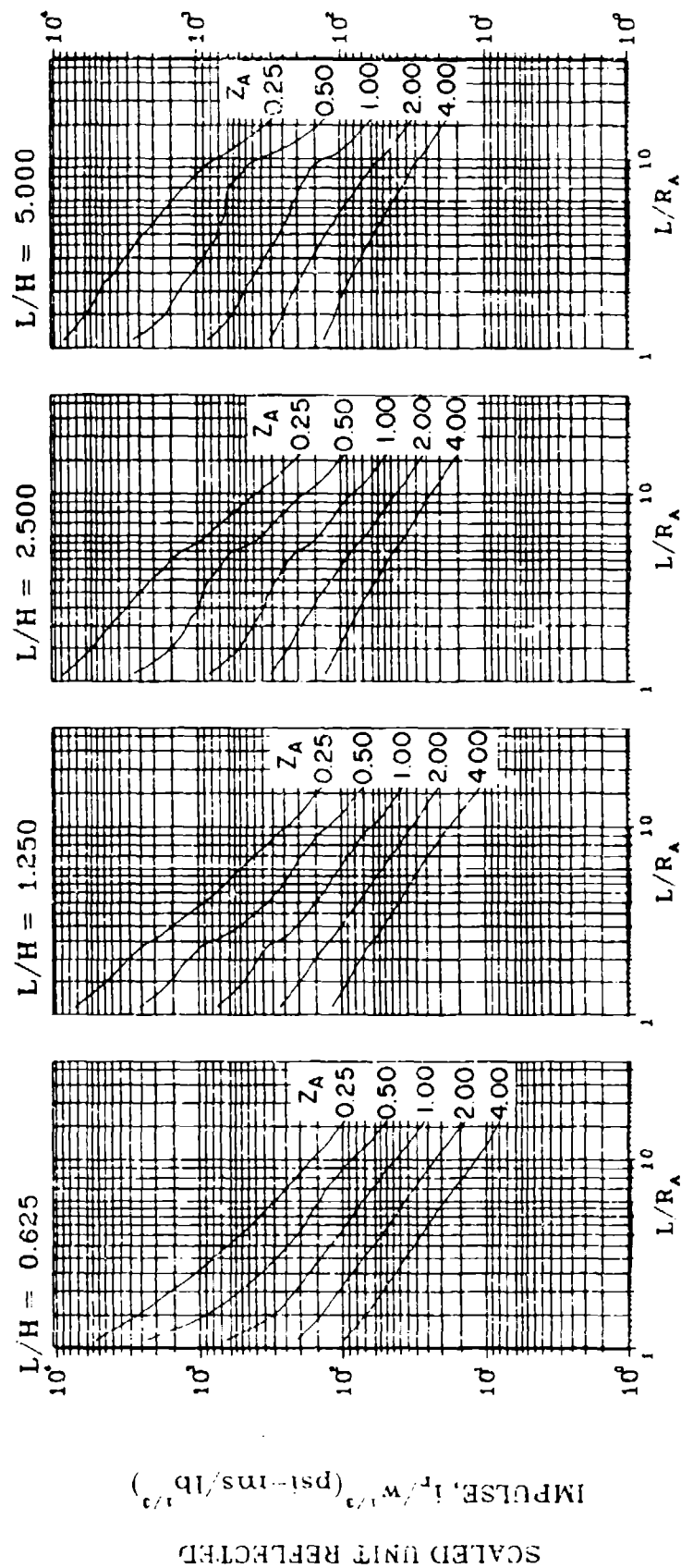


Figure 2-147 Scaled average unit reflected impulse
($N = 4$, $L/L = 0.10$, $h/H = 0.50$)

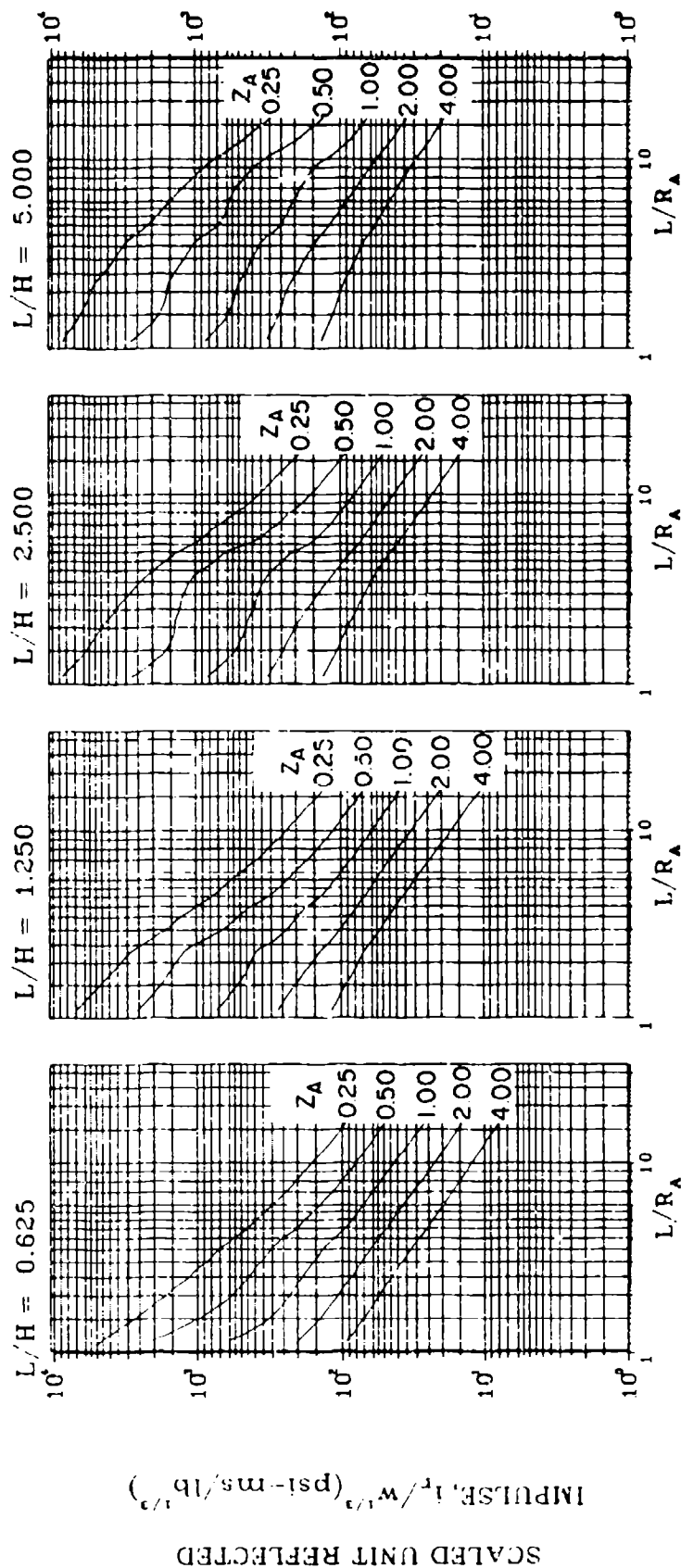


Figure 2-148 Scaled average unit reflected impulse
($N = 4$, $\ell/L = 0.25$ and 0.75 , $h/H = 0.50$)

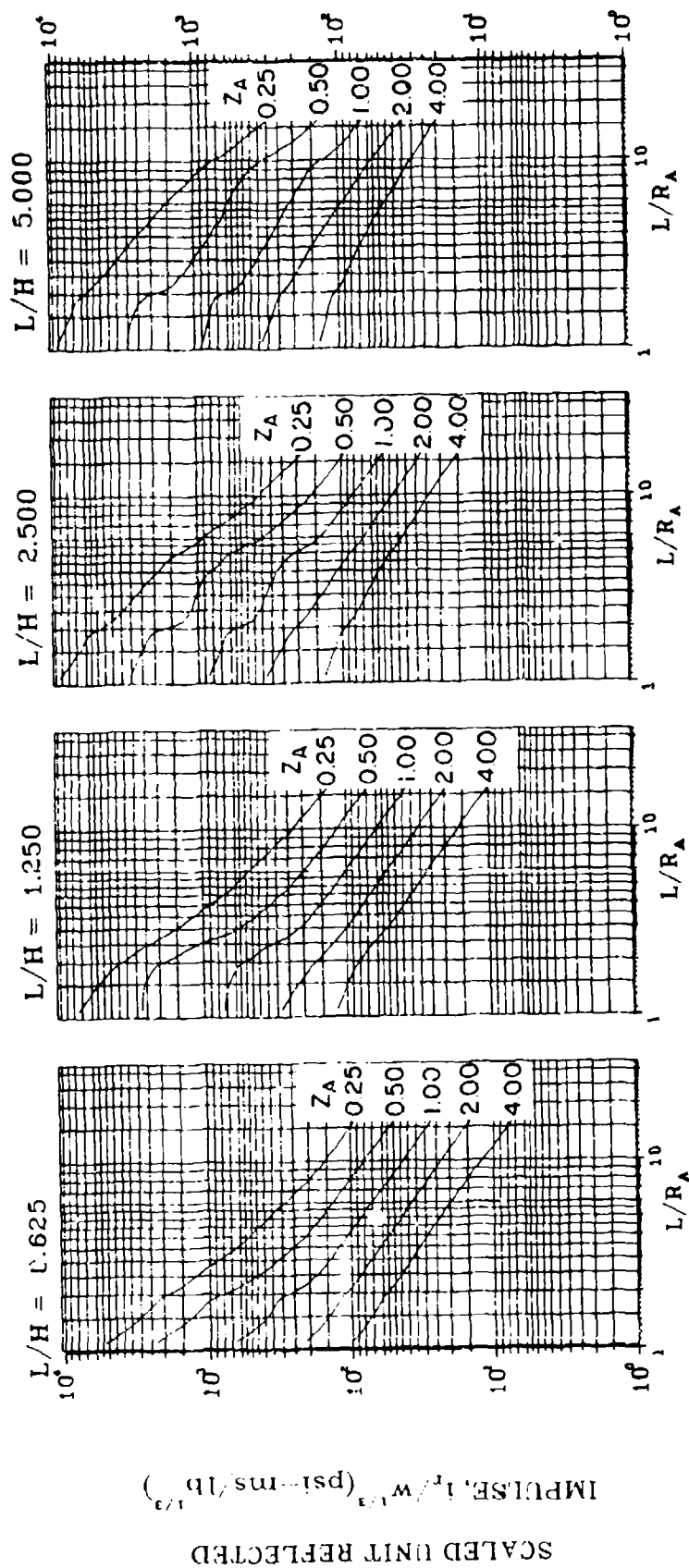


Figure 2-149 Scaled average unit reflected impulse
($N = 4$, $l/L = 0.50$, $h/H = 0.50$)

2-14.2.2 Frangibility. A frangible element, as defined here, is an element that exhibits a resistance to internal shock loads equal to or less than 25 pounds per square foot and will undergo significant displacement during the loading time of the shock pressures and, thereby, reduce the effects of the shock pressures acting on both the frangible panel itself and reflections to other elements of the structure.

The following are design procedures for determining the magnitude of applied shock pressures which will contribute to the displacement of the frangible element:

1. Determine the peak average reflected pressure P_r and average impulse i_r acting on the frangible element assuming that the element is rigid (figures 2-52 through 2-149)
2. Calculate the unit weight of the frangible element and divide this weight by the sixth root of charge weight, $W_F/W^{1/6}$.
3. Determine the fictitious scaled distance Z from figure 2-7, which corresponds to the average impulse determined in Step 1.
4. Using the value of $W_F/W^{1/6}$ from Step 2 and the fictitious scaled distance of Step 3 and utilizing figure 2-150, determine the value of the factor f_r , of average impulse contributing to the translation of the frangible element (may require interpolation)
5. Calculate the value of the average impulse contributing to the translation of the frangible element by multiplying the values of i_r and f_r of steps 1 and 4 respectively
6. The value of the peak average pressure contributing to the translation of the frangible element is assumed to be equal to the value of P_r of Step 1.

The step by step procedure for determining the shock loads being reflected from a frangible element to an adjacent element is:

1. Determine the average peak reflected pressure P_r and the average reflected impulse i_r acting on the element in question, assuming that the adjoining frangible element will remain in place (figures 2-52 through 2-149)
2. Determine the average impulse acting on the element in question assuming that the adjoining frangible element is removed (figures 2-52 through 2-149)

3. Subtract the average impulse determined in Step 2 from the average impulse determined in Step 1
4. Calculate the unit weight of the frangible element and divide this weight by the sixth root of the charge weight, $W_F/W^{1/6}$
5. Calculate the normal scaled distance Z between the center of the charge and the surface of the frangible element
6. Utilizing figure 2-150, determine the value of the fraction f_r of the average impulse reflected to the element in question using the scaled weight density and scaled distance of Steps 4 and 5 respectively (may require interpolation)
7. Determine the magnitude of the impulse load reflected to the element in question from the frangible element by multiplying the value of the average impulse of Step 3 by the value of f_r of Step 6
8. Determine the total impulse load acting on the element in question by adding the impulse loads determined in Steps 2 and 7.
9. The peak average reflected pressure of the shock loads acting on the element in question may be taken equal to the value of P_r of Step 1.

In the above procedure, it is assumed that the frangible element will remain intact while being displaced away from the structure. If the element fails while being translated, then the portion of the shock pressure impulse displacing the element as well as that portion of the impulse being reflected to other elements will be reduced due to additional venting area produced by the element's "break up".

2-14.2.3 TNT Equivalency. The shock loads presented in figure 2-52 through 2-149 pertain to the blast effects of bare spherical TNT explosives and must be extended to include other potentially mass-detonating materials. However, only a limited amount of testing has been performed to determine the TNT equivalency of confined explosives. Therefore, as an interim procedure, it is suggested that the determination of shock pressures for confined explosives other than TNT utilize equivalencies based on Equation 2-1.

The above relationship assumes that the explosive in question is a bare charge and spherical in shape. If the charge is not spherical, then it is suggested that the explosive be subdivided into several segments which will have approximately equal dimensions and that the reflected impulse for any segment be calculated, as previously discussed. The reflected impulse of the total charge is then determined by multiplying the impulse of the individual segments by the total number of segments. The peak average reflected pressure is calculated by assuming the total charge as having a spherical shape. The impulse load for multiple explosives is obtained in a similar manner except that the locations of the individual charges are considered in calculation.

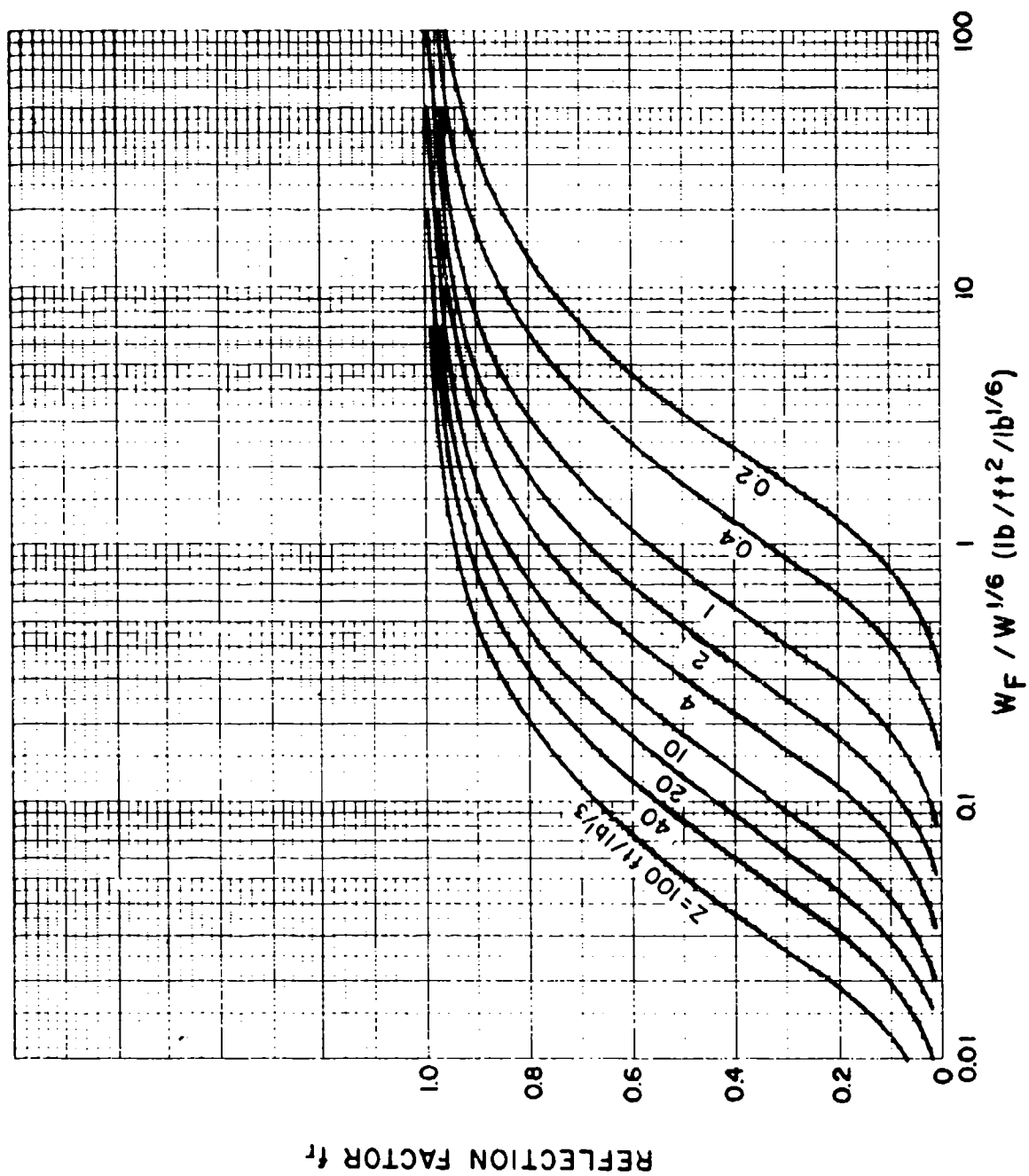


Figure 2-150 Reflection factor for shock loads on frangible elements

ing their individual impulse load. The impulse load of the total charge is determined by adding together the individual impulse loads. The average peak reflected pressure is calculated using the total weight of the explosive located at the centroid of the individual charges.

The explosive casing will have an effect on the magnitude of the shock pressures. These effects are dependent on the properties of the casing such as material, thickness, shape, etc. A review of a limited amount of surface detonated test data has indicated that the effects of the casing are not severe and, therefore, for design purposes it is recommended that casing effects be neglected.

2-14.2.4 Multiple Explosions

The blast pressures and impulse loads, acting on various elements of cubicle or other similar structures, which are produced by multiple explosions, will usually differ from those produced by a single explosion of the same amount of explosives.

Although the magnitude of the total combined impulse produced by the multiple explosions will usually be larger than that produced by the single explosion, the damage to a protective element due to the impulse of the multiple detonation may be either greater, equal to, or less than that produced by the impulse of the single explosion. For a given total impulse, the degree of damage to a protective element will be defined by the duration of the entire load relative to the response time of the element (time to reach maximum deflection).

A minimum amount of theoretical and experimental data is available concerning the degree of damage sustained by structural elements due to multiple explosions. However, results of response tests of reinforced concrete slabs have indicated that if the total combined duration of the blast loads produced by simultaneously or near simultaneously exploded charges is equal to or less than one-third the response time (time to reach maximum deflection) of the element, then the total combined impulse acting on the element can be estimated by numerically adding the impulse loads produced by the individual explosions. However, if the total combined duration of the blast loads is greater than one-third the response time, the actual pressure-time relationship of the combined loads approximated by a fictitious peaked triangular pressure pulse (similar to that of a single explosion) should be considered. The blast loads produced by charges that are not simultaneously or near simultaneously exploded may be considered as two or more impulse loads, two or more pressure-time loads, or a combination of impulse and pressure-time loads depending on the time delay and the duration of the individual loads compared to the response time of the element. A load or group of loads should be treated as an impulse load if the duration (one load or the combined duration of two or more loads) of the loading is less than one-third the time interval between the onset of the load or group of loads and the response time of the member.

The duration of the blast loads due to multiple explosions may be approximated by considering the interrelationship between (a) the time intervals between individual explosions, (b) arrival times of the blast waves of the individual explosions at the element and (c) the fictitious duration of the pressure load from individual explosions. Because of the many variables involved, a

relationship cannot be given to obtain the duration of the blast loads due to multiple explosions. Each situation will require a series of computations involving the time increments outlined above.

2-14.3 Gas Pressures

2-14.3.1 Blast Loads. When an explosion occurs within a confined area, gaseous products will accumulate and a temperature within the structure will rise, thereby forming blast pressures whose magnitude is generally less than that of the shock pressures but whose duration is significantly longer. The magnitude of the gas pressures as well as their durations is a function of the size of the vent openings in the structure. For very small openings or no openings at all, the duration of the gas pressures will be very long in comparison to the fundamental periods of the structure's elements and, therefore, may be considered as a long duration load similar to that associated with a nuclear event.

These conditions usually occur in total or near containment type structures. In the former, the internal blast pressures must be contained because of the presence of toxic or other harmful materials in the structure. In near containment structures, the leakage of pressure flow out of the structure usually must be limited because of either personnel or frangible structures are located immediately adjacent to the donor structure. In other cases, however, openings in structures may be quite large, thereby minimizing the products' accumulation and limiting the temperature rise, hence producing gas pressures with limited duration or no duration at all. The structures without gas pressure buildup are referred to as fully vented structures.

A typical pressure-time record at a point on the interior surface of a partially vented chamber is shown in figure 2-151. The high peaks are the multiple reflections associated with shock pressures. The gas pressure, denoted as p_g , is used as the basis for design and is a function of the charge weight and the contained net volume of the chamber.

Figure 2-152 shows an experimentally fitted curve based upon test results of partially vented chambers with small venting areas where the vent properties ranged between:

$$0 \leq A_f/V_f^{2/3} \leq 0.022 \quad 2-3$$

The values of A and V_f are the chamber's total vent area and free volume which is equal to the total volume minus the volume of all interior equipment, structural elements, etc. The maximum gas pressure, P_g , is plotted against the charge weight to free volume ratio.

Figures 2-153 through 2-164 provide the relationship of the gas pressure scaled impulse $i_g/W^{1/3}$ as a function of the charge weight to free volume ratio W/V_f , scaled value of the vent opening $A/V_f^{2/3}$, the scaled unit weight of the cover $W_f/W^{1/3}$ over the opening, and the scaled average reflected impulse

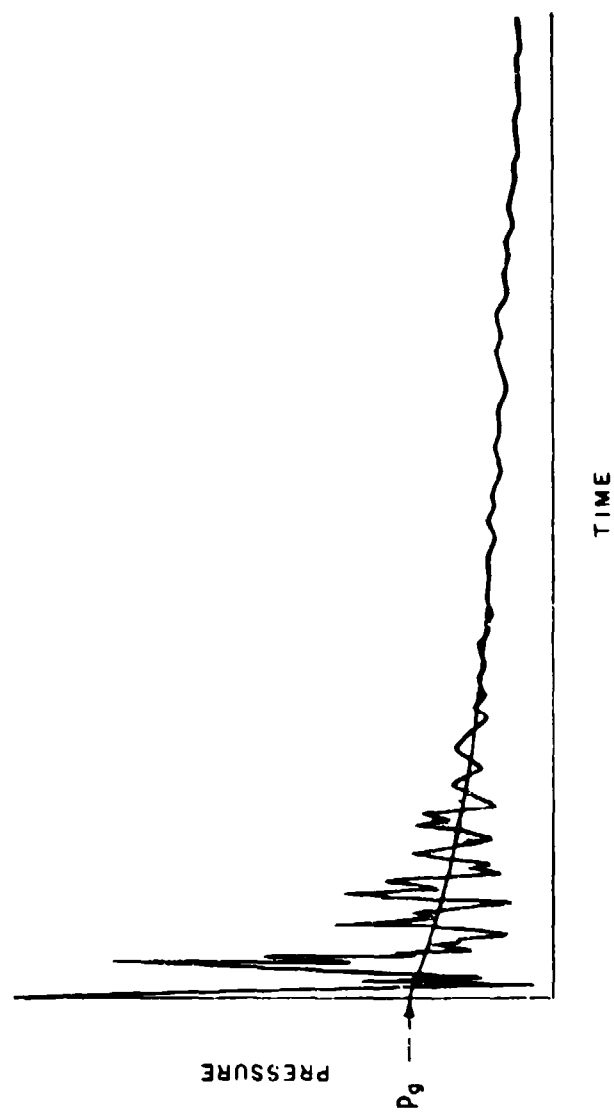
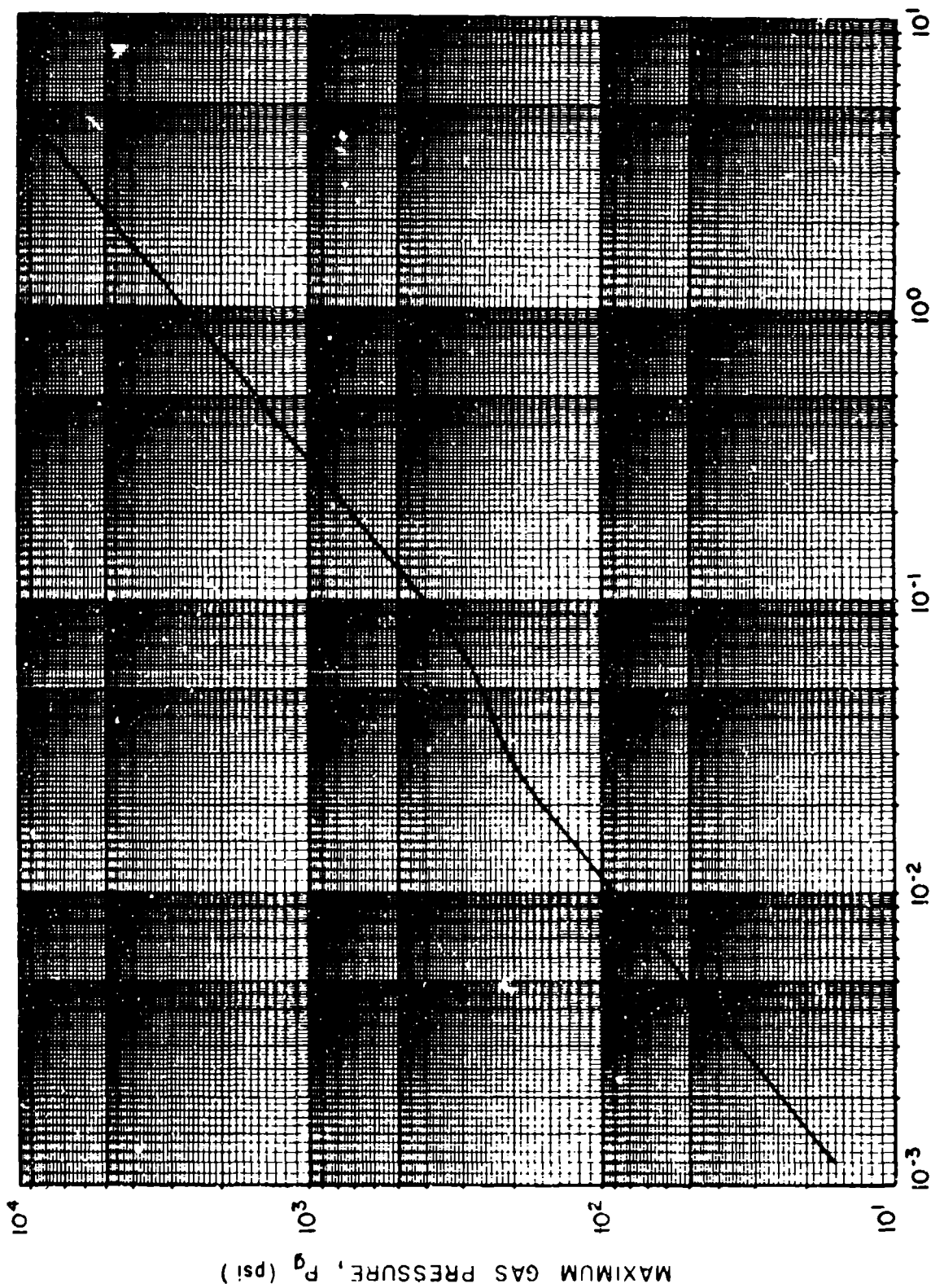


Figure 2-151 Pressure-time variation for a partially vented explosion



CHARGE WEIGHT TO FREE VOLUME, W/V_f (lbs/cu ft)

Figure 2-152 Peak gas pressure produced by a TNT detonation in a partially contained chamber

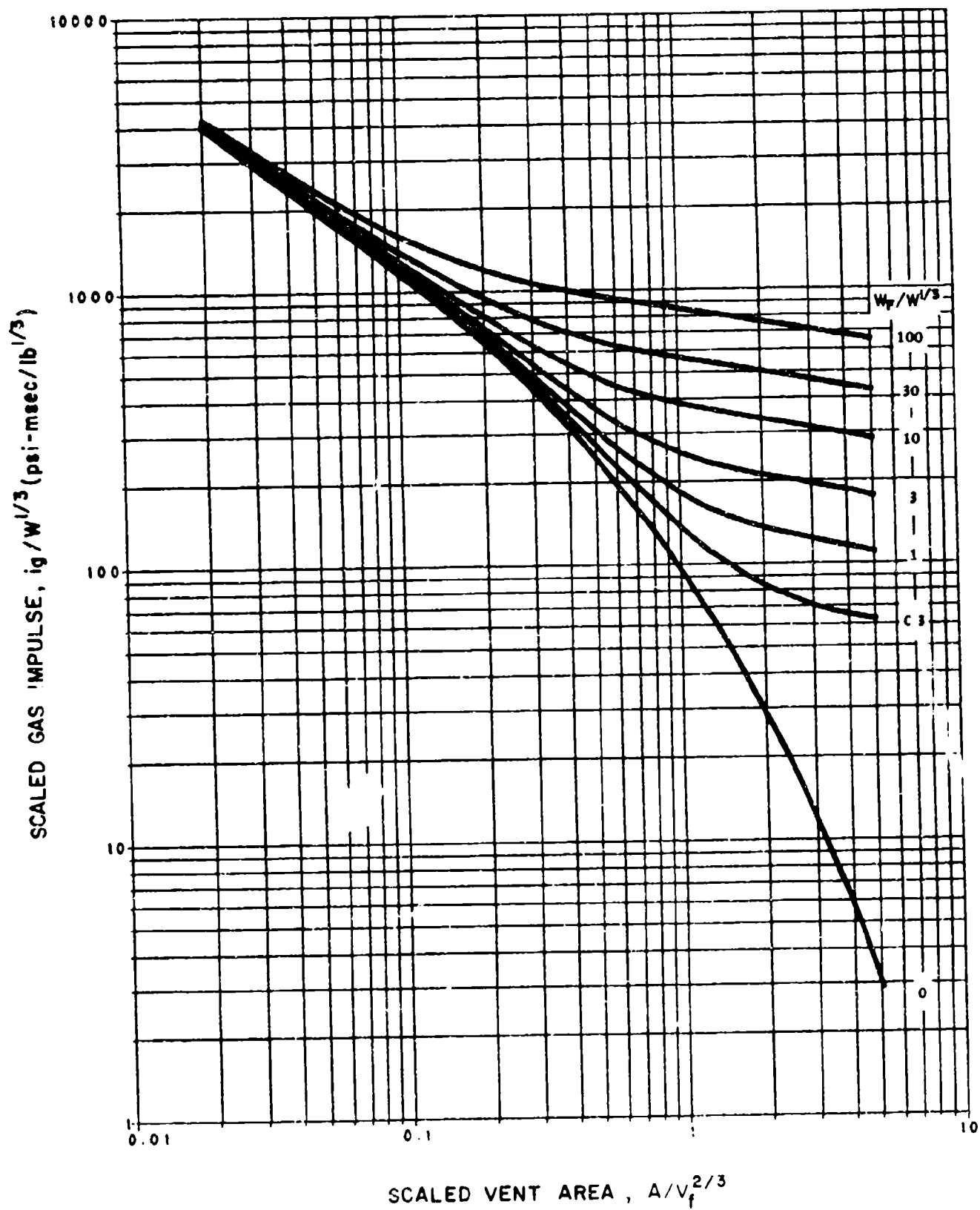


Figure 2-153 Scaled gas impulse ($W/V_f = 0.002$, $i_L/W^{1/3} = 20$)

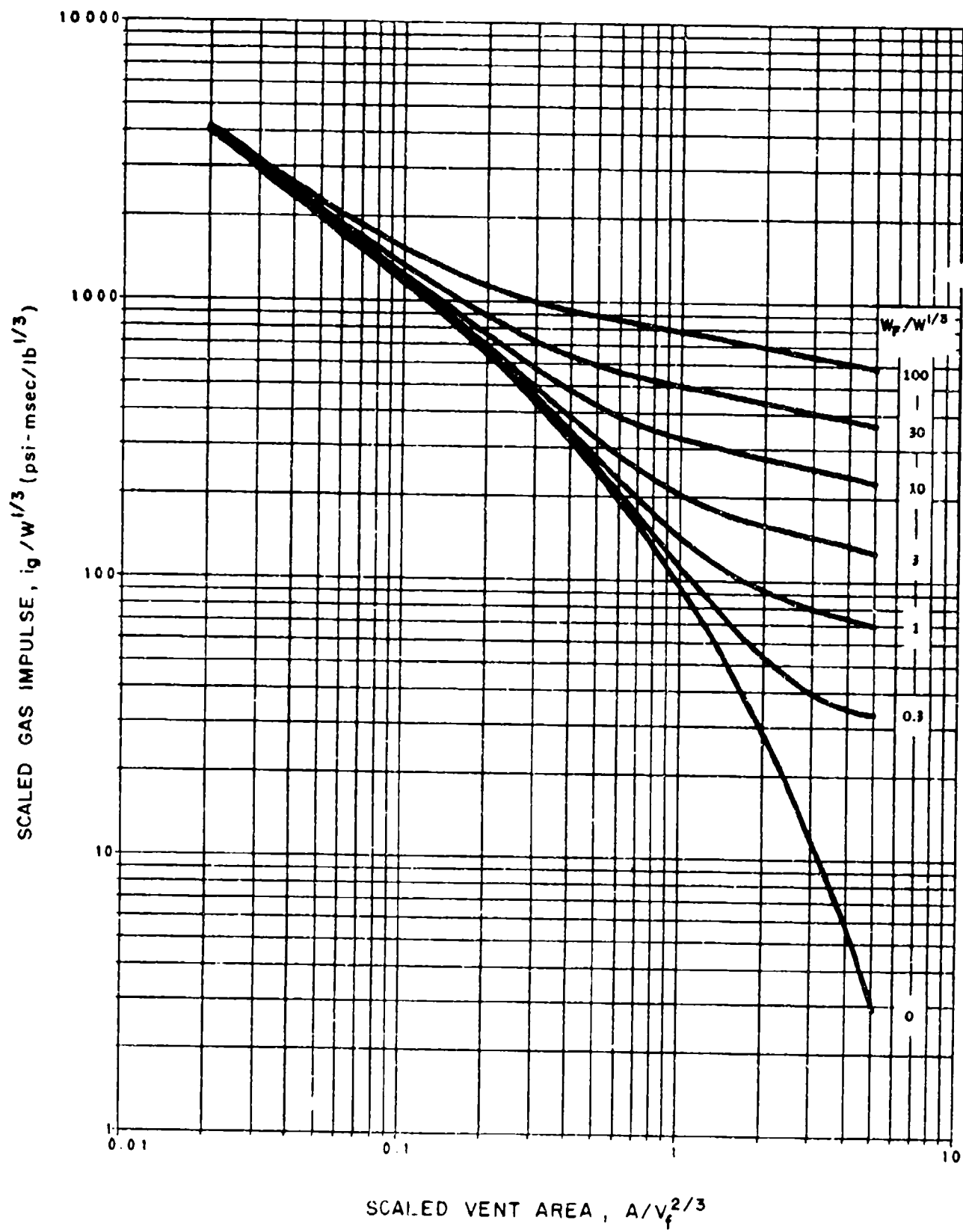


Figure 2-154 Scaled gas impulse ($W/V_f = 0.002$, $i_r/W^{1/3} = 100$)

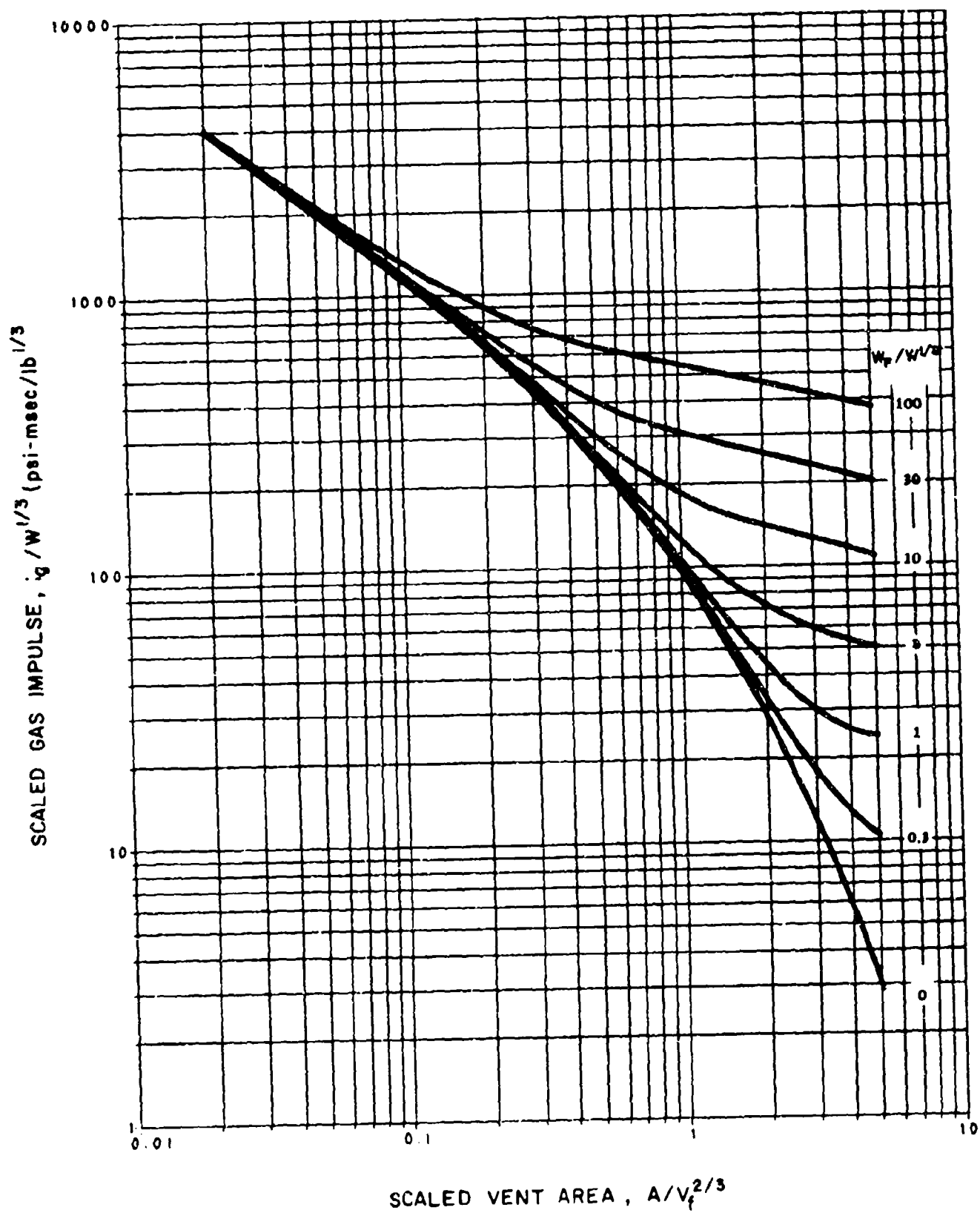


Figure 2-155 Scaled gas impulse ($W/V_f = 0.002$; $i_r/W^{1/3} \approx 600$)

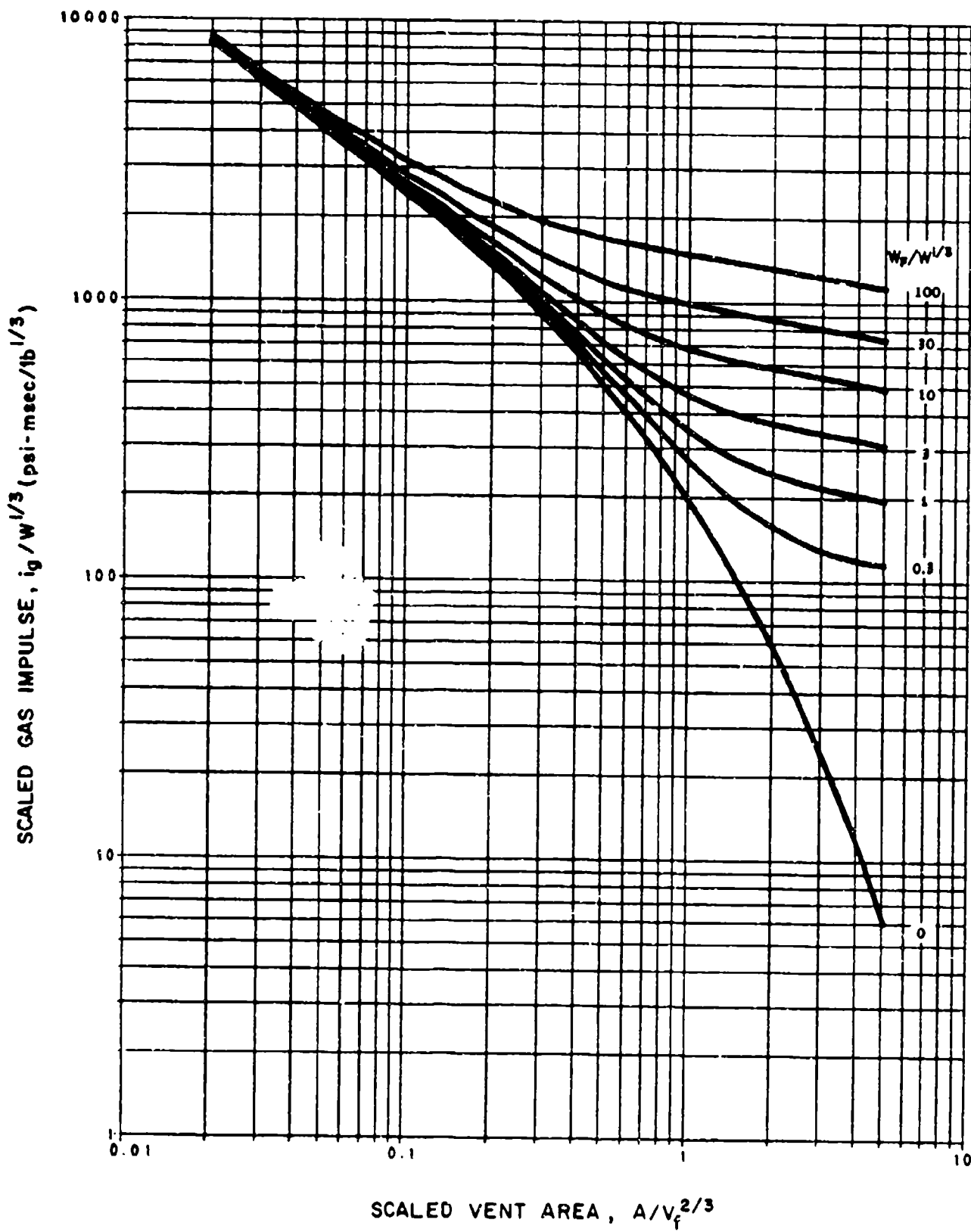


Figure 2-156 Scaled gas impulse ($W/V_f = 0.015$, $i_r/W^{1/3} = 20$)

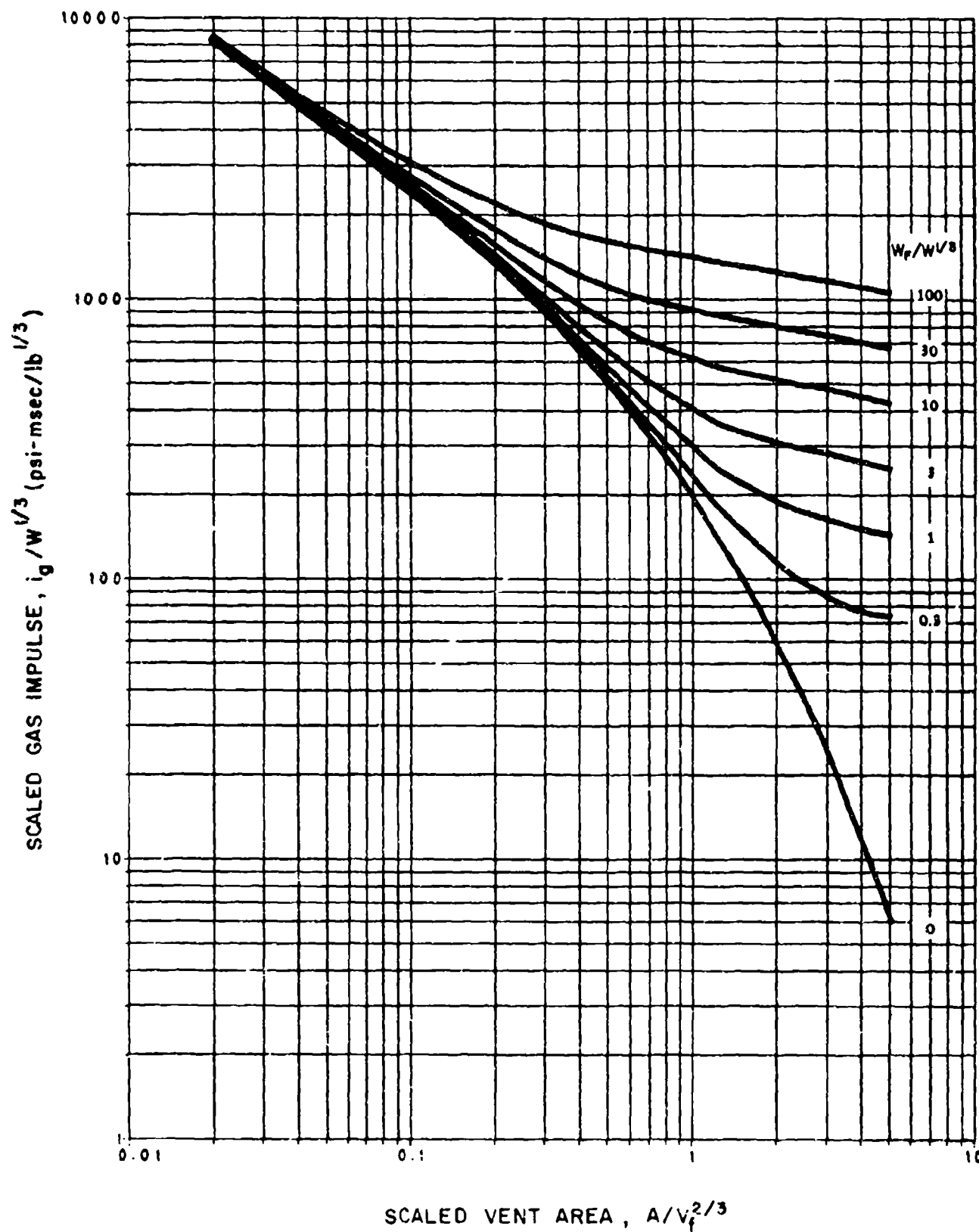


Figure 2-157 Scaled gas impulse ($W/V_F = 0.015$, $i_r/W^{1/3} = 100$)

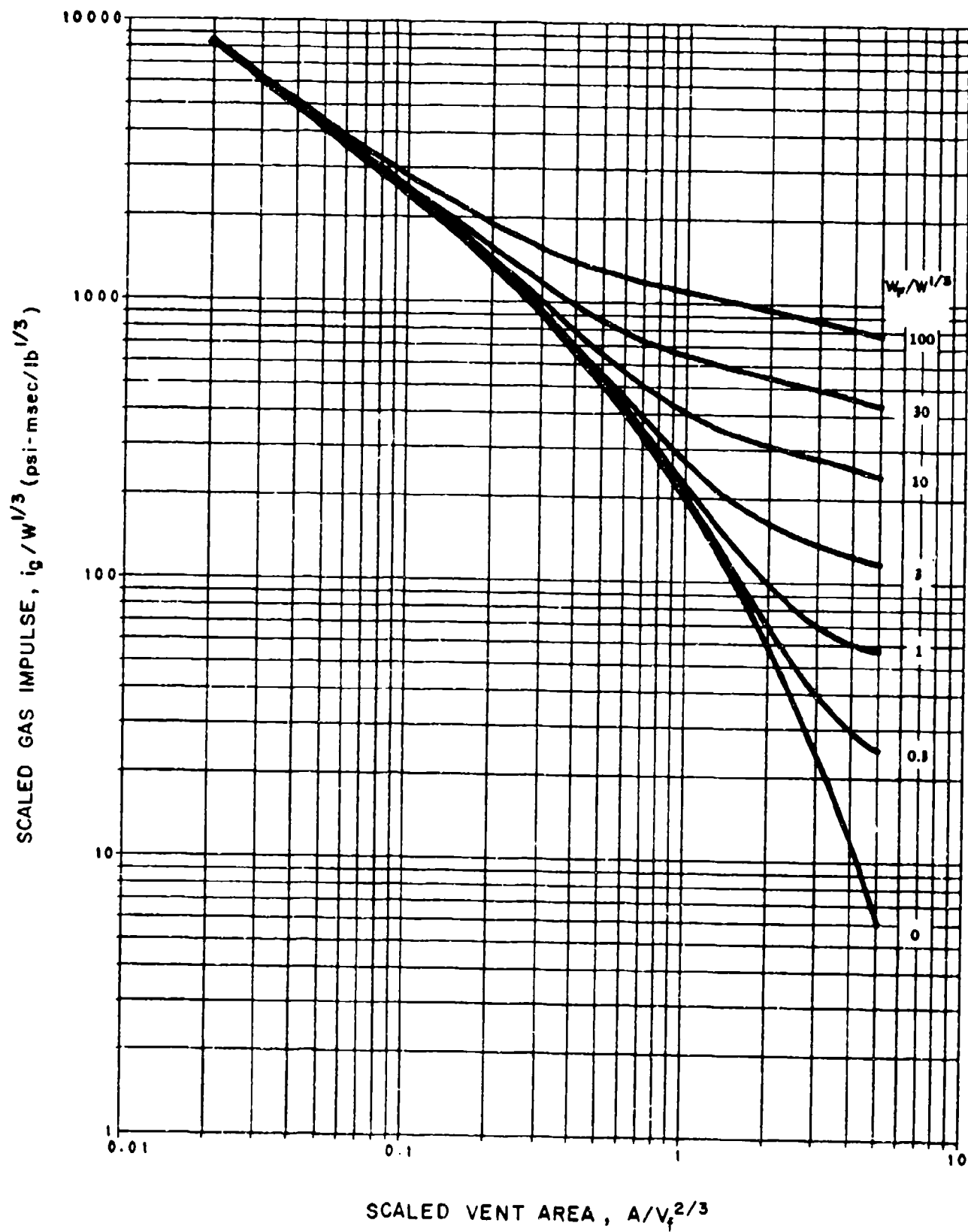


Figure 2-158 Scaled gas impulse ($W/V_f = 0.015$, $i_1/W^{1/3} = 600$)

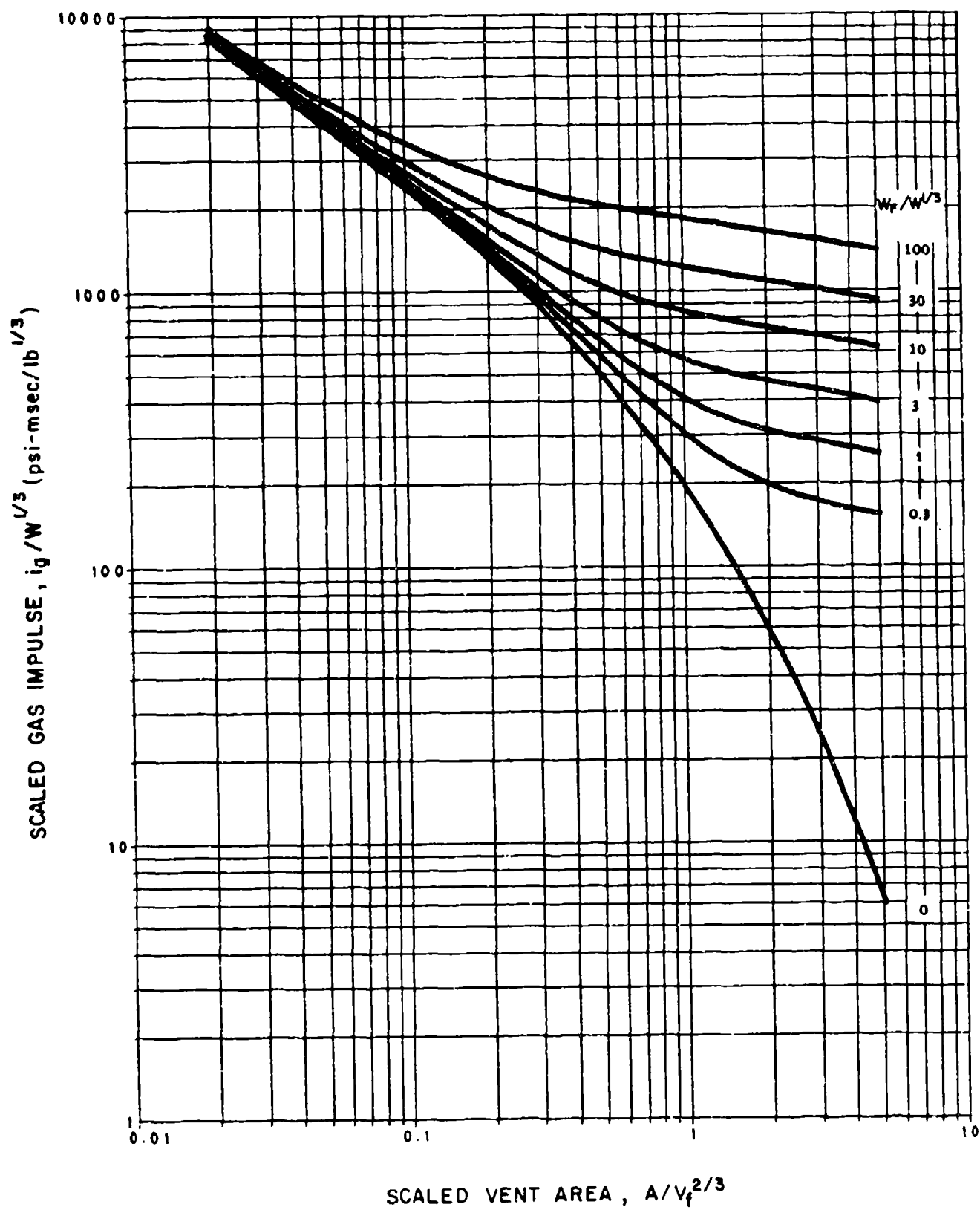


Figure 2-159 Scaled gas impulse ($W/V_f = 0.15$, $i_r/W^{1/3} = 20$)

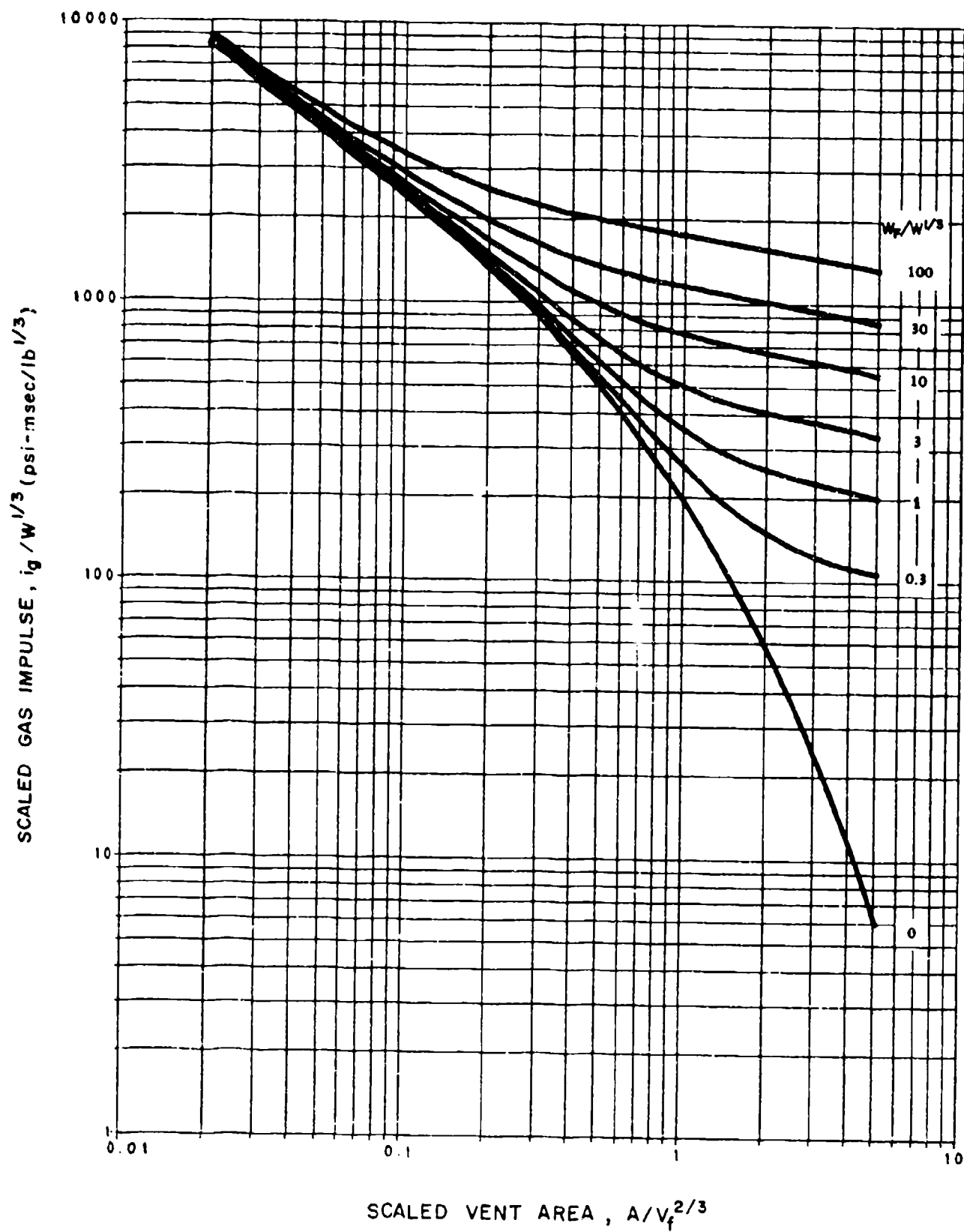


Figure 2-160 Scaled gas impulse ($W/V_f = 0.15$, $i_r/W^{1/3} = 100$)

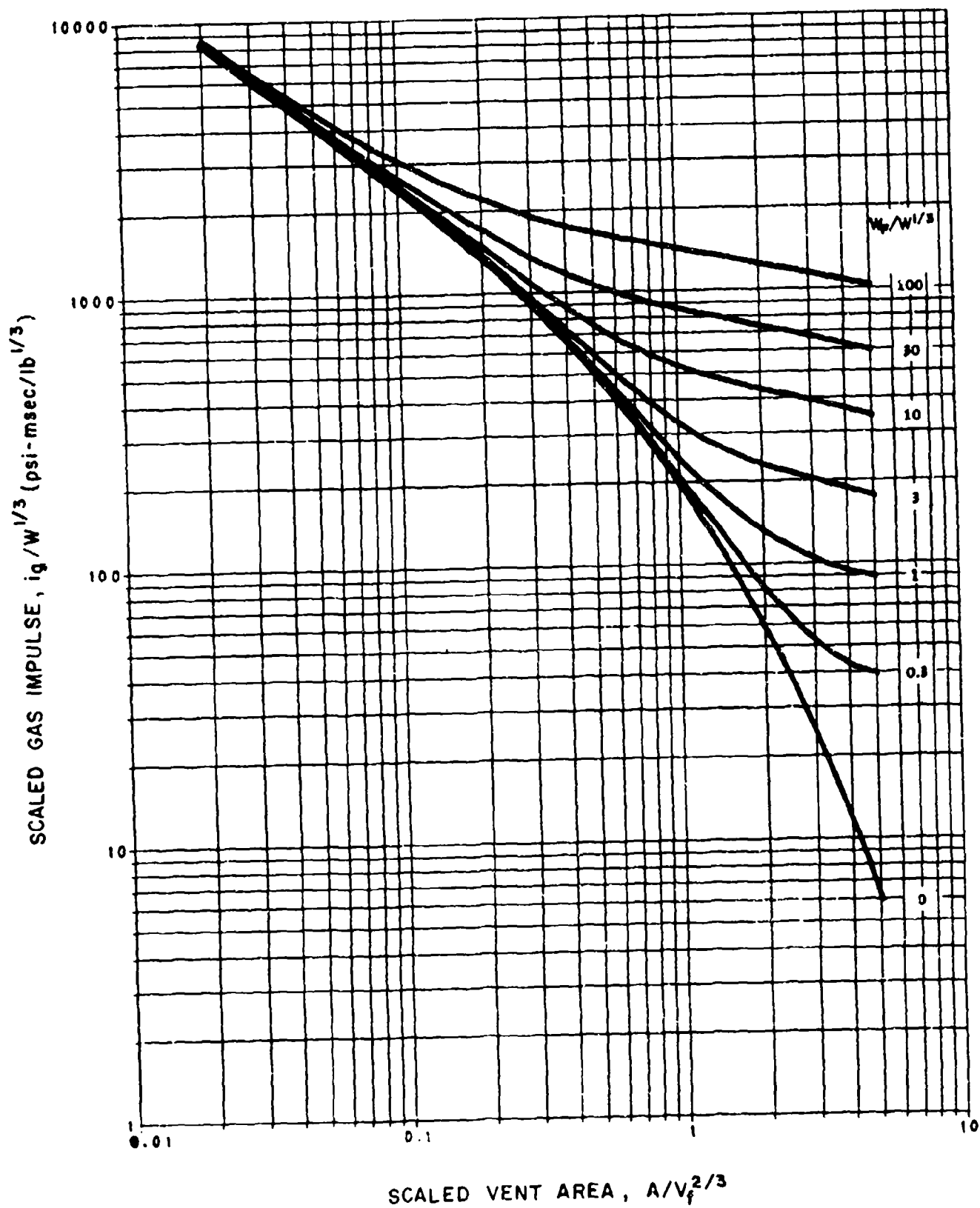


Figure 2-161 Scaled gas impulse ($W/V_f = 0.15$, $i_r/W^{1/3} = 600$)

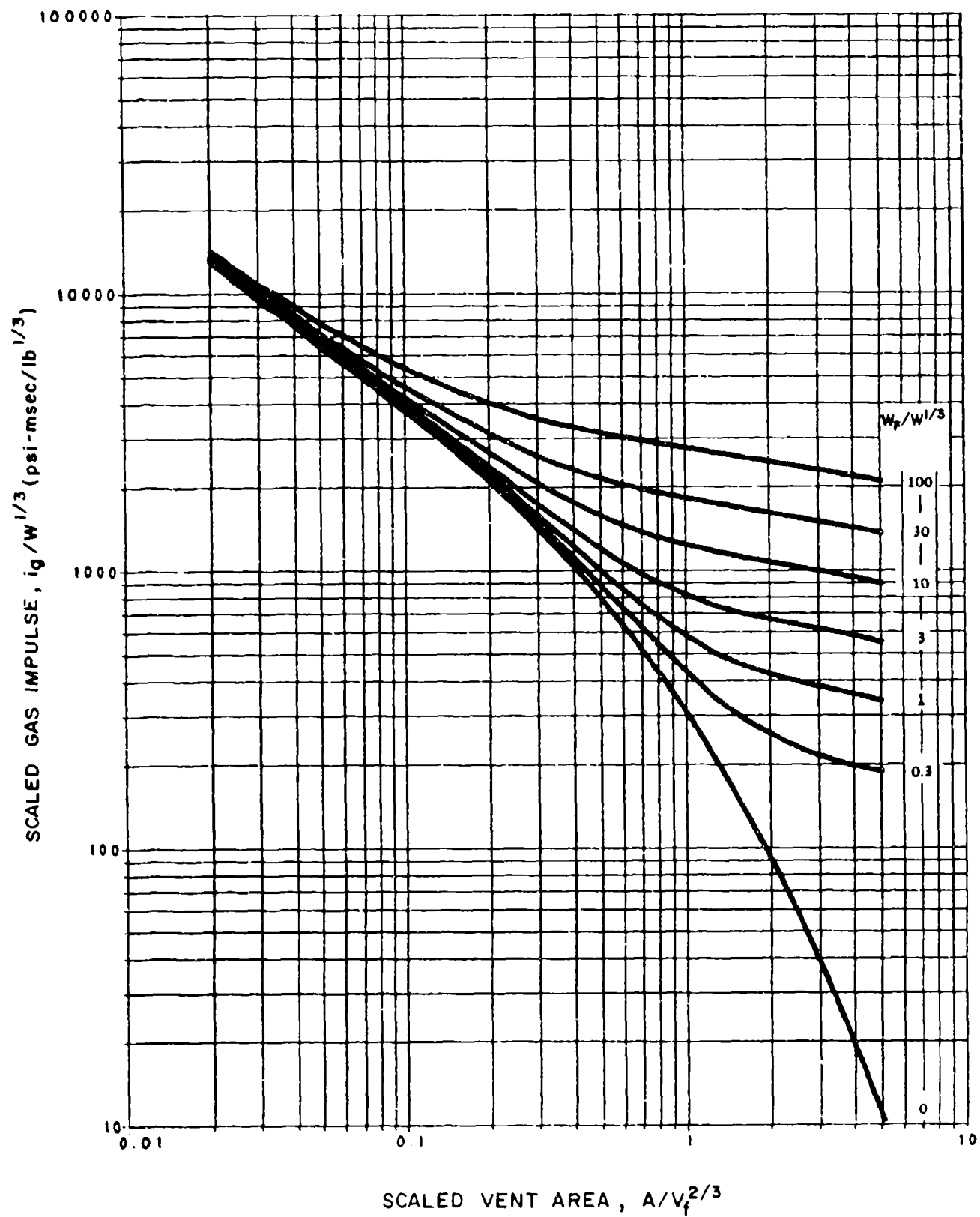


Figure 2-162 Scaled gas impulse ($W/V_f = 1.0$, $i_r/W^{1/3} = 100$)

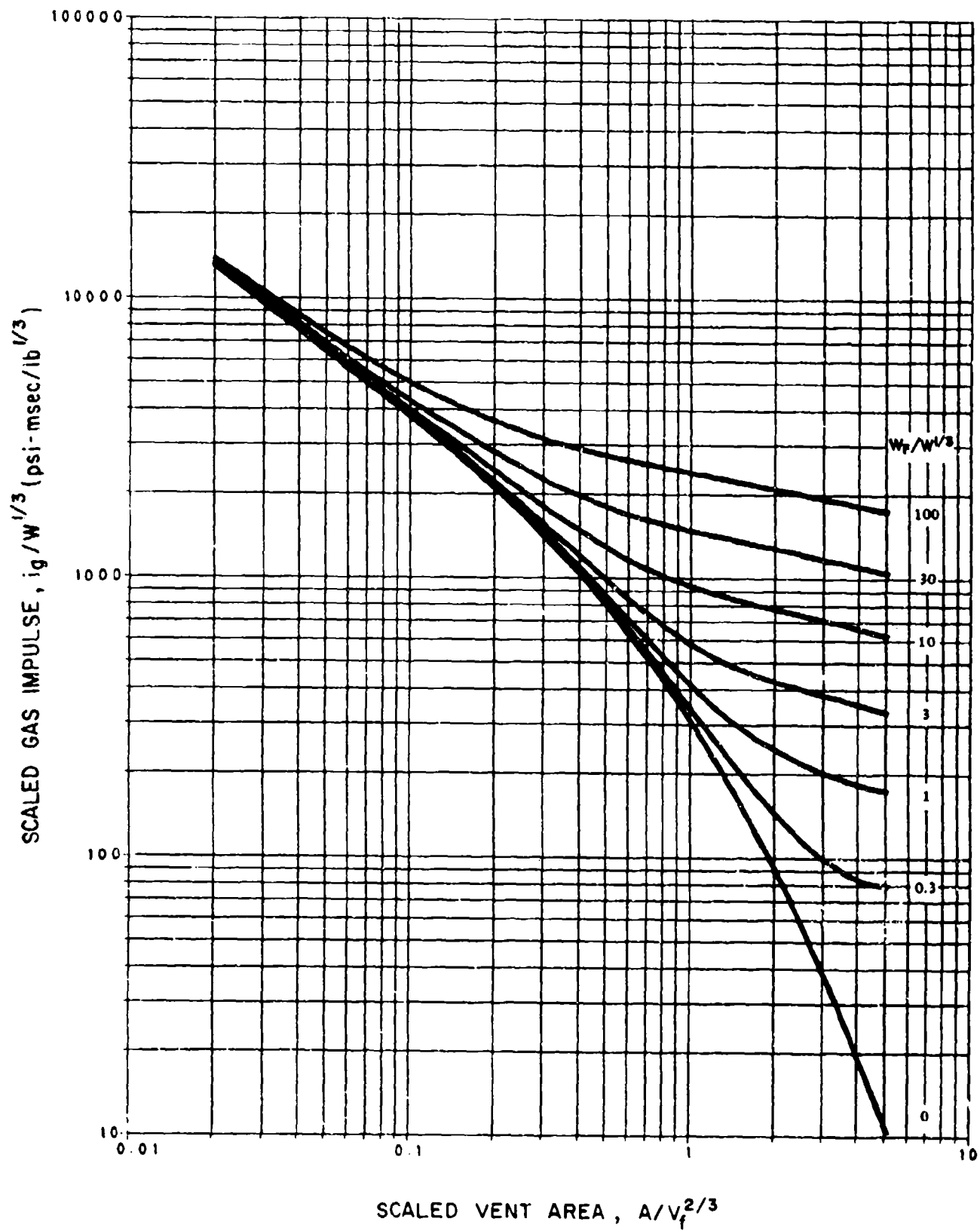


Figure 2-163 Scaled gas impulse ($W/V_f = 1.0$, $i_r/W^{1/3} = 600$)

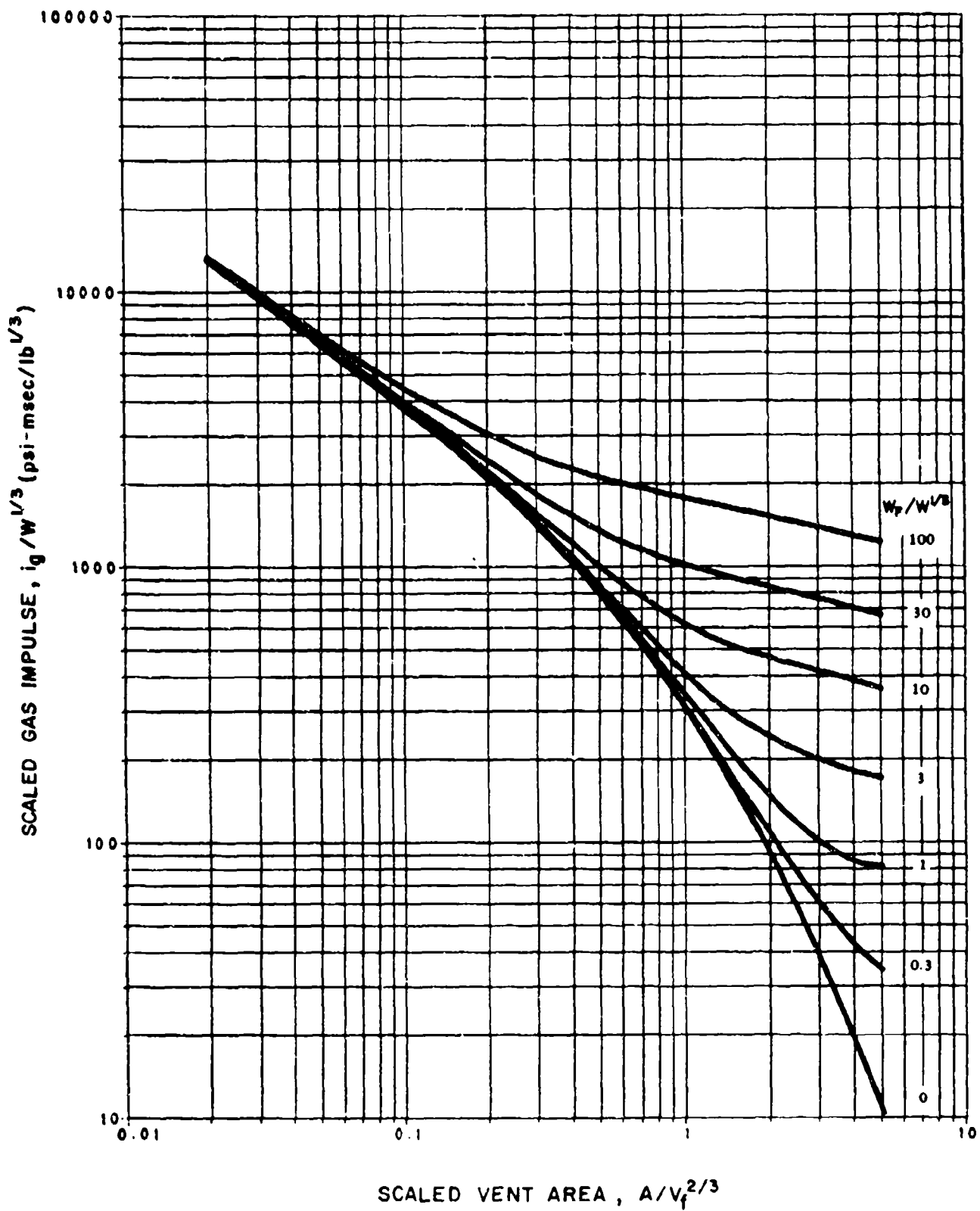


Figure 2-164 Scaled gas impulse ($W/V_F = 1.0$, $i_r/W^{1/3} = 2000$)

$i_p/W^{1/3}$ of the shock pressures acting on the frangible wall (Section 2-14.2.2) or a non-frangible wall with a vent opening. For a full containment type structure the impulse of the gas pressure will be infinite in comparison to the response time of the elements (long duration load). For near containment type structures where venting is permitted through vent openings without covers, then the impulse loads of the gas pressures are determined using the scaled weight of the cover equal to zero. The impulse loads of the gas pressures corresponding to scaled weight of the cover greater than zero relates to frangible covers and will be discussed later. The effects on the gas pressure impulse caused by the shock impulse loads will vary. The gas impulse loads will have greater variance at lower shock impulse loads than at higher loads. Interpolation will be required for the variation of gas impulse as a function of the shock impulse loads. This interpolation can be performed in a manner similar to the interpolation for the shock pressures.

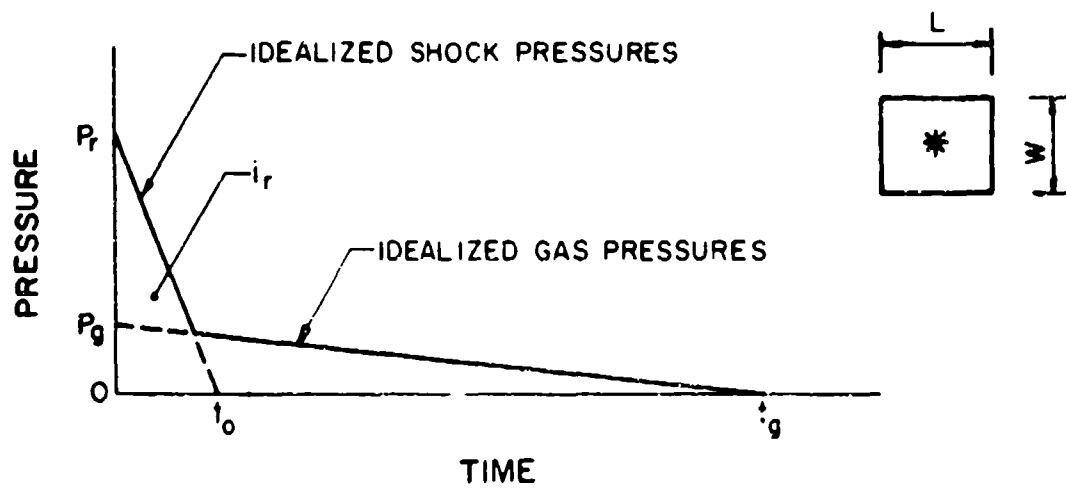
A computer program is available which executes the interpolation procedure. Availability of this program is listed in Section 2-4.

The actual duration and the pressure-time variation of the gas pressures is not required for the analysis of most structural elements. Similar to the shock pressures, the actual pressure-time relationship can be approximated by a fictitious peak triangular pulse. The peak gas pressure is obtained from figure 2-152 and the impulse from figures 2-153 through 2-164 and the fictitious duration is calculated from the following:

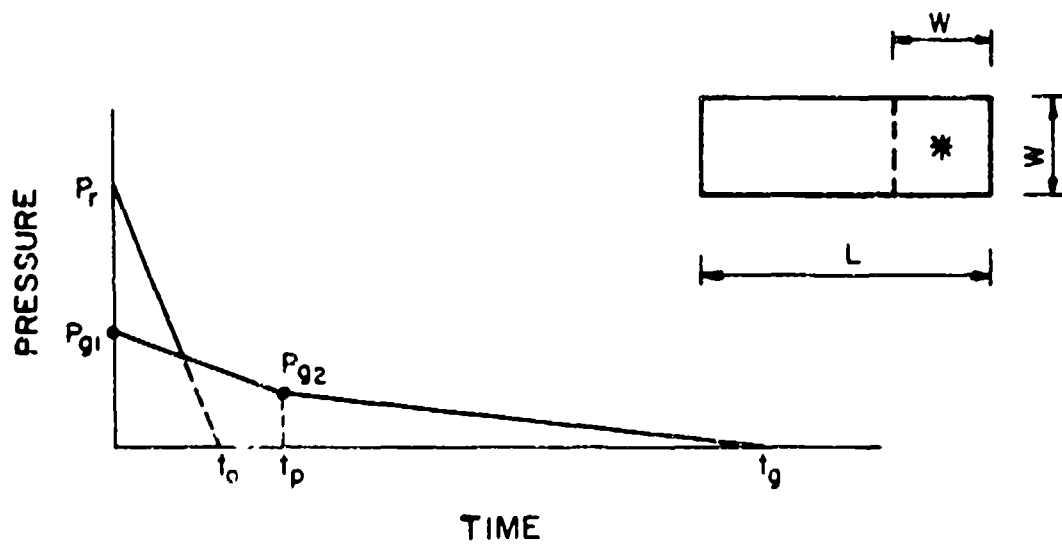
$$t_g = \frac{2 I_g}{P_g}$$

Figure 2-165a illustrates an idealized pressure-time curve considering both the shock and gas pressures. As the duration of the gas pressures approach that of the shock pressures, the effects of the gas pressures on the response of the elements diminishes until the duration of both the shock and gas pressures are equal and the structure is said to be fully vented.

If a chamber is relatively small and/or square in plan area then the magnitude of the gas pressure acting on an individual element will not vary significantly. For design purposes the gas pressures may be considered to be uniform on all members. When the chamber is quite long in one direction and the explosion occurs at one end of the structure, the magnitude of the gas pressures will initially vary along the length of the structure. At the end where the explosion occurs, the peak gas pressure is P_{g1} (fig. 2-165b) which after a finite time decays to P_{g2} , and finally decays to zero. The gas pressure P_{g2} is based on the total volume of the structure and is obtained from figure 2-152 while the time for this pressure to decay to zero is calculated from equation 2-4 where the impulse is obtained from figures 2-153 through 2-164 again for the total volume of the structure. The peak gas pressure P_{g1} is obtained from figure 2-152 based on a pseudo volume (fig. 2-165b) whose length is equal to its width and the height is the actual height of the structure. The time t_p for the gas pressure to decay from P_{g1} to P_{g2} is taken as the actual length of the structure minus the width divided by the velocity of sound (1.12 fpm/s).



a) SMALL AND/OR SQUARE CHAMBER



b) LONG RECTANGULAR CHAMBER

Figure 2-165 Combined shock and gas pressures

At the end where the explosion occurs, the peak gas pressures (P_{g1} , figure 2-165b) will be a maximum and, after a finite time, they will decay to a value (P_{g2} , figure 2-165b) which is consistent with full volume of the structure; after which they will decay to zero. The magnitude of the peak gas pressures (P_{g1}) may be evaluated by utilizing figure 2-152 and a pseudo volume whose length is equal to its width and the height is the actual height of the chamber. The length of time t_p between the two peak gas pressures may be taken as the length minus the width of the structure divided by the velocity of sound (1 fpm).

2-14.3.2 Frangibility. Similar to shock pressures, an element can be considered frangible if it is designed such that its resistance to internal blast forces does not exceed 25 psf and that it will undergo significant displacement during the shock and gas loading phases. Figures 2-153 through 2-164 present the method for determining the gas pressure impulse acting on the interior surfaces of the donor structure. These impulse loads will vary as the mass of the cover over the vent opening varies; that is, the heavier the vent opening cover, the larger the gas pressure impulse. Like the vented structures, the internal gas pressure impulse loads produced by a frangible cover must be interpolated as a function of the shock pressure impulse loads.

2-14.3.3 TNT Equivalency. The data presented in figure 2-152 and figures 2-153 to 2-164 are for TNT only and must be extended to include other potentially mass-detonating materials. Similar to the shock pressures, only a limited amount of data is available regarding the TNT equivalency of confined explosions and in particular the effects produced on gas pressures. It has been suggested that the TNT equivalency of explosives relating to gas pressures is a function of both the heat of detonation as well as the heat of combustion, while for the shock pressures, the TNT equivalency is a function of the former only. A relationship has been developed based on a limited amount of testing as follows:

$$W_{Eg} = \frac{\phi[H_{EXP}^c - H_{EXP}^d] + H_{EXP}^d}{\phi[H_{TNT}^c - H_{TNT}^d] + H_{TNT}^d} W_{EXP} \quad 2-5$$

where:

- W_{Eg} -- effective charge weight for gas pressure
- H_{TNT}^c -- heat of combustion of TNT
- H_{EXP}^c -- heat of combustion of explosive in question
- ϕ_d -- TNT conversion factor (figure 2-166)
- H_{TNT}^d -- heat of detonation of TNT

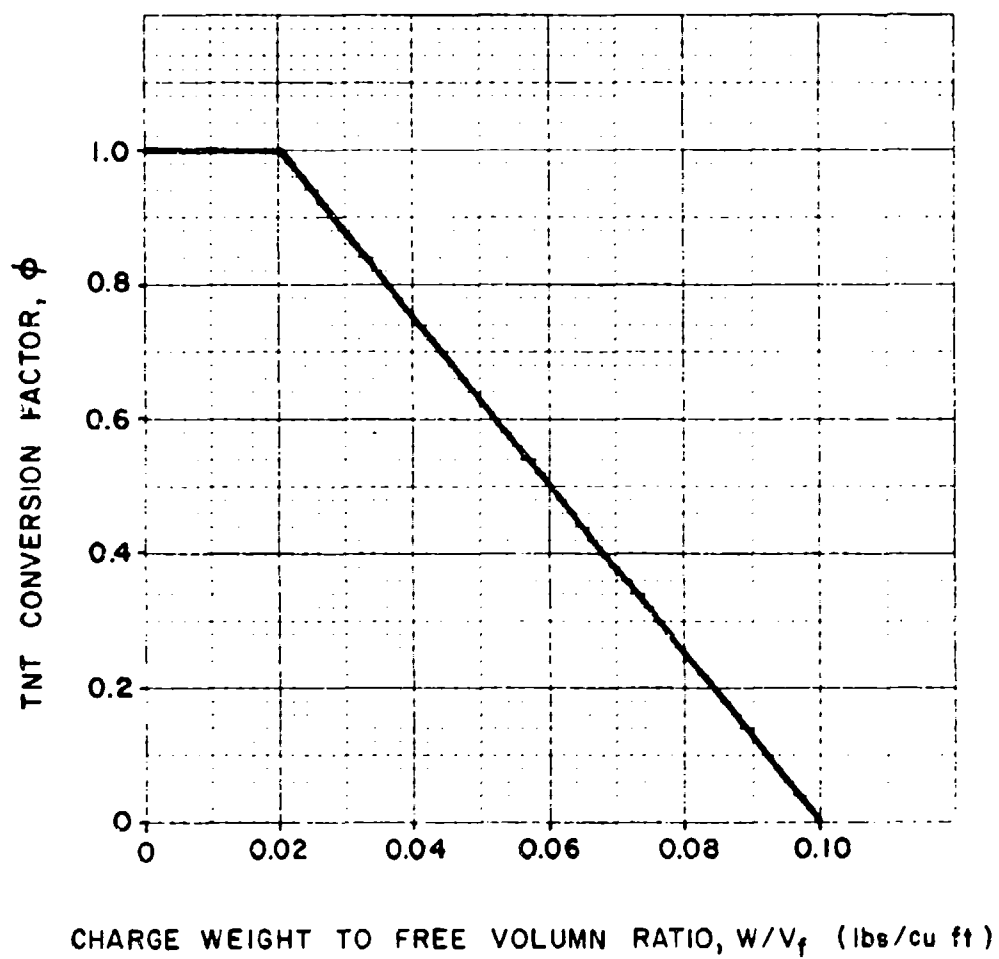


Figure 2-166 TNT conversion factor for charges

- H_{EXP}^d - heat of detonation of explosion in question
- W_{EXP} - weight of explosive in question

Gas pressures will be increased due to casings and in particular if the casing is combustible. Since only unrelated data is available concerning the effects on gas pressures by the casing, a method of compensating for these effects is to adjust the heat of combustion of the given explosive material in Equation 2-5 to account for the heat of combustion of the casing material. This adjustment should be made by chemically combining the heat of combustion of the explosive and casing.

12-14.3.4 Multiple Explosions

The gas pressure produced by the release of the gaseous products of multiple explosions in a confined area may be approximated by considering the explosion to be produced by a single explosive whose weight is equal to the combined weights of the individual charges. This approximation is accurate if the individual charges are positioned in the immediate vicinity of one another and if near simultaneous detonation of the individual charges occurs. If the individual charges are not close to one another and/or positioned at one end of the structure, the magnitude of the gas pressures will initially vary along the length or width of the structure. This variation may be determined in a manner similar to that described in Section 2-14.3.1.

2-14.4 Leakage Pressures

2-14.4.1 Introduction. When an explosion occurs inside a vented chamber, shock pressures escape to the outside along with venting of the gas pressures. Trailing shocks overrun and coalesce with the lead shock at some distance from a single diverging shock wave. Close to the structure, the blast pressures are affected by the structure itself as the shock pressures spill around the edges of the structure and form highly turbulent vortices. At further distances, this effect is no longer present and the shock pressure decreases with increasing distances. The leakage pressures are enhanced in the direction of venting (front) and reduced to the side and rear. The enhancement of pressures in the front and reduction of pressures to the side and rear are less extreme as the distance away from the structure is increased.

The blast environment outside of cubicles containing fully and partially vented explosions is presented in this section. Pressures and impulses acting on the ground surface are provided as a function of distance from the explosion, direction (front, side, back) relative to the vent opening in the structure, area of the vent opening and volume of the structure. For design purposes, the remaining blast parameters corresponding to the pressure and impulse acting on the ground surface may be obtained from figures 2-15 and 2-16 in exactly the same manner as a surface burst of an explosive other than TNT.

Explosions in three and four wall cubicles are considered. Three wall cubicles are fully vented structures. The blast environment is furnished for cu-

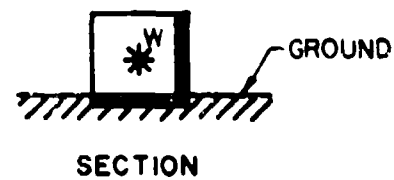
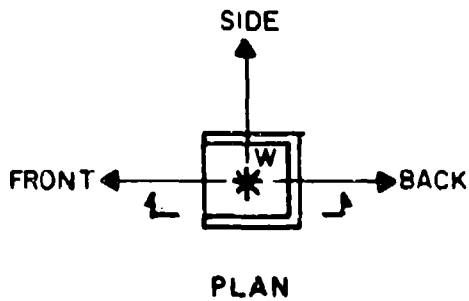
bicles with or without roofs. Four wall cubicles with a vent opening located either in the roof or one wall are considered. The size of the vent opening is varied from that of a fully vented cubicle through a full range of partially vented structures.

The data presented is based on tests in which the vent openings were completely open. There were no frangible covers over the vent area which might inhibit the pressure flow. Vent openings in protective structures are normally covered with frangible panels for weather protection, separation of operations, etc. These panels will affect the leakage pressures. However, it is assumed that these frangible panels will reduce the shock pressures leaking through the opening to a greater extent than the increase in the internal gas pressure buildup. Therefore, use of this data will predict conservative leakage pressures from cubicles with frangible covers.

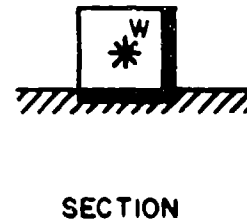
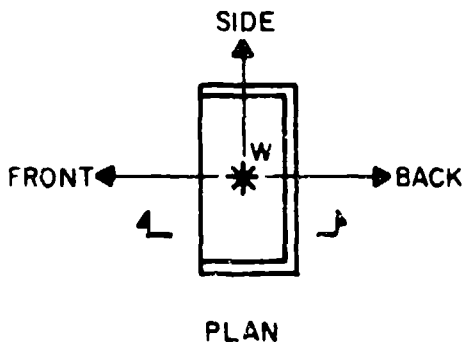
2-14.4.2 Fully Vented Three Wall Cubicles. For cubicle-type structures where full venting is provided through the frangible or open portion of the structure, the resulting blast wave exterior of the cubicle will be appreciably modified as compared to an unbarricaded detonation. As the blast wave propagates out from the center of the explosion, the shock front will collide with the interior surfaces of the structure. These collisions will reflect and reinforce the initial loads (pressure and impulse). Eventually these pressures will spill over and around the blast walls, and in the event of rapid collapse of frangible walls, through the structure to the surrounding area. The exterior pressures will not initially have a definite shock front but will, at some distance from the structure, shock-up with frontal pressures similar to those produced by a surface burst. The pressure distance gradients away from the explosion will vary in all directions. This variation is defined by the configuration (shape, openings, etc.) of the protective structure containing the explosion.

A series of tests have been performed on three wall cubicle type structures illustrated in figure 2-167. Cubic and rectangular three wall cubicles with and without a roof were tested. The results indicated that several parameters were important:

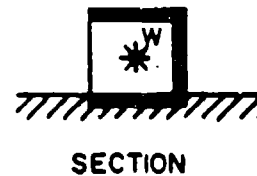
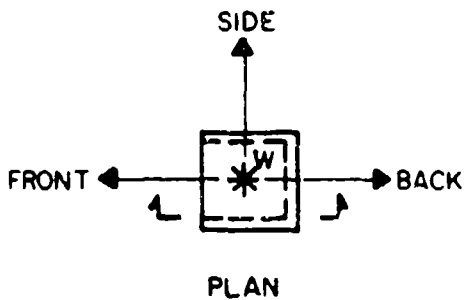
- (1) Direction - Three directions illustrated in Figure 2-167 are considered. The direction normal to the open wall is called the front. The directions perpendicular to the front normal are called the sides. The direction opposite the normal to the open wall is called the back. The blast pressures out the front are greater than that to the side which, in turn, are greater than that to the back.
- (2) Structure geometry - Differences were found in the blast environment depending upon whether the structure was cubic or rectangular in shape. This was true for pressure and impulse measurements to the side and back, and only impulse to the front. There were no differences in pressure out the front for the cubic and rectangular structures. The difference in pressures to the side and back occur only close to the structure. Far from the structure, there is no effect on pressure in any direction due to structure shape. However, impulse does not converge with distance for differences in cubicle shape.



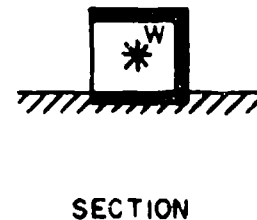
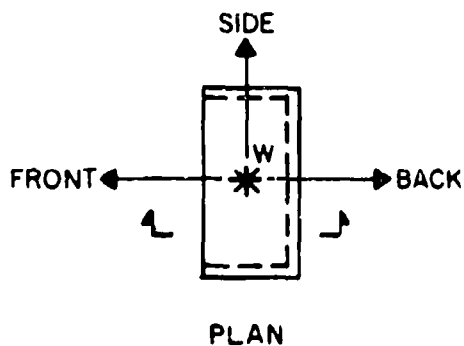
a) CUBIC THREE WALL CUBICLE WITHOUT A ROOF



b) RECTANGULAR THREE WALL CUBICLE WITHOUT A ROOF



c) CUBIC THREE WALL CUBICLE WITH A ROOF



d) RECTANGULAR THREE WALL CUBICLE WITH A ROOF

Figure 2-167 Fully vented three-wall cubicles and direction of blast wave propagation

- (3) Charge weight to volume ratio W/V and distance - The ratio W/V does not have an effect on the pressure to the front of any cubicle. There is an effect of W/V on pressure to the side and back of all cubicles, but only close to the structure. For a particular W/V , the pressure is affected differently for a cubic or rectangular structure. Thus, the effect on pressure close in depends both on structure size and W/V . But, for further out, neither affect the pressures. For all values of Z , there is a measured effect of W/V on impulse.
- (4) Venting through the roof - For any direction, cubicle shape, and W/V value, there are differences in blast pressure and impulse based solely on whether or not venting could occur through the roof.
- (5) Scaled distance Z - Both blast pressure and scaled impulse are affected by scaled distance from the explosion. This parameter is not independent of other factors.

The pressure variation in the front, side and back direction of any three wall cubicle without a roof is given in figure 2-168 while for a three wall cubicle with a roof the pressure variation is given in figure 2-169. Due to interferences from the side and back walls which cause complex vortices near the structure and coalescence of shock waves in close, there is a maximum pressure produced in the side and back directions. These pressures are a function of the charge weight to cubicle volume ratio, W/V , and the configuration of the cubicle. The maximum peak pressure in the side or back directions of three wall cubicles with or without a roof are given in figure 2-170.

The scaled peak positive impulse in the front, side and back direction of three wall cubicles is given in figures 2-171 through 2-182. The scaled impulse is given as a function of scaled distance from the explosion for various values of charge weight to structure volume ratio. The curves are presented in two groups; three wall cubicles without roofs and then cubicles with roofs. For each direction, the impulse is given for explosions in cubic and rectangular cubicles, respectively.

2-14.4.3 Partially vented four wall cubicles - vent opening in roof. Four wall cubicles with a vent opening located in the roof will produce blast pressures on the ground surface which are symmetric about the vent opening. Leakage pressures were determined for a below ground cubicle with its roof flush with the ground surface (fig. 2-183a). The vent opening was centrally located in the roof and various vent areas were considered. The blast pressure was determined to be a strong function of the vent area divided by the structure volume to the two-thirds power ($A/V^{2/3}$) and the scaled distance, and a very weak function of the charge weight to volume ratio W/V which can be ignored with negligible error.

The leakage pressures resulting from an explosion in a partially vented below-ground cubicle with a vent opening in its roof is given in figure 2-184 while the impulse is given in figure 2-185. The scaled ground distance as indicated in figure 2-183a is used in these charts for the below-ground structures.

Figures 2-184 and 2-185 may also be used to determine the pressure and impulse acting on the ground surface for above-ground four wall cubicles (fig 2-183b). For an above-ground structure, the shock front must travel a longer distance than a below-ground structure. Therefore, the scaled distance that must be used in figures 2-184 and 2-185 is approximated by the addition of the slant and horizontal distances indicated in figure 2-183b.

The above charts are useful in selecting the degree of venting required to limit leakage pressures outside roof-vented four wall cubicles to a specified safe level at some given distance. From a knowledge of the pressure and impulse on the ground surface, the blast load acting on a structure may be obtained from the procedures given in this report. Thus, an adjacent structure may be designed to resist a blast load resulting from a given vent opening or the vent opening may be varied to suit the capacity of an adjacent structure.

2-14.4.4 Partially vented four wall cubicle - vent opening through wall. Leakage pressures resulting from an explosion in a partially vented four wall cubicle where the vent opening is located in a wall (fig. 2-186) have not been documented. These leakage pressures have a variation in direction similar to a three wall cubicle with a roof and a variation with vent opening similar to a roof vented four wall cubicle. Extrapolation of the data for these types of cubicles have resulted in figures 2-187 through 2-189. These charts present a reasonable estimate of the pressures produced in the front, side and back directions (fig. 2-186). In addition to direction, these pressures are a function of scaled distance and the vent area divided by the volume to the two-thirds power ($A/V^{2/3}$).

2-15 External Blast Loads on Structures

2-15.1 General

The blast loading on a structure caused by a high-explosive detonation is dependent upon several factors:

- (1) the magnitude of the explosion,
- (2) location of the explosion relative to the structure in question (unconfined or confined),
- (3) the geometrical configuration of the structure, and
- (4) the structure orientation with respect to the explosion and the ground surface (above, flush with, or below the ground).

The procedures presented here for the determination of the external blast loads on structures are restricted to rectangular structures positioned above the ground surface where the structures will be subjected to a plane wave shock front. The procedures can be extended to include structures of other shapes (cylindrical, arch, spherical, etc.) as well as structures positioned at and below the ground surface.

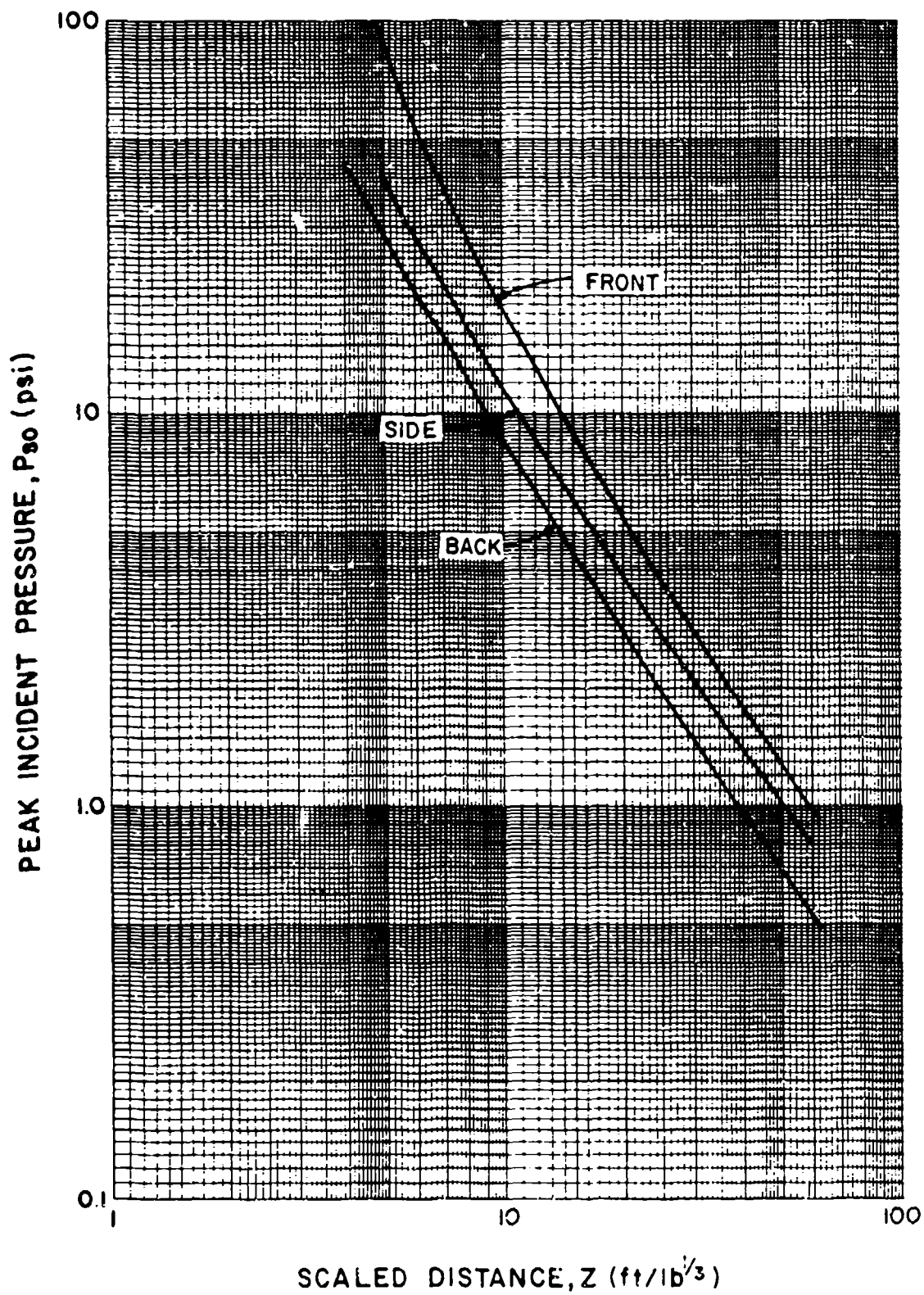


Figure 2-168 Envelope curves for peak positive pressure outside three-wall cubicles without a roof

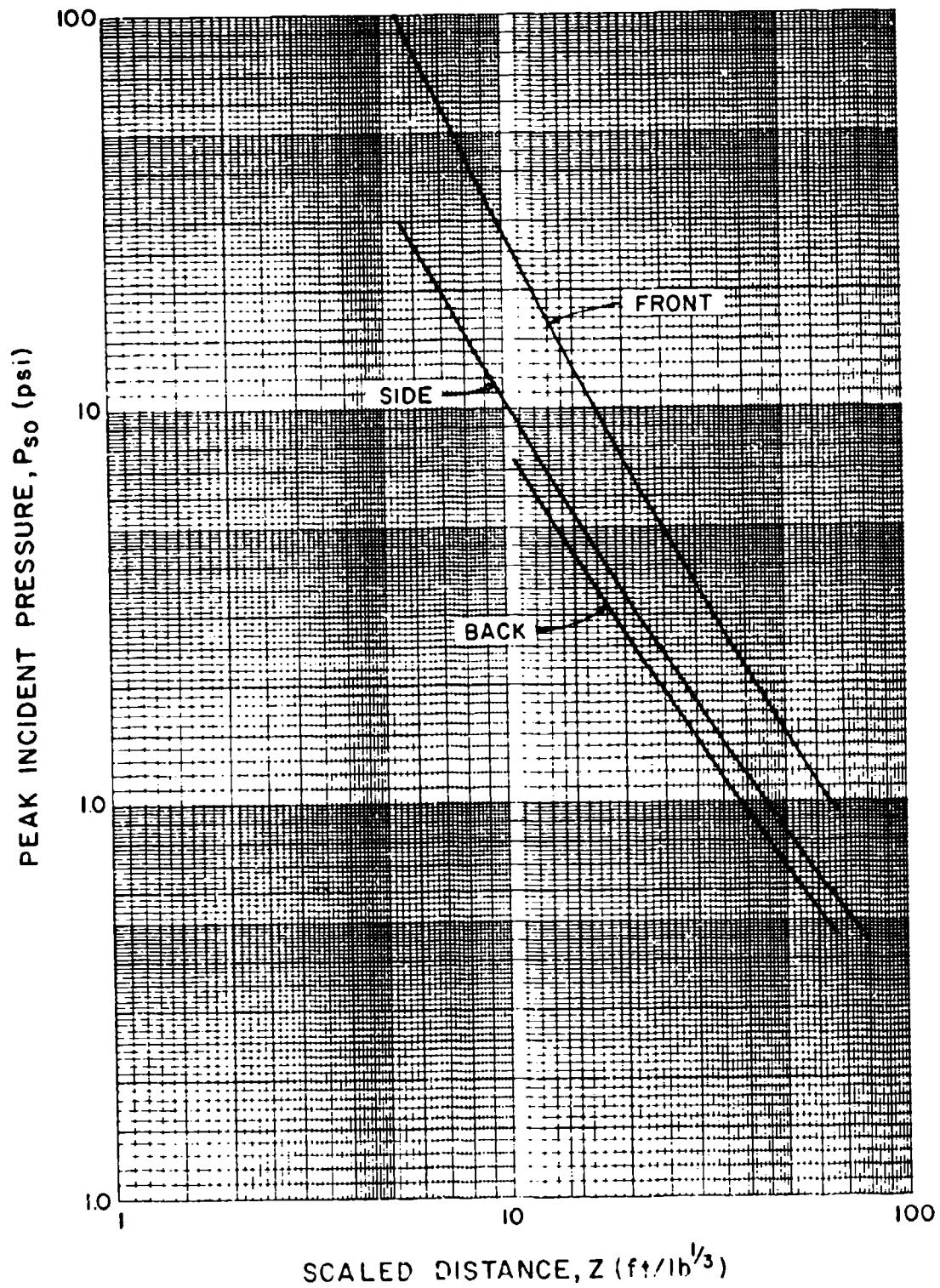
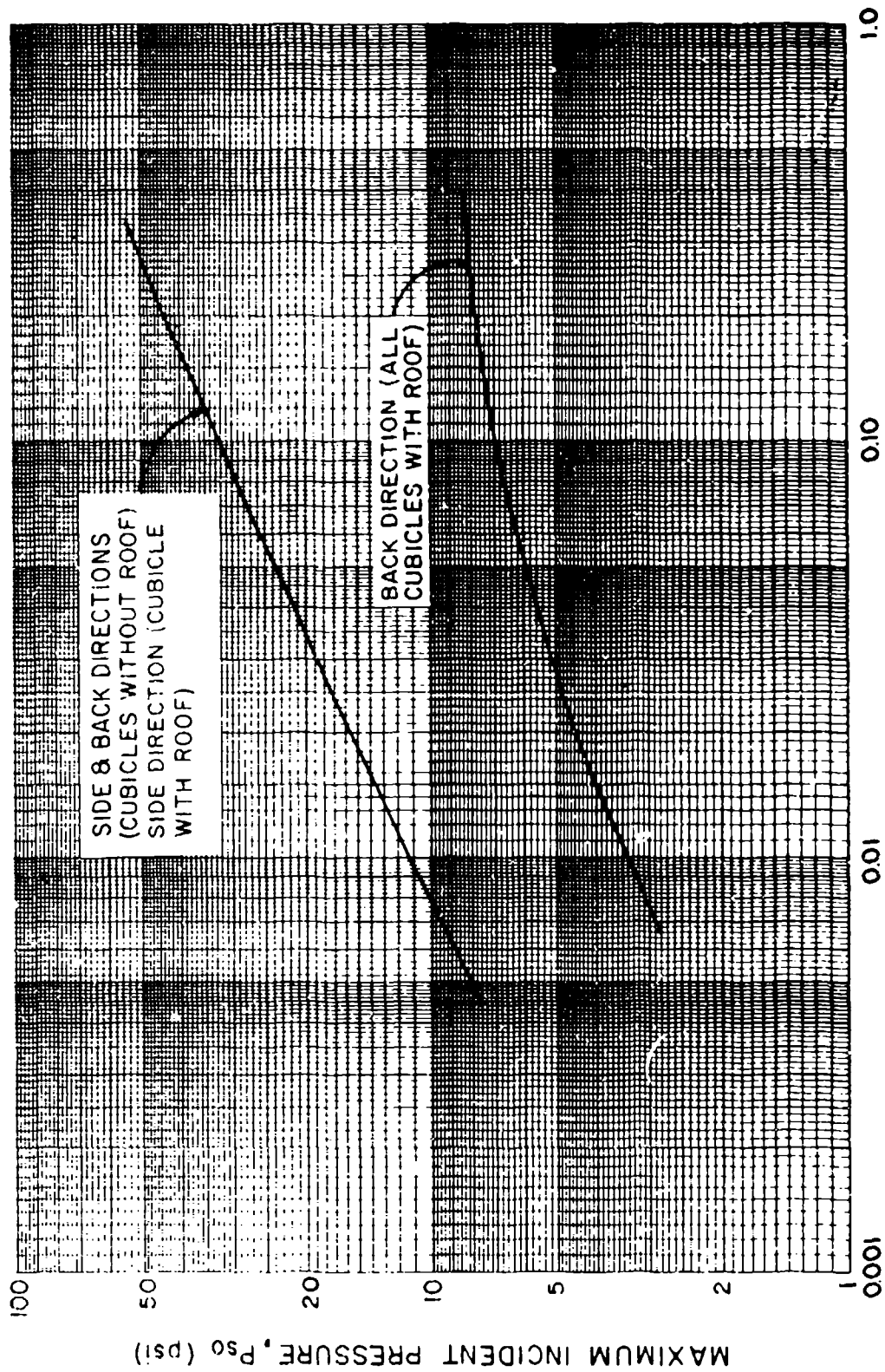


Figure 2-169 Envelope curves for peak positive pressure outside three-wall cubicles with a roof



CHARGE WEIGHT TO CUBICLE VOLUME, W/V (lb/ft^3)

Figure 2-170 Envelope curves for maximum peak pressure
outside three-wall cubicles

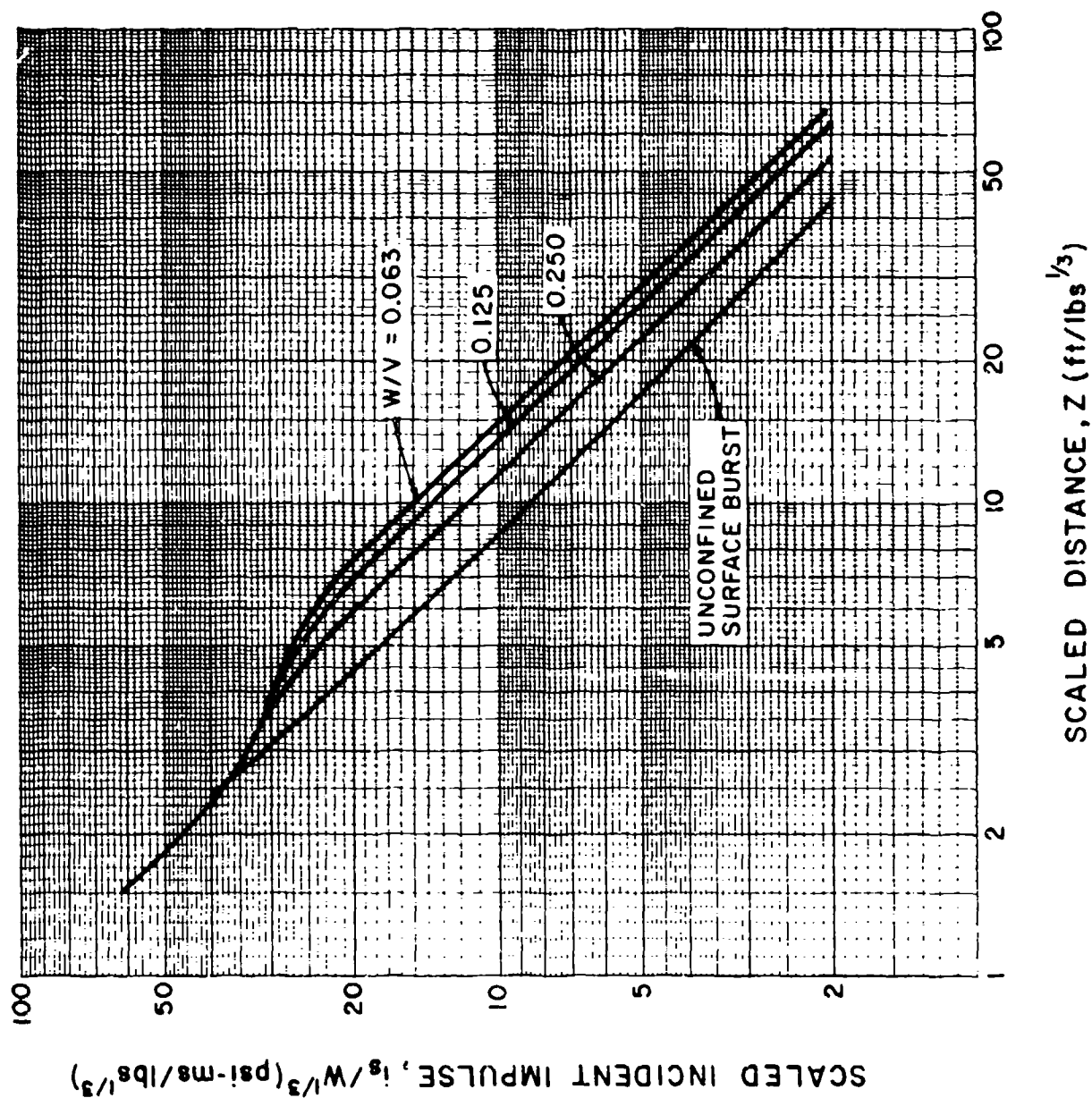


Figure 2-171 Scaled peak positive impulse out the open front of cubic three-wall cubicle without a roof

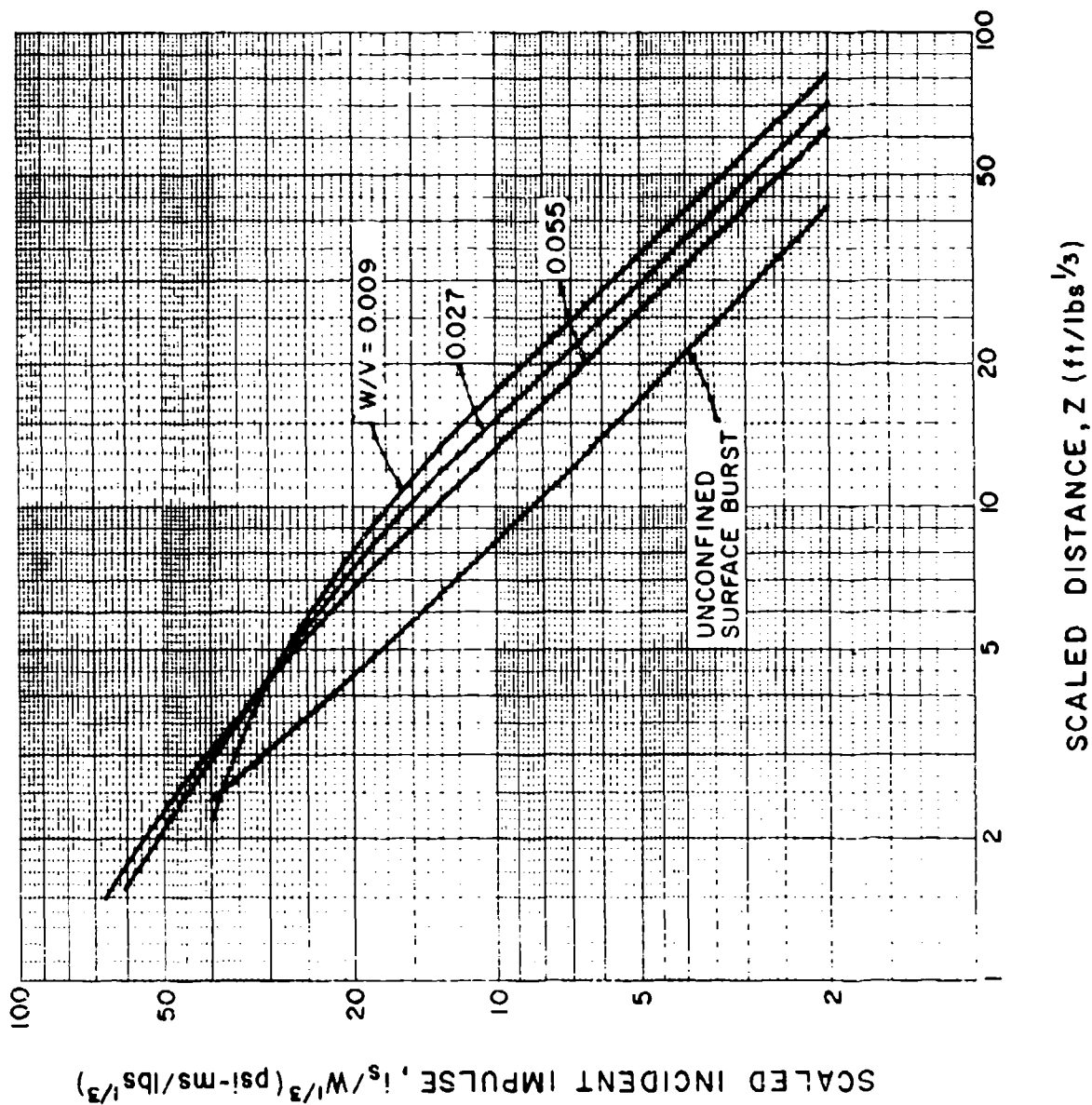


Figure 2-172 Scaled peak positive impulse out the open front of rectangular three-wall cubicle without a roof

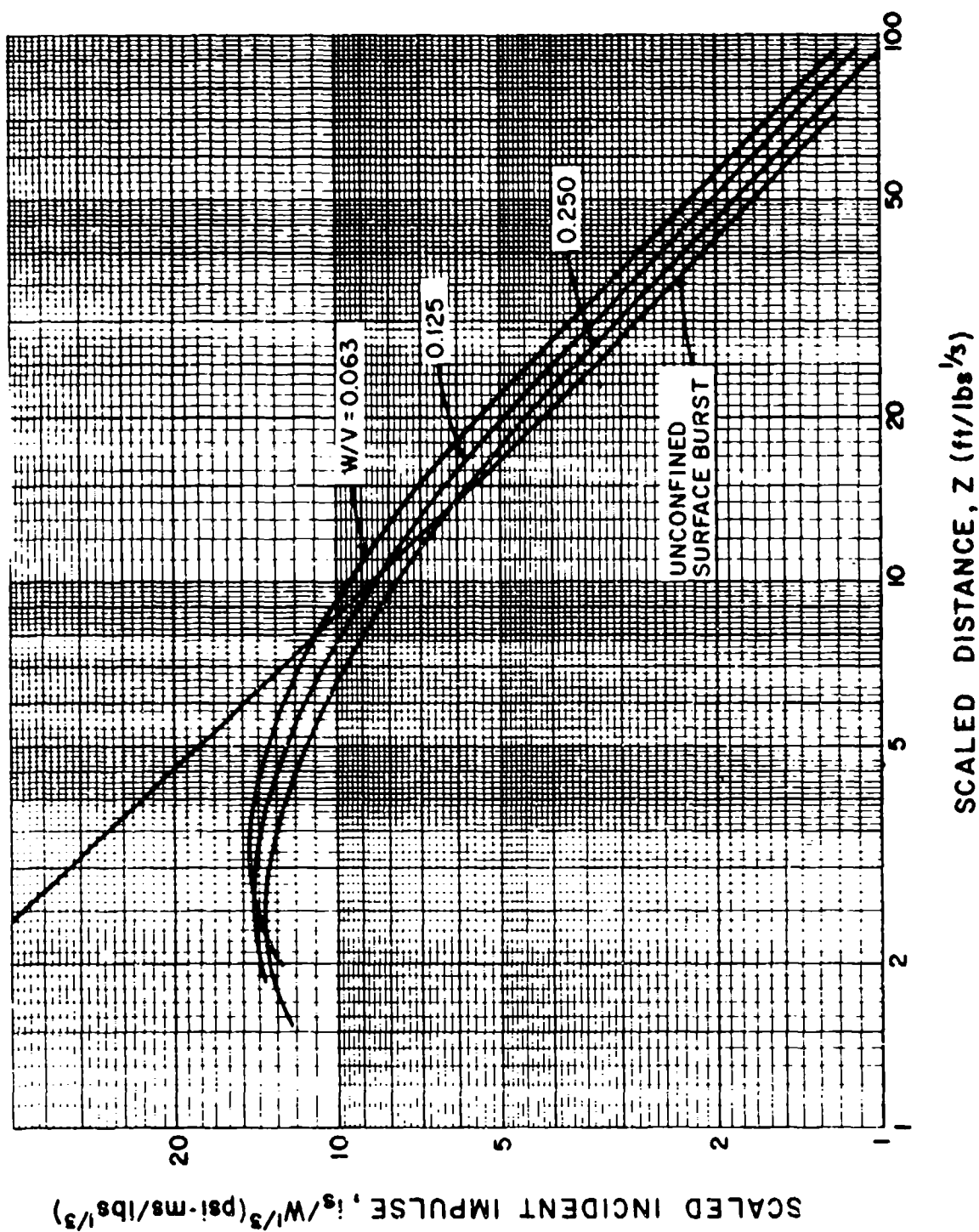


Figure 2-173 Scaled peak positive impulse behind sidewall of cubic three-wall cubicle without a roof

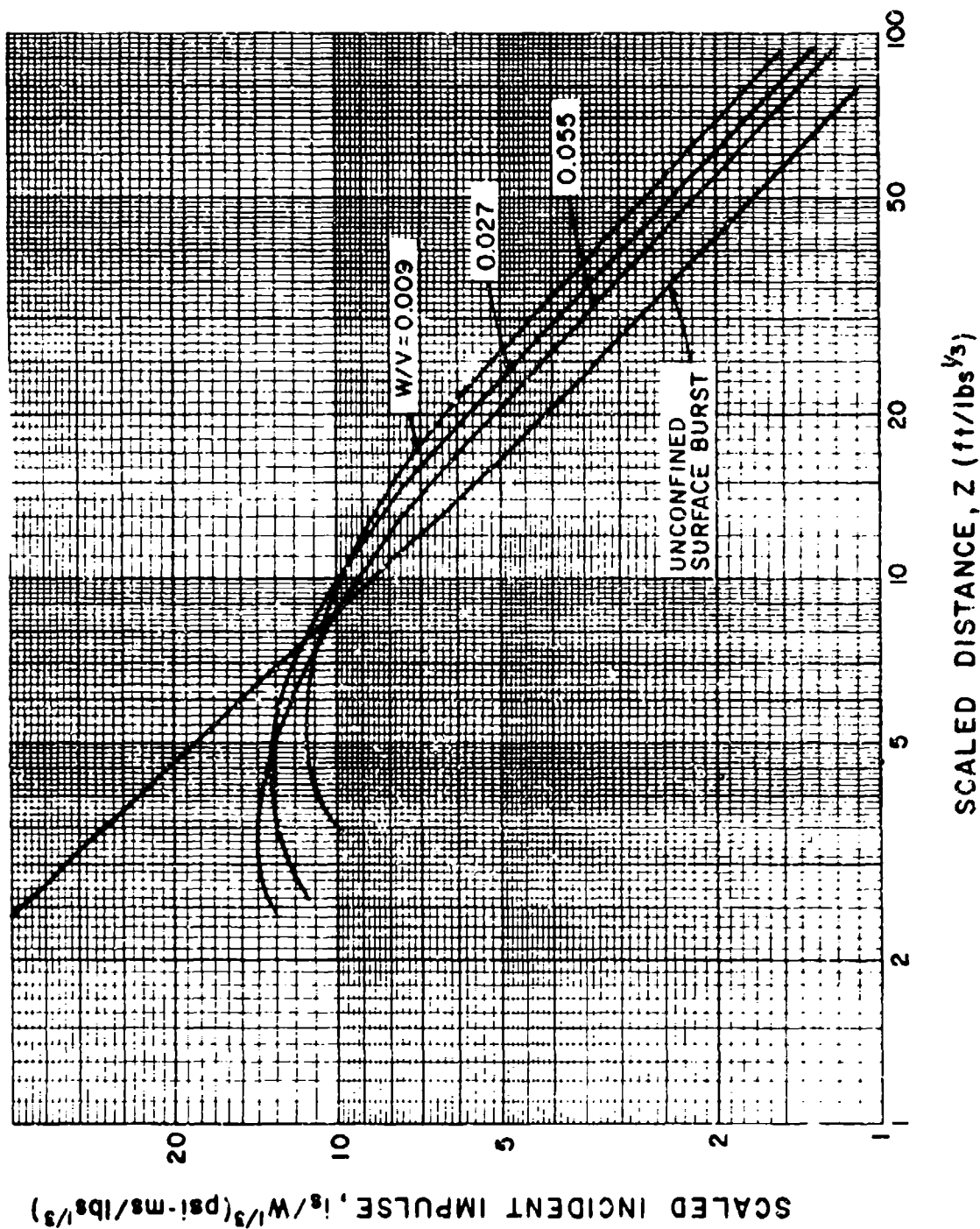


Figure 2-174 Scaled peak positive impulse behind sidewall of rectangular three-wall cubicle without a roof

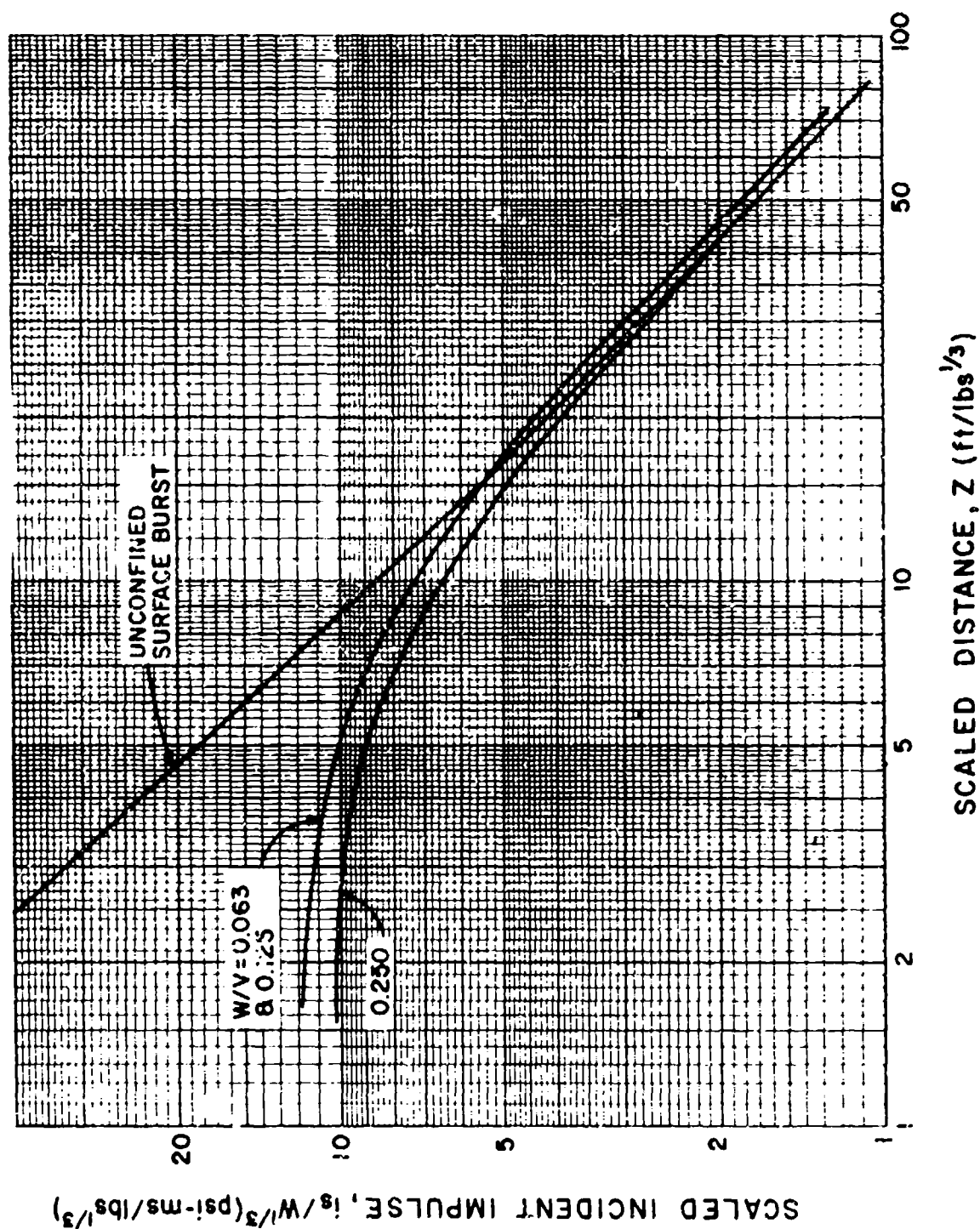


Figure 2-175 Scaled peak positive impulse behind backwall of cubic three-wall cubicle without a roof

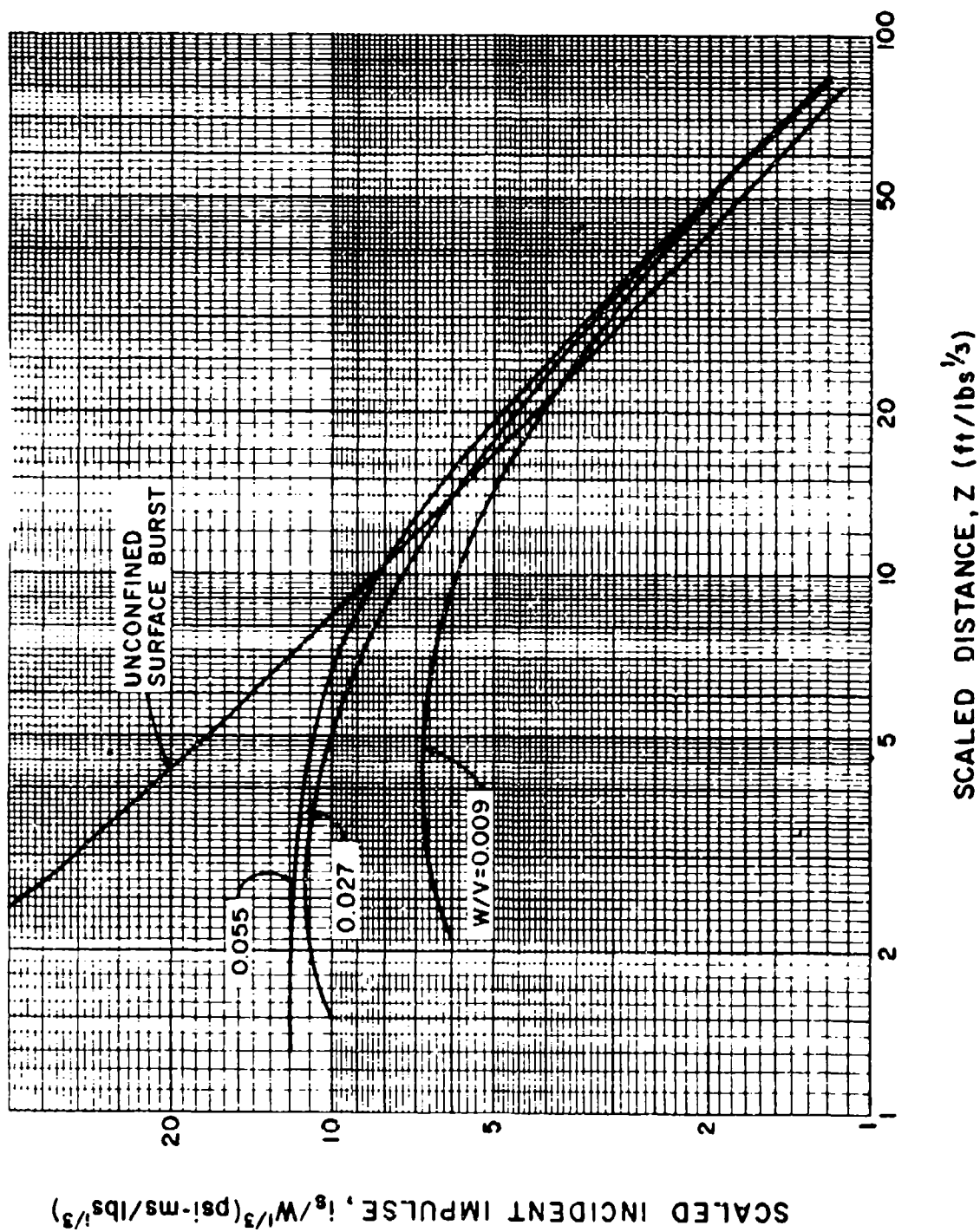


Figure 2-176 Scaled peak positive impulse behind backwall of rectangular three-wall cubicle without a roof

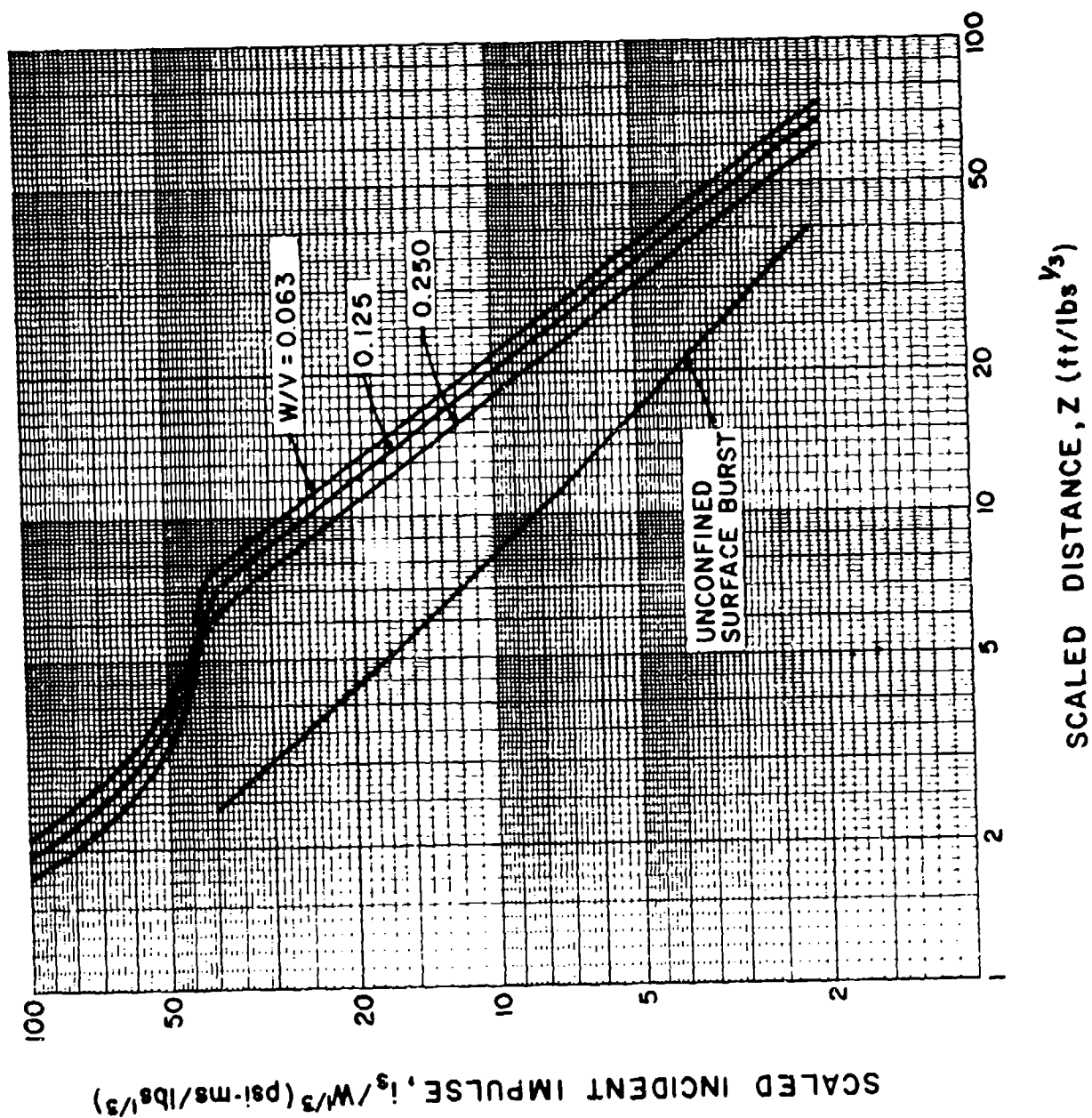


Figure 2-177 Scaled peak positive impulse out the open front of cubic three-wall cubicle with a roof

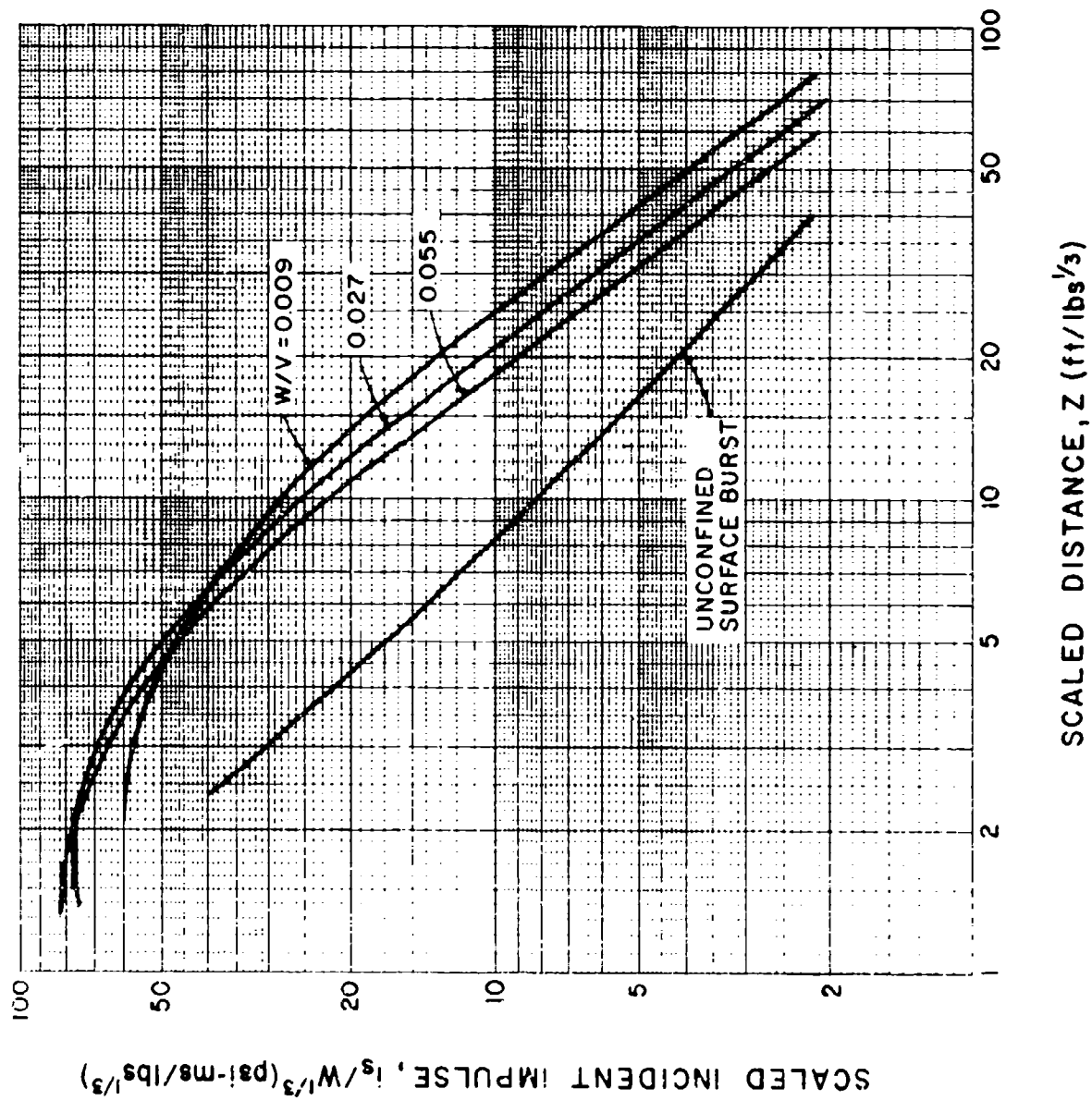


Figure 2-178 Scaled peak positive impulse out the open front of rectangular three-wall cubicle with a roof

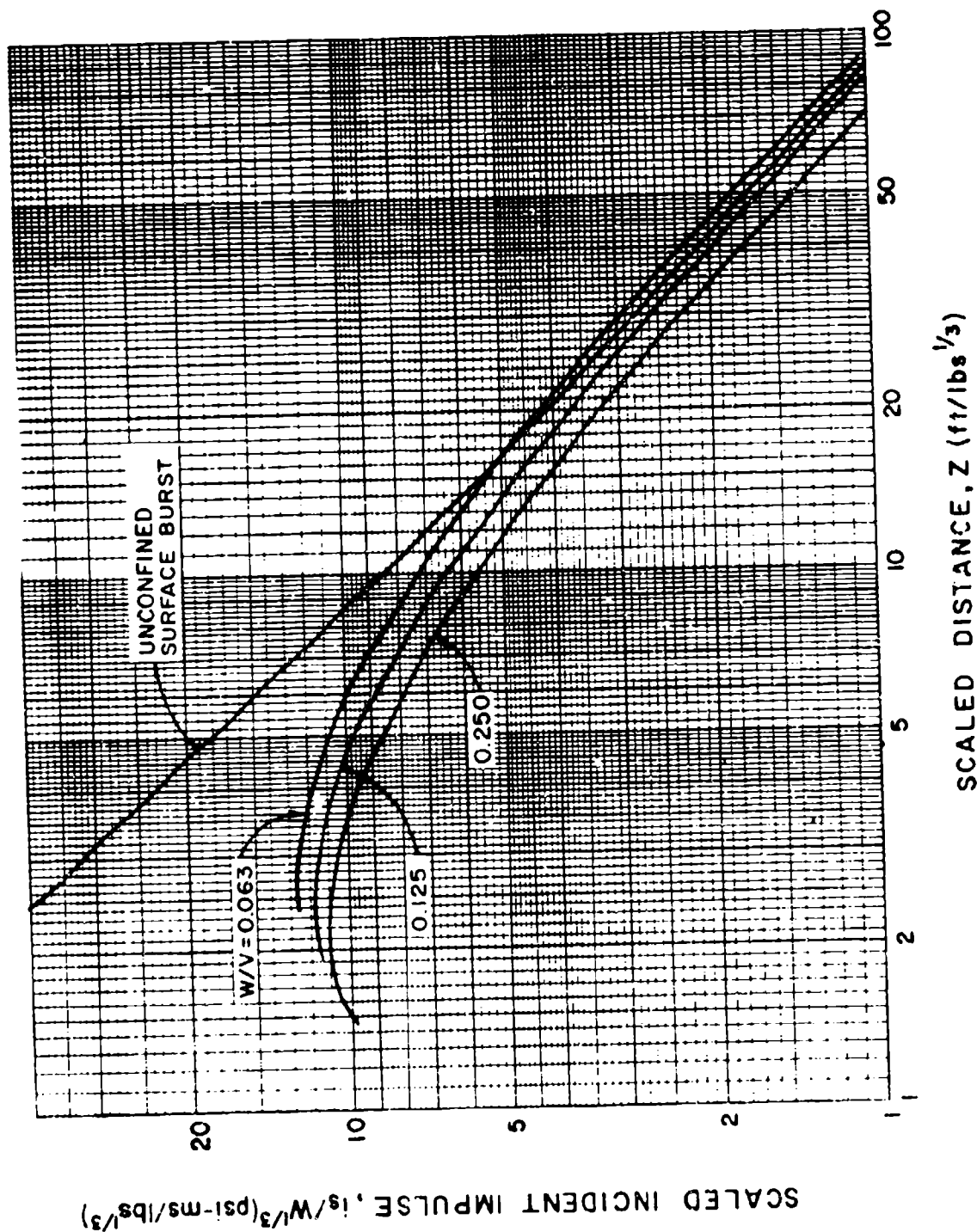


Figure 2-179 Scaled peak positive impulse behind sidewall of cubic three-wall cubicle with a roof

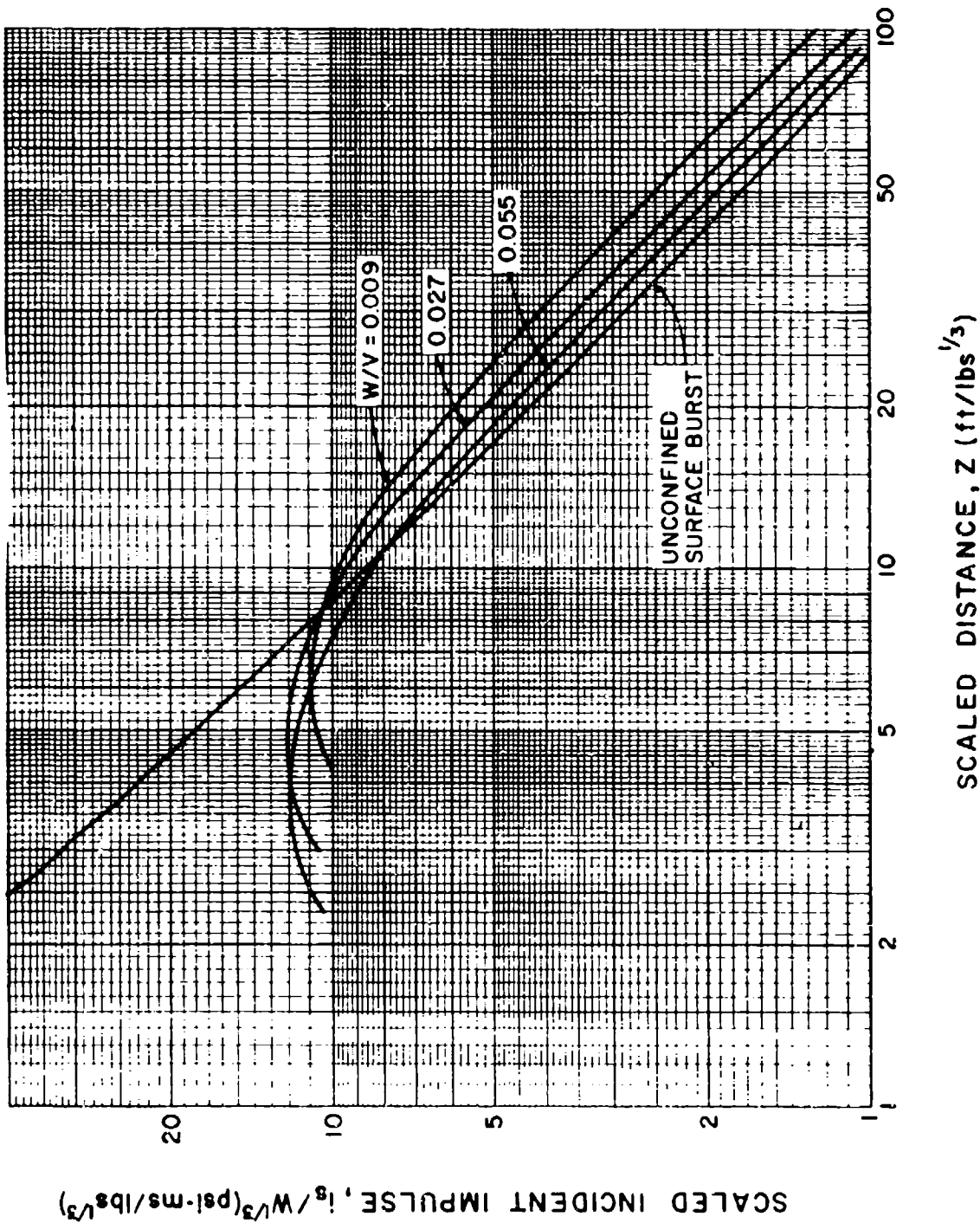


Figure 2-180 Scaled peak positive impulse behind sidewall of rectangular three-wall cubicle with a roof

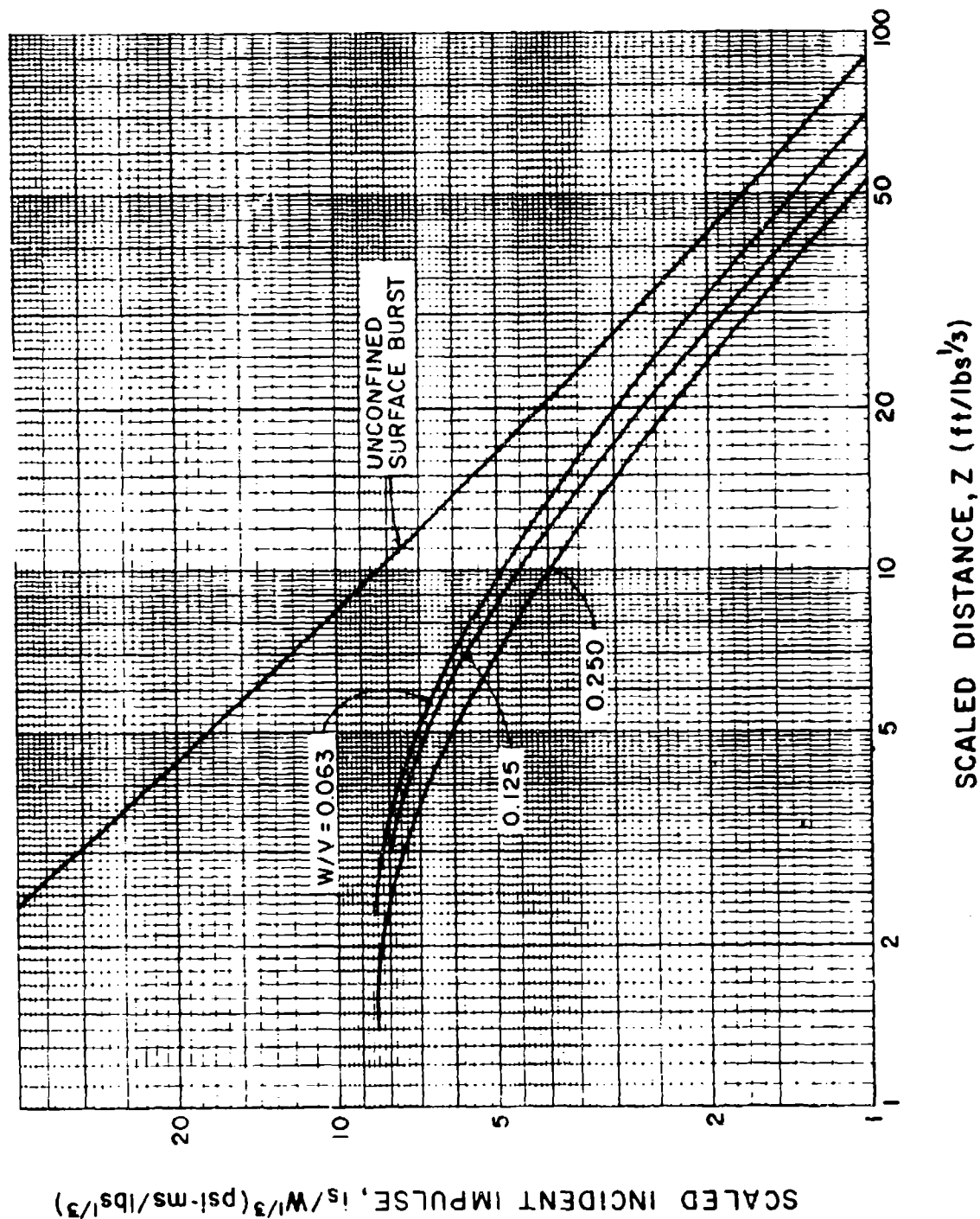


Figure 2-181 Scaled peak positive impulse behind backwall of cubic three-wall cubicle with a roof

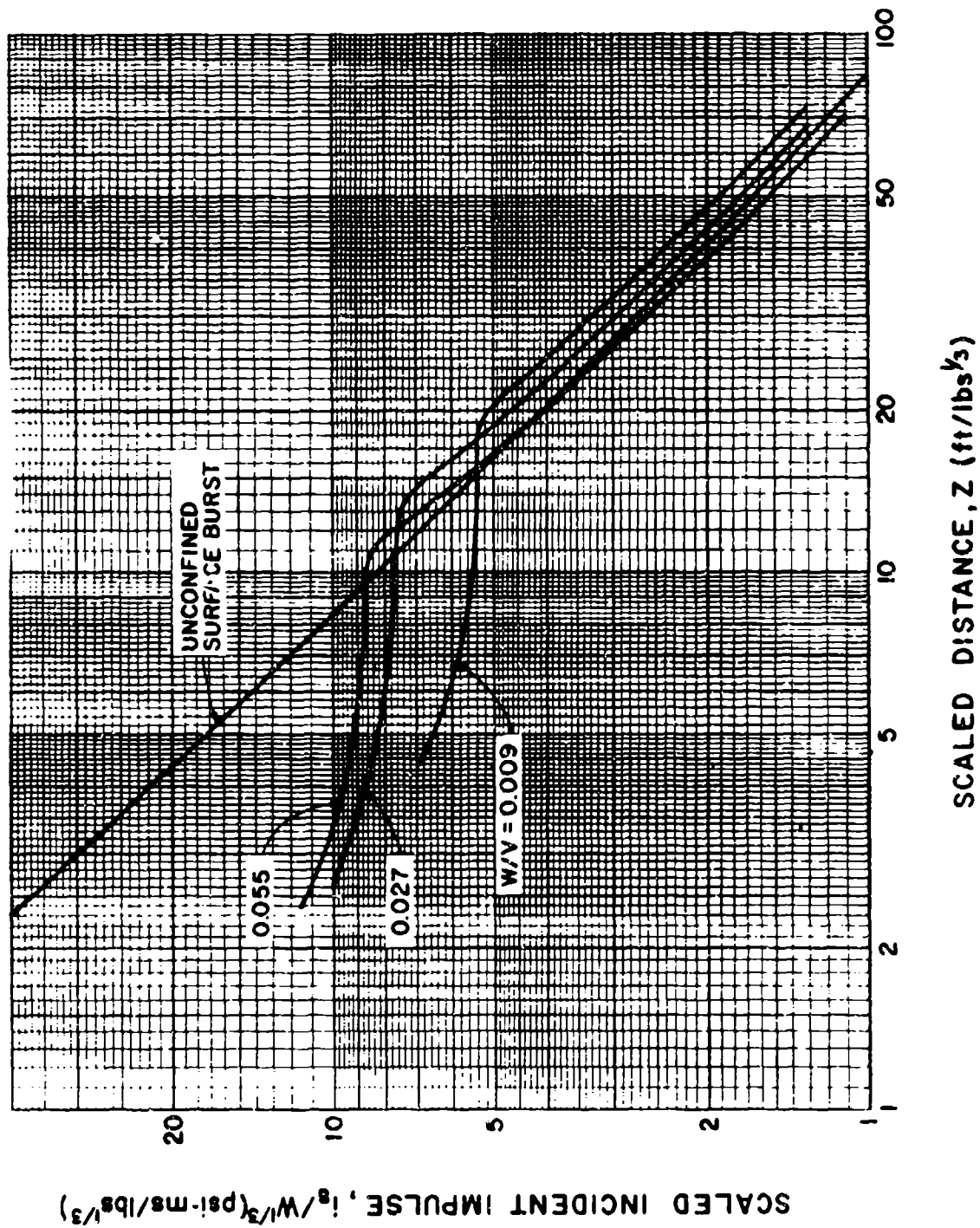
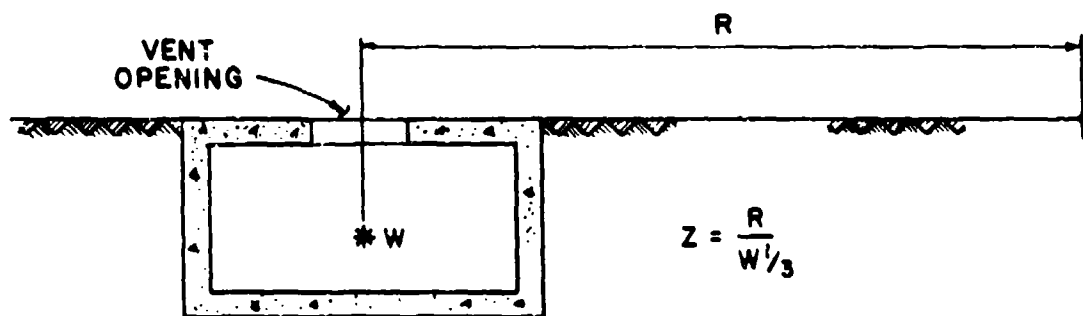
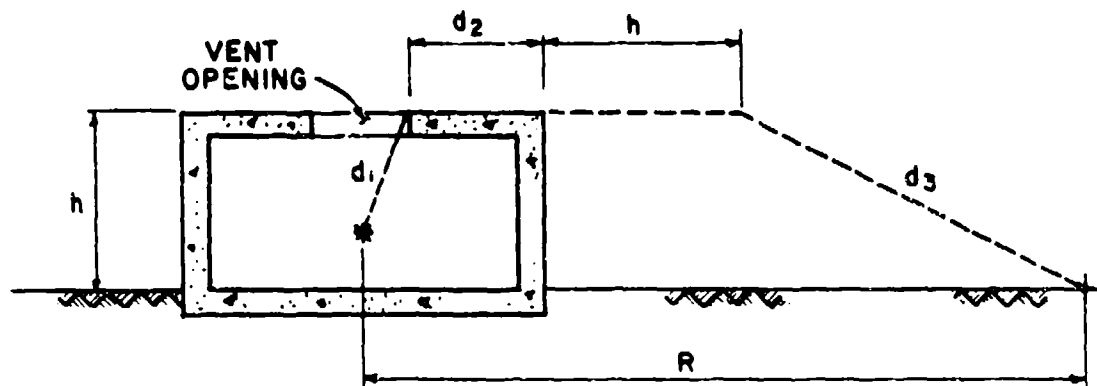


Figure 2-182 Scaled peak positive impulse behind backwall of rectangular three-wall cubicle with a roof



a) BELOW GROUND STRUCTURE WITH ROOF AT GROUND SURFACE



b) ABOVE GROUND STRUCTURE

Figure 2-183 Four wall cubicle vented through its roof

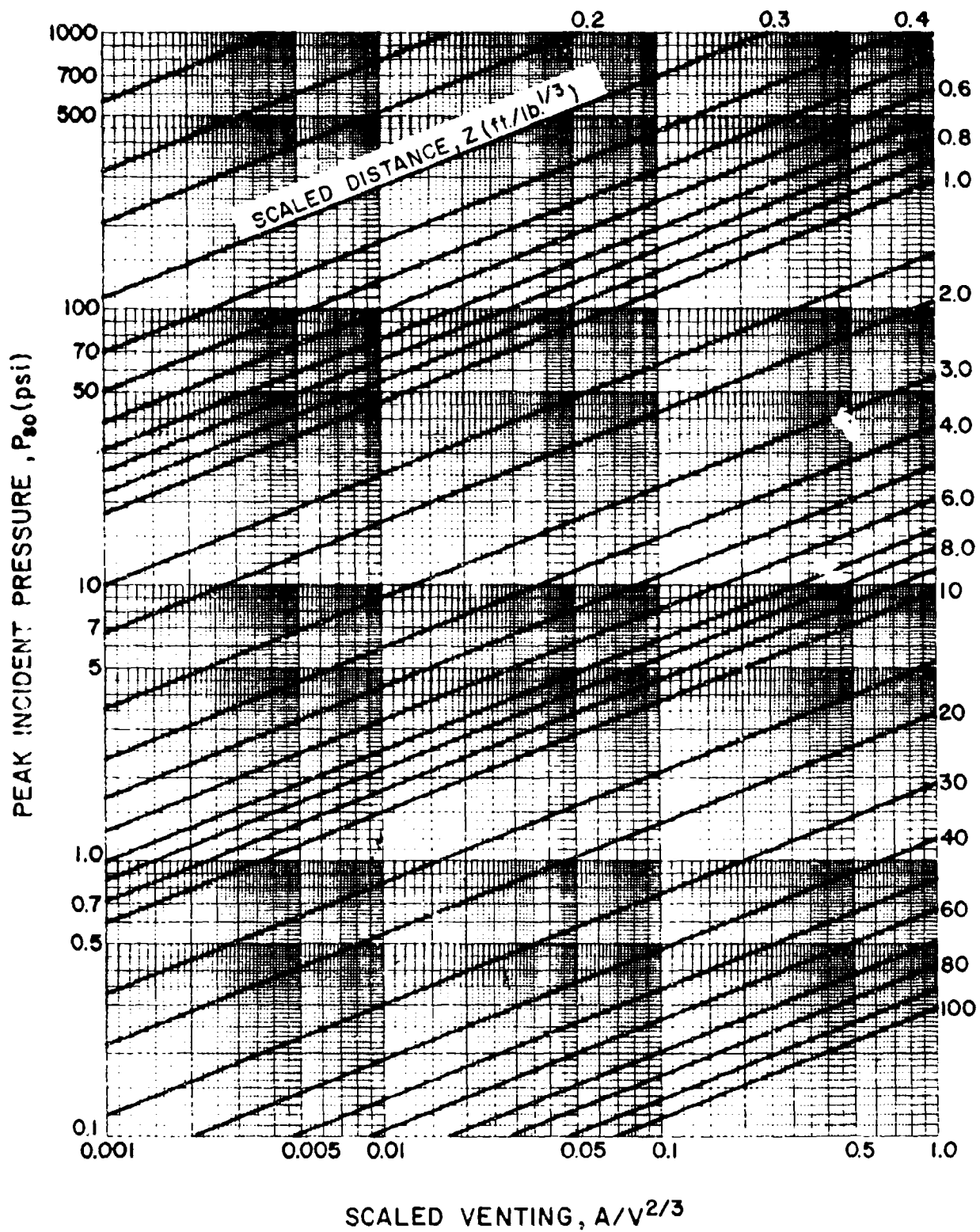
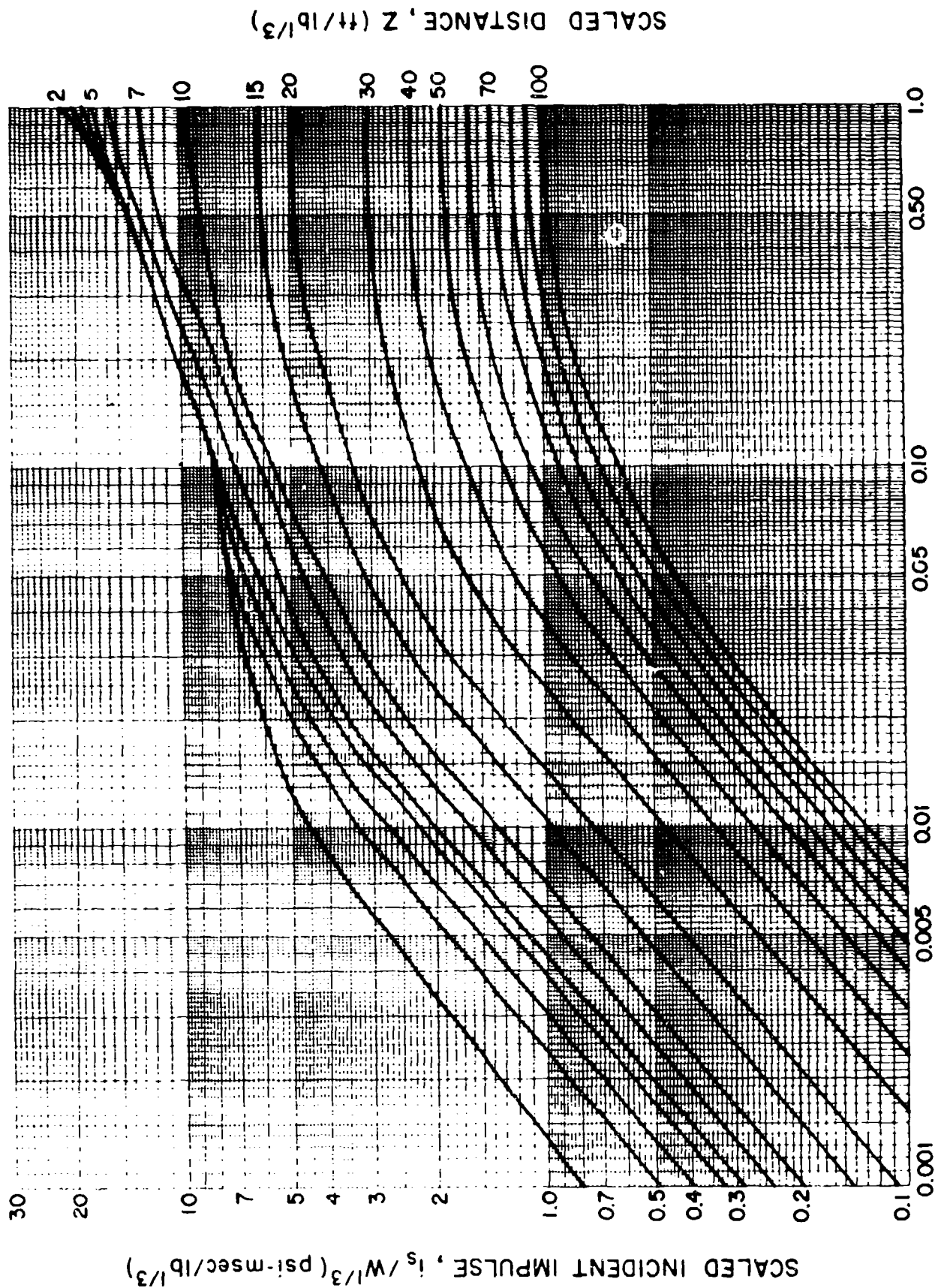


Figure 2-184 Peak positive pressure outside of a four-wall cubicle vented through its roof



SCALED DEGREE OF VENTING, $AW^{1/3}/V$ ($lb^{1/3}/ft$)

Figure 2-185 Scaled positive impulse outside of a four-wall cubicle vented through its roof

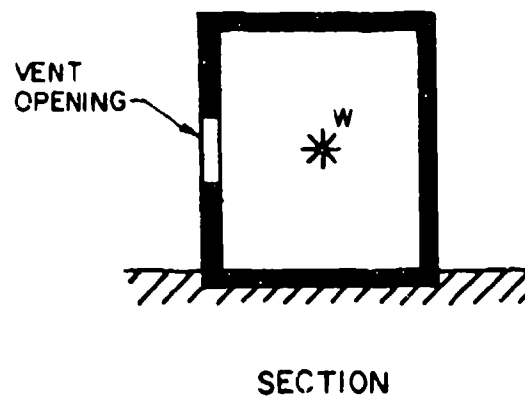
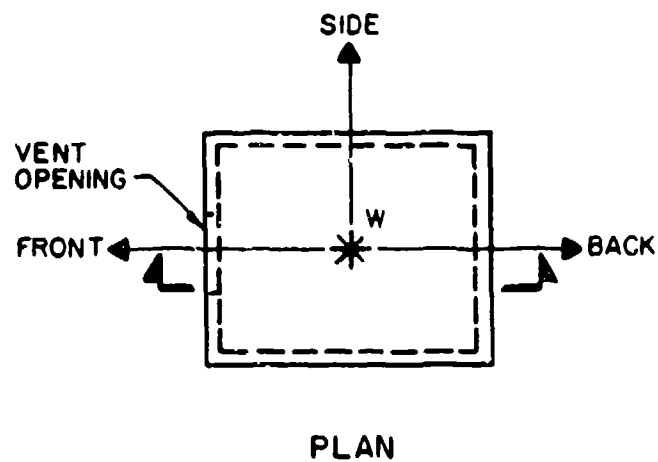


Figure 2-186 Four wall cubicle vented through a wall and direction of blast wave propagation

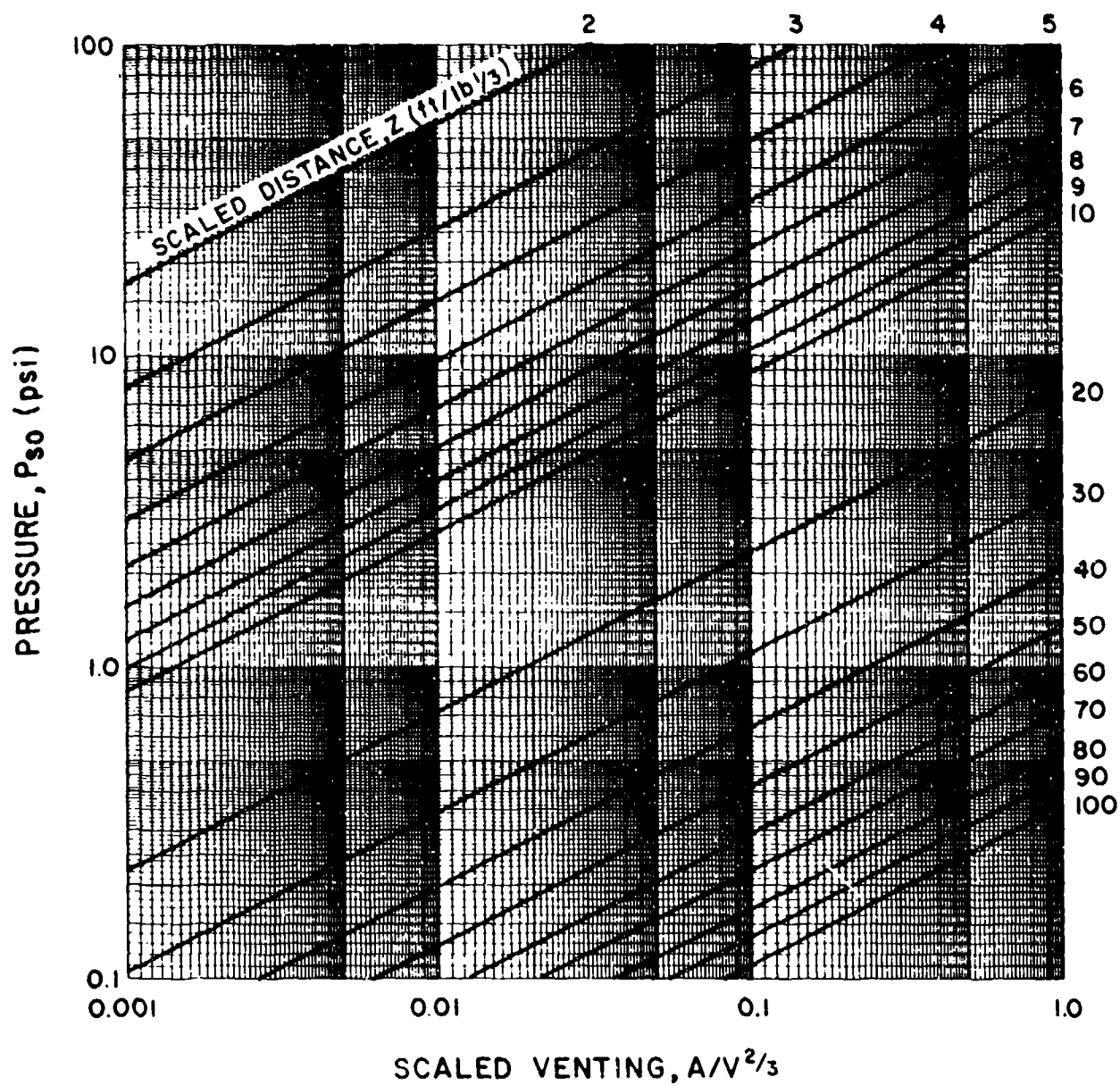


Figure 2-187 Peak positive pressure at the front of a partially vented four-wall cubicle

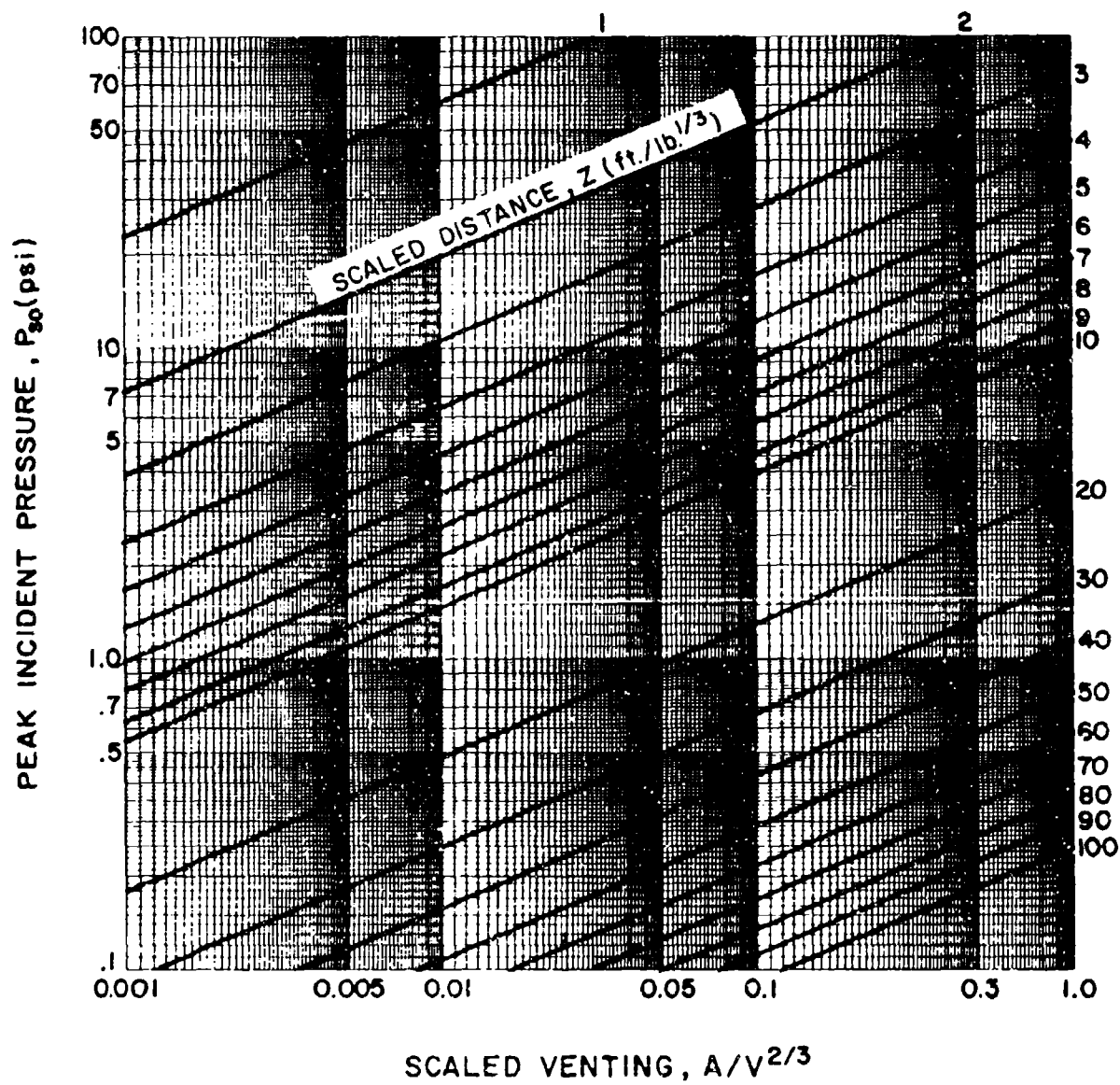


Figure 2-188 Peak positive pressure at the side of a partially vented four-wall cubicle

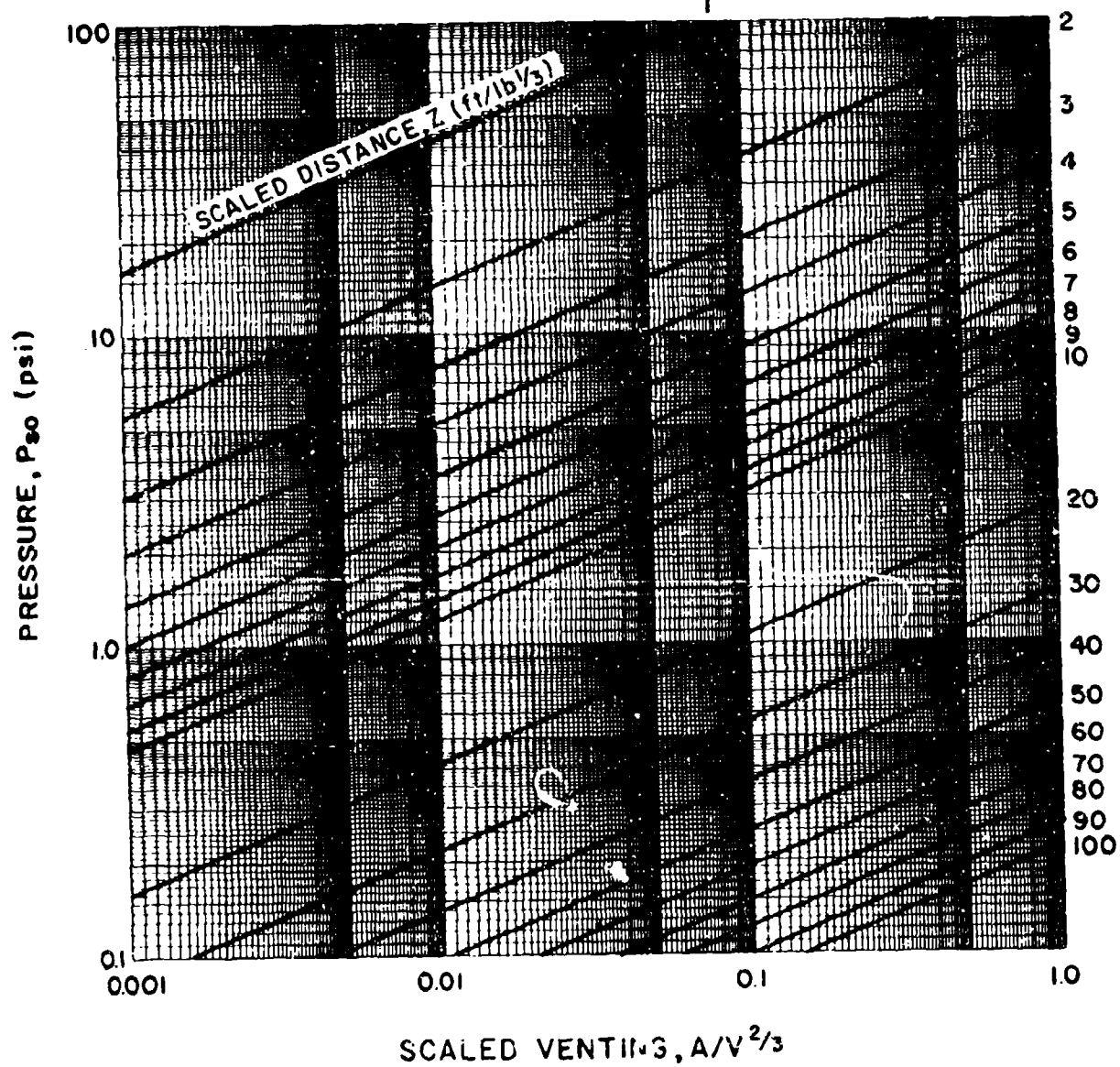


Figure 2-189 Peak positive pressure at the back of a partially vented four wall cubicle

2-15.2 Forces Acting on Structure

The forces acting on a structure associated with a plane shock wave are dependent upon both the peak pressure and the impulse of the incident and dynamic pressures acting in the free-field. The peak pressures and impulses associated with the free-field shock wave have been presented for various explosives.

For each pressure range there is a particle or wind velocity associated with the blast wave that causes a dynamic pressure on objects in the path of the wave. In the free field, these dynamic pressures are essentially functions of the air density and particle velocity. For typical conditions, standard relationships have been established between the peak incident pressure, P_{s0} , the peak dynamic pressure q_0 , the particle velocity, and the air density behind the shock front. The magnitude of the dynamic pressures, particle velocity and air density is solely a function of the peak incident pressure, and, therefore, independent of the explosion size. Figure 2-3 gives the values of the parameters versus the peak incident pressure. Of the three parameters, the dynamic pressure is the most important for determining the loads on structures.

For design purposes, it is necessary to establish the variation or decay of both the incident and dynamic pressures with time since the effects on the structure subjected to a blast loading depend upon the intensity-time history of the loading as well as on the peak intensity. The form of the incident blast wave (fig. 2-190) is characterized by an abrupt rise in pressure to a peak value, a period of decay to ambient pressure and a period in which the pressure drops below ambient (negative pressure phase).

The rate of decay of the incident and dynamic pressures, after the passage of the shock front, is a function of the peak pressure (both positive and negative phases) and the size of the detonation. For design purposes, the actual decay of the incidental pressure may be approximated by the rise of an equivalent triangular pressure pulse. The actual positive duration is replaced by a fictitious duration which is expressed as a function of the total positive impulse and peak pressure:

$$t_{of} = 21/p$$

2-6

the above relationship for the equivalent triangular pulse is applicable to the incident as well as the reflected pressures; however, in the case of the latter, the value of the pressure and impulse used with equation 2-6 is equivalent to that associated with the reflected wave. The fictitious duration of

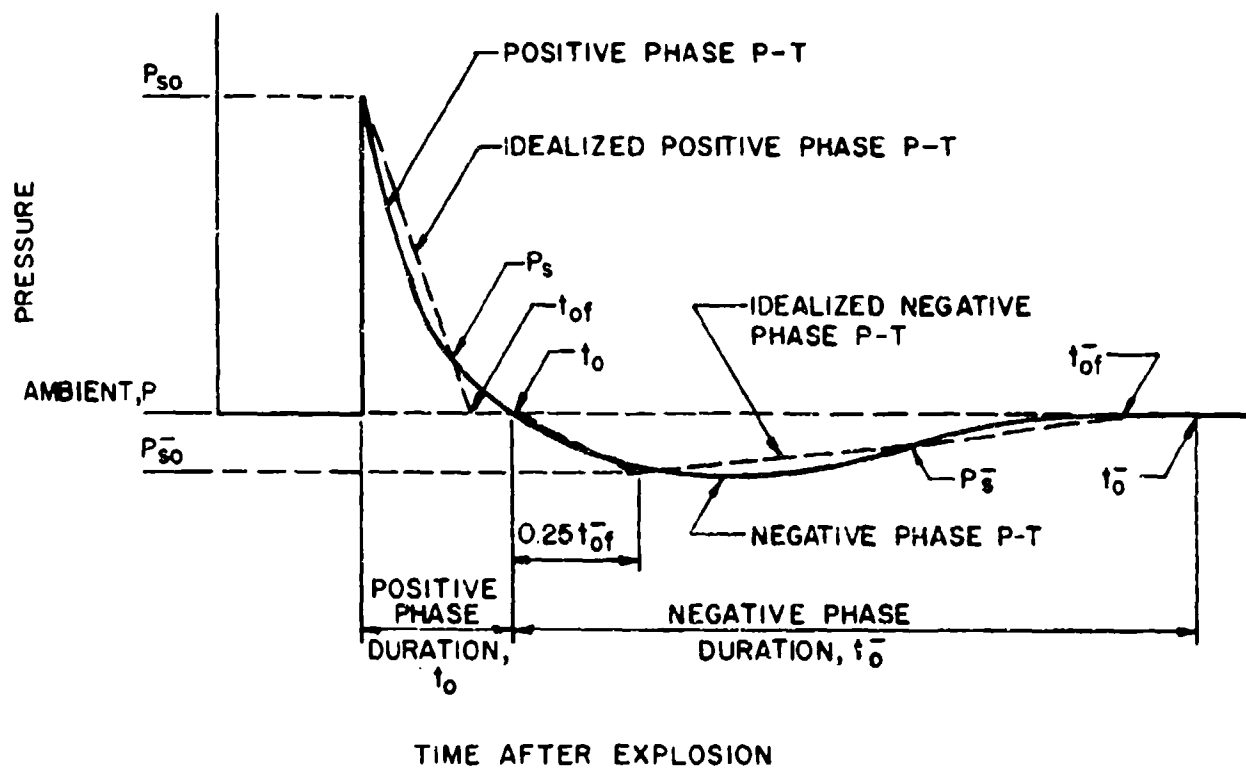


Figure 2-190 Idealized pressure-time variation

the dynamic pressure may be assumed to be equal to that of the incident pressure.

For determining the pressure-time data for the negative phase, a similar procedure as used in the evaluation of the idealized positive phase may be utilized. The equivalent negative pressure-time curve will have a time of rise equal to $0.25 t_{of}^-$ whereas the fictitious duration t_{of}^- is given by the triangular equivalent pulse equation:

$$t_{of}^- = 2i^-/p^- \quad 2-7$$

where i^- and p^- are the total impulse and peak pressure of the negative pulse of either the incident or reflected waves. The effects of the dynamic pressure in the magazine phase region usually may be neglected.

Since the fictitious duration of the positive phase will be smaller in magnitude than the actual duration, a time gap will occur between the fictitious duration and the onset of the negative phase. This time gap, which is illustrated in figure 2-190, should be maintained in an analysis for consistency of the onset of the various load phasings.

2-15.3 Above-Ground Rectangular Structure Without Openings

2-15.3.1 General For any given set of free-field incident and dynamic pressure pulses, the forces imparted to an above-ground structure can be divided into four general components: (a) the force resulting from the incident pressure, (b) the force associated with the dynamic pressures, (c) the force resulting from the reflection of the incident pressure impinging upon an interfering surface, and (d) pressures associated with the negative phase of the shock wave. The relative significance of each of these components is dependent upon the geometrical configuration and size of the structure, the orientation of the structure relative to the shock front, and the design purpose of the blast loads.

The interaction of the incident blast wave with a structure is a complicated process. To reduce the complex problem of blast to reasonable terms, it will be assumed here that: (a) the structure is generally rectangular in shape, (b) the incident pressure of interest is in the order of 200 psi or less, (c) the structure being loaded is in the region of the Mach stem, and (d) the Mach stem extends above the height of the building.

2-15.3.2 Front Wall For a rectangular above-ground structure at low pressure ranges, the variation with time on the side facing the detonation (front face) when this side is parallel to the shock front (normal reflection) is illustrated in figure 2-191a. At the moment the incident shock front strikes the front wall, the pressure immediately rises from zero to the normal reflected pressure, P_r , which is a function of the incident pressure (fig. 2-15). The clearing time, t_c , required to relieve the reflected pressure is represented as:

$$t_c = \frac{4S}{(1 + R)C_r}$$

2-8

where:

S = clearing distance and is equal to H or W (fig. 2-191a) whichever is the smallest

H = height of the structure

R = ratio of S/G where G is equal to H or W (fig. 2-191) whichever is the larger

C_r = sound velocity in reflected region (fig. 2-192)

The pressure acting on the front wall after time t_c is the algebraic sum of the incident pressure P_s and the drag pressure $C_D q$ or:

$$P = P_s + C_D q$$

2-9

The drag coefficient C_D gives the relationship between the dynamic pressure and the total translational pressure in the direction of the wind produced by the dynamic pressure and varies with the Mach number (or with the Reynold's number at low incident pressures) and the relative geometry of the structure. A value of $C_D=1$ for the front wall is considered adequate for the pressure ranges considered in this manual. At higher pressure ranges, the above procedure may yield a fictitious pressure-time curve because of the extremely short pressure pulse durations involved. Therefore, the pressure-time curve constructed must be checked to determine its accuracy. The comparison is made by constructing a second curve (dotted triangle as indicated in fig. 2-191a) using the total reflected pressure impulse i_r from figure 2-15 for a normal reflected shock wave (fig. 2-191a). The fictitious duration t_{rf} for the normal reflected wave is calculated from:

$$t_{rf} = \frac{2i_r}{P_r}$$

2-10

where P_r is the peak normal reflected pressure (fig. 2-15). Whichever curve (fig. 2-191a) gives the smallest value of the impulse (area under curve), that curve should be used in calculating the wall loading.

If the shock front approaches the structure at an oblique angle (fig. 2-191b), then the peak pressure will be a function of the incident pressure and the incident angle between the front and the front wall and is obtained from figure 2-193.

An equation similar to that used for the manual shock front may be used when the angle of obliquity is greater than zero as follows:

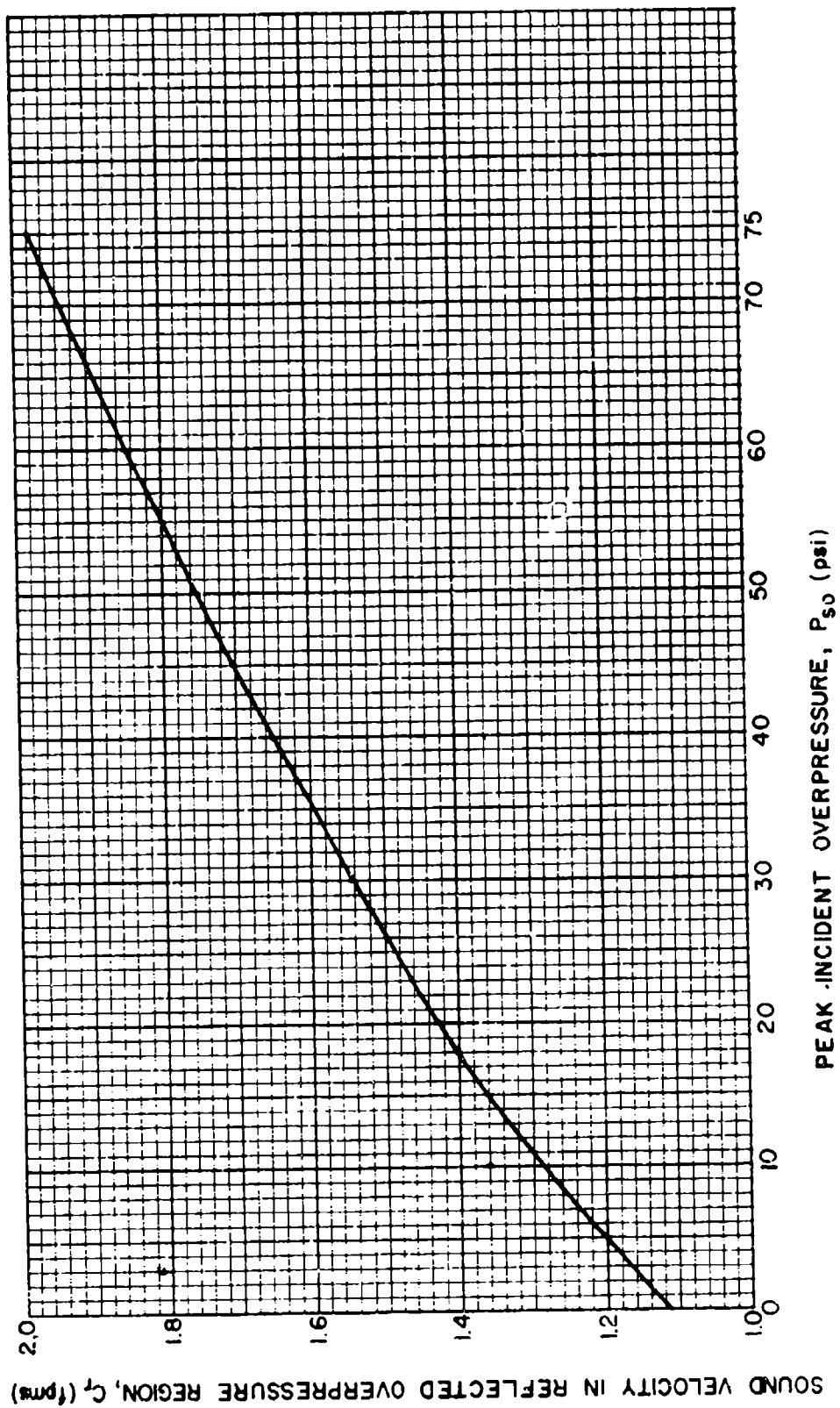


Figure 2-192 Velocity of sound in reflected overpressure region versus peak incident overpressure

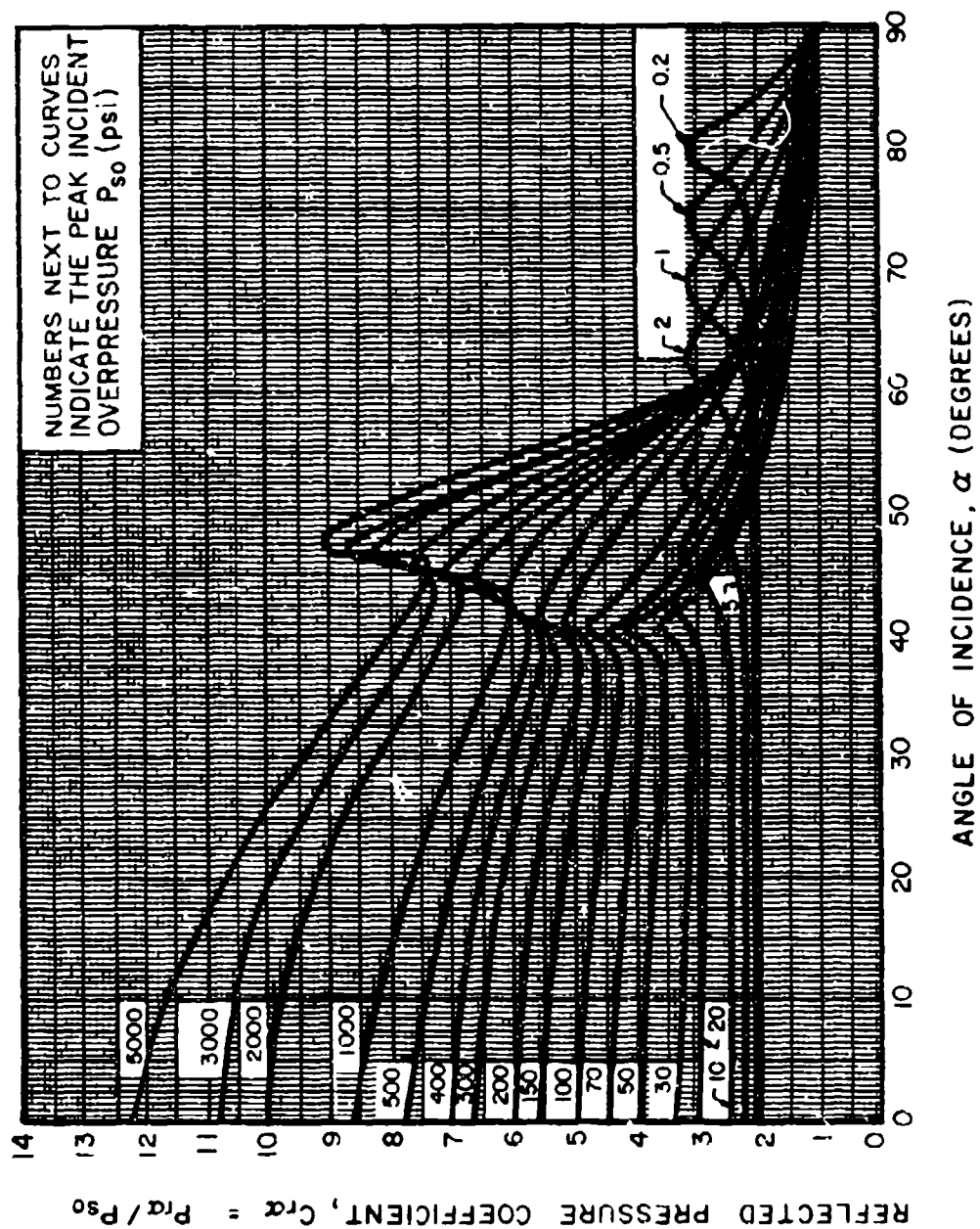


Figure 2-193 Reflected pressure coefficient versus angle of incidence

$$t_{rf} = \frac{2i_{ra}}{P_{ra}}$$

2-11

where peak reflected impulse i_{ra} is obtained from figure 2-194.

Usually only the positive pulse of the pressure-time relationship of figure 2-191b is utilized for the front wall design since the negative pulse seldom affects the design. For determining the overall motions of the structure, however, the effects of negative pressures should be included. The peak negative reflected pressure (fig. 2-190) and reflected impulse are obtained from figure 2-16 and correspond to the peak incident pressure (fig. 2-15) acting on the front wall. The rise time and decay of the negative pressures are similarly calculated as described in Section 2-15.2.

2-15.3.3 Roof and Side Walls. As the shock front traverses a structure a pressure is imparted to the roof slab and side walls equal to the incident pressure at a given time at any specified point reduced by a negative drag pressure. The portion of the surface loaded at a particular time is dependent upon the magnitude of the shock front incident pressure, the location of the shock front and the wavelengths (L_w and L_w^-) of the positive and negative pulses.

To determine accurately the overall loading on a surface, a step-by-step analysis of the wave propagation across the surface should be made. This analysis includes an integration of the pressures at various points (fig. 2-195a) on the surface and at various times to determine the equivalent uniform incident pressure acting on a span L as a function of time (fig. 2-195b). Since the point of inflection of the element will vary as the shock front traverses the surface, in order to make the assumption of the uniform pressure valid, the reinforcement on both faces must be continuous across the span length.

As the shock wave traverses the roof, the peak value of the incident pressure decays and the wave length increases. As illustrated in figure 2-195b, the equivalent uniform pressure will increase linearly from time t_f when the blast wave reaches the beginning of the element (point f) to time t_d when the peak equivalent uniform pressure is reached when the shock front arrives at point d. The equivalent uniform pressure will then decrease to zero where the blast load at point b on the element decreases to zero.

To simplify the calculations, the equivalent uniform pressure has been expressed as a function of the blast wave parameters at point f. The equivalent load factor C_E , the rise time and duration of the equivalent uniform pressure are obtained from figures 2-196, 2-197 and 2-198, as a function of the wave length-span ratio L_{wf}/L .

The peak value of the pressure acting on the roof P_R is the sum of contribution of the equivalent uniform pressure and drag pressure:

$$P_R = C_E P_{sof} + C_D q_{of}$$

2-12

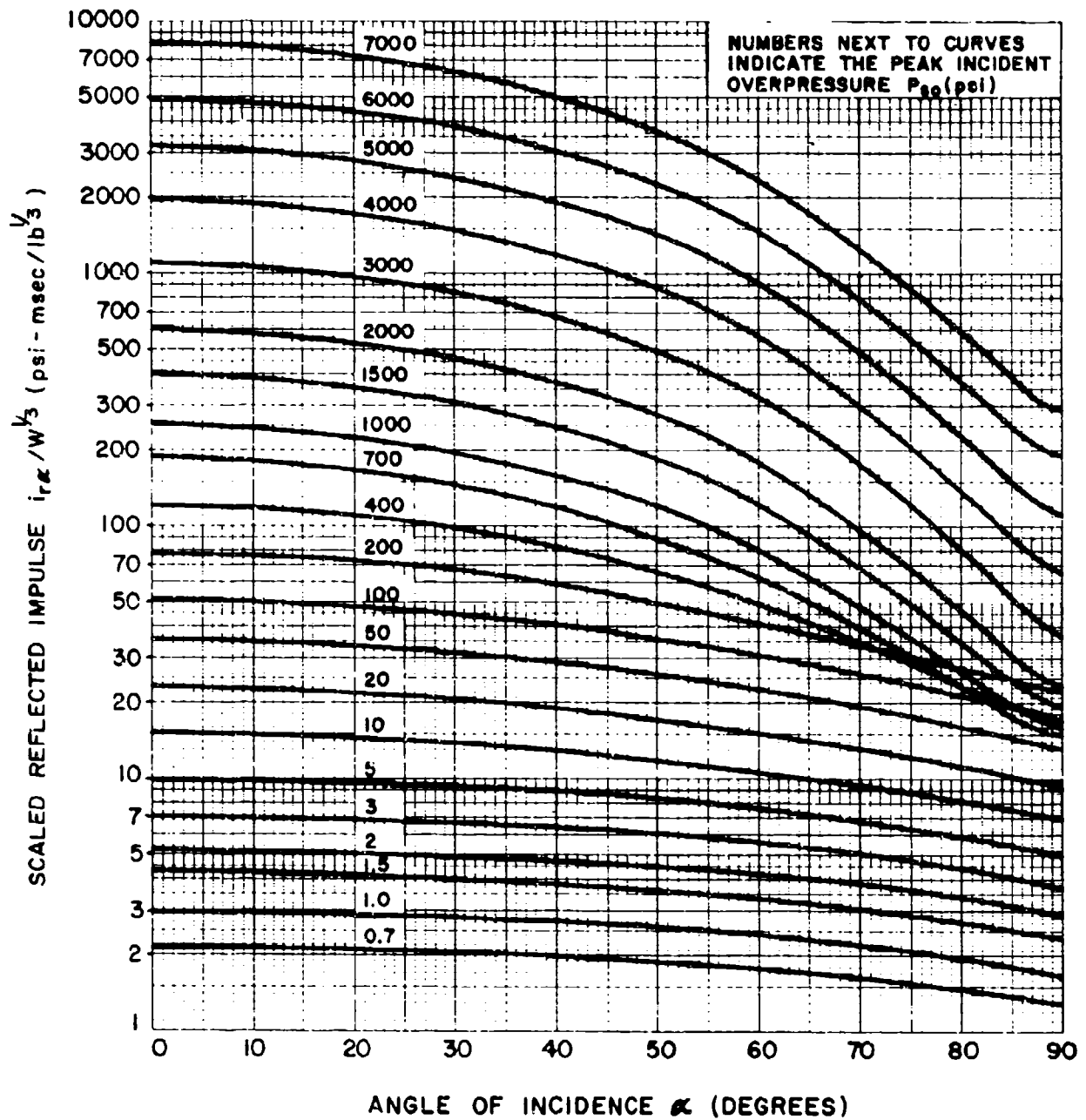
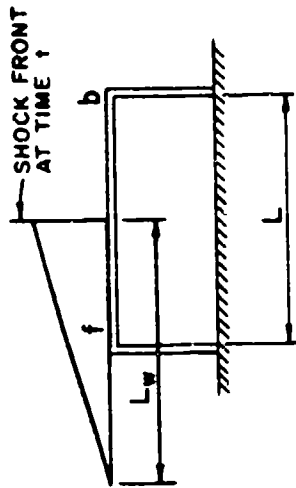
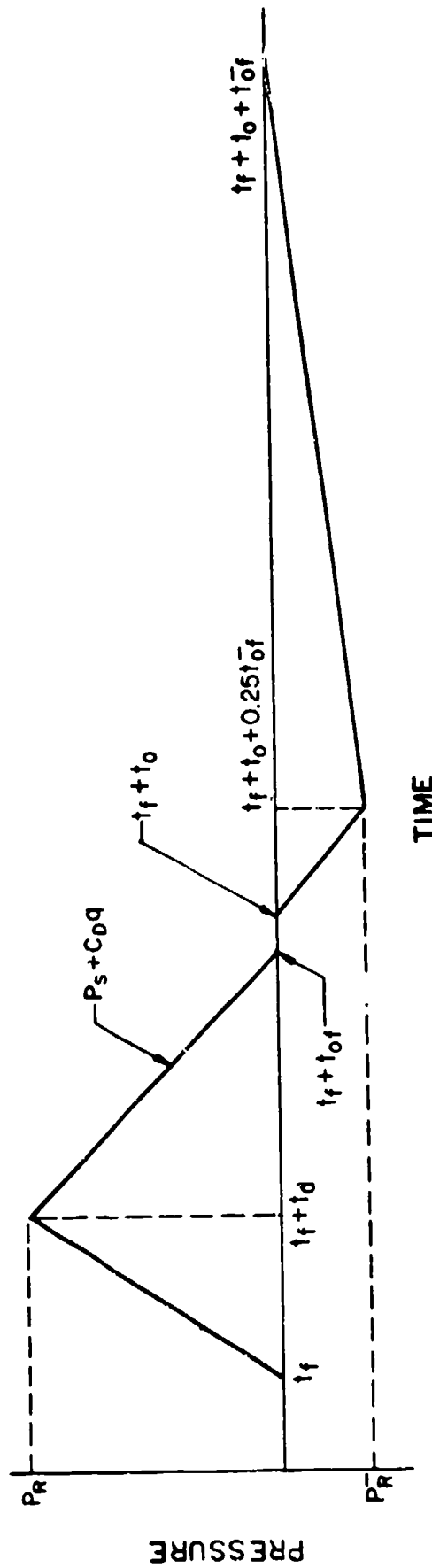


Figure 2-194 Reflected scaled impulse versus angle of incidence



a) SECTION THROUGH STRUCTURE



b) AVERAGE PRESSURE - TIME VARIATION

Figure 2-195 Roof and side wall loading

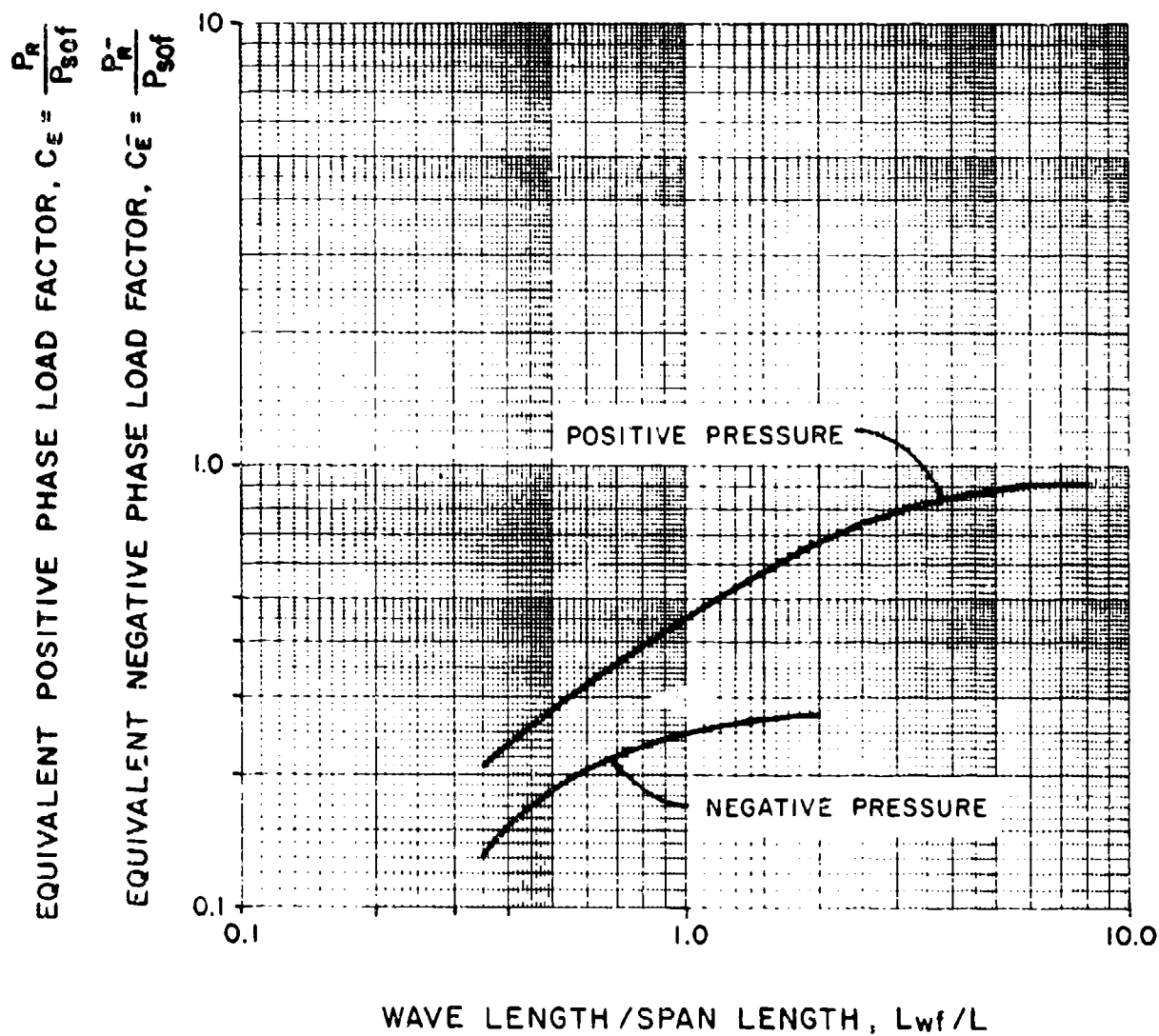


Figure 2-196 Peak equivalent uniform roof pressures

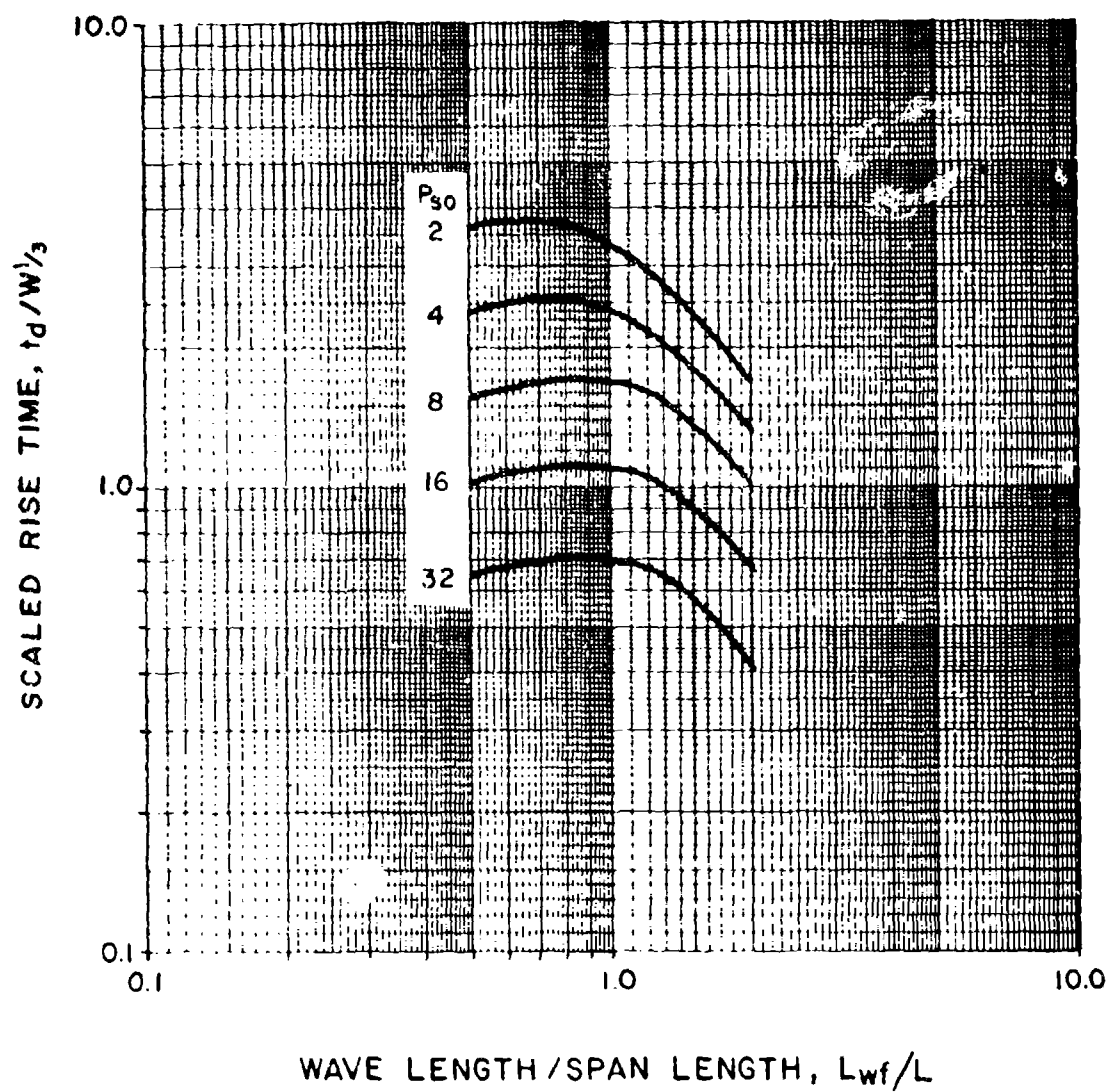


Figure 2-197 Scaled rise time of equivalent uniform positive roof pressures

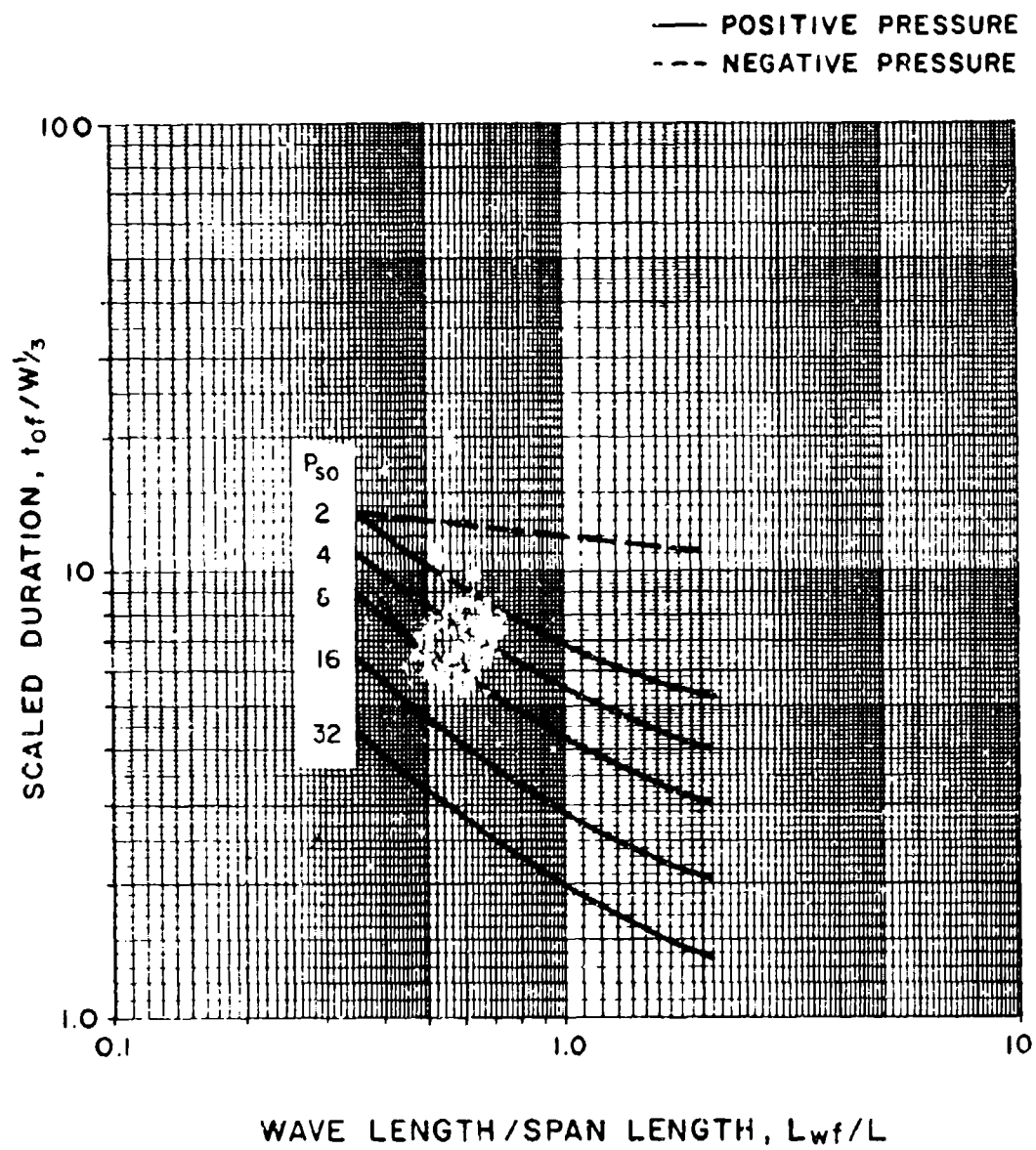


Figure 2-198 Scaled duration of equivalent uniform roof pressures

where P_{sof} is the incident pressure occurring at point f and q_{of} is the dynamic pressure corresponding to $C_E P_{sof}$.

The drag coefficient C_D for the roof and side walls is a function of the peak dynamic pressure. Recommended values are as follows:

| Peak dynamic pressure | Drag coefficient |
|-----------------------|------------------|
| 0-25 psi | -0.40 |
| 25-50 psi | -0.30 |
| 50-130 psi | -0.20 |

The data presented above for the equivalent uniform roof and side wall blast pressures are used principally for the design of individual elements. For overall motions of a structure, the effects of the negative phase pressures should be included. The equivalent load factor C_E for the peak equivalent uniform negative pressure is obtained from figure 2-196 as a function of the wave length-span ratio L_{wf}/L . The value of the negative pressure acting on the roof, P_R^- , is equal to $C_E^- P_{sof}$ where the value of C_E^- is a minus value. The value of the equivalent negative pressure duration t_{of} is obtained from figure 2-198. The value is not a function of the peak incident pressure at point f. The rise time of the negative phase is equal to $0.25 t_{of}$.

If a side wall is positioned at an oblique angle to the shock front then blast loads acting on the side wall are calculated in the same manner as that described for front walls.

2-15.3.4 Rear Wall. As the shock front passes over the rear edges of the roof and/or side walls the pressure front will expand, forming secondary waves which propagate over the rear wall. In the case of long buildings, the secondary wave enveloping the back wall essentially results from the spillover from the roof, and the side walls. In both cases, the secondary waves are reinforced due to their impingement with reflecting surfaces. The reinforcement of the spillover wave from the roof is produced by its reflection from the ground surface at the base of the rear wall, whereas the reinforcement of the secondary waves from the side walls is produced by their collision near the center of the wall and/or their interaction with the wave from the roof. Little information is available on the overall effects on the rear wall loading produced by the reflections of the secondary waves.

In most design cases, the primary reason for determining the blast loads acting on the rear wall is to determine the overall drag effects (both front and rear wall loadings) on the building. For this purpose, a procedure may be used where the blast loading on the rear wall figure (2-199a) is calculated using the equivalent uniform method used for computing the blast loads on the roof and side walls. Here the peak pressure of the equivalent uniform pressure-time curve (fig. 2-199b) is calculated using the peak pressure that would accrue at the back edge of the roof slab P_{sob} . The equivalent uniform load factors C_E and C_E^- are based on the wave length of the peak pressure above and the height of the rear wall H_g as are the time rises and durations of both the positive and negative phases.

Like the roof and side walls, the blast loads acting on the rear wall are a function of the drag pressures in addition to the incident pressure. The dynamic pressure of the drag corresponds to that associated with the equivalent pressure $C_E P_{sob}$, while the recommended drag coefficients are the same as used for the roof and side walls.

In the event that the back wall is positioned at an oblique angle to the shock front, then peak incident pressure at point b should be calculated at the mid width.

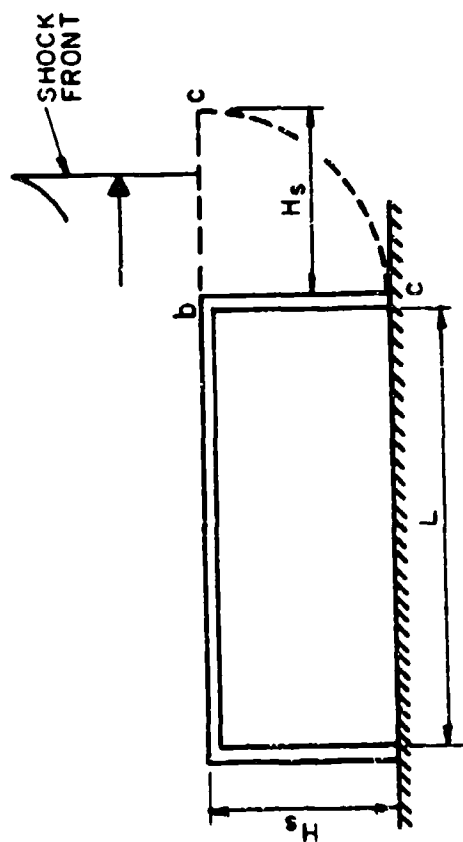
2-15.3.5 Multiple Explosions

As previously mentioned, the blast loads, produced by multiple explosions, acting on structures located far from an explosion may consist of a series of separate pressure pulses rather than a single pulse blast load. However, the multiple pressure-pulse loading is usually associated with weights of explosives which are very small (several pounds) and, therefore, will not be the usual design situation. For large charge weights, however, the single pressure pulse loading with multiple peak pressures will occur. At the present time no specific method has been devised which will enable one to evaluate this type of blast loading. In the interim, it is suggested that the multiple peak pressure type loading be replaced by the pressure-pulse which is associated with the merged shock wave. The parameters of this shock wave and corresponding pressures are determined assuming a single explosion, the explosive weight of which is equal to the combined weight of the individual charges.

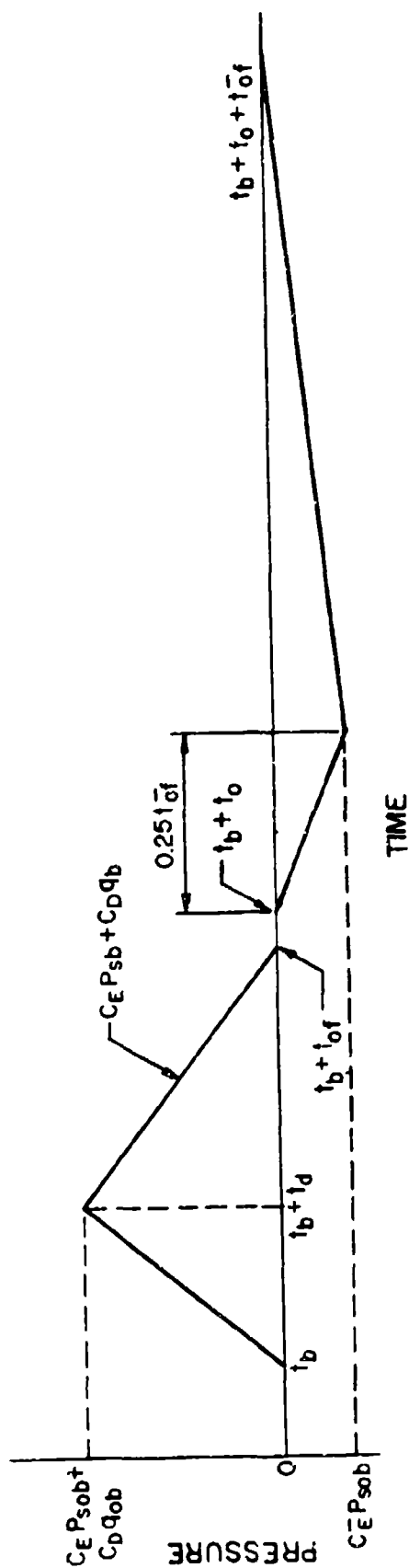
2-15.4 Above Ground Rectangular Structures with Openings.

2-15.4.1 General. Two structural configurations are usually encountered when blast loads are determined on structures with unsealed or unprotected openings in its exterior. The first configuration includes windows, doors or other openings located in both the front and rear walls as well as along the side walls of the structure. The second would include openings located only in the front face of the structure. The remaining surfaces are void of openings. The second configuration is the one most likely to be encountered since interior partitions will restrict the flow of the blast wave through the structure. Increased interior blast loads are produced due to the reflection of the blast wave on interior components. The blast loads associated with the second configuration are primarily discussed in this section with comments regarding the loads pertaining to the first configuration.

When a shock front strikes the front wall of a structure, the incident pressure is amplified. Windows and doors will fail almost immediately (approximately one millisecond) after the onset of the shock front unless they were designed to resist the applied load. As a result, blast pressures will flow into the structure through these openings. This sudden release of high pressure will cause a shock front to form inside of each opening. Each individual front will expand and tend to combine into a single front which will further expand throughout the structure's interior. This interior shock is initially weaker than the incident pressure at the building's exterior. However, the interior pressure will tend to get stronger due to reflections off interior building components.



a) SECTION THROUGH STRUCTURE



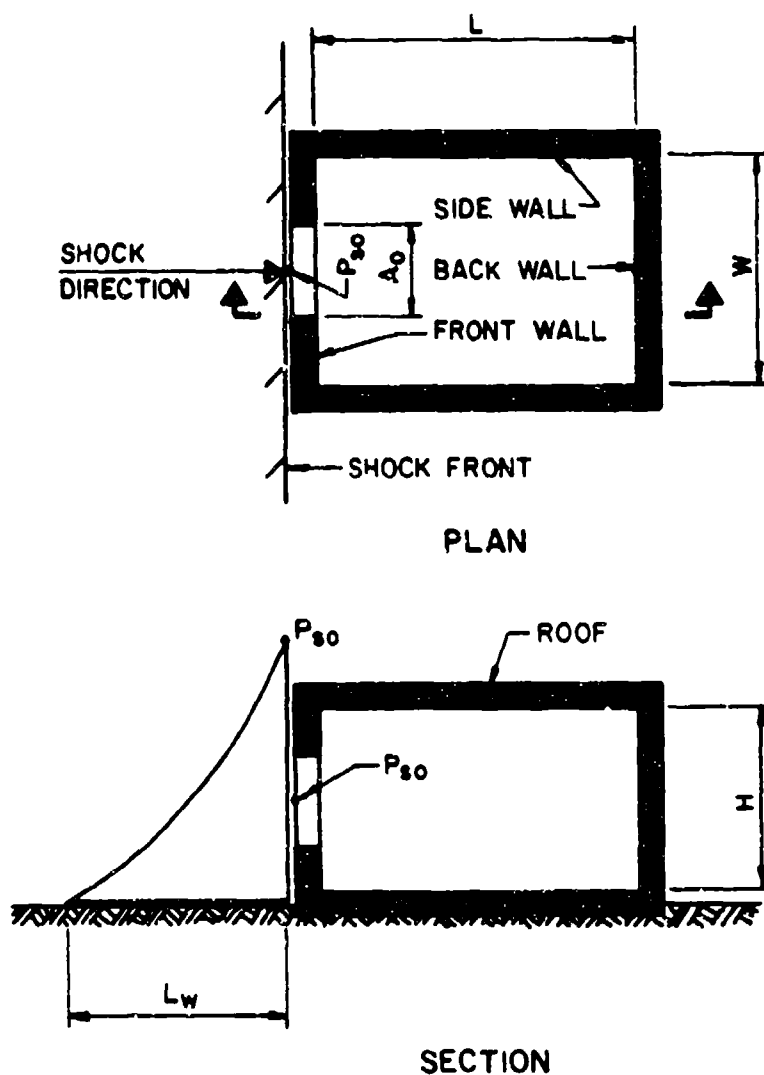
b) AVERAGE PRESSURE - TIME VARIATION

Figure 2-199 Rear wall loading

An idealized structure configuration is shown in figure 2-200. The incident shock front arriving at the front wall of the structure has an incident pressure P_{s0} and wave length L_w . As the shock front sweeps across the structure, blast pressures enter the interior of the building through the opening in the front wall of area A_0 . The areas of multiple openings are added to obtain a fictitious single opening located at the center of the front wall. The blast pressures entering the building first load the interior surface of the front wall, followed by the interior surface of the side walls and roof, and finally the interior surface of the back wall. The idealized pressure-time load curves for these surfaces are presented in figure 2-201. The procedures necessary to obtain the magnitude of the parameters given on the idealized load curves for a particular explosion are presented in the remainder of this section. Except for the front wall, the blast pressures acting on the exterior of the structure are not affected by the opening and are determined according to the procedures of the previous section.

The primary purpose of this section is to provide the blast loading on the interior surface of an exterior wall so that the maximum outward motion of the wall may be determined. It is not the intent to use these interior loads to reduce the exterior positive phase loading. Except for the front wall, accurate phasing of the interior and exterior blast loads are not possible. The interior loads will always lag the exterior positive phase loading and, due to reflections off interior components, the duration of the interior load is always longer. For design, the interior blast loads should be added to the negative phase exterior loading to obtain the maximum outward motion (negative response) of a side wall, roof or back wall. The maximum positive response should be determined for the exterior positive phase loading without any reductions due to internal pressures. In most instances, interior partitions are required to withstand the blast pressures leaking into a structure. The procedures presented in this section may be used to determine the design blast load acting on these elements. An interior partition located parallel to the front wall will reflect the shock front and, therefore, is considered as a back wall. The length of the side wall would then be taken as the distance between the front wall and this partition. An interior partition(s) perpendicular to and framing into the front wall may be considered as a side wall(s). The length of the front wall would then be taken as the distance between an interior partition and a side wall or between two interior partitions. In both cases, only the openings located between these partition walls would be considered as the vent opening.

The procedures presented in this section to determine interior blast loads acting on a structure with an opening in the front wall were developed for a shock front striking the front wall head-on. For the same size opening in a front wall, this orientation of the approaching shock front results in the most severe interior shock wave effects. The use of these procedures for shock fronts approaching at all other angles will result in conservative estimates of the blast loadings acting on the interior of the structure.



NOMENCLATURE:

L , LENGTH OF SIDE WALL

W , WIDTH OF BACK WALL AND FRONT WALL

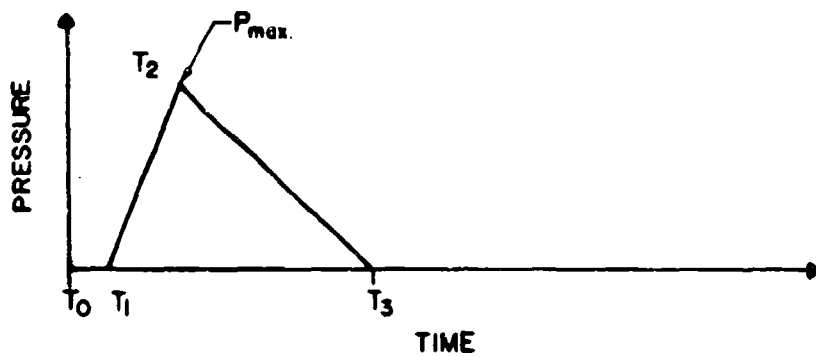
H , HEIGHT OF ALL WALLS

A_0 , AREA OF OPENING IN FRONT WALL

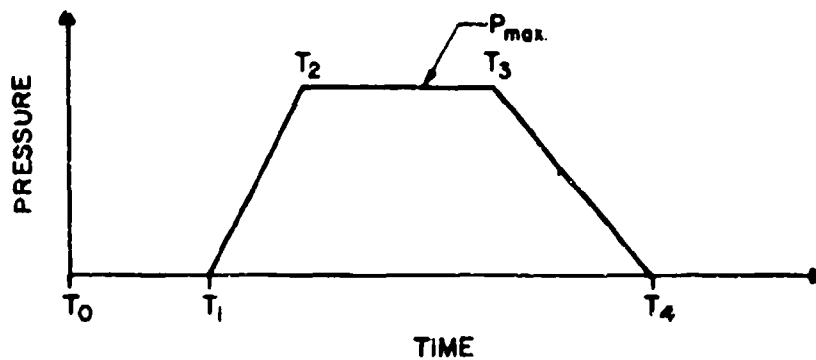
A_w , AREA OF BACK WALL

L_w , WAVE LENGTH OF SHOCK WAVE OF INCIDENT PRESSURE, P_{s0} ,
AT EXTERIOR FACE OF FRONT WALL

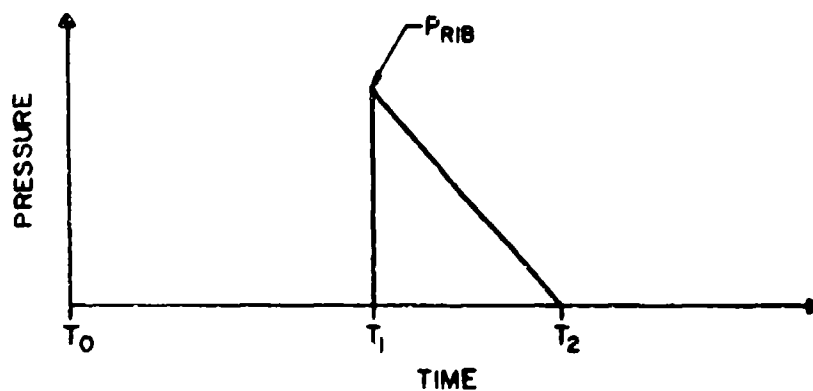
Figure 2-200 Idealized structure configuration for interior blast loads



a. INTERIOR FRONT WALL SURFACE



b. INTERIOR SIDE WALL OR ROOF SURFACE



c. INTERIOR BACK WALL SURFACE

Figure 2-201 Idealized interior blast loads

2-15.4.2 *Exterior Front Wall Loads.* The time required for reflected pressures to clear a solid front wall is expressed in multiples of the time necessary for a rarefaction wave to sweep the wall. When walls with openings are considered, clearing takes place around the edges of the opening in addition to the edges of the wall. Depending upon the size of the overall wall and the openings, the clearing time of the reflected pressures may be significantly reduced.

The pressure-time relationship of the applied blast load acting on the front wall of a structure with openings is the same as that of a solid front wall (fig. 2-191) except the clearing time will be reduced. To evaluate this reduced time, the value of S' is introduced into equation 2-8. This value is the weighted average distance that the rarefaction wave must travel to cover the wall assuming immediate access of the incident shock to the interior of the structure. If frangible covers (windows, doors, etc.) do not fail immediately, the clearing time should not be reduced.

The method for evaluating S' is illustrated in figure 2-202 where the face of the front wall is divided into rectangular areas. These areas are determined by the location and dimensions of the openings in the wall, and by consideration of the direction along which the reflected pressure clears around the area in the shortest possible time. The individual areas are labeled depending upon the number and location of the clearing sides of the individual areas. Clearing factors δ_n are established for these areas as follows:

| Area | δ_n | Number of Clearing Sides |
|-------|--------------------|--------------------------|
| 1 1.0 | Two adjacent sides | |
| 2 0.5 | Two opposite sides | |
| 3 1.0 | One side | |
| 4 1.0 | None | |

The weighted average clearing distance S' is expressed as:

$$S' = \frac{\sum \delta_n h_n A_n}{A_f} \leq S \quad 2-13$$

where

S' = weighted average clearing distance with openings

δ_n = clearing factor

h_n = average clearing distance for individual areas as follows:

Area 1 - width or height of area whichever is smaller

Area 2 - distance between opposite sides where clearing occurs

Area 3 - distance between side where clearing occurs
and opposite side

Area 4 - same as Area 1

A_n = area of individual wall subdivision

A_f = net area of the wall excluding openings

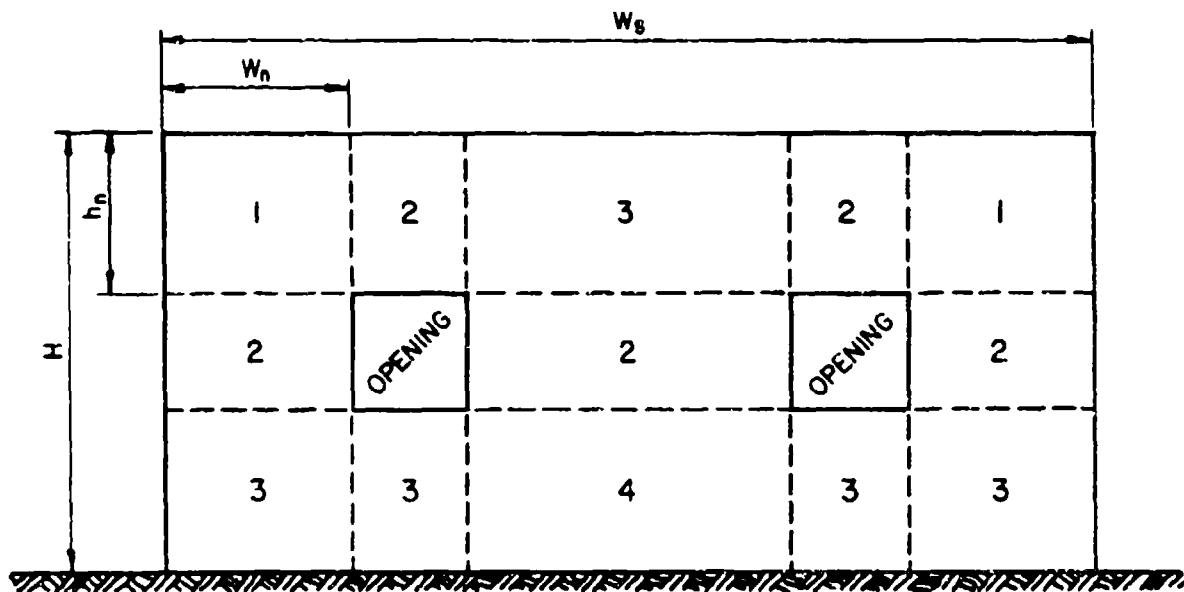


Figure 2-202 Sub-division of typical front wall with openings

The clearing time t'_c for a front wall with openings is calculated from equation 2-8 in which S' is substituted for S or

$$t'_c = \frac{4S'}{(1+R)C_r} \quad 2-14$$

where all components of equation 2-14 have been previously defined. It should be realized that the load acting on the front wall with openings is still the same as that shown on figure 2-191 except with the reduced clearing time, t'_c . The curve which represents the wall loading is still the curve which gives the lower impulse.

As previously stated, window breakage will require a finite length of time. This time may be evaluated using the resisting functions of Volume VI and the dynamic procedures of Volume III. This time must be accounted for in determining the window contribution to the blast pressures acting on the wall.

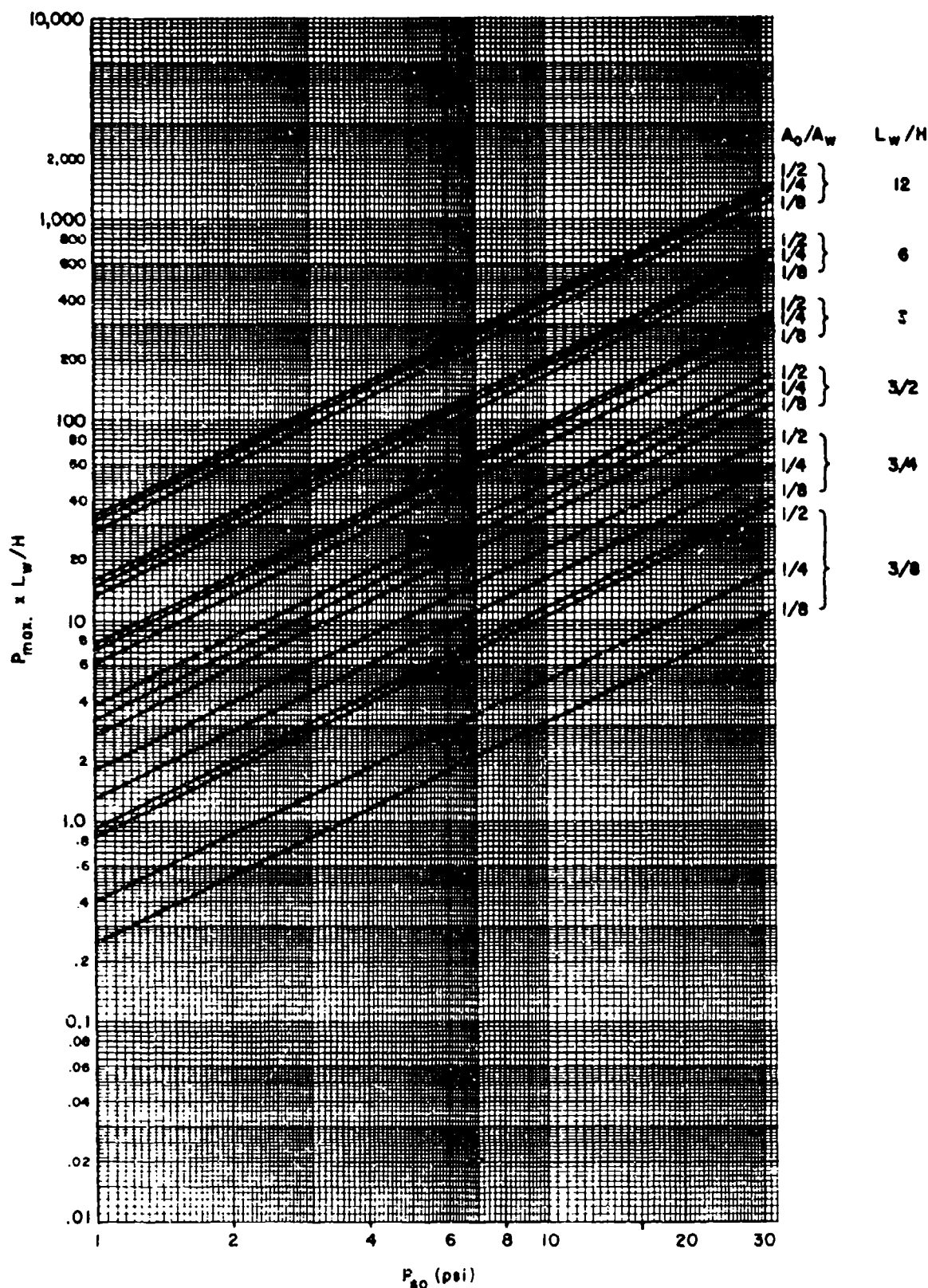
2-15.4.3 Interior Front Wall Loads. The average pressure acting on the interior face of the front wall will initially build up in a similar manner as the average pressure on the exterior back wall of a closed structure. However, vortices are located all around the interior edges of all openings in the front wall. The effect of these vortices, which tend to reduce the blast load, have been neglected.

The shock front entering through the opening in the front wall travels along the interior face of the front wall, thereby subjecting the wall to incident pressures. When the front reaches the side wall, it is reflected back. The length of wall loaded by this reflected wave is a function of the wave length, L_w . The average pressure acting on the wall is determined assuming a single opening of area A_0 located at the center of the wall. In the case of multiple openings, a single opening equal to the combined area of all openings is located in the center of the front wall.

The idealized pressure-time blast load acting on the interior face of the front wall is shown on figure 2-201a. The time at which the shock front arrives at the exterior surface of the front wall is taken as zero ($T_0 = 0$).

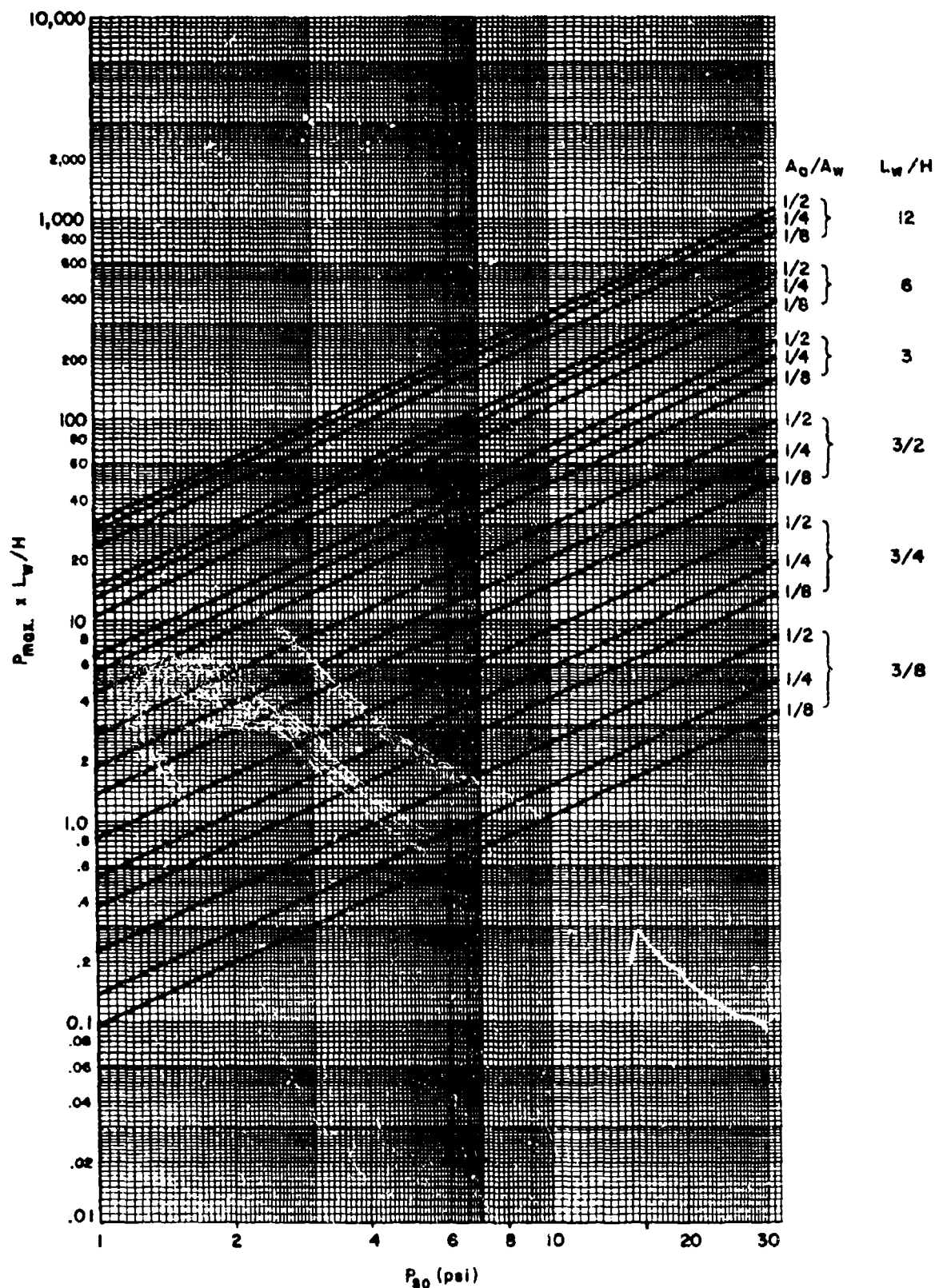
The blast load acting on the wall begins at time T_1 . This time represents the time it takes for the shock front to enter the structure through the opening A_0 . The pressure buildup is linear from time T_1 to a maximum pressure P_{max} at time T_2 , and then decays linearly to zero at time T_3 .

The maximum average pressure P_{max} acting on the interior face of the front wall varies as a function of the incident pressure P_{so} and the wave length L_w corresponding to that pressure, and the geometry of the wall. Figures 2-203 through 2-206 give the maximum pressure P_{max} acting on front walls having width to height ratios W/H equal to $3/4$, $3/2$, 3 and 6 , respectively.



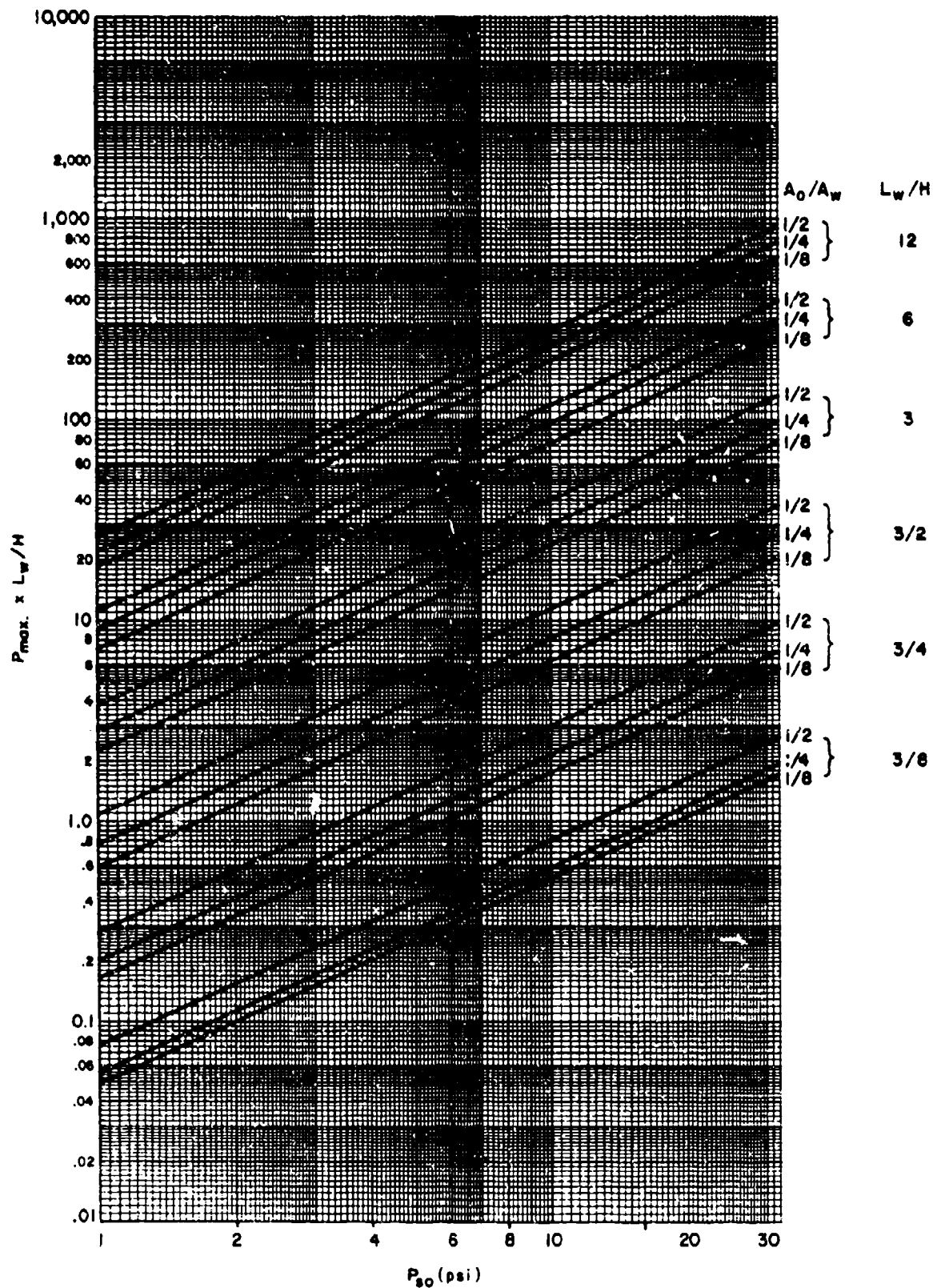
EXTERNAL INCIDENT PRESSURE AT FRONT FACE OF BUILDING, P_{s0} (psi)

Figure 2-203 Maximum average pressure on interior face of front wall ($W/H = 3/4$)



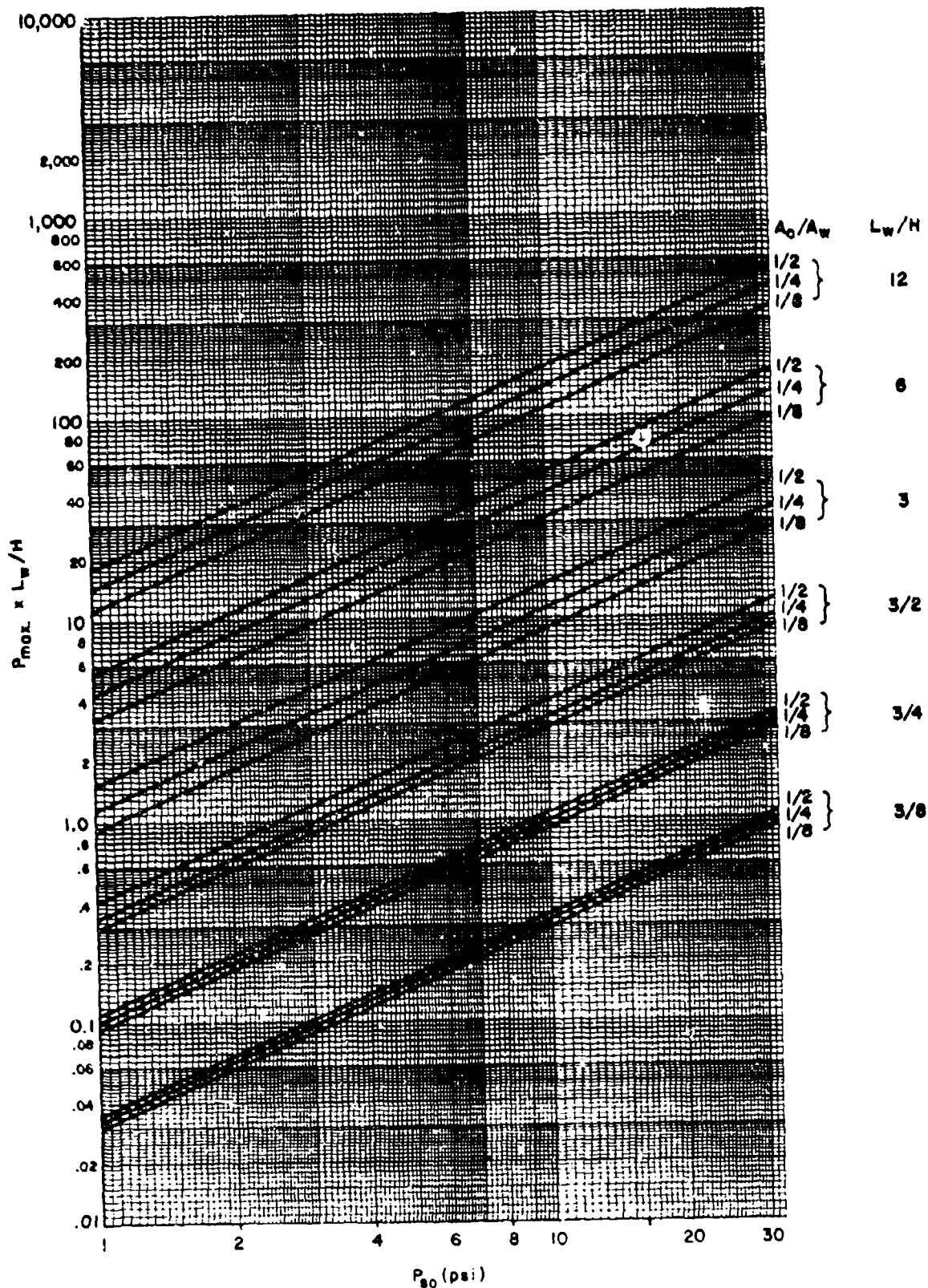
EXTERNAL INCIDENT PRESSURE AT FRONT FACE OF BUILDING, P_{so} (psi)

Figure 2-204 Maximum average pressure on interior face of front wall ($W/H = 3/2$)



EXTERNAL INCIDENT PRESSURE AT FRONT FACE OF BUILDING, P_{so} (psi)

Figure 2-205 Maximum average pressure on interior face of front wall ($W/H = 3$)



EXTERNAL INCIDENT PRESSURE AT FRONT FACE OF BUILDING, $P_{80} \text{ (psi)}$

Figure 2-206 Maximum average pressure on interior face of front wall ($W/H = 6$)

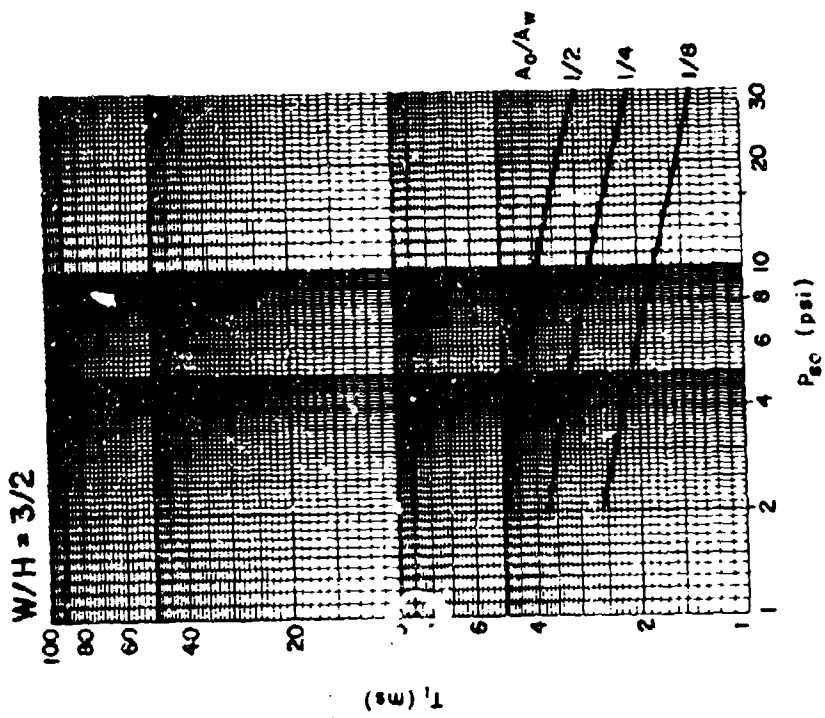
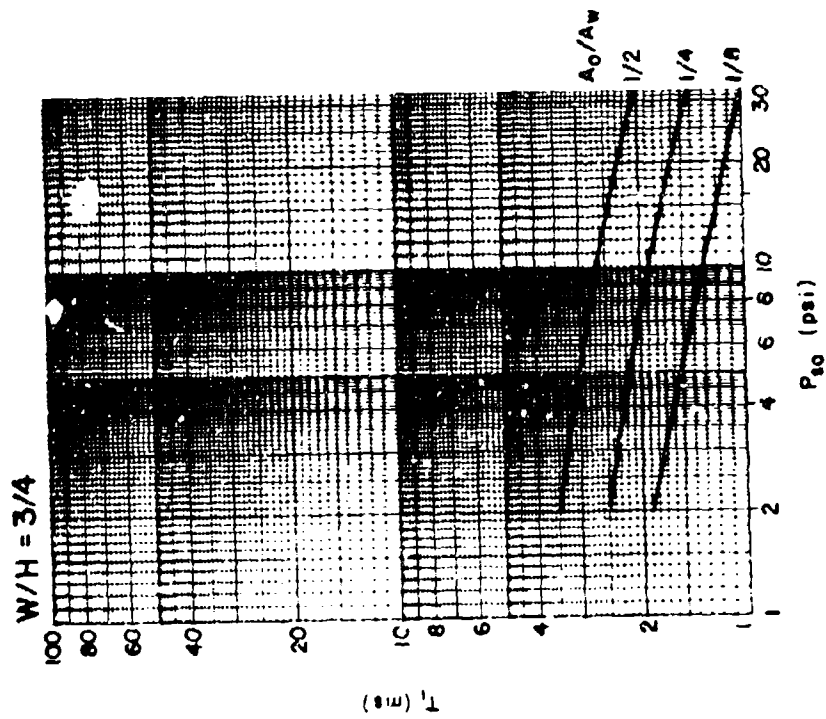
The idealized times T_1 , T_2 and T_3 are also obtained from plots of front walls having width to height ratios W/H equal to $3/4$, $3/2$, 3 and 6 . The arrival time T_1 of the load is given in figures 2-207 and 2-208 as a function of the incident pressure acting on the exterior surface of the front wall P_{s0} for various opening to wall area ratios A_o/A_w . The rise time of the load, $T_2 - T_1$ is given in figures 2-209 and 2-210 as a function of P_{s0} and various wave length to width of front ratios L_w/W . Finally, the duration of the load $T_3 - T_1$ is given in figures 2-211 and 2-212 again as a function of P_{s0} and L_w/W . The times T_2 and T_3 are obtained from subtracting T_1 from the rise time and duration, respectively.

Failure of the cover sealing openings in a building (windows, doors, etc.) will affect the onset of the blast load acting on the interior surface of the front wall. Due to the time required to cause failure of the covers, the onset of the interior pressures may not be in phase with the onset of the exterior blast load. Therefore, care must be taken to arrive at a combined loading for the structural element.

2-15.4.4 Interior Side Wall and Roof Loads. The blast pressures entering the interior of the building through the opening in the front wall (multiple openings are combined to form a single opening) must travel along the interior face of the front wall before arriving at the side wall. The incident pressures arriving at the side wall are increased due to reflection off the wall itself. The front expands and travels across the side wall until it reaches the back wall. It is then reflected off the back wall and the reflected wave travels back across the side wall towards the front wall. The length of side wall loaded by this reflected wave is a function of the wave length L_w .

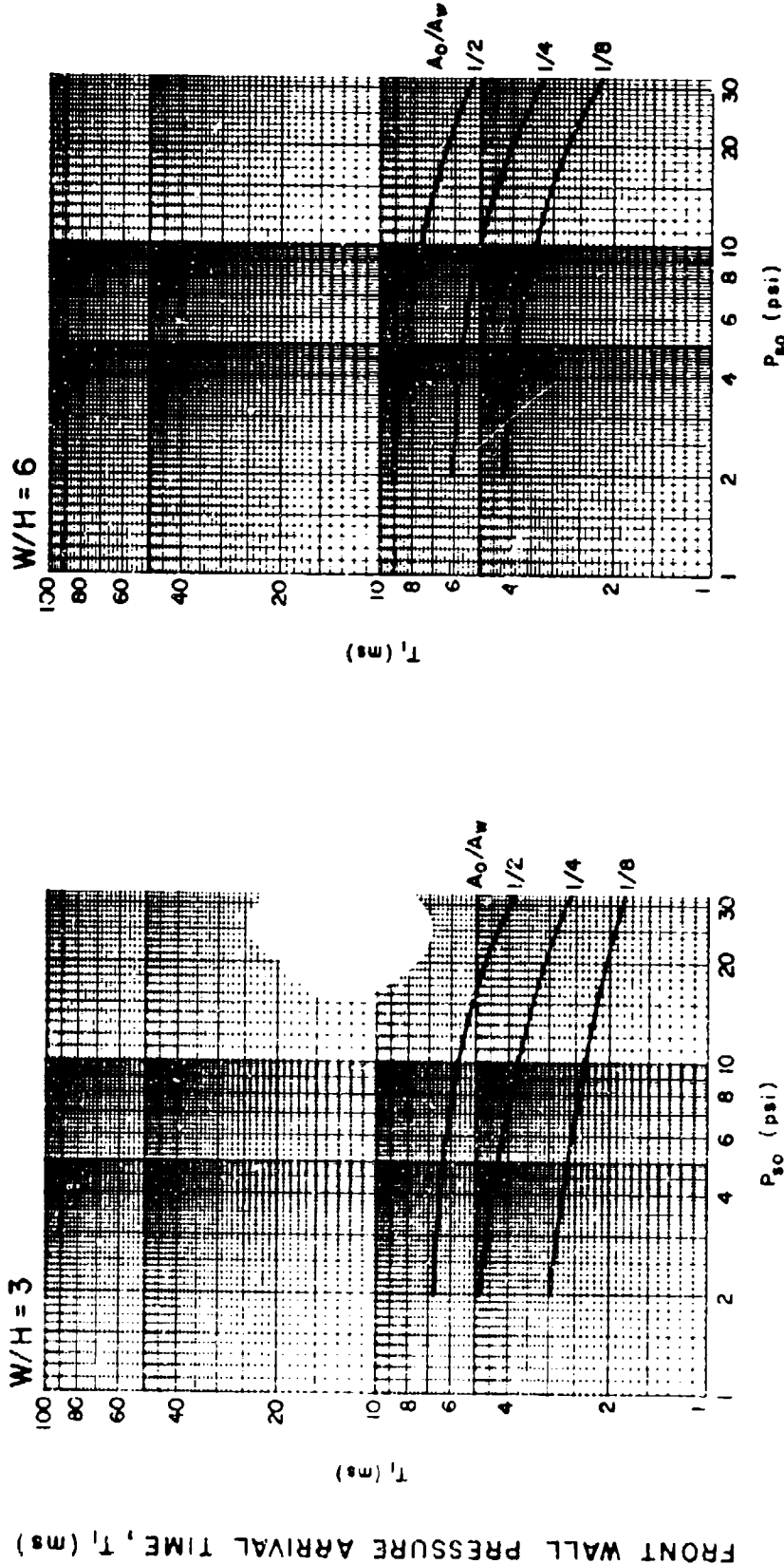
The idealized pressure-time blast load acting on the interior face of the side wall and roof is shown on figure 2-201b. The same assumption is made for the side wall and roof as for the interior front wall. That is, the time at which the shock front arrives at the front wall of the structure is taken as zero ($T_0 = 0$). The time T_1 represents the time it takes the shock front to travel from the opening across the interior face of the front wall to the side wall (or roof). The pressure build up is linear from time T_1 to a maximum pressure P_{max} at time T_2 , remains constant until time T_3 and decays linearly to zero at time T_4 . This idealized curve applies to both the side walls and roof. The structure configuration parameters as given in figure 2-200 apply for side wall loadings. However, to determine the roof loading, the structure must be rotated 90 degrees so that the roof takes the position of a side wall. The width and height of the structure must be interchanged. All other parameters are not effected.

FRONT WALL PRESSURE ARRIVAL TIME, T_1 (ms)



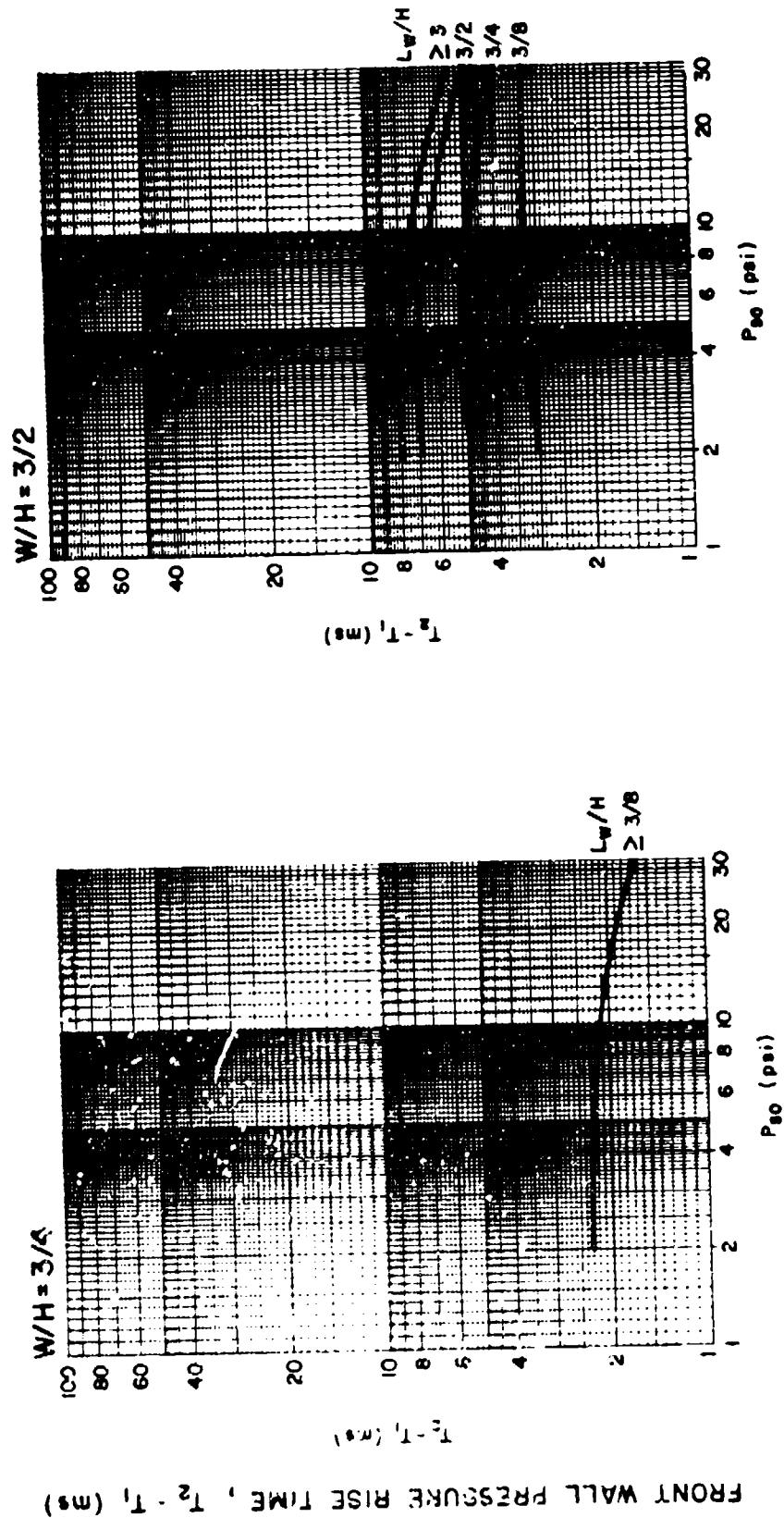
EXTERNAL INCIDENT PRESSURE AT FRONT FACE OF BUILDING, P_{so} (psi)

Figure 2-207 Arrival time, T_1 , for interior front wall blast load ($W/H = 3/4$ and $3/2$)



EXTERNAL INCIDENT PRESSURE AT FRONT FACE OF BUILDING, P_{30} (psi)

Figure 2-208 Arrival time, T_1 , for interior front wall blast load
($W/H = 3$ and 6)



EXTERNAL INCIDENT PRESSURE AT FRONT FACE OF BUILDING, P_{00} (psi)

Figure 2-209 Idealized rise time, $T_2 - T_1$, for interior front wall
blast load ($W/H = 3/4$ and $3/2$)

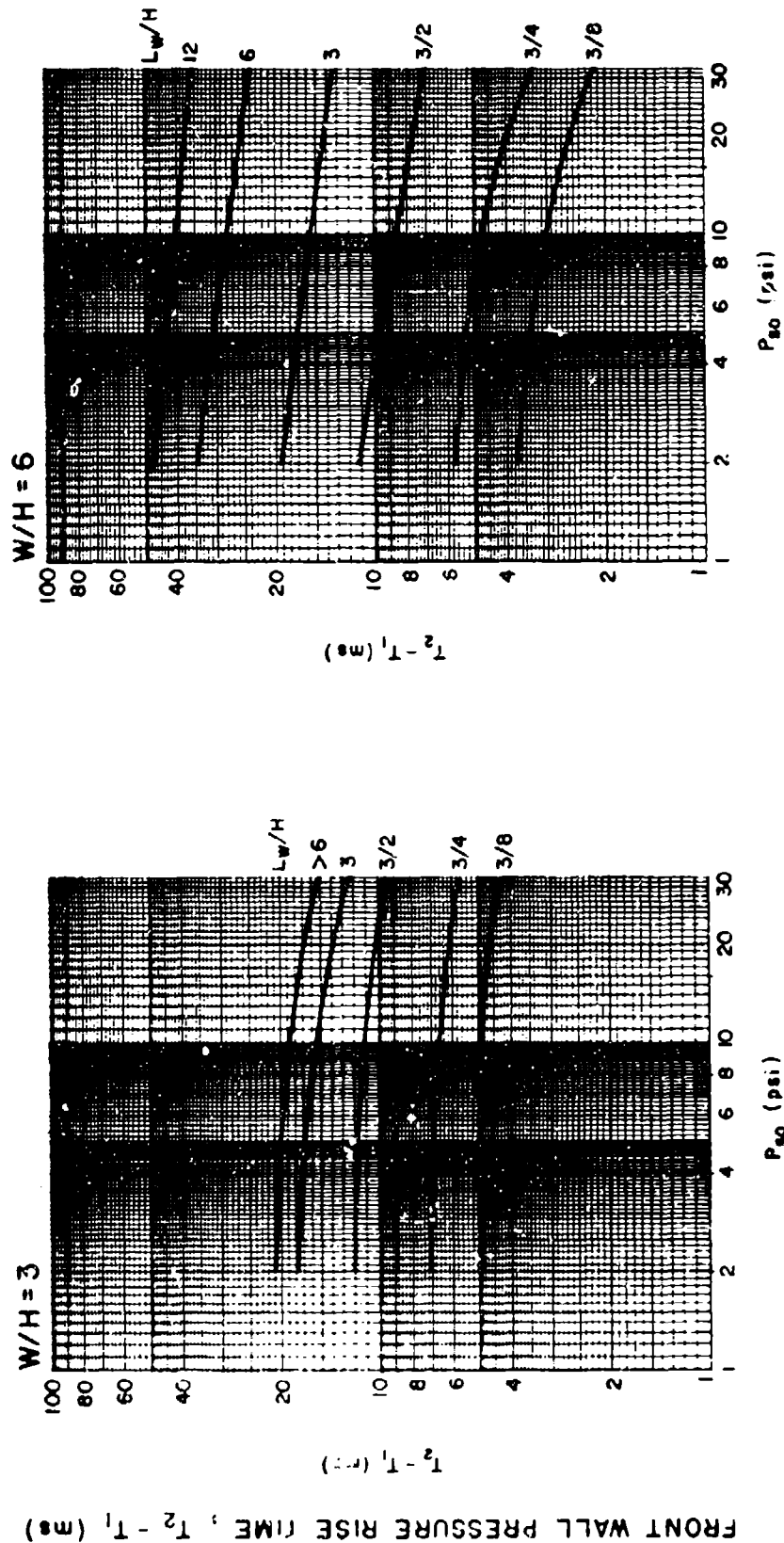
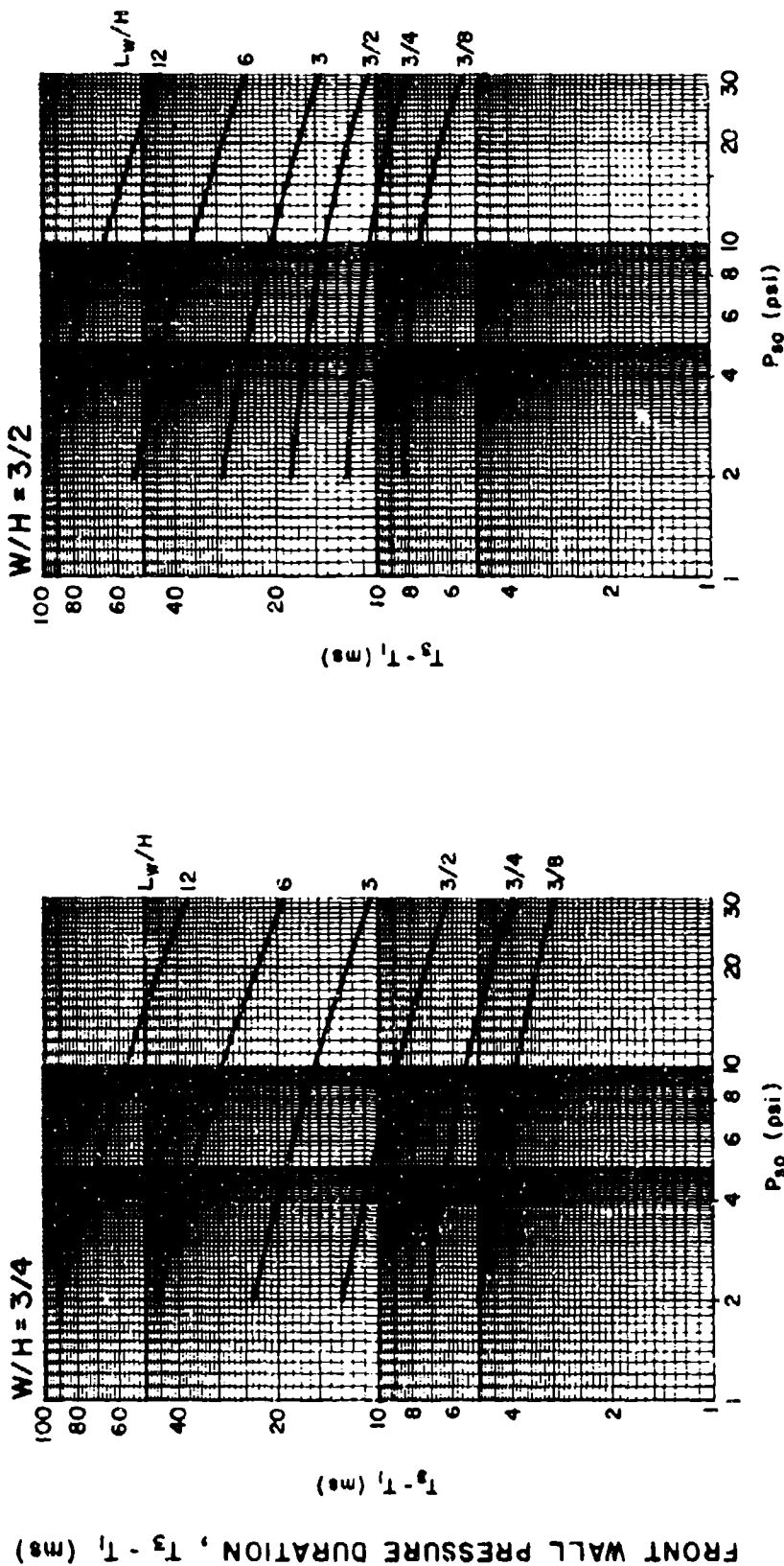
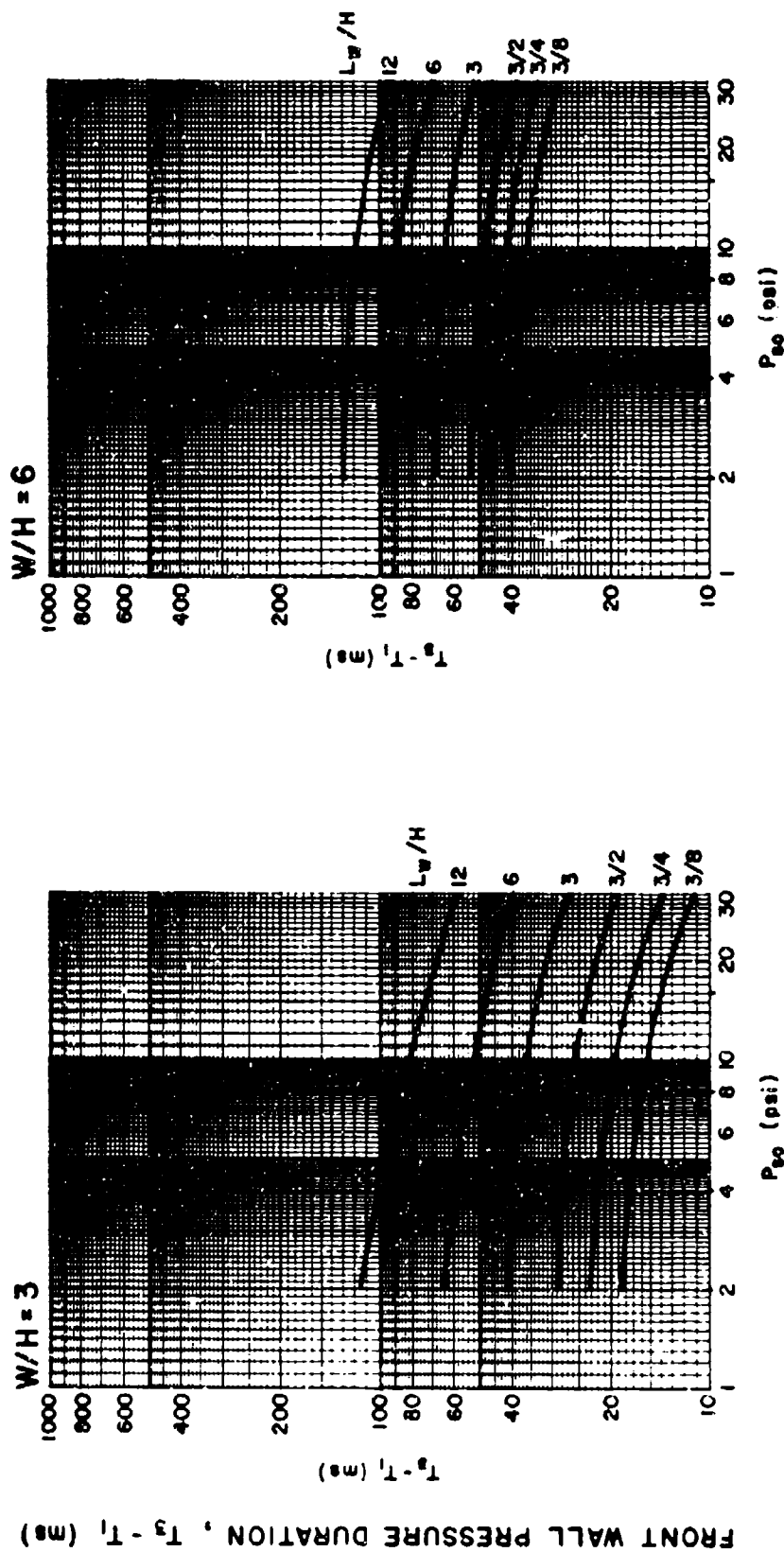


Figure 2-210 Idealized rise time, $T_2 - T_1$, for interior front wall blast load ($W/H = 3$ and 6)



EXTERNAL INCIDENT PRESSURE AT FRONT FACE OF BUILDING, P_{s0} (psi)

Figure 2-211 Idealized duration, $T_3 - T_1$, for interior front wall blast load ($W/H = 3/4$ and $3/2$)



EXTERNAL INCIDENT PRESSURE AT FRONT FACE OF BUILDING, P_{ao} (psi)

Figure 2-212 Idealized duration, $T_3 - T_1$, for interior front wall
blast load ($W/H = 3$ and 6)

The maximum average pressure P_{\max} acting on the interior face of the side wall (or roof) varies as a function of the incident pressure P_{so} acting on the exterior face of the front wall, the wavelength L_w corresponding to P_{so} , and the geometry of the structure. Since a large number of plots would be required to describe P_{\max} for the blast and geometric parameters involved, an equation has been developed. The value of P_{\max} is given by:

$$P_{\max} = K / (L_w / L) \quad 2-15$$

For $6 \geq W/H \geq 3/2$

$$K = [A + (B \times (L_w / L)^C)] \times D \times E \times P_{so}^{1.025} \quad 2-16$$

where:

$$A = [0.002 (W/H)^{1.4467}] - 0.0213 \quad 2-17$$

$$B = 2.2075 - [1.902 (W/H)^{-0.085}] \quad 2-18$$

$$C = 1.231 + [0.0008 (W/H)^{2.678}] \quad 2-19$$

$$D = [2.573 (L/H)^{-0.444}] - 0.3911 \quad 2-20$$

$$E = 0.4221 + [1.241 (A_o / A_w)^{0.367}] \quad 2-21$$

For $W/H = 3/4$

$$K = A \times B \times C^E \times F^H \times P_{so}^{0.9718} \quad 2-22$$

where:

$$A = [0.5422 (L_w / L)^{1.2944}] - 0.001829 \quad 2-23$$

$$B = [0.654 + 2.616 (A_o / A_w) - 4.928 (A_o / A_w)^2] \quad 2-24$$

$$[2.209 (L/H)^{-0.3451} - 0.739]$$

$$C = 0.829 + 0.104 (L_w/L)^{1.6} \quad 2-25$$

$$+ [0.00124 + 0.00414 (L_w/L)^{3.334}] [L/H]^D$$

$$D = 2.579 - 0.0534 (L_w/L)^{3.891} \quad 2-26$$

$$E = 999 (A_o/A_w)^{9.964} \quad 2-27$$

$$F = 1.468 - 1.6627 (A_o/A_w)^{0.7801} \quad 2-28$$

$$+ [1.8692 - 1.1735 (A_o/A_w)^{-0.2226}] [L_w/L]^G$$

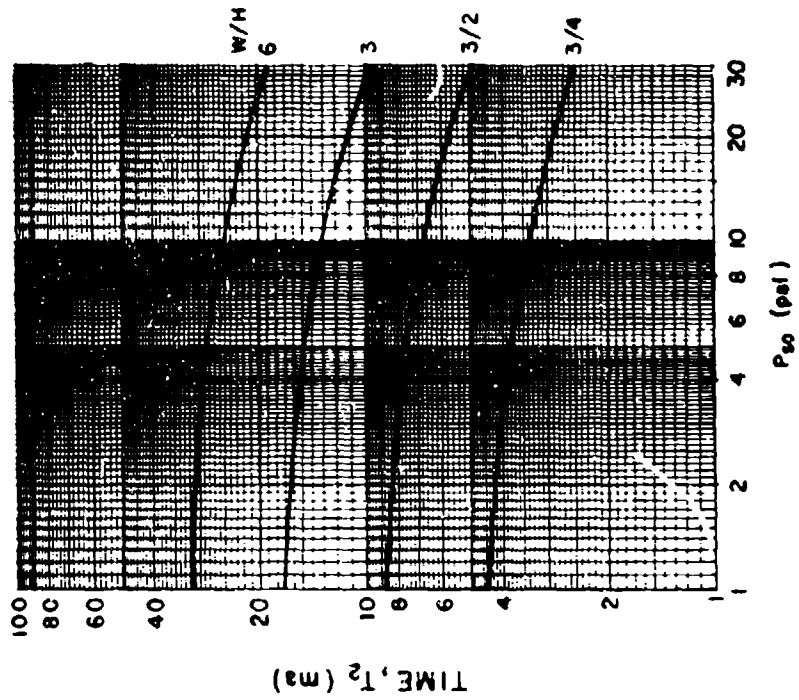
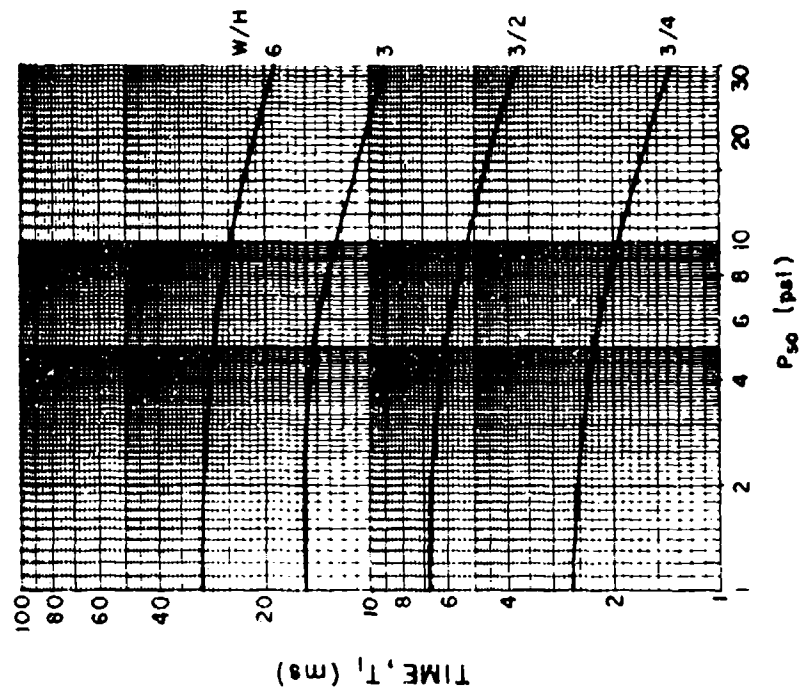
$$G = 0.2979 (A_o/A_w)^{-1.4872} - 0.8351 \quad 2-29$$

$$H = (5.425 \times 10^{-4}) + (1.001 \times 10^{-9}) (L/H)^{9.965} \quad 2-30$$

For $3/2 > W/H > 3/4$, graphical interpolation is required to determine P_{\max} . Several values of P_{\max} are determined from equation 2-15 for values of W/H equal to $3/4$, $3/2$ and preferably two values greater than $3/2$. A plot of P_{\max} versus W/H is prepared and the value of P_{\max} is read for the required W/H .

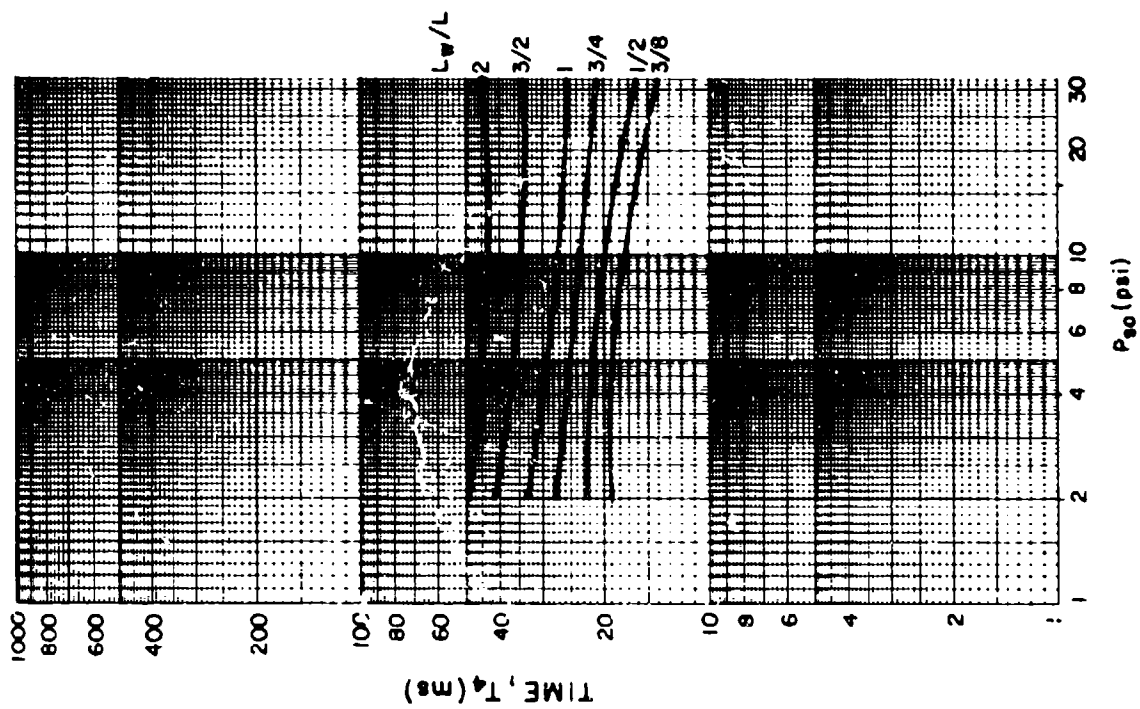
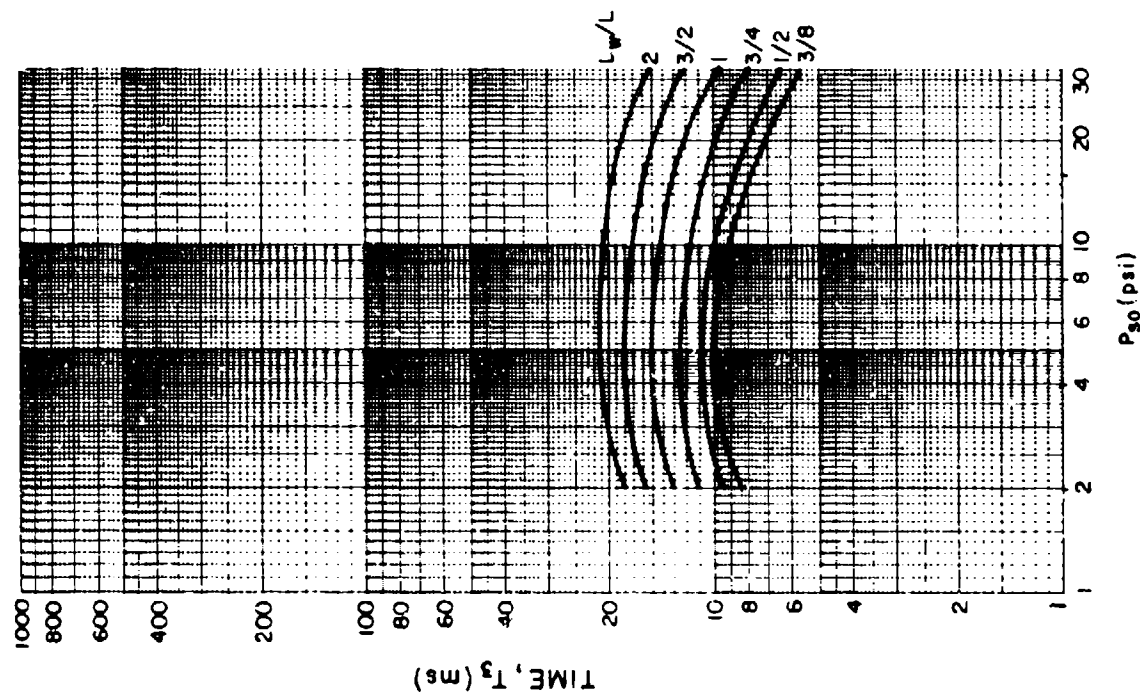
The idealized times T_1 and T_2 are determined from figure 2-213. These times are presented as a function of the incident pressure P_{s0} arriving at the exterior of the building and the width to height ratio W/H of the front wall. Since the distance that the shock front must travel across the front wall is taken from the center of the opening, times T_1 and T_2 are not a function of the area of the opening. This assumption will not result in significant errors since the openings considered are comparatively small.

The idealized times T_3 and T_4 are determined from figures 2-214 through 2-229. Each figure is prepared for a given structure configuration defined by the length to height ratio of the side wall L/H and the width to height ratio of the front wall W/H . The times T_3 and T_4 are given on each figure as a function of the incident pressure P_{s0} and various values of the wave length to side wall length ratio L_w/L . As explained above, these times are not a function of the area of the opening. For ease of reference, these figures are listed in table 2-4 for the various L/H and W/H ratios provided. In most



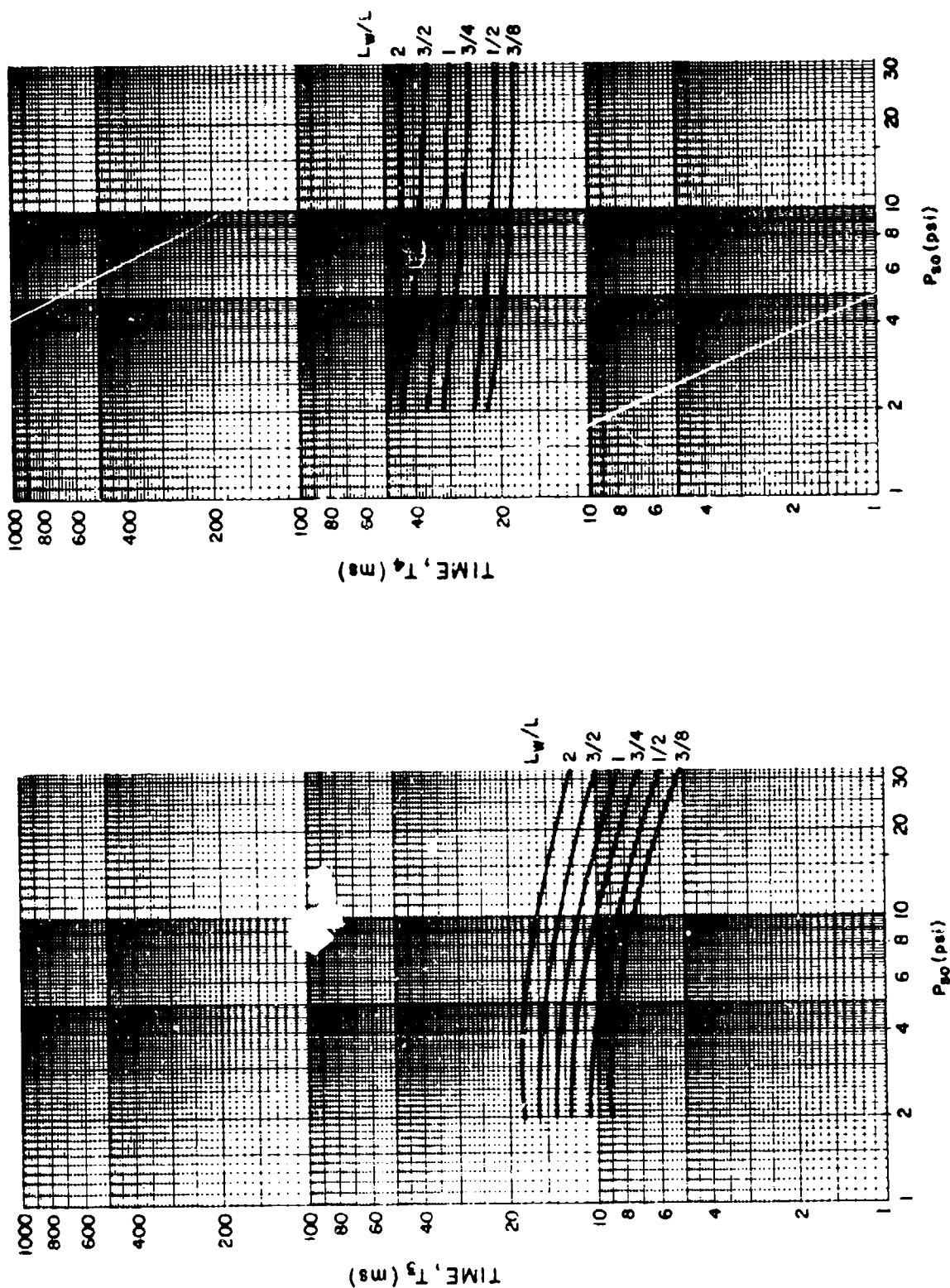
EXTERNAL INCIDENT PRESSURE AT FRONT FACE OF BUILDING, P_{50} (psi)

Figure 2-213 Idealized times T_1 and T_2 for interior side wall blast load



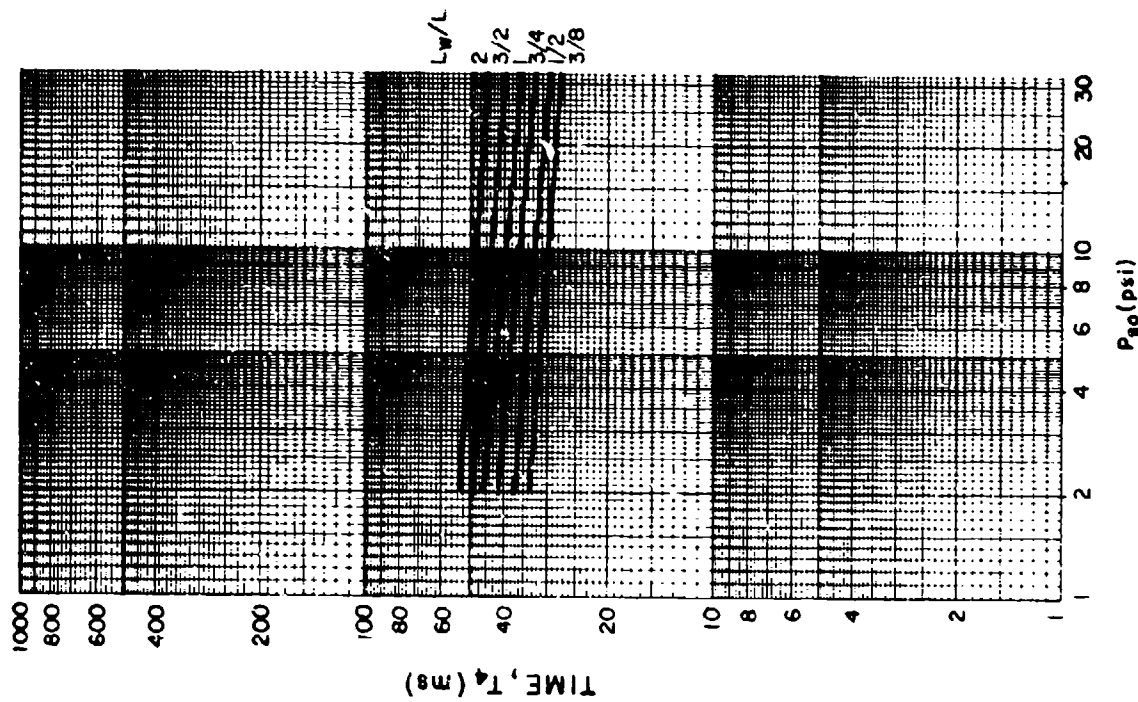
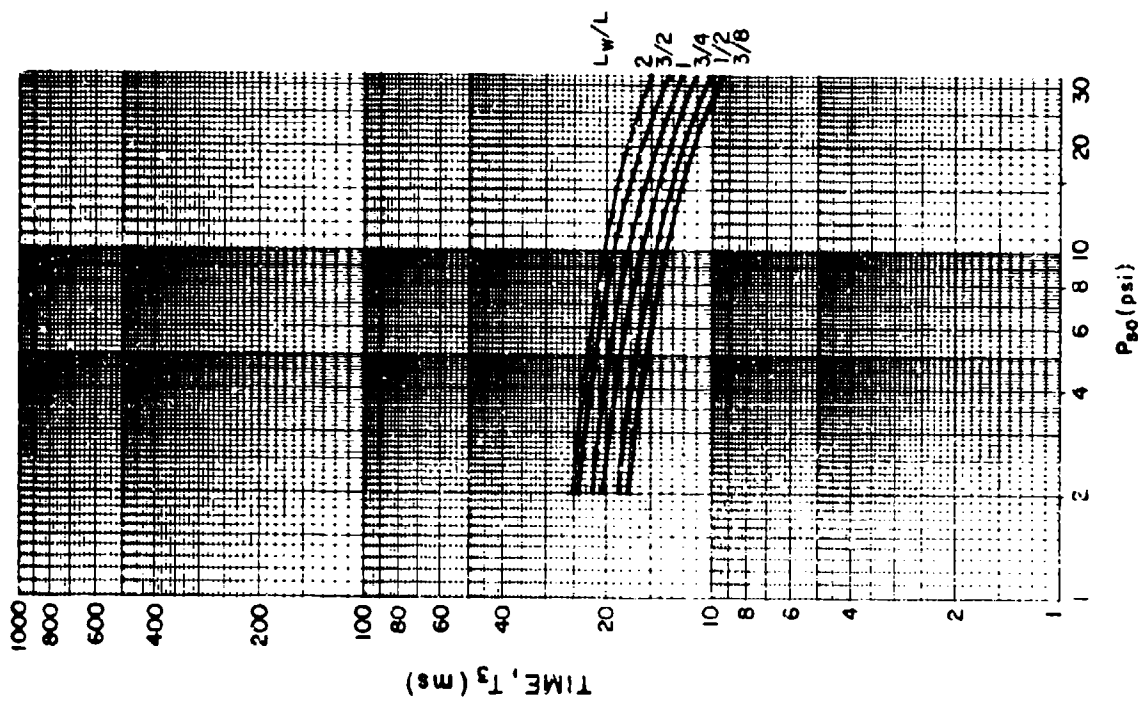
EXTERNAL INCIDENT PRESSURE AT FRONT FACE OF BUILDING, P_{so} (psi)

Figure 2-214 Idealized times T_3 and T_4 for interior side wall blast load
($L/H = 1$, $W/H = 3/4$)



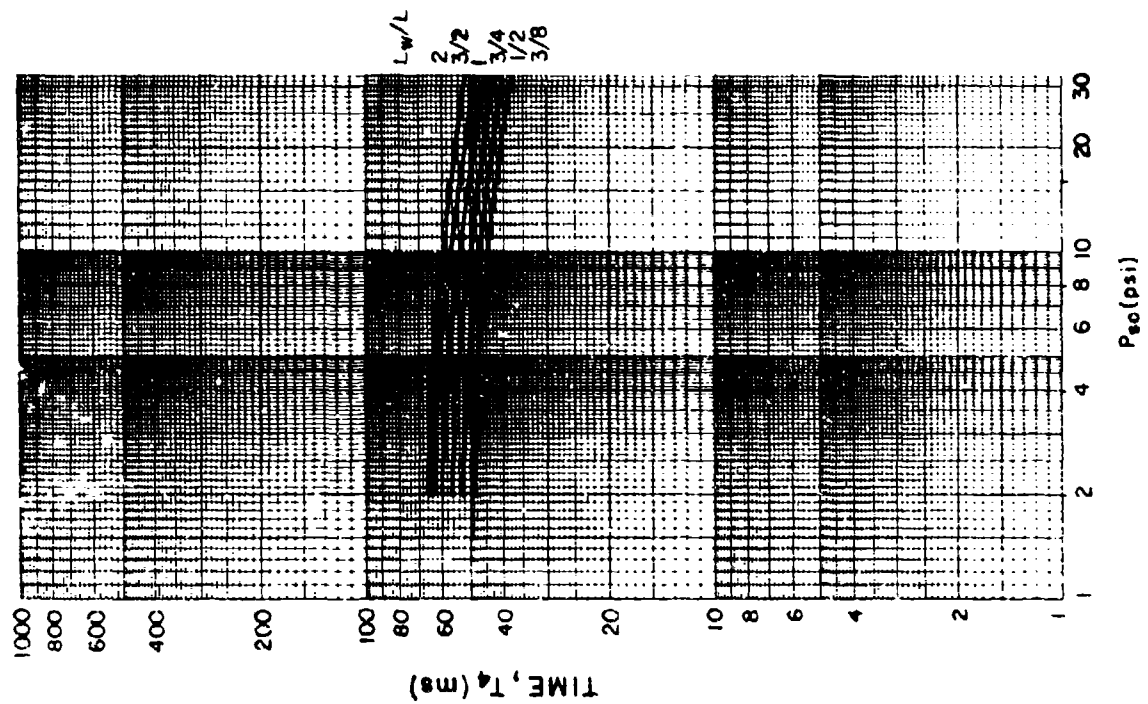
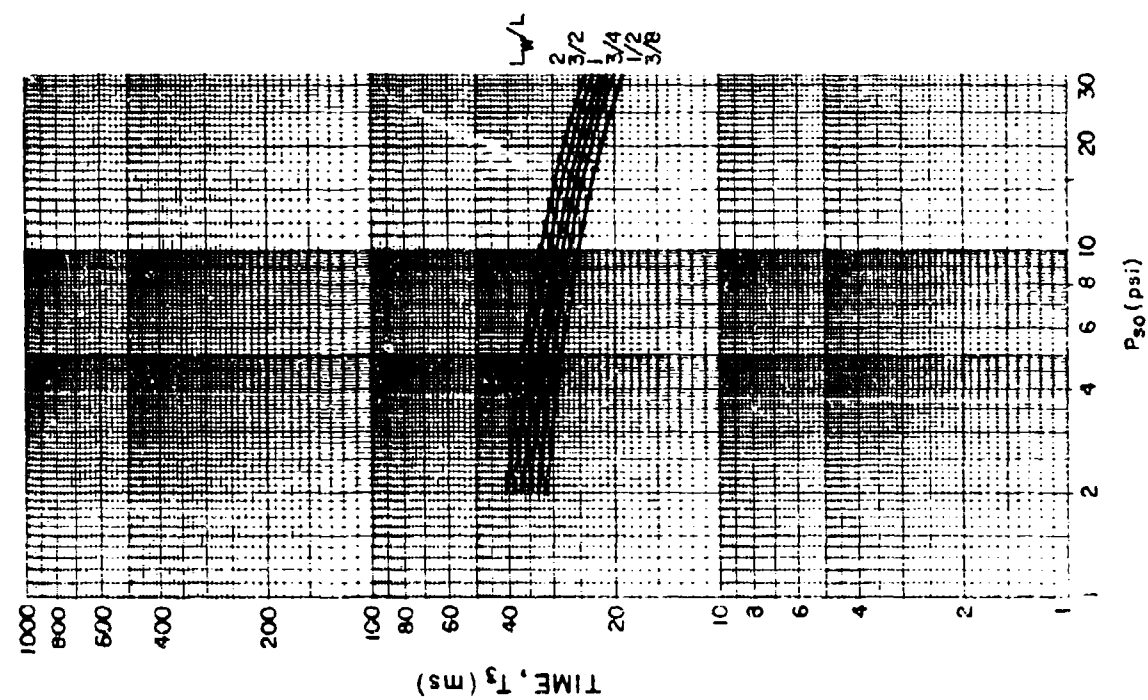
EXTERNAL INCIDENT PRESSURE AT FRONT FACE OF BUILDING, P_{30} (psi)

Figure 2-215 Idealized times T_3 and T_4 for interior side wall blast load
($L/H = 1$, $W/H = 3/2$)



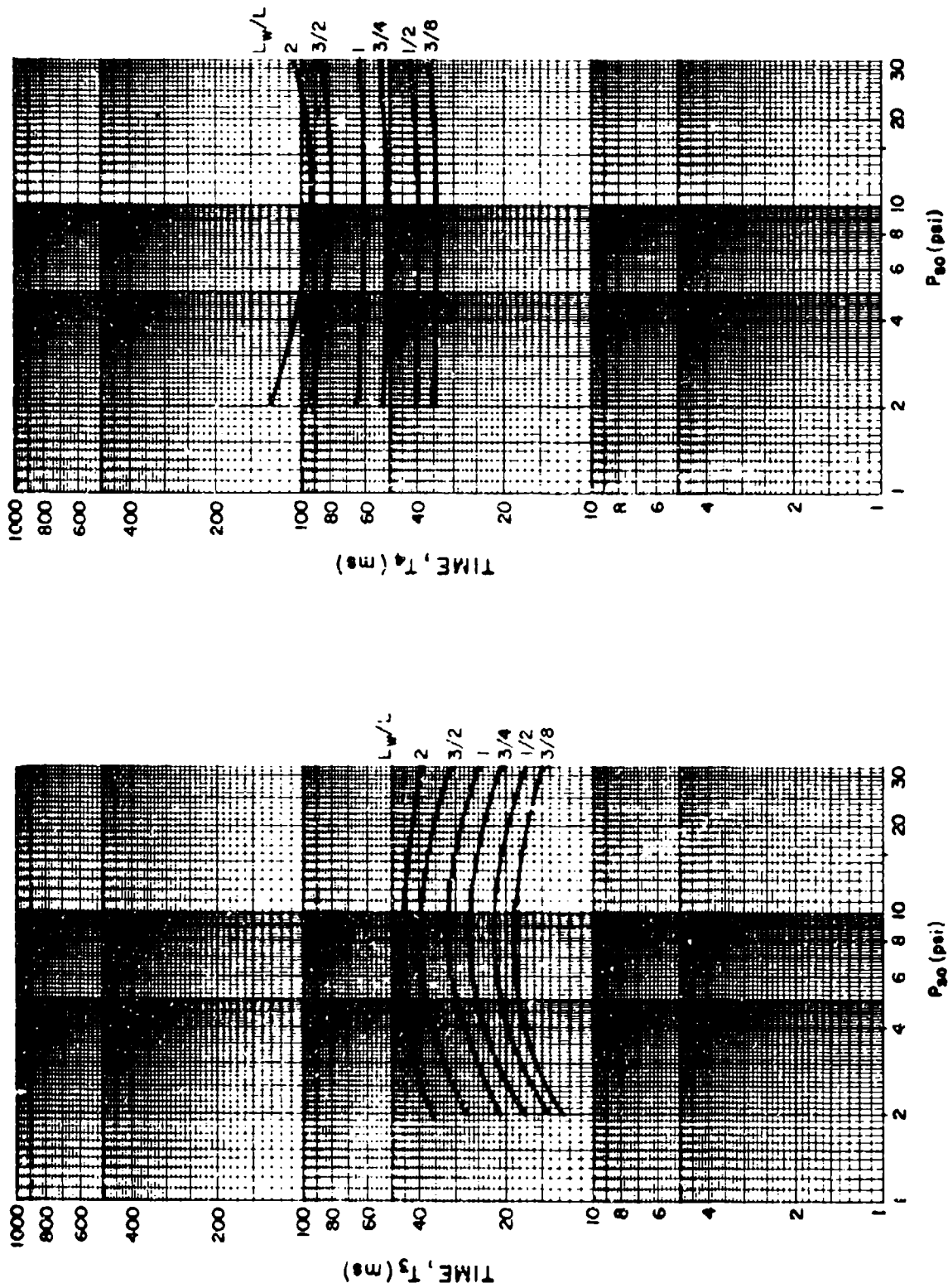
EXTERNAL INCIDENT PRESSURE AT FRONT FACE OF BUILDING, P_{so} (psi)

Figure 2-216 Idealized times T_3 and T_4 for interior side wall blast load
($L/H = 1$, $W/H = 3$)



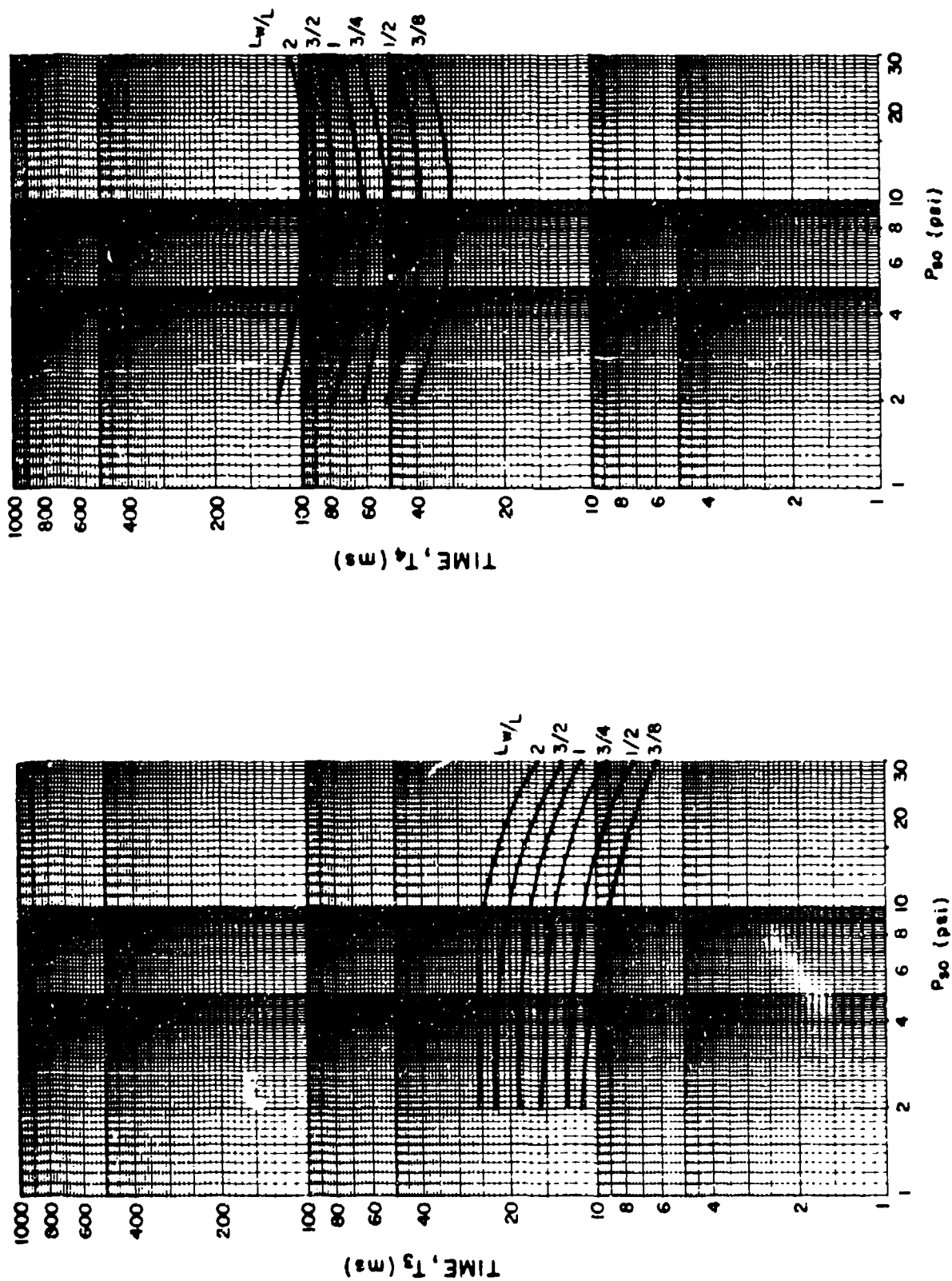
EXTERNAL INCIDENT PRESSURE AT FRONT FACE OF BUILDING, P_{so} (psi)

Figure 2-217 Idealized times T_3 and T_4 for interior side wall blast load
($L/H = 1$, $W/H = 6$)



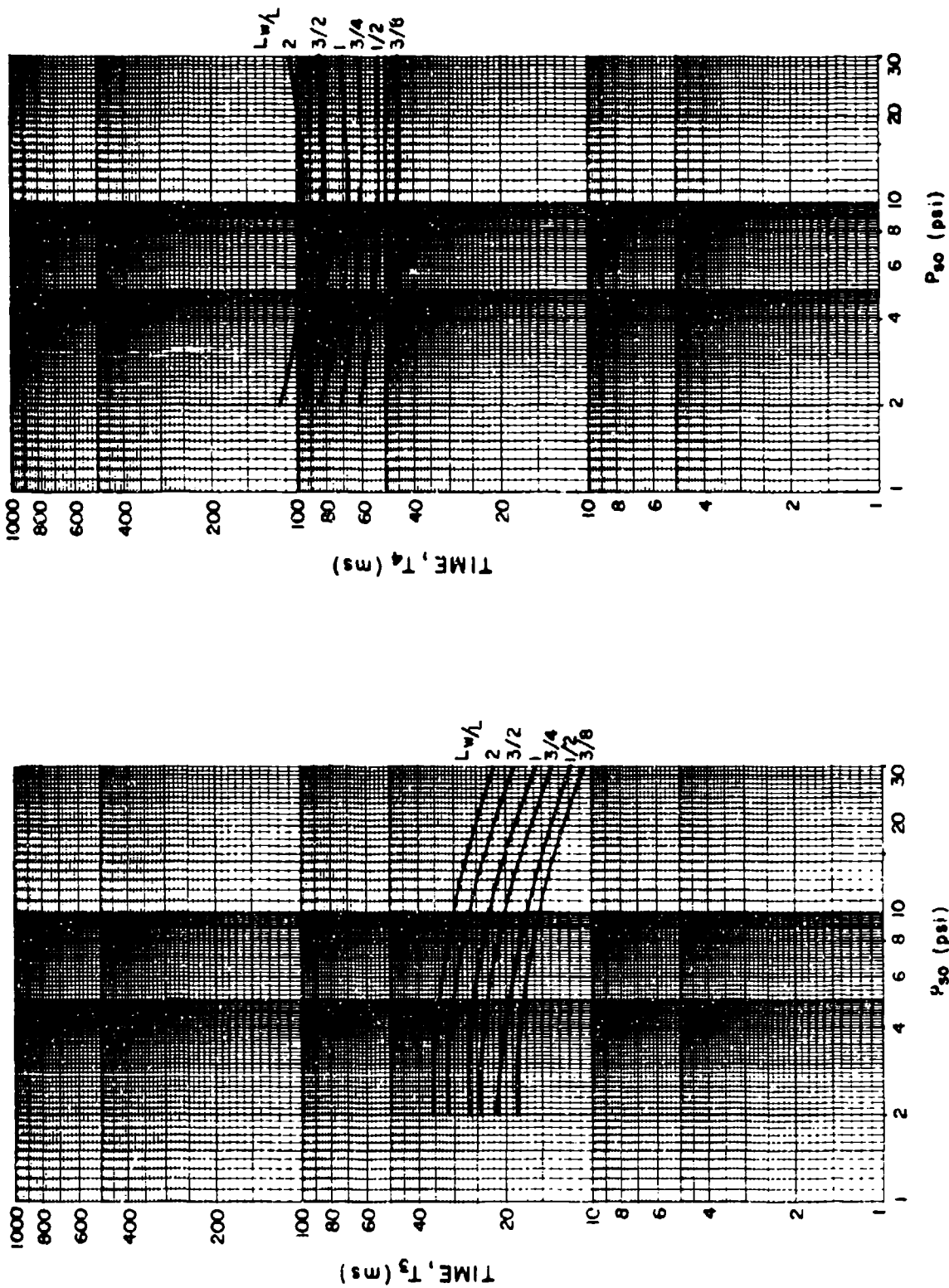
EXTERNAL INCIDENT PRESSURE AT FRONT FACE OF BUILDING, P₃₀ (psi)

Figure 2-218 Idealized times T₃ and T₄ for interior side wall blast load
(L/H = 2, W/H = 3/4)



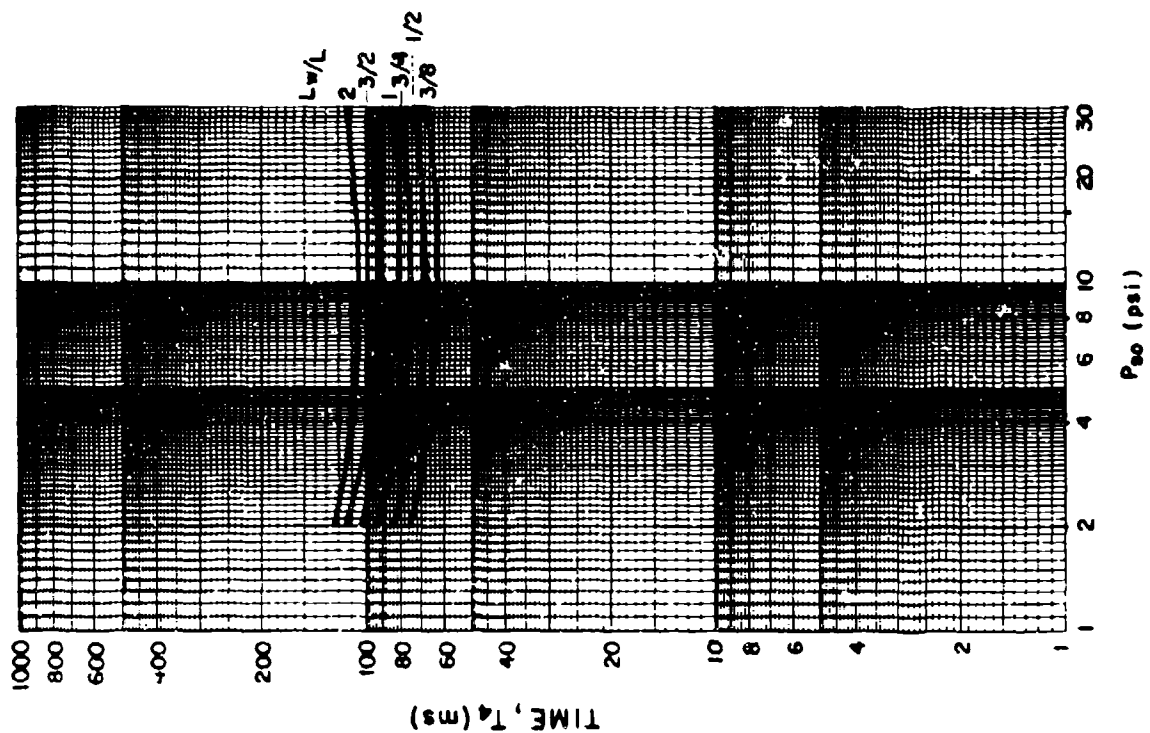
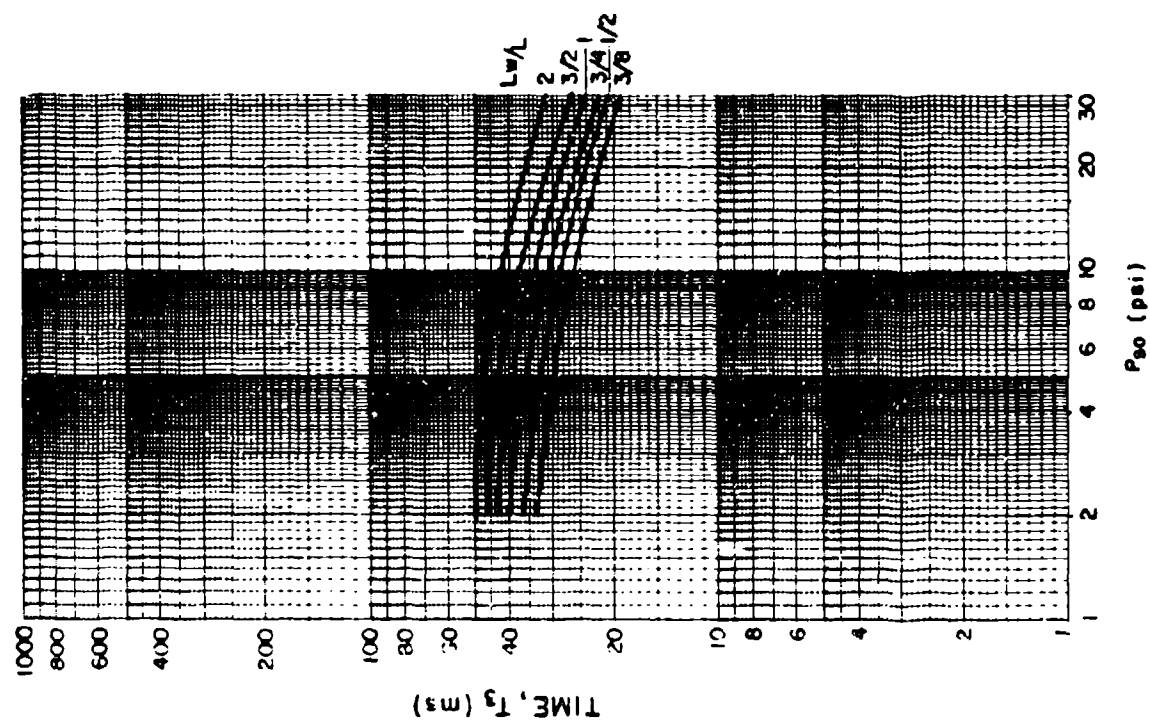
EXTERNAL INCIDENT PRESSURE AT FRONT FACE OF BUILDING, P₅₀ (psi)

Figure 2-219 Idealized times T₃ and T₄ for interior side wall blast load
(L/H = 2, W/H = 3/2)



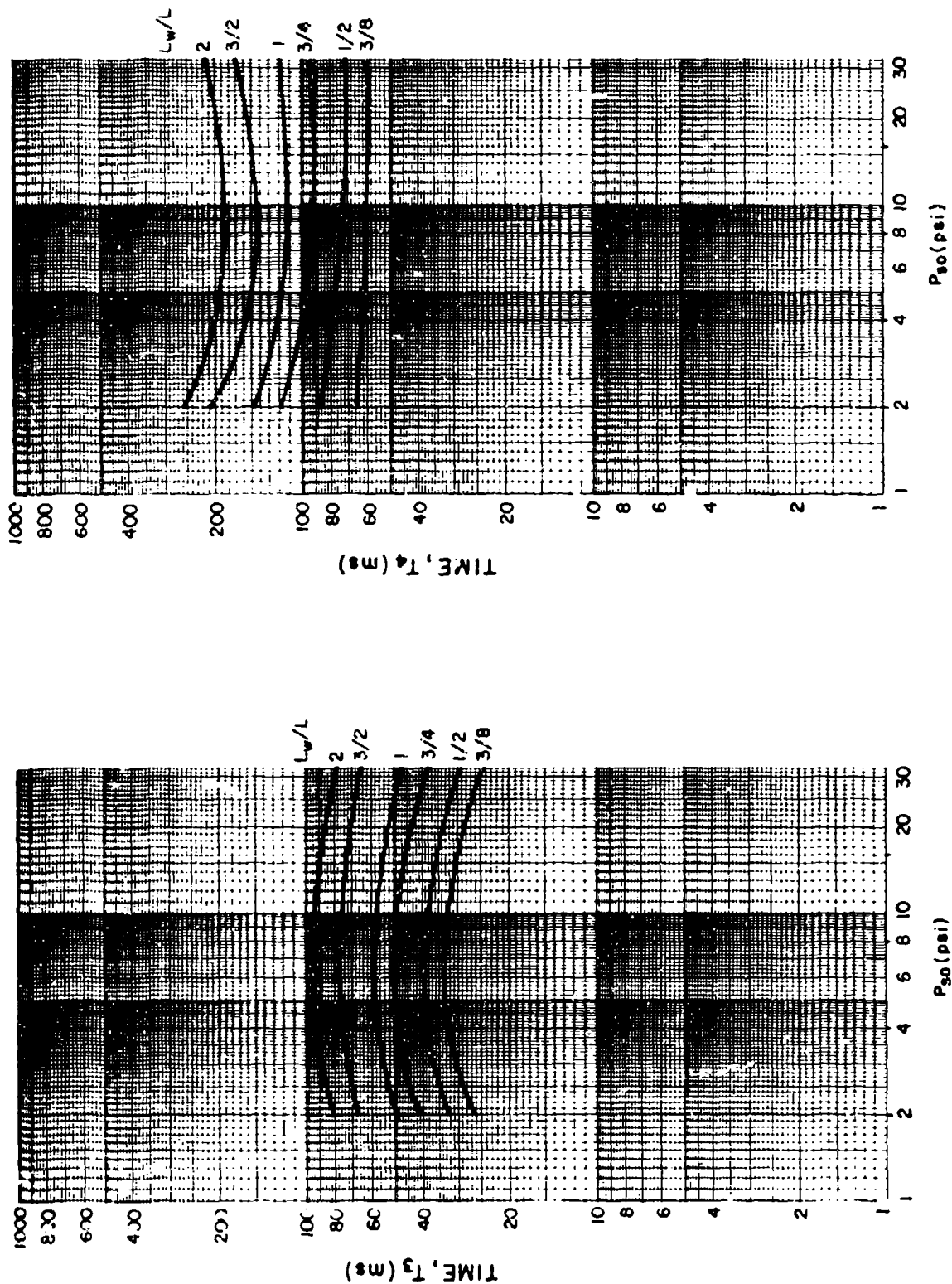
EXTERNAL INCIDENT PRESSURE AT FRONT FACE OF BUILDING, P_{so} (psi)

Figure 2-220 Idealized times T_3 and T_4 for interior side wall blast load
($L/H = 2$, $W/H = 3$)



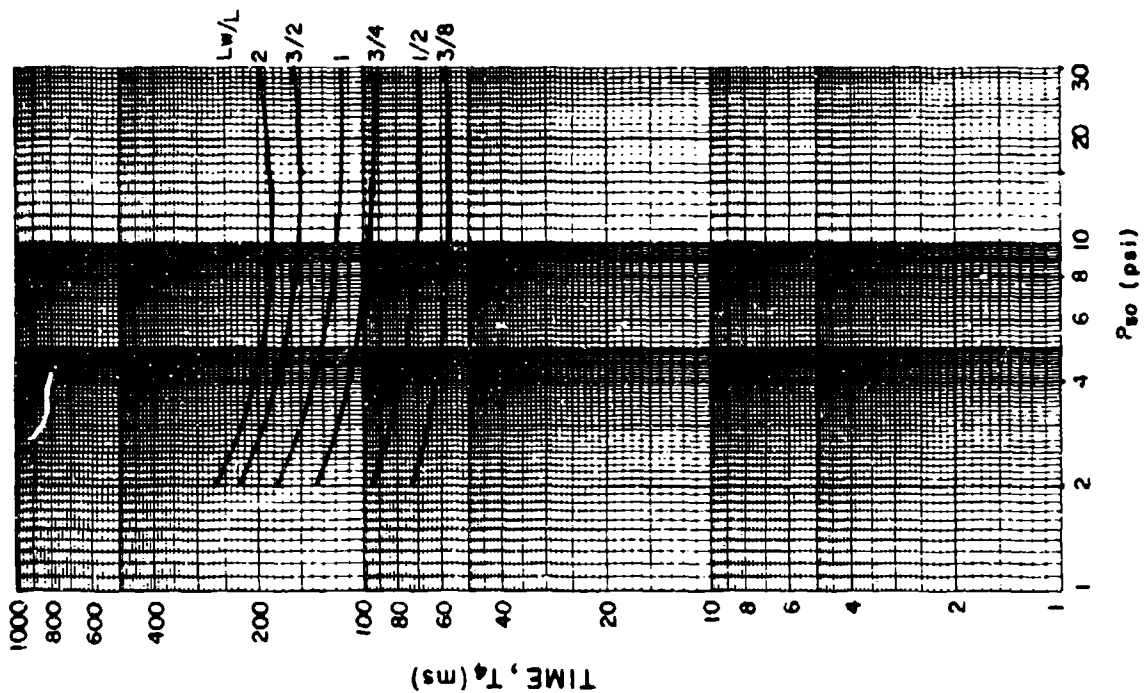
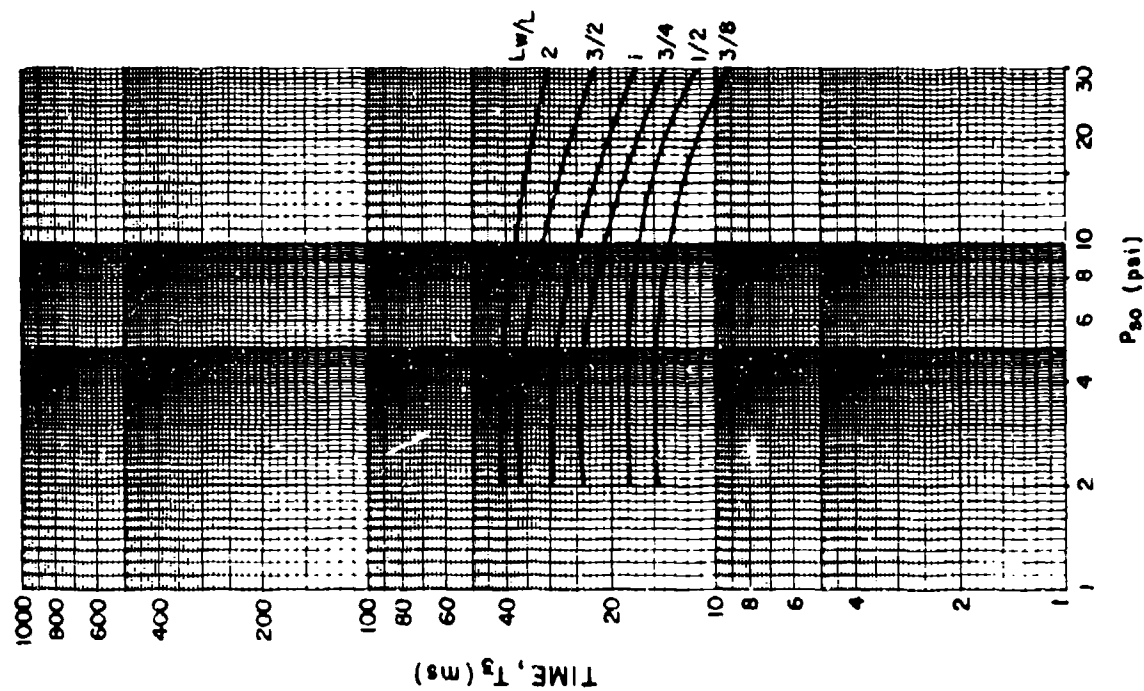
EXTERNAL INCIDENT PRESSURE AT FRONT FACE OF BUILDING, P_{so} (psi)

Figure 2-221 Idealized times T_3 and T_4 for interior side wall blast load
($L/H = 2$, $W/H = 6$)



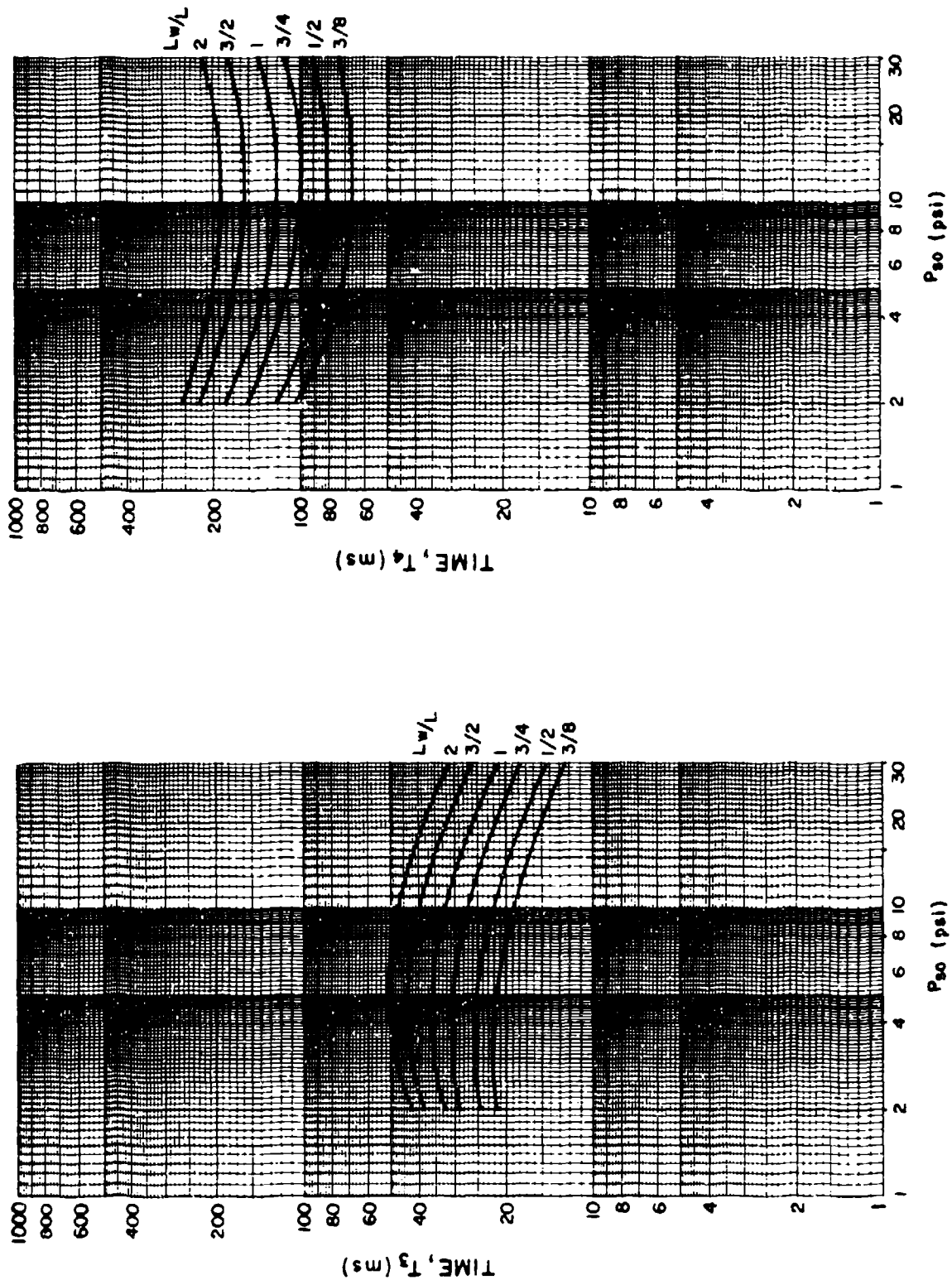
EXTERNAL INCIDENT PRESSURE AT FRONT FACE OF BUILDING, P_{so} (psi)

Figure 2-222 Idealized times T_3 and T_4 for interior side wall blast load
($L/H = 4$, $W/H = 3/4$)



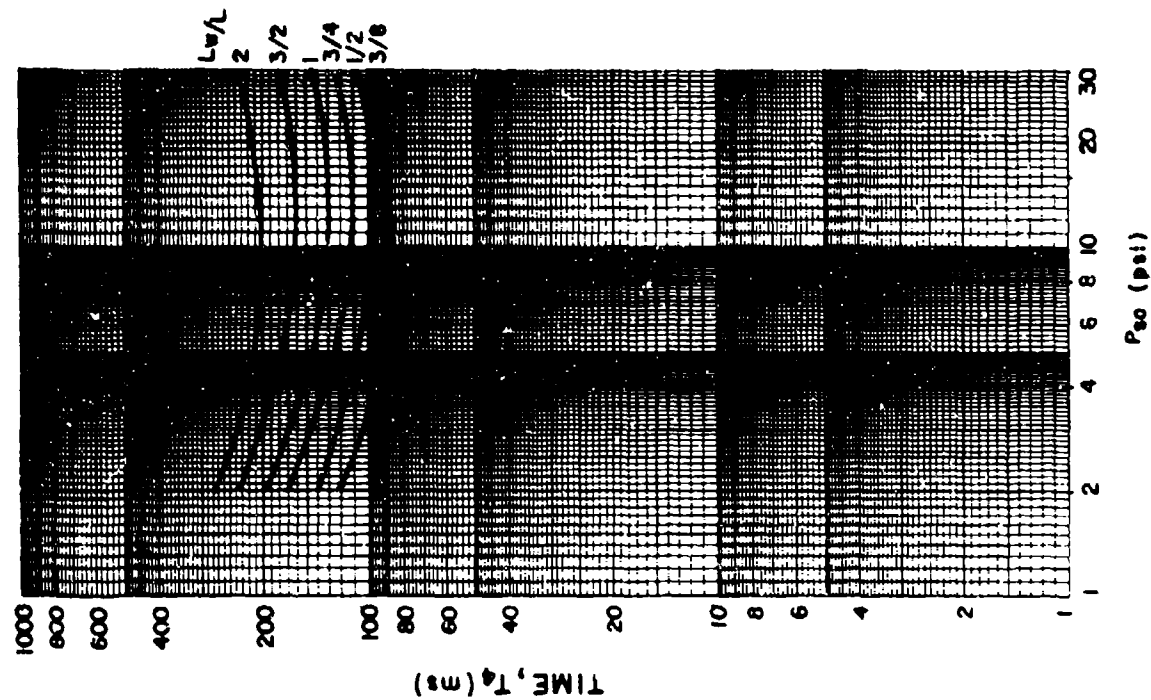
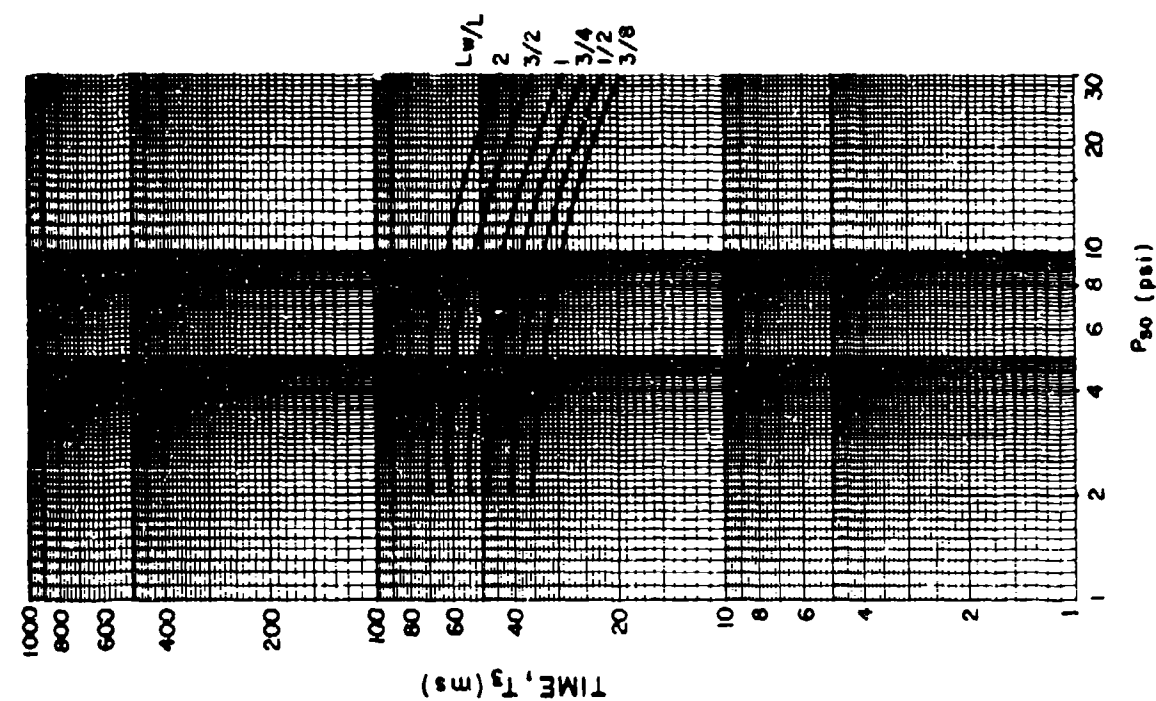
EXTERNAL INCIDENT PRESSURE AT FRONT FACE OF BUILDING, P_{so} (psi)

Figure 2-223 Idealized times T_3 and T_4 for interior side wall blast load
($L/H = 4$, $W/H = 3/2$)



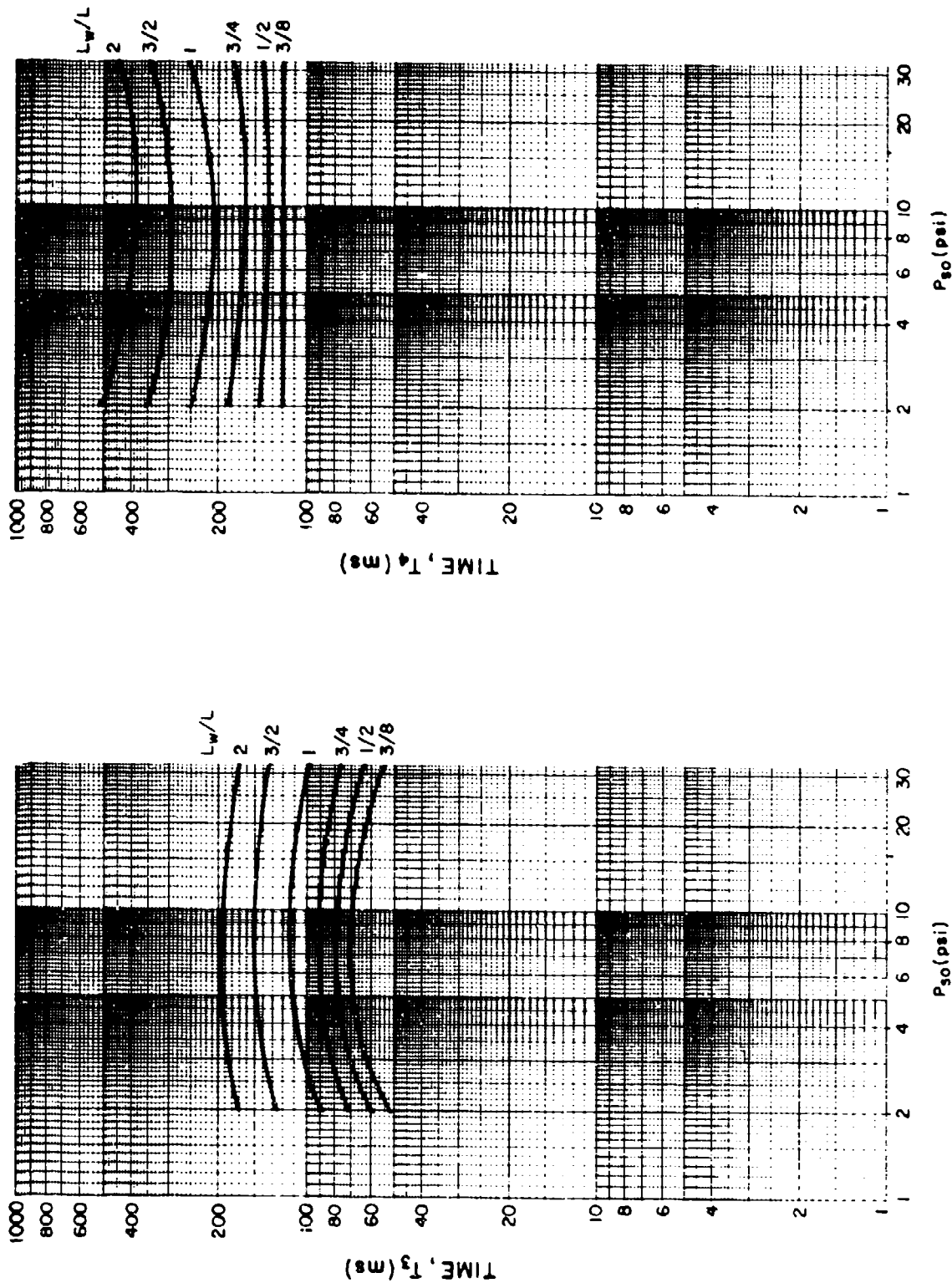
EXTERNAL INCIDENT PRESSURE AT FRONT FACE OF BUILDING, P_{so} (psi)

Figure 2-224 Idealized times T_3 and T_4 for interior side wall blast load
($L/H = 4$, $W/H = 3$)



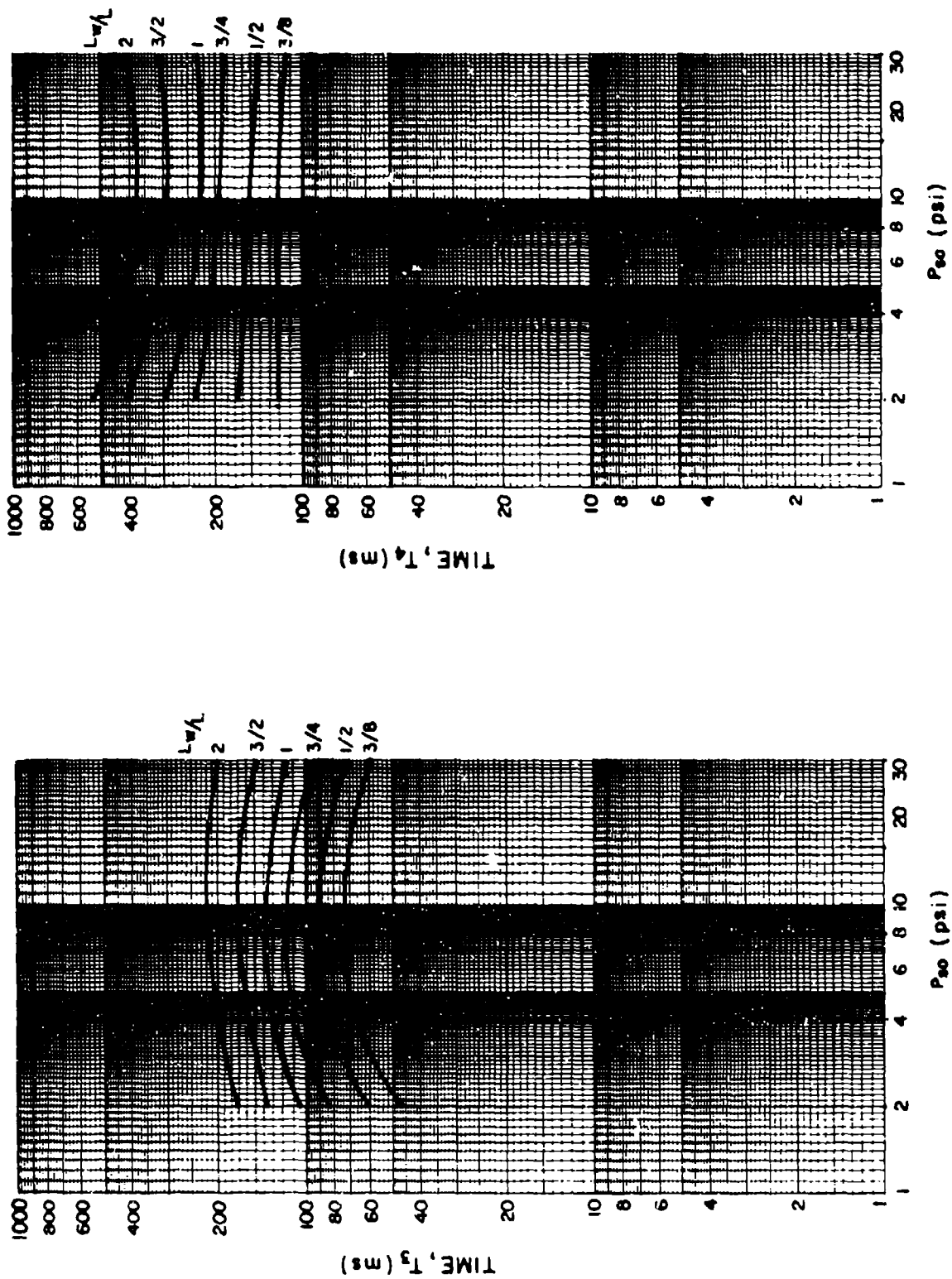
EXTERNAL INCIDENT PRESSURE AT FRONT FACE OF BUILDING, P_{so} (psi)

Figure 2-225 Idealized times T_3 and T_4 for interior side wall blast load
($L/H = 4$, $W/H = 6$)



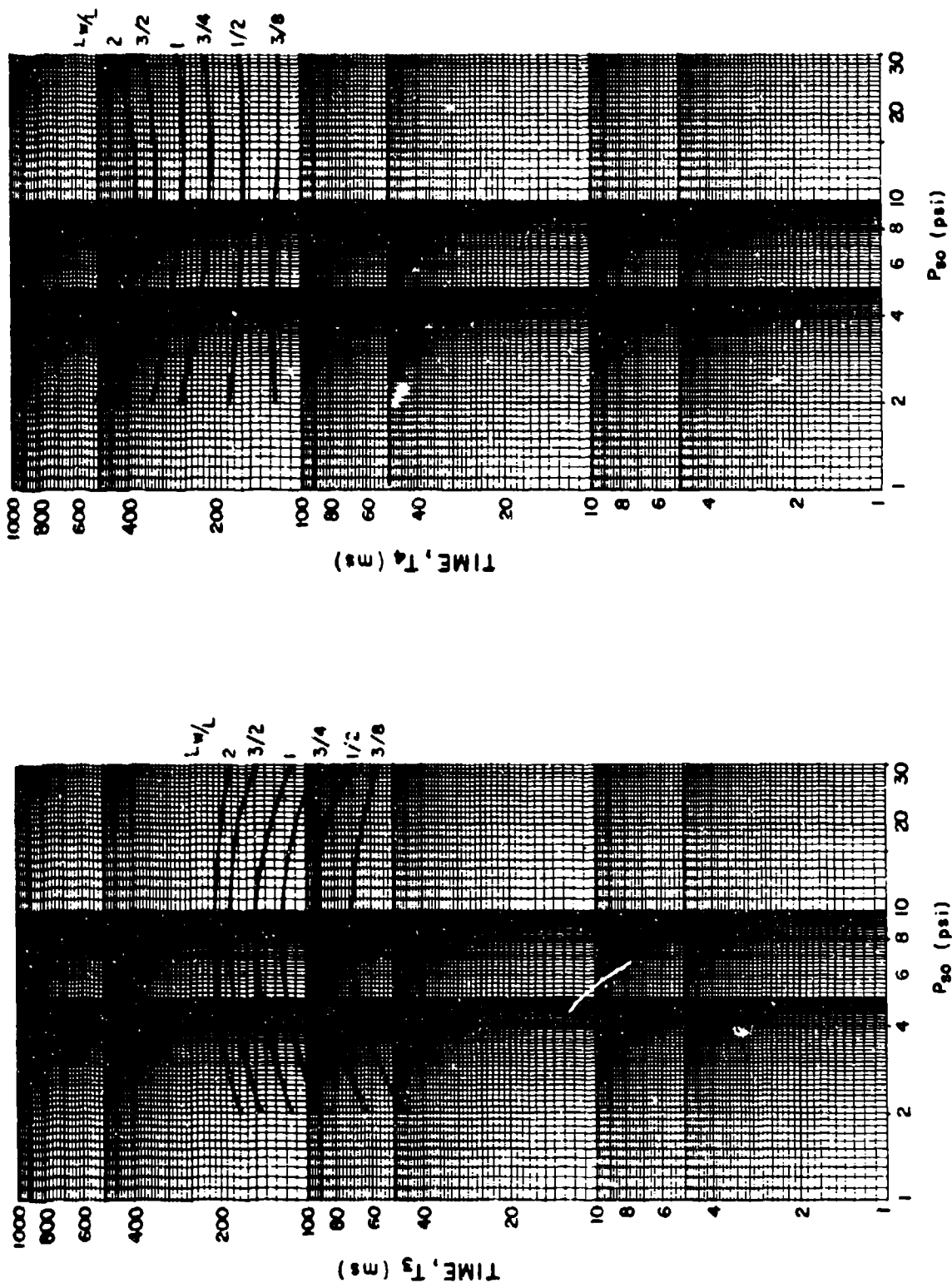
EXTERNAL INCIDENT PRESSURE AT FRONT FACE OF BUILDING, P_{30} (psi)

Figure 2-226 Idealized times T_3 and T_4 for interior side wall blast load
($L/H = 8$, $W/H = 3/4$)



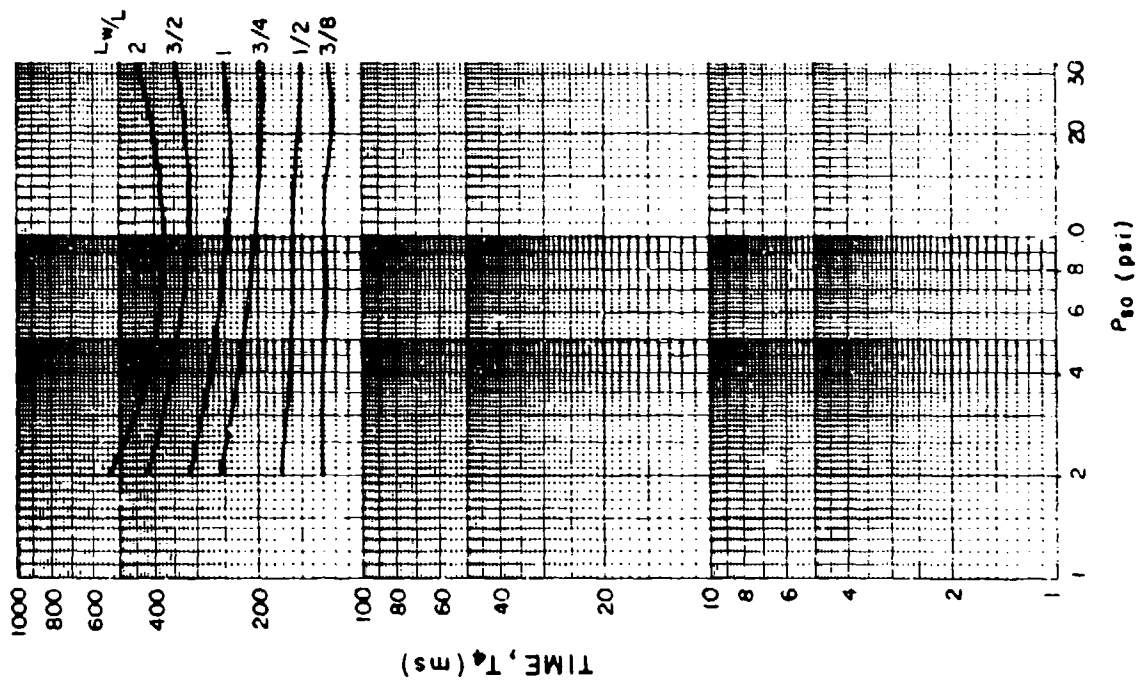
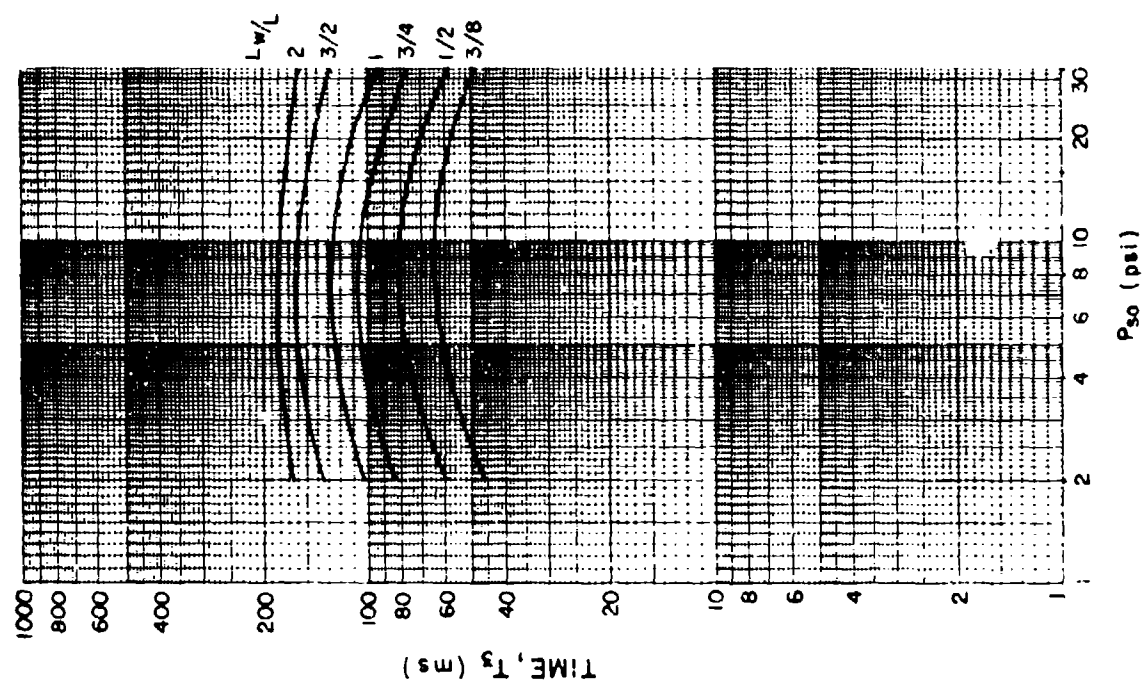
EXTERNAL INCIDENT PRESSURE AT FRONT FACE OF BUILDING, P_{so} (psi)

Figure 2-227 Idealized times T₃ and T₄ for interior side wall blast load
(L/H = 8, W/H = 3/2)



EXTERNAL INCIDENT PRESSURE AT FRONT FACE OF BUILDING, P_{so} (psi)

Figure 2-228 Idealized times T₃ and T₄ for interior side wall blast load
(L/H = 8, W/H = 3)



EXTERNAL INCIDENT PRESSURE AT FRONT FACE OF BUILDING, P_{so} (psi)

Figure 2-229 Idealized times T_3 and T_4 for interior side wall blast load
($L/H = 8$, $W/H = 6$)

cases, interpolation will be required to obtain the correct values of T_3 and T_4 for the given structure configuration.

**Table 2-4 List of Illustrations for Interior Side Wall
Idealized Times T_3 and T_4**

| L/H | W/H | | | |
|-----|-------|-------|-------|-------|
| | 3/4 | 3/2 | 3 | 6 |
| 1 | 2-214 | 2-215 | 2-216 | 2-217 |
| 2 | 2-218 | 2-219 | 2-220 | 2-221 |
| 4 | 2-222 | 2-223 | 2-224 | 2-225 |
| 8 | 2-226 | 2-227 | 2-228 | 2-229 |

2-15.4.5 Interior Back Wall. The blast pressures entering the interior of the building through the opening in the front wall must travel the full length of the building before arriving at the back wall. The incident pressure arriving at the back wall is essentially uniform over the wall. This pressure is immediately increased to the normal reflected pressure when it strikes the back wall.

The idealized pressure-time blast load acting on the interior face of the back wall is shown on figure 2-201c. Again, the time at which the shock front arrives at the front wall of the structure is taken as zero ($T_0 = 0$). The time T_1 represents the time it takes the shock front to travel from the opening to the back wall. The pressure build up is instantaneous to P_{RIB} due to the normal reflection of the shock front and then decays to zero at time T_2 . This loading is similar to the loading of an exterior front wall except that clearing is not possible.

The maximum average pressure P_{RIB} acting on the back wall is obtained from figures 2-230 and 2-231. Each figure is prepared for a given value of L/H . The ratio of the maximum average pressure on the back wall to the incident pressure P_{RIB}/P_{SO} is given as a function of P_{SO} for various values of A_O/A_W . Interpolation between figures may be necessary for a given structural configuration.

The idealized time T_1 is determined from figures 2-232 and 2-233. Each figure is prepared for a given value of the width to height ratio of the wall W/H . The time T_1 is given as a function of the incident pressure P_{SO} for various values of the wall length to height ratio L/H and the ratio of the opening area to the wall area A_O/A_W . The duration of the load T_2-T_1 is determined from figure 2-234. The time is given as a function of the incident pressure P_{SO} for various values of A_O/A_W . Since the back wall is located at the greatest distance from the front wall, the area of the opening has a significant effect on these times and must be considered.

2-15.5 Pressure Buildup in Structures

2-15.5.1 General. The procedures in Section 2-15.4 are for determining the net effects of shock loads entering openings in structures from windows or doors which are not designed to withstand the applied blast loads. In certain cases, structures may have closures which are designed to resist the blast loading, but have very small openings due to vents, ducts, etc., which will not withstand the blast. In this case, the small opening will not allow the shock front to develop inside the structure. However, the structure experiences an increase in its ambient pressure (a "filling" pressure) in a time that is a function of the structure volume, area of the openings, and applied exterior pressure and duration. Since personnel exhibit a tolerance limit to such pressure increases, a method of determining the average pressure inside the structure is needed. It should be noted that the interior pressures immediately adjacent to the openings will be higher than the average pressure.

2-15.5.2 Method of Calculation. The following procedure is applicable for structures with small area - volume ratios and applied blast pressures less than 150 psi. The change in pressure ΔP_i inside the structure within a time interval Δt is a function of the pressure difference at the openings, $P-P_i$, and the area-volume ratio, A_O/V_O :

$$\Delta P_i = C_L (A_O/V_O) \Delta t \quad 2-31$$

where:

C_L = leakage pressure coefficient and a function of the pressure difference $P-P_i$ and is obtained from figure 2-235

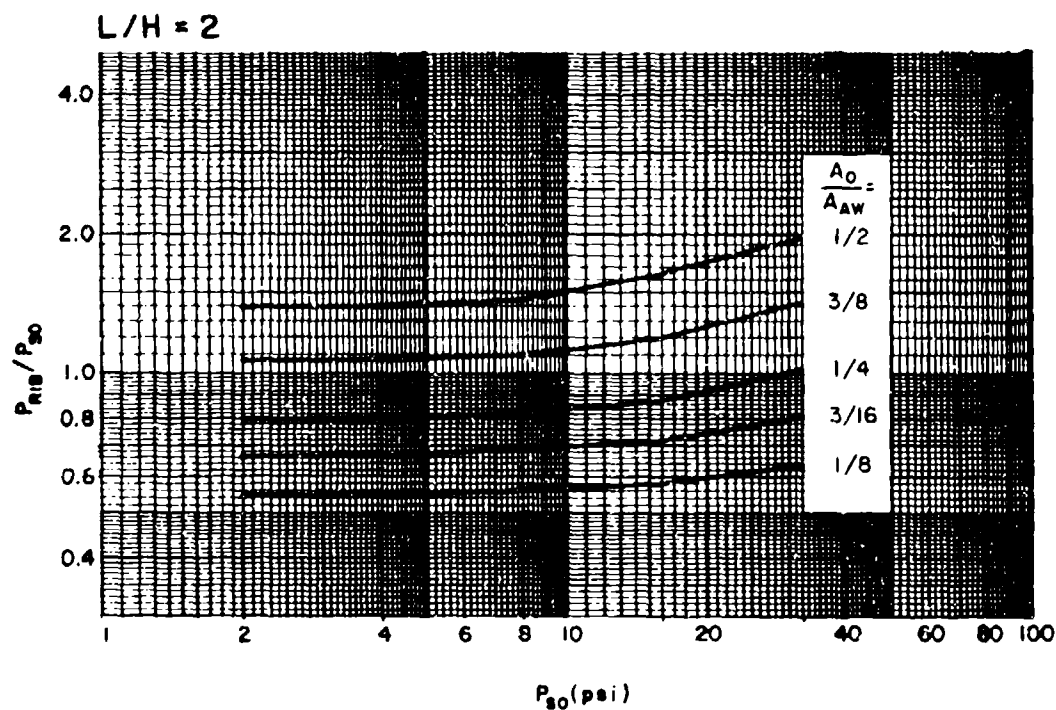
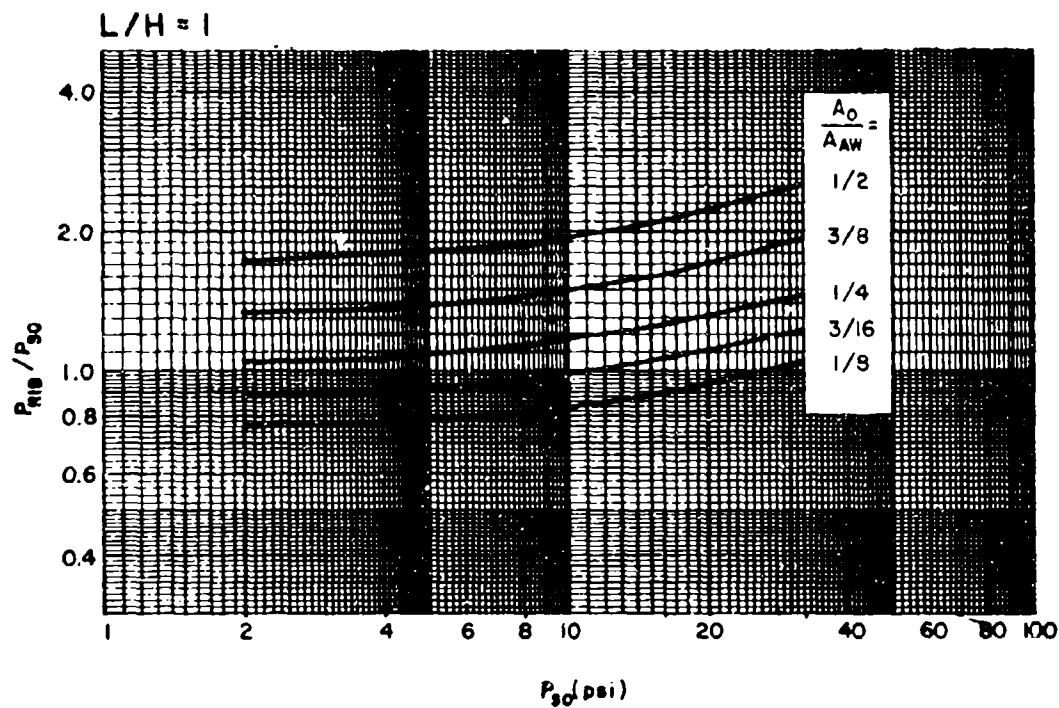
- P = applied exterior pressure
- P_i = interior pressure
- ΔP_i = interior pressure increment
- A_o = area of openings
- V_o = structure volume
- Δt = time increment

The interior pressure-time curve is calculated as follows:

1. Determine the pressure-time history of the applied blast pressures P acting on the surface surrounding the opening as presented in Section 2-15.3.
 2. Divide the duration t_o of the applied pressure into n equal intervals (Δt), each interval being approximately $t_o/10$ to $t_o/20$, and determine the pressures at the end of each interval.
 3. For each time interval, compute the pressure differential $P - P_i$, determine the corresponding value of C_L from figure 2-235, and calculate ΔP_i from equation 2-31 using the proper values of A_o/V_o and Δt . Add ΔP_i to P_i for the interval being considered to obtain the new value of P_i for the next interval.
 4. Repeat for each interval using the proper values of P and P_i .
- Note: when $P - P_i$ becomes negative during the analysis, the value of C_L must also be taken as negative.

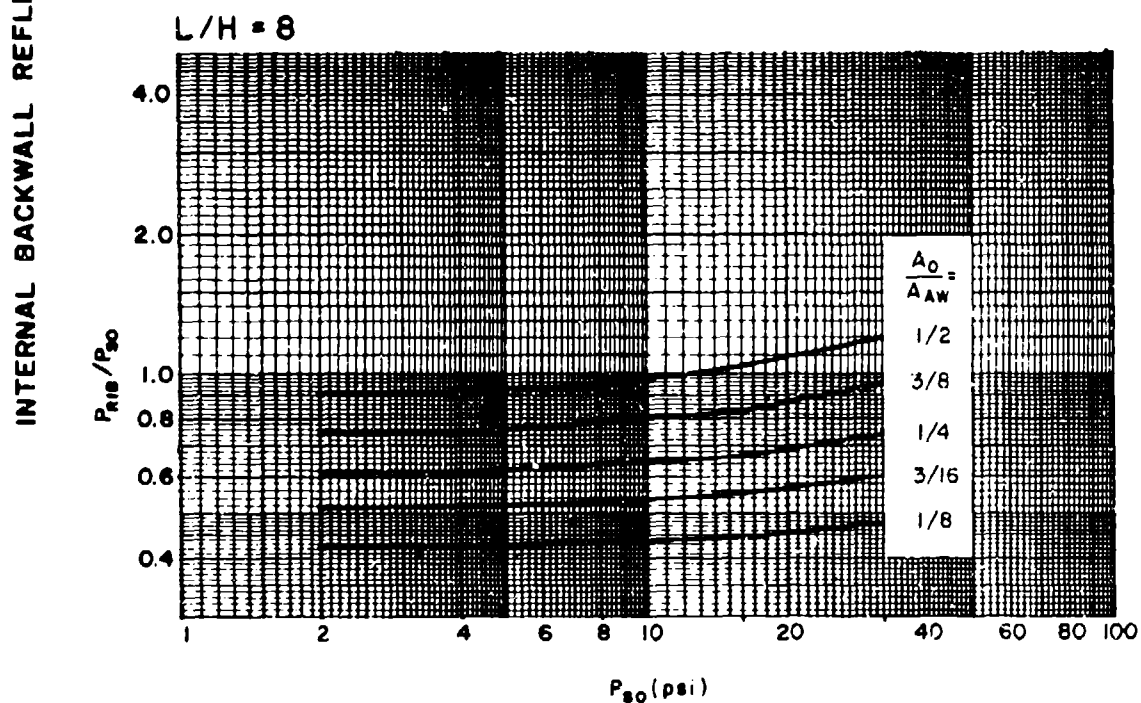
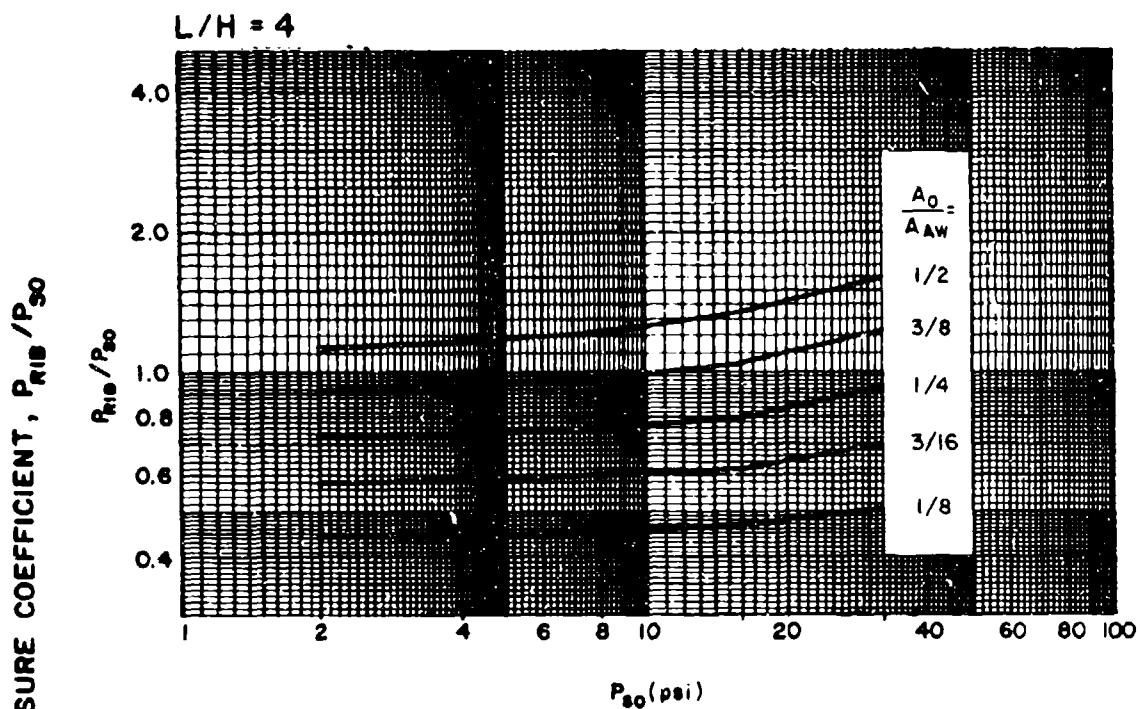
The above procedure is most easily accomplished by using a tabular arrangement for the required computations. An illustrative example is presented in Appendix 2A.

INTERNAL BACKWALL REFLECTED PRESSURE COEFFICIENT, P_{RIB}/P_{S0}



EXTERNAL INCIDENT PRESSURE AT FRONT FACE OF BUILDING, P_{S0} (psi)

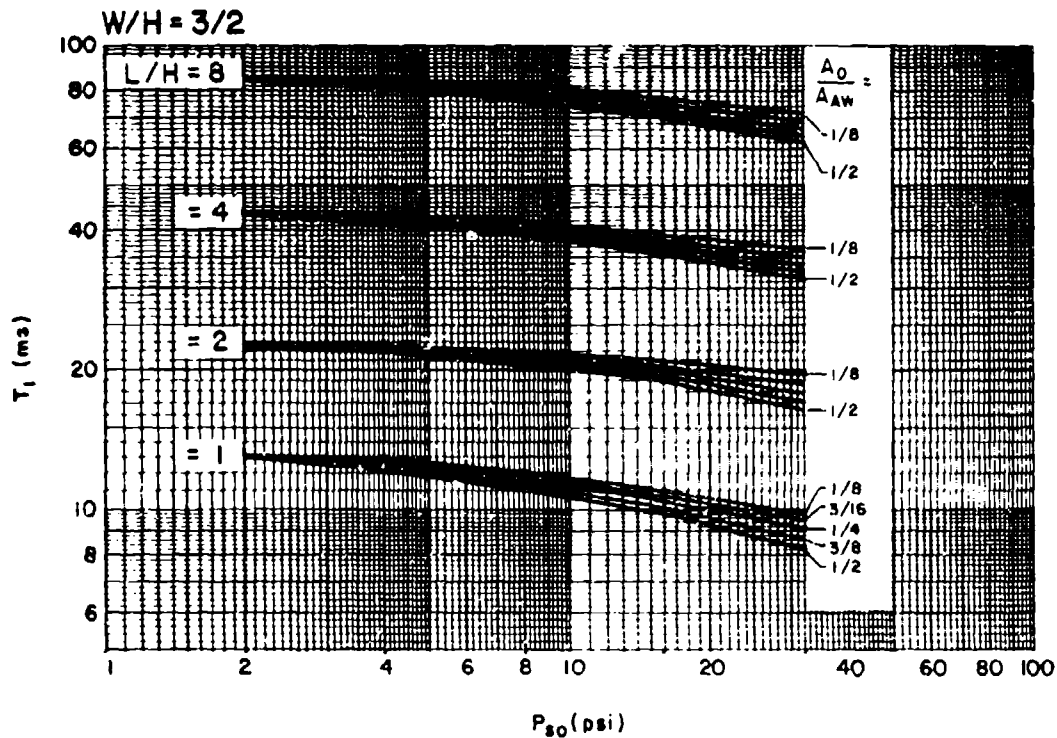
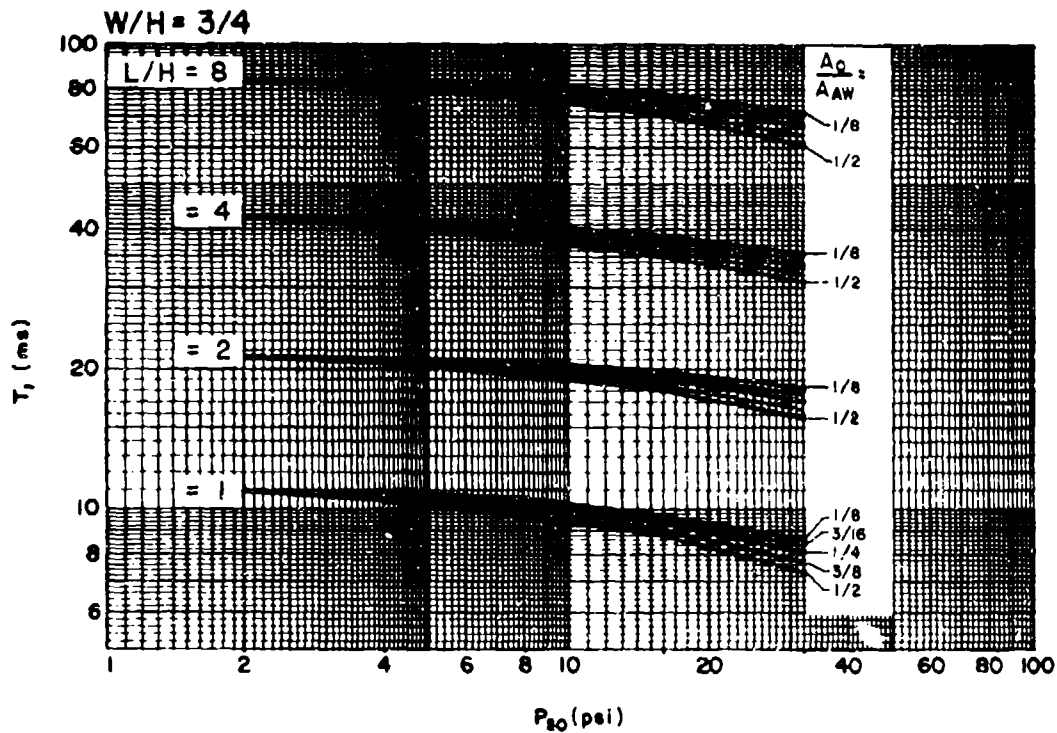
Figure 2-230 Idealized pressure coefficient for back wall interior blast load ($L/H = 1$ and 2)



EXTERNAL INCIDENT PRESSURE AT FRONT FACE OF BUILDING, $P_{80}(\text{psi})$

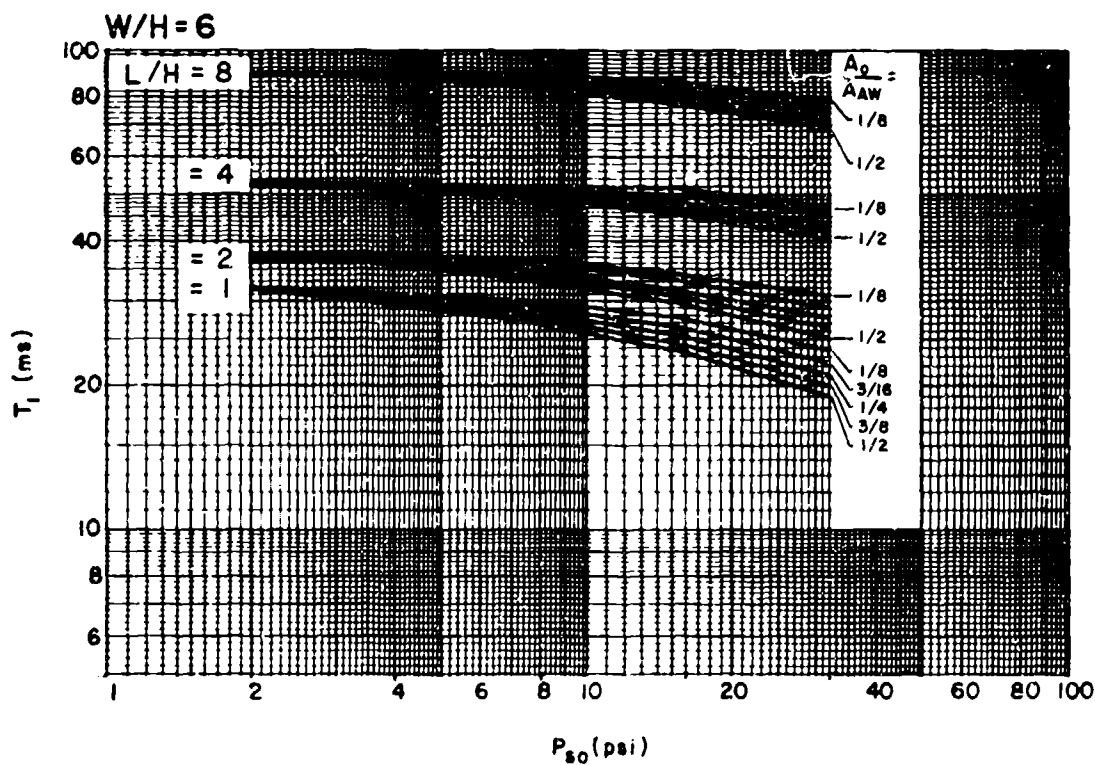
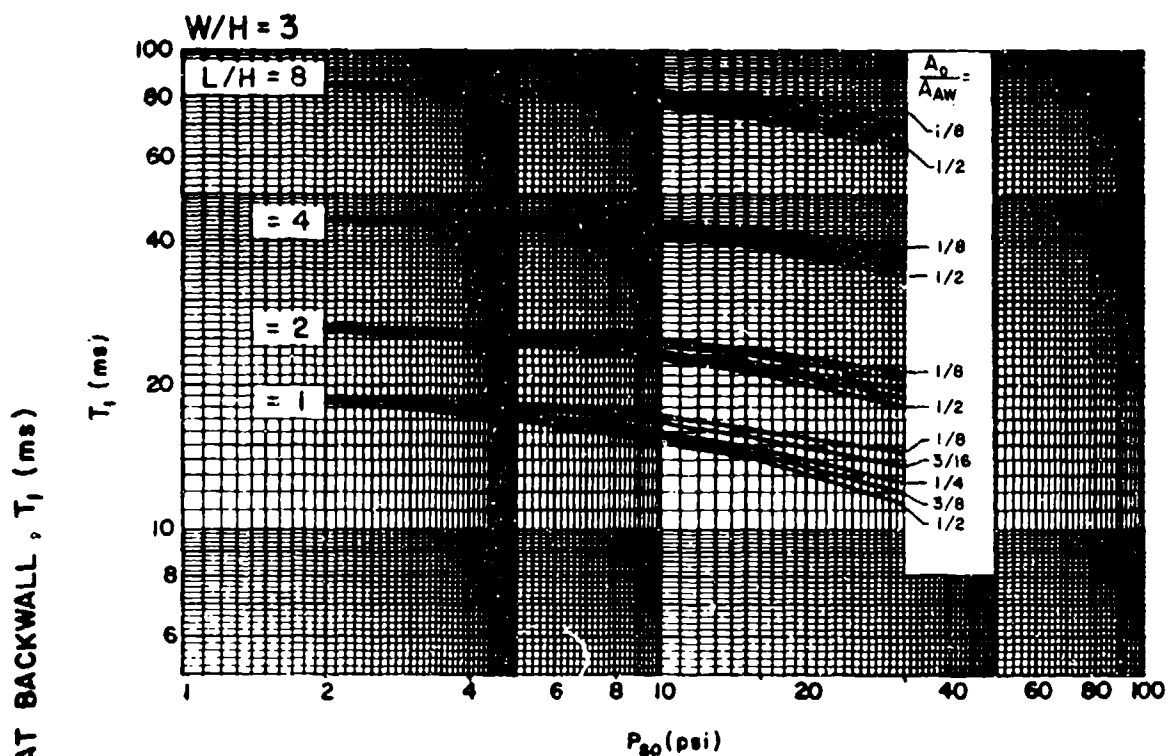
Figure 2-231 Idealized pressure coefficient for back wall interior blast load
($L/H = 4$ and 8)

ARRIVAL TIME OF SHOCK FRONT AT BACKWALL, T_1 (ms)



EXTERNAL INCIDENT PRESSURE AT FRONT FACE OF BUILDING, P_{80} (psi)

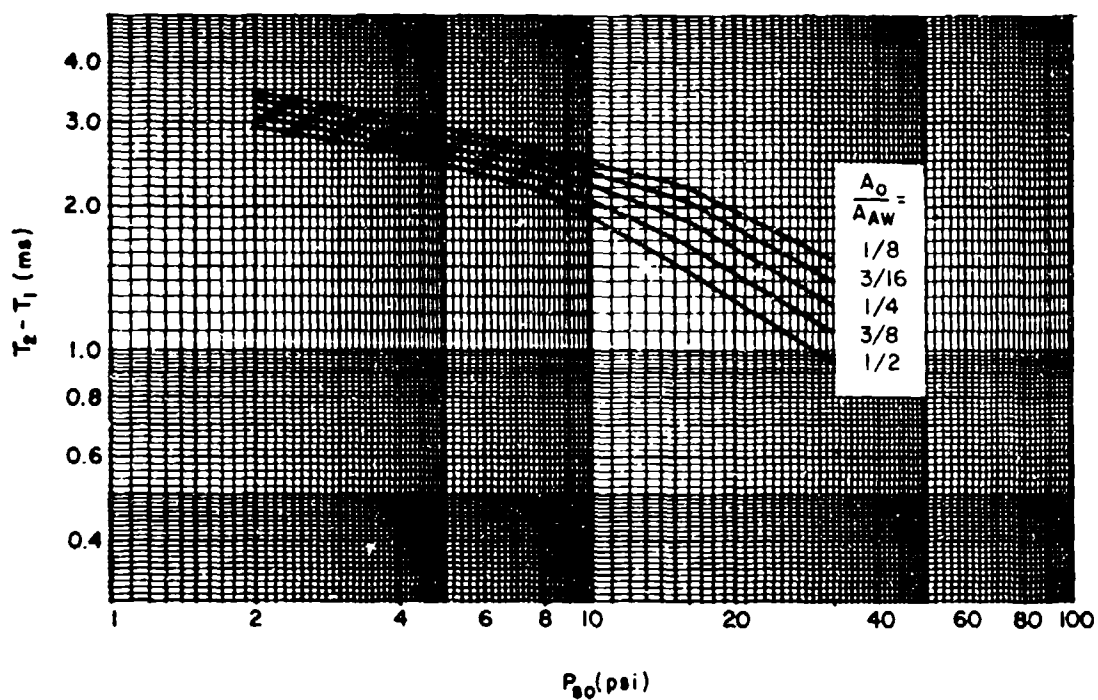
Figure 2-232 Arrival time, T_1 , for interior back wall blast load ($W/H = 3/4$ and $3/2$)



EXTERNAL INCIDENT PRESSURE AT FRONT FACE OF BUILDING, P_{s0} (psi)

Figure 2-233 Arrival time, T_1 , for interior back wall blast load
(W/H = 3 and 6)

BACKWALL SCALED REFLECTED PRESSURE DURATION, $T_2 - T_1$ (ms)



EXTERNAL INCIDENT PRESSURE AT FRONT FACE OF BUILDING, P_{so} (psi)

Figure 2-234 Idealized time $T_2 - T_1$ for interior back wall blast load

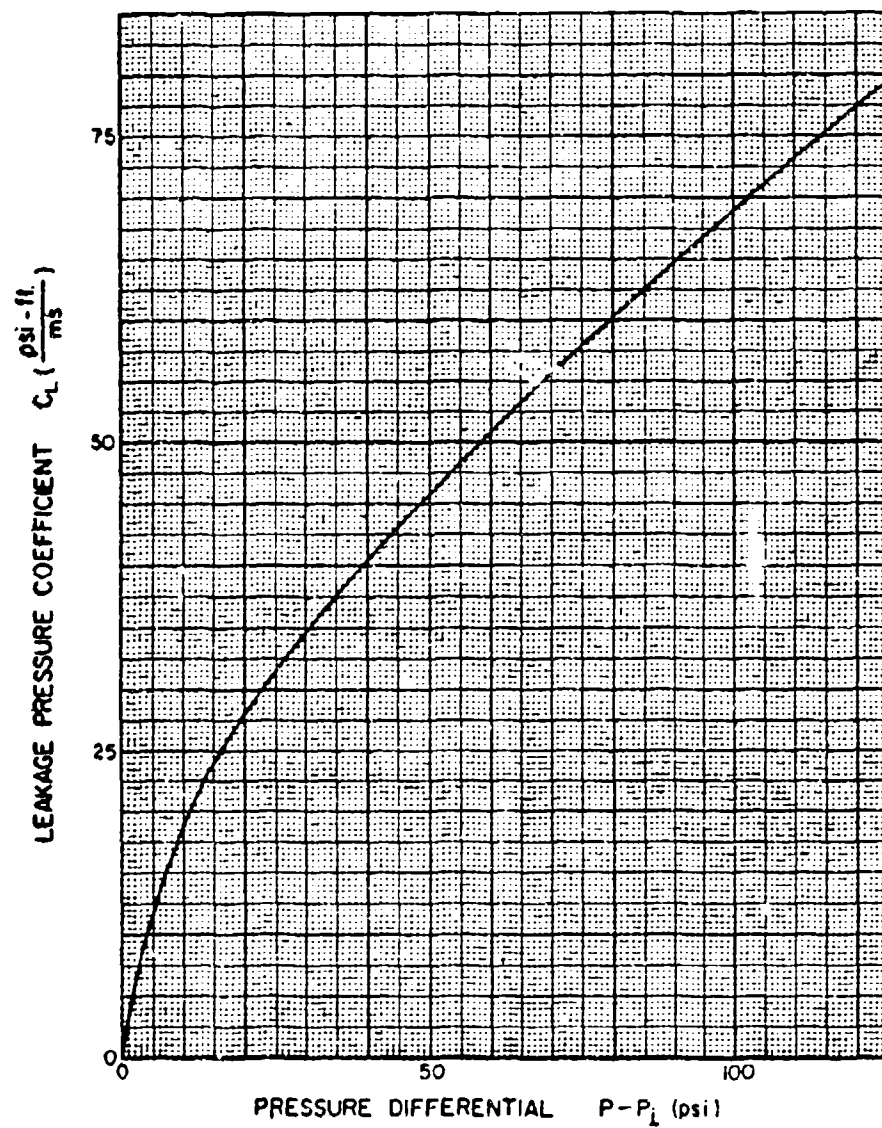


Figure 2-235 Leakage pressure coefficient vs. pressure differential

PRIMARY AND SECONDARY FRAGMENTS

2-16 General

Previous sections in this volume have discussed explosive accident predictions in reference to studies of blast waves and their effects. Significant damage from accidental explosions can also be caused by the impact of fragments or objects which were generated during the explosions and hurled against structures or other receivers at high speed.

Fragments resulting from accidental explosions can be divided into two categories. The term "primary fragment" denotes a fragment from a casing or container of an explosive source or a fragment from an object in contact with an explosive. If the source is a true high explosive, the container or casing usually ruptures into a large number of small primary fragments which can be projected at velocities up to several thousand feet per second by the explosion. For bomb and shell casings, typical weights of damaging fragments recovered in field tests are about 0.032 oz. These primary fragments, though irregular, are usually of "chunky" geometry, i.e., all linear dimensions are of the same order.

Containers or casings which fragment or burst during explosions are not the only sources of fragments and missiles. Other potentially damaging objects, known as "secondary missiles" or "secondary fragments" can also be produced due to the blast wave interaction with objects or structures located near the explosive source. These objects can be torn loose from their moorings, if they are attached, and accelerated to velocities high enough to cause impact damage. The objects could be pieces of machinery, small tools, materials such as pipes and lumber, parts of buildings or other structures disrupted by the explosions, large pieces of equipment, etc. Characteristics of both primary and secondary fragments (often referred to as secondary "debris" to distinguish them from primary "fragments") will be discussed in this section.

2-17 Primary Fragments

2-17.1 General

The explosion of a cased donor charge results in the formation of primary fragments which are produced by the shattering of the explosive container. The container may be the casing of conventional munitions, the kettles, hoppers and other metal containers used in the manufacture of explosives, metal housing of rocket engines, etc.

Primary fragments are characterized by very high initial velocities (in the order of thousands of feet per second), a large number of fragments, and relatively small sizes in comparison to secondary fragments and concrete fragments formed due to partial failure or total collapse of protective elements. The initial velocity and size of the fragments are functions of the thickness of the metal container, the shape of the explosive as a whole (spherical, cylindrical, prismatic), and the sections of the container (ends, middle, etc.) from which the fragments are formed. The size and shape of the fragments will depend greatly on the metallographic history of the casing, its physical condition (such as dents, grooves, bends, or internal cracks or flaws), and the condition of joints, most notably welded joints.

Upon detonation of a cased explosive, the casing breaks up into fragments with varying weights and velocities. The destructive potential of these fragments is a function of their shapes, materials, momentum and kinetic energy distributions. Since only the larger fragments have the momentum necessary to perforate a barrier and/or cause propagation of explosions, they are usually the only fragments of concern in design of a protective system. Therefore, through testing or analysis, the velocity and weight of the "worst case" fragment must be determined and used as a design criterion.

2-17.2 Initial Fragment Velocity

2-17.2.1 Explosives with Uniform Cylindrical Containers. The most common technique for calculating the initial velocity of fragments in contact with an explosive charge is the Gurney method. The initial velocity of primary fragments resulting from the detonation of a cased explosive is a function of the explosive output and the ratio of the explosive charge weight to casing weight.

The initial velocity of primary fragments resulting from a high-order detonation of a cylindrical casing with evenly distributed explosives is expressed as:

$$v_o = (2E')^{1/2} \left(\frac{W/W_c}{1 + 0.5 W/W_c} \right)^{1/2} \quad 2-32$$

and, applying a 20 percent factor of safety, the design charge weight is:

$$W = 1.2W_{ACT} \quad 2-33$$

where:

v_o = initial velocity of fragments

$(2E')^{1/2}$ = Gurney' Energy Constant from table 2-5

W = design charge weight

W_c = weight of casing

W_{ACT} = actual quantity of explosive

The ratio of Gurney energy to the heat of detonation $E'/\Delta H$, represents the conversion efficiency of chemical energy to "Gurney" energy. If E' is unknown for a particular explosive, and ΔH is known, $E'/\Delta H$ may be determined for a similar explosive (i.e., similar heat of detonation) and the value used to estimate the Gurney energy.

2-17.2.2 Explosives with Non-Uniform Cylindrical Containers. Cylinders are the most common shape of cased explosives. Along the length of the cylinder, there may be a large variation in the thickness of the casing and its outside diameter. In such cases, the cylinder is divided into a series of equivalent cylinders. This method is further discussed in Section 2-17.3.2.

Table 2-5 Specific Weight and Gurney Energy Constant
for Various Explosives

| Explosive | Specific Weight | $\sqrt{2E'}$ |
|------------------|-----------------------|--------------|
| | (lb/in ³) | (ft/sec) |
| Composition B | 0.0621 | 9100 |
| Composition C-3 | 0.0578 | 8800 |
| HMX | 0.0682 | 9750 |
| Nitromethane | 0.0411 | 7900 |
| PBX-9404 | 0.0664 | 9500 |
| PETN | 0.0635 | 9600 |
| RDX | 0.0639 | 9600 |
| TACOT | 0.0581 | 7000 |
| Tetryl | 0.0585 | 8200 |
| TNT | 0.0588 | 8000 |
| Trimonite No. 1 | 0.0397 | 3400 |
| Tritonal | 0.0621 | 7600 |
| (TNT/Al = 80/20) | | |

Gurney's equations were developed for cased explosives where the explosive is in direct contact with the outer metal casing. Several conditions are illustrated in figure 2-236 where the explosive and outer casing are separated by an incompressible fluid. The initial velocity of primary fragments resulting from the detonation of such items may be approximated by using the Gurney equations with slight modifications. The actual weight of the explosive is increased by the required 20 percent factor of safety. The design charge weight is.

$$W = 1.2 W_{ACT}$$

2-34

and, the weight of the casing is increased to include the weight of the fluid and the weight of the inner casing which surrounds the explosive, if present, or:

$$W_C = W_{CO} + W_{CI} + W_A$$

2-35

where:

W = design charge weight

W_{ACT} = actual quantity of explosive

W_C = total weight of casing

W_{CO} = weight of outer casing

W_{CI} = weight of inner casing

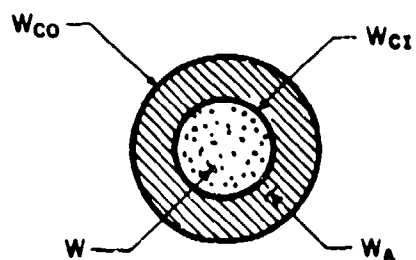
W_A = weight of fluid

2-17.2.3 Explosives with Non-Cylindrical Containers. Gurney formulas for some additional geometries are given in table 2-6. A plot of velocity versus casing to charge weight ratio for various geometries is shown in figure 2-237.

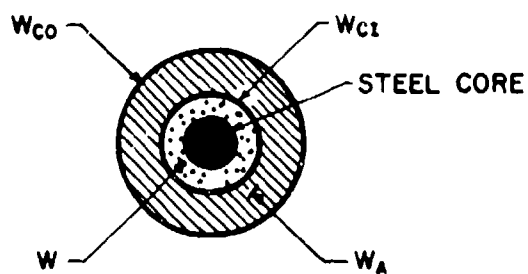
The shapes considered in figure 2-237 are assumed to have an evenly distributed explosive and also a uniform container (casing) or plate thickness. However, for those cases where the shape is slightly non-uniform, the initial velocity of the resulting fragments may be estimated by using the average cross-sectional dimensions.

2-17.3 Fragment Mass Distribution

2-17.3.1 Explosives with Uniform Cylindrical Containers. The fragmentation pattern and the weight of the largest fragment, resulting from the high-order detonation of an evenly-distributed explosive in a cylindrical metal case of uniform thickness, have been calculated according to relationships developed on the basis of theoretical considerations confirmed with a large number of tests. The number of fragments produced by a cylindrical cased charge weighing more than a given design fragment is:





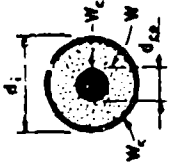
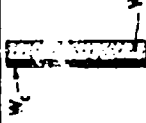

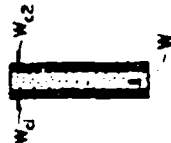
a. CYLINDER OR SPHERE



b. STEEL CORED CYLINDER

Figure 2-236 Explosive outer casing separated by incompressible fluid

Table 2-6 Initial Velocity of Primary Fragments for Various Geometries

| Type | Cross-sectional shape | Initial fragment velocity v_0 | Maximums | Remarks |
|----------------------|---|--|---------------------------------------|---|
| Cylinder |  | $\sqrt{2E} \left[\frac{\frac{W}{W_c}}{1 + \frac{3W}{2W_c}} \right]^{\frac{1}{3}}$ | $\sqrt{2E} \sqrt{3}$ | See paragraph 2-17.2 |
| Sphere |  | $\sqrt{2E} \left[\frac{\frac{W}{W_c}}{1 + \frac{3W}{2W_c}} \right]^{\frac{1}{3}}$ | $\sqrt{2E} \sqrt{3}$ | |
| Steel cored cylinder |  | $\sqrt{2E} \left[\frac{\frac{W}{W_c}}{1 + \frac{(2+a)W}{6(1+a)W_c}} \right]^{\frac{1}{3}}$ where $a = \frac{d_1}{d_2}$ | $\sqrt{2E} \sqrt{\frac{3(1+a)}{2+a}}$ | If the steel core is many times more massive than the explosive, this expression for the initial velocity should be modified by multiplying it by the expression: $\sqrt{1 - \frac{0.025W}{W_c}}$ where W_c is the weight of the steel core (lbs.). |
| Plate |  | $\sqrt{2E} \left[\frac{\frac{3W}{5W_c}}{1 + \frac{4W}{5W_c} + \frac{W}{5W_c}} \right]^{\frac{1}{3}}$ | $\sqrt{2E} \sqrt{3}$ | This expression applies for a rectangular explosive in contact with a metal plate having the same surface area. It is assumed that the entire system is suspended in free air and its thickness is small in comparison to its surface area so that the resulting motions are essentially normal to the plane of the plate. |
| Hollow cylinder |  | — | — | Although an expression to predict the velocity of fragments is not available, an upper limit of the initial velocity may be obtained using the expression for a solid cylinder and a lower limit from the expression for a single plate. The ratio of the explosive weight to the casing weight (W/W_c) of the hollow cylindrical charge is used in both expressions. |
| Steel web plate |  | If $W_c \neq W_{c2}$ $\sqrt{2E} \left[\frac{\frac{W}{W_c}}{W_c + W_{c2} + \frac{W}{3} (1 - \rho + \rho^2)} \right]^{\frac{1}{3}}$ where $\rho = \frac{W_c + \frac{W}{2}}{W_c + \frac{W}{2}}$ If $W_c = W_{c2} = W$, $\sqrt{2E} \left[\frac{\frac{W}{2W_c}}{1 + \frac{W}{6W_c}} \right]^{\frac{1}{3}}$ | $\sqrt{2E} \sqrt{3}$ | This expression applies for a rectangular explosive sandwiched between two metal plates having the same surface area as the explosive. It is assumed that the entire system is suspended in free air and its thickness is small in comparison to its surface area so that the resulting motions are essentially normal to the plane of the plates. Note: $W = E = \text{Explosive weight}$ $W_c = C = \text{Casing weight}$ $W, W_c, W_{c2}, W_{c1}, W_{c2}$ (lbs.) d_1, d_{c2} (lbs.) $v_0, \sqrt{2E}$ (ft./sec) |

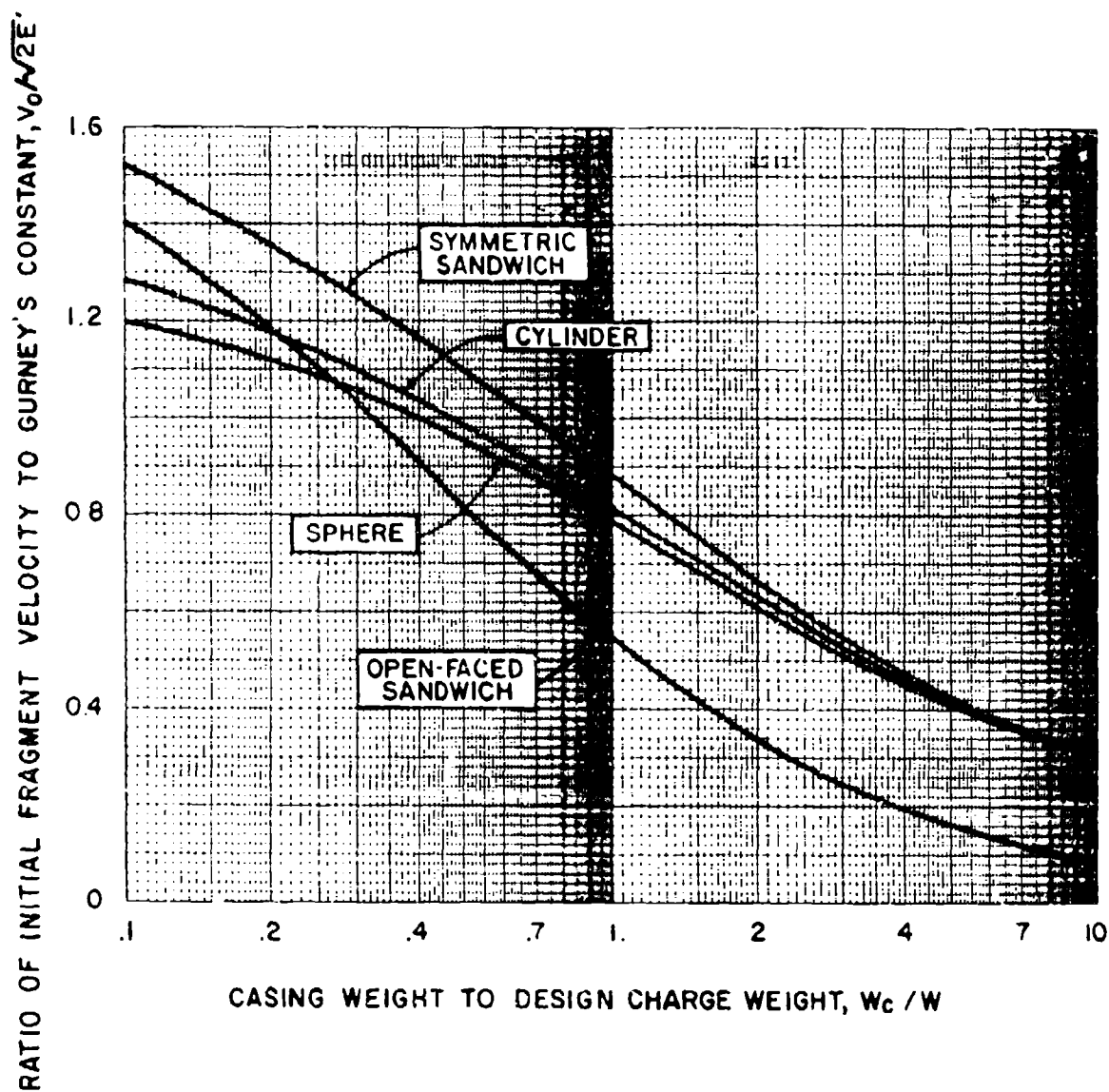


Figure 2-237 Initial velocity of primary fragments for various geometries

$$N_f = \frac{8W_c e^{-[(W_f)^{1/2}/M_A]}}{M_A^2} \quad 2-36$$

and:

$$M_A = B t_c^{5/6} d_1^{1/3} \left(1 + \frac{t_c}{d_1}\right) \quad 2-37$$

where:

N_f = number of fragments with weight greater than W_f

W_c = casing weight

W_f = design fragment weight

M_A = fragment distribution factor

B = explosive constant from table 2-7

t_c = average casing thickness

d_1 = average inside diameter of casing

The largest fragment produced by an explosion can be found by setting $N_f = 1$. Thus, the weight of the largest fragment is given by:

$$W_f = \left[M_A \ln \left(\frac{8W_c}{M_A^2} \right) \right]^2 \quad 2-38$$

Setting the fragment weight W_f equal to zero, the following expression for the total number of fragments is obtained:

$$N_T = 8W_c / M_A^2 \quad 2-39$$

where: N_T = total number of fragments

Hence, the average particle weight can be found:

$$\bar{W}_f = 16W_c / N_T = 2M_A^2 \quad 2-40$$

where:

\bar{W}_f = average fragment weight

**Table 2-7 Mott Scaling Constants for Mild Steel Casings
and Various Explosives**

| Explosive | A | B |
|-------------------|------------------------------|------------------------------|
| | (oz ^{1/2} in. -3/2) | (oz ^{1/2} in. -7/6) |
| Baratol | - | 0.512 |
| Composition A-3 | - | 0.220 |
| Composition B | 0.214 | 0.222 |
| Cyclotol (75/25) | - | 0.197 |
| H-6 | - | 0.276 |
| HBX-1 | - | 0.256 |
| HBX-3 | - | 0.323 |
| Pentolite (50/50) | 0.238 | 0.248 |
| PTX-1 | - | 0.222 |
| PTX-2 | - | 0.227 |
| RDX | 0.205 | 0.212 |
| Tetryl | 0.265 | 0.272 |
| TNT | 0.302 | 0.312 |

For design purposes, a confidence level CL, where $(0 < CL < 1)$, can be defined as the probability that the weight, W_f , is the largest weight fragment released. The expression for the design fragment weight corresponding to a prescribed design confidence level (CL) is given as.

$$CL = 1 - N_f/N_T = 1 - e^{-[(W_f)^{1/2}/M_A]} \quad 2-41$$

or rearranging terms:

$$W_f = M_A^2 \ln^2 (1 - CL) \quad 2-42$$

Equation 2-42 can then be used to calculate the design fragment weight for a prescribed design confidence level. Note that equation 2-42 uses an infinite distribution to describe a physical phenomenon which has a finite upper limit. Equation 2-42 may be used for $CL \leq 0.9999$. If $CL > 0.9999$, use:

$$W_f = M_A^2 \ln^2 [1 - CL (1 - e^{-[4(W_c)^{1/2}/M_A]})] \quad 2-43$$

The number of fragments with weight greater than W_f is:

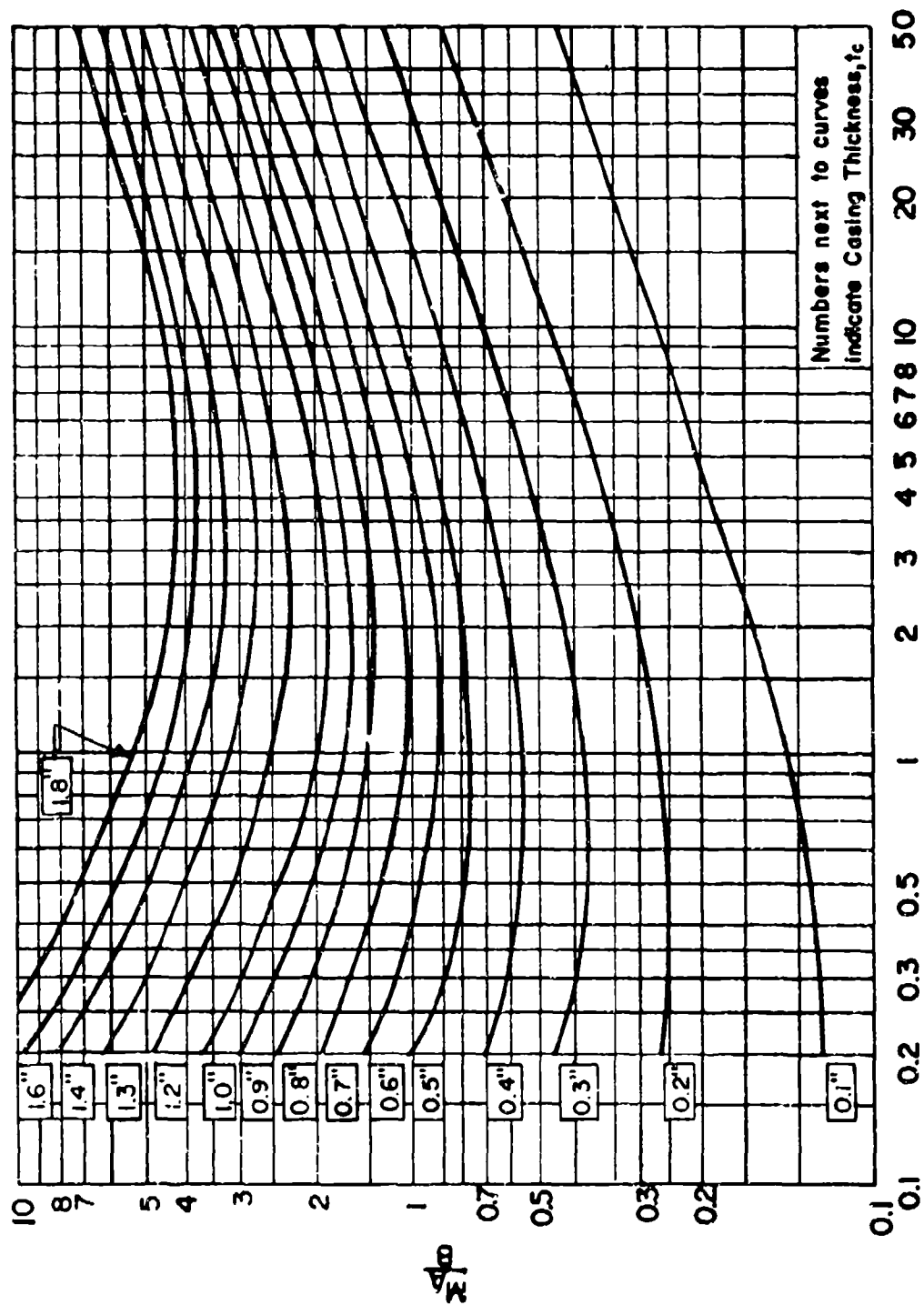
$$N_f = N_T (1 - CL) \quad 2-44$$

It should be noted that equations 2-41 through 2-44 are not applicable to casings designed to fragment in a specific pattern.

In order to facilitate design calculations, figure 2-238 is available for determining the quantity M_A/B for a given cylindrical casing geometry and figures 2-239 and 2-240 provide the value of W_f/M_A^2 corresponding to a specified confidence level. Figure 2-239 is applicable for a wide range of confidence levels $(0.3 < CL < 1.0)$ whereas figure 2-240 is applicable for high confidence levels $(0.986 \leq CL \leq 1)$.

To calculate the actual number of fragments with a weight greater than the design fragment weight, equation 2-36 can be applied directly. Alternatively, figure 2-241 presents a plot of the quantity $B^2 N_T / W_c$ versus the casing geometry. The number of fragments with weight greater than W_f can then be calculated from equation 2-44.

2-17.3.2 Explosives with Non-Uniform Cylindrical Containers. The equations in Section 2-17.3.1 were developed assuming a uniform cross-section along the axis of the cylinder with evenly distributed explosive in direct contact with the outer casing. Actual cased explosives rarely conform to these ideal conditions. If there is only slight variation in the casing thickness and/or



INSIDE DIAMETER OF CASING, d_i (in.)

Figure 2-238 M_A/B versus cylindrical casing geometry

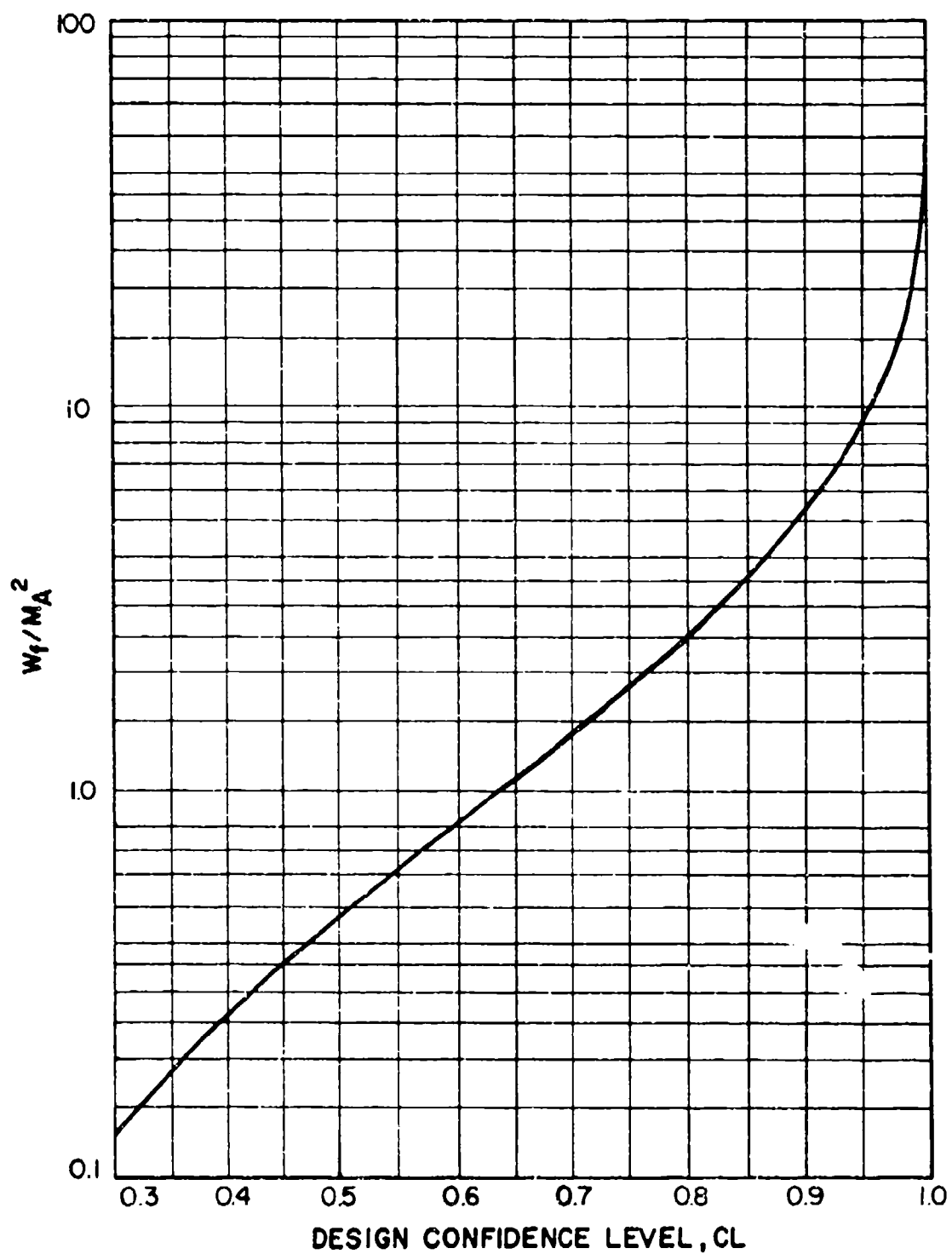


Figure 2-239 Design fragment weight versus design confidence level
($0.3 \leq CL \leq 1$)

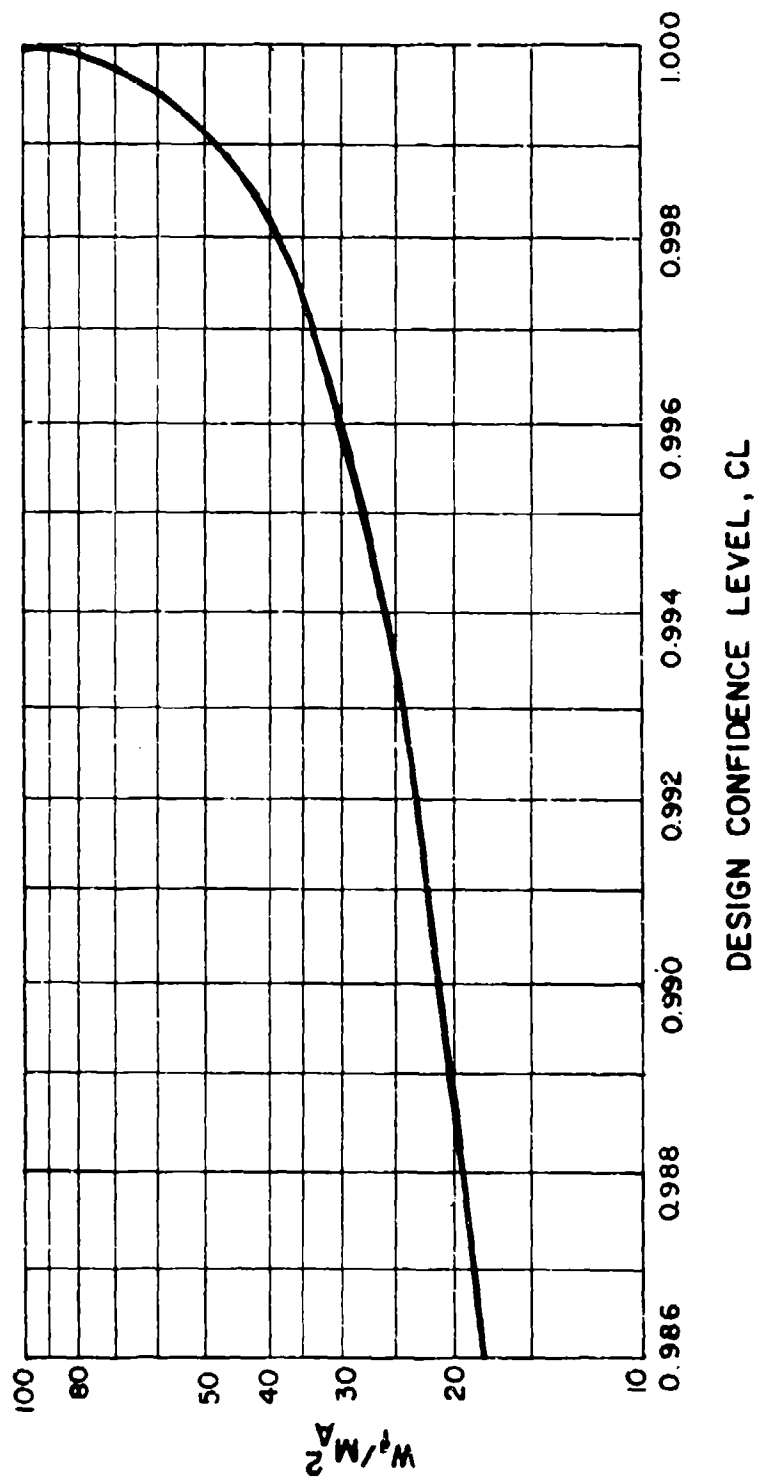


Figure 2-240 Design fragment weight versus design confidence level
($0.986 \leq CL \leq 1$)

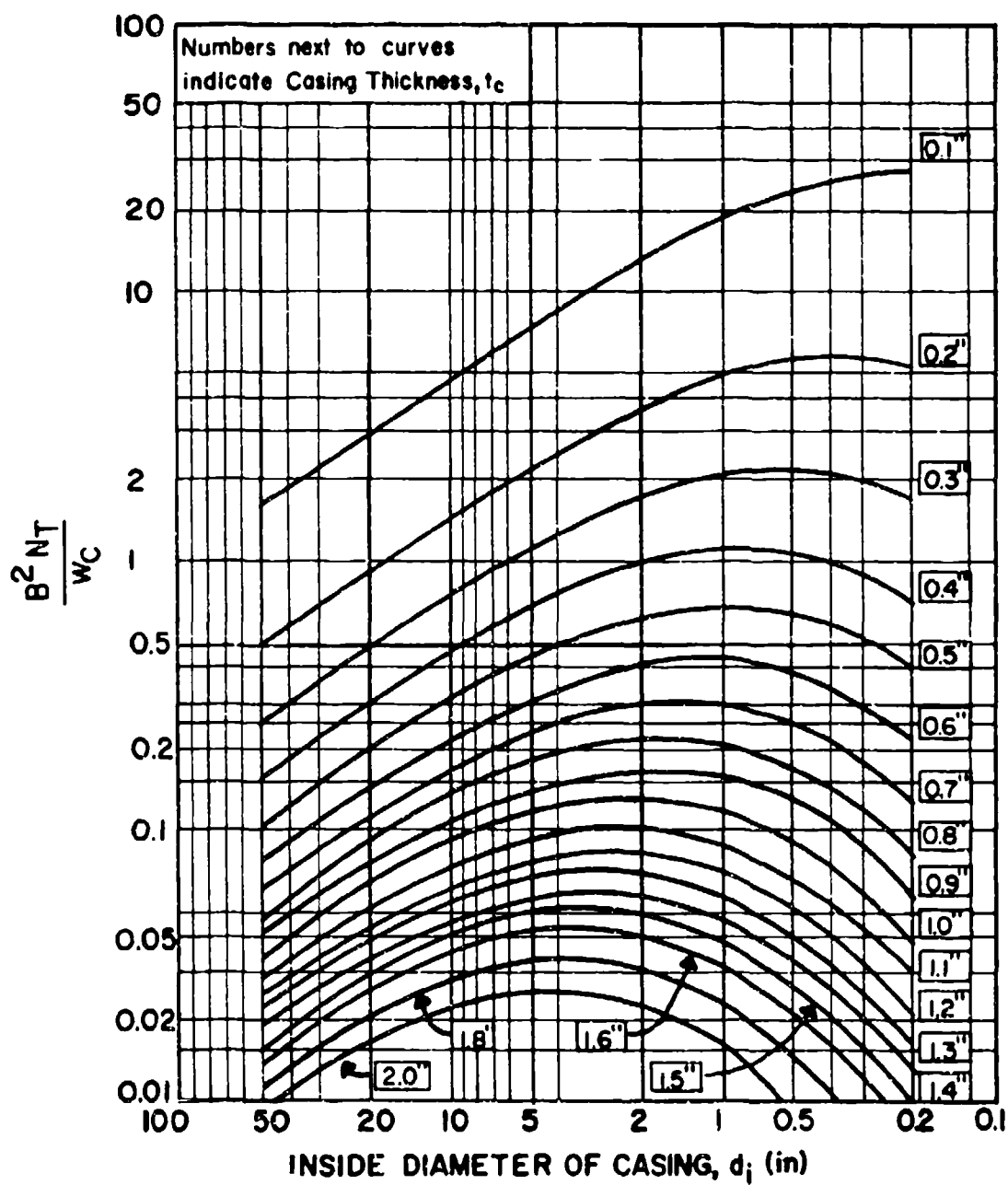


Figure 2-241 $B^2 N_T / W_C$ versus casing geometry

casing diameter, the fragment weight may be estimated using an average casing thickness and diameter in equation 2-37.

If the cross-section varies greatly, the container is treated as a series of equivalent cylinders, representing the actual shape as closely as possible (see fig. 2-242). Using the average casing thickness and diameter of each section, the velocity and weight of the design fragment must be determined for each section. The worst case fragment of the equivalent cylinders is then taken as the design fragment for the entire container.

Cylindrical explosives with steel and hollow cores are shown in table 2-6. The fragment mass distribution may be estimated for these shapes using the uniform cylinder equations of Section 2-17.3.1. In applying these equations, the same procedures as outlined above for non-uniform cylinders are employed, except that the steel or hollow cores are neglected in the calculations.

Figure 2-236 illustrates the cased explosive where the explosive and outer casing are separated by an incompressible fluid. The outer casing is much thicker than the inner casing which encloses the explosive. Here again, the fragment mass distribution may be estimated using the uniform cylinder equations of Section 2-17.3.1 except as indicated below. The heaviest fragment will fracture from the outer casing. Thus, W_c should be the weight of the outer casing only. The thin inner casing is neglected in the calculations. In addition, since the ratio of explosive weight to casing weight (W/W_c) is small, the fragment distribution factor (M_A) should be the larger of that given in equation 2-36 and equation 2-44 as follows:

$$M_A = A t_c \frac{(d_i + t_c)^{3/2}}{d_i} \left(1 + \frac{W}{2W_c}\right)^{1/2} \quad 2-45$$

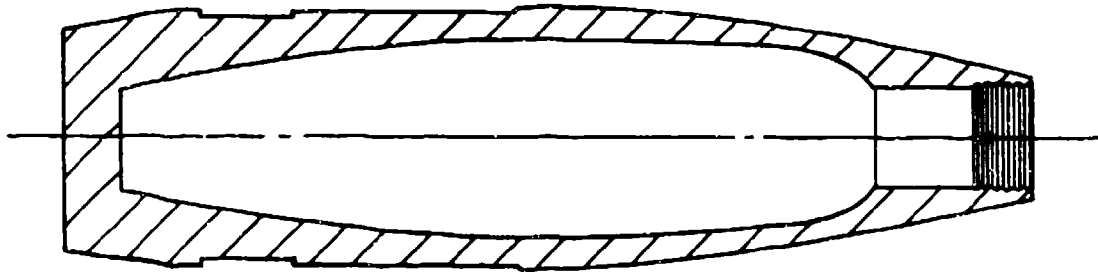
where:

A = explosive composition constant from table 2-7

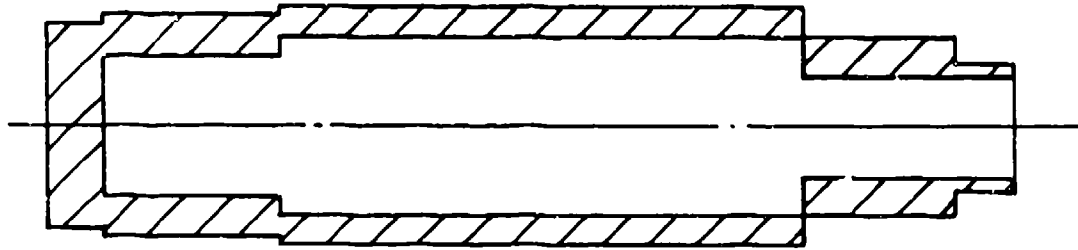
and all other terms are as previously defined.

2-17.3.3 Explosives with Non-Cylindrical Containers. Information is not presently available for evaluating the number and weight of fragments from charges other than those having a cylindrical casing.

The equations of Section 2-17.3.1 can only be employed to calculate masses of primary fragments which evolve from accidents involving an explosive detonation within a container of some sort, like a casing, storage tank, or a confining piece of machinery such as a centrifuge or press. Weights of fragments created as a result of a given quantity of explosive detonating while being machined or in an unconfined space must be estimated using other methods.



(a) ACTUAL CONFIGURATION



(b) IDEALIZED CONFIGURATION

Figure 2-242 Equivalent cylindrical explosive casings

2-17.4 Variation of Fragment Velocity with Distance

When an explosion is located close to an object (acceptor explosive, barrier, etc.), the velocity v_s at which a fragment strikes the object is approximately equal to the initial velocity v_o . However, if the detonation is located at a relatively large distance from the object, then the impact or striking velocity of the fragment may be substantially less than its velocity immediately after the explosion. This variation in velocities, which is primarily a result of air resistance, is also a function of the physical properties of the casing and the distance between the donor explosive and the object.

When the protective barriers are located 20 feet or less from a detonation, the variation between striking and initial velocities usually may be neglected. On the other hand, for determining the effects of primary fragment impact on structures further away from a detonation, the variation of fragment velocity with distance should be included in the design. The fragment velocity of major concern is the velocity with which the "design fragment(s)" (the worst case fragment(s) which the structure must be designed to withstand) strikes the protective structure. This striking velocity is expressed as:

$$v_s = v_o e^{-12k_v R_f} \quad 2-46$$

and:

$$k_v = (A/W_f) \rho_a C_D \quad 2-47$$

where:

v_s = fragment velocity at a distance R_f from the center of detonation

v_o = initial (maximum) fragment velocity

R_f = distance from the center of detonation

k_v = velocity decay coefficient

A = presented area of the fragment

W_f = fragment weight

A/W_f = fragment form factor

ρ_a = specific density of air

C_D = drag coefficient

The decay coefficient can be evaluated as:

$$A/W_f = 0.78/W_f^{1/3} \text{ for a random mild steel fragment}$$

$$\rho_a = 0.00071 \text{ oz/in}^3$$

$$C_D = 0.6 \text{ for primary fragments}$$

The resulting expression for the striking velocity is:

$$v_s = v_o e^{-0.004 R_f / W_f^{1/3}} \quad 2-48$$

Figure 2-243 shows the variation of primary fragment velocity with distance. The term initial velocity refers to the maximum fragment velocity as the fragment is ejected from the charge. Due to the extremely high rates of fragment acceleration, this velocity is considered to be attained by the fragment prior to moving appreciably from its initial position.

2-17.5 Primary Fragments - Shape, Caliber Density and Impact Angle

2-17.5.1 General. In order to determine the damage potential of primary fragments, it is necessary to evaluate the caliber density, shape and angle of obliquity of the fragments as well as the previously described weight and striking velocity. When a container fragments, a random distribution of fragment shapes results. Section 2-17.3 contained a method for determining the weight distribution of primary fragments. From the weight of the fragment and shape of the containment vessel, one can estimate the size of individual fragments. This section discusses a method for performing an engineering estimate of a standard design fragment(s) for use in fragment impact damage.

2-17.5.2 Shape of Primary Fragments. Two possible fragment shapes are shown in figure 2-244 for explosives in contact with the outer casing. The blunt fragment shape in figure 2-244 is considered as the standard shape in the design charts presented in the following section. While the standard fragment has a milder nose shape than the alternate fragment, the standard fragment is generally considered appropriate for use in design since: (a) only a small number of fragments will strike the structure nose-on, and (b) only a small fraction of these fragments will have a more severe nose shape than the standard fragment. In addition, the length-to-diameter ratio of these fragments is felt to be more representative of an average fragment configuration. For convenience, a plot of fragment weight versus fragment diameter for these two fragment shapes is given in figure 2-245.

There is little data available concerning the shape of a fragment ejected from a cased explosive where the explosive is not in direct contact with the casing (fig. 2-236). Consequently, the worst possible shape is assumed, a thin rectangular or circular rod. The diameter of the cross-section (the thickness of a rectangular cross-section) is equal to the casing thickness at rupture.

The fragmentation pattern of this type of cased explosive somewhat resembles that of a ruptured pressure vessel. The casing diameter typically expands before rupturing and, therefore, to conserve mass, the casing thickness must be decreased.

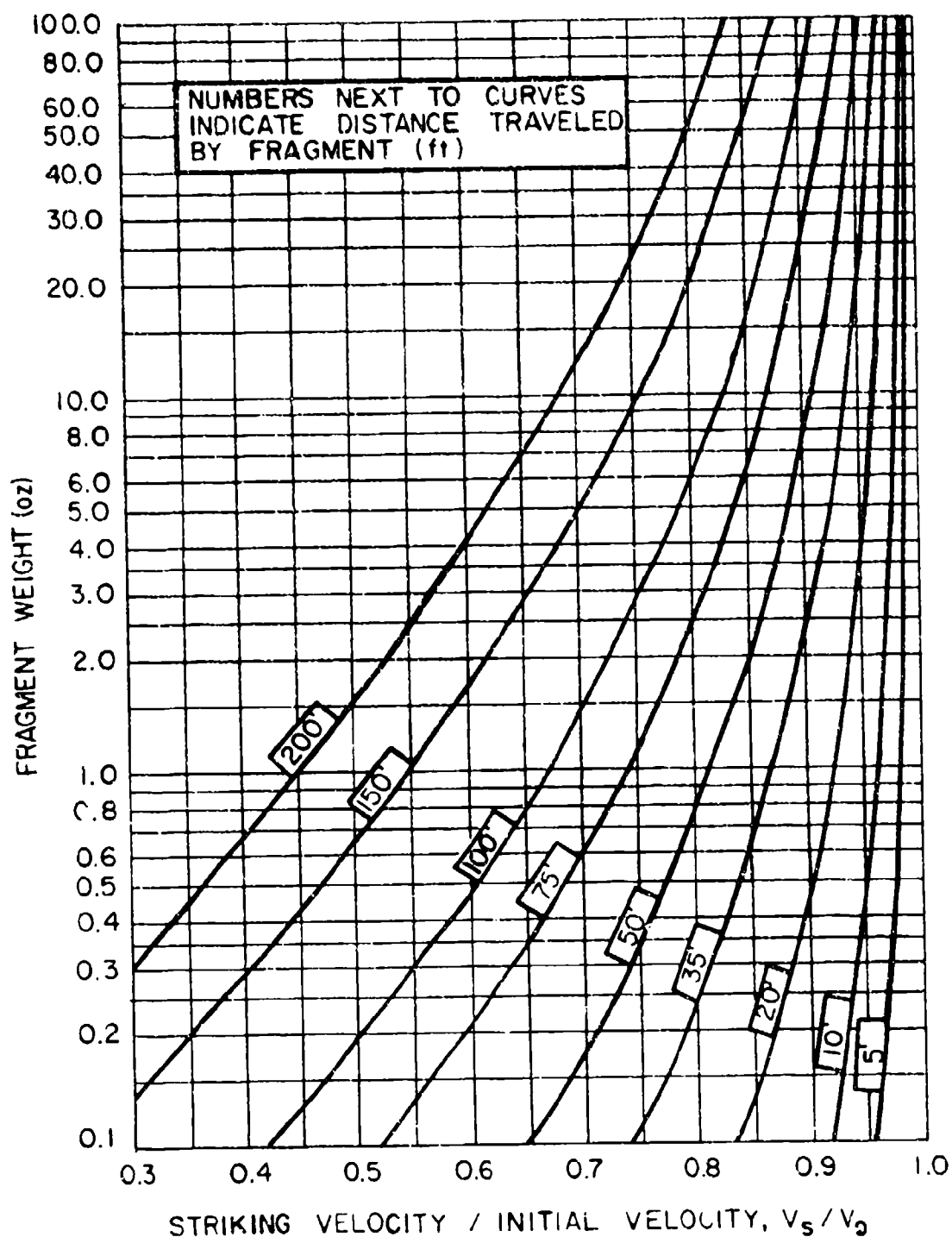
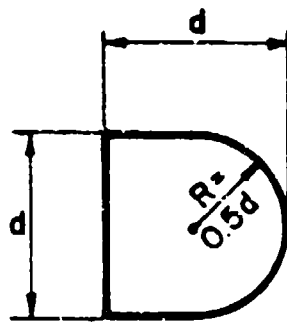
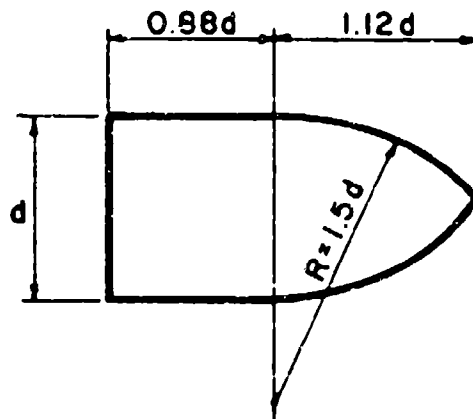


Figure 2-243 Variation of primary fragment velocity with distance



$$\begin{aligned}
 n &= 0.5 \\
 N &= 0.845 \\
 \text{Volume} &= 0.654d^3 \\
 \text{Weight} &= 0.654d^3 \gamma = 0.186d^3 \\
 D &= 0.186 \text{ lb./in.}^3
 \end{aligned}$$

(a) STANDARD FRAGMENT SHAPE



$$\begin{aligned}
 n &= 1.5 \\
 N &= 1.00 \\
 \text{Volume} &= 1.2d^3 \\
 \text{Weight} &= 1.2d^3 \gamma = 0.34d^3 \\
 D &= 0.34 \text{ lb./in.}^3
 \end{aligned}$$

(b) ALTERNATE FRAGMENT SHAPE

NOTE:

$$N = \text{Nose shape factor} = 0.72 + 0.25 \sqrt{n - 0.25}$$

$$n = \text{Caliber radius of the tangent ogive of the fragment nose} = R/d$$

$$D = \text{Caliber density} = W_f / d^3$$

Figure 2-244 Primary fragment shapes

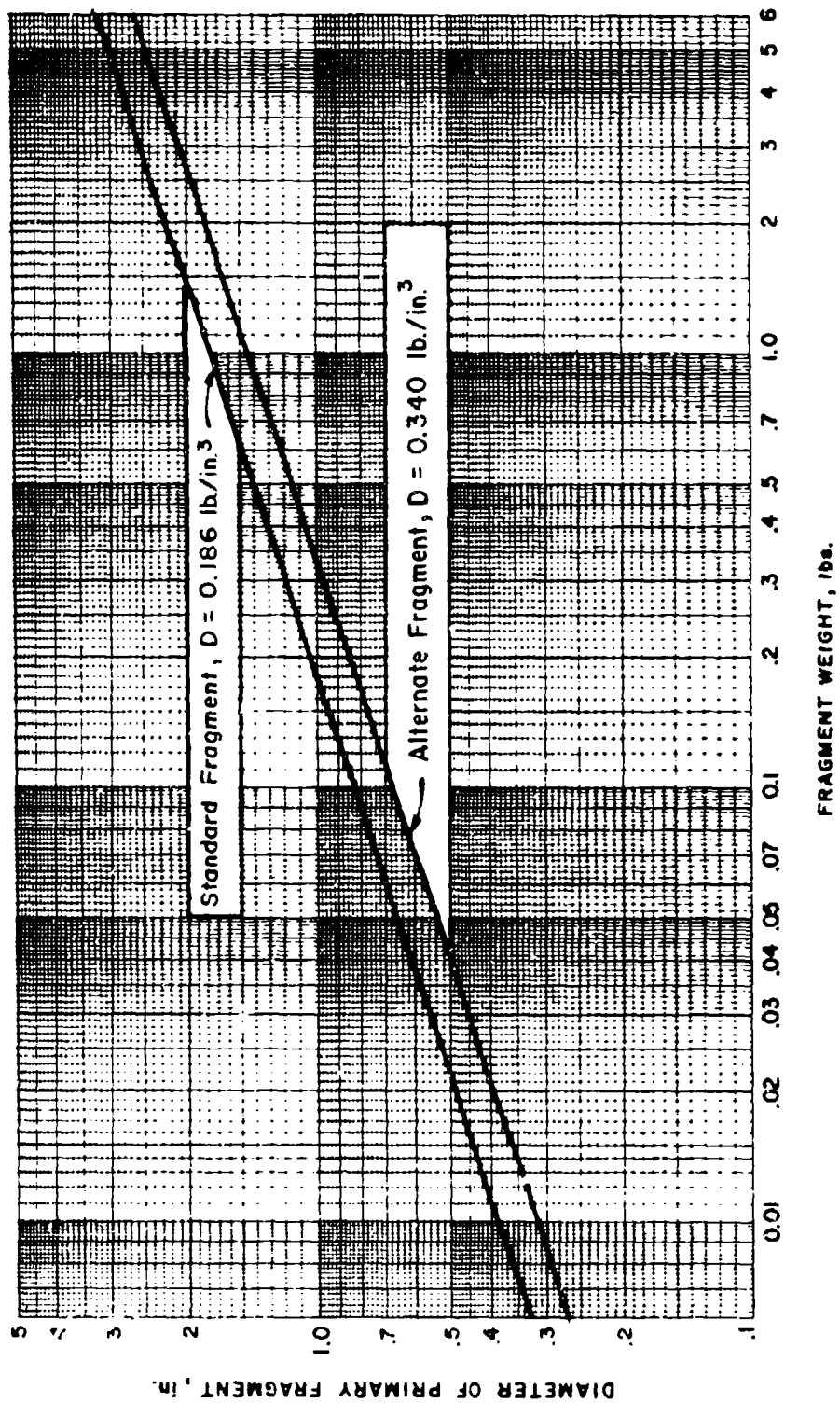


Figure 2-245 Relationship between fragment weight and fragment diameter

It is assumed that the outside diameter expands to 1.5 times the original diameter. Thus, the adjusted inside diameter is:

$$d'_1 = [1.25 (d_1 + 2t_c)^2 + d_1^2]^{1/2} \quad 2-49$$

where:

d'_1 = adjusted inside diameter of casing

d_1 = original inside diameter of casing

t_c = original casing thickness

The adjusted or "necked-down" thickness is:

$$t'_c = 0.75(d_1 + 2t_c) - 0.5d'_1 \quad 2-50$$

where:

t'_c = adjusted casing thickness

Assuming a circular cross-section, the length of the fragment is:

$$L_f = \frac{4W_f}{\pi \rho_c (t'_c)^2} \leq L_{cyl} \quad 2-51$$

where:

L_f = length of the fragment

W_f = weight of the fragment from Section 2-17.3

ρ_c = density of casing material

L_{cyl} = length of the cylinder or equivalent cylinder

If assuming a circular cross-section, the length L_f calculated is longer than the length of the cylinder, then a rectangular cross-section is assumed where the width is equal to:

$$b_f = \frac{W_f}{\rho_c t'_c L_{cyl}} \quad 2-52$$

where:

b_f = width of the fragment

2-17.5.3 Caliber Density. The influence of the fragment weight to fragment diameter ratio is expressed in terms of the caliber density of the fragment which is defined as:

$$D = W_f/d^3 \quad 2-53$$

where:

D = caliber density

d = fragment diameter

2.17.5.4 Nose Shape Factor. The nose shape factor expresses the influence of the shape of the primary fragment and is defined as:

For flat-nosed, solid fragments:

$$N = 0.72 \quad 2-54$$

For fragments with special nose shapes:

$$N = 0.72 + 0.25 (n - 0.2)^{1/2} < 1.17 \quad 2-55$$

where:

N = nose shape factor

n = caliber radius of the tangent ogive of the assumed fragment nose

2-17.5.5 Impact Angle. The angle of obliquity refers to the angle between the path of the fragment and a normal to the surface; thus, a normal impact corresponds to an angle of obliquity of zero degrees. A normal impact is usually assumed in penetration calculations in order to conservatively design for the worst case condition.

2-18 Secondary Fragments

2-18.1 General

The explosion of HE during some manufacturing or forming process (i.e., nitration, centrifuging, pressing, machining on lathe, etc.) can result in a large number of secondary fragments which vary greatly in size, shape, initial velocity and range. Each of these parameters affects the damage potential of an accidental explosion and, therefore, should be considered in the design of protective structures.

The current state-of-the-art for assessing damage potential requires that the design engineer estimate the conditions which are likely to exist at the time of the accident, and perform a structural assessment of any equipment which will be involved. Some of the initial factors to consider are:

1. Type and amount of HE.
2. Configuration of HE (i.e., sphere, cylinder, cased, uncased, etc.).
3. Location of HE (i.e., attached to lathe, resting on support table, contained in centrifuge, proximity to walls and other equipment).
4. Type of propagation after initiation (i.e., high order, burning, partial detonation, etc.).

If the fragmentation pattern varies with the initial conditions, the Architectural Engineer must examine several likely scenarios to evaluate the damage potential.

To estimate the weight, shape, and velocity of fragments which result from detonation of an HE during a manufacturing or forming process, one would perform the following steps:

1. Determine distance (R_i) from the center of the explosive to the i^{th} point of interest (refer to structural details of the machine and/or architectural drawings).
2. Determine the size and shape of the expected fragment (refer to structural details of the machine).
3. Determine the fragment velocity (refer to sections 2-18.2 and 2-18.3).

2-18.2 *Velocity of Unconstrained Secondary Fragments*

To predict velocities of objects accelerated by an explosion, the interaction of blast waves with solid objects must first be considered. Figure 2-246 shows the interaction of a blast wave with an irregular object. The interaction is shown in three phases as the wave passes over the object. As the wave first strikes the object, a portion is reflected from the front face, and the remainder diffracts around the object. In the diffraction process, the incident wave front closes in behind the object, greatly weakened locally, and a pair of trailing vortices is formed. Rarefaction waves sweep across the front face, attenuating the initial reflected blast pressure. After passage of the front, the object is immersed in a time-varying flow field. Maximum pressure on the front face during this "drag" phase of loading is the stagnation pressure.

To predict the effect of a blast wave on the object, it is necessary to examine the net transverse pressure on the object as a function of time. This loading, somewhat idealized, is shown in figure 2-247. After the time arrival t_a , the net transverse pressure rises from zero to a maximum peak reflected pressure P_r in time $(T_1 - t_a)$. For an object with a flat face nearest the approaching blast wave, this time interval is zero. Pressure then falls linearly to drag pressure in time $(T_2 - T_1)$ and decays more slowly to zero in time $(T_3 - T_2)$.

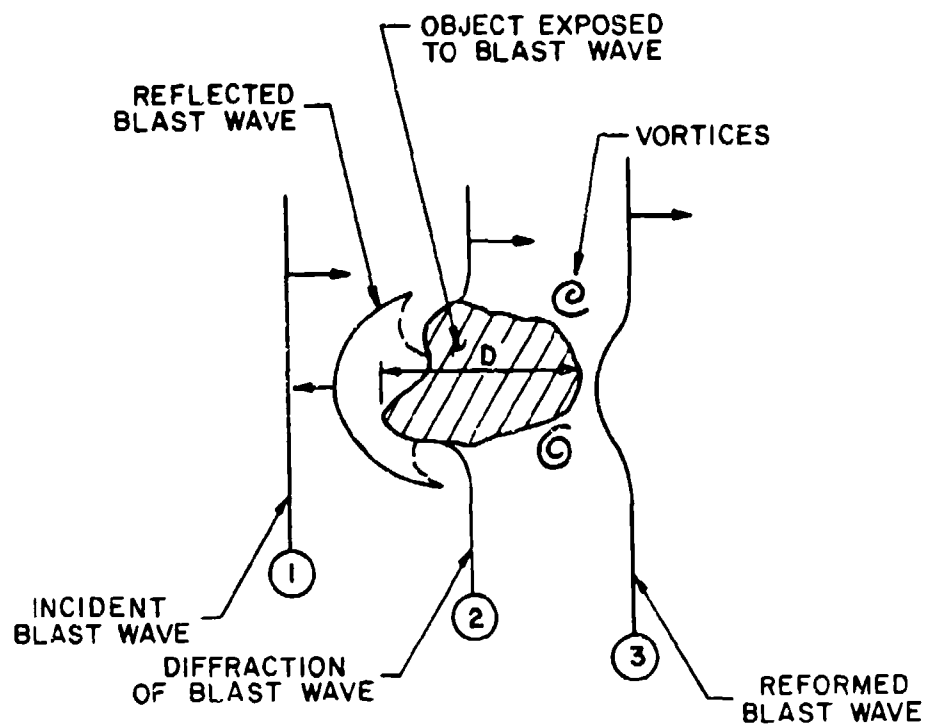


Figure 2-246 Interaction of blast wave with an irregular object

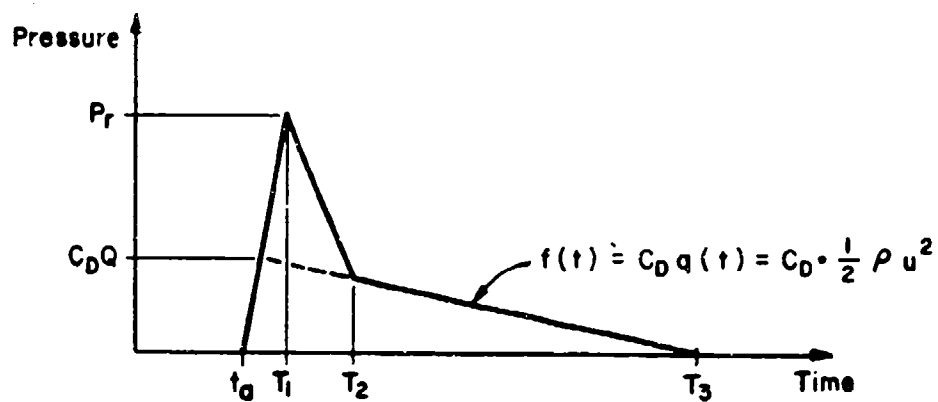


Figure 2-247 Idealized pressure-time loading on an irregular fragment.

The basic assumptions for unconstrained secondary fragments are: (1) the object behaves as a rigid body, (2) none of the energy in the blast wave is absorbed in breaking the object loose from its moorings or deforming it elastically or plastically, and (3) gravity effects can be ignored during the acceleration phase of the motion. The equation of motion of the object is then:

$$A p(t) = Ma \quad 2-56$$

where:

A = area of object presented to blast front

$p(t)$ = pressure-time history of blast wave acting on object

M = mass of object

a = acceleration of object

Rearranging terms and integrating:

$$v(T_3) = \int_{t_a}^{T_3} a dt = \frac{A}{M} \int_{t_a}^{T_3} p(t) dt = \frac{A}{M} i_d \quad 2-57$$

where:

$v(T_3)$ = initial velocity of the object

i_d = total drag and diffraction impulse

The integral in equation 2-57 is the area under the curve of pressure-time relationship. Equation 2-57 can be integrated explicitly if the pressure-time history can be described by suitable mathematical functions or it can be evaluated graphically or numerically if $p(t)$ cannot be easily written in function form.

For intermediate strength shocks, the solution of equation 2-57 can be determined from a rather long equation. For computational purposes that equation is presented here in graphical form as figure 2-248, where:

P_{s0} = peak incident overpressure

p_a = atmospheric pressure

C_D = drag coefficient

i_s = incident specific impulse

a_0 = velocity of sound in air

K = constant (4 if object is on the ground or reflecting surface
and 2 if object is in the air)

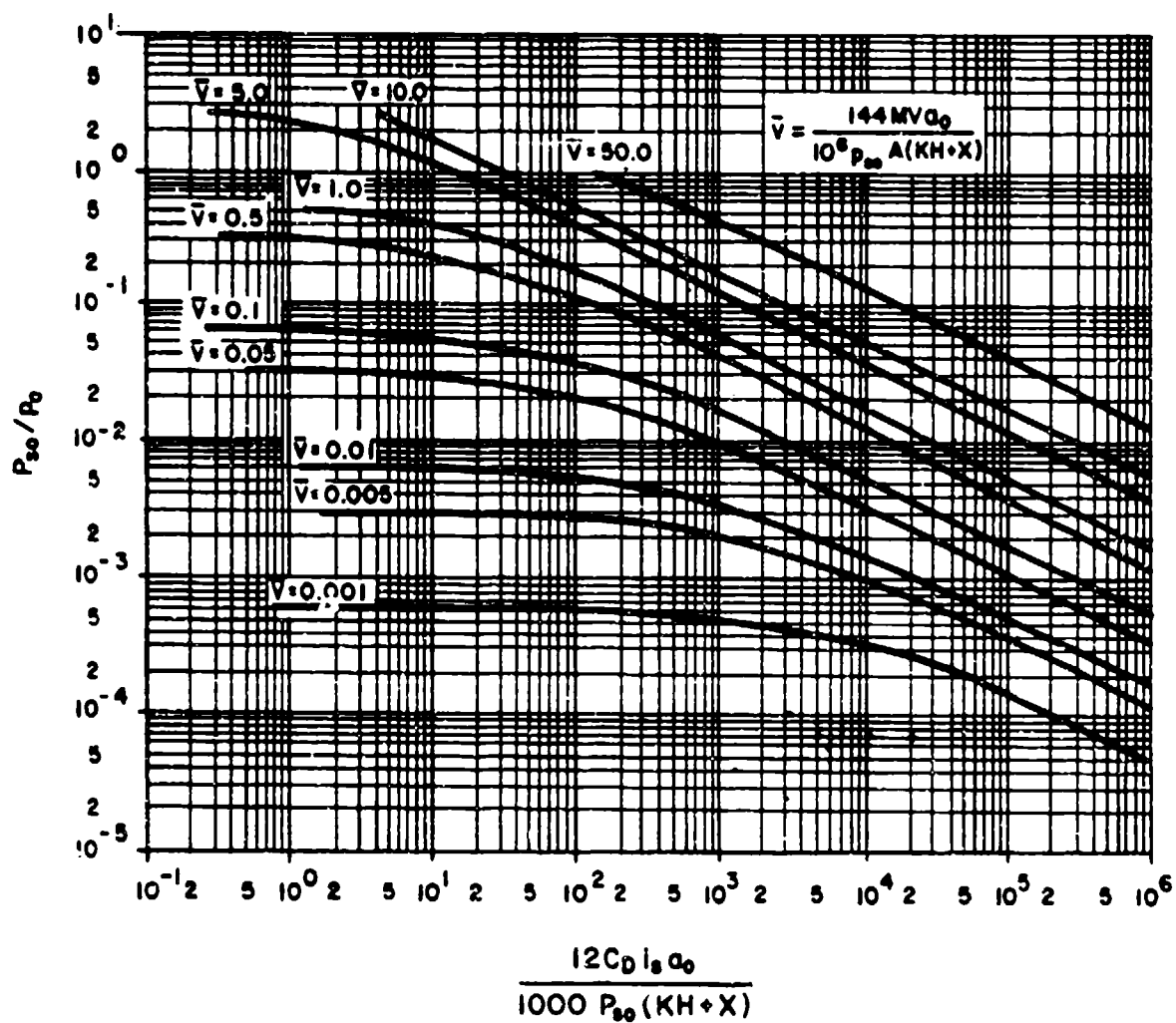


Figure 2-248 Nondimensional object velocity, \bar{V} , as a function of pressure and impulse

H = minimum transverse dimension of the mean presented area of object

X = distance from the front of the object to the location of its largest cross-section normal to the plane of the shock front

M = mass of object

A = mean presented area of object

v_o = initial velocity of object

The peak incident pressure P_s and the incident specific impulse i_s can be determined from figure 2-7 knowing the scaled distance to the object. Values for the drag coefficient C_D for several common shapes are given in table 2-8.

This analysis is appropriate for objects "far" from the explosive charge; thus, the object is not in a high velocity flow field and C_D is essentially a constant. Figure 2-248 can be used in most cases where the distance from the object to the center of a spherical charge is greater than 20 charge radii, which is normally considered to be "far" from the charge. For objects close to a charge, the initial velocity is a function of the impulse on the target, and the actual pressure-time variation across the object is unimportant. For this close-in range the impulse acting on the object is equal to the applied momentum.

$$i = \frac{MV}{AB} \quad 2-58$$

Thus, the velocity in terms of the actual target shape is:

$$v_o = \frac{1000i\beta A}{12M} \quad 2-59$$

where:

i = specific acquired impulse

β = target shape factor from figure 2-249



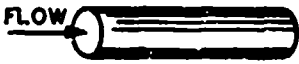
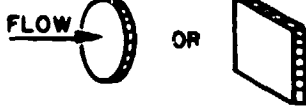





A = area of the target

M = mass of the target

v_o = velocity of the target

To calculate the specific impulse imparted to a close-in target, the following equations were developed based on experimental data:

Table 2-8 Drag Coefficient, C_D , for Various Shapes

| SHAPE | SKETCH | C_D |
|---|--|-------|
| CIRCULAR CYLINDER (LONG ROD), SIDE-ON |  | 1.20 |
| SPHERE |  | 0.47 |
| ROD, END-ON |  | 0.82 |
| DISC, FACE-ON |  | 1.17 |
| CUBE, FACE-ON |  | 1.05 |
| CUBE, EDGE-ON |  | 0.80 |
| LONG RECTANGULAR MEMBER, FACE-ON |  | 2.05 |
| LONG RECTANGULAR MEMBER, EDGE-ON |  | 1.55 |
| NARROW STRIP, FACE-ON |  | 1.98 |

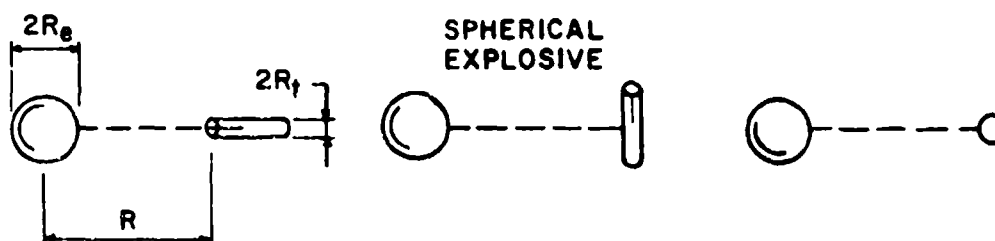
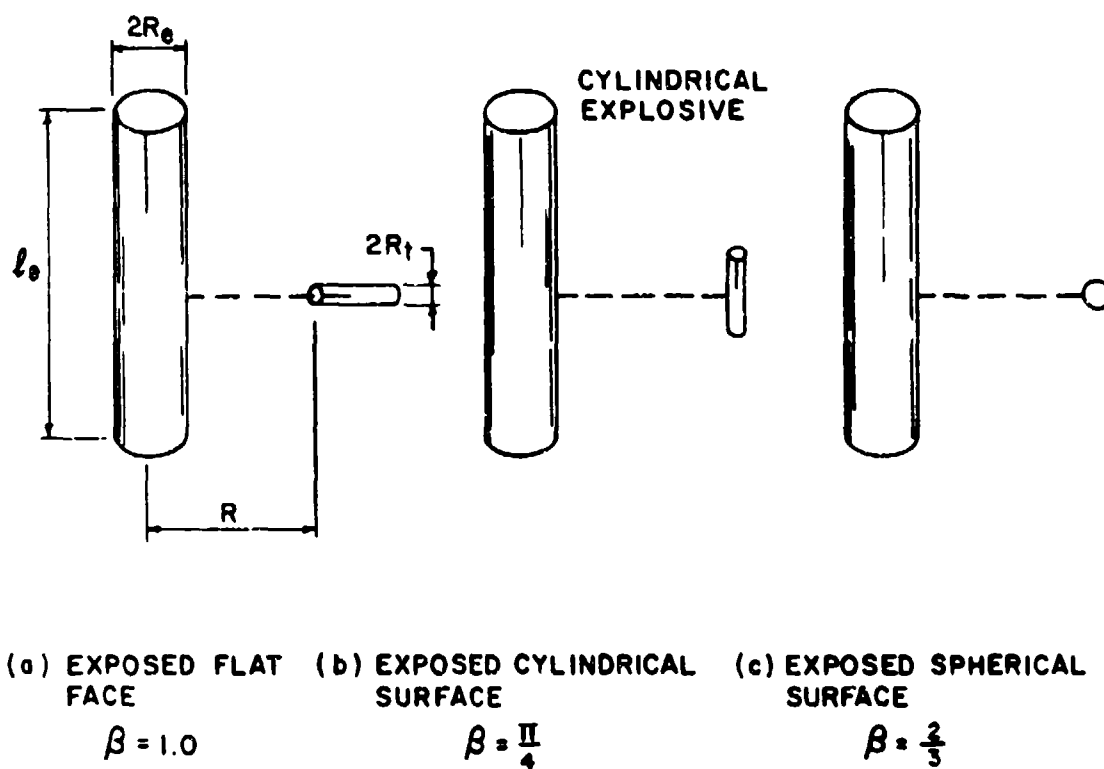


Figure 2-249 Target shape factor for unconstrained fragments

For spherical charges with $R/R_e \leq 5.07$:

$$\frac{1}{\beta R_{\text{eff}}} \left(\frac{R_e}{R_t} \right)^{0.158} = 38,000 \left(\frac{R_e}{R} \right)^{1.4} \quad 2-60$$

and:

$$R_{\text{eff}} = R_e \quad 2-61$$

For cylindrical charges with $R/R_e \leq 5.25$:

$$\frac{1}{\beta R_{\text{eff}}} \left(\frac{R_e}{R_t} \right)^{0.158} = 46,500 \frac{R_e}{R} \quad 2-62$$

For cylindrical charges with $5.25 < R/R_e \leq 10$:

$$\frac{1}{\beta R_{\text{eff}}} \left(\frac{R_e}{R_t} \right)^{0.158} = 161,700 \left(\frac{R_e}{R} \right)^{1.75} \quad 2-63$$

and:

$$R_{\text{eff}} = 0.909 \left(\frac{l_e}{R_e} \right)^{0.333} R_e \quad 2-64$$

where:

i = specific acquired impulse

β = non-dimensional shape factor of the target from figure 2-249

R_{eff} = effective radius

R_e = radius of the explosive

R = standoff distance

R_t = target radius

l_e = length of cylindrical explosive

The effective radius R_{eff} is the radius of an equivalent sphere of explosive which could be formed from a cylinder of radius R_e and length l_e .

The specific impulse imparted to a target, as given by equations 2-60, and 2-62 and 2-63 for spherical and cylindrical charges respectively, is plotted in figure 2-250. This experimentally derived data should not be used beyond the distances shown on the figure. When these standoff distances are exceeded, the specific acquired impulse may be approximated by using the normal reflected impulse obtained from figure 2-7.

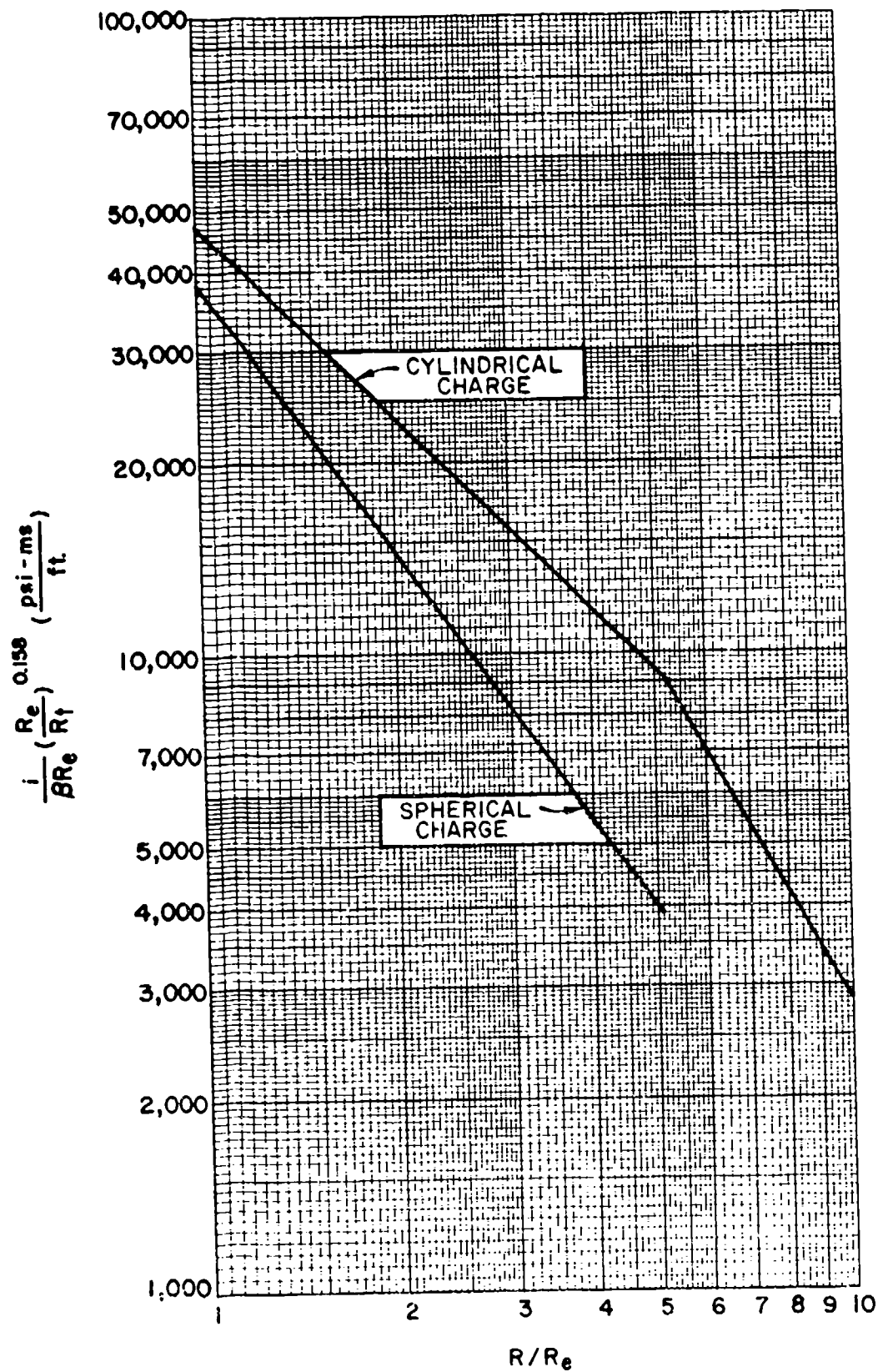


Figure 2-250 Specific acquired impulse versus distance

2-18.3 Velocity of Constrained Secondary Fragments

The method used to predict initial velocities of a constrained secondary fragments close to an explosion must first consider the amount of energy applied to each fragment as well as the energy consumed in freeing the fragment from its support. This relationship can be expressed using the conservation of momentum and allowing the structural constraint to reduce the imparted impulse, as follows:

$$I - I_{st} = mV_o \quad 2-65$$

where:

I = total impulse of the blast applied to the fragment

I_{st} = impulse consumed by the fragment support connection

m = mass of the fragment

V_o = velocity of the fragment after break away

The value of I_{st} must be established experimentally. Based on tests, an empirical expression has been developed for cantilever beams subjected to close-in effects:

$$v_o = \frac{1000}{12} \left[\frac{T}{\rho_f} \right]^{1/2} \left\{ C_1 + C_2 \left[\frac{ib_f}{A (\rho_f T)^{1/2}} \right] \left[\frac{2L_f}{b_f} \right]^{0.3} \right\} \quad 2-66$$

where:

T = toughness of material (area under the stress-strain curve)
from table 2-9

ρ_f = mass density of the fragment

i = unit impulse acting on the member

b_f = width of fragment exposed to the blast

L_f = length of fragment exposed to the blast

A = cross-sectional area in the plan perpendicular to the long axis of the fragment

C_1 = constant equal to -0.2369

C_2 = constant equal to +0.3931

Equation 2-66 is adequate for determining the fragment velocity, when:

$$\left[\frac{1b_f}{A (\rho_f T)^{1/2}} \right] \left[\frac{2L_f}{b_f} \right]^{0.3} \geq 0.602$$

2-67

When equation 2-67 is less than 0.602, the magnitude of the velocity is equal to zero which indicates that disengagement of the fragment will not occur.

The constants in equation 2-66 were derived from experimental data and can only be used for cantilevered beams of steel or aluminum.

An equation similar to that of equation 2-66 has been developed for clamped-clamped fragments except that the value of C_1 is equal to -0.6498 and C_2 is equal to 0.4358.

A plot of equation 2-66 for both cantilever and clamped-clamped fragments is presented in figure 2-251.

Table 2-9 Steel Toughness

| <u>Steel</u> | <u>Toughness in-lb/in³</u> |
|-------------------|---------------------------------------|
| ASTM A 36 | 12,000 |
| ASTM A 441 | 15,000 |
| ASTM A514 Grade F | 19,000 |

2-19 Fragment Trajectories

Once primary fragments or secondary missiles have been formed and accelerated by an explosion, they will move along a specific trajectory until they impact a target (receiver), or the ground. The forces acting on the fragments and affecting their trajectories are inertia, gravitation, and fluid dynamic forces. The fluid dynamic forces are determined by the instantaneous velocity of the fragment at each instant in time. Generally, fragments are quite irregular in shape and may be tumbling, so a completely accurate description of the fluid dynamics forces during flight is difficult, if not impossible. In the trajectory analysis for fragment flight, one usually resorts to some simplified description of the fluid dynamic forces, and uses the concepts from aerodynamics of division of these forces into components called drag (along the trajectory or normal to the gravity vector) and lift (normal to the trajectory or opposing gravity). Then the force components are given at any instant by:

$$F_L = C_L A_L (1/2) \rho v^2 \quad 2-68$$

and

$$F_D = C_D A_D (1/2) \rho v^2 \quad 2-69$$

where:

$$F_L = \text{lift force}$$

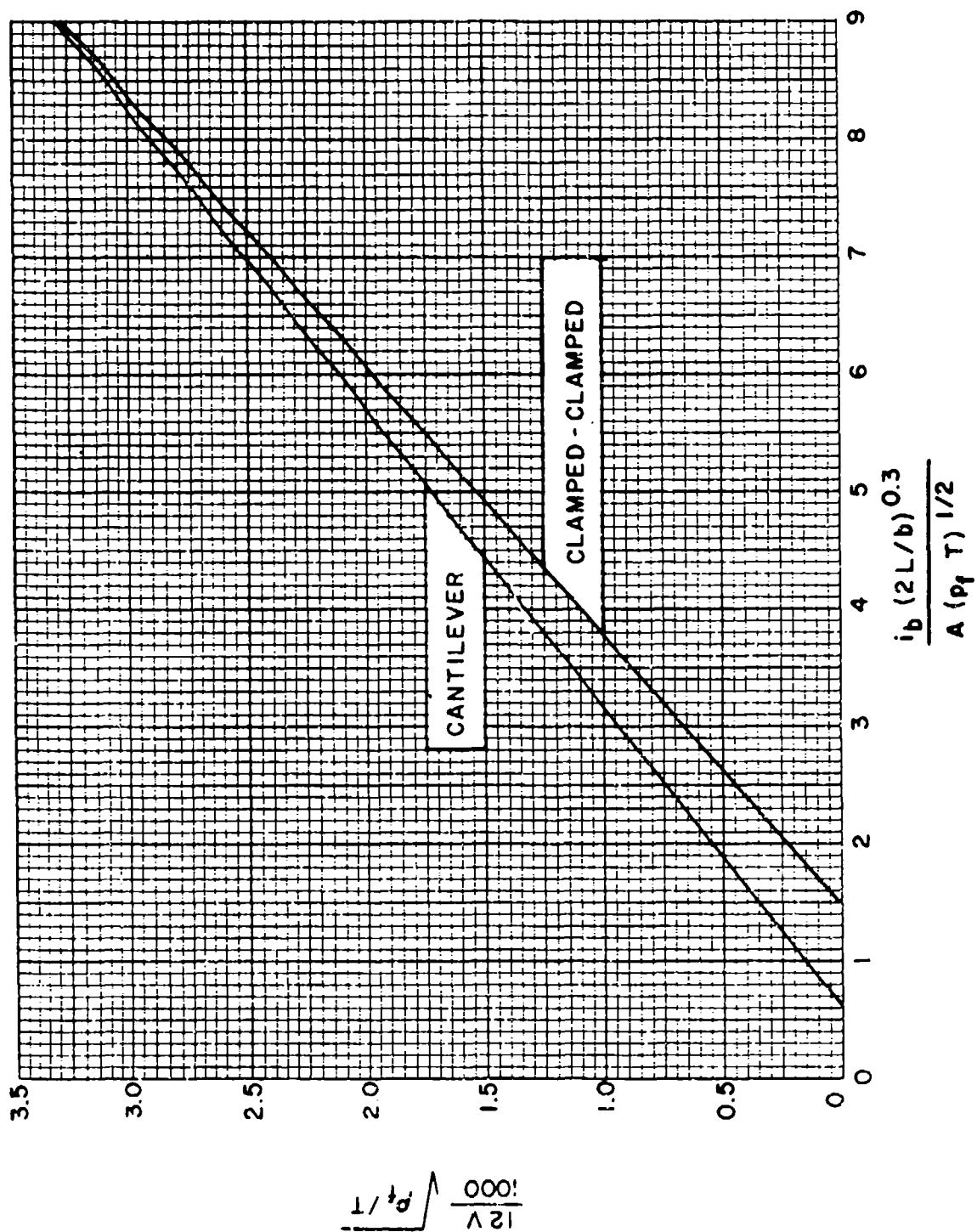


Figure 2-251 Scaled fragment velocities for constrained fragments

F_D = drag force

C_L = lift coefficient

C_D = drag coefficient

A_L = lift area

A_D = drag area

ρ = density of the medium through which the fragment is traveling

v = velocity of the fragment

The lift and drag coefficients are determined empirically as a function of shape and orientation with respect to the velocity vector, and the magnitude of the velocity v . Fragments discussed in sections 2-17 and 2-18 are generally of chunky shape, so that $C_D \gg C_L$ for any flight orientation. Thus, they are called drag-type fragments. The lift force on drag-type fragments is very small and may be neglected.

In a simplified trajectory problem, where the fragment is considered to move in one plane, equations of motion can be written for acceleration in the X and Y directions.

The acceleration in the X direction (drag only) is:

$$a_x = - \frac{A_D C_D \rho_0 (v_x^2 + v_y^2)}{2M} \cos \alpha \quad 2-70$$

and for the Y direction (drag only):

$$a_y = - 1.2 \times 10^{-5} g - \frac{A_D C_D \rho_0 (v_x^2 + v_y^2)}{2M} \sin \alpha \quad 2-71$$

where:

a_x, a_y = acceleration in the X and Y directions, respectively

ρ_0 = mass density of the medium through which the fragment travels

v_x, v_y = velocity in the X and Y directions, respectively

g = gravity force (32.2 ft./sec.²)

M = mass of the fragment

α = trajectory angle

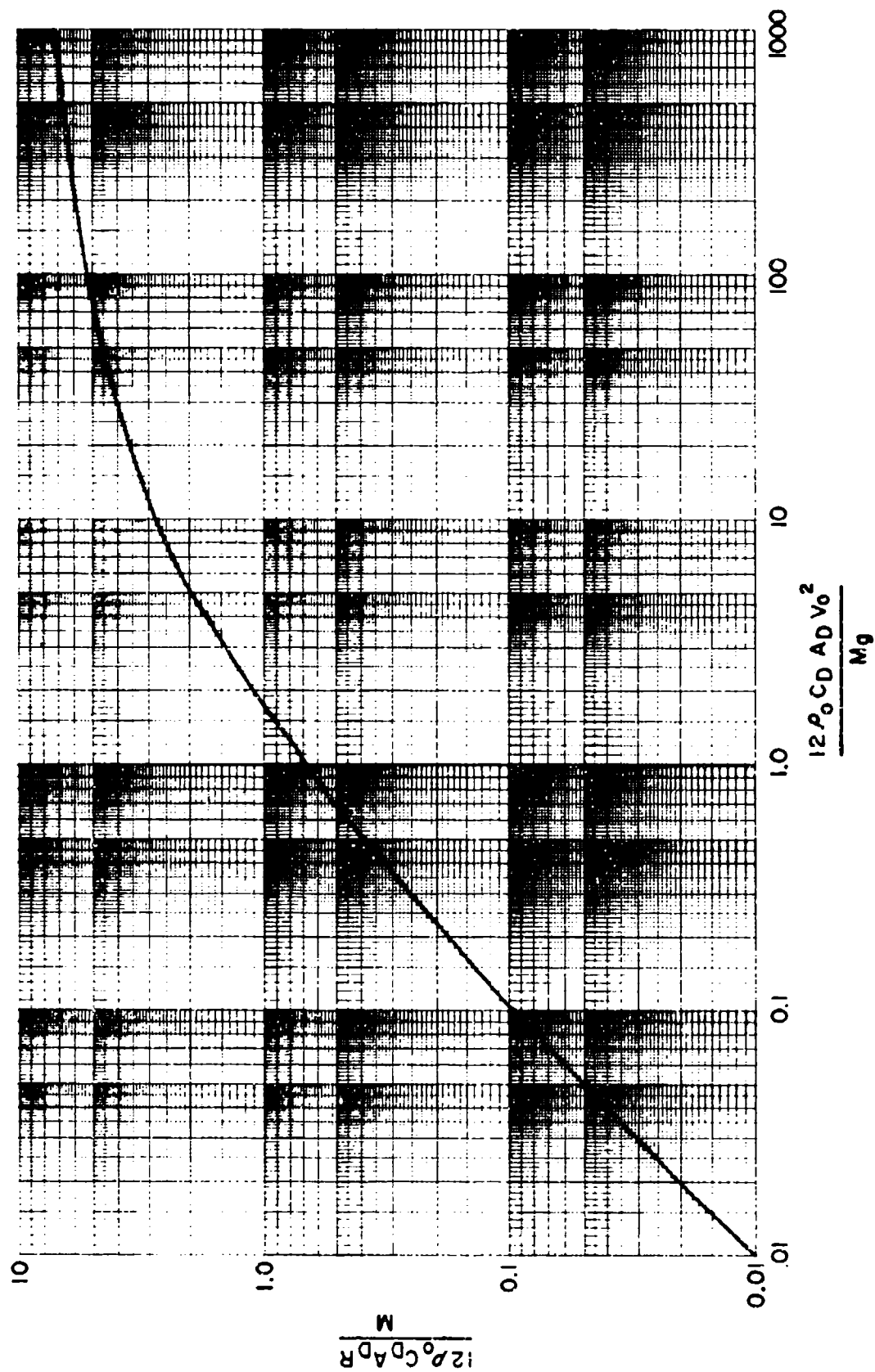


Figure 2-252 Fragment range prediction

At $t = 0$:

$$v_x = v_0 \cos \alpha_0 \quad 2-72$$

$$v_y = v_0 \sin \alpha_0 \quad 2-73$$

where:

v_0 = initial velocity

α_0 = initial trajectory angle

The equations shown above can be solved simultaneously to eventually determine the distance traveled by the fragment. These equations are valid for fragment velocities up to Mach 1 for standard conditions. Figure 2-252 summarizes the results of fragment range R for numerous sets of initial conditions for fragments affected only by drag forces. It should be noted that, in this curve, several initial trajectory angles were used in the analysis to obtain the maximum range R for the respective fragments. Thus, one need not know the initial trajectory angle of a fragment in order to use figure 2-252.

SHOCK LOADS

2-20 Introduction

The strong air blast waves and high speed fragments are the primary hazards of accidental explosions. The exterior of a protective structure is designed primarily for the blast pressures. In some situations, the fragments may be just as important as the pressures in determining the configuration of a protective facility. While the contents of the structure are protected from the direct effects of blast pressures and fragments by the structure's exterior, the contents are subject to effects of the building's motion. These structure motions can cause injury to personnel, damage to equipment as well as dislodgement of the structure's interior components including interior partitions, hung ceilings, light fixtures, ductwork, piping, electrical lines, etc.

Structure motions are caused by what is normally termed shock loads. These are loads which cause transient or short-duration vibratory motions of the ground surface and the structure. They do not cause significant structural damage but instead induce motion which, as stated above, can damage the structure's interior contents.

There are two distinct types of shock loads: ground shock and air shock. Ground shock results from the energy which is imparted to the ground by an explosion. Some of this energy is transmitted through the ground as direct-induced ground shock. Both of these forms of ground shock when imparted to a structure will cause the structure to move in both a vertical and horizontal direction. Air shock results from the blast overpressures striking the building. Vertical, horizontal and overturning motions result from the shock impact. The vertical and overturning motions are usually not significant and can be neglected while the horizontal motions must be considered. Large displacements can result when a structure slides relative to the ground surface.

The net motion of the structure is a combination of the motions due to the air induced and direct-induced ground shock, and the air shock. Curves which describe the ground motion (acceleration versus time, velocity versus time, and displacement versus time curves) are not readily calculated. However, these relationships are not required since the design of protective structures to resist shock loads is based on the peak values of the induced motion rather than the actual motion-time relationships.

The procedures presented in this section are applicable for uniform motions. The shock loads and resulting structure motions apply to rigid concrete structures located at the low- and intermediate-pressure design ranges. At distances corresponding to these pressures, the shock loads are uniform across the structure. A rigid concrete structure acts as a rigid body, that is, all components of the structure have essentially the same motion. The procedures can be applied to structures located close to an explosion and to non-rigid structures. However, the local effects associated with these conditions must be accounted for in the analysis.

2-21 Ground Shock

2-21.1 Introduction

When an explosion occurs at or near the ground surface, ground shock results from the energy imparted to the ground by the explosion. Some of this energy is transmitted through the air in the form of air-induced ground shock and some is transmitted through the ground as direct-induced ground shock.

Air-induced ground shock results when the air-blast shock wave compresses the ground surface and sends a stress pulse into the underlying media. The magnitude and duration of the stress pulse in the ground depends on the character of the air-blast pulse and the ground media. Generally, the air-induced ground motions are downward. They are maximum at the ground surface and attenuate with depth. However, the presence of a shallow water table, a shallow soil-rock interface, or other discontinuities can alter the normal attenuation process. The properties of the incident overpressure pulse and the surface soil layer usually determine the character of air-induced ground shock on aboveground structures.

Direct-induced ground shock results from the explosive energy being transmitted directly through the ground. This motion includes both the true direct-induced motions and cratering-induced motions. The latter generally have longer durations and are generated by the crater formation process in cratering explosions. The induced ground motion resulting from both types have a longer duration than air-blast-induced ground shock and the waveforms tend to be sinusoidal.

The net ground shock experienced by a point on the ground surface is a combination of the air-blast-induced and direct-induced shock. The relative magnitudes and sequencing of the motions are functions of the media (air and soil) through which the shock travels and the distance from the point of detonation. At ranges close to the blast, the highly compressed air permits the air-blast-shock front to propagate at speeds greater than the seismic velocity of the ground. In this region, the super-seismic region, the air blast arrives at a given point before the direct-induced ground shock. As the air-blast shock

front moves farther from the point of detonation, the shock front velocity decreases, and the direct-induced ground shock catches and "outruns" the air blast. This latter region is called the outrunning region. Waveforms in the outrunning region are generally a complex combination of both types of induced shock. The combined motion can be obtained from consideration of the arrival time of each wave. The arrival time of the air blast is determined from the data presented for unconfined explosions. Whereas, the arrival time of the direct-induced ground shock can be estimated by assuming that the ground shock travels at the seismic velocity of the ground media. The combined ground motion in both the superseismic and outrunning region are illustrated in figure 2-253.

2-21.2 Air Blast-Induced Ground Shock

One-dimensional wave propagation theory is used to estimate air blast-induced ground shock. For surface structures located on ground media having uniform properties, the expressions to define this motion take very simple forms. Using this approach, the maximum vertical velocity at the ground surface, V_V , can be expressed as

$$V_V = \frac{P_{s0}}{\rho C_p} \quad 2-74$$

where

V_V = maximum vertical velocity of the ground surface

P_{s0} = peak positive incident pressure (fig. 2-15)

ρ = mass density of the soil

C_p = compression wave seismic velocity in the soil

The mass density, ρ , for typical soils and rock are presented in table 2-10 while the seismic velocities are presented in table 2-11.

The maximum vertical displacement, D_V , is obtained by integrating the above expression with respect to time. The integral of the pressure with respect to time is simply the total positive phase impulse, so that:

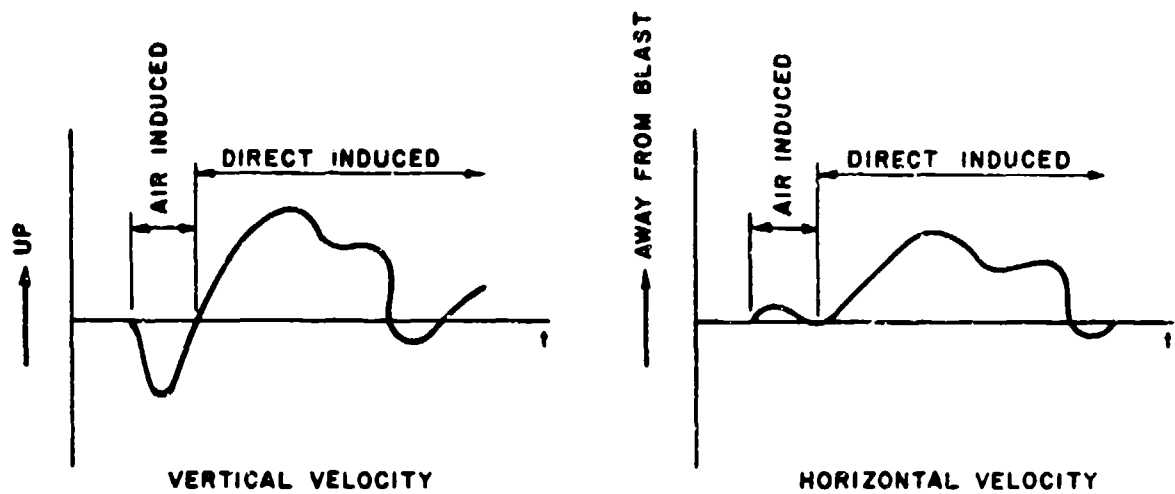
$$D_V = \frac{i_s}{1,000 \rho C_p} \quad 2-75$$

where

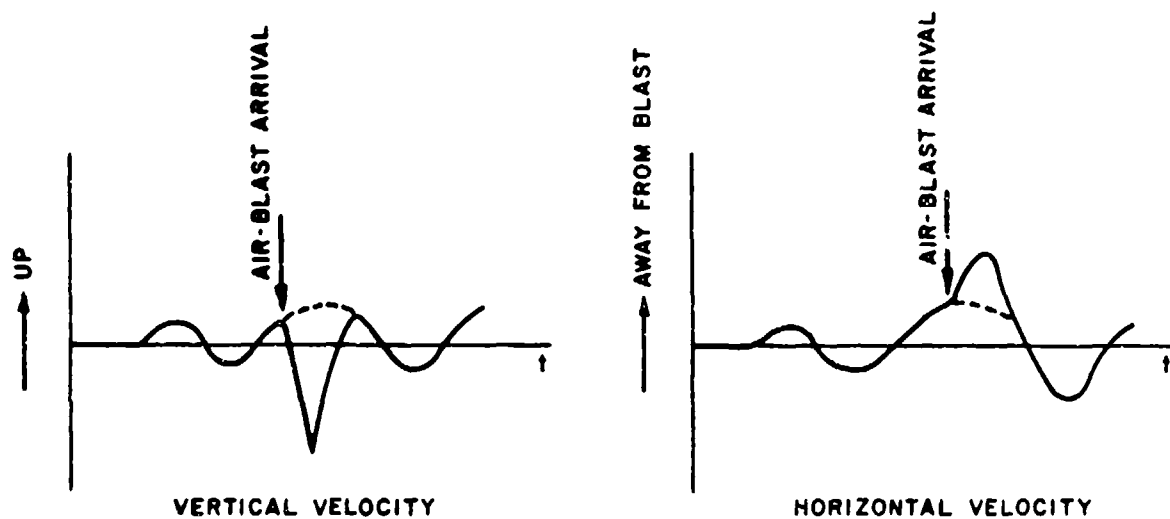
D_V = maximum displacement of the ground surface

i_s = unit positive incident impulse (fig. 2-15)

The maximum vertical acceleration, A_V , is based on the assumption of a linear velocity increase during a rise time equal to one millisecond. The resulting



(a) SUPERSEISMIC GROUND SHOCK



(b) OUTRUNNING GROUND SHOCK

Figure 2-253 Net ground motions produced by an explosion at the ground surface

Table 2-10 Mass Density for Typical Soils and Rocks

| Material | Mass Density, ρ (lb-sec ²)/in. ⁴ |
|-----------------------|---|
| Loose, dry sand | 1.42×10^{-4} |
| Loose, saturated sand | 1.79×10^{-4} |
| Dense, dry sand | 1.65×10^{-4} |
| Dense, saturated sand | 2.02×10^{-4} |
| Dry clay | 1.12×10^{-4} |
| Saturated clay | 1.65×10^{-4} |
| Dry, sandy silt | 1.57×10^{-4} |
| Saturated, sandy silt | 1.95×10^{-4} |
| Basalt | 2.56×10^{-4} |
| Granite | 2.47×10^{-4} |
| Limestone | 2.25×10^{-4} |
| Sandstone | 2.10×10^{-4} |
| Shale | 2.17×10^{-4} |
| Concrete | 2.25×10^{-4} |

Table 2-11 Typical Seismic Velocities for Soils and Rocks

| Material | Seismic Velocity |
|------------------------------|-------------------------|
| | in./sec |
| Loose and dry soils | 7,200 to 39,600 |
| Clay and wet soils | 30,000 to 75,600 |
| Coarse and compact soils | 36,000 to 102,000 |
| Sandstone and cemented soils | 36,000 to 168,000 |
| Shale and marl | 72,000 to 210,000 |
| Limestone-chalk | 84,000 to 252,000 |
| Metamorphic rocks | 120,000 to 252,000 |
| Volcanic rocks | 120,000 to 270,000 |
| Sound plutonic rocks | 156,000 to 300,000 |
| Jointed granite | 9,600 to 180,000 |
| Weathered rocks | 24,000 to 120,000 |

acceleration is increased by 20 percent to account for nonlinearity during the rise time. Accelerations are expressed in multiples of the gravitational constant, so that,

$$A_V = \frac{100 P_{so}}{\rho C_p g} \quad 2-76$$

where

A_V = maximum vertical acceleration of the ground surface

g = gravitational constant equal to 32.2 ft/sec²

The above equation is adequate for predicting the acceleration in dry soil. However, the equation underestimates the acceleration in saturated soils and rock. To approximate the acceleration of saturated soils and rock, it is recommended that the value of the acceleration obtained from the equation 2-76 be doubled.

The maximum horizontal ground motions are expressed in terms of the maximum vertical motions as a function of the seismic velocity of the soil and the shock wave velocity, so that

$$D_H = D_V \tan [\sin^{-1} (C_p/12,000 U)] \quad 2-77$$

$$V_H = V_V \tan [\sin^{-1} (C_p/12,000 U)] \quad 2-78$$

$$A_H = A_V \tan [\sin^{-1} (C_p/12,000 U)] \quad 2-79$$

where U = shock front velocity (fig. 2-15).

For $(C_p/12,000 U)$ greater than one, horizontal and vertical motions are approximately equal. Therefore, it is recommended that for all values of the above function greater than one, the horizontal motion is set equal to the calculated vertical motion.

The equations which describe the air-induced ground shock are a function of the density and seismic velocity of the soil. However, a wide range of seismic velocities is given in table 2-11 for each of the soils listed. In a final design, soil tests are required to accurately determine the density and seismic velocity of the particular soil at the site. In lieu of tests, the mass density given in table 2-10 may be used. However, since the range of seismic velocities given table 2-11 is so large, it is recommended that the lower bound value of the velocity be used to produce a conservative estimate of the induced motion.

2-21.3 Direct-Induced Ground Motion

Empirical equations have been developed to predict direct-induced ground motions. The equations apply for TNT detonations at or near the ground surface. Three types of ground media have been considered; dry soil, saturated soil and rock. The ground shock parameters are expressed in terms of the charge weight and distance from the explosion.

The maximum vertical displacement, D_V , of the ground surface for a rock media is given by

$$D_V = \frac{0.025 R_G^{1/3} W^{1/3}}{Z_G^{1.3}} \quad 2-80$$

in which

$$Z_G = \frac{R_G}{W^{1/3}} \quad 2-81$$

where

R_G = ground distance from the explosion

W = weight of TNT charge

Z_G = scaled distance from the explosion

and the maximum horizontal displacement, D_H of the ground surface is equal to one-half of the maximum vertical displacement or

$$D_H = 0.5 D_V \quad 2-82$$

When the ground media consists of either dry or saturated soil, the maximum vertical displacement is given by

$$D_V = \frac{0.17 R_G^{1/3} W^{1/3}}{Z_G^{2.3}} \quad 2-83$$

while the maximum horizontal displacement D_H is equal to the maximum vertical displacement or,

$$D_H = D_V \quad 2-84$$

The maximum vertical velocity, V_V , for all ground media is given by

$$V_V = \frac{150}{Z_G^{1.5}} \quad 2-85$$

and the maximum horizontal velocity, V_H , is equal to the maximum vertical velocity for all ground media or

$$V_H = V_V \quad 2-86$$

Finally, the maximum vertical acceleration, A_V , of the ground surface for all media is given by

$$A_V = \frac{10,000}{W^{1/3} Z_G^2} \quad 2-87$$

while for dry soil, the maximum horizontal acceleration, A_H , is equal to one-half of the maximum vertical acceleration, or

$$A_H = 0.5 A_V \quad 2-88$$

however, for a wet soil or a rock media, the horizontal and vertical acceleration is equal, or

$$A_H = A_V \quad 2-89$$

2-22 Air Shock

2-22.1 Introduction

When an air blast strikes an above ground protective structure, motions are imparted to the building. The most severe motion is due to the response of the individual elements which make up the exterior shell of the structure. Procedures for the design of these elements are presented in subsequent volumes of this manual. This section is concerned with the gross motion of the structure on its supporting soil due to the impact of the air blast. This gross motion is in addition to the ground induced motions.

Vertical, horizontal and overturning motions are imparted to the structure by the air blast. However, since the vertical motion of the structure is restricted by the ground which is already compressed due to the dead load of the structure and its contents, vertical motions must necessarily be small and can be safely neglected. Overturning motions are also neglected in this section. These motions are most significant in tall structures with small plan dimensions which are not common in protective construction. This section is concerned solely with horizontal sliding motions which can be quite significant.

Horizontal motion results from an unbalanced blast load acting on the structure. The tendency of the structure to slide is resisted by the friction forces developed between the foundation and the underlying soil. For structures with deep foundations, additional resistance to sliding is afforded by active and passive soil pressures developed at the leeward side of the structure.

2-22.2 Method of Analysis

The gross horizontal motion of a structure is computed in this manual using a method of numerical integration, namely, the acceleration-impulse extrapolation method. This method of dynamic analysis is comprehensively presented in Volume III. Briefly, the equation of motion for a single-degree-of-freedom system is given as

$$F - R - D = Ma$$

2-90

where

F = applied blast load as a function of time

R = resistance of the system to motion as a function of displacement

D = damping force as a function of velocity

M = mass of the single-degree-of-freedom system

a = acceleration of the system

The numerical method of solving the equation of motion involves a step-by-step integration procedure. The integration is started at time zero where the displacement and velocity are known to be zero. The time scale is divided into small intervals. The values of F, R and M (D is not included) are calculated for each time step. The integration is started by first approximating the acceleration for the first time interval and progresses by successively calculating the acceleration at each time step. The change in velocity and displacement associated with each incremental acceleration is calculated. The accumulated velocity and displacement is obtained for each time step until the maximum values have been obtained.

The first step in the analysis is to describe the blast loads acting on the structure. The pressure-time variation of the blast load is computed as the shock front sweeps across the structure. The unbalanced load in the horizontal direction is computed as a function of the blast loads acting on the front and back walls (windward and leeward walls), respectively. The average blast load action of the roof of the structure is computed as the shock front traverses the building. The procedure used to describe these loading conditions have been presented in previous sections of this volume.

The second step in the problem is the determination of the resistance of the building to horizontal motion. The tendency of the base of the structure to slide is resisted by friction forces on the foundation and earth pressure at the rear (leeward side) of the structure. For structures with shallow foundations, the resistance to sliding is afforded primarily by friction between the horizontal surfaces of the concrete foundation and underlying soil. The earth pressure resistance at the rear of the structure is small and can be conservatively neglected. For structures with deep foundations, the passive pressure at the rear of the structure is significant and greatly reduces the displacement of the building.

The friction force developed between the horizontal surfaces of the concrete foundation and underlying soil is given by

$$F_f = \mu F_N$$

2-91

where

- F_f = frictional force resisting horizontal motion
- μ = coefficient of friction between concrete and type of supporting soil
- F_N = vertical load supported by the foundation

The coefficient of friction, μ , for the horizontal surface between the concrete foundation and the underlying soil is given in Table 2-12 for various types of soil. The coefficient is not a function of time or displacement. However, the structure must slide a finite amount before the frictional force is generated. The structure should slide approximately one-quarter of an inch before the frictional force is taken into account.

The vertical load, F_N supported by the foundation consists of the dead weight of the structure, the weight of the building's interior contents, and the blast load acting on the roof of the structure. Since the blast load is a function of time, the building's resistance to sliding (frictional force F_f) is also a function of time. In addition, the blast load acting on the roof greatly increases the foundation loads, and consequently, significantly increases the building's resistance to sliding.

2-23 Structure Motions

2-23.1 Introduction

The net motion of a structure is a combination of the motions due to the air-induced and direct-induced ground shock, and the air shock. Since the methods of analysis described in this section are applicable to rigid concrete structures located at comparatively large distances from an explosion, the structure motions are taken equal to the ground motions in the vicinity of the building. In the case of air shock, the structure motions are computed directly.

The motion of structures located at comparatively close distances to an explosion as well as the motion of non-rigid structures may be determined. However, the local effects associated with these conditions such as motions due to cratering, fragment impact, etc. must be accounted for in the determination of the structure motions.

2-23.2 Net Ground Shock

The net ground shock associated with an accidental explosion is a combination of the air-induced and direct-induced ground shock. The time at which the shock is felt at adjacent structures and the magnitude and duration of the motion is a function of the quantity of explosives detonating, the absolute distance between the detonation and adjacent structure and the soil media at the site.

The air-induced ground shock is a function of the air blast. Consequently, the arrival time and duration of the ground shock may be taken equal to the arrival time t_A and duration t_O of the air blast. For an explosion occurring at or near the ground surface, the arrival time and duration are obtained from figure 2-15 for the scaled ground distance Z_G between the explosion and the structure. Figure 2-15 provides the blast parameters associated with the detonation of hemispherical TNT charge located on the ground surface.

The direct-induced ground shock is a function of the soil media. The arrival time of the shock load at the structure is a function of the seismic velocity in the soil and the distance from the explosion. The arrival time is expressed as

$$t_{AG} = \frac{12,000 R_G}{C_p} \quad 2-92$$

where t_{AG} = arrival time of the ground shock

R_G = ground distance from the explosion

C_p = compression wave seismic velocity in the soil (table 2-11)

As previously explained, the seismic velocity of the soil should be obtained from soil tests for a final design. In lieu of tests, it is recommended that the entire range of velocities given in table 2-11 be investigated to determine if the direct-induced ground shock can be in phase with the air-induced ground shock.

The actual duration of the shock load is not readily available. However, it is sufficient to realize that the duration is long, that is, many times larger than the duration of the air-induced shock.

The net ground shock is obtained from consideration of the arrival time and duration of each type of induced shock. If $t_A + t_O$ is less than t_{AG} , the structure is subjected to superseismic ground shock (fig. 2-253). The air induced ground shock arrives at the structure first and is dissipated by the time that the direct-induced ground shock arrives. The structure feels the effect of each shock separately. If t_A is greater than t_{AG} , the structure is subjected to outrunning ground shock (fig. 2-253). The direct-induced ground shock arrives at the structure first and, since its duration is long, the air-induced ground shock will arrive at the structure while the direct-induced ground shock is still acting. The structure feels the combined effects of the induced shocks. If t_A is slightly less than t_{AG} and $t_A + t_O$ is greater than t_{AG} , the air-induced ground shock will still be acting when the direct-induced ground shock arrives. For design purposes, this latter case should be treated as an outrunning ground shock.

**Table 2-12 Coefficient of Friction for Concrete Foundation
and Underlying Soils**

| Soil Material | Coefficient of Friction, μ |
|--|--|
| Clean sound rock 0.70 | |
| Clean gravel, gravel-sand mixture, coarse sand | 0.55 to 0.60 |
| Clean fine to medium sand, silty medium to coarse sand, silty or clayey gravel | 0.45 to 0.55 |
| Clean fine sand, silty or clayey fine to medium sand | 0.35 to 0.45 |
| Fine sandy silt, nonplastic silt | 0.30 to 0.35 |
| Very stiff and hard residual or preconsolidated clay | 0.40 to 0.50 |
| Medium stiff and stiff clay and silty clay | 0.30 to 0.35 |

2-23.3 Maximum Structure Motion

The design of protective structures to resist the effect of shock loads is based on the peak values of the induced motion rather than the actual motion-time relationships. In fact, the actual time history of the motion is not known nor can it be approximated with any degree of accuracy. Consequently, the phasing of the various shocks cannot be accomplished accurately. Therefore, for design purposes the peak values of the in-phase motions are added.

For the case of air-induced ground shock and air shock, the maximum values of horizontal displacement, velocity and acceleration are always added. These shock motions must be in phase since they are caused by the same source, namely, the air blast.

In the case of superseismic ground shock where the air-induced and direct-induced ground shock are completely separated, the maximum motion may be due to either source. The maximum value of displacement, velocity or acceleration is the numerically larger value regardless of its source.

In the case of outrunning ground, the structure motion results from the combined effect of the air-induced and direct-induced ground shock as well as the air shock. The maximum motions in the vertical and horizontal direction is the algebraic sum of the maximum value of displacement, velocity and acceleration from each source of motion in the vertical and horizontal directions.

2-24 Shock Response Spectra

2-24.1 Introduction

For the purposes of assessing the effects of shock on structures, one of the simplest interpretations of motion data involves the concept of the response spectrum. A response spectrum is a plot of the maximum response of a simple linear oscillator subjected to a given input motion against frequency. Hence, a response spectrum depicts only maximum response values, not a time-dependent history of the motion of the oscillator. The use of these maximum values is sufficient to insure a reasonable and safe design for shock loads.

2-24.2 Definition of Shock Spectra Grid

Response spectra are constructed from consideration of the response of a simple linear oscillator. For a protective structure subjected to shock loads, a piece of equipment or any interior component can be considered as the mass of a simple oscillator. The load-deflection properties of the structural system which connects the component to the protective structure determines the spring constant of the oscillator.

The maximum displacement of the mass (building component) relative to the base (protective structure) is called the spectrum displacement, D , and the maximum acceleration of the mass is called the spectrum acceleration, A . The maximum velocity of the mass is approximately equal to the more useful quantity called the spectrum pseudo-velocity, V , which is given by

$$V = 2 \pi f D$$

2-93

where V = velocity of the mass
 f = natural frequency of vibration of the oscillator
 D = displacement of the mass

For an undamped system, the displacement and acceleration are related by

$$A = \frac{(2\pi f)^2 Dg}{387} \qquad 2-94$$

where A = acceleration of the mass in g's
 g = gravitational constant

When damping is present, the above relationship between acceleration and displacement is approximate. However, the relationship may still be used to develop shock spectra.

Plots of the three quantities, displacement D, velocity V, and acceleration A, against frequency f, are then shock spectra. They may be plotted individually or, more conveniently, on a single plot by means of the type of chart shown in figure 2-254. Any point on this logarithmic grid represents a simultaneous solution to equations 2-93 and 2-94. The log-log grid must be proportioned to satisfy the solution of the equations. The grid is constructed from standard log-log paper on which a second log-log grid is superimposed and rotated 45 degrees. The width of a log cycle on this rotated grid is 0.707 times the width of a cycle on the standard grid.

2-24.3 Response Spectra

A response spectrum is a plot of the maximum response of a single-degree-of-freedom system to a given input motion. The given input motion is the air shock, and the air-induced and direct-induced ground shocks. Since the maximum values of the free-field displacement, velocity and acceleration (input motion) are used to construct the spectra, a response spectrum envelope is produced. The spectrum takes a trapezoidal shape and is shown on figure 2-254 by the lines labeled D, V and A. The three sides of this trapezoid can be related to the maximum free-field input motion parameters of displacement, velocity and acceleration.

Relationships between the spectrum envelope bounds and the characteristics of the time dependent free-field input motions (displacements, velocities, and accelerations) clearly indicate that as the variation of the free-field motion parameters versus time is defined, the definition of the corresponding spectrum envelope can be refined. However, in the general case of blast-induced motions, the variation of the input motions with time cannot visually be described in significant detail. Consequently, it is recommended that for the elastic response of systems, the spectrum be defined by the following three straight lines as illustrated in figure 2-254.

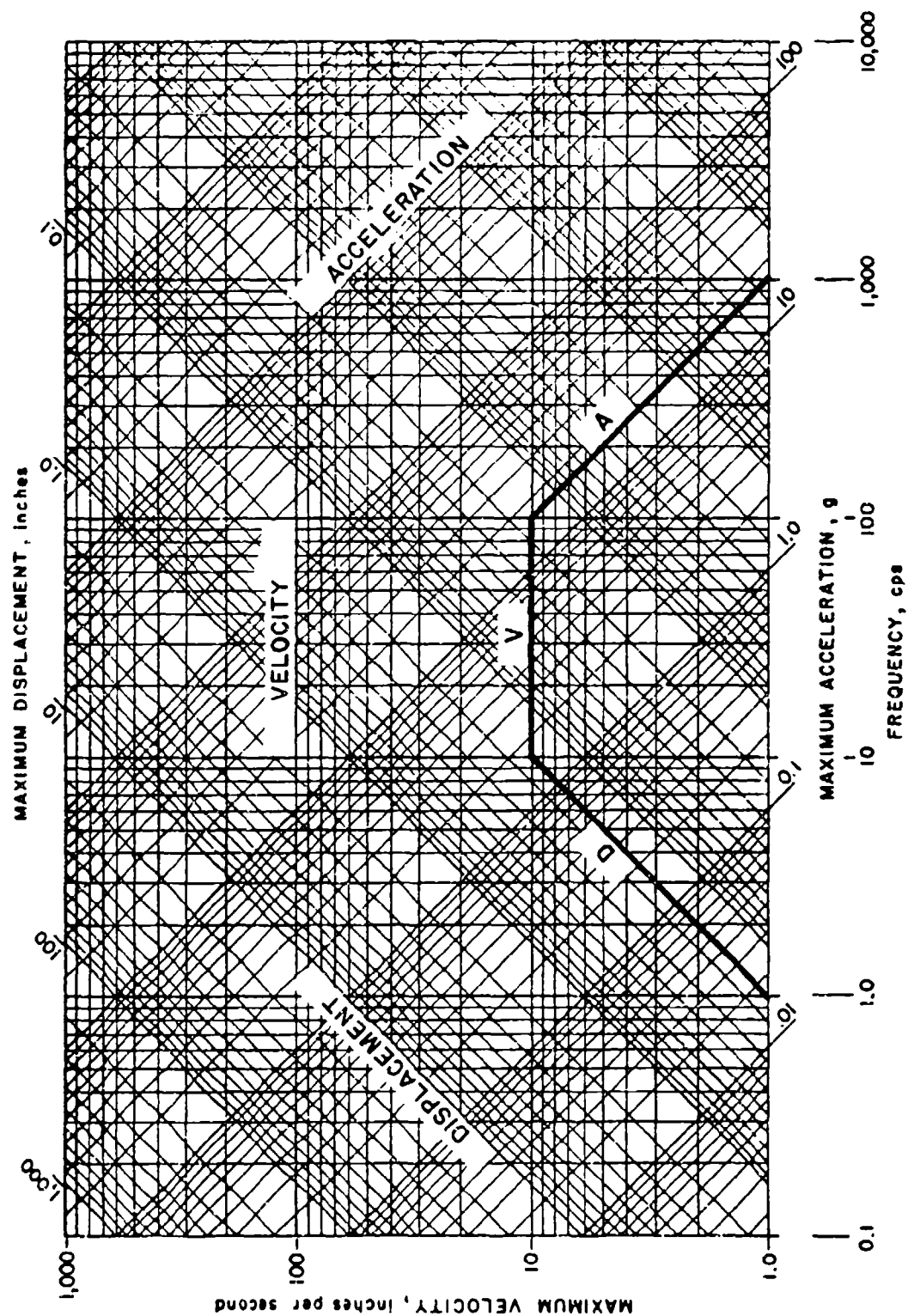


Figure 2-254 Typical response shock spectra

- (1) Line "D" is drawn parallel to lines of constant displacement with a magnitude equal to the maximum free-field (building) displacement.
- (2) Line "V" is drawn parallel to lines of constant velocity (actually pseudo velocity) with a magnitude equal to one and one-half (1.5) times the maximum free-field (building) velocity.
- (3) Line "A" is drawn parallel to lines of constant acceleration with a magnitude equal to two (2) times the maximum free-field (building) acceleration.

A spectrum defined in this manner is clearly an approximation, however, its accuracy is considered to be consistent with the accuracy of the input free-field (building) motions on which it is based. In those cases where the input motions can be defined with greater confidence, the spectrum identified above can be defined to reflect the greater accuracy.

In most cases, interior components of the structure and/or equipment and equipment supports are designed elastically. Therefore, the shock spectra described above will suffice. However, when a very large explosion causes large structure motions, interior systems may require inelastic designs. These conditions will usually not arise for the charge capacities considered in this report. Therefore, methods for calculating inelastic shock spectra have not been presented. It is recommended that the bibliography given at the end of this volume be consulted for further data on this subject.

APPENDIX 2A. EXPLOSIVE EFFECTS -
ILLUSTRATIVE EXAMPLES

Problem 2A-1. Free-Air Burst

Problem: Determine incident blast wave parameters for a point of interest in the air for a free air burst.

Procedure:

Step 1. Determine the charge weight and height of burst H_C . Select point of interest in the air relative to the charge.

Step 2. Apply a 20% safety factor to the charge weight.

Step 3. For the point of interest, calculate slant distance R and scaled slant distance Z :

$$Z = R/W^{1/3}$$

Step 4. Determine incident blast wave parameters from figures 2-7 and 2-8 for the calculated value of the scaled slant distance Z .

From figure 2-7 read:

Peak positive incident pressure P_{s0}

Shock front velocity U

Scaled unit positive incident impulse $i_s/W^{1/3}$

Scaled positive phase duration $t_o/W^{1/3}$

Scaled arrival time $t_A/W^{1/3}$

Scaled wave length of positive phase $L_w/W^{1/3}$

From figure 2-8 Read:

Peak negative incident pressure P_{s0}^-

Scaled unit negative incident impulse $i_s^-/W^{1/3}$

Scaled negative phase duration $t_o^-/W^{1/3}$

Scaled wave length of negative phase $L_w^-/W^{1/3}$

Multiply scaled values by $W^{1/3}$ to obtain absolute values.

Example 2A-1. Free-Air Burst

Required: Incident blast wave parameters P_{s0} , P_{s0^-} , U , i_s , i_s^- , t_0 , t_0^- , t_A , L_W^- at a point 30 ft. below and 45 ft. away in the air from an air burst of 290 lbs. at a height of burst of 60 ft. above the ground.

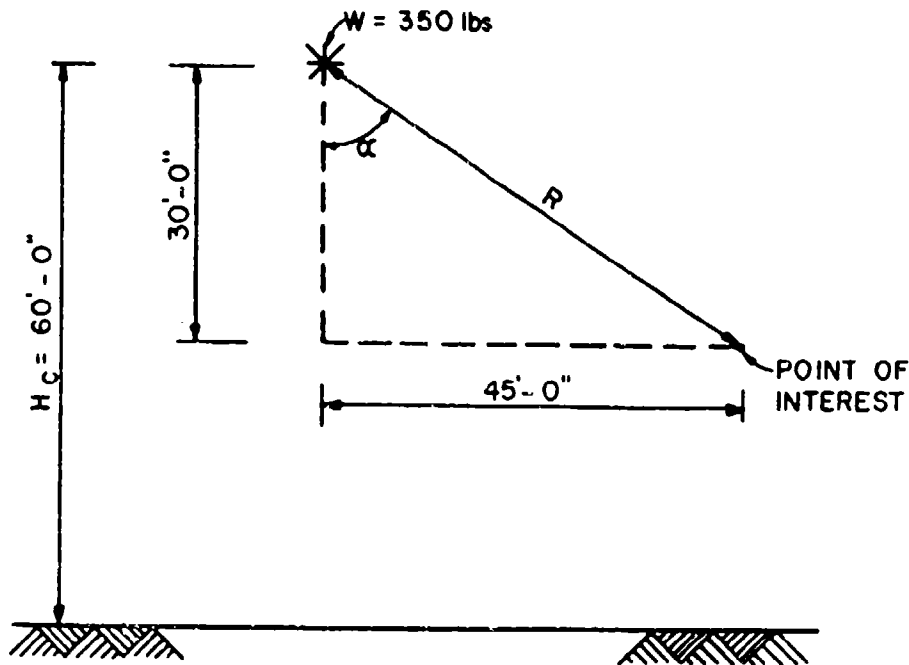


Figure 2A-1

Solution:

Step 1. Given: Charge weight = 290 lbs., $H_C = 60$ ft.

Step 2. $W = 1.2 (290) = 350$ lbs.

Step 3. For the point of interest:

$$R = ((45)^2 + (30)^2)^{1/2} = 54.1 \text{ ft.}$$

$$Z = \frac{R}{W^{1/3}} = \frac{54.1}{(350)^{1/3}} = 7.67 \text{ ft./lb.}^{1/3}$$

Step 4. Determine incident blast wave parameters for

$$Z = 7.67 \text{ ft./lb.}^{1/3}$$

From figure 2-7:

$$P_{s0} = 11.2 \text{ psi}$$

$$U = 1.34 \text{ ft./ms}$$

$$i_s/W^{1/3} = 7.0 \text{ psi-ms/lb.}^{1/3}, i_s = 7.0 (350)^{1/3} = 49.3 \text{ psi-ms}$$

$$t_o/W^{1/3} = 2.05 \text{ ms/lb.}^{1/3}, t_o = 2.05 (350)^{1/3} = 14.45 \text{ ms.}$$

$$t_A/W^{1/3} = 3.15 \text{ ms/lb.}^{1/3}, t_A = 3.15 (350)^{1/3} + 22.2 \text{ ms}$$

$$L_W/W^{1/3} = 2.0 \text{ ft/lb.}^{1/3}, L_W = 14.09 \text{ ft}$$

From figure 2-8:

$$P_{s0}^- = 1.63 \text{ psi}$$

$$i_s^-/W^{1/3} = 7.2 \text{ psi-ms/lb.}^{1/3}, i_s^- = 7.2 (350)^{1/3} = 50.74 \text{ psi-ms}$$

$$t_o^-/W^{1/3} = 8.4 \text{ ms/lb.}^{1/3}, t_o^- = 8.4 (350)^{1/3} = 59.20 \text{ ms}$$

$$L_W^-/W^{1/3} = 5.8 \text{ ft/lb.}^{1/3}, L_W^- = 5.8 (350)^{1/3} = 40.87 \text{ ft.}$$

Problem 2A-2. Air Burst

Problem: Determine free-field blast wave parameters at a point on the ground for an air burst.

Procedure:

Step 1. Select point of interest on the ground relative to the charge. Determine the charge weight, height of burst H_C , and ground distance R_G .

Step 2. Apply a 20% safety factor to the charge weight.

Step 3. Calculate scaled height of burst and angle of incidence α :

$$H_C/W^{1/3}$$

$$\alpha = \tan^{-1} (R_G/H_C)$$

Step 4. Determine peak reflected pressure P_{ra} and scaled unit positive reflected impulse $i_{ra}/W^{1/3}$ in Mach front from figures 2-9 and 2-10, respectively, for corresponding scaled height of burst and angle of incidence α :

Read P_{ra} and $i_{ra}/W^{1/3}$

Multiply scaled value by $W^{1/3}$ to obtain absolute value.

Step 5. Read scaled distance Z from figure 2-7 for corresponding peak incident pressure $P_{so} = P_{ra}$ in the Mach front.

Step 6. Determine shock front velocity U and scaled time of arrival of blast wave $t_A/W^{1/3}$ from figure 2-7 for value Z from step 5. Multiply scaled value of $W^{1/3}$ to obtain absolute value.

Step 7. Read scaled distance Z from figure 2-7 for corresponding scaled unit positive incident impulse $i_s/W^{1/3} = i_{ra}/W^{1/3}$ in the Mach front.

Step 8. Determine scaled positive duration of positive phase from figure 2-7 for the value of Z from step 7.

Multiply scaled value of $W^{1/3}$ to obtain absolute value.

Example 2A-2. Air Burst

Required: Free-field blast wave parameters P_{so} , U , i_s , t_o , t_A for an air burst of 20,800 lbs. at a ground distance of 300 ft. and a height of burst of 90 ft.

Solution:

Step 1. Given: Charge weight = 20,800 lb. $R_G = 300$ ft, $H_C = 90$ ft.

Step 2. $W = 1.20 (20,800) = 25,000$ lbs.

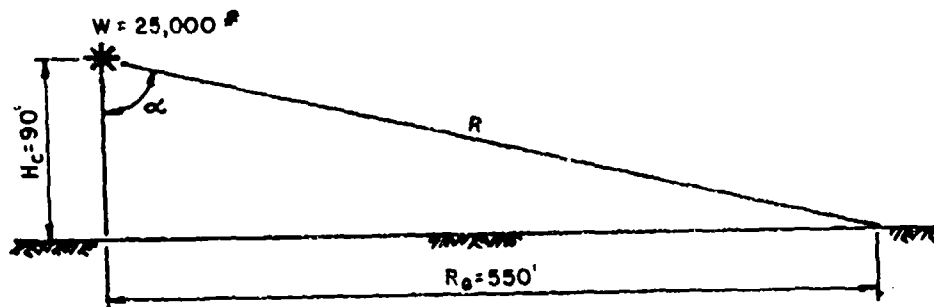


Figure 2A-2

Step 3. For point of interest

$$H_c/W^{1/3} = 90/(25,000)^{1/3} = 3.08 \text{ ft/lb}^{1/3}$$

$$\alpha = \tan^{-1} \left[\frac{R_G}{H_c} \right] = \tan^{-1} \left[\frac{550}{90} \right] = 73.3^\circ$$

Step 4. Determine reflected pressure P_{ra} and reflected impulse in the Mach front from figure 2-9 and 2-10.

$$H_c/W^{1/3} = 3.08 \text{ ft/lb}^{1/3} \text{ and } \alpha = 73.3^\circ$$

$$P_{ra} = 10.1 \text{ psi}$$

$$\frac{i_{ra}}{W^{1/3}} = 9.2 \text{ psi-ms/lb}^{1/3}, i_{ra} = 9.2 (25,000)^{1/3} = 269.0 \text{ psi-ms}$$

Step 5. Read scaled distance Z from figure 2-7 corresponding to

$$P_{so} = P_{ra} = 10.1 \text{ psi}$$

$$Z = 7.8 \text{ ft/lb}^{1/3}$$

Step 6. Determine U and $t_A/W^{1/3}$ from figure 2-7 corresponding to $Z = 7.8 \text{ ft/lb}^{1/3}$

$$U = 1.38 \text{ ft/ms}$$

$$t_A/W^{1/3} = 300 \text{ ms/lb}^{1/3}, t_A = 300 (25,000)^{1/3} = 8772.05 \text{ ms.}$$

Step 7. Read scaled distance Z from Fig. 2-7 corresponding to

$$i_s/W^{1/3} = i_{ra}/W^{1/3} = 9.2 \text{ psi-ms/lb}^{1/3}$$

$$Z = 5.7 \text{ ft/lb}^{1/3}$$

Step 8. Determine $t_o/W^{1/3}$ from Figure 2-7 corresponding to

$$Z = 5.7 \text{ ft/lb}^{1/3}$$

$$t_o/W^{1/3} = 155 \text{ ms/lb}^{1/3}, t_o = 155(25,000)^{1/3} = 4532.23 \text{ ms}$$

Problem 2A-3. Surface Burst

Problem: Determine free-field blast wave parameters for a surface burst.

Procedure:

Step 1. Select point of interest on the ground relative to the charge. Determine the charge weight, and ground distance R_G .

Step 2. Apply a 20% safety factor to the charge weight.

Step 3. Calculate scaled ground distance Z_G :

$$Z_G = \frac{R_G}{W^{1/3}}$$

Step 4. Determine free-field blast wave parameters from figure 2-15 for corresponding scaled ground distance Z_G :

Read:

Peak positive incident pressure P_{so}

Shock front velocity U

Scaled unit positive incident impulse $i_s/W^{1/3}$

Scaled positive phase duration $t_o/W^{1/3}$

Scaled arrival time $t_A/W^{1/3}$

Multiply scaled values by $W^{1/3}$ to obtain absolute values.

Example 2A-3. Surface Burst

Required: Free-field blast wave parameters P_{so} , U , i_s , t_o , t_A for a surface burst of 20,800 lbs at a distance of 530 ft.

Solution:

Step 1: Given: Charge weight = 20,800 lb. $R_G = 530$ ft.

Step 2. $W = 1.20 (20,800) = 25,000$ lbs.

Step 3. For point of interest:

$$Z_G = \frac{R_G}{W^{1/3}} = \frac{530}{(25,000)^{1/3}} = 18.1 \text{ ft/lb}^{1/3}$$

Step 4. Determine blast wave parameters from figure 2-15 for $Z_G = 18.1 \text{ ft/lb}^{1/3}$

$$P_{so} = 3.45 \text{ psi}$$

$$U = 1.22 \text{ ft/ms}$$

$$\frac{i_s}{W^{1/3}} = 4.7 \text{ psi-ms/lb}^{1/3} \quad i_s = 4.7(25,000)^{1/3} = 137.4 \text{ psi-ms}$$

$$\frac{t_o}{W^{1/3}} = 3.3 \text{ ms/lb}^{1/3} \quad t_o = 3.3(25,000)^{1/3} = 96.5 \text{ ms}$$

$$\frac{t_A}{W^{1/3}} = 10.6 \text{ ms/lb}^{1/3} \quad t_A = 10.6(25,000)^{1/3} = 310 \text{ ms}$$

Problem 2A-4 Shock Loads on Cubicle Walls

Problem: Determine the average peak reflected pressure and average scaled reflected impulse acting on the wall of a cubicle from an internal explosion. The cubicle is fully vented.

Procedure:

Step 1. Select from figure 2-51 the structural configuration which will define the number N and location of effective reflecting surfaces for the wall of the structure in question. Determine the charge weight, and, as defined by the structural configuration chosen above, the charge location parameters R_A , h , l and the structural parameters L , H .

Step 2. Apply a 20% safety factor to the charge weight.

Step 3. Calculate the chart parameters $\frac{h}{H}$, $\frac{l}{L}$, $\frac{L}{R_A}$, and the scaled distance Z_A .

Note:

Use of the average pressure and impulse charts may require interpolation in many cases. Interpolation may be achieved by inspection for the scaled distance Z_A and by a graphical procedure for the chart parameters L/H , l/L , and h/H using 2 cycle x 2 cycle logarithmic graph paper. The following procedure will illustrate the interpolation of all three chart parameters.

Step 4. From table 2-3 determine the appropriate pressure and impulse charts for the number of adjacent reflecting surfaces N . Determine and tabulate the values of the average pressure P_r and average scaled impulse $i_r/W^{1/3}$ from these charts for the required L/R_A and Z_A and the following variables:

$$L/H = 0.625, 1.25, 2.50, \text{ and } 5.00$$

$$l/L = 0.10, 0.25, 0.50, \text{ and } 0.75$$

$$h/H = 0.10, 0.25, 0.50, \text{ and } 0.75$$

- Step 5.
- Prepare four 2-cycle log-log charts with $\frac{L}{R_A}$ as the lower abscissa, $\frac{l}{L}$ as the upper abscissa, and P_r as the ordinate (one chart for each of the $\frac{h}{H}$ ratios). On each chart for constant $\frac{h}{H}$ and Z_A , plot \bar{i}_b versus $\frac{L}{R_A}$ for all $\frac{l}{L}$ values. Repeat with the ordinate labeled as $i_r/W^{1/3}$.
 - Using chart for $\frac{h}{H} = 0.10$, read values of P_r and $i_r/W^{1/3}$ versus $\frac{l}{L}$ for required $\frac{L}{R_A}$. Tabulate results.

- c. Repeat step 3b for charts $\frac{h}{H} = 0.25, 0.50, \text{ and } 0.75$.
Tabulate results.
- d. On each $\frac{h}{H}$ chart, plot P_r and $i_r/W^{1/3}$ versus $\frac{l}{L}$ from steps 5b and 5c.
- e. On each $\frac{h}{H}$ chart, read P_r and $i_r/W^{1/3}$ for required $\frac{l}{L}$ ratio.
- f. On a fifth chart, plot P_r and $i_r/W^{1/3}$ from step 5e versus $\frac{h}{H}$.

Step 6. For required $\frac{h}{H}$ ratio, read P_r and $i_r/W^{1/3}$ from chart of step 5f.

Step 7. Calculate duration of load on element from equation 2-2.

Example 2A-4 (A) Shock Loads on Cubicle Walls

Required: Average peak reflected pressure and average scaled reflected impulse on the side wall of a three-wall cubicle from an explosive charge of 205 lbs. The cubicle is fully vented.

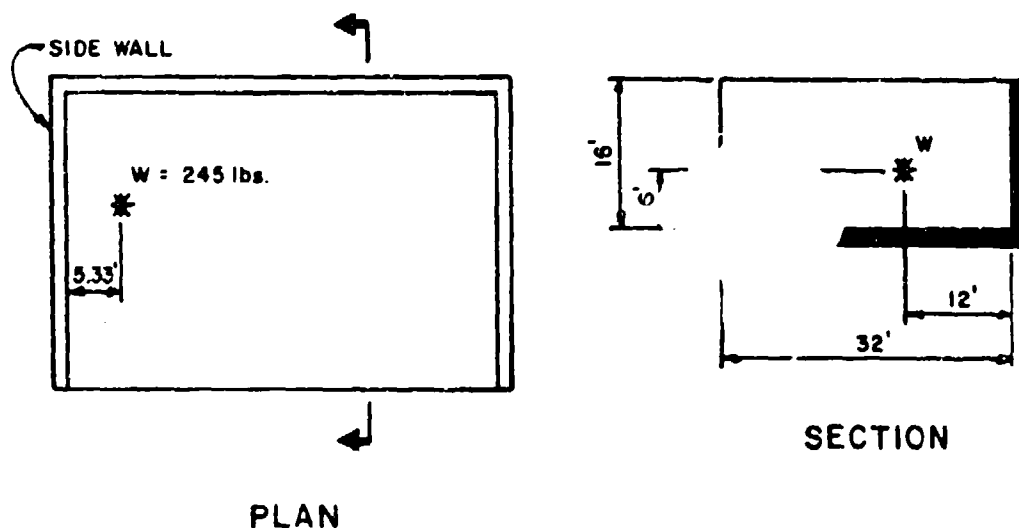


Figure 2A-3

Solution:

Step 1. $H = 16 \text{ ft.}$ $L = 32 \text{ ft.}$ Charge Weight = 205 lbs.
 $h = 6 \text{ ft.}$ $l = 12 \text{ ft.}$ $R_A = 5.33 \text{ ft.}$

Note:

For definition of terms, see figure 2-51 (side wall of three wall cubicle, $N = 2$).

Step 2. $W = 1.20 (205) = 245 \text{ lbs.}$

Step 3. $\frac{h}{H} = 0.375 \quad \frac{l}{L} = 0.375 \quad \frac{L}{R_A} = 6.00 \quad \frac{L}{H} = 2.00$

$$Z_A = \frac{R_A}{W^{1/3}} = \frac{5.33}{(245)^{1/3}} = 0.85 \text{ ft/lb}^{1/3}$$

Interpolation is required for Z_A , $\frac{L}{H}$, $\frac{l}{L}$, and $\frac{h}{H}$.

Step 4. Determine and tabulate the values of P_r and $i_r/W^{1/3}$ from pressure and impulse charts (see table 2-3 for $N = 2$) for:

$$L/R_A = 6.00, Z_A = 0.85$$

(interpolate by inspection) and for values given for L/H , l/L and h/H . The results are tabulated in tables 2A-1 and 2A-2.

- Step 5.
- Plot P_r and $i_r/W^{1/3}$ versus $\frac{L}{H}$ for the values of l/L and constant h/H (fig. 2A-4 and 2A-5).
 - Determine P_r and $i_r/W^{1/3}$ for $\frac{L}{H} = 2.00$, $\frac{h}{H} = 0.10$, and various $\frac{l}{L}$ ratios by entering figure 2A-4a and 2A-5a with $\frac{L}{H} = 2.00$
 - Repeat above step for $\frac{h}{H} = 0.25, 0.50$, and 0.75 by entering figures 2A-4b through d and 2A-5b through d with $\frac{L}{H} = 2.00$ (tabulation of results not shown).
 - On each h/H chart, plot P_r and $i_r/W^{1/3}$ (steps 5b and 5c) versus l/L (upper abscissa of figures 2A-4a through d and 2A-5a through d).
 - Determine P_r and $i_r/W^{1/3}$ for $\frac{l}{L} = 0.375$ on each h/H chart of figures 2A-4 and 2A-5 with $\frac{l}{L} = 0.375$ and reading curves plotted in step 5d.

Table 2A-1 Average Pressure

| h/H t/L L/H | 0.10 | | | | | | | | 0.25 | | | | | | | | 0.50 | | | | | | | | 0.75 | | | | | | | |
|-------------------|------|------|------|------|------|------|------|------|------|------|------|------|------|------|------|------|------|------|------|------|------|------|------|------|------|------|------|------|------|------|------|------|
| | 0.10 | | 0.25 | | 0.50 | | 0.75 | | 0.10 | | 0.25 | | 0.50 | | 0.75 | | 0.10 | | 0.25 | | 0.50 | | 0.75 | | 0.10 | | 0.25 | | 0.50 | | 0.75 | |
| | 0.10 | 0.25 | 0.50 | 0.75 | 0.10 | 0.25 | 0.50 | 0.75 | 0.10 | 0.25 | 0.50 | 0.75 | 0.10 | 0.25 | 0.50 | 0.75 | 0.10 | 0.25 | 0.50 | 0.75 | 0.10 | 0.25 | 0.50 | 0.75 | 0.10 | 0.25 | 0.50 | 0.75 | 0.10 | 0.25 | 0.50 | 0.75 |
| 0.625 | 462 | 569 | 598 | 569 | 533 | 665 | 701 | 665 | 546 | 681 | 718 | 681 | 533 | 665 | 701 | 665 | 533 | 665 | 701 | 665 | 533 | 665 | 701 | 665 | 533 | 665 | 701 | 665 | 533 | 665 | 701 | 665 |
| 1.25 | 749 | 932 | 980 | 932 | 943 | 1176 | 1238 | 1178 | 1017 | 1267 | 1333 | 1267 | 943 | 1178 | 1238 | 1178 | 943 | 1178 | 1238 | 1178 | 943 | 1178 | 1238 | 1178 | 943 | 1178 | 1238 | 1178 | 943 | 1178 | 1238 | 1178 |
| 2.50 | 1200 | 1488 | 1562 | 1428 | 1432 | 1796 | 1881 | 1796 | 1609 | 2028 | 2120 | 2028 | 1432 | 1796 | 1881 | 1796 | 1432 | 1796 | 1881 | 1796 | 1432 | 1796 | 1881 | 1796 | 1432 | 1796 | 1881 | 1796 | 1432 | 1796 | 1881 | 1796 |
| 5.00 | 2032 | 2519 | 2635 | 2519 | 1870 | 2334 | 2437 | 2334 | 1987 | 2456 | 2563 | 2456 | 1870 | 2334 | 2437 | 2334 | 1870 | 2334 | 2437 | 2334 | 1870 | 2334 | 2437 | 2334 | 1870 | 2334 | 2437 | 2334 | 1870 | 2334 | 2437 | 2334 |
| Fig. | 2-64 | 2-65 | 2-66 | 2-67 | 2-68 | 2-69 | 2-70 | 2-71 | 2-72 | 2-73 | 2-74 | 2-75 | 2-76 | 2-77 | 2-78 | 2-79 | 2-76 | 2-77 | 2-78 | 2-79 | 2-76 | 2-77 | 2-78 | 2-79 | 2-76 | 2-77 | 2-78 | 2-79 | 2-76 | 2-77 | 2-78 | 2-79 |

Table 2A-2 Average Unit Impulses

| h/H L/L L/H | 0.10 | | | | 0.25 | | | | 0.50 | | | | 0.75 | | | |
|-------------------|-------|-------|-------|-------|-------|-------|-------|-------|-------|-------|-------|-------|-------|-------|-------|-------|
| | 0.10 | 0.25 | 0.50 | 0.75 | 0.10 | 0.25 | 0.50 | 0.75 | 0.10 | 0.25 | 0.50 | 0.75 | 0.10 | 0.25 | 0.50 | 0.75 |
| | 0.10 | 0.25 | 0.50 | 0.75 | 0.10 | 0.25 | 0.50 | 0.75 | 0.10 | 0.25 | 0.50 | 0.75 | 0.10 | 0.25 | 0.50 | 0.75 |
| 0.625 | 73 | 71 | 70 | 66 | 65 | 61 | 59 | 55 | 64 | 61 | 58 | 54 | 59 | 56 | 53 | 49 |
| 1.25 | 96 | 92 | 90 | 84 | 96 | 92 | 90 | 83 | 93 | 87 | 83 | 76 | 87 | 79 | 76 | 70 |
| 2.50 | 126 | 121 | 121 | 111 | 139 | 131 | 129 | 120 | 129 | 120 | 118 | 109 | 117 | 106 | 103 | 95 |
| 5.00 | 172 | 164 | 164 | 153 | 167 | 153 | 154 | 143 | 186 | 168 | 168 | 158 | 201 | 189 | 189 | 179 |
| F15. | 2-113 | 2-114 | 2-115 | 2-116 | 2-117 | 2-118 | 2-119 | 2-120 | 2-121 | 2-122 | 2-123 | 2-124 | 2-125 | 2-126 | 2-127 | 2-128 |

313.

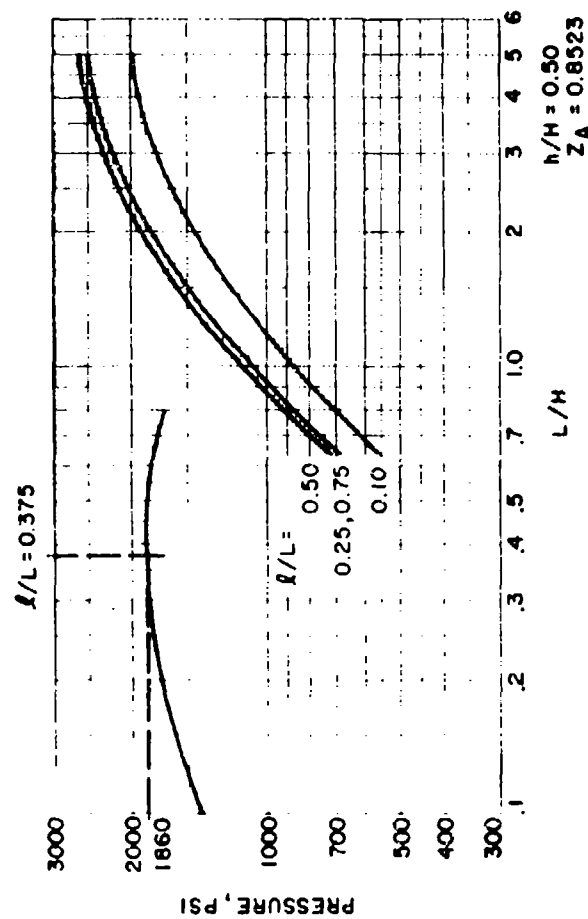
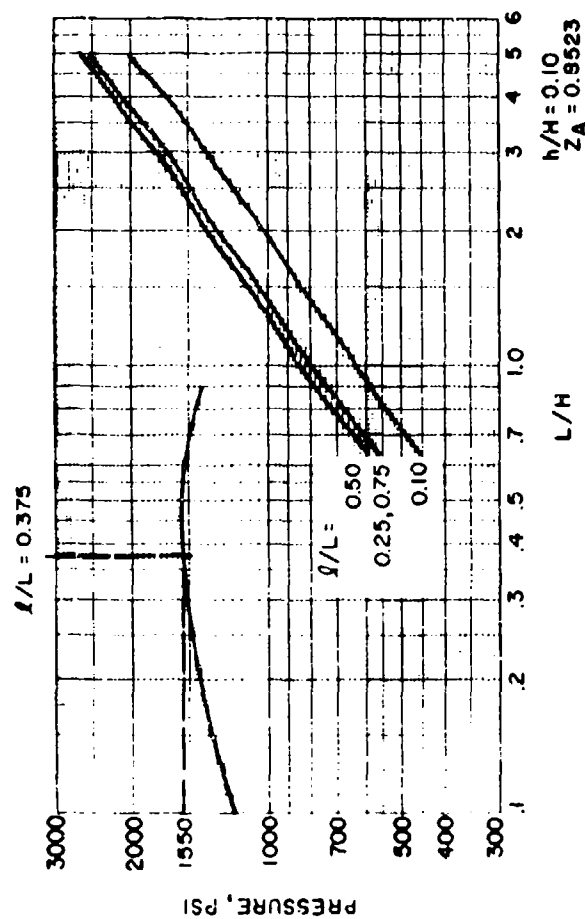
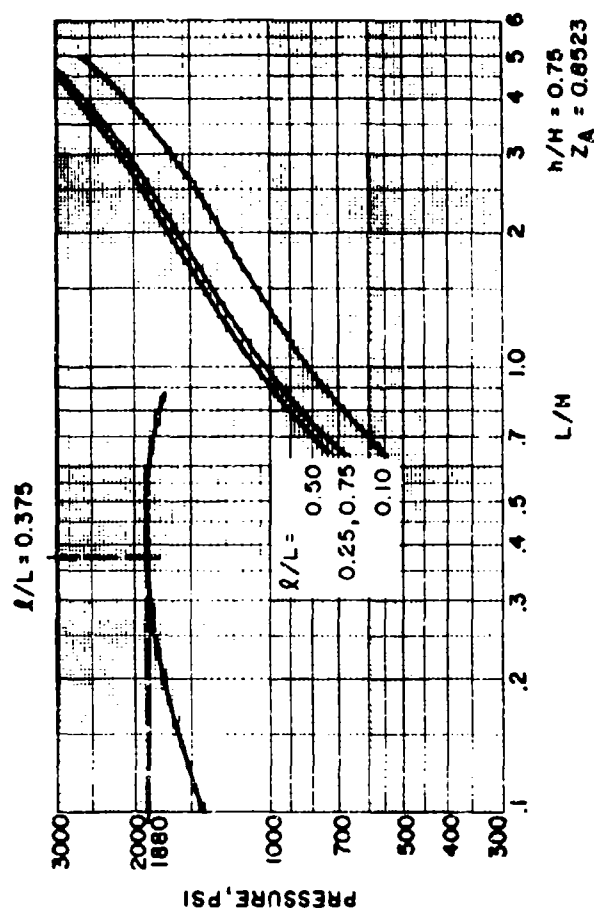
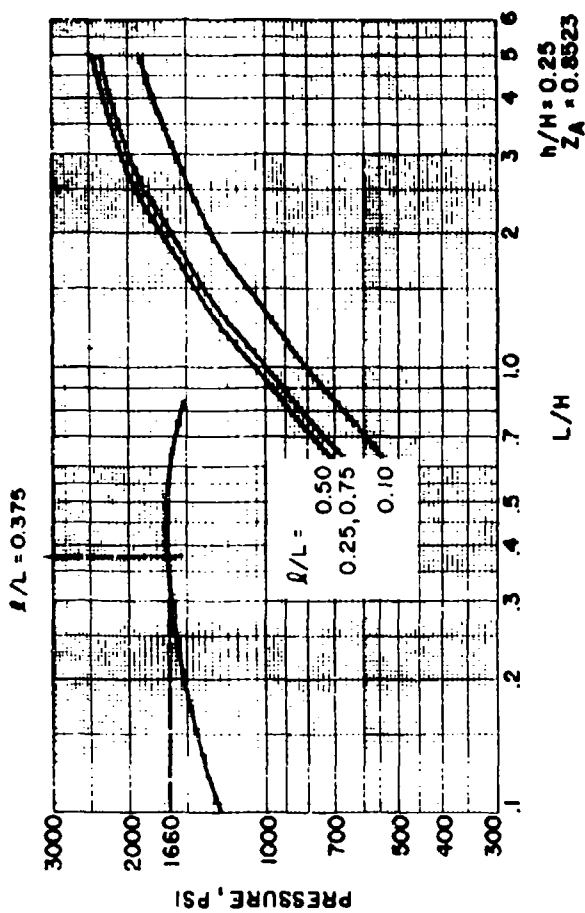


FIGURE 2A-4

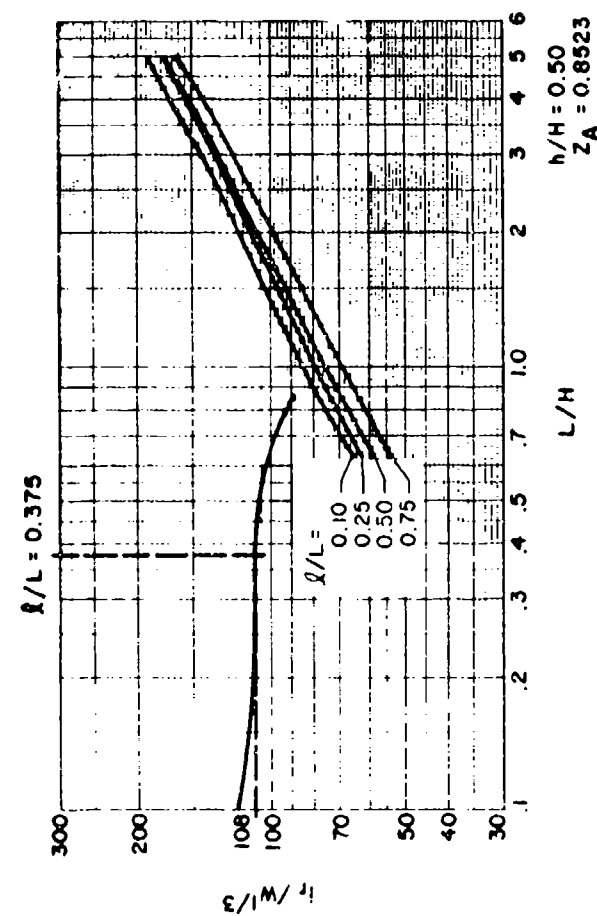
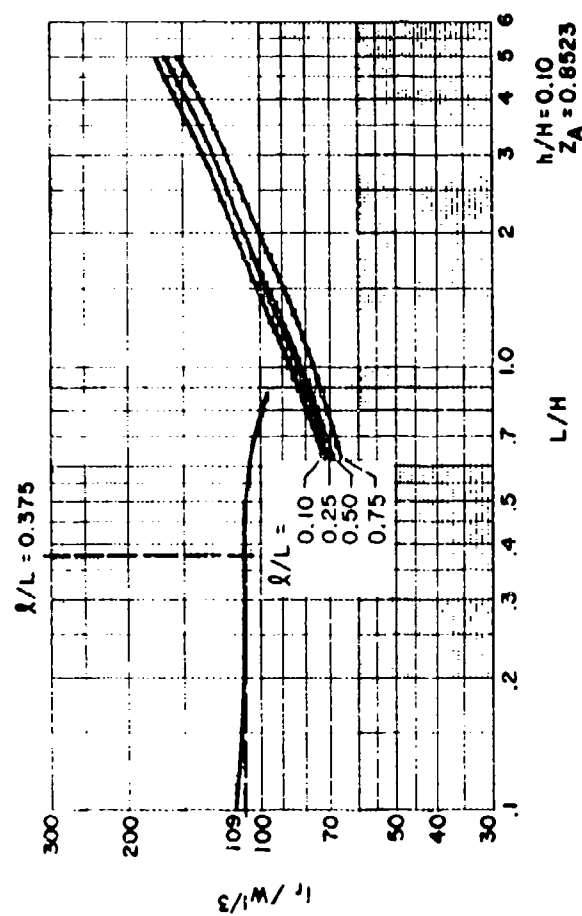
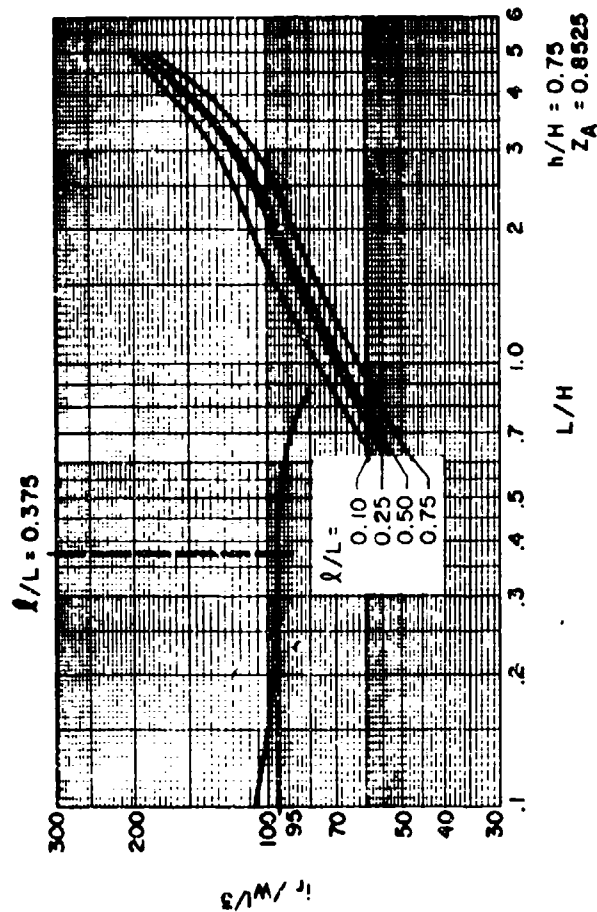
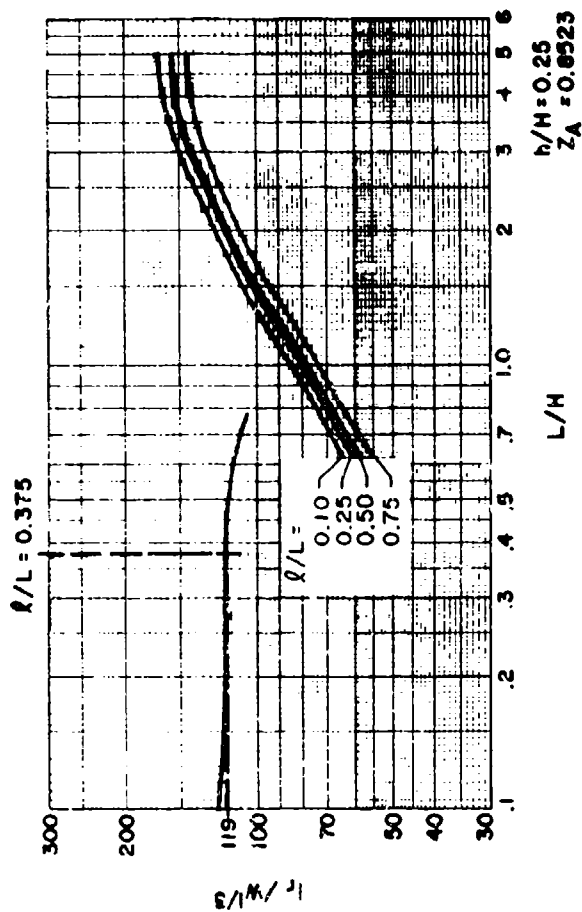


FIGURE 2A-5

| h/H | P_r | $i_r/W^{1/3}$ |
|-------|-------|---------------|
| 0.10 | 1550 | 109 |
| 0.25 | 1660 | 119 |
| 0.50 | 1860 | 108 |
| 0.75 | 1880 | 95 |

f. Plot P_r and $i_r/W^{1/3}$ (step 5e) versus $\frac{h}{H}$ (fig. 2A-7).

Step 6. For $\frac{h}{H} = 0.375$ read $P_r = 1800$ psi on figure 2A-7 and read $i_r/W^{1/3} = 115$ psi-ms/lb^{1/3} on figure 2A-7

Step 7. Calculate duration of load on wall.

$$t_o = 2(i_r/W^{1/3})(W)^{1/3}/P_r = 2(115)(245)^{1/3}/1800 = 0.80 \text{ ms}$$

Example 2A-4(B). Shock Loads on Cubicle Walls

Required: Average peak reflected pressure and average scaled reflected impulse on the back wall of a three-wall cubicle from an explosive charge of 3,750 lbs. The cubicle is fully vented and shown in figure 2A-6.

Solution:

Step 1. $H = 16$ ft. $L = 36$ ft. Charge weight = 3,750 lbs.
 $h = 4$ ft. $l = 9$ ft. $R_A = 16.5$ ft.

Note:

For definition of terms, see figure 2-51 (back wall of three-wall cubicle, $N = 3$).

Step 2. $W = 1.20(3,750) = 4,500$ lbs.

Step 3. $\frac{h}{H} = 0.25$ $\frac{l}{L} = 0.25$ $\frac{L}{R_A} = 2.18$ $\frac{L}{H} = 2.25$

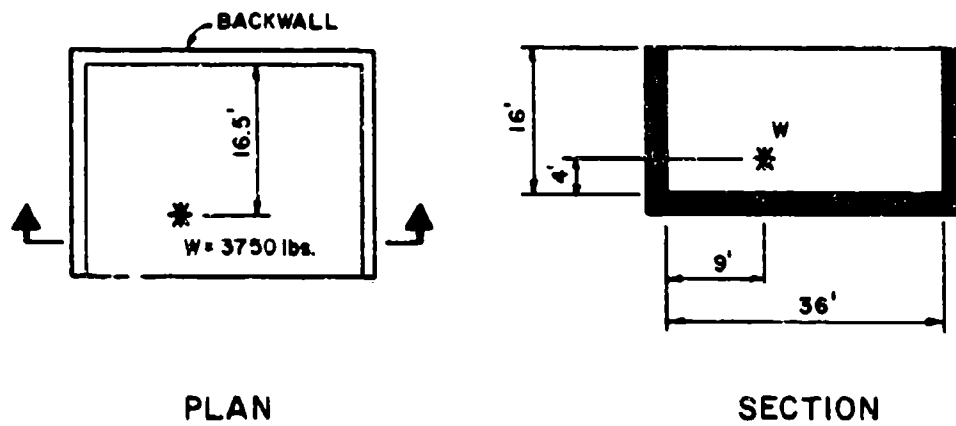
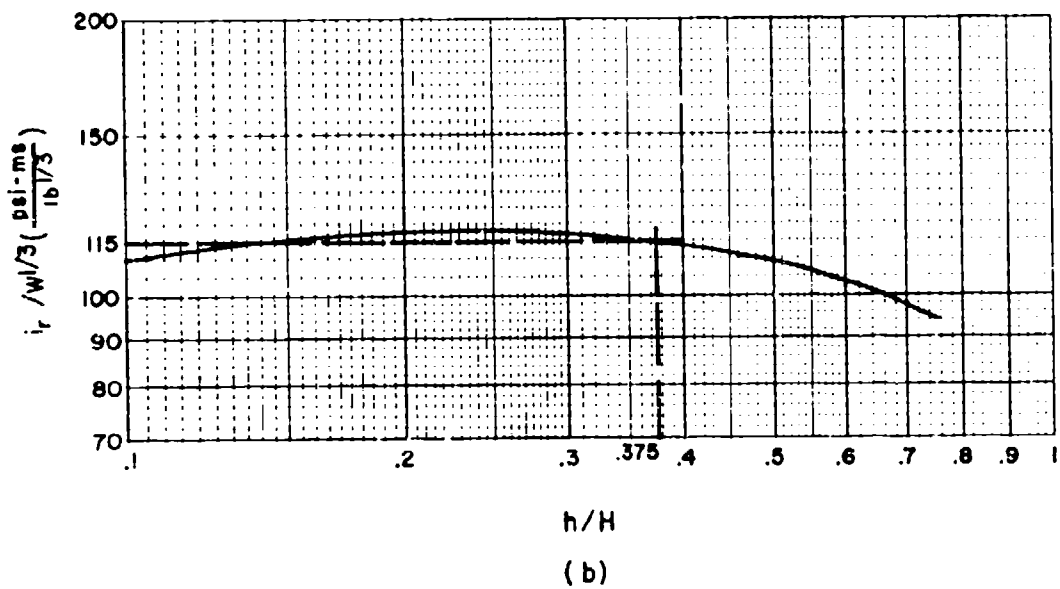
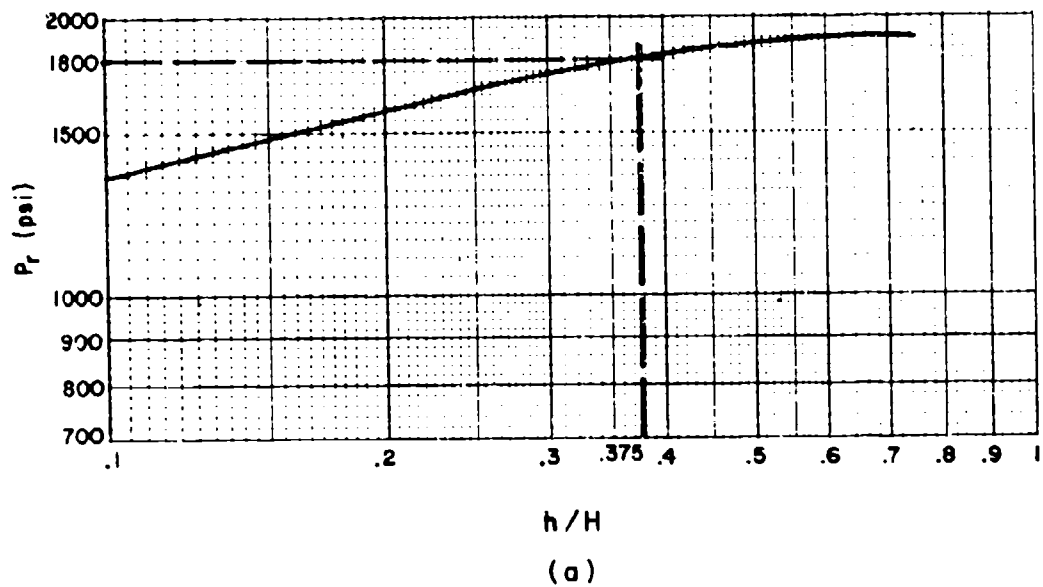


FIGURE 2A-6



$R/A = 4.0$ $L/H = 2.0$
 $L/R = 6.0$ $q/L = 0.375$
 $Z/A = 0.85$ $h/H = 0.375$

FIGURE 2A-7

$$Z_A = \frac{R_A}{W^{1/3}} = \frac{16.5}{(4,500)^{1/3}} = 1.00 \text{ ft/lb}^{1/3}$$

Interpolation is required for $\frac{L}{H}$

- Step 4. Determine the values of P_r and $i_r/W^{1/3}$ from figures 2-84 and 2-133 (determined from table 2-3 for $N = 3$, $h/H = 0.25$, $l/L = 0.25$) for $\frac{L}{H}$ ratios of 0.625, 1.25, 2.50 and 5.00.
- Step 5. Plot P_r and $i_r/W^{1/3}$ versus $\frac{L}{H}$ (fig. 2A-8).
- Step 6. For $\frac{L}{H} = 2.25$ read, $P_r = 3700 \text{ psi}$ and $i_r/W^{1/3} = 295 \text{ psi-ms/lb}^{1/3}$ and on figure 2A-8.
- Step 7. Calculate duration of load on wall (equation 2-2).

$$t_o = 2(i_r/W^{1/3}) W^{1/3}/P_r = 2(295)(4500)^{1/3}/3700 = 2.63 \text{ ms}$$

Problem 2A-5 Effect of Frangibility on Shock Loads

Problem: Determine average peak reflected pressure and average reflected impulse acting on the wall of a cubicle due to an internal explosion. One of the reflection surfaces is a frangible wall.

Procedure:

- Step 1. Determine the average peak reflected pressure P_r and the average reflected impulse acting on the element in question according to the procedure in problem 2A-4 assuming that the adjoining frangible element will remain in place and provide full reflection.
- Step 2. Determine the average reflected impulse acting on the element in question according to the procedure in problem 2A-4 assuming that the adjoining frangible element is not in place.
- Step 3. Subtract the average impulse determined in step 2 from the one in step 1.

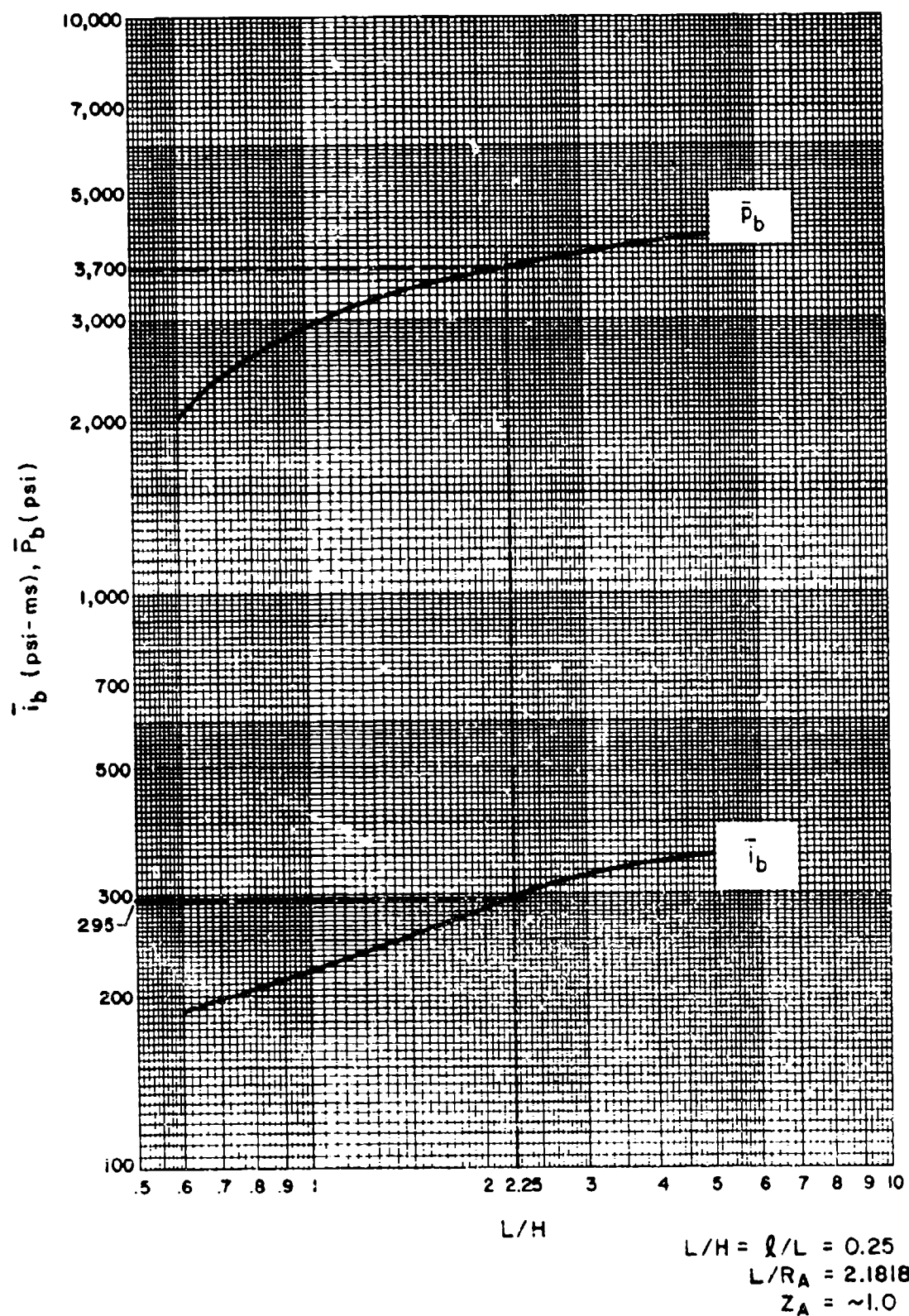


FIGURE 2A-8

- Step 4. Calculate unit weight of the frangible element W_F and divide by the sixth root of the charge weight (apply a 20% factor of safety to the charge weight).
- Step 5. Calculate the normal scaled distance Z between the center of the charge and the surface of the frangible element.
- Step 6. Determine the reflection factor f_r from figure 2-150 for the values of $W_F/W^{1/6}$ from step 4 and Z from step 5. Interpolate for value of Z if required.
- Step 7. Determine the magnitude of the impulse load reflected from the frangible element to the element in question by multiplying the value of the average impulse from step 3 and f_r from step 6.
- Step 8.
- Determine the total impulse load acting on the element in question by adding the impulse values from steps 2 and 7.
 - The peak average reflected pressure of the shock load is equal to the value of P_r in step 1.
 - Determine the duration of the load from equation 2-2.

Example 2A-5 Effect of Frangibility on Shock Loads

Required: Average peak reflected pressure and average reflected impulse on the back wall of the cubicle described in example 2A-4B except the left side wall is a 10 psf frangible element. The charge weight is 3,750 lbs (see figure 2A-6).

Solution:

- Step 1. Assuming the frangible side wall provides full reflection of the blast wave, P_r and i_r for the back wall according to the procedure in problem 2A-4 are:

$$P_r = 3700.0 \text{ psi}$$

$$i_r = 4870.3 \text{ psi-ms}$$

- Step 2. Assuming no left side wall, the average reflected impulse on the back wall, according to procedure in problem 2A-4 is:

$$i_r = 3962.3 \text{ psi-ms}$$

- Step 3. Calculate the reflected impulse contributed by the left side wall by subtracting the impulse value of step 2 from step 1.

$$\Delta i_r = 4870.3 - 3962.3 = 908.0 \text{ psi-ms}$$

- Step 4.
- a. $W_F = 10 \text{ lb/ft}^2$ (given)
 - b. $W = 3,750 \times 1.20 = 4,500 \text{ lbs}$
 - c. Calculate $W_F/W^{1/6}$ ratio:

$$W_F/W^{1/6} = 10/(4500)^{1/6} = 2.46$$

- Step 5.
- a. $R = 9.0 \text{ feet}$ (see figure 2A-6)
 - b. Calculate normal scale distance Z :

$$Z = \frac{R}{W^{1/3}} = \frac{9}{(4500)^{1/3}} = 0.545 \text{ ft/lbs}^{1/3}$$

- Step 6. From figure 2-150 where $W_F/W^{1/6} = 2.46$ and $Z = 0.545$ read:

$$f_r = 0.68$$

- Step 7. Determine the magnitude of the impulse reflected from the frangible left side wall, using $f_r = 0.68$ and the impulse from step 3.

$$i_r (\text{left side wall}) = 908 (0.68) = 617.4 \text{ psi-ms}$$

- Step 8.
- a. Calculate total reflected impulse on the back wall by adding impulse values from steps 2 and 7.

$$i_r (\text{back wall}) = 3962.3 + 617.4 = 4579.7 \text{ psi-ms}$$

- b. Peak reflected pressure from step 1:

$$p_r = 3700 \text{ psi}$$

- c. Calculate duration of load on wall:

$$t_o = \frac{2i_r}{p_r} = \frac{2 (4579.7)}{3700} = 2.48 \text{ ms}$$

Problem 2A-6 Shock Loads on Frangible Elements

Problem: Determine the average peak reflected pressure and average reflected impulse acting on the frangible wall of a cubicle due to an internal explosion.

Procedure:

- Step 1. Determine the average peak reflected pressure P_r and the average reflected impulse acting on the element in question according to the procedure in problem 2A-4, assuming that the wall will remain intact.
- Step 2. Calculate the unit weight of the frangible element W_F and divide by the sixth root of the charge weight (apply a 20% factor of safety to the charge weight).
- Step 3. From figure 2-7 determine the fictitious scaled distance Z which corresponds to the average scaled impulse determined in step 1.
- Step 4. Using the value of $W_F/W^{1/6}$ from step 2 and the Z from step 3, determine the reflection factor f_r from figure 2-150. Interpolate for value of Z if required.
- Step 5.
- Calculate the value of the average impulse contributing to the translation of the frangible element by multiplying the values of i_r and f_r of steps 1 and 4 respectively.
 - The peak average reflected pressure of the shock load is equal to the value of P_r in step 1.
 - Determine the duration of the load from equation 2-2.

Example 2A-6 Shock Loads on Frangible Elements

Required: Average peak reflected pressure and average scaled reflected impulse on the back wall of the cubicle described in example 2A-4 except the back wall is a 10 psf frangible wall. The charge weight is 3,750 lbs (see figure 2A-6).

Solution:

- Step 1. P_r and i_r for the back wall, assuming it is a rigid element, according to procedure in problem 2A-4 are:

$$P_r = 3700.0 \text{ psi}$$

$$i_r/W^{1/3} = 295.0 \text{ psi-ms/lb}^{1/3}$$

$$i_r = 4870.3 \text{ psi-ms}$$

Step 2. a. $W_F = 10.0 \text{ lb/ft}^2$ (given)

b. $W = 3,750 \times 1.20 = 4,500 \text{ lbs}$

c. Calculate $W_F/W^{1/6}$ ratio:

$$W_F/W^{1/6} = 10/(4500)^{1/6} = 2.46$$

Step 3. Read the fictitious scaled-distance Z corresponding to $i_r/W^{1/3} = 295$ from figure 2-7.

$$Z = 0.82 \text{ ft/lb}^{1/3}$$

Step 4. From figure 2-150 where $W_F/W^{1/6} = 2.46$ and $Z = 0.82$ read:

$$f_r = 0.74$$

Step 5. a. Calculate reflected impulse on the frangible back wall by multiplying the value of impulse from step 1 and $f_r = 0.74$

$$i_r \text{ (frangible back wall)} = 4870.3 (0.74) = 3604.0 \text{ psi-ms}$$

b. Peak reflected pressure from step 1.

$$P_r = 3700 \text{ psi}$$

c. Calculate duration of load on wall.

$$t_o = \frac{2i_r}{P_r} = \frac{2 (3604.0)}{3700} = 1.95 \text{ ms}$$

Problem 2A-7 Gas Pressure

Problem: Determine the gas pressure-time loading inside a cubicle, with a small vent opening, due to an internal explosion. The vent opening may be sealed or unsealed with a frangible panel or cover.

Procedure:

Step 1. Apply a 20% factor of safety to the charge weight.

- Step 2. Calculate the free volume inside the cubicle V_f .
- Step 3. Determine the charge weight to free volume ratio W/V_f .
- Step 4. Determine the peak gas pressure P_g from figure 2-152 using the value of W/V_f from step 3.
- Step 5. Determine vent area A .
- Step 6. Determine scaled value of the vent area $A/V^{2/3}$.
- Step 7. a. Calculate the unit weight of the frangible panel W_F , if any.
b. Calculate the scaled unit weight of the frangible panel or cover $W_F/W^{1/3}$. Use $W_F/W^{1/3} = 0$ for no cover.
- Step 8. Determine the scaled average reflected impulse on the element containing the vent opening with no cover according to the procedure outlined in Problem 2A-4 or on the frangible panel (cover) using the procedure of Problem 2A-6.
- Step 9. Determine the scaled gas impulse from figures 2-153 to 2-164. Use the values of W/V_f from step 3, $W_F/W^{1/3}$ from step 7, $A/V^{2/3}$ from step 6 and $i_r/W^{1/3}$ from step 8. Interpolate for values of W/V_f and $i_r/W^{1/3}$ if required. Multiply by $W^{1/3}$ to calculate gas impulse.
- Step 10. Calculate the fictitious gas duration using equation 2-4 and values of P_g and i_g from steps 4 and 9 respectively.

Example 2A-7 (A) Gas Pressure (Small Vent Opening)

Required: Gas pressure-time loading inside a 10' x 10' x 10' cubicle with a 2' x 2' vent opening on the rear wall. The charge weight is 833.3 pounds.

Solution:

Step 1. Charge weight:

$$W = 833.3 \times 1.20 = 1,000 \text{ lbs}$$

Step 2. Free volume inside the structure:

$$V_f = 10' \times 10' \times 10' = 1,000 \text{ ft}^3$$

Step 3. Charge weight to free volume ratio:

$$W/V_f = 1000.0/1000.0 = 1.0$$

Step 4. Read P_g from fig. 2-152 for $W/V_f = 1.0$.

$$P_g = 2,650 \text{ psi}$$

Step 5. Vent area of 2' x 2' opening:

$$A = 2' \times 2' = 4 \text{ ft}^2$$

Step 6. Calculate scaled vent area:

$$A/V^{2/3} = 4/1000^{2/3} = .04 \text{ ft}^2/\text{ft}^2$$

Step 7. a. Vent has no cover.

b. Scaled weight of the cover:

$$W_F/W^{1/3} = 0$$

Step 8. Scaled average reflected impulse of the rear wall from procedure outlined in problem 2A-4:

$$i_r/W^{1/3} = 1225 \text{ psi-ms/lb}^{1/3}$$

Step 9. Read scaled gas impulse from figures 2-162 to 2-164 for $A/V^{2/3} = 0.04$ and $W_F/W^{1/3} = 0.0$. Interpolate for scaled impulse of $i_g/W^{1/3} = 1225$.

$$i_g/W^{1/3} = 7500 \text{ psi-ms/lb}^{1/3}$$

$$\therefore i_g = 7,500 \times 1,000^{1/3} = 75,000.0 \text{ psi-ms}$$

Step 10. Calculate fictitious duration of gas load from equation 2-4.

$$t_g = \frac{21}{P_g} = \frac{2 \times 75,000.0}{2,650} = 56.6 \text{ ms}$$

Example 2A-7 (B) Gas Pressure (Frangible Wall)

Required: Gas pressure-time loading inside a 10' x 10' x 10' cubicle with a frangible wall of 10 psf as the rear wall. The charge weight is 833.3 pounds.

Solution:

Step 1. Charge weight:

$$W = 833.3 \times 1.2 = 1,000 \text{ lbs}$$

Step 2. Free volume inside the structure:

$$V_f = 10' \times 10' \times 10' = 1,000 \text{ ft}^3$$

Step 3. Charge weight to free volume ratio:

$$W/V_f = 1000/1000 = 1.0$$

Step 4. Read P_g from fig. 2-152 for $W/V_f = 1.0$.

$$P_g = 2650 \text{ psi}$$

Step 5. Vent area of frangible wall:

$$A = 10' \times 10' = 100 \text{ ft}^2$$

Step 6. Calculate scaled vent area:

$$A/V^{2/3} = 100/1000^{2/3} = 1.0 \text{ ft}^2/\text{ft}^2$$

Step 7. a. Unit density of the frangible wall:

$$W_F = 10.0 \text{ lbs/ft}^2 \text{ (given)}$$

b. Scaled weight of the frangible wall:

$$W_F/W^{1/3} = 10/1000^{1/3} = 1.0$$

Step 8. Scaled average reflected impulse of the rear frangible wall from procedure outlined in problem 2A-6:

$$i_r/W^{1/3} = 784 \text{ psi-ms/lb}^{1/3}$$

- Step 9. a. Read scaled gas impulse from figures 2-162 to 2-164 for $A/V^{2/3} = 1.0$ and $W_F/W^{1/3} = 1.0$. Interpolate for scaled impulse of $i_r/W^{1/3} = 784$.

$$i_g/W^{1/3} = 400.0 \quad \text{psi-ms/lb}^{1/3}$$

$$\therefore i_g = 400.0 \times 1000^{1/3} = 4000 \quad \text{psi-ms}$$

- Step 10. Calculate fictitious duration of gas load from equation 2-4.

$$t_g = \frac{21}{P_g} = \frac{2 \times 4000}{2650} = 3.02 \text{ ms}$$

Problem 2A-8 Leakage Pressures from Fully Vented Three Wall Cubicle

Problem: Determine free-field blast wave parameters at a distance from a fully vented explosion inside a three wall cubicle.

Procedure:

- Step 1. Determine charge weight, distance in the desired direction and volume of structure.
- Step 2. Apply a 20% safety factor to the charge weight.
- Step 3. Calculate scaled distance and W/V ratio.
- Step 4. Determine peak positive pressures using figures 2-168 or 2-169.
- Step 5. Determine maximum peak pressure for side and back directions from figure 2-170 using W/V ratio.
- Step 6. For W/V ratio determine scaled positive impulses using figures 2-171 to 2-182. Multiply by $W^{1/3}$ to calculate actual value of impulses.
- Step 7. Determine shock parameters from Figure 2-15 corresponding to the peak pressure from step 4, except for the normal reflected impulse where the scaled impulse from step 6 should be used.

Example 2A-8 Leakage Pressures from Fully Vented Three Wall Cubicle

Required: Blast wave parameters at a distance of 200 ft. from an explosion located at the center of a three wall cubicle with no roof. The charge weight is 833.3 lbs. and the interior dimensions of the cubicle are 17.5 ft. x 17.5 ft. x 13 ft. high. Calculate the parameters at the front, side and back of the cubicle.

Solution:

Step 1. Given:

- a. Charge weight = 833.3 lbs.
- b. $R = 200$ ft. in all directions.
- c. $V = 17.5 \times 17.5 \times 13 = 3.980 \text{ ft}^3$.

Step 2. Calculate W :

$$W = 1.20 \times \text{Charge Weight} = 1.20 \times 833.3 = 1000 \text{ lbs.}$$

Step 3. Calculate:

- a. Scaled distance Z ,

$$Z = \frac{R}{W^{1/3}} = \frac{200}{(1000)^{1/3}} = 20 \text{ ft/lbs}^{1/3}$$

- b. W/V ratio,

$$W/V = 1000/3,980 = 0.25 \text{ lbs/ft}^3$$

Step 4. Determine peak incident pressure from figure 2-168:

$$P_{so} \text{ (front)} = 5.5 \text{ psi}$$

$$P_{so} \text{ (side)} = 4.0 \text{ psi}$$

$$P_{so} \text{ (back)} = 2.8 \text{ psi}$$

Step 5. For $W/V = 0.25$, read the maximum peak incident pressures from figure 2-170:

$$(P_{so})_{\max} \text{ (back and side)} = 47.0 \text{ psi} > 4.0 > 2.8$$

Step 6. Scaled positive impulse, for $Z = 20 \text{ ft/lbs}^{1/3}$ and $W/V = 0.25 \text{ lbs/ft}^3$

$$i_s/W^{1/3} \text{ (front)} = 5.5 \text{ psi-ms/lb}^{1/3} \quad \text{figure 2-171}$$

$$i_s \text{ (front)} = 5.5 \times 1000^{1/3} = 55 \text{ psi-ms}$$

$$i_s/W^{1/3} \text{ (side)} = 4.5 \text{ psi-ms/lb}^{1/3} \quad \text{figure 2-173}$$

$$i_s \text{ (side)} = 4.5 \times 1000^{1/3} = 45 \text{ psi-ms}$$

$$i_s/W^{1/3} \text{ (back)} = 3.8 \text{ psi-ms/lb}^{1/3} \quad \text{figure 2-175}$$

$$i_s \text{ (back)} = 3.8 \times 1000^{1/3} = 38 \text{ psi-ms}$$

Step 7. For peak positive pressures (P_{s0}) read shock parameters from figure 2-15 at front, side and back directions.

a. For P_{s0} (front) = 5.5 psi (Step 4)

$$U = 1.28 \text{ ft/ms}$$

$$t_o/W^{1/3} = 2.95 \text{ ms/lb}^{1/3}$$

$$t_o = 2.95 \times 1000^{1/3} = 29.5 \text{ ms}$$

$$t_A/W^{1/3} = 7.00 \text{ ms/lb}^{1/3}$$

$$t_A = 7.00 \times 1000^{1/3} = 70.0 \text{ ms}$$

b. For P_{s0} (side) = 4.0 psi (Step 4)

$$U = 1.24 \text{ ft/ms}$$

$$t_o/W^{1/3} = 3.20 \text{ ms/lb}^{1/3}$$

$$t_o = 3.2 \times 1000^{1/3} = 32.0 \text{ ms}$$

$$t_A/W^{1/3} = 9.30 \text{ ms/lb}^{1/3}$$

$$t_A = 9.3 \times 1000^{1/3} = 93.0 \text{ ms}$$

c. For P_{so} (back) = 2.8 psi

$$U = 1.20 \text{ ft/ms}$$

$$t_o/W^{1/3} = 3.45 \text{ ms/lb}^{1/3}$$

$$t_o = 3.45 \times 1000^{1/3} = 34.5 \text{ ms}$$

$$t_A/W^{1/3} = 12.90 \text{ ms/lb}^{1/3}$$

$$t_A = 12.9 \times 1000^{1/3} = 129.0 \text{ ms}$$

Problem 2A-9 Leakage Pressure from Partially Vented Four Wall Cubicle

Problem: Determine free-field blast wave parameters at a distance from a partially vented explosion inside a four wall cubicle.

Procedure:

- Step 1. Determine charge weight, distance to point in question, vent area and volume of structure.
- Step 2. Apply a 20% safety factor to the charge weight.
- Step 3. Calculate distance Z , $\frac{A}{V^{2/3}}$ ratio and $AW^{1/3}/V$ ratio.
- Step 4. Determine peak positive pressure using figure 2-184.
- Step 5. Determine scaled positive impulses using figure 2-185. Multiply

by $W^{1/3}$ to calculate actual value of impulses.

- Step 6. Determine shock parameters from figure 2-15. Use the peak pressure from step 4, except for normal reflected impulse where the scaled impulse(s) from step 5 should be used.

**Example 2A-9 Leakage Pressure from Partially Vented
Four Wall Cubicle**

Required: Blast wave parameters at distance of 200 ft. from a charge located in an above ground four wall cubicle. The circular vent is located at the center of the roof and has a diameter of 4 ft. The charge is 833.3 lbs and located at the center of 17.5' x 17.5' x 13' cubicle. Top of the roof is 15 feet above the ground level.

Solution:

Step 1. Given (see figure 2-183b for parameters):

a. Charge weight = 833.3 lbs.

b. $R = 200$ ft., $h = 15$ ft.

$$d_1 = \left[\left(\frac{17.5}{2} \right)^2 + (15 - 13/2)^2 \right]^{1/2} = 8.73 \text{ ft.}$$

$$d_2 = (17.5 - 4)/2 = 6.75 \text{ ft.}$$

$$d_3 = \left[(15)^2 + (200 - 4/2 - 6.75 - 15)^2 \right]^{1/2} = 176.89 \text{ ft.}$$

$$R' = d_1 + d_2 + h + d_3 = 8.73 + 6.75 + 15 + 176.89 = 207.37 \text{ ft.}$$

c. $A = \pi(2)^2 = 12.57 \text{ ft}^2$

d. $V = 17.5 \times 17.5 \times 13 = 3,980 \text{ ft}^3$

Step 2. Calculate W:

$$W = 1.20 \times \text{charge weight} = 1.20 \times 833.3 = 1000 \text{ lbs.}$$

Step 3. Calculate:

a. Scaled distance Z.

$$Z = \frac{R'}{W^{1/3}} = \frac{207.37}{1000^{1/3}} = 20.7 \text{ ft/lb}^{1/3}$$

$$b. \quad A/V^{2/3} = 12.57/(3980)^{2/3} = 0.05$$

$$c. \quad AW^{1/3}/V = 12.57 (1000)^{1/3}/3,980 = 0.0316 \text{ lbs}^{1/3}/\text{ft}$$

Step 4. Peak positive pressure from figure 2-184 for $Z = 20.7$ and $A/V^{2/3} = .050$.

$$\therefore P_{s0} = 0.95 \text{ psi}$$

Step 5. Peak positive pressure impulse from figure 2-185 for $Z = 20.7$ and $AW^{1/3}/V = .0316$.

$$i_s/W^{1/3} = 1.80 \text{ psi-ms/lb}^{1/3}$$

$$i_s = 1.8 \times 1000^{1/3} = 18.0 \text{ psi-ms}$$

Step 6. For peak positive pressure $P_{s0} = .95 \text{ psi}$, read shock parameters from figure 2-15.

$$U = 1.12 \text{ ft/ms}$$

$$t_o/W^{1/3} = 4.5 \text{ ms/lb}^{1/3}$$

$$t_o = 4.5 \times 1000^{1/3} = 45.0 \text{ ms}$$

$$t_A/W^{1/3} = 35.0 \text{ ms/lb}^{1/3}$$

$$t_A = 35.0 \times 1000^{1/3} = 350.0 \text{ ms}$$

Problem 2A-10 External Blast Loads on Structures

Problem: Determine the pressure-time blast loading curves on a rectangular structure from an external explosion.

Procedure:

- Step 1. Determine the charge weight, ground distance R_G , height of burst H_G (for air burst) and structure dimensions.
- Step 2. Apply a 20% safety factor to the charge weight.
- Step 3. Select several points on the structure (front wall, roof, rear wall, etc.) and determine free-field blast wave parameters for each point. For air burst, follow the procedure outlined in problem 2A-2; a surface burst, problem 2A-3; and leakage pressures, problem 2A-8 or 2A-9.

Step 4. For the front wall:

- a. Calculate peak positive reflected pressure $P_{ra} = C_{ra} \times P_{so}$. Read value of C_{ra} for P_{so} and α from figure 2-193.
- b. Read scaled unit positive reflected impulse $i_{ra}/W^{1/3}$ from figure 2-194 for P_{so} and α . Multiply scaled value by $W^{1/3}$ to obtain absolute value.

Note: If wave front is not plane, use average values.

Step 5. Determine positive phase of front wall loading.

- a. Determine sound velocity in reflected overpressure region C_r from figure 2-192 for peak-incident pressure P_{so} .
- b. Calculate clearing time t_c :

$$t_c = \frac{4S}{(1 + R) C_r} \text{ (ms)} \quad (\text{eq. 2-3})$$

where:

S = height of front wall or one-half its width, whichever is smaller.

G = maximum of wall height or one-half its width

$R = S/G$

- c. Calculate fictitious positive phase duration t_{of} :

$$t_{of} = \frac{2i_s}{P_{so}} \quad (\text{eq. 2-6})$$

- d. Determine peak dynamic pressure q_0 from figure 2-3 for P_{so} .

- e. Calculate $P_{so} + C_D q_0$. Obtain C_D from paragraph 2-15.3.2.
- f. Calculate fictitious duration t_{rf} of the reflected pressure.

$$t_{rf} = \frac{2i_{ra}}{P_{ra}} \quad (\text{eq. 2-11})$$

- g. Construct the positive pressure-time curve of the front wall similar to figure 2-191. The actual loading is the smaller of the impulse (area under curve) due to reflected pressure or cleared reflected pressure plus incident pressure.

Step 6. Determine negative phase of the front wall loading.

- a. Read the values of Z from figure 2-15 for the value of P_{ra} from step 4a and $i_{ra}/W^{1/3}$ from step 4b.
- b. Determine P_{ra}^- and $i_{ra}^-/W^{1/3}$ from figure 2-16 for the corresponding values of Z from step 6a. Multiply scaled value of the negative impulse by $W^{1/3}$ to obtain absolute value.
- c. Calculate the fictitious duration of the negative reflected pressure.

$$t_{rf}^- = 2i_{ra}^-/P_{ra}^- \quad (\text{eq. 2-7})$$

- d. Calculate rise time of the negative pressure by multiplying t_{rf}^- by 0.27 (Section 2-15.3.2).
- e. Construct the negative pressure-time curve similar to figure 2-191.

Step 7. Determine positive phase of side wall loading.

- a. Calculate the wave length to span length ratio L_{wf}/L at front of the span.
- b. Read values of C_E , $t_d/W^{1/3}$ and $t_{of}/W^{1/3}$ from figures 2-196, 2-197 and 2-198 respectively.
- c. Calculate P_R , t_r and t_o .
- d. Determine dynamic pressure q_0 from figure 2-3 for P_R .
- e. Calculate $P_R = C_E P_{sof} + C_D q_0$ (eq. 2-12). Obtain C_D from paragraph .
- f. Construct positive phase pressure-time curve similar to figure 2-195.

- Step 8. Determine negative phase of side wall loading.
- Determine value of C_E and $t_{of}/W^{1/3}$ for the value of L_{wf}/L from step 7a from figures 2-196 and 2-198 respectively.
 - Calculate $P_r = C_E \times P_{sof}$ and t_{of} .
 - Calculate rise time of negative phase equal to $0.27 t_{of}$ (section 2-15.3.2).
 - Construct the negative pressure-time curve similar to figure 2-195.
- Step 9. Determine roof loading. Follow procedure outlined for side wall loading.
- Step 10. Determine rear wall loading. Follow procedure outlined for side wall loading. For the purpose of calculations, assume that the back wall is rotated to a horizontal position (see figure 2-199).

Example 2A-10 External Blast Loads on Structures

Required: Determine pressure-time blast loading curves for the front wall, roof, rear half of the side walls and rear wall of the structure shown in figure 2A-9 for a surface burst of 5,000 lbs. at a distance from the front wall of 155 ft. Structure width is 30 ft. and the shock front is plane.

- Step 1. Given: Charge weight = 5,000 lbs., $R_G = 155$ ft.
- Step 2. $W = 1.2 (5,000) = 6,000$ lbs.
- Step 3. Determine free-field blast wave parameters P_{so} , t_A , L_w and t_o at points 1 through 3 and i_g at point 1.

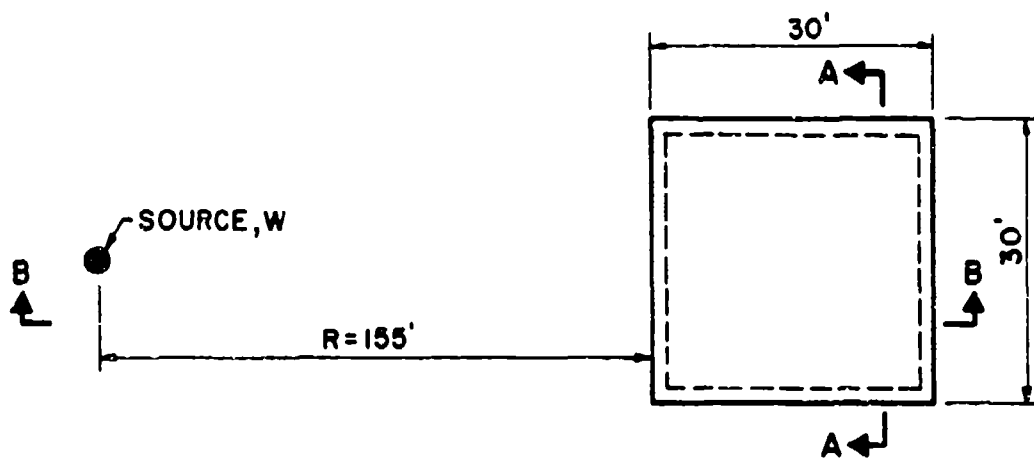
For point 1:

$$a. \quad Z_G = \frac{R_G}{W^{1/3}} = \frac{155}{6000^{1/3}} = 8.53 \text{ ft/lb}^{1/3}$$

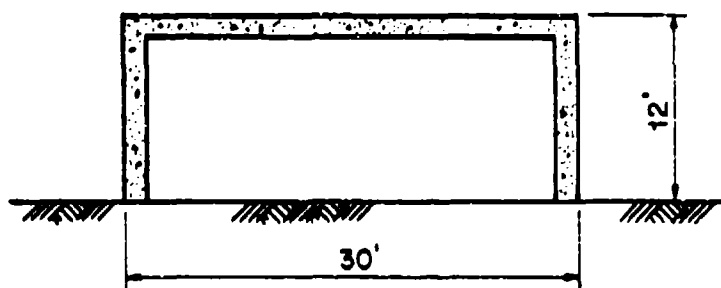
- b. Determine free-field blast wave parameters from figure 2-15 for $Z_G = 8.53 \text{ ft/lb}^{1/3}$

$$P_{so} = 12.8 \text{ psi}$$

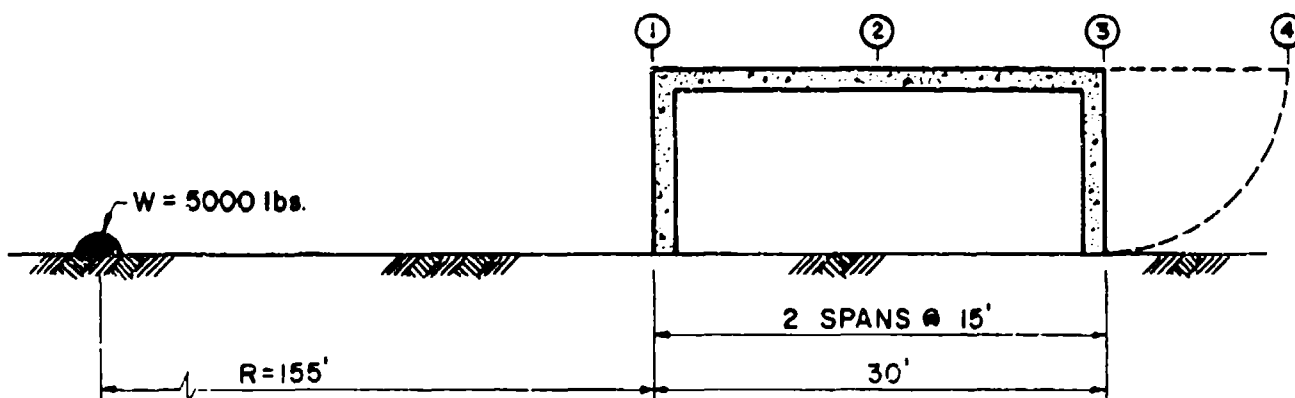
$$t_A/W^{1/3} = 3.35 \text{ ms/lb}^{1/3} \therefore t_A = 3.35 (6000)^{1/3} = 60.9 \text{ ms}$$



PLAN



SECTION A-A



SECTION B-B

FIGURE 2A-9

$$L_w/W^{1/3} = 2.10 \text{ ft/lb}^{1/3} \therefore L_w = 2.10 (6000)^{1/3} = 38.2 \text{ ft}$$

$$t_o/W^{1/3} = 2.35 \text{ ms/lb}^{1/3} \therefore t_o = 2.35 (6000)^{1/3} = 42.7 \text{ ms}$$

- c. Determine incident impulse from figure 2-15 for $Z_G = 8.53 \text{ ft/lb}^{1/3}$.

$$\frac{i_s}{W^{1/3}} = 9.0 \text{ psi-ms/lb}^{1/3} \therefore i_s = 9.0 (6000)^{1/3} = 163.5 \text{ psi-ms}$$

- d. Repeat steps 3a and 3b for points 2 and 3. Results are tabulated below.

| Point No. | R_G (ft) | Z (ft) | P_{so} (psi) | $t_A/W^{1/3}$ (ms/lb ^{1/3}) | t_A (ms) |
|-----------|------------|----------|----------------|---------------------------------------|------------|
| 1 | 155.0 | 8.53 | 12.8 | 3.35 | 60.9 |
| 2 | 170.0 | 9.35 | 10.8 | 3.90 | 70.9 |
| 3 | 185.0 | 10.18 | 9.0 | 4.60 | 83.6 |

| $L_w/W^{1/3}$ (ft/lb ^{1/3}) | L_w (ft) | $t_o/W^{1/3}$ (ms/lb ^{1/3}) | t_o (ms) | $i_s/W^{1/3}$ (psi-ms/lb ^{1/3}) | i_s (psi-ms) |
|---------------------------------------|------------|---------------------------------------|------------|---|----------------|
| 2.10 | 38.2 | 2.35 | 42.7 | 9.00 | 163.5 |
| 2.24 | 40.7 | 2.48 | 45.1 | - | - |
| 2.35 | 42.7 | 2.62 | 47.6 | - | - |

Step 4. Determine front wall reflected pressure and impulse.

- a. Read C_{ra} for $P_{so} = 12.8 \text{ psi}$ and $\alpha = 0^\circ$ from figure 2-193 for point 1.

$$C_{ra} = 2.70 \text{ then } P_{ra} = C_{ra} \times P_{so} = 2.70 \times 12.8 = 34.6 \text{ psi}$$

- b. Read $i_{ra}/W^{1/3}$ for $P_{so} = 12.8 \text{ psi}$ and $\alpha = 0^\circ$ from figure 2-194 for point 1.

$$i_{ra}/W^{1/3} = 17.0 \text{ then } i_{ra} = 17.0 (6,000)^{1/3} = 308.9 \text{ psi-ms}$$

Step 5. Front wall loading, positive phase.

- a. Calculate sound velocity in reflected overpressure region C_r from figure 2-192 for $P_{so} = 12.8$ psi.

$$C_r = 1.325 \text{ ft/ms}$$

- b. Calculate clearing time t_c from eq.

$$t_c = \frac{4S}{(1+R)C_r} \quad (\text{eq. 2-3})$$

where:

$$S = 12.0 \text{ ft} < \frac{30.}{2}$$

$$G = \frac{30.}{2} = 15.0 \text{ ft} > 12.0 \text{ ft.}$$

$$R = S/G = 12./15. = .80$$

then:

$$t_c = \frac{4 \times 12}{(1 + 0.80) 1.325} = 20.1 \text{ ms}$$

- c. Calculate t_{of} from eq. 2-11. Use impulse from step 3c.

$$t_{of} = \frac{2I_s}{P_{so}} = \frac{2 \times 163.5}{12.8} = 25.5 \text{ ms}$$

- d. Determine q_o from figure 2-3 for $P_{so} = 12.8$ psi.

$$q_o = 3.5 \text{ psi}$$

- e. Calculate $P_{so} + C_D q_o$:

$$C_D = 1.0 \text{ from section 2-15.3.2}$$

then,

$$P_{so} + C_D q_o = 12.8 + (1.0 \times 3.5) = 16.3 \text{ psi}$$

- f. Calculate t_{rf} from eq. 2-11 and results of step 4.

$$t_r = \frac{2I_{ra}}{P_{ra}} = \frac{2 \times 308.9}{34.6} = 17.9 \text{ ms}$$

- g. Construct the pressure time curve. See figure 2A-10.

Note: The reflected pressure-time curve is used for design since the reflected impulse is less than the impulse produced by the clearing time.

Step 6. Negative phase loading, front wall.

- a. Read the values of Z corresponding to $P_{ra} = 34.6$ (step 4a) and $i_{ra}/W^{1/3} = 17.0$ (step 4b) from figure 2-15.

$$P_{ra} = 34.6 \text{ then, } Z(P_{ra}) = 8.5$$

$$i_{ra}/W^{1/3} = 17.0 \text{ then, } Z(i_{ra}/W^{1/3}) = 10.4$$

- b. Using the Z values from step 6a and figure 2-16 determine values of P_{ra}^- and i_{ra}^- (Peak pressure and impulse in negative phase).

$$Z(P_{ra}) = 8.5 \text{ then, } P_{ra}^- = 3.25 \text{ psi}$$

$$Z(i_{ra}/W^{1/3}) = 10.4 \text{ then, } i_{ra}^-/W^{1/3} = 14.6 \text{ psi-ms/lb}^{1/3}$$

and

$$i_{ra}^- = 14.6 \times (6,000)^{1/3} = 265.3 \text{ psi-ms}$$

- c. Calculate fictitious duration t_{rf}^- .

$$t_{rf}^- = \frac{2 i_{ra}^-}{P_{ra}^-}$$

$$t_{rf}^- = \frac{2 \times 265.3}{3.25} = 163.3 \text{ ms}$$

- d. Calculate negative phase rise time:

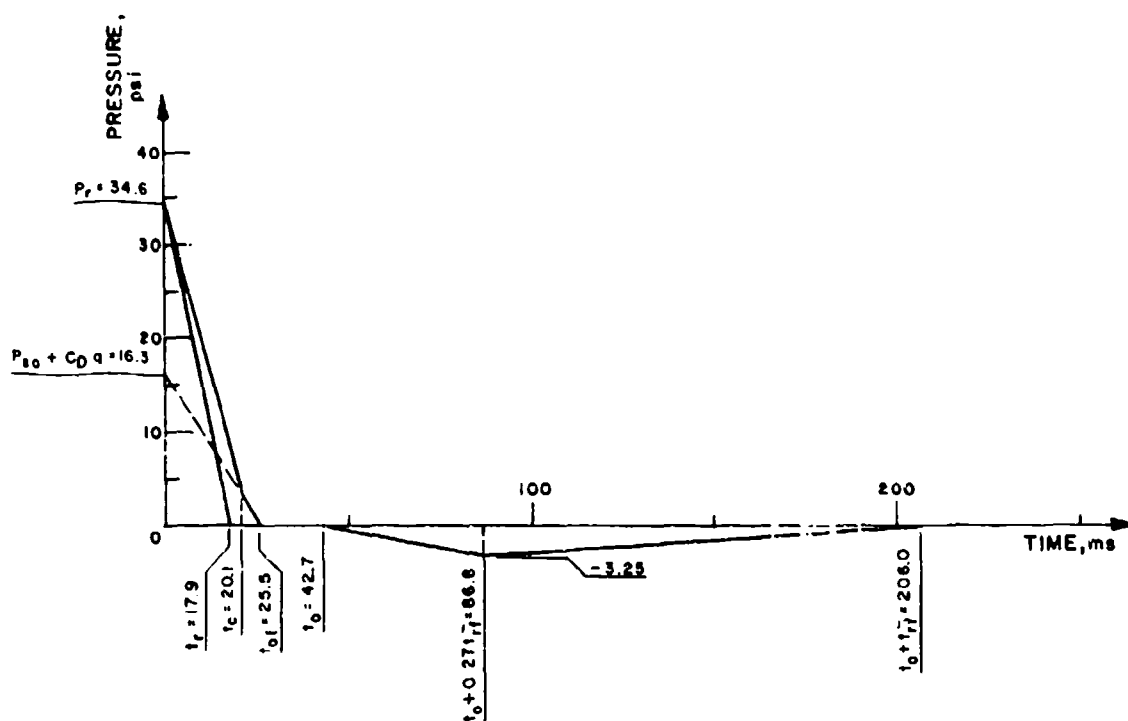


FIGURE 2A-10

$$0.27 \times t_{rf} = .27 \times 163.3 = 44.1 \text{ ms}$$

- e. Construct the negative pressure-time curve.

$$t_o = 42.7 \text{ ms (Point 1, step 3d)}$$

$$t_o + 0.27 t_{rf} = 42.7 + 44.1 = 86.8 \text{ ms}$$

$$t_o = t_{rf} = 42.7 + 163.3 = 206.0 \text{ ms}$$

The negative pressure-time curve is plotted in figure 2A-10.

- Step 7. Side wall loading, positive phase, calculate the loading on the rear-half of the wall (Point 2 to 3, figure 2A-9).

- a. Calculate L_{wf}/L ratio:

$$L = 15.0 \text{ ft (Point 2 to 3)}$$

$$L_{w2} = 40.7 \text{ ft (step 3d)}$$

then,

$$L_{wf}/L = \frac{40.7}{15.0} = 2.71$$

- b. Read C_E , $t_d/W^{1/3}$ and $t_{of}/W^{1/3}$ for $L_{wf}/L = 2.71$ and $P_{sof} = 10.8$ (step 3d, Point 2)

$$C_E = .76 \text{ fig. 2-196}$$

$$t_d/W^{1/3} = .66 \text{ fig. 2-197}$$

$$t_{of}/W^{1/3} = 2.47 \text{ fig. 2-198}$$

- c. Calculate $C_E P_{sof}$, t_d and t_{of} using results of step 7b.

$$\therefore C_E P_{sof} = .76 \times 10.8 = 8.2$$

$$\therefore t_r = .66 \times (6,000)^{1/3} = 12.0 \text{ ms}$$

$$\therefore t_{of} = 2.47 \times (6,000)^{1/3} = 44.9 \text{ ms}$$

d. Determine q_o from figure 2-3 for $C_E P_{sof} = 8.2 \text{ psi}$.

$$q_o = 1.55 \text{ psi}$$

e. Calculate peak positive pressure from eq. 2-12.

$$C_D = -0.40 \text{ from section 2-15.3.2}$$

$$C_E P_{sof} + C_D q_o = .76 \times 10.8 + (-0.40 \times 1.55) = 7.6 \text{ psi}$$

f. Construct the pressure-time curve.

See figure 2A-11 below.

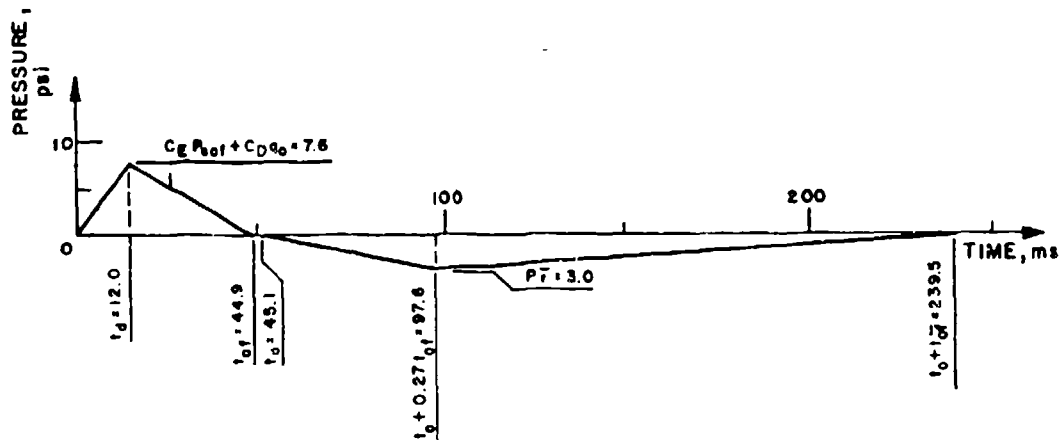


Figure 2A-11

Step 8. Negative phase loading on the rear-half of the side wall.

- a. Read values of C_E and $t_{of}^-/W^{1/3}$ for $L_{wf}/L = 2.71$ (Step 7a) from figures 2-196 and 2-198 respectively.

$$C_E = .28$$

$$t_{of}^-/W^{1/3} = 10.7 \text{ ms/lb}^{1/3}$$

- b. Calculate P_r^- and t_{of}^- :

$$P_r^- = C_E \times P_{sof} = .28 \times 10.8 = 3.0 \text{ psi}$$

$$t_{of}^- = 10.7 \times (6,000)^{1/3} = 194.4 \text{ ms}$$

- c. Negative phase rise time:

$$0.27 t_{of}^- = .27 \times 194.4 = 52.5 \text{ ms}$$

- d. Construct the negative pressure-time curve.

$$t_o = 45.1 \text{ ms (Point 2, step 3d)}$$

$$t_o + 0.27 t_{of}^- = 45.1 + 52.5 = 97.6 \text{ ms}$$

$$t_o + t_{of}^- = 45.1 + 194.4 = 239.5 \text{ ms}$$

The negative pressure-time curve is plotted in figure 2A-11.

Step 9. Calculate roof loading. (Point 1 to 3, figure 2A-9)

- a. Calculate L_{wf}/L ratio:

$$L = 30.0 \text{ ft (Point 1 to 3)}$$

$$L_{w1} = 38.2 \text{ ft (step 3d) then,}$$

$$L_{wf}/L = \frac{38.2}{30.0} = 1.27$$

- b. Read C_E , $t_d/W^{1/3}$ and $t_{of}/W^{1/3}$ for $L_{wf}/L = 1.27$ and $P_{sof} = 12.8$ psi (step 3d, Point 1) then,

$$C_E = .52 \text{ fig. 2-196}$$

$$t_d/W^{1/3} = 1.25 \text{ fig. 2-197}$$

$$t_{of}/W^{1/3} = 3.10 \text{ fig. 2-198}$$

- c. Calculate $C_E P_{sof}$, t_d and t_{of} using results of step 9b.

$$C_E P_{sof} = .52 \times 12.8 = 6.66$$

$$t_d = 1.25 \times (6,000)^{1/3} = 22.7 \text{ ms}$$

$$t_{of} = 3.10 \times (6,000)^{1/3} = 56.3 \text{ ms}$$

- d. Determine q_0 from figure 2-3 for $C_E P_{sof} = 6.66$ psi.

$$q_0 = 1.05 \text{ psi}$$

- e. Calculate maximum pressure from eq. 2-12:

$$C_D = -0.40 \quad \text{From section 2-15.3.2}$$

$$C_E P_{sof} + C_D q_0 = .52 \times 12.8 + (-0.40 \times 1.05) = 6.24 \text{ psi}$$

- f. Construct the pressure-time curve.

See figure 2A-12 below.

- g. Read values of C_E^- and $t_{of}^-/W^{1/3}$ for $L_{wf}/L = 1.27$ (step 9a) from figures 2-196 and 2-198 respectively.

$$C_E^- = .26$$

$$t_{of}^-/W^{1/3} = 11.7 \text{ ms/lb}^{1/3}$$

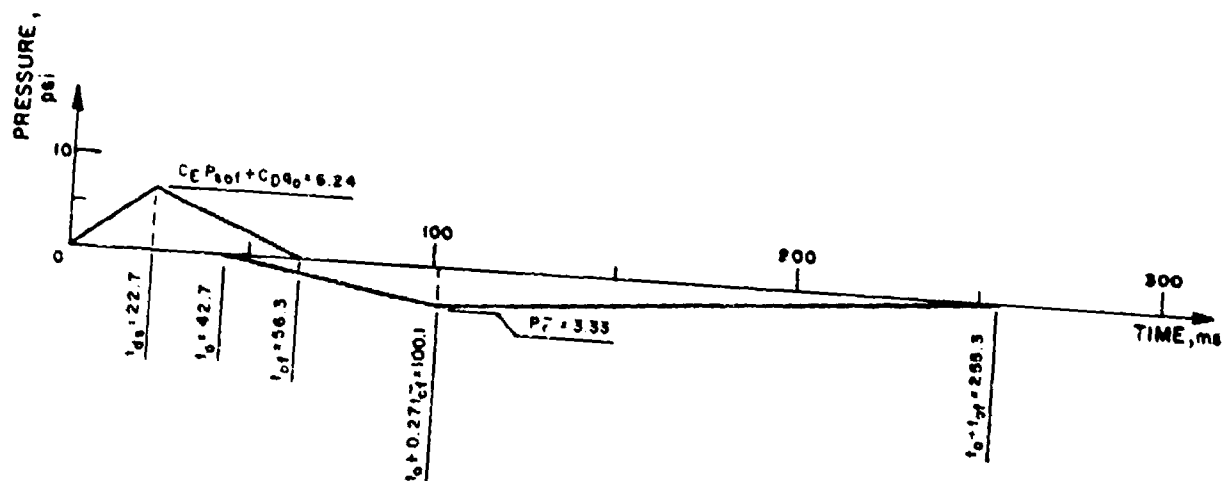


FIGURE 2A-12

- h. Calculate P_r^- and t_{of}^- :

$$P_r^- = C_E^- \times P_{sof} = .26 \times 12.8 = 3.33 \text{ psi}$$

$$t_{of}^- = 11.7 \times (6,000)^{1/3} = 212.6 \text{ ms}$$

- i. Negative phase rise time:

$$0.27 t_{of}^- = .27 \times 212.6 = 57.4 \text{ ms}$$

- j. Construct the negative pressure-time curve.

$$t_o = 42.7 \text{ ms (Point 1, step 3d)}$$

$$t_o + .27 t_{of}^- = 42.7 + 57.4 = 100.1 \text{ ms}$$

$$t_o + t_{of}^- = 42.7 + 212.6 = 255.3 \text{ ms}$$

The negative pressure-time curve is plotted in figure 2A-12

Step 10. Calculate rear wall loading (Point 3 to 4, figure 2A-9). Assume rear wall is rotated to a horizontal position.

- a. Calculate L_{wf}/L ratio:

$$L = 12.0 \text{ ft (Point 3 to 4 or height of the structure)}$$

$$L_{w3} = 42.7 \text{ ft (step 3d), then,}$$

$$L_{wf}/L = \frac{42.7}{12.0} = 3.56$$

- b. Read C_E , $t_d/W^{1/3}$ and $t_{of}/W^{1/3}$ for $L_{wf}/L = 3.56$ and $P_{sob} = 9.0$ psi (step 3d, point 3).

$$C_E = .83$$

fig. 2-196

$$t_d/W^{1/3} = .51$$

fig. 2-197

$$t_{of}/W^{1/3} = 2.45$$

fig. 2-198

c. Calculate $C_E P_{sob}$, t_r and t_o using results of step 10b.

$$\therefore C_E P_{sob} = .83 \times 9.0 = 7.47 \text{ psi}$$

$$\therefore t_d = .51 \times (6,000)^{1/3} = 9.3 \text{ ms}$$

$$\therefore t_{of} = 2.45 \times (6,000)^{1/3} = 44.5 \text{ ms}$$

d. Determine q_o from figure 2-3 for $C_E P_{sob} = 7.47 \text{ psi}$

$$q_o = 1.30 \text{ psi}$$

e. Calculate maximum pressure from eq. 2-12:

$$C_D = -0.40 \quad \text{from section 2-15.3.2}$$

$$C_E P_{sob} + C_D q_o = .83 \times 9.0 + (-0.40 \times 1.30) = 6.95 \text{ psi}$$

f. Construct the pressure-time curve.

See figure 2A-13 below.

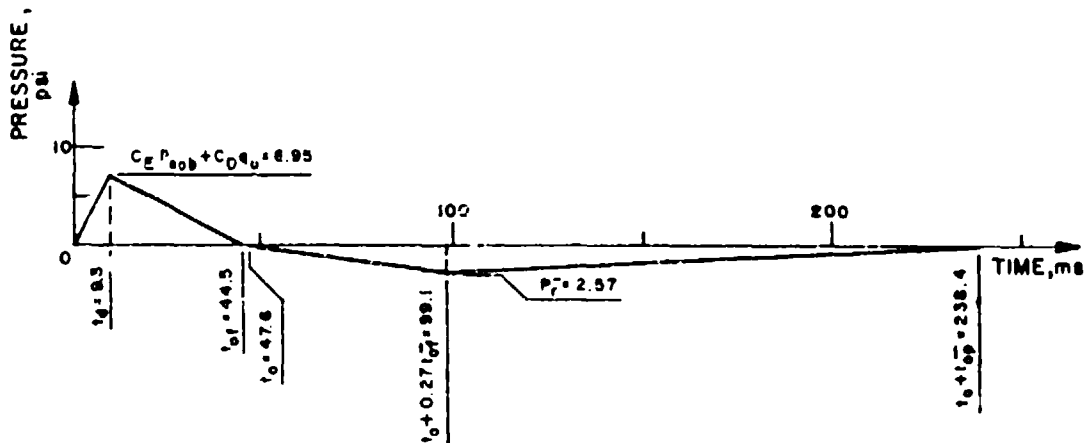


Figure 2A-13

- g. Read values of C_E and $t_{of}^-/W^{1/3}$ for $L_{wf}/L = 3.56$ (step 10a) from figures 2-196 and 2-198 respectively.

$$C_E = .285$$

$$t_{of}^-/W^{1/3} = 10.5 \text{ ms/lb}^{1/3}$$

- h. Calculate P_r^- and t_{of}^- :

$$P_r^- = C_E \times P_{sob} = .285 \times 9.0 = 2.57 \text{ psi}$$

$$t_{of}^- = 10.5 \times (6,000)^{1/3} = 190.8 \text{ ms}$$

- i. Negative phase rise time:

$$0.27 t_{of}^- = .27 \times 190.8 = 51.5 \text{ ms}$$

- j. Construct the negative pressure-time curve.

$$t_o = 47.6 \text{ ms (Point 3, step 3d)}$$

$$t_o + .27 t_{of}^- = 47.6 + 51.5 = 99.1 \text{ ms}$$

$$t_o + t_{of}^- = 47.6 + 190.8 = 238.4 \text{ ms}$$

The negative pressure-time curve is plotted in figure 2A-13.

Problem 2A-11 Blast Loads on a Structure with Front Wall Openings

Problem: Determine the pressure-time loads acting on the exterior front wall and all interior surfaces of a rectangular structure with front wall openings due to an external shock load.

Step 1. Charge weight:

- Determine TNT equivalent charge weight, W ;
- Increase charge weight by 20% safety factor, $W = 1.20 \times W$;
- Determine charge weight scaling factor, $W^{1/3}$.

Step 2. Determine free field blast parameters:

- a. For an air burst, use Problem 2A-2 procedure; for a surface burst, use Problem 2A-3 procedure; for leakage pressures, use Problem 2A-8 or 2A-9 procedures.
- b. Evaluate the angle of incidence, α , as the angle between the ground distance from the charge to the center of the front wall, and the normal distance from the charge to the front wall.

Step 3. Front wall idealized pressure-time blast loads:

A. Exterior Blast Load:

- a. Determine peak positive reflected pressure, P_r , as a function of P_{SO} and α , using Figure 2-193.
- b. Determine peak positive reflected scaled unit impulse, $i_{ra}/(W^{1/3})$, as a function of P_{SO} and α , using Figure 2-194.
- c. Determine the absolute positive reflected impulse by multiplying the scaled unit impulse by $(W^{1/3})$.
- d. Determine the sound velocity of the reflected pressure wave, C_r , as a function of P_{SO} , using Figure 2-192.
- e. Determine the reflected pressure clearing time, T'_C , from equation 2-14.
- f. Construct the exterior blast pressure-time load. Follow the procedure in Problem 2A-10.
- g. Determine the scaled wave length of the incident wave, $L_w/(W^{1/3})$, as a function of P_{SO} , using Figure 2-15, irrespective of how the external incident wave was created.
- h. Determine the absolute wave length by multiplying the scaled wave length by $(W^{1/3})$.

B. Interior Blast Load:

- a. Determine the following parameters: L_w/L , L_w/H , A_o/A_w , W/H , and L/H , where A_o is the total area of openings in the front wall, and A_w is the area H by W .

- b. Determine the idealized factored average peak pressure, $(P_{\max} \times (L_w/H))$, as a function of W/H , P_{s0} , A_o/A_w , and L_w/H , using Figures 2-203 to 2-206. Calculate $P_{\max} = (P_{\max} \times L_w/H)/(L_w/H)$.
- c. Determine the arrival time, T_1 , as a function of W/H , P_{s0} , and A_o/A_w , using Figures 2-207 and 2-208.
- d. Determine the rise time, $T_2 - T_1$, as a function of W/H , P_{s0} , and, L_w/H , from Figures 2-209 and 2-210.
- e. Determine the duration time, $T_3 - T_1$, as a function of W/H , P_{s0} , and L_w/H , from Figures 2-211 and 2-212.
- f. Using times T_1 , $T_2 - T_1$, $T_3 - T_1$, and P_{\max} , construct the idealized pressure-time blast load. See Figure 2-201A for general configuration of this blast load.

Step 4. Side Wall Idealized Interior Pressure-Time Blast Load:

- a. Determine the maximum average sidewall pressure, P_{\max} , from equation 2-15.
- b. Determine the idealized times T_1 and T_2 for W/H , using Figure 2-213.
- c. Determine the idealized times T_3 and T_4 for W/H , using Figures 2-214 to 2-229.
- d. Using times T_1 , T_2 , T_3 , T_4 , and P_{\max} , construct the idealized pressure-time load. See Figure 2-201b for general configuration of this blast load.

Step 5: Back Wall Idealized Interior Pressure-Time Blast Load:

- a. Determine the maximum average positive reflected pressure coefficient, P_{RIB}/P_{s0} , as a function of L/H , P_{s0} , and A_o/A_w , using Figures 2-233 and 2-234.
- b. Determine the maximum average pressure, P_{RIB} , by multiplying the pressure coefficient, P_{RIB}/P_{s0} , by P_{s0} .
- c. Determine the idealized time T_1 as a function of W/H , P_{s0} , L/H , and A_o/A_w , using Figure 2-230.
- d. Determine the idealized pressure duration, $T_2 - T_1$, as a function of P_{s0} , and A_o/A_w , using Figure 2-232.

- e. Using times T_1 , $T_2 - T_1$, and P_{RIB} , construct the idealized pressure-time blast load. See Figure 2-201c for general configuration of this blast load.

Step 6. Roof Idealized Interior Pressure-Time Blast Load:

- a. Determine the W/H ratio for the roof as the inverse of W/H ratio of the side wall.
- b. Repeat Step 4 using the W/H ratio of the roof.

Example 2A-11 Blast Loads on a Structure with Front Wall Openings

Required: For the structure and charge as is shown in Figure 2A-14, determine the idealized positive external blast load on the front wall, and the idealized positive internal blast load on the front wall, side wall, roof and back wall.

Step 1. Charge weight

- a. $W = 5000$ lbs. TNT
- b. $W = 1.20 \times 5000 = 6000$ lbs. TNT
- c. $W^{1/3} = 18.1712$ lbs. $^{1/3}$

Step 2. Free field blast parameters - surface burst

- a. Procedure from Problem 2A-3.

Blast parameters: P_{so} , U , i_s , t_o , t_A , for $W = 6000$ lbs., $R_G = 155'$ $Z_G = R_G/W^{1/3} = 155/18.1712 = 8.53$ (say 8.5)

From Figure 2-15 for hemispherical surface burst

$$P_{so} = f_1(Z_G) = 12.6 \text{ psi}$$

$$U = f_2(Z_G) = 1.46 \text{ ft/ms}$$

$$i_s/W^{1/3} = f_3(Z_G) = 9.0 \text{ psi-ms/lb}^{1/3}, i_s = 163.54 \text{ psi-ms}$$

$$t_o/W^{1/3} = f_4(Z_G) = 2.40 \text{ ms/lb}^{1/3}, t_o = 43.61 \text{ ms}$$

$$t_A/W^{1/3} = f_5(Z_G) = 3.40 \text{ ms/lb}^{1/3}, t_A = 61.78 \text{ ms}$$

- b. Charge to wall center ground distance = 155.0'

Charge to wall normal distance = 155.0'

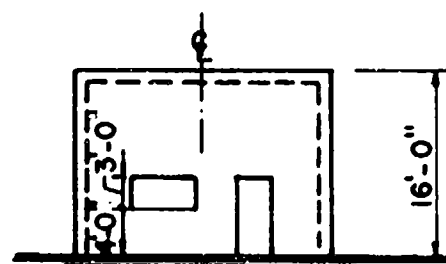
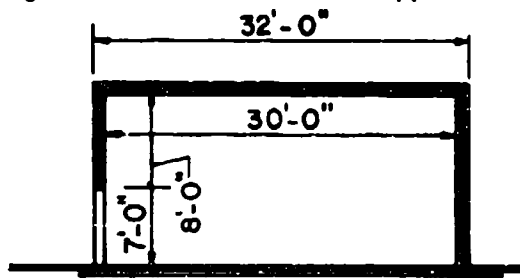
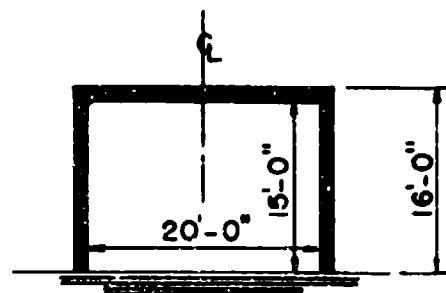
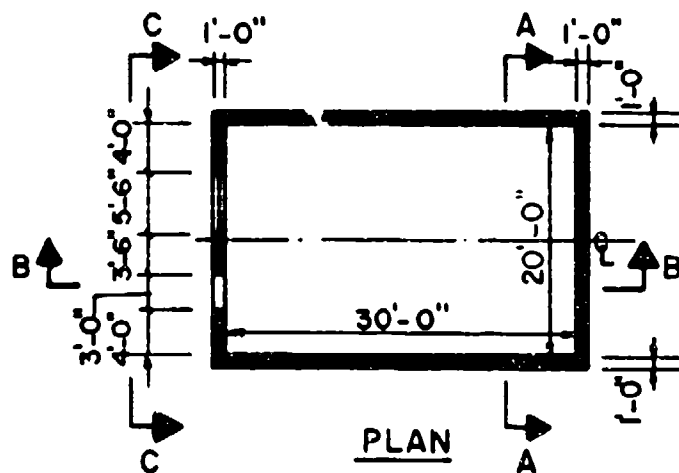
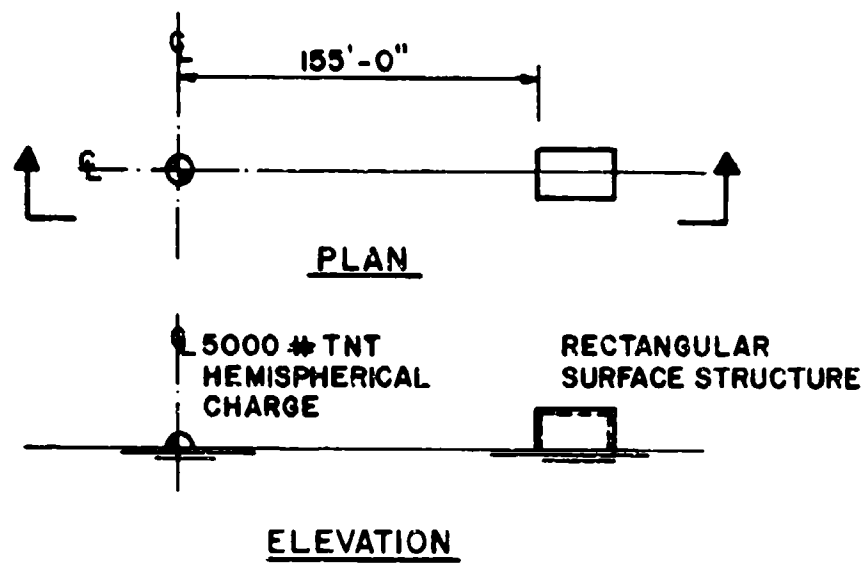
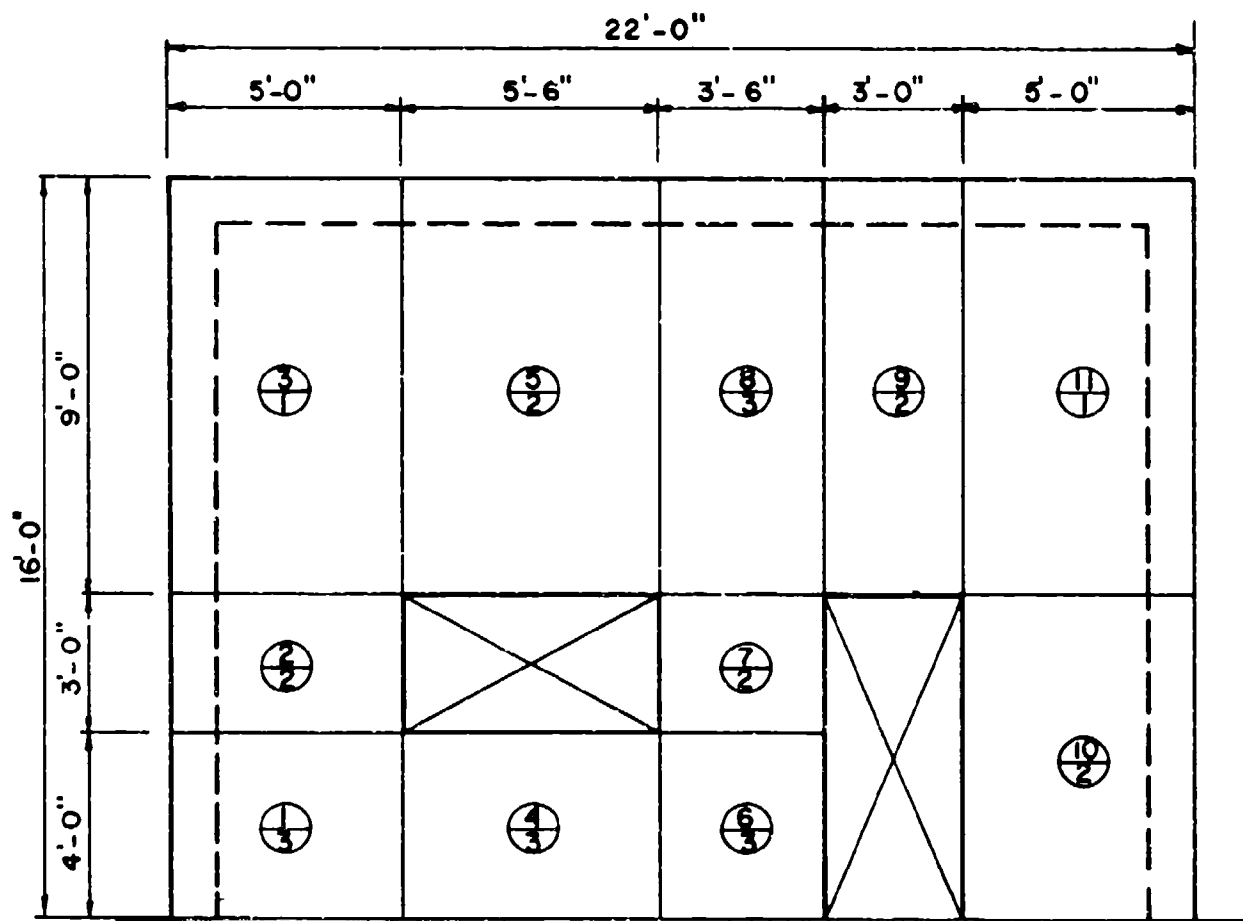
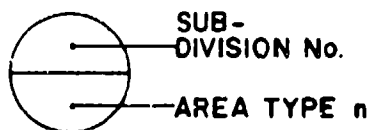


FIGURE 2A-14



ELEVATION



WALL SUB-DIVISION
NOMENCLATURE

FIGURE 2A - 15

$$\alpha = \cos^{-1} (155/155) = 0^\circ$$

Step 3. Front wall idealized pressure-time blast load

A. Exterior Blast Load

- a. From Figure 2-193, for $\alpha = 0^\circ$ and $P_{so} = 12.6$ psi, determine
 $C_{ra} = P_{ra}/P_{so}$

| | | | |
|----------|------|------|------|
| P_{so} | 10.0 | 12.6 | 20.0 |
|----------|------|------|------|

| | | | |
|----------|------|---|------|
| C_{ra} | 2.40 | ? | 2.90 |
|----------|------|---|------|

$$C_{ra} = \langle (2.9 - 2.4) \times (12.6 - 10.0) / (20.0 - 10.0) \rangle + 2.40$$

$$= 0.130 + 2.40 = 2.53$$

$$P_{ra} = P_r = C_{ra} \times P_{so} = 2.53$$

$$\times 12.6 = 31.878 \text{ psi, say } 31.9 \text{ psi}$$

- b. From Figure 2-194, for $\alpha = 0^\circ$, read $i_{ra}/W^{1/3}$ for $P_{so} = 10$ and 20 psi and interpolate for $i_{ra}/W^{1/3}$ at $P_{so} = 12.6$ psi

| | |
|----------|------------------|
| P_{so} | $i_{ra}/W^{1/3}$ |
|----------|------------------|

| | |
|-----|--------------------------|
| psi | psi-ms/lb ^{1/3} |
|-----|--------------------------|

| | |
|----|------|
| 10 | 15.2 |
|----|------|

| | |
|------|---|
| 12.6 | ? |
|------|---|

| | |
|----|----|
| 20 | 23 |
|----|----|

$$i_{ra}/W^{1/3} = \langle [23.0 - 15.2] \times [12.6 - 10.0] / [20.0 - 10.0] \rangle + 15.2 = 2.028$$

$$+ 15.2 = 17.228 \text{ psi-ms/lb}^{1/3}$$

- c. Determine absolute impulse,

$$i_{ra} = (i_{ra}/W^{1/3}) \times (W^{1/3}) = 17.228 \times 18.1712 = 313.1 \text{ psi-ms}$$

- d. For $P_{so} = 12.6$ psi, $C_r = 1.325$ ft/ms from Figure 2-192.

- e. Using Figure 2A-15 as the front wall sub-divisioning, determine h_n , W_n , δ_n , h'_n , A_n , $\delta_n h'_n A_n$, $\sum \delta_n h'_n A_n$, A_f , S' , S , R , and T'_C .

| Subdivision No. | Type n | δ_n - | h'_n ft | h_n ft | W_n ft | A_n ft ² | $\delta_n h'_n A_n$ ft ³ |
|----------------------------------|--------|--------------|-----------|----------|----------|-----------------------|-------------------------------------|
| 1 | 3 | 1.0 | 5.0 | 4.0 | 5.0 | 20.0 | 100.0 |
| 2 | 2 | 0.50 | 5.0 | 3.0 | 5.0 | 15.0 | 37.50 |
| 3 | 1 | 1.0 | 5.0 | 9.0 | 5.0 | 45.0 | 225.0 |
| 4 | 3 | 1.0 | 4.0 | 4.0 | 5.5 | 22.0 | 88.0 |
| 5 | 2 | 0.50 | 9.0 | 9.0 | 5.5 | 49.50 | 222.750 |
| 6 | 3 | 1.0 | 3.50 | 4.0 | 3.5 | 14.0 | 49.0 |
| 7 | 2 | 0.50 | 3.50 | 3.0 | 3.5 | 10.5 | 18.3750 |
| 8 | 3 | 1.0 | 9.0 | 9.0 | 3.5 | 31.5 | 283.50 |
| 9 | 2 | 0.50 | 9.0 | 9.0 | 3.0 | 27.0 | 121.50 |
| 10 | 2 | 0.50 | 5.0 | 7.0 | 3.0 | 35.0 | 87.50 |
| 11 | 1 | 1.0 | 5.0 | 9.0 | 3.0 | 45.0 | 225.0 |
| $\sum_{n=1}^n \delta_n h'_n A_n$ | | | | | | | = 1458.1250 |

$$A_f = (16 \times 32) - (3 \times 5.5) - (7.0 \times 3.0)$$

$$= 512 - 16.5 - 21.0$$

$$= 512 - 37.5$$

$$= 474.5 \text{ ft}^2$$

$$S' = \left(\sum_{n=1}^{11} \delta_n h'_n A_n \right) / A_f = 1458.1250 / 474.5 = 3.073 \text{ ft}$$

$$H = 15.0', W = 20.0', H < W \therefore S = H = 15.0', S' < S \text{ O.K.}$$

$$W > H \therefore G = W = 20.0'$$

$$R = S/G = 15.0/20.0 = 0.75; C_r = 1.325 \text{ ft/ms}$$

$$t'_C = 4S' / \langle (1 + R) \times C_r \rangle = (4 \times 3.073) / (1.75 \times 1.325) = 5.301 \text{ ms}$$

- f. Following general procedure problem 2A-10, Step 5 required previously determined values are:

$$P_{so} = 12.6 \text{ psi}$$

$$i_s = 163.5 \text{ psi-ms}$$

$$P_{ra} = 31.9 \text{ psi}$$

$$i_{ra} = 313.1 \text{ psi-ms}$$

Determine

$$t_{of} = 2i_s/P_{so} = 2 \times 163.5/12.6 = 26 \text{ ms, Eq. 2-b,}$$

$$t_{rf} = 2i_{ra}/P_{ra} = 2 \times 313.1/31.9 = 19.6 \text{ ms, eq. 2-11,}$$

$$q_o = f(P_{so}) = 3.4 \text{ psi, Fig. 2-3}$$

$$C_D = 1.0, \text{ Paragraph 2-15.3.2,}$$

$$P_{so} + C_D q_o = 16 \text{ psi, Paragraph 2-15.3.2}$$

Construct infinite surface impulse and theoretic bi-linear actual surface impulse. Minimum value is design impulse.

Infinite surface fictitious impulse = $i_{ra} = 313.1 \text{ psi-ms}$

Bi-linear theoretic actual surface impulse is area under curve P_{ra} to t'_c on line $P_{so} + C_D q_o$ to t_{of}

$$\begin{aligned} \text{Let } P &= (P_{so} + C_D q_o) < 1 - (t'_c/t_{of}) > \\ &= 16.0 < 1 - (5.3/26) > = 12.7 \text{ psi} \end{aligned}$$

$$\begin{aligned} i_{BL} &= [<P_{ra} - P><t'_c/2>] + <Pt'_c> + [<t_{of} - t'_c><P/2>] \\ &= [(31.9 - 12.7)(5.3/2)] + (12.7 \times 5.3) \\ &\quad + [<26 - 5.3><12.7/2>] = 50.9 + 67.3 + 131.4 \\ &= 250 \text{ psi-ms} \end{aligned}$$

$i_{BL} < i_{ra}$, use bi-linear pressure-time as design blast load.

See Figure 2A-16

$$\text{g. For } P_{so} = 12.6 \text{ psi, } L_w/W^{1/3} = 2.10 \text{ ft/lb}^{1/3}, \text{ Fig 2-15}$$

$$\text{h. } L_w = (L_w/W^{1/3})(W^{1/3}) = 2.10 \times 18.1712 = 38.16, \text{ say } 38.2 \text{ ft.}$$

B. Interior Blast Load

a. From previous steps: $L_w = 38.2 \text{ ft, } L = 30 \text{ ft, } H = 15 \text{ ft, } W = 20 \text{ ft.}$



FICTICIOUS INFINITE
SURFACE IMPULSE



THEORETIC ACTUAL
SURFACE IMPULSE

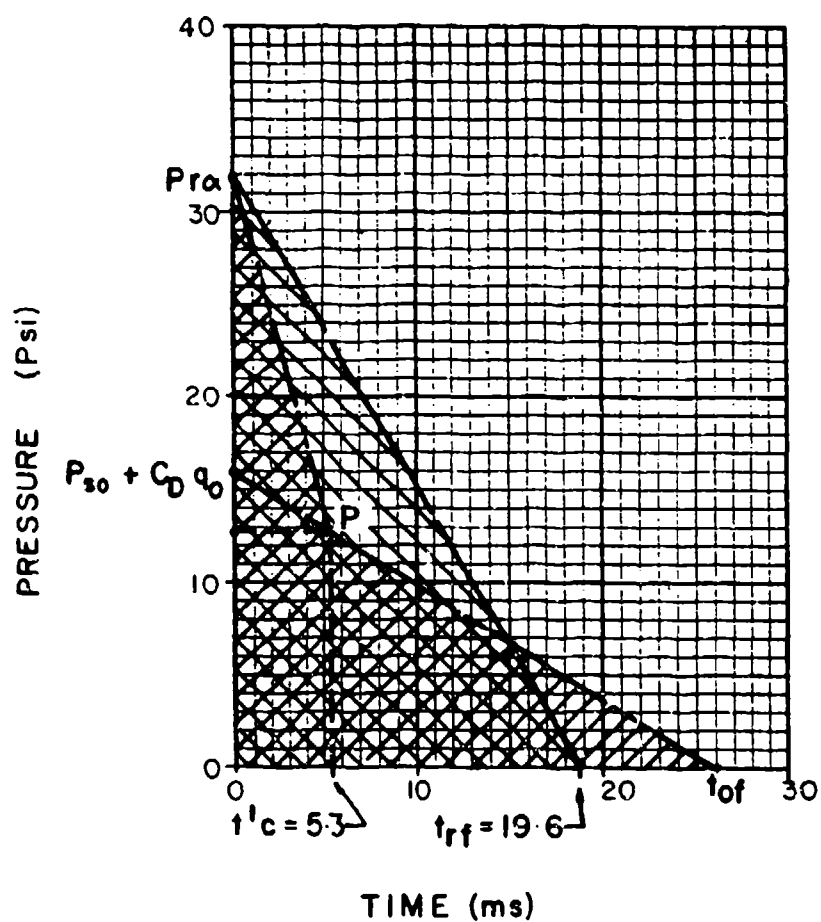


FIGURE 2A-16

A_o = Door opening area + window opening area

$$= (7 \times 3) + (3 \times 5'5) = 37'5 \text{ ft}^2$$

$$A_w = H \times W = 15 \times 20 = 300 \text{ ft}^2$$

$$A_o/A_w = 37'5/300 = 0'125$$

$$L_w/L = 38'2/30 \approx 1'27$$

$$L_w/H = 38'2/15 \approx 2'54$$

$$W/H = 20/15 = 1'33$$

$$L/H = 30/15 = 2'00$$

b' For $W/H = 1'33 < P_{so} = 12'6 \text{ psi} < A_o/A_w = 0'125 < \text{and } L_w/H = 2'54$
 summarize factored maximum average pressure $< P_{max} \times L_w/H <$ for
 W/H and L_w/H equal to '75 < 1'5 < 3 and 6'

| Figure No' | W/H | L_w/H | $P_{max} \times L_w/H$ |
|------------|------|---------|------------------------|
| 2-203 | 0'75 | 0'75 | 15'0 |
| | | 1'50 | 38'5 |
| | | 3'0 | 88'0 |
| | | 6'0 | 190'0 |
| 2-204 | 1'50 | 0'75 | 4'70 |
| | | 1'50 | 17'0 |
| | | 3'0 | 55'0 |
| | | 6'0 | 121'0 |
| 2-205 | 3'0 | 0'75 | 2'0 |
| | | 1'50 | 7'0 |
| | | 3'0 | 27'0 |
| | | 6'0 | 85'0 |
| 2-206 | 6'0 | 0'75 | 1'0 |
| | | 1'50 | 3'20 |
| | | 3'0 | 10'0 |
| | | 6'0 | 35'0 |

Plot Figure 2A-17 (a), and interpolate to determine $P_{\max} \times L_w/H$ at $L_w/H = 2.54$ for $W/H = .75, 1.5, 3$ and 6 .

| | | | | |
|-------------------------|-----|-----|----|-----|
| W/H | .75 | 1.5 | 3 | 6 |
| $P_{\max} \times L_w/H$ | 74 | 44 | 19 | 7.5 |

Plot Figure 2A-17 (b) from above values, and interpolate to determine $P_{\max} \times L_w/H = 48$ for $W/H = 1.33$.

Determine $P_{\max} = (P_{\max} \times L_w/H)/(L_w/H) = 48/2.54 = 18.9$ psi.

- c. For $P_{s0} = 12.6$ psi and $A_o/A_w = 1/8$, determine T_1 for $W/H = .75, 1.5$, and 3 , from Figures 2-207 and 2-208

| | | | |
|-------|------|------|------|
| W/H | .75 | 1.5 | 3 |
| T_1 | 1.25 | 1.70 | 2.26 |

Plot Figure 2A-18 with above values, and determine $T_1 = 1.60$ for $W/H = 1.33$.

- d. For $P_{s0} = 12.6$ psi, determine $T_2 - T_1$ for W/H and $L_w/H = .75, 1.5$, and 3 , from Figures 2-209 and 2-210

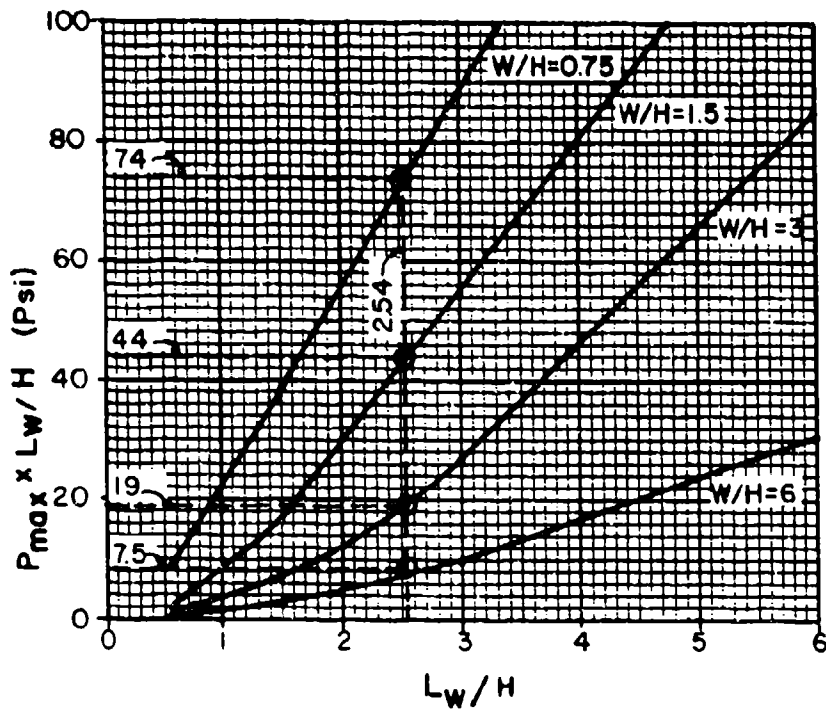
| | | | | | | | | | |
|-------------|------|------|------|------|------|-----|------|------|------|
| W/H | .75 | | | 1.5 | | | 3 | | |
| L_w/H | .75 | 1.5 | 3 | .75 | 1.5 | 3 | .75 | 1.5 | 3 |
| $T_2 - T_1$ | 2.07 | 2.07 | 2.07 | 4.70 | 6.20 | 7.0 | 6.50 | 10.8 | 15.0 |

Plot Figure 2A-19 with above values, and interpolate to determine $T_2 - T_1$ at $L_w/H = 2.54$ for $W/H = .75, 1.5$ and 3 , as summarized below.

| | | | |
|-------------|------|------|------|
| W/H | .75 | 1.5 | 3 |
| $T_2 - T_1$ | 2.07 | 6.75 | 14.0 |

Plot Figure 2A-19 with above values, and determine $T_2 - T_1 = 5.80$ ms for $W/H = 1.33$.

- e. For $P_{s0} = 12.6$ psi, determine $T_3 - T_1$ for $W/H = .75, 1.5$, and 3 , and $L_w/H = .75, 1.5$, and 3 , from Figures 2-211 and 2-212, as summarized below.



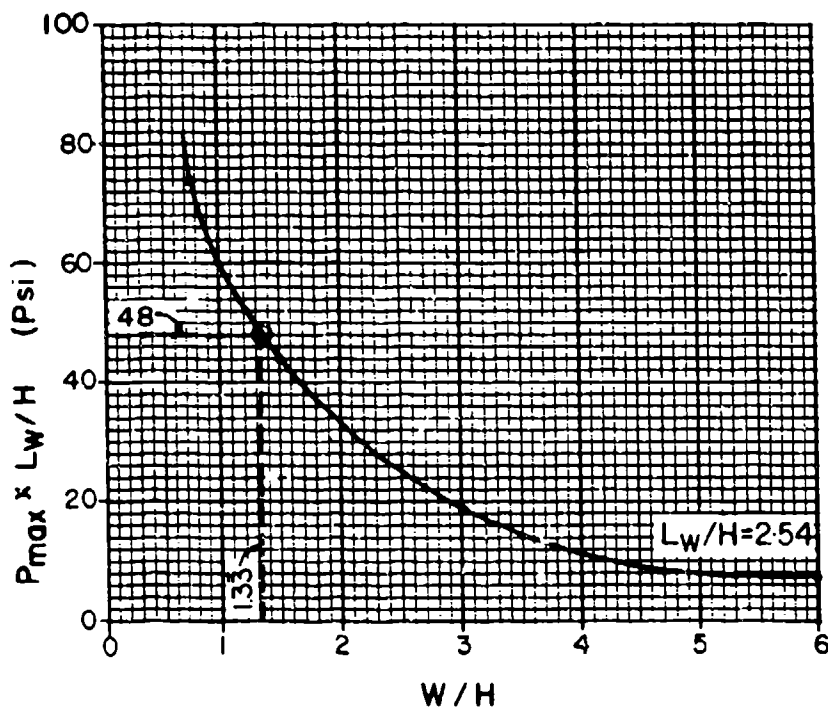
(a)

NOTE:

SEE EXAMPLE 2A-II,
STEP 3, PART B, ITEM b

FOR $L_W/H = 2.54$ GRAPHIC
INTERPOLATION YIELDS
 $P_{max} L_W/H = f(W/H)$, AS
SUMMARIZED BELOW.

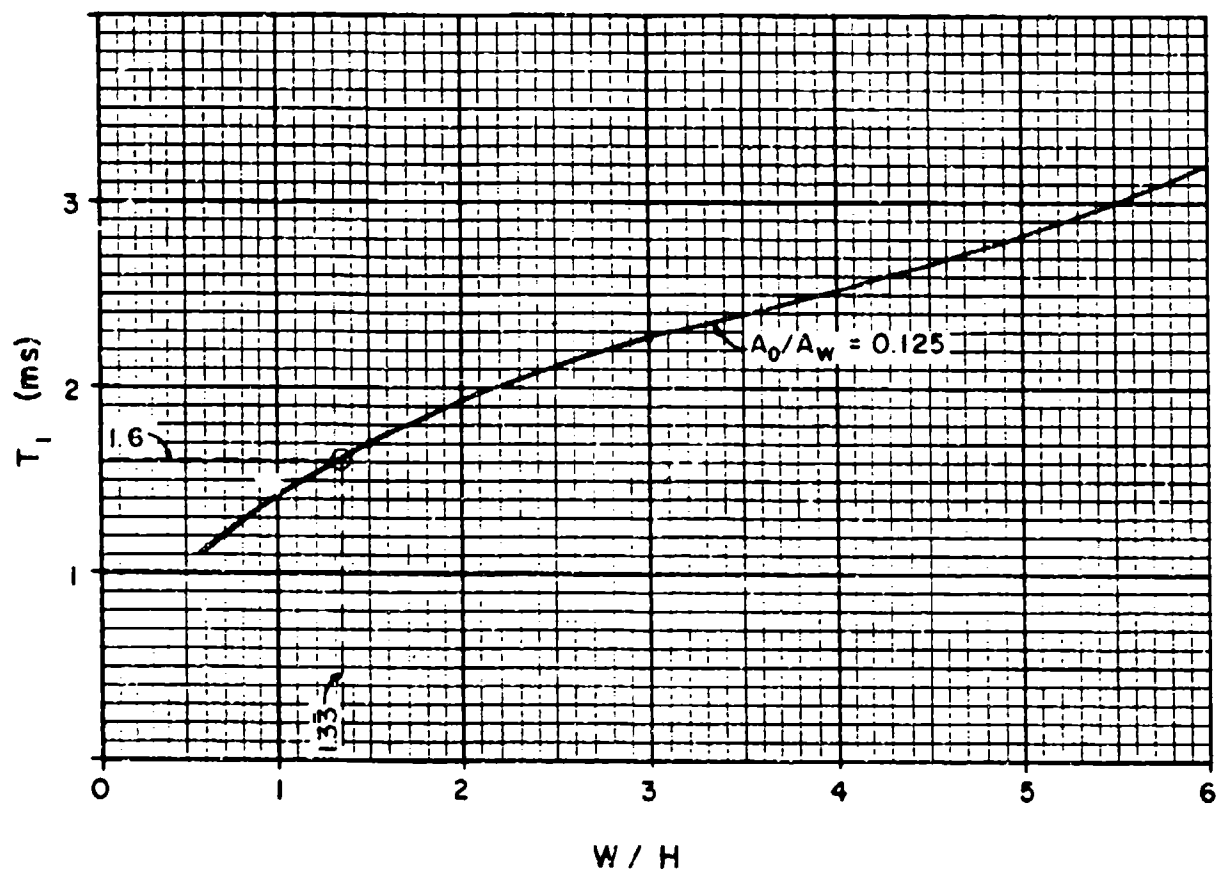
| W/H | $P_{max} L_W/H$ |
|-------|-----------------|
| 0.75 | 74 |
| 1.5 | 44 |
| 3 | 19 |
| 6 | 7.5 |



(b)

FOR $L_W/H = 2.54$, AND
 $W/H = 1.33$, GRAPHIC
INTERPOLATION YIELDS
 $P_{max} L_W/H = 48$

FIGURE 2A-17

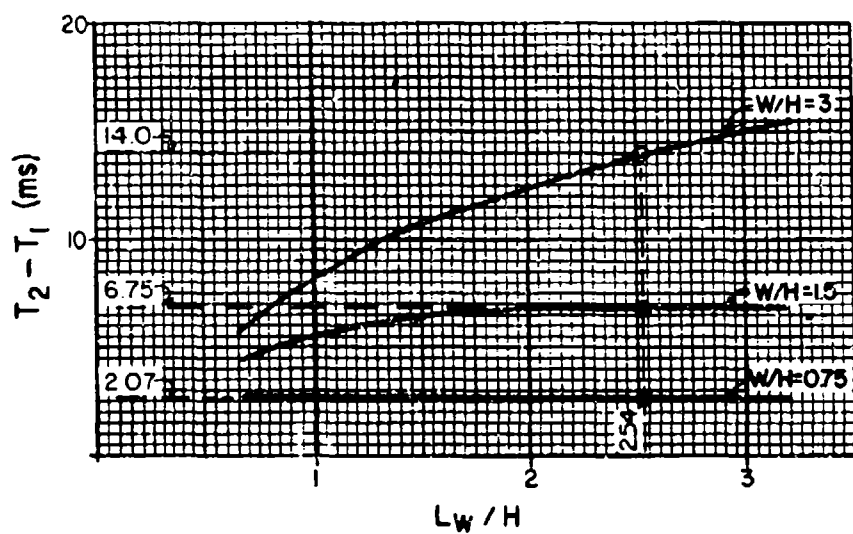


NOTE:

SEE EXAMPLE 2A-II, STEP 3, PART B, ITEM c

FOR $A_0/A_w = 0.125$, FOR $W/H = 1.33$,
GRAPHIC INTERPOLATION YIELDS $T_1 = 1.60$ ms

FIGURE 2 A -18

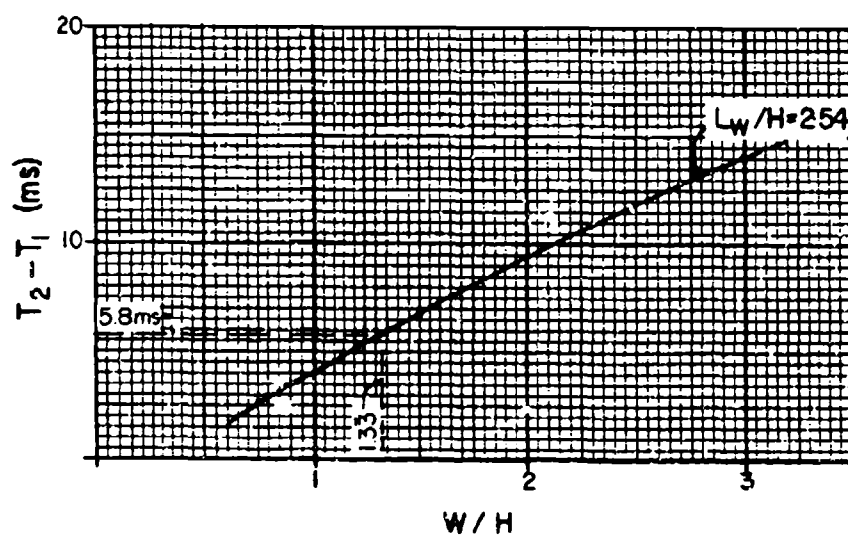


(a)

NOTE:

SEE EXAMPLE 2A-11
STEP 3, PART B, ITEM d.
FOR $L_w/H = 2.54$, GRAPHIC
INCORPORATION YIELDS
 $T_2 - T_1$ SUMMARIZED
BELOW

| W/H | $T_2 - T_1$ |
|-------|-------------|
| 0.75 | 2.07 |
| 1.5 | 6.75 |
| 3 | 14.0 |



(b)

NOTE:

FOR $W/H = 1.33$
 $T_2 - T_1 = 5.8$ ms

FIGURE 2A - 19

| | | | | | | | | | |
|-------------|-----|-----|------|------|------|------|------|------|------|
| W/H | .75 | | | 1.5 | | | 3 | | |
| L_w/H | .75 | 1.5 | 3 | .75 | 1.5 | 3 | .75 | 1.5 | 3 |
| $T_3 - T_1$ | 5.2 | 8.2 | 14.5 | 10.0 | 13.5 | 19.5 | 18.6 | 24.8 | 34.8 |

Plot Figure 2A-20 with above values, and graphically interpolate to determine $T_3 - T_1$ at $L_w/H = 2.54$ for $W/H = .75, 1.5,$ and 3 , as summarized below.

| | | | |
|-------------|------|------|------|
| W/H | .75 | 1.5 | 3 |
| $T_3 - T_1$ | 12.8 | 17.5 | 31.7 |

Plot Figure 2A-20 with above values, and determine $T_3 - T_1 = 16.3$ ms at $W/H = 1.33$.

f. Determine times T_2 and T_3 from T_1 , $T_2 - T_1$, and $T_3 - T_1$.

$$T_1 = 1.60 \text{ ms}$$

$$T_2 - T_1 = 5.80 \text{ ms}$$

$$T_3 - T_1 = 16.30 \text{ ms}$$

$$T_2 = 5.80 + 1.60 = 7.40 \text{ ms}$$

$$T_3 = 16.30 + 1.60 = 17.9 \text{ ms}$$

Plot Figure 2A-23 using above values and $P_{\max} = 18.9$ psi.

Step 4. Sidewall idealized interior pressure-time blast load.

a. Using equation 2-15, with $P_{so} = 12.6$ psi, $A_o/A_w = 1/8$, $L_w/L = 1.27$, $L/H = 2.0$, solve for P_{\max} for $W/H = .75, 1.5$, and 3 .

$$\text{Equation 2-15: } P_{\max} = K/(L_w/L)$$

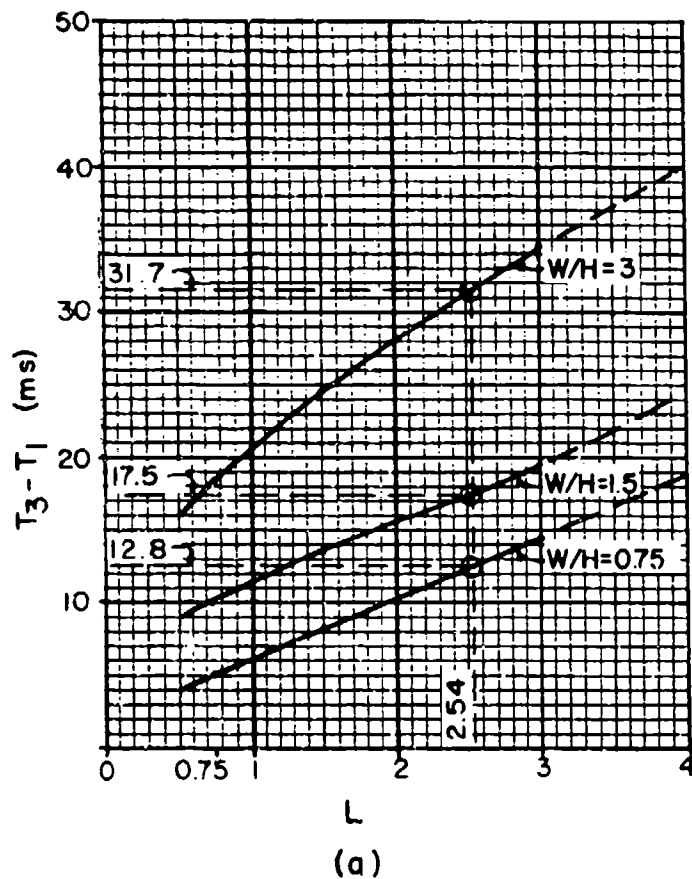
For $W/H = .75$, $K = A \times B \times C^E \times F^H \times P_{so}^{0.9718}$, where:

$$A = [0.5422 (L_w/L)^{1.2944}] - 0.001829 = 0.7385$$

$$B = [0.654 + 2.616 (A_o/A_w) - 4.928 (A_o/A_w)^2] \\ \times [2.209 (L/H)^{-0.3451} - 0.739] = 0.9040$$

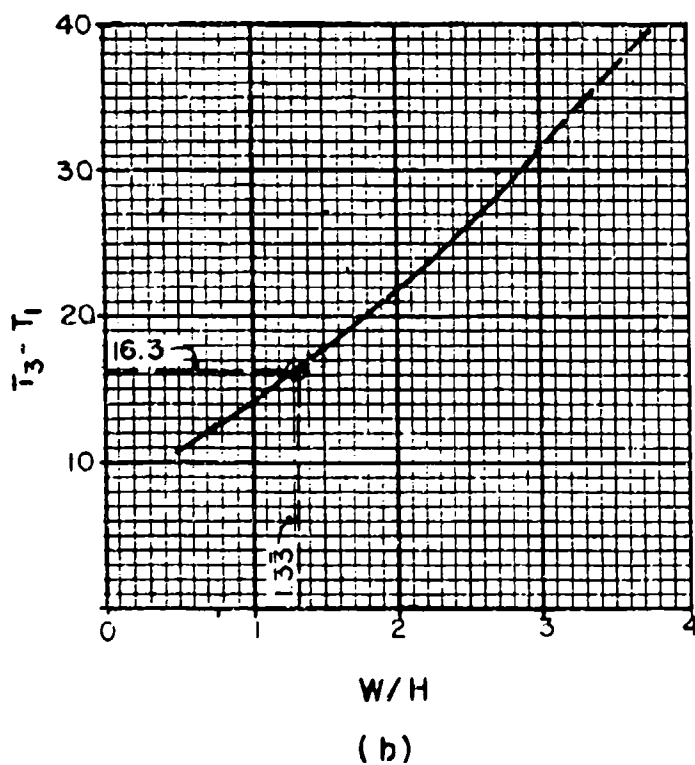
$$C = [0.829 + 0.104 (L_w/L)^{1.6}] + [0.00124 + 0.00414 (L_w/L)^{3.334}] \\ \times [L/H]^D = 1.0398$$

$$D = 2.579 - .0534 (L_w/L)3.891 = 2.4428$$



NOTE:
SEE EXAMPLE 2A-II,
STEP 3, PART B, ITEM e,
FOR $L_w/H = 2.54$, GRAPHIC
INTERPOLATION YIELDS
 $T_3 - T_1$ SUMMARIZED BELOW

| W/H | $T_3 - T_1$ |
|------|-------------|
| 0.75 | 12.8 |
| 1.5 | 17.5 |
| 3 | 31.7 |
| 6 | 56.5 |



NOTE:
FOR $W/H = 1.33$
 $T_3 - T_1 \approx 16.3$ ms

FIGURE 2A - 20

$$E = 999 (A_o/A_w)^{9.964} = 0.000001002$$

$$F = 1.468 - 1.6627 (A_o/A_w)^{0.7801} + [1.8692 - 1.1735 (A_o/A_w)^{-0.2226}] \times [L_w/L]^G = 1.1592$$

$$G = 0.2979 (A_o/A_w)^{-1.4872} - 0.8351 = 5.7286$$

$$H = (5.425 \times 10^{-4}) + (1.001 \times 10^{-3}) (L/H)^{9.965} = 0.0005435$$

$$K = 0.7385 \times 0.9040 \times 1.0388^{0.000001002} \times 1.1592^{0.0005435} \times 12.6^{0.9718} = 7.83$$

$$P_{\max} = 7.83/1.27 = 6.2 \text{ psi, for } W/H = .75$$

For 1.5

$$\leq W/H \leq 6, K = [A + [B \times (L_w/L)^C]] \times D \times E \times P_{so}^{1.025} \text{ where,}$$

$$A = 0.002 (W/H)^{1.4467} - 0.0213$$

$$B = 2.2075 - < 1.902 < W/H >^{-0.085} >$$

$$C = 1.231 + < 0.0008 < W/H >^{2.678} >$$

$$D = < 2.573 < L/H >^{-0.444} > -0.3911$$

$$E = 0.4221 + < 1.241 < A_o/A_w >^{0.367} >$$

For $W/H = 1.5, 3, \text{ and } 6$, determine values for A to E , and K and P_{\max} , as summarized below.

| W/H | A | B | C | D | E | K | P_{\max} |
|-------|---------|--------|--------|--------|--------|--------|------------|
| 1.5 | -0.0177 | 0.3700 | 1.2334 | 1.5003 | 1.0006 | 9.6743 | 7.60 |
| 3 | -0.0115 | 0.4751 | 1.2462 | 1.5003 | 1.0006 | 12.690 | 9.98 |

Plot Figure 2A-21 with above values of P_{\max} vs $W/H = .75, 1.5, \text{ and } 3$, and determine $P_{\max} = 7.30 \text{ psi}$ for $W/H = 1.33$.

- b. For $P_{s0} = 12.6 \text{ psi}$, determine T_1 and T_2 for $W/H = .75, 1.5, \text{ and } 3$ from Figure 2-213, as summarized below.

| | | | |
|-------|------|------|------|
| W/H | .75 | 1.5 | 3 |
| T_1 | 1.82 | 4.95 | 11.7 |
| T_2 | 3.20 | 6.50 | 12.5 |

Plot Figure 2A-21 using above values of W/H and T_1 and T_2 , and determine $T_1 = 4.4 \text{ ms}$ and $T_2 = 5.9 \text{ ms}$ for $W/H = 1.33$.

- c. For $P_{s0} = 12.6 \text{ psi}$ and $L/H = 2$, determine T_3 and T_4 for $W/H = .75, 1.5 \text{ and } 3$ and $L_w/L = .75, 1, 1.5, \text{ and } 2$, from figures 2-218 to 2-221, as summarized below:

Plot figure 2A-21 with above values, and interpolate to determine T_3 and T_4 , for $L_w/L = 1.27$ for $W/H = .75, 1.5, \text{ and } 3$, as summarized below.

| | | | |
|-------|-----|-----|------|
| W/H | .75 | 1.5 | 3 |
| T_3 | 35 | 18 | 24 |
| T_4 | 71 | 71 | 74.5 |

Plot figure 2A-21 with above values, and determine $T_3 = 19 \text{ ms}$ and $T_4 = 71 \text{ ms}$, for $W/H = 1.33$.

- d. For $P_{\max} = 7.3 \text{ psi}$, $T_1 = 4.4 \text{ ms}$, $T_2 = 5.9 \text{ ms}$, $T_3 = 19 \text{ ms}$ and $T_4 = 71 \text{ ms}$ plot figure 2A-23.

Step 5. Back wall idealized interior pressure-time blast load.

- a. For $L/H = 2$, $P_{s0} = 12.6 \text{ psi}$ and $A_o/A_w = 1/8$, determine $P_{RIB}/P_{s0} = 0.575$ from Figure 2-234.
- b. $P_{RIB} = (P_{RIB}/P_{s0}) \times P_{s0} = 0.575 \times 12.6 = 7.5 \text{ psi}$.

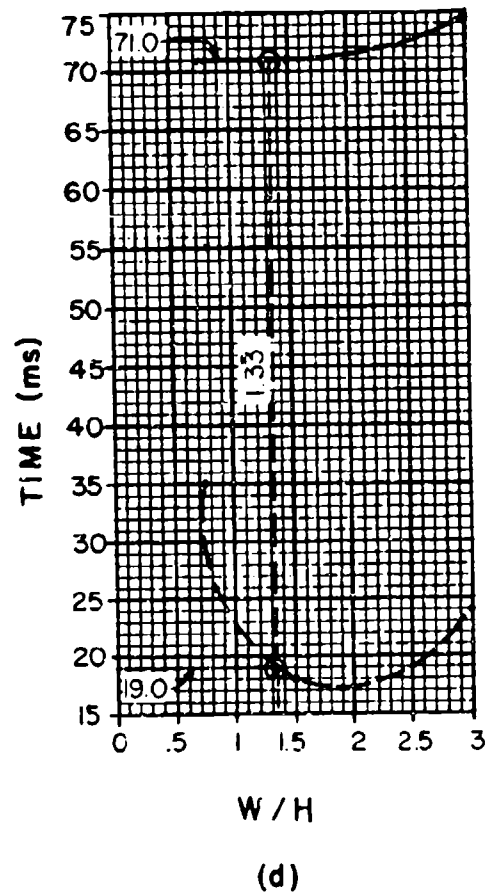
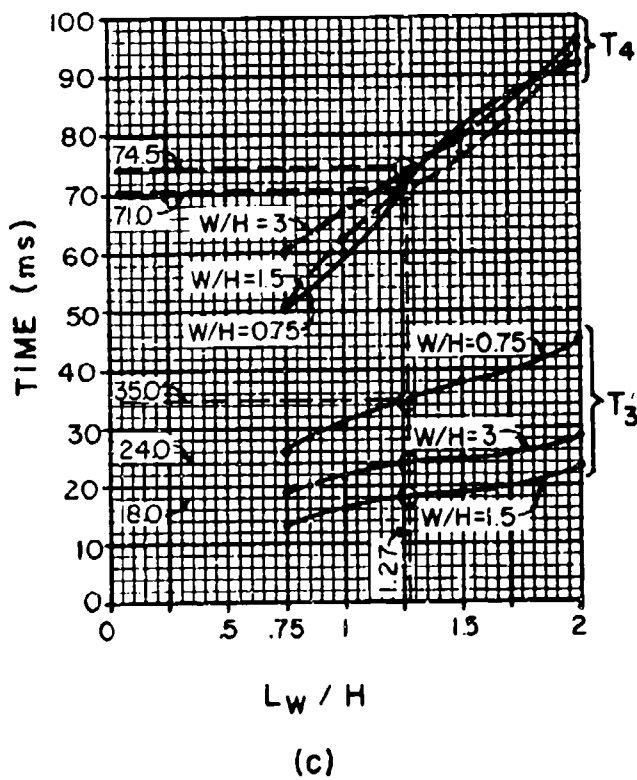
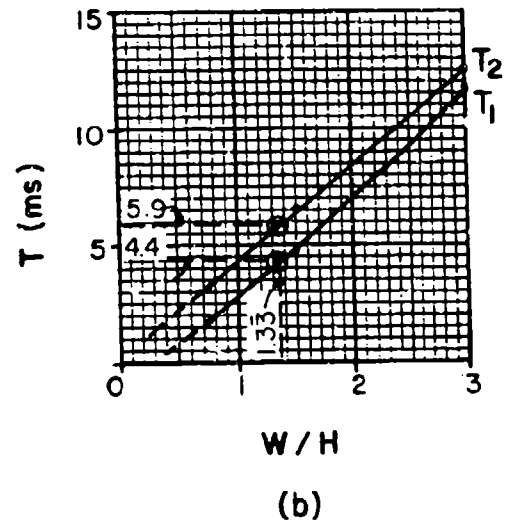
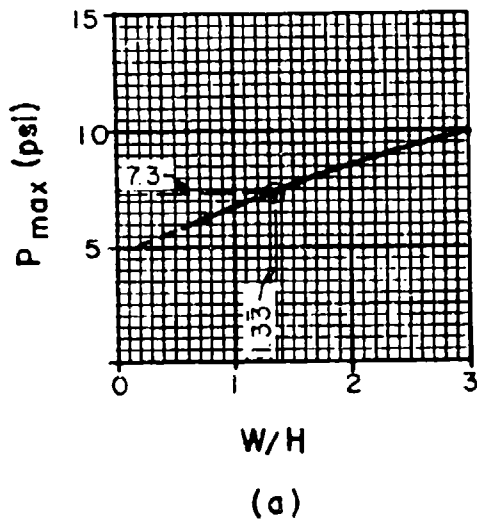


FIGURE 2A-21

- c. For $P_{SO} = 12.6$ psi, $L/H = 2$, and $A_O/A_W = 1/8$, determine T_1 for $W/H = .75, 1.5$ and 3 from Figures 2-230 and 2-231, as is shown below.

| | | | |
|-------|------|------|------|
| W/H | .75 | 1.5 | 3 |
| T_1 | 19.0 | 21.5 | 24.0 |

Plot figure 2A-22 using above values, and determine $T_1 = 21.1$ ms for $W/H = 1.33$.

- d. For $P_{SO} = 12.6$ psi and $A_O/A_W = 1/8$, determine $T_2 - T_1 = 2.35$ ms from figure 2-232.

Determine $T_2 = (T_2 - T_1) + T_1 = 2.35$ ms + 21.1 ms = 23.5 ms.

- e. Plot figure 2A-23 using $P_{RIB} = 7.5$ psi, $T_1 = 21.1$ ms and $T_2 = 23.5$ ms.

Step 6. Roof idealized interior pressure-time blast load

- a. Sidewall $W/H = 1-1/3 = 4/3$

Roof $W/H = 1/(4/3) = 3/4$

- b. Repeat Step 4 with $W/H = 3/4$

For $W/H = 3/4$, $L/H = 2.0$, $A_O/A_W = 1/8$, $L_W/L = 1.272$ and $P_{SO} = 12.6$,

$P_{max} = 6.2$ psi

For $W/H = 3/4$ and $P_{SO} = 12.6$ psi

$T_1 = 1.82$ and $T_2 = 3.20$ ms

For $W/H = 3/4$, $P_{SO} = 12.6$ psi, and $L_W/L = 1.27$

$T_3 = 35$ and $T_4 = 65$ ms

Plot figure 2A-23 with above values.

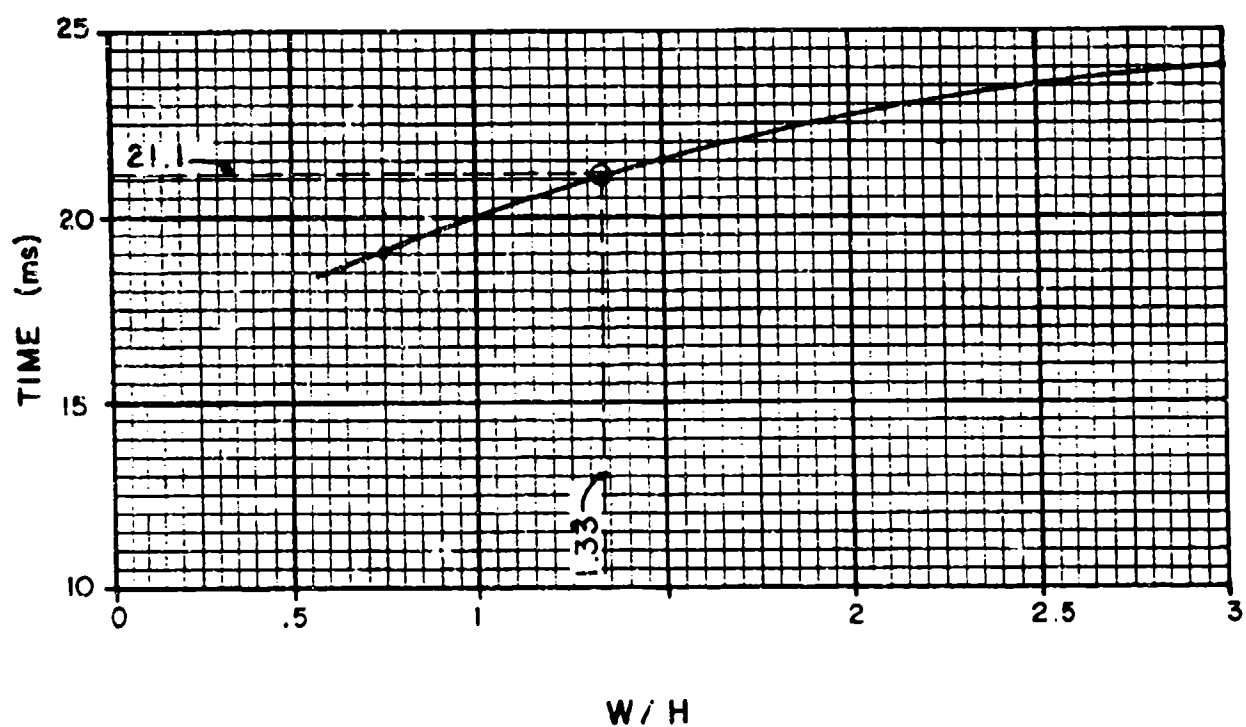
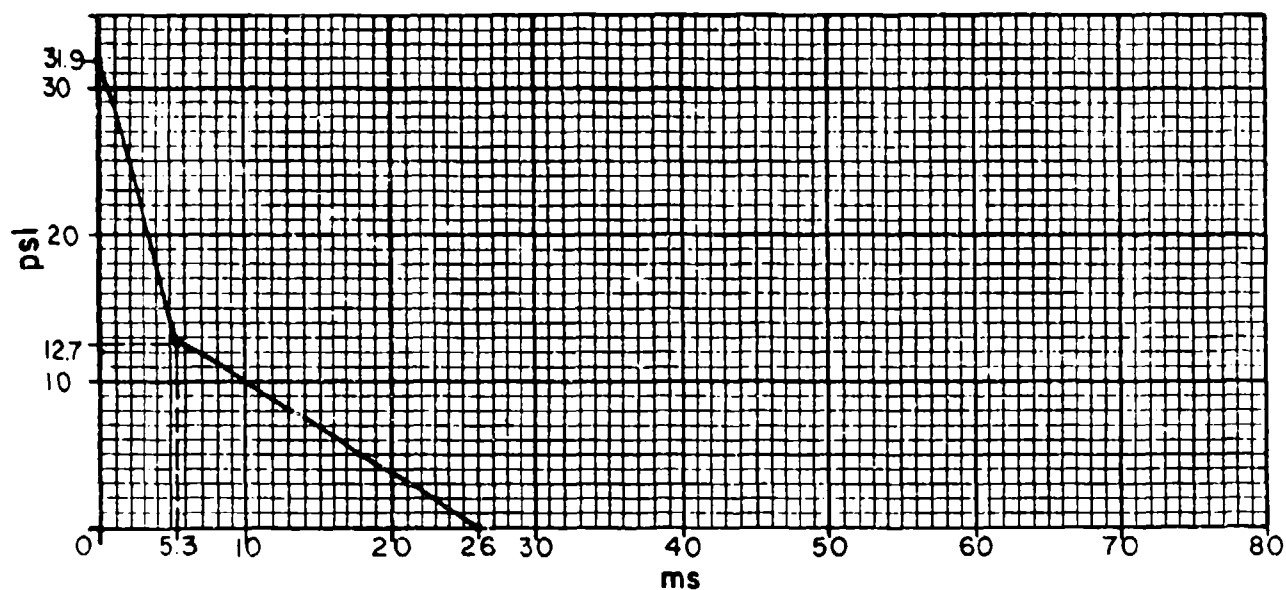
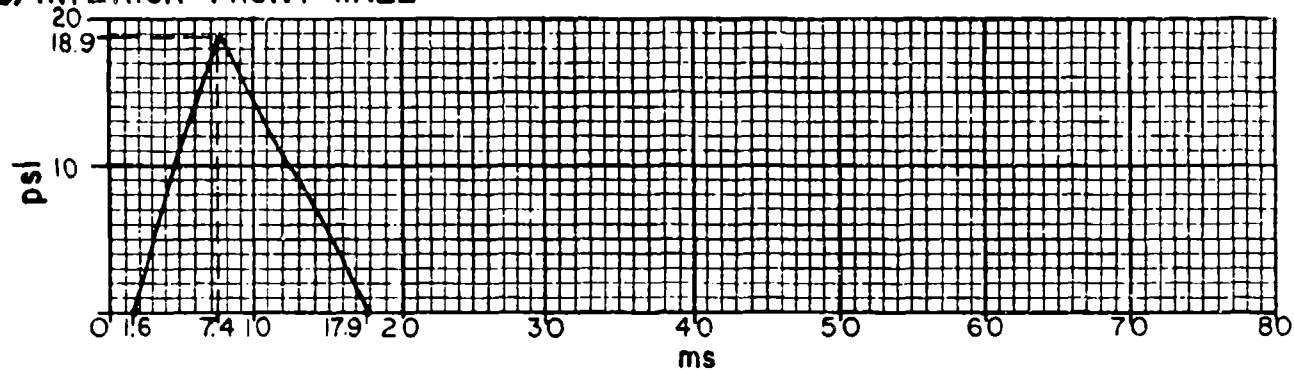


FIGURE 2A-22

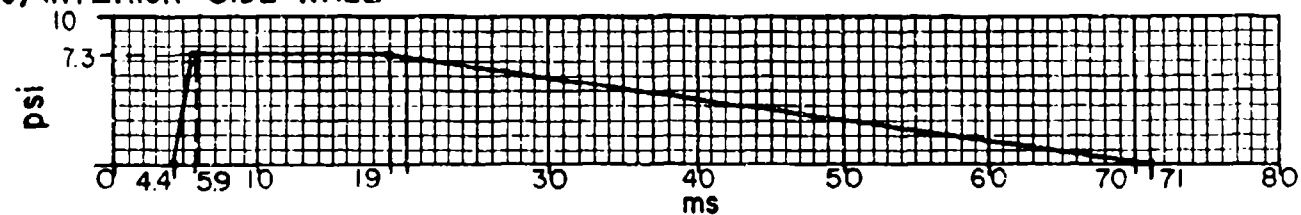
(a) EXTERIOR FRONT WALL



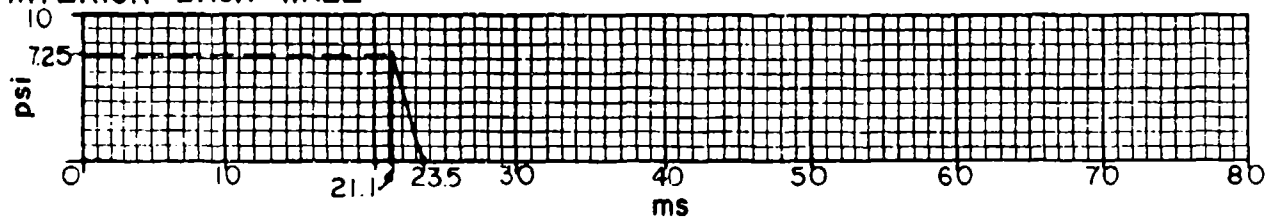
(b) INTERIOR FRONT WALL



(c) INTERIOR SIDE WALL



(d) INTERIOR BACK WALL



(e) INTERIOR ROOF

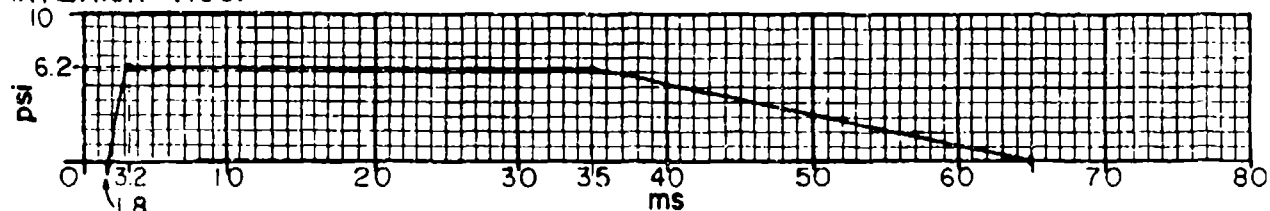


FIGURE 2A-23 BLAST LOAD SUMMARY

Problem 2A-12, Interior Pressure Buildup in a Structure

Problem: Determine the interior pressure-time curve for a structure with an opening in one of its walls and subjected to an applied blast pressure.

Procedure:

Step 1. Determine the pressure-time history of the applied blast pressure P acting on the wall surrounding the opening in the structure as presented in problem 2A-10. Also the area of the opening A_O and the volume of the structure V_O must be known.

Step 2. Divide the duration t_O of the applied pressure into n equal intervals Δt , each interval being approximately $t_O/10$ to $t_O/20$, and determine the pressures at the end of each interval.

Step 3. Compute the pressure differential $P-P_i$ where P_i is the interior pressure. Obtain the leakage pressure coefficient C_L for each $P-P_i$ from figure 2-235.

Step 4. Calculate ΔP_i from

$$\Delta P_i = C_L \left(\frac{A_O}{V_O} \right) \Delta t \quad (\text{eq. 2-31})$$

using the proper values for C_L and Δt . Add ΔP_i to P_i for the interval being considered to obtain the new value of P_i for the next interval.

Step 5. Repeat steps 3 and 4 for each interval using the proper values of P and P_i . Plot curve of pressure buildup.

Note:

When $P-P_i$ becomes negative, the value of C_L must be taken as negative also.

Example 2A-12, Interior Pressure Buildup in a Structure

Required: Interior pressure-time curve for a structure with an opening in one of its walls and subjected to an applied blast pressure.

Solution:

Step 1. The curve of the applied blast pressure P for the wall in question is shown in figure 2A-24. (Only the positive phase of the blast wave is considered in this example.)

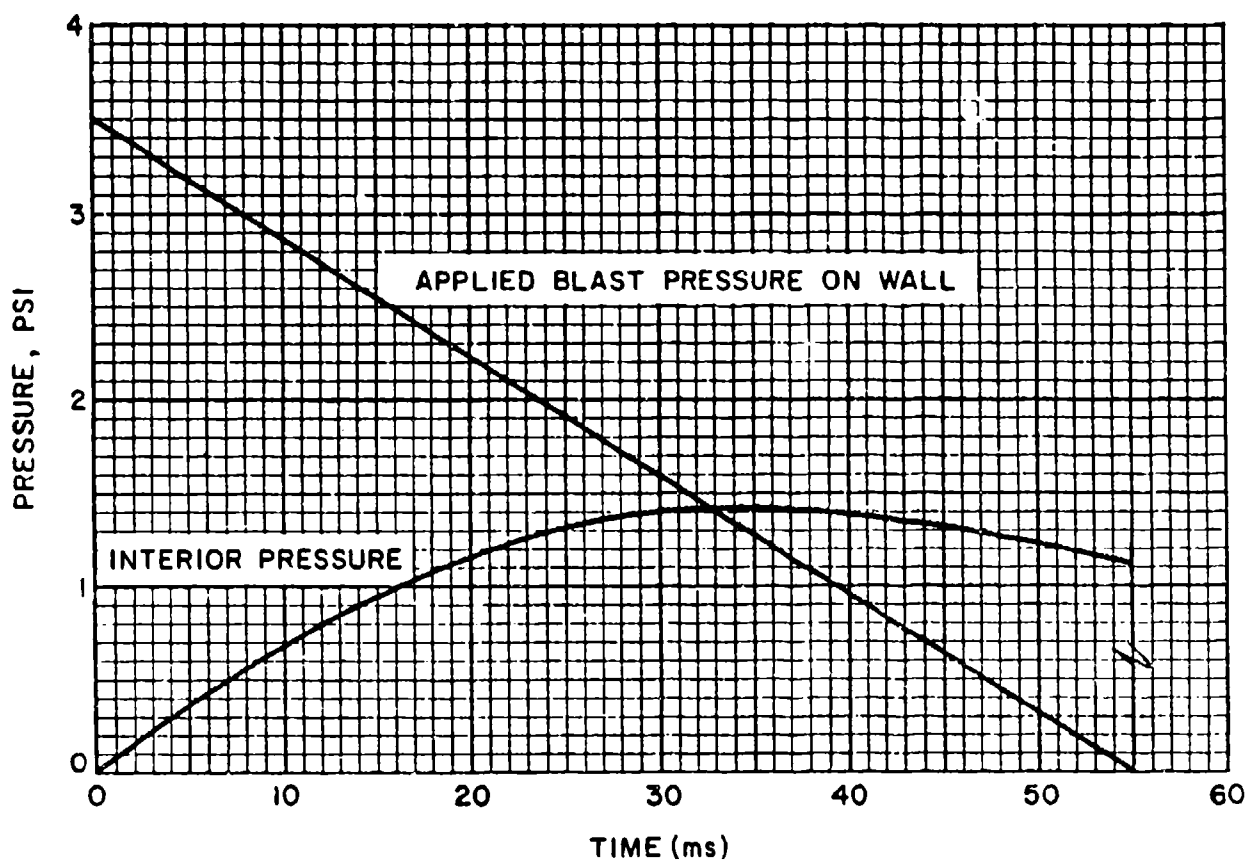


FIGURE 2A - 24

Area of opening $A_o = 3' \times 3' = 9 \text{ sq ft.}$

Volume of structure $V_o = 10' \times 10' \times 10'$
 $V_o = 1,000 \text{ cu ft}$

Step 2. $t_o = 55 \text{ ms}$

Use $n = 10$ $\Delta t = 5.5 \text{ ms}$

For the first interval, $P = 3.5 \text{ psi}$ at $t = 0$

Step 3. $P_i = 0$ for the first interval

$$\therefore P - P_i = 3.50 - 0 = 3.50 \text{ psi}$$

$$C_L = 8.75$$

(fig. 2-235)

Step 4. $\Delta P_i = C_L \frac{A_o}{V_o} \Delta t$

(eq. 2-31)

$$\Delta P_i = 8.75 \left(\frac{9.0}{1000} \right) (5.5) = 0.433 \text{ psi}$$

$$\therefore \text{new } P_i = 0 + 0.433 = 0.433 \text{ psi}$$

Step 5. The remainder of the analysis is presented in tabular form below and the pressure buildup within the structure is plotted in figure 2A-24.

| $t(1)$ | P | P_i | $P - P_i$ | C_L | ΔP_i |
|--------|-------|-------|-----------|-------------|--------------|
| (ms) | (psi) | (psi) | (psi) | (psi-ft/ms) | (psi) |
| 0. | 3.50 | 0. | 3.50 | 8.75 | 0.433 |
| 5.5 | 3.15 | 0.433 | 2.72 | 7.00 | 0.347 |
| 11.0 | 2.80 | 0.780 | 2.02 | 5.45 | 0.270 |
| 16.5 | 2.45 | 1.05 | 1.40 | 3.78 | 0.187 |
| 22.0 | 2.10 | 1.24 | 0.86 | 2.32 | 0.115 |
| 27.5 | 1.75 | 1.36 | 0.39 | 1.05 | 0.052 |
| 33.0 | 1.40 | 1.41 | -0.01 | -0.027 | -0.0013 |
| 38.5 | 1.05 | 1.41 | -0.36 | -0.972 | -0.048 |
| 44.0 | 0.70 | 1.36 | -0.66 | -1.78 | -0.088 |
| 49.5 | 0.35 | 1.27 | -0.92 | -2.48 | -0.123 |
| 55.0 | 0. | 1.14 | -1.14 | -3.50 | -.173 |
| 60.5 | 0. | .97 | -.97 | -3.00 | -.148 |
| 66.0 | 0. | .82 | -.82 | -2.50 | -.124 |
| 71.5 | 0. | .70 | -.70 | -2.25 | -.111 |
| 77.0 | 0. | .59 | -.59 | -2.00 | -.099 |
| 82.5 | 0. | .49 | -.49 | -1.80 | -.089 |

| $t(1)$ | P | P_1 | $P-P_1$ | C_L | ΔP_1 |
|--------|-------|-------|---------|-------------|--------------|
| (ms) | (psi) | (psi) | (psi) | (psi-ft/ms) | (psi) |
| 88.0 | 0. | .40 | -.40 | -1.60 | -.079 |
| 93.5 | 0. | .32 | -.32 | -1.45 | -.071 |
| 99.0 | 0. | .25 | -.25 | -1.30 | -.064 |
| 104.5 | 0. | .19 | -.19 | -1.15 | -.056 |
| 110.0 | 0. | .13 | -.13 | -1.0 | -.050 |
| 115.5 | 0. | .08 | -.08 | -.85 | -.042 |
| 121.0 | 0. | .04 | -.04 | -.05 | -.025 |
| 126.5 | 0. | .01 | -.01 | -.2 | -.01 |
| 132.0 | 0. | 0. | 0. | 0. | 0. |

(1) Maximum P_1 occurs between $t = 27.5$ and $t = 33.0$ ms

Problem 2A-13 Primary Fragments from Cased Cylindrical Charges

Problem: Determine the average fragment weight for a primary fragment ejected from a uniform cylindrical steel casing; the total number of fragments, the design fragment weight and the number of fragments weighing more than the design fragment.

Procedure:

Step 1. Establish design parameters:

- type of explosive.
- average casing thickness, t_c .
- average inside diameter of casing, d_i .
- total casing weight, W_c .
- confidence level, CL.

Step 2. Determine the value of the explosive constant B for the given type of explosive from table 2-6. With this value and the values of t_c and d_i from step 1, calculate the fragment distribution M_A from

$$M_A = B t_c^{5/6} d_i^{1/3} \left[1 + \frac{t_c}{d_i} \right] \quad (\text{eq. 2-37})$$

Step 3. With the value of M_A from step 2, calculate the average weight of the fragments from

$$\bar{W}_f = 2M_A^2 \quad (\text{eq. 2-40})$$

Step 4. Calculate the total number of fragments using the value of W_c from step 1d and M_A from step 2 and equation 2-37.

$$N_T = 8W_c/M_A^2 \quad (\text{eq. 2-39})$$

or: With the values of d_i and t_c from step 1, enter figure 2-241 and determine $B^2 N_T / W_c$. From this value, the value of B from step 2 and W_c from step 1 find N_T .

Step 5. Find the design fragment weight for the confidence level CL , given in step 1, using the value of M_A and

$$W_f = M_A^2 \ln^2 (1 - CL) \text{ for } CL \leq 0.9999 \quad (\text{eq. 2-42})$$

or equation 2-43 if $CL > 0.9999$

Step 6. Using the value of W_c from step 1, M_A from step 2 and W_f from step 5, determine the number of fragments which weigh more than the design fragment from

$$N_f = \frac{8W_c e^{-[(W_f)^{1/2}/M_A]}}{M_A^2} \quad (\text{eq. 2-36})$$

or: Calculate the number of fragments which weigh more than the design fragment using the confidence level of step 1, the total number of fragments from step 4 and equation 2-244.

Example 2A-13 Primary Fragments from Cased Cylindrical Charges

Required: The average fragment weight, the total number of fragments, the design fragment weight and the number of fragments weighing more than the design fragment.

Solution:

Step 1. Given:

- a. type of explosive: Comp B
- b. average casing thickness: $t_c = 0.50$ inch
- c. average inside diameter of casing: $d_i = 12.0$ inches

d. total casing weight: $W_c = 65.0$ lbs

e. confidence level: $CL = 0.95$

Step 2. For Comp B, $B = 0.22$ (table 2-7)

$$M_A = B t_c^{5/6} d_1^{1/3} \left(1 + \frac{t_c}{d_1}\right) \quad (\text{eq. 2-37})$$

$$= 0.22 (0.5)^{5/6} (12)^{1/3} \left(1 + \frac{0.5}{12}\right) = 0.294$$

Step 3. Average weight of fragments.

$$\bar{W}_f = 2M_A^2 = 2 \times (0.294)^2 = 0.17 \text{ oz} \quad (\text{eq. 2-40})$$

Step 4. Total number of fragments.

$$N_T = 8W_c/M_A^2 = 8 \times 65/0.294^2 = 6016 \text{ fragments} \quad (\text{eq. 2-39})$$

or:

$$\frac{B^2 N_T}{W_c} = 0.28 \quad (\text{fig. 2-37})$$

$$N_T = 0.28 \times (65 \times 16)/.22^2 = 6016 \text{ fragments}$$

Step 5. Design fragment weight.

$$W_f = M_A^2 \ln^2 (1 - CL) = 0.294^2 \ln^2 (1 - 0.95) = 0.78 \text{ oz} \quad (\text{eq. 2-42})$$

Step 6. Number of fragments weighing more than $W_f = 0.78$ oz.

$$N_f = \frac{8W_c e^{-[(W_f)^{1/2}/M_A]}}{M_A^2} = \frac{(8 \times 65) e^{- (0.78)^{1/2}/0.294}}{(0.294)^2} \\ = 298 \text{ fragments} \quad (\text{eq. 2-36})$$

or: $C_L = 1 - N_f/N_T$ (eq. 2-44)

$$N_f = N_T (1 - C_L) = 6016 (1 - 0.95) = 301 \text{ fragments}$$

Problem 2A-14 Primary Fragment Velocity

Problem: Determine the initial velocity of a primary fragment and its striking velocity.

Procedure:

Step 1. Establish design parameters.

- a. shape of charge
- b. dimensions of charge
- c. type and density of explosive
- d. type and density of casing
- e. distance from center of charge to impact location
- f. weight of fragment

Step 2. Calculate the total weight of the explosive W and increase it 20%. Find the weight of the casing W_c . Also calculate the ratio of the explosive weight to the casing weight W/W_c .

Step 3. Determine the Gurney Energy Constant $(2E')^{1/2}$ for the explosive charge from table 2-5. With this value and the value of W/W_c from step 2, calculate the initial v_o of the primary fragments from the equation chosen from table 2-6.

or: Calculate the casing to charge weight ratio W_c/W . With W_c/W , find the initial velocity from figure 2-237, for proper shape.

Step 4. For the distance traveled by the fragment R_f , calculate the striking velocity v_s using the initial velocity from step 3, the weight of the fragment from step 1g and

$$v_s = v_o e^{-.004 R_f/W_f^{1/3}} \quad (\text{eq. 2-48})$$

or: With the fragment weight W_f and striking distance R_f from step 1, enter figure 2-243 and find the ratio of the striking velocity to initial velocity. Multiply the ratio by the initial velocity v_0 from step 3 to find the striking velocity v_s .

Example 2A-14 Primary Fragment Velocity

Required: The initial velocity and striking velocity of a primary fragment.

Solution:

Step 1. Given:

- a. spherical charge
- b. inner diameter of charge: $d_i = 6$ inches
average casing thickness: $t_c = 0.25$ inches
- c. type of explosive TNT
density of explosive = 0.0558 lb/in^3
- d. mild steel casing
density of casing = 0.283 lb/in^3
- e. striking distance $R_f = 35$ ft.
- f. weight of fragment, $W_f = 2$ oz

Step 2. a. weight of the explosive

$$W = \frac{4}{3} \pi \left(\frac{6}{2}\right)^3 \times 0.0558 = 6.31 \text{ lbs}$$

b. Increase weight of explosive 20 percent

$$W = 1.20 \times 6.31 = 7.57 \text{ lb}$$

c. Weight of casing

$$W_c = \frac{4}{3} \pi (3.5^3 - 3^3) \times 0.283 = 18.82 \text{ lb}$$

d. Explosive weight to casing weight ratio.

$$W/W_c = 7.57/18.82 = 0.402$$

Step 3. For TNT, $(2E')^{1/2} = 8000$ (table 2-5)

Initial velocity from table 2-6

$$v_o = (2E')^{1/2} \left[\frac{W/W_c}{1 + \frac{3W}{5W_c}} \right]^{1/2}$$

$$v_o = (8000) \left[\frac{0.40}{1 + 0.40(3/5)} \right]^{1/2} = 4500 \text{ ft/sec}$$

or: $W_c/W = 18.82/7.57 = 2.49$

from figure 2-237

$$v_o / (2E')^{1/2} = 0.56$$

$$v_o = 0.56 \times 8000 = 4500 \text{ ft/sec}$$

Step 4. Striking velocity

$$v_s = v_o e^{-0.004 R_f/W_f^{1/3}} = 4500 e^{-0.004 \times 35/2^{1/3}} \quad (\text{eq. 2-48})$$

$$v_s = 4030 \text{ ft/sec}$$

or: from figure 2-243

$$v_s/v_o = 0.895$$

$$v_s = 0.895 \times 4500 = 4030 \text{ ft/sec}$$

Problem 2A-15 Unconstrained Secondary Fragments "Close" to a Charge

Problem: Determine the velocity of an unconstrained object close to an explosive charge and its maximum range.

Procedure:

- Step 1. Establish design parameters
- weight W and shape of TNT equivalent explosive
 - radius of explosive R_e
 - shape, dimensions and weight of target
 - distance from the center of the explosive charge to the surface of the target, R
 - orientation of target with respect to the explosive charge
 - mass density of air ρ_o
- Step 2. Calculate the ratio of standoff distance to radius of the explosive R/R_e using the values from step 1.
- Step 3. From figure 2-249, determine target shape factor, β .
- Step 4
- If R/R_e is less than or equal to 10 for cylindrical charges, or less than equal to 5.0 for spherical charges, determine the specific acquired impulse either from figure 2-250 or equations 2-60, or 2-61.
 - If $10 < R/R_e \leq 20$ for a cylindrical charge, or $5 < R/R_e \leq 20$ for a spherical charge, calculate the scaled standoff distance $Z_A = R/W^{1/3}$. With that value of Z_A , obtain the normal reflected impulse from figure 2-7. The normal reflected impulse is then used as the specific acquired impulse.
- Step 5. Calculate the mean presented area A of the target and the mass M using the values of step 1.
- Step 6. With the area and mass from step 4, the target shape factor β from step 2 and the impulse from step 3, calculate the velocity from
- $$v_o = \frac{1000 A \beta i}{12 M} \quad (\text{eq. 2-59})$$
- Step 7. Determine the drag coefficient C_D from table 2-8. Using that value of C_D , the area and mass of the target from step 5, the velocity from step 6 and the mass density of air from step 1f, evaluate the term: $12 \rho_o C_D A_D v_o^2 / Mg$.

Step 8. With the term calculated in step 7, enter figure 2-252 and read the value of $12 \rho_0 C_D A_D R/M$ from which the range R is calculated.

Example 2A-15 Unconstrained Secondary Fragments "Close" to a Charge

Required: The velocity and maximum range of a steel tool holder resting on a lathe when a charge being held by the lathe explodes.

Solution:

Step 1. Given:

a. spherical charge of TNT

$$W = 15 \text{ lbs}$$

b. radius of explosive: $R_e = 0.33 \text{ ft}$

c. cylindrical target; length = 8.0 in

$$R_t = 1.0 \text{ in} = 0.083 \text{ ft}$$

$$W_t = 7.13 \text{ lb}$$

d. standoff distance: $R = 1.0 \text{ ft}$

e. tool holder is resting so that its longitudinal axis is perpendicular to the radial line from the charge

f. mass density of air: $\rho_0 = 0.115 \text{ lb} - \text{ms}^2/\text{in}^4$

Step 2. Ratio of standoff distance to radius of explosive:

$$R/R_e = 1.0/0.33 = 3.03$$

Step 3. Target shape factor.

$$\beta = \pi/4 \text{ from figure 2-512}$$

Step 4. Determine specific acquired impulse

$$a. \frac{i}{\beta R_{\text{eff}}} \left(\frac{R_e}{R_t} \right)^{0.158} = 8000 \frac{\text{psi} - \text{ms}}{\text{ft}} \quad (\text{fig 2-250})$$

$$b. R_{\text{eff}} = R_e = 0.33 \text{ ft} \quad (\text{eq. 2-61})$$

$$c. \quad i = \frac{\pi}{4} (0.33 \text{ ft}) \left(\frac{0.083}{0.33} \right)^{0.158} \times 8000 \frac{\text{psi-ms}}{\text{ft}}$$

$$i = 1667 \text{ psi-ms}$$

Step 5. Calculate area and mass of target.

a. Mean presented area

$$A = 2.0 \text{ in} \times 8.0 \text{ in} = 16 \text{ in}^2$$

b. Mass

$$M = \frac{W_t}{g} = \frac{7.13 \text{ lb}}{32.2 \times 12 \times 10^{-6} \frac{\text{in}}{\text{ms}^2}} = 18,450 \frac{\text{lb-ms}^2}{\text{in}}$$

Step 6. Find the velocity.

$$v_o = \frac{1000 A \beta i}{12 M} = \frac{1000 \times 16 \times (\pi/4) \times 1667}{12 \times 18450} \quad (\text{eq. 2-59})$$

$$v_o = 95 \text{ ft/sec}$$

Step 7. Evaluate the term $12 \rho_o C_D A_D v_o^2 / Mg$.

a. $C_D = 1.2$ (table 2-8)

$$b. \quad \frac{12 \rho_o C_D A_D v_o^2}{Mg} = \frac{0.115 (1.2) (16) (95)^2 12}{18450 \times 32.2} = 0.40$$

Step 8. Calculate the range.

$$a. \quad \frac{12 \rho_o C_D A_D R}{M} = 0.33 \quad (\text{fig. 2-252})$$

$$b. \quad R = 0.33M / (12 \rho_o C_D A_D)$$

$$= 0.33 (18450) / [12 (0.115) 1.2 (16)] = 230 \text{ ft.}$$

Problem 2A-16 Unconstrained Secondary Fragments "Far" from a Charge

Problem: Determine the velocity of an unconstrained object "far" from an explosive charge.

Procedure:

Step 1. Establish design parameters:

- a. weight W of TNT equivalent explosive
- b. shape, dimensions and weight of target
- c. distance from the center of explosive charge to surface of the target
- d. orientation and location of target with respect to the explosive charge
- e. velocity of sound in air, a_0
- f. atmospheric pressure, p_0

Step 2. Calculate the scaled standoff distance from:

$$Z_A = R_A / W^{1/3}$$

From figure 2-7, and the scaled distance find the peak incident overpressure and the incident specific impulse.

Step 3. Determine the drag coefficient C_D from table 2-8 based on the shape and orientation of target (step 1).

Step 4. Calculate the mass of the target. Determine the distance from the front of the target to the location of its largest cross-sectional area, X . Also, determine the minimum transverse distance of the mean presented area, H , and the presented area.

Step 5. Determine the constant K , which is equal to 4 if the object is on the ground or reflecting surface. If the target is in the air, K is equal to 2.

Step 6. With the peak incident overpressure P_{S0} from step 2 and the atmospheric pressure p_0 from step 1f, find P_{S0}/p_0 .

Step 7. Evaluate the term $12C_D i_s a_o / 10^3 [P_{so}(KH + X)]$ using i_s and P_{so} from step 2, C_D from step 3, a_o from step 1e, K from step 5 and H and X from step 4.

Step 8. With two terms calculated in steps 6 and 7 enter figure 2-248 and read $144v_o Ma_o / [10^6 P_o A(KH + X)]$ from which the velocity is calculated.

Example 2A-16 Unconstrained Secondary Fragments "Far" from Charge

Required: The initial velocity of a steel tool holder resting on a nearby table, when a charge explodes.

Solution:

Step 1. Given:

- a. weight of explosive: $W = 15$ lbs of TNT
- b. cylindrical target: length = 8.0 in
 $R_t = 1.0$ in
 $W_t = 7.13$ lb
- c. standoff distance: $R = 10$ ft
- d. tool holder is resting on a table so that its longitudinal axis is perpendicular to the radial line from the charge
- e. velocity of sound in air: $a_o = 1100$ ft/sec
- f. atmospheric pressure: $p_o = 14.7$ psi

Step 2. Find the peak incident overpressure and the incident specific impulse.

- a. Scaled distance

$$Z_A = R/W^{1/3} = 10/(15)^{1/3} = 4.05 \text{ ft/lb}^{1/3}$$

- b. Peak incident overpressure.

$$P_{so} = 39 \text{ psi} \quad (\text{fig. 2-7})$$

- c. Incident specific impulse.

$$i_s/W^{1/3} = 12 \text{ psi-ms/lb}^{1/3} \quad (\text{fig. 2-7})$$

$$i_s = 12 (15)^{1/3} = 29.6 \text{ psi-ms}$$

Step 3. Drag coefficient.

$$C_D = 1 \quad (\text{from table 2-8 for cylinder loaded perpendicular to axis.})$$

Step 4. a. Mass of target.

$$M = \frac{W_t}{g} = \frac{7.13 \text{ lb}}{32.2 \times 12 \times 10^{-6} \frac{\text{in}}{\text{ms}^2}} = 18,450 \frac{\text{lb-ms}^2}{\text{in}}$$

b. Location of largest cross-section.

$$X = 1 \text{ in} \quad (\text{radius of object in this case - see fig. 2A-21})$$

c. Transverse distance of presented area.

$$H = 2.0 \text{ in} \quad (\text{diameter of object in this case - see fig. 2A-25}).$$

d. Mean presented area.

$$A = 2 \times 8 = 16 \text{ in}^2$$

Step 5. Reflection constant.

Target is resting on table which is a reflecting surface so:

$$K = 4$$

Step 6. Evaluate P_{so}/p_o

$$P_{so}/p_o = 39/14.7 = 2.65$$

Step 7. Evaluate $12C_D 1_s a_o / [10^3 P_{so} (KH + X)]$

$$\frac{12C_D 1_s a_o}{10^3 P_{so} (KH + X)} = \frac{12 (1.2) (29.6) (1100)}{10^3 (39) (2 \times 4 + 1)} = 1.34$$

Step 8. Calculate the velocity.

$$\frac{144 v_o M a_o}{10^6 p_o A (KH + X)} = 6.0 \quad (\text{fig. 2-248})$$

$$v_o = \frac{6.0 p_o A (KH + X) 10^6}{144 M a_o} = \frac{10^6 (6.0) (14.7) (16) (2 \times 4 + 1)}{(144) (18450) (1100)}$$

$$v_o = 4.34 \text{ ft/sec}$$

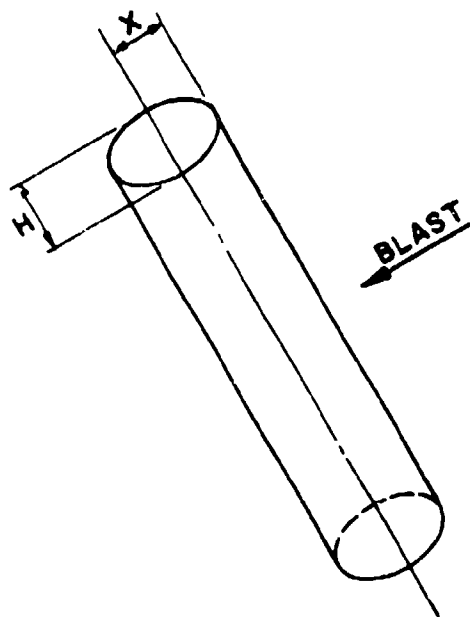


FIGURE 2A-25

Problem 2A-17 Constrained Secondary Fragments

Problem: Determine the velocity of a constrained object close to an exploding charge.

Procedure:

Step 1. Establish design parameters:

- a. fragment material.
- b. dimensions of object.
- c. boundary condition, cantilever or fixed-fixed.
- d. specific impulse imparted to object.

Step 2. Determine the fragment toughness T from table 2-9 and the fragment mass density ρ_f .

Step 3. Calculate the loaded area of the object.

Step 4. Evaluate the term $1b(2L/b)^{0.3}/[A(\rho_f T)^{0.5}]$, using the specific impulse and object dimensions from step 1, the fragment density and toughness from step 2 and the loaded area from step 3. With this term, enter figure 2-251 and read the value of $\frac{12V}{1000}(\rho_f/T)^{0.5}$ from which the velocity is calculated.

or: Using the specific impulse and object dimensions from step 1, the fragment density and toughness from step 2, and the loaded area from step 3, calculate the velocity of the object from equation 2-66.

Example 2A-17 Constrained Secondary Fragments

Required: The velocity of a cylindrical tool holder after it breaks free of its moorings.

Solution:

Step 1. Given:

- a. fragment material; A36 steel
- b. dimensions of object: $b = 2.0$ inches
 $L = 8.0$ inches
- c. boundary conditions; cantilever
- d. specific impulse: $i = 1667$ psi-ms (see step 4 of example 2A-15).

Step 2. a. Fragment toughness.

$$T = 12,000 \text{ in-lb/in}^3 \quad (\text{table 2-9})$$

b. Mass density of steel.

$$\rho_f = \frac{490 \text{ lb/ft}^3 \left(\frac{\text{ft}^3}{1728 \text{ in}^3} \right)}{32.2 \text{ ft/s}^2 \left(\frac{12 \text{ in/ft}}{10^6 \text{ ms}^2} \right)} = 734 \frac{\text{lb-ms}^2}{\text{in}^4}$$

Step 3. Loaded area.

$$A = \pi r^2 = \pi (1.0)^2 = 3.14 \text{ in}^2$$

Step 4. Calculate the velocity.

$$\frac{\text{ib}}{A(\rho_f T)^{0.5}} \left(\frac{2L}{b} \right)^{0.3} = \frac{1667 \times 2.0}{3.14(734 \times 12,000)^{0.5}} \left(\frac{2 \times 8}{2} \right)^{0.3} = 0.668$$

from figure 2-251

$$\frac{12}{1000} \left[\frac{\rho_f}{T} \right]^{1/2} V = 0.025$$

$$\text{so } V = \frac{1000}{12} \left[\frac{T}{\rho_f} \right]^{1/2} 0.025 = \frac{1000}{12} \left(\frac{12,000}{734} \right)^{1/2} 0.025 = 8.4 \text{ fps}$$

or from equation 2-66

$$\begin{aligned} V &= \frac{1000}{12} \left[\frac{T}{\rho_f} \right]^{1/2} \left\{ -0.2369 + 0.3931 \left[\frac{\text{ib}}{(\rho_f T)^{1/2} A} \right] \left[\frac{2L}{b} \right]^{0.3} \right\} \\ &= \frac{1000}{12} \left[\frac{12,000}{734} \right]^{1/2} (-0.2369 + 0.3931 \times 0.668) \end{aligned}$$

$$V = 8.6 \text{ fps}$$

Problem 2A-18 Ground Shock Load

Problem: Determine the air blast and direct induced ground shock parameters.

Procedure: Air blast-induced ground shock.

Step 1. Determine the charge weight, ground distance R, height of burst H_0 , if any, and structure dimensions.

Step 2. Apply a 20% safety factor to the charge weight.

Step 3. Calculate the scaled distance Z.

Read: From fig. 2-15

a. Peak positive incident pressure P_{so} .

b. Scaled unit positive incident impulse $i_s/W^{1/3}$. Multiply scaled value by $W^{1/3}$ to obtain absolute value.

c. Shock front velocity U.

Step 4. Determine the maximum vertical ground motions.

a. Calculate maximum vertical velocity.

$$V_V = \frac{P_{so}}{\rho C_p} \quad (\text{eq. 2-74})$$

where:

ρ = Mass density of soil (table 2-10)

C_p = Compression wave seismic velocity in the soil (table 2-11)

b. Calculate maximum vertical displacement

$$D_V = \frac{i_s}{1,000 \rho C_p} \quad (\text{eq. 2-75})$$

- c. Calculate maximum vertical acceleration of the ground surface.

$$A_V = \frac{100P_{so}}{\rho C_p g} \quad (\text{eq. 2-76})$$

where:

g = Gravitational constant equal to 32.2 ft/sec²

- Step 5. Determine the maximum horizontal ground motions parameters.

- a. Check $C_p/12000 U > .707$
 b. Calculate maximum horizontal velocity.

$$V_H = V_V \tan [\sin^{-1}(C_p/12,000 U)] \quad (\text{eq. 2-77})$$

- c. Calculate maximum horizontal displacement.

$$D_H = D_V \tan [\sin^{-1}(C_p/12,000 U)] \quad (\text{eq. 2-78})$$

- d. Calculate maximum horizontal acceleration.

$$A_H = A_V \tan [\sin^{-1}(C_p/12,000 U)] \quad (\text{eq. 2-79})$$

- Step 6. Determine arrival time t_A and duration t_O :

- a. Read from fig. 2-15.

$t_A/W^{1/3}$ scaled time of arrival of blast wave and,

$t_O/W^{1/3}$ scaled duration of positive phase.

- b. Multiply scaled value by $W^{1/3}$ to obtain absolute value.

Direct-Induced Ground Shock

- Step 7. Determine the maximum vertical ground motions.

- a. Calculate maximum vertical displacement.

$$D_V = \frac{0.025 R_G^{1/3} W^{1/3}}{Z_G^{1.3}} \quad (\text{eq. 2-80, rock media})$$

or

$$D_V = \frac{0.17 R_G^{1/3} W^{1/3}}{Z_G^{2.3}} \quad (\text{eq. 2-83, dry or saturated soil})$$

b. Calculate the maximum vertical velocity.

$$V_V = 150/Z_G^{1.5} \quad (\text{eq. 2-85})$$

c. Calculate the maximum vertical acceleration.

$$A_V = 10,000/W^{1/3} Z_G^2 \quad (\text{eq. 2-87})$$

Step 8. Determine the maximum horizontal ground motion parameters.

a. Calculate the maximum horizontal displacement.

$$D_H = 0.5 D_V \quad (\text{eq. 2-82, rock media})$$

or

$$D_H = D_V \quad (\text{eq. 2-84, dry or saturated soil})$$

b. Calculate the maximum horizontal velocity.

$$V_H = V_V \quad (\text{eq. 2-86, all ground media})$$

c. Calculate the maximum horizontal acceleration.

$$A_H = 0.5 A_V \quad (\text{eq. 2-88, dry soil})$$

$$A_H = A_V \quad (\text{eq. 2-89, wet soil or rock media})$$

Step 9. Determine arrival time t_{AG} :

$$t_{AG} = 12000 R_G / C_p$$

(eq. 2-92)

Example 2A-18 Ground Shock Loads

Required: Maximum acceleration, velocity, and displacement at a point 155 ft. away from a surface burst of 5,000 lbs. Also required are; times of arrival and duration of air-blast induced ground shock.

Solution:

Air blast-induced ground shock.

Step 1. Given: Charge weight = 5,000 lbs., $R = 155$ ft., $H_G = 12$ ft.

Step 2. $W = 1.2 (5,000) = 6,000$ lbs.

Step 3. Calculate the scaled distance Z .

$$Z = \frac{R}{W^{1/3}} = \frac{155}{(6,000)^{1/3}} = 8.53 \text{ ft/lb}^{1/3}$$

Read from figure 2-15.

a. $P_{so} = 13$ psi

b. $\frac{i_s}{W^{1/3}} = 9 \text{ psi-ms/lb}^{1/3}$

$$i_s = 9 \times W^{1/3} = 9 \times (6,000)^{1/3} = 163.54 \text{ psi-ms}$$

c. $U = 1.5$ ft/ms

Step 4. Determine the maximum vertical ground motion.

a. $V_V = \frac{P_{so}}{\rho C_p}$ (eq. 2-74)

$$V_V = \frac{13}{1.65 \times 10^{-4} \times 70,000} = 1.125 \text{ in/sec}$$

b. $D_V = \frac{i_s}{1,000 \rho C_p}$ (eq. 2-75)

$$D_V = \frac{163.5}{1,000 (1.65 \times 10^{-4}) 70,000} = 0.0142 \text{ in}$$

$$c. \quad A_V = \frac{100 P_{so}}{\rho C_p g} \quad (\text{eq. 2-76})$$

$$A_V = \frac{100 \times 12.8}{(1.65 \times 10^{-4}) 70,000 \times 32.2} = 3.44 \text{ g}$$

Step 5. Determine the maximum horizontal ground motion.

$$a. \quad \text{Check } C_p / 12000 U > .707$$

$$70,000 / 12,000 \times 1.5 = 3.89 > .707$$

$$b. \quad V_H = V_V = 1.125 \text{ in/sec}$$

$$c. \quad D_H = D_V = 0.0142 \text{ in}$$

$$d. \quad A_H = A_V = 3.44 \text{ g}$$

Step 6. Arrival time t_A

$$a. \quad \text{Read from figure 2-15.}$$

$$\frac{t_A}{W^{1/3}} = 3.35 \text{ ms/lb}^{1/3}$$

$$t_O / W^{1/3} = 2.35 \text{ ms/lb}^{1/3}$$

$$b. \quad t_A = 3.35 \times W^{1/3} = 3.35 (6,000)^{1/3}$$

$$t_A = 60.90 \text{ ms}$$

$$t_O = 2.35 \times W^{1/3} = 2.35 \times (6,000)^{1/3}$$

$$t_o = 42.70 \text{ ms}$$

Direct-induced ground shock.

Step 7. Maximum vertical ground motions.

$$a. \quad D_V = \frac{0.17 R_G^{1/3} W^{1/3}}{Z_G^{2.3}} \quad (\text{eq. 2-83})$$

$$= \frac{0.17 (155)^{1/3} (6,000)^{1/3}}{(8.53)^{2.3}} = 0.1198 \text{ in}$$

$$b. \quad V_V = \frac{150}{Z_G^{1.5}} \quad (\text{eq. 2-85})$$

$$V_V = \frac{150}{(8.53)^{1.5}} = 6.020 \text{ in/sec}$$

$$c. \quad A_V = \frac{10,000}{W^{1/3} Z_G^2} \quad (\text{eq. 2-87})$$

$$A_V = \frac{10,000}{(6,000)^{1/3} (8.53)^2} = 7.56 \text{ g}$$

Step 8. Horizontal ground motions.

$$a. \quad D_H = D_V \quad (\text{eq. 2-84})$$

$$D_H = 0.1198 \text{ in.}$$

$$b. \quad V_H = V_V \quad (\text{eq. 2-86})$$

$$V_H = 6.020 \text{ in/sec}$$

$$c. \quad A_H = 0.5 A_V \quad (\text{eq. 2-88})$$

$$A_H = 0.5 (7.56)$$

$$A_H = 3.78 g$$

Step 9. Arrival time t_{AG}

$$t_{AG} = 12,000 R_G / C_p = \frac{12,000 \times 155}{70,000} \quad (\text{eq. 2-92})$$

$$t_{AG} = 26.6 \text{ ms}$$

Problem 2A-19 Structure Motion Due to Air Shock

Problem: Determine the maximum horizontal acceleration, displacement and velocity of an above ground structure subjected to air shock.

Procedure:

- Step 1. Determine external loadings acting on the roof, front and rear walls according to the procedure outlined in problem 2A-10.
- Step 2. Construct the horizontal force-time load curve by combining the front and rear wall loadings from step 1 applied over the area of front and rear walls. Use times of arrival to phase these two loads.
- Step 3. Calculate the dead weight and mass of the structure.
- Step 4. Construct the downward force-time curve by adding the weight of the structure and total roof load. The roof load is the pressure-time loading from step 1 applied over the total area of the roof.
- Step 5. Determine the coefficient of friction between soil and the structure from table 2-12.
- Step 6. Determine maximum horizontal acceleration, displacement and velocity using the acceleration impulse extrapolation method outlined in Volume III, Article 3-19.2.1.2 of this manual. The resisting force at each time interval is equal to the value of downward force curve of step 4 multiplied by the coefficient of friction determined in step 5. The resisting force is assumed to be effective when the total horizontal movement is equal to or larger than 1/4 inch as mentioned in paragraph

Example 2A-19 Structure Motion Due to Air Shock

Required: Maximum horizontal acceleration, velocity and displacement of the square structure shown in figure 2A-9 from problem 2A-10 for a surface burst of 5,000 lbs at a distance from the front wall of 155 ft. Assume a coarse and compact soil. Roof, floor slab and side walls are 1 foot thick reinforced concrete slabs and assume a 50 psf of internal dead load for the structure.

Step 1. External loadings on the structure are determined according to the procedure in example 2A-10. See figures 2A-10, 2A-12 and 2A-13. The arrival time (t_A) for these loads are tabulated in step 3d of example 2A-10.

$$\therefore t_{Af} \text{ (front wall)} = 60.9 \text{ ms}$$

$$\therefore t_{Ab} \text{ (rear wall)} = 83.6 \text{ ms}$$

Step 2. a. Calculate area of front and rear walls.

$$\text{Area (front and rear)} = 30 \times 12 \times (12)^2 = 51840 \text{ in}^2$$

b. Calculate the time difference between the rear and front walls from step 1.

$$\Delta t = t_{Ab} - t_{Af} = 83.6 - 60.9 = 22.7 \text{ ms}$$

c. Construct the horizontal force-time load curve by multiplying the values of the front and rear wall curves from step 1 by the area from step 2a. Rear wall load starts at time equal to $\Delta t = 22.7$ from step 2b. See figure 2A-26.

Step 3. a. Calculate dead weight of structure W_d . Assume concrete weight is 150 psf.

$$W_d = 150 [4 (30 - 1) (12 - 1) + 2 (30)^2] + 50 (30 - 2)^2 = 500,600 \text{ lbs}$$

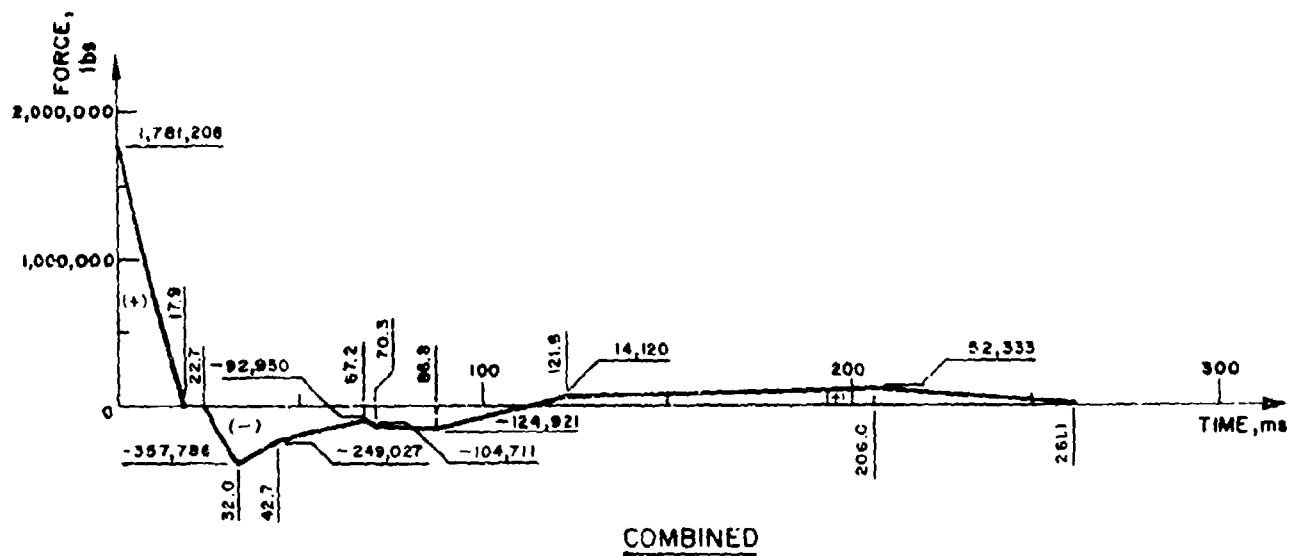
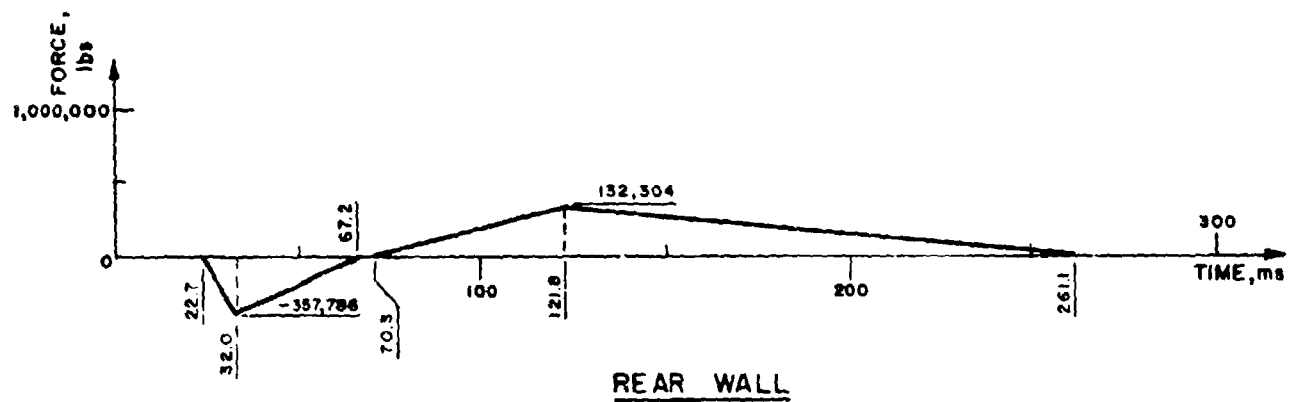
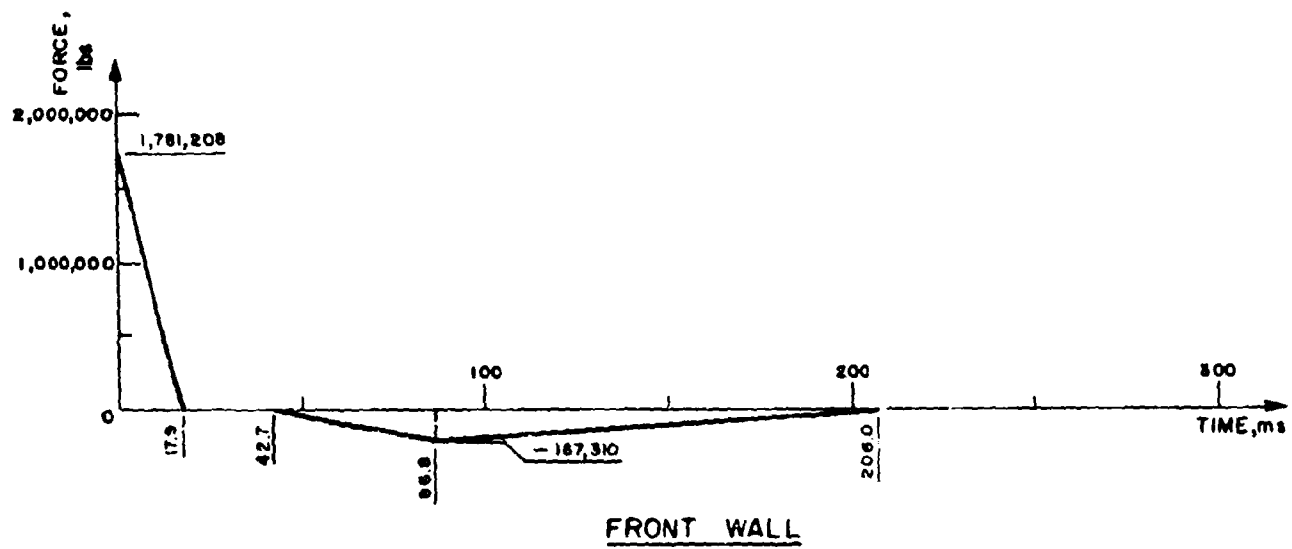


FIGURE 2A-26

b. Calculate total mass.

$$m = \frac{W_d}{g} = \frac{500,600 (1000)^2}{32.2 \times (12)} = 1295.55 \times 10^6 \frac{\text{lb ms}^2}{\text{in}}$$

Step 4. a. Calculate area of the roof.

$$\text{Area (roof)} = 30^2 \times (12)^2 = 129,600 \text{ in}^2$$

b. Construct the downward force-time curve by multiplying the values of the roof curve from step 1 by the roof area from step 4a, and adding the dead weight of structure $W_d = 500,600$ lbs from step 3a. (If the resulting value is negative, assume zero). See figure 2A-27 below.

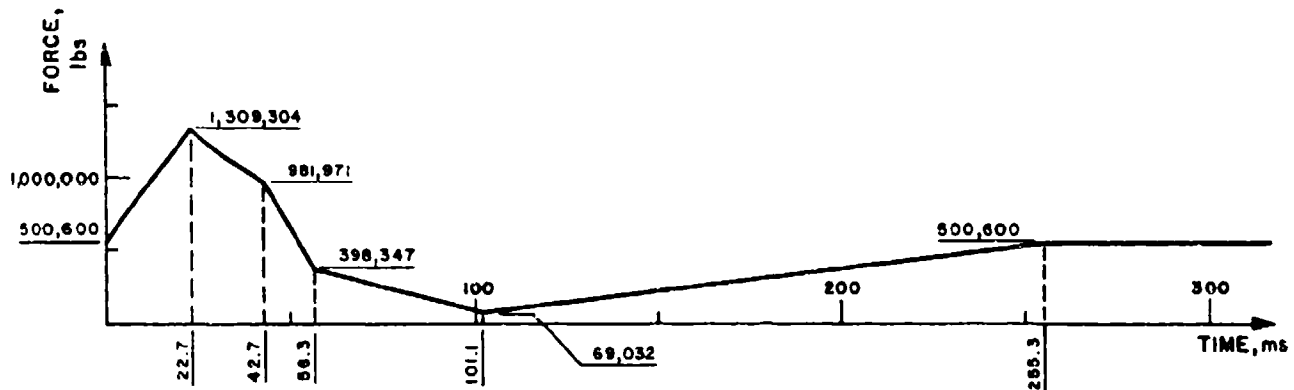


Figure 2A-27

Step 5. Coefficient of friction μ from table 2-12 for coarse and compact soil.

$$\therefore \mu = 0.60$$

Step 6. Using the acceleration impulse extrapolation method from Volume III of this manual determine maximum horizontal acceleration, displacement and velocity of the structure due to load curve (P) from step 2c. Resisting force R is the friction force produced due to the downward load curve F from step 4b after an initial lateral translation of $1/4$ inch. Use two ms time intervals for extrapolation. The following are the equations used in the extrapolation shown in Table 2A-3.

$$P_n - R_n = ma_n$$

$$R_n = \mu F_n$$

$$X_n + 1 = 2X_n - X_{n-1} + a_n (\Delta t)^2$$

$$V_n = V_{n-1} + a_n (\Delta t)$$

where

P_n = Load at time of step n (step 2c)

R_n = Resisting Friction Force at time step n

m = Mass from (step 3b)

a_n = Acceleration at time step n

μ = Friction coefficient (step 5)

F_n = Downward force at time step n (step 4b)

X_n = Deflection at time step n

V_n = Velocity at time step n

The maximum motions from Table 2A-3 are:

$$a_{\max} = .00122 \text{ in/ms}^2 \ll 101.67 \text{ ft/sec}^2 \ll 3.16 \text{ g's}$$

$$V_{\max} = .01231 \text{ in/ms} \ll 1.026 \text{ ft/sec}$$

$$D_{\max} = .355 \text{ in}$$

Problem 2A-20 Shock Response Spectra

Problem: Construct the elastic shock response spectra for the interior components of an above ground structure subject to an external explosion.

Procedure:

Table 2A-3

| n | t | P _n | R _n | P _n R _n | $a_n = \frac{P_n - \bar{P}_n}{n}$ | $a_n (\Delta t)^2$ | Σa_n | Σa_n^2 | Σa_n^3 | Σa_n^4 | Σa_n^5 | Σa_n^6 |
|----|----|----------------|----------------|-------------------------------|-----------------------------------|--------------------|--------------|----------------|--------------------|--------------------|----------------|----------------|
| - | ms | lbs | lbs | lbs | in/ms ² | in | in | in | in | in | in | in |
| 0 | 0 | 1,781,208 | 0 | 1,781,208 | $\frac{.0138}{2}$ | $\frac{.00550}{2}$ | 0 | 0 | $\frac{.00275}{2}$ | $\frac{.00275}{2}$ | 0 | .00138 |
| 1 | 2 | 1,582,190 | 0 | 1,582,190 | .00122 | .00499 | .00550 | .00244 | .00138 | .00382 | .00382 | .00382 |
| 2 | 4 | 1,383,173 | 0 | 1,383,173 | .00107 | .00427 | .02077 | .00214 | .00382 | .00596 | .00596 | .00596 |
| 3 | 6 | 1,184,155 | 0 | 1,184,155 | .00091 | .00356 | .04458 | .00182 | .00596 | .00778 | .00778 | .00778 |
| 4 | 8 | 985,137 | 0 | 985,137 | .00076 | .00304 | .07571 | .00152 | .00778 | .00930 | .00930 | .00930 |
| 5 | 10 | 786,120 | 0 | 786,120 | .00061 | .00243 | .11292 | .00122 | .00930 | .01052 | .01052 | .01052 |
| 6 | 12 | 587,102 | 0 | 587,102 | .00045 | .00181 | .15497 | .00090 | .01052 | .01142 | .01142 | .01142 |
| 7 | 14 | 388,084 | 0 | 388,084 | .00030 | .00120 | .20064 | .00060 | .01142 | .01202 | .01202 | .01202 |
| 8 | 16 | 189,067 | 0 | 189,067 | .00015 | .00059 | .24870 | .00029 | .01202 | .01231 | .01231 | .01231 |
| 9 | 18 | 0 | 0 | 0 | 0 | 0 | .29793 | 0 | .01231 | .01231 | .01231 | .01231 |
| 10 | 20 | 0 | 0 | 0 | 0 | 0 | .34716 | 0 | .01231 | .01231 | .01231 | .01231 |
| 11 | 22 | 0 | 0 | 0 | 0 | 0 | .39640 | 0 | .01231 | .01231 | .01231 | .01231 |
| 12 | 24 | -50,013 | 0 | -50,013 | -.00004 | -.00015 | .44564 | -.00008 | .01231 | .01223 | .01223 | .01223 |
| 13 | 26 | -126,956 | 0 | -126,956 | -.00010 | -.00039 | .49456 | -.00020 | .01223 | .01203 | .01203 | .01203 |
| 14 | 28 | -203,890 | 733,536 | -937,426 | -.00072 | -.00289 | .54270 | -.00142 | .01203 | .01061 | .01061 | .01061 |
| 15 | 30 | -280,843 | 713,896 | -994,739 | -.00077 | -.00307 | .58505 | -.00153 | .01061 | .00908 | .00908 | .00908 |
| 16 | 32 | -357,786 | 694,256 | -1,052,042 | -.00081 | -.00325 | .62126 | -.00162 | .00908 | .00746 | .00746 | .00746 |
| 17 | 34 | -337,457 | 674,617 | -1,012,074 | -.00078 | -.00312 | .65096 | -.00155 | .00746 | .00590 | .00590 | .00590 |
| 18 | 36 | -317,128 | 654,977 | -972,105 | -.00075 | -.00300 | .67441 | -.00150 | .00590 | .00440 | .00440 | .00440 |
| 19 | 38 | -296,780 | 635,337 | -932,117 | -.00072 | -.00288 | .69186 | -.00144 | .00440 | .00296 | .00296 | .00296 |
| 20 | 40 | -276,471 | 615,697 | -892,168 | -.00069 | -.00275 | .70354 | -.00138 | .00296 | .00158 | .00158 | .00158 |
| 21 | 42 | -256,142 | 596,057 | -852,199 | -.00066 | -.00263 | .70972 | -.00132 | .00158 | .00036 | .00036 | .00036 |
| 22 | 44 | -240,745 | 555,710 | -796,455 | -.00061 | -.00244 | .71064 | -.00122 | .00036 | .00006 | .00006 | .00006 |
| 23 | 46 | -218,004 | 504,214 | -722,218 | | | .70664 | | | | | |
| 24 | 48 | -215,263 | 452,718 | -668,001 | | | .35332 | | | | | |

- Step 1. Determine maximum acceleration, velocity and displacement due to ground shock according to procedure outlined in Problem 2A-18.
- Step 2. Determine maximum acceleration, velocity and displacement due to air shock according to the procedure outlined in Problems 2A-10 and 2A-19.
- Step 3. Determine if the ground shock is outrunning or superseismic (paragraph 2-23.2). For outrunning ground shock the maximum values of displacement, velocity and acceleration in horizontal and vertical directions are the algebraic summation of the maximum motions from steps 1 and 2. Otherwise proceed to step 4.
- Step 4. For superseismic ground shock the maximum values of displacement, velocity and acceleration are the numerically larger values of direct-induced ground shock or the algebraic sum of the maximum motions from air shock and air-burst induced ground shock.
- Step 5. Calculate the magnitude of acceleration, velocity and displacement for response spectra in horizontal and vertical directions by multiplying the maximum values of motions from step 3 or step 4 by their appropriate factor from paragraph 2-24.3.
- Step 6. Draw the horizontal and vertical shock response spectras.

Example 2A-20 Shock Response Spectra

Required: Shock response spectra for the structure defined in Examples 2A-18 and 2A-19.

Solution:

Step 1. Maximum values of motion in vertical and horizontal directions due to ground shock according to the procedure outlined in Example 2A-18 are:

a. Air blast-induced

$$A_H = A_V = 3.44 \text{ g}$$

$$V_H = V_V = 1.125 \text{ in/sec}$$

$$D_H = D_V = .014 \text{ in}$$

b. Direct-induced

$$A_H = 3.78 \text{ g}$$

$$A_V = 7.56 \text{ g}$$

$$V_H = V_V = 6.02 \text{ in/sec}$$

$$D_H = D_V = .120 \text{ in}$$

Step 2. Maximum horizontal acceleration, velocity and displacement due to air shock following the procedure outlined in Examples 2A-10 and 2A-19.

$$A_{\text{max}} = 3.16 \text{ g}$$

$$V_{\text{max}} = 12.31 \text{ in/sec}$$

$$D_{\text{max}} = .355 \text{ in}$$

Step 3. a. Check for outrunning ground shock

$$T_{AG} < T_A:$$

From Example 2A-18

$$T_{AG} = 26.6 \text{ ms}$$

$$T_A = 60.9 \text{ ms}$$

$$\therefore T_{AG} < T_A \text{ Outrunning ground shock}$$

b. Add the values of maximum motions from step 1 and step 2.

$$\therefore A_H \text{ max} = 3.16 + 3.44 + 3.78 = 10.38 \text{ g}$$

$$\therefore V_H \text{ max} = 12.310 + 1.108 + 6.020 = 19.438 \text{ in/sec}$$

$$\therefore D_H \text{ max} = .355 + .014 + .120 = .489 \text{ in}$$

and

$$\therefore A_V \text{ max} = 3.44 + 7.56 = 11.00 \text{ g}$$

$$\therefore V_V \text{ max} = 1.108 + 6.020 = 7.128 \text{ in/sec}$$

$$\therefore D_V \text{ max} = .014 + .120 = .134 \text{ in}$$

Step 4. Does not apply, the ground shock is not superseismic.

Step 5. Magnitude of the motions for response spectra.

$$A_H = 10.38 \times 2.0 = 20.76 \text{ g}$$

$$V_H = 19.438 \times 1.5 = 29.157 \text{ in/sec}$$

$$D_H = .489 \times 1.0 = .489 \text{ in}$$

and

$$A_V = 11.00 \times 2.0 = 22.00 \text{ g}$$

$$V_V = 7.128 \times 1.5 = 10.692 \text{ in/sec}$$

$$D_V = .134 \times 1.0 = .134 \text{ in}$$

Step 6. See the shock response spectra for the values from step 6 in figure 2A-28.

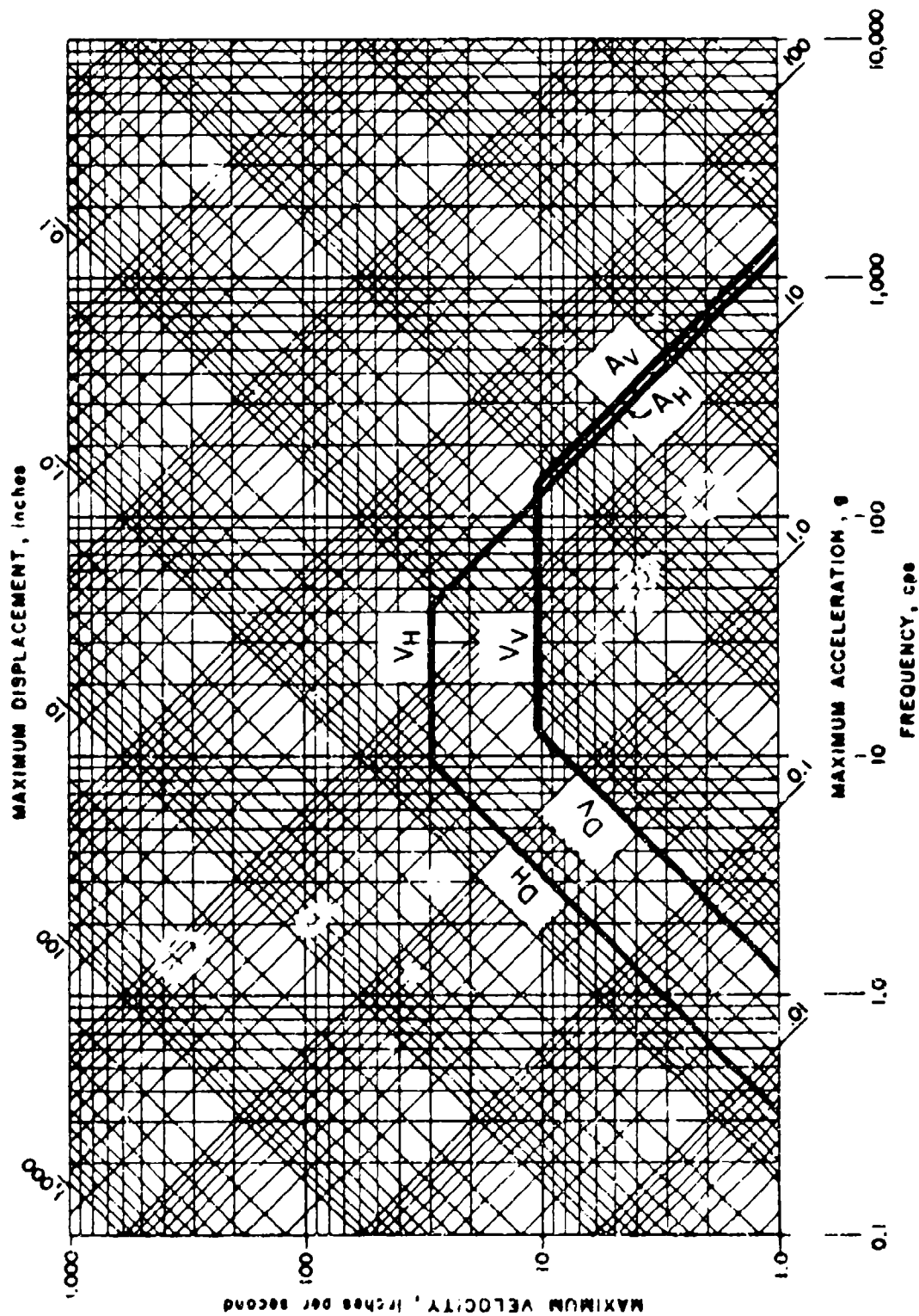


FIGURE 2A-28

APPENDIX 2B - LIST OF SYMBOLS

| | |
|-----------------------------|---|
| a | (1) acceleration (in./ms ²) (2) depth of equivalent rectangular stress block (in.) (3) long span of a panel (in.) |
| a ₀ | velocity of sound in air (ft./sec.) |
| a _x | acceleration in x direction (in./ms ²) |
| a _y | acceleration in y direction (in./ms ²) |
| A | (1) area (in. ²) (2) explosive composition factor (oz. ^{1/2} -in. ^{-3/2}) |
| A _a | area of diagonal bars at the support within a width b (in. ²) |
| A _b | area of reinforcing bar (in. ²) |
| A _d | (1) door area (in. ²) (2) area of diagonal bars at the support within a width b (in. ²) |
| A _D | drag area (in. ²) |
| A _F | net area of wall excluding openings (ft. ²) |
| A _G | area of gross section (in. ²) |
| A _H | maximum horizontal acceleration of ground surface (g's) |
| A _l | area of longitudinal torsion reinforcement (in. ²) |
| A _L | lift area (in. ²) |
| A _{ti} | (1) net area of section (in. ²) (2) area of individual wall subdivision (ft. ²) |
| A _O | area of openings (ft. ²) |
| A _{ps} | area of prestressed reinforcement (in. ²) |
| A _s | area of tension reinforcement within a width b (in. ²) |
| A _s ' | area of compression reinforcement within a width b (in. ²) |
| A _s ⁻ | area of rebound reinforcement (in. ²) |
| A _{sH} | area of flexural reinforcement within a width b in the horizontal direction on each face (in. ²)* |
| A _{sp} | area of spiral reinforcement (in. ²) |
| A _{st} | total area of reinforcing steel (in. ²) |

* See note at end of symbols.

| | |
|---------------|--|
| A_{SV} | area of flexural reinforcement within a width b in the vertical direction on each face (in.^2)* |
| A_t | area of one leg of a closed tie resisting torsion within a distance s (in.^2) |
| A_v | total area of stirrups or lacing reinforcement in tension within a distance, s_s or s_ℓ and a width b_s or b_ℓ (in.^2) |
| A_y | maximum vertical acceleration of the ground surface (g 's) |
| A_w | area of wall (ft.^2) |
| A_I, A_{II} | area of sector I and II, respectively (in.^2) |
| b | (1) width of compression face of flexural member (in.) (2) width of concrete strip in which the direct shear stresses at the supports are resisted by diagonal bars (in.) (3) short span of a panel (in.) |
| b_f | width of fragment (in.) |
| b_s | width of concrete strip in which the diagonal tension stresses are resisted by stirrups of area A_v (in.) |
| b_ℓ | width of concrete strip in which the diagonal tension stresses are resisted by lacing of area A_v (in.) |
| b_o | failure perimeter for punching shear (in.) |
| b_t | center-to-center dimension of a closed rectangular tie along b (in.) |
| B | explosive constant defined in table 2-7 ($\text{oz.}^{1/2} \text{ in.}^{-7/6}$) |
| c | (1) distance from the resultant applied load to the axis of rotation (in.) (2) damping coefficient (3) width of column capital (in.) |
| c_I, c_{II} | distance from the resultant applied load to the axis of rotation for sectors I and II, respectively (in.) |
| c_g | dilatational velocity of concrete (ft./sec.) |
| C | (1) shear coefficient (2) deflection coefficient for flat slabs |
| C_C | deflection coefficient for the center of interior panel of flat slab |
| C_{cr} | critical damping |

* See note at end of symbols.

| | |
|------------|---|
| C_d | shear coefficient for ultimate shear stress of one-way elements |
| C_D | drag coefficient |
| C_{Dq} | drag pressure (psi) |
| C_{Dq_0} | peak drag pressure (psi) |
| C_E | equivalent load factor |
| C_f | post-failure fragment coefficient ($\text{lb.}^2\text{-ms}^4/\text{in.}^8$) |
| C_H | shear coefficient for ultimate shear stress in horizontal direction for two-way elements* |
| C_L | (1) leakage pressure coefficient from figure 2-235 (2) deflection coefficient for midpoint of long side of interior flat slab panel (3) lift coefficient. |
| C_M | maximum shear coefficient |
| C_m | equivalent moment correction factor |
| C_p | compression wave seismic velocity in the soil from Table 2-10 (in./sec.) |
| C_r | sound velocity in reflected region from figure 2-192 (ft./ms) |
| C_R | force coefficient for shear at the corners of a window frame |
| C_{ra} | peak reflected pressure coefficient at angle of incidence α |
| C_s | shear coefficient for ultimate support shear for one-way elements |
| C_{sH} | shear coefficient for ultimate support shear in horizontal direction for two-way elements* |
| C_{sV} | shear coefficient for ultimate support shear in vertical direction for two-way elements* |
| C_S | deflection coefficient for midpoint of short side of interior flat slab panel |
| C_u | impulse coefficient at deflection X_u ($\text{psi-ms}^2/\text{in.}^2$) |
| C'_u | impulse coefficient at deflection X_m ($\text{psi-ms}^2/\text{in.}^2$) |
| C_v | shear coefficient for ultimate shear stress in vertical direction for two-way elements* |
| C_x | shear coefficient for the ultimate shear along the long side of window frame |

* See note at end of symbols.

| | |
|----------|--|
| C_y | shear coefficient for the ultimate shear along the short side of window frame |
| CL | confidence level |
| C_1 | (1) impulse coefficient at deflection X_1 (psi-ms ² /in. ²) (2) ratio of gas load to shock load |
| C_1 | impulse coefficient at deflection X_m (psi-ms ² /in. ²) |
| C_2 | ratio of gas load duration to shock load duration |
| d | (1) distance from extreme compression fiber to centroid of tension reinforcement (in.) (2) diameter (in.) (3) fragment diameter (in.) |
| d' | distance from extreme compression fiber to centroid of compression reinforcement (in.) |
| d_b | diameter of reinforcing bar (in.) |
| d_c | distance between the centroids of the compression and tension reinforcement (in.) |
| d_{cH} | distance between the centroids of the horizontal compression and tension reinforcement (in.) |
| d_{co} | diameter of steel core (in.) |
| d_{cV} | distance between the centroids of the vertical compression and tension reinforcement (in.) |
| d_e | distance from support and equal to distance d or d_c (in.) |
| d_i | average inside diameter of explosive casing (in.) |
| d_i' | adjusted inside diameter of casing (in.) |
| d_p | distance between center lines of adjacent lacing bends measured normal to flexural reinforcement (in.) |
| d_p | distance from extreme compression fiber to centroid of prestressed reinforcement (in.) |
| d_{sp} | depth of spalled concrete (in.) |
| d_1 | diameter of cylindrical portion of primary fragment (in.) |
| D | (1) unit flexural rigidity (lb-in.) (2) location of shock front for maximum stress (ft.) (3) minimum magazine separation distance (ft.) (4) caliber density (lb/in. ³) (5) overall diameter of circular section (in.) (6) damping force (lb.) |

| | |
|---------------|--|
| | (7) displacement of mass from shock load (in.) |
| D_E | equivalent loaded width of structure for non-planar wave front (ft.) |
| D_H | maximum horizontal displacement of the ground surface (in.) |
| DIF | dynamic increase factor |
| D_S | diameter of the circle through centers of reinforcement arranged in a circular pattern (in.) |
| D_{sp} | diameter of the spiral measured through the centerline of the spiral bar (in.) |
| DLF | dynamic load factor |
| D_V | maximum vertical displacement of the ground surface (in.) |
| e | (1) base of natural logarithms and equal to 2.71828... |
| | (2) distance from centroid of section to centroid of pre-stressed reinforcement (in.) |
| | (3) actual eccentricity of load (in.) |
| e_b | balanced eccentricity (in.) |
| $(2E')^{1/2}$ | Gurney Energy Constant (ft./sec.) |
| E | (1) modulus of elasticity |
| | (2) internal work (in.-lbs.) |
| E_c | modulus of elasticity of concrete (psi) |
| E_m | modulus of elasticity of masonry units (psi) |
| E_s | modulus of elasticity of reinforcement (psi) |
| f | (1) unit external force (psi) |
| | (2) frequency of vibration (cps) |
| f'_c | static ultimate compressive strength of concrete at 28 days (psi) |
| f'_{dc} | dynamic ultimate compressive strength of concrete (psi) |
| f'_{dm} | dynamic ultimate compressive strength of masonry units (psi) |
| f_{ds} | dynamic design stress for reinforcement (a function of f_y , f_u and θ) (psi) |
| f_{du} | dynamic ultimate stress of reinforcement (psi) |
| f_{dy} | dynamic yield stress of reinforcement (psi) |
| f'_m | static ultimate compressive strength of masonry units (psi) |
| f_n | natural frequency of vibration (cps) |
| f_{ps} | average stress in the prestressed reinforcement at ultimate |

| | |
|----------|---|
| | load (psi) |
| f_{pu} | specified tensile strength of prestressing tendon (psi) |
| f_{py} | yield stress of prestressing tendon corresponding to a 1 per- cent elongation (psi) |
| f_r | reflection factor |
| f_s | static design stress for reinforcement (psi) |
| f_{se} | effective stress in prestressed reinforcement after allowances for all prestress losses (psi) |
| f_u | static ultimate stress of reinforcement (psi) |
| f_y | static yield stress of reinforcement (psi) |
| F | (1) total external force (lbs.) (2) coefficient for moment of inertia of cracked section (3) function of C_2 and C_1 for bilinear triangular load |
| F_o | force in the reinforcing bars (lbs.) |
| F_E | equivalent external force (lbs.) |
| F_D | drag force (lbs.) |
| F_F | frictional force (lbs.) |
| F_L | lift force (lbs.) |
| F_N | vertical load supported by foundation (lbs.) |
| g | acceleration due to gravity (32.2 ft./sec. ²) |
| G | shear modulus (psi) |
| h | (1) charge location parameter (ft.) (2) height of masonry wall |
| h_n | average clearing distance for individual areas of openings from Section 2-15.4.2 |
| h_t | center-to-center dimension of a closed rectangular tie along h (in.) |
| h' | clear height between floor slab and roof slab |
| H | (1) span height (in.)* (2) distance between reflecting surface(s) and/or free edge(s) in vertical direction (ft.) (3) minimum transverse dimension of mean presented area of object (ft.) |
| H_c | height of charge above ground (ft.) |
| H_s | height of structure (ft.) |

| | |
|----------------|--|
| H_T | height of triple point (ft.) |
| H_w | height of wall (ft.) |
| H^c | heat of combustion (ft.-lb./lb.) |
| H^d | heat of detonation (ft.-lb./lb.) |
| i | unit positive impulse (psi-ms) |
| i_a | sum of blast impulse capacity of the receiver panel and the least impulse absorbed by the sand (psi-ms) |
| i_{ba} | blast impulse capacity of receiver panel (psi-ms) |
| i^- | unit negative impulse (psi-ms) |
| \bar{i}_a | sum of scaled unit blast impulse capacity of receiver panel and scaled unit blast impulse attenuated through concrete and sand in a composite element (psi-ms/lb. ^{1/3}) |
| i_b | unit blast impulse (psi-ms) |
| \bar{i}_b | scaled unit blast impulse (psi-ms/lb. ^{1/3}) |
| \bar{i}_{ba} | scaled unit blast impulse capacity of receiver panel of composite element (psi-ms/lb. ^{1/3}) |
| \bar{i}_{bd} | scaled unit blast impulse capacity of donor panel of composite element (psi-ms/lb. ^{1/3}) |
| \bar{i}_{bt} | total scaled unit blast impulse capacity of composite element (psi-ms/lb. ^{1/3}) |
| i_c | impulse capacity of an element (psi-ms) |
| i_d | total drag and diffraction impulse (psi-ms) |
| i_e | unit excess blast impulse (psi-ms) |
| i_{fs} | required impulse capacity of fragment shield (psi-ms) |
| i_g | gas impulse (psi-ms) |
| i_r | unit positive normal reflected impulse (psi-ms) |
| i_r^- | unit negative normal reflected impulse (psi-ms) |
| i_{ra} | peak reflected impulse at angle of incidence α (psi-ms) |
| i_s | unit positive incident impulse (psi-ms) |
| i_s^- | unit negative incident impulse (psi-ms) |
| i_{st} | impulse consumed by fragment support connection (psi-ms) |
| I | (1) moment of inertia (in. ⁴ /in. for slabs) (in. ⁴ for beams) (2) total impulse applied to fragment |

* See note at end of symbols.

| | |
|--------------|---|
| I_a | average of gross and cracked moments of inertia ($\text{in.}^4/\text{in.}$ for slabs) (in.^4 for beams) |
| I_c | moment of inertia of cracked concrete section ($\text{in.}^4/\text{in.}$ for slabs) (in.^4 for beams) |
| I_{CH} | moment of inertia of cracked concrete section in horizontal direction ($\text{in.}^4/\text{in.}$)* |
| I_{CV} | moment of inertia of cracked concrete section in vertical direction ($\text{in.}^4/\text{in.}$)* |
| I_g | moment of inertia of gross concrete section ($\text{in.}^4/\text{in.}$ for slabs) (in.^4 for beams) |
| I_m | mass moment of inertia ($\text{lb.-ms}^2\text{-in.}$) |
| I_n | moment of inertia of net section of masonry unit (in.^4) |
| I_s | gross moment of inertia of slab ($\text{in.}^4/\text{in.}$) |
| I_{st} | impulse consumed by the fragment support connection (psi-ms) |
| I_w | gross moment of inertia of wall ($\text{in.}^4/\text{in.}$) |
| j | ratio of distance between centroids of compression and tension forces to the depth d |
| k | (1) constant depending on the casing metal (2) effective length factor |
| k_v | velocity decay coefficient |
| K | (1) unit stiffness (psi/in. for slabs) (lb./in./in. for beams) (lb./in. for springs) (2) constant defined in paragraph 2-18.2 |
| K_e | elastic unit stiffness (psi/in. for slabs) (lb./in./in. for beams) |
| K_{ep} | elasto-pastic unit stiffness (psi/in. for slabs) (lb./in./in. for beams) |
| K_E | (1) equivalent elastic unit stiffness (psi/in. for slabs) (lb./in./ in. for beams) (2) equivalent spring constant (lb./in.) |
| K_L | load factor |
| K_{LM} | load-mass factor |
| $(K_{LM})_u$ | load-mass factor in the ultimate range |

* See note at end of symbols.

| | |
|------------------|---|
| $(K_{LM})_{up}$ | load-mass factor in the post-ultimate range |
| K_M | mass factor |
| K_R | resistance factor |
| KE | kinetic energy |
| l | charge location parameter (ft.) |
| l | (1) length of the yield line (in.) (2) width of 1/2 of the column strip (in.) |
| l_d | basic development length of reinforcing bar (in.) |
| l_{dh} | development length of hooked bar (in.) |
| l_c | length of cylindrical explosive (in.) |
| l_p | spacing of same type of lacing bar (in.) |
| l_s | span of flat slab panel (in.) |
| L | (1) span length (in.)* (2) distance between reflecting surface(s) and/or free edge(s) in horizontal direction (ft.) |
| L_{cyl} | length of cylinder (in.) |
| L_f | length of fragment (in.) |
| L_H | clear span in short direction (in.) |
| L_l | length of lacing bar required in distance s_l (in.) |
| L_L | clear span in long direction (in.) |
| L_o | embedment length of reinforcing bars (in.) |
| L_s | length of shaft (in.) |
| L_u | unsupported length of column (in.) |
| L_w | wave length of positive pressure phase (ft.) |
| L_w^- | wave length of negative pressure phase (ft.) |
| L_x | clear span in long direction (in.) |
| L_y | clear span in short direction (in.) |
| L_{wb}, L_{wd} | wave length of positive pressure phase at points b and d, respectively (ft.) |
| L_1 | total length of sector of element normal to axis of rotation (in.) |
| m | (1) unit mass (psi-ms ² /in. for slabs) [beams, (lb./in-ms ²)/in.] |

* See note at end of symbols.

| | |
|------------------|---|
| | (2) ultimate unit moment (in.-lbs./in.) |
| | (3) mass of fragment (lbs.-ms ² /in.) |
| m_a | average of the effective elastic and plastic unit masses (psi-ms ² /in. for slabs) [beams, (lb./in-ms ²)/in] |
| m_e | effective unit mass (psi-ms ² /in. for slabs) [beams, (lb/in-ms ²)/in] |
| m_{sp} | mass of spalled fragments (psi-ms ² /in.) |
| m_u | effective unit mass in the ultimate range (psi-ms ² /in. for slabs) [beams, (lb/in-ms ²)/in.] |
| m_{up} | effective unit mass in the post-ultimate range (psi-ms ² /in.) |
| M | (1) unit bending moment (in.-lbs./in. for slabs) (in.-lbs. for beams) |
| | (2) total mass (lb.-ms ² /in.) |
| | (3) design moment (in.-lbs.) |
| M_e | effective total mass (lb.-ms ² /in.) |
| M_u | ultimate unit resisting moment (in.-lbs./in. for slabs) (in.-lbs. for beams) |
| M_u | ultimate unit rebound moment (in.-lbs./in. for slabs) (in.-lbs. for beams) |
| M_c | moment of concentrated loads about line of rotation of sector (in.-lbs.) |
| M_A | fragment distribution factor |
| M_E | equivalent total mass (lb.-ms ² /in.) |
| M_{HN} | ultimate unit negative moment capacity in horizontal direction (in.-lbs./in.)* |
| M_{HP} | ultimate unit positive moment capacity in horizontal direction (in.-lbs./in.)* |
| M_{OH}, M_{OL} | total panel moment for direction H and L respectively (in.-lbs.) |
| M_N | ultimate unit negative moment capacity at supports (in.-lbs./in. for slabs) (in.-lbs. for beams) |
| M_P | ultimate unit positive moment capacity at midspan (in.-lbs./in.) |

* See note at end of symbols.

| | |
|----------|--|
| | for slabs) (in.-lbs. for beams) |
| M_{VN} | ultimate unit negative moment capacity in vertical direction (in.-lbs./in.)* |
| M_{VP} | ultimate unit positive moment capacity in vertical direction (in.-lbs./in.)* |
| M_1 | value of smaller end moment on column |
| M_2 | value of larger end moment on column |
| n | (1) modular ratio |
| | (2) number of time intervals |
| | (3) number of glass pane tests |
| | (4) caliber radius of the tangent ogive of fragment nose |
| N | (1) number of adjacent reflecting surfaces |
| | (2) nose shape factor |
| N_f | number of primary fragments larger than W_f |
| N_u | axial load normal to the cross section |
| N_T | total number of fragments |
| p | reinforcement ratio equal to $\frac{A_s}{bd}$ or $\frac{A_s}{bd_c}$ |
| p' | reinforcement ratio equal to $\frac{A'_s}{bd}$ or $\frac{A'_s}{bd_c}$ |
| p_b | reinforcement ratio producing balanced conditions at ultimate strength |
| p_o | ambient atmospheric pressure (psi) |
| p_p | prestressed reinforcement ratio equal to A_{ps}/bd_p |
| p_m | mean pressure in a partially vented chamber (psi) |
| p_{mo} | peak mean pressure in a partially vented chamber (psi) |
| p_r | average peak reflected pressure (psi) |
| p_H | reinforcement ratio in horizontal direction on each face* |
| p_T | total reinforcement ratio equal to $p_H + p_V$ |
| p_V | reinforcement ratio in vertical direction on each face* |
| $p(x)$ | distributed load per unit length |
| P | (1) pressure (psi) |

* See note at end of symbols.

| | |
|-----------------------------|--|
| | (2) concentrated load (lbs.) |
| P_- | negative pressure (psi) |
| P_c | critical axial load causing buckling (lbs.) |
| P_g | maximum gas pressure (psi) |
| P_i | interior pressure within structure (psi) |
| ΔP_i | interior pressure increment (psi) |
| P_f | fictitious peak pressure (psi) |
| P_{max} | maximum average pressure acting on interior face of wall (psi) |
| P_o | (1) peak pressure (psi) (2) maximum axial load (lbs.) (3) atmospheric pressure (psi) |
| P_r | peak positive normal reflected pressure (psi) |
| P_{r-} | peak negative normal reflected pressure (psi) |
| $P_{r\alpha}$ | peak reflected pressure at angle of incidence α (psi) |
| P_{RIB} | maximum average pressure on backwall (psi) |
| P_s | positive incident pressure (psi) |
| P_{sb}, P_{se} | positive incident pressure at points b and e, respectively (psi) |
| P_{so} | peak positive incident pressure (psi) |
| P_{so-} | peak negative incident pressure (psi) |
| $P_{sob}, P_{sod}, P_{soe}$ | peak positive incident pressure at points b, d, and e, respectively (psi) |
| P_u | ultimate axial load at actual eccentricity c (lbs.) |
| P_x | ultimate load when eccentricity e_x |
| P_y | ultimate load when eccentricity e_y is present (lbs.) |
| q | dynamic pressure (psi) |
| q_b, q_e | dynamic pressure at points b and e, respectively (psi) |
| q_o | peak dynamic pressure (psi) |
| q_{ob}, q_{oe} | peak dynamic pressure at points b and e, respectively (psi) |
| r | (1) unit resistance (psi) (2) radius of spherical TNT [density equals 95 lb./ft. ³] charge (ft.) (3) radius of gyration of cross section of column (in.) |
| r_- | unit rebound resistance (psi, for slabs) (lb./in. for beams) |
| r_{avail} | dynamic resistance available (psi) |

| | |
|---------------|--|
| Δr | change in unit resistance (psi, for slabs) (lb./in. for beams) |
| r_d | radius from center of impulse load to center of door rotation (in.) |
| r_{DL} | uniform dead load (psi) |
| r_e | elastic unit resistance (psi, for slabs) (lb./in. for beams) |
| r_{ep} | elasto-plastic unit resistance (psi, for slabs) (lb./in. for beams) |
| r_{fs} | ultimate unit resistance of fragment shield (psi) |
| r_s | radius of shaft (in.) |
| r_T | tension membrane resistance (psi) |
| r_u | ultimate unit resistance (psi, for slabs) (lb./in. for beams) |
| r_{up} | post-ultimate unit resistance (psi) |
| r_1 | radius of hemispherical portion of primary fragment (in.) |
| R | (1) total internal resistance (lbs.) (2) slant distance (ft.) (3) ratio of S/G (4) standoff distance (ft.) |
| R_{eff} | effective radius (ft.) |
| R_f | (1) distance traveled by primary fragment (ft.) (2) distance from center of detonation (ft.) |
| R_g | uplift force at corners of window frame (lbs.) |
| R_l | radius of lacing bend (in.) |
| R_t | target radius (ft.) |
| R_A | normal distance (ft.) |
| R_E | equivalent total internal resistance (lbs.) |
| R_G | ground distance (ft.) |
| R_u | total ultimate resistance (lb.) |
| R_I, R_{II} | total internal resistance of sectors I and II, respectively (lbs.) |
| s | (1) sample standard deviation (2) spacing of torsion reinforcement in a direction parallel to the longitudinal reinforcement (in.) (3) pitch of spiral (in.) |
| s_s | spacing of stirrups in the direction parallel to the longitu- |

| | |
|-----------------|---|
| | dinal reinforcement (in.) |
| s_1 | spacing of lacing in the direction parallel to the longitudinal reinforcement (in.) |
| S | height of front wall or one-half its width, whichever is smaller (ft.) |
| S' | weighted average clearing distance with openings (ft.) |
| SE | strain energy |
| t | time (ms) |
| Δt | time increment (ms) |
| t_a | any time (ms) |
| t_b, t_e, t_f | time of arrival of blast wave at points b, e, and f, respectively (ms) |
| t_c | (1) clearing time for reflected pressures (ms) (2) average casing thickness of explosive charges (in.) |
| t'_c | (1) adjusted casing thickness (in.) (2) Clearing time for reflected pressures adjusted for wall openings (ms) |
| t_d | rise time (ms) |
| t_E | time to reach maximum elastic deflection (ms) |
| t_g | fictitious gas duration (ms) |
| t_m | time at which maximum deflection occurs (ms) |
| t_o | duration of positive phase of blast pressure (ms) |
| t_o^- | duration of negative phase of blast pressure (ms) |
| t_{of} | fictitious positive phase pressure duration (ms) |
| t_{of}^- | fictitious negative phase pressure duration (ms) |
| t_r | fictitious reflected pressure duration (ms) |
| t_u | time at which ultimate deflection occurs (ms) |
| t_y | time to reach yield (ms) |
| t_A | time of arrival of blast wave (ms) |
| t_{AG} | time of arrival of ground shock (ms) |
| t_1 | time at which partial failure occurs (ms) |
| T | (1) duration of equivalent triangular loading function (ms) (2) thickness of masonry wall (in.) (3) toughness of material (psi-in./in.) |
| T_c | thickness of concrete section (in.) |

| | |
|--------------|--|
| \bar{T}_c | scaled thickness of concrete section (ft./lb. ^{1/3}) |
| T_g | thickness of glass (in.) |
| T_H | force in the continuous reinforcement in the short span direction (lbs.) |
| T_i | angular impulse load (lb.-ms-in.) |
| T_L | force in the continuous reinforcement in the long span direction (lbs.) |
| T_N | effective natural period of vibration (ms) |
| T_{pf} | minimum thickness of concrete to prevent perforation by a given fragment (in.) |
| T_r | rise time (ms) |
| T_s | (1) thickness of sand fill (in.) (2) thickness of slab (in.) |
| T_{sp} | minimum concrete thickness to prevent spalling (in.) |
| \bar{T}_s | scaled thickness of sand fill (ft./lb. ^{1/3}) |
| T_u | total torsional moment at critical section (in.-lbs.) |
| T_w | thickness of wall (in.) |
| T_y | force of the continuous reinforcement in the short direction (lbs.) |
| u | particle velocity (ft./ms) |
| u_u | ultimate flexural or anchorage bond stress (psi) |
| U | shock front velocity (ft./ms) |
| U_s | strain energy |
| v | velocity (in./ms) |
| v_a | instantaneous velocity at any time (in./ms) |
| v_b | boundary velocity for primary fragments (ft./sec.) |
| v_c | ultimate shear stress permitted on an unreinforced web (psi) |
| v_f | maximum post-failure fragment velocity (in./ms) |
| v_f (avg.) | average post-failure fragment velocity (in./ms) |
| v_i | velocity at incipient failure deflection (in./ms) |
| v_o | initial velocity of primary fragment (ft./sec.) |
| v_r | residual velocity of primary fragment after perforation (ft./sec.) |
| v_s | striking velocity of primary fragment (ft./sec.) |
| v_{tc} | maximum torsion capacity of an unreinforced web (psi) |

| | |
|----------|--|
| v_{tu} | nominal torsion stress in the direction of v_u (psi) |
| v_u | ultimate shear stress (psi) |
| v_{uH} | ultimate shear stress at distance d_e from the horizontal support (psi)* |
| v_{uV} | ultimate shear stress at distance d_e from the vertical support (psi)* |
| v_x | velocity in x direction (in./ms.) |
| v_y | velocity in y direction (in./ms.) |
| V | (1) volume of partially vented chamber (ft. ³) (2) velocity of compression wave through concrete (in./sec.) (3) velocity of mass under shock load (in./sec.) |
| V_d | ultimate direct shear capacity of the concrete of width b (lbs.) |
| V_{dH} | shear at distance d_e from the vertical support on a unit width (lbs./in.)* |
| V_{dV} | shear at distance d_e from the horizontal support on a unit width (lbs./in.)* |
| V_f | free volume (ft. ³) |
| V_H | maximum horizontal velocity of the ground surface (in./sec.) |
| V_O | volume of structure (ft. ³) |
| V_S | shear at the support (lb./in., for panels) (lbs. for beam) |
| V_{SH} | shear at the vertical support on a unit width (lbs./in.)* |
| V_{SV} | shear at the horizontal support on a unit width (lbs./in.)* |
| V_u | total shear on a width b (lbs.) |
| V_V | maximum vertical velocity of the ground surface (in./sec.) |
| V_x | unit shear along the long side of window frame (lb./in.) |
| V_y | unit shear along the short side of window frame, (lbs./in.) |
| w | applied uniform load (lbs.-in. ²) |
| w_c | (1) unit weight (psi, for panels) (lb./in. for beam) (2) weight density of concrete (lbs./ft. ³) |
| w_s | weight density of sand (lbs./ft. ³) |
| W | (1) design charge weight (lbs.) (2) external work (in.-lbs.) |

* See note at end of symbols.

| | |
|------------------|--|
| | (3) width of wall (ft.) |
| W_A | weight of fluid (lbs.) |
| W_{ACT} | actual quantity of explosives (lbs.) |
| W_C | total weight of explosive containers (lbs.) |
| W_E | effective charge weight (lbs.) |
| W_{EG} | effective charge weight for gas pressure (lb.) |
| W_{EXP} | weight of explosive in question (lbs.) |
| W_f | weight of primary fragment (oz.) |
| \bar{W}_f | average fragment weight (oz.) |
| W_F | weight of frangible element (lb./ft. ²) |
| W_{CI} | weight of inner casing (lbs.) |
| W_{CO} | total weight of steel core (lbs.) |
| W_{CO} | weight of outer casing (lbs.) |
| W_{C1}, W_{C2} | total weight of plates 1 and 2, respectively (lbs.) |
| W_s | width of structure (ft.) |
| WD | work done |
| x | yield line location in horizontal direction (in.)* |
| X | (1) deflection (in.) (2) distance from front of object to location of largest cross section to plane of shock front (ft.) |
| X_a | any deflection (in.) |
| X_c | lateral deflection to which a masonry wall develops no resistance (in.) |
| X_{DL} | deflection due to dead load (in.) |
| X_e | elastic deflection (in.) |
| X_E | equivalent elastic deflection (in.) |
| X_{ep} | elasto-plastic deflection (in.) |
| X_f | maximum penetration into concrete of armor-piercing fragments (in.) |
| $X_{f,}$ | maximum penetration into concrete of fragments other than armor-piercing (in.) |
| X_m | maximum transient deflection (in.) |
| X_p | plastic deflection (in.) |

* See note at end of symbols.

| | |
|------------------------------|---|
| x_s | (1) maximum penetration into sand of armor-piercing fragments (in.) (2) static deflection (in.) |
| x_u | ultimate deflection (in.) |
| x_1 | (1) partial failure deflection (in.) (2) deflection at maximum ultimate resistance of masonry wall (in.) |
| y | yield line location in vertical direction (in.)* |
| y_t | distance from the top of section to centroid (in.) |
| z | scaled slant distance (ft./lb. ^{1/3}) |
| z_A | scaled normal distance (ft./lb. ^{1/3}) |
| z_G | scaled ground distance (ft./lb. ^{1/3}) |
| α | (1) angle formed by the plane of stirrups, lacing, or diagonal reinforcement and the plane of the longitudinal reinforcement (deg) (2) angle of incidence of the pressure front (deg) (3) acceptance coefficient (4) trajectory angle (deg.) |
| α_{ec} | ratio of flexural stiffness of exterior wall to flat slab |
| $\alpha_{ecH}, \alpha_{ecL}$ | ratio of flexural stiffness of exterior wall to slab in direction H and L respectively |
| β | (1) coefficient for determining elastic and elasto-plastic resistances (2) particular support rotation angle (deg) (3) rejection coefficient (4) target shape factor from figure 2-212 |
| β_1 | factor equal to 0.85 for concrete strengths up to 4,000 psi and is reduced by 0.05 for each 1,000 psi in excess of 4,000 psi |
| γ | coefficient for determining elastic and elasto-plastic deflections |
| γ_p | factor for type of prestressing tendon |
| δ | moment magnifier |

* See note at end of symbols.

| | |
|----------------|--|
| δ_{11} | clearing factor |
| Δ | deflection at sector's displacement (in.) |
| ϵ'_c | average strain rate for concrete (in./in./ms) |
| ϵ_m | unit strain in mortar (in./in.) |
| ϵ'_s | average strain rate for reinforcement (in./in./ms) |
| ϵ_u | rupture strain (in./in./ms) |
| θ | (1) support rotation angle (deg) (2) angular acceleration (rad/ms ²) |
| θ_{max} | maximum support rotation angle (deg) |
| θ_H | horizontal rotation angle (deg)* |
| θ_V | vertical rotation angle (deg)* |
| λ | increase in support rotation angle after partial failure (deg) |
| μ | (1) ductility factor (2) coefficient of friction |
| ν | Poisson's ratio |
| ρ | (1) mass density (lbs.-ms. ² /in. ⁴) (2) density of air behind shock front (lbs/ft. ³) |
| ρ_a | density of air (oz./in. ³) |
| ρ_c | density of casing (oz./in. ³) |
| ρ_f | mass density of fragment (oz./in. ³) |
| ρ_o | mass density of medium (lb.-ms. ² /in. ⁴) |
| σ_u | fracture strength of concrete (psi) |
| Σ_o | effective perimeter of reinforcing bars (in.) |
| ΣM | summation of moments (in.-lbs.) |
| ΣM_N | sum of the ultimate unit resisting moments acting along the negative yield lines (in.-lbs.) |
| ΣM_P | sum of the ultimate unit resisting moments acting along the positive yield lines (in.-lbs.) |
| τ_s | maximum shear stress in the shaft (psi) |
| ϕ | (1) capacity reduction factor (2) bar diameter (in.) (3) TNT conversion factor |
| ϕ_r | assumed shape function for concentrated loads |

* See note at end of symbols.

$\phi(x)$ assumed shape function for distributed loads free edge

ω angular velocity (rad./ms)

simple support

fixed support

either fixed, restrained, or simple support

* Note. This symbol was developed for two-way elements which are used as walls. When roof slabs or other horizontal elements are under consideration, this symbol will also be applicable if the element is treated as being rotated into a vertical position.

APPENDIX 2C - BIBLIOGRAPHY

Blast Loads

1. Armendt, B. R., Hippensteel, R. G., Hoffman, A. J., and Keefer, J. H., Project White Tribe: Air Blast From Simultaneously Detonated Large-Scale Explosive Charges, BRL Report 1145, Aberdeen Proving Ground, Maryland, September 1961.
2. Armendt, B. R., Hippensteel, R. G., Hoffman, A. J., and Kingery, C. N., The Air Blast From Simultaneously Detonated Explosive Spheres, BRL Report 1294, Aberdeen Proving Ground, Maryland, August 1960.
3. Armendt, B. R., Hippensteel, R. G., Hoffman, A. J., and Schlueter, S.D., The Air Blast From Simultaneously Detonated Explosive Spheres: Part II - Optimization, BRL Memorandum Report 1384, Department of the Army Project No. 503-04-002, Aberdeen Proving Ground, Maryland, January 1962.
4. Ayvazyan, H.E., Dobbs N., Computer Program Impres, special publication ARLCD-SP-84001, prepared by Ammann & Whitney, New York, New York, for U.S. Army Armament Research and Development Center, Large Caliber Weapon Systems Laboratory, Dover, New Jersey.
5. Baker, W. E., Explosions in Air, University of Texas Press, Austin, Texas 1973.
6. Baker, W. E., Prediction and Scaling of Reflected Impulse From Strong Blast Waves, International Journal of Mechanical Science, 9, 1967, pp. 45-51.
7. Bleakney, W., The Diffraction of Shock Waves Around Obstacles and the Transient Loading of Structures, Princeton University, March 1950, (Published and Distributed by the Armed Forces Special Weapons Project).
8. Coulter, G.A., Air Shock and Flow in Model Rooms, BRL Memorandum Report 1987, Aberdeen Proving Ground, Maryland, June 1969.
9. Coulter, G. A., Air Shock Filling of Model Rooms, BRL Memorandum Report 1916, Aberdeen Proving Ground, Maryland, March 1968.
10. Coulter, G. A. and Peterson, R.L., Blast Fill Time of a One-Room Structure, Operation Prairie Flat Project Officers Report, Project LN 111 POR-2102, Ballistic Research Laboratory, Aberdeen Proving Ground, Maryland, November 1964.
11. Coulter, G. A., Bulmash G., and Kingery C., Feasibility Study of Shock Wave Modification in the BRL 2.44 m Blast Simulator, Memorandum Report ARBRL-MR-0339, prepared by U.S. Army Armament Research and Development Center, Ballistic Research Laboratory, Aberdeen Proving Ground, Maryland, March 1984.
12. Cranz, C., Lehrbuch der Ballistik, Springer-Verlag, Berlin, 1926.

13. Dewey, J.M., Johnson, O.T., and Patterson, J.D. II, Mechanical Impulse Measurements Close to Explosive Charges, BRL Report 1182, Aberdeen Proving Ground, Maryland, November 1962.
14. Dobratz, B.M., LLNL Explosives Handbook, Properties of Chemical Explosives and Explosive Simulants, URCL-52997, Lawrence Livermore National Laboratory, Livermore, California, March 1981.
15. Engineering Design Handbook, Principles of Explosive Behavior, AMCP 706-180, Headquarters, U.S. Army Material Command, Washington, D.C., April 1972.
16. Goodman, H. J., Compiled Free Air Blast Data on Bar Spherical Pentolite, BRL Report 1092, Aberdeen Proving Ground, Maryland, 1960.
17. Granstorm, S. A., Loading Characteristics of Air Blasts From Detonating Charges, Transactions of the Royal Institute of Technology, Stockholm, Sweden, Nr.100, 1956.
18. Hokanson, J.C., Esparza, E. D., and Wenzel, A. B., Blast Effects of Simultaneous Multiple-Charge Detonations, Contractor Report ARLCD-CR-78032, ARRADCOM, Dover, New Jersey, AD E400232, October 1978.
19. Hokanson, J.C., Esparza, E.D., Baker W.E., Sandoval, N.R. and Anderson, C.E., Determination of Blast Loads in the Damaged Weapons Facility, Vol 3, Final Report, Purchase Order F0913400, SWRI-6578, prepared by Southwest Research Institute, San Antonio, Texas, for Mason & Hanger - Silas Mason Company, Inc., Pantex Plant, Amarillo, Texas, July 1982.
20. Hokanson, J. C., Esparza, E. D., and Wenzel, A. B., Reflected Blast Measurements Around Multiple Detonating Charges, Minutes of the Eighteenth Explosives Safety Seminar, Volume I, September 1978, pp. 447-471.
21. Hokanson, J. C., Esparza, E. D., Wenzel, A. B. (Southwest Research Institute), Price, P. D. (ARRADCOM), Blast Effects of Simultaneous Multiple-Charge Detonations, Contractor Report ARLCD-CR-78032, prepared by U.S. Army Armament Research and Development Command, Large Caliber Weapon Systems Laboratory, Dover, New Jersey, October 1978.
22. Hopkinson, B. British Ordnance Board Minutes, 13565, 1915.
23. Iwanski, E. C., et al., Blast Effects on Buildings and Structures Operation of 6-Foot and 2-Foot Shock Tubes: High Pressure Tests on Simple Shapes, Report No. 54, Final Test Report No. 10, ARF Project No. D087, Armour Research Foundation of Illinois Institute of Technology.
24. Jack, W. H., Jr., Measurements of Normally Reflected Shock Waves From Explosive Charges, BRL Memorandum Report 1499, Aberdeen Proving Ground, Maryland, AD 422886, July 1963.
25. Jack, W. H., Jr. and Armendt, B. F., Jr., Measurements of Normally Reflected Shock Parameters Under Simulated High Altitude Conditions, BRL Report 1280, Aberdeen Proving Ground, Maryland, AD 469014, April 1965.

26. Johansson, C. H. and Persson, P.A., Detonics of High Explosives, Academic Press, London, England, and New York, New York, 1970.
27. Johnson, O.T., Patterson, J.D. II, and Olson, W.C., A Simple Mechanical Method for Measuring the Reflected Impulse of Air Blast Waves, BRL Report 1099, Aberdeen Proving Ground, Maryland, July 1957.
28. Kaplan, K., Lewis, K. S., and Morris, P. J., Blast Loading and Response of Military Equipment, Draft Final Report URS 7339-6, URS Research Company, San Mateo, California, Prepared for Ballistic Research Laboratory, December 1973.
29. Kaplan, K. and Price, P.D., Accidental Explosions and Effects of Blast Leakage Into Structures, Contractor Report ARLCD-CR-79009, U.S. Army ARRADCOM, Dover, New Jersey, AD E400320, June 1979.
30. Keenan, W. A., and Tancreto, J. E., Blast Environment From Fully and Partially Vented Explosions in Cubicles, Technical Report R 828, prepared by Civil Engineering Laboratory, Naval Construction Battalion Center, Port Hueneme, California, sponsored by Department of the Army Picatinny Arsenal, November 1975.
31. Keenan, W., Tancreto, J., Meyers, G., Johnson, F., Hopkins, J., Nickerson, H., and Armstrong, W., NCEL Products Supporting DOD Revision of NAVFAC P-397, Program No. Y0995-01-003-201, Technical Memorandum 2591TM, sponsored by Naval Facilities Engineering Command, Alexandria, Virginia, and Naval Civil Engineering Laboratory, Port Hueneme, California, March 1983.
32. Kingery, C.N., and Bulmash G., Airblast Parameters from TNT Spherical Air Burst and Hemispherical Surface Burst, Technical Report ARBRL-TR-02555, prepared by U.S. Army Armament Research and Development Center, Ballistic Research Laboratory, Aberdeen Proving Ground, Maryland, April 1984.
33. Kingery, C. N. and Coulter G. A., Reflected Overpressure Impulse on a Finite Structure, Technical Report ARBRL-TR-02537, prepared by U. S. Army Armament Research and Development Center, Ballistic Research Laboratory, Aberdeen Proving Ground Maryland, December 1983.
34. Kingery, C. N. and Coulter G. A., Enhanced Blast as a Function of Multiple Detonations and Shape for Bare Pentolite Charges, Memorandum Report BRL-MR-3539, prepared by U.S. Army Ballistic Research Laboratory, Aberdeen Proving Ground, Maryland, July 1986.
35. Kingery, C. N., Bulmash G., and Muller P., Blast Loading on Above Ground Barricaded Munition Storage Magazines, Technical Report ARBL-TR-02557, prepared by U.S. Army Armament Research and Development Center, Ballistic Research Laboratory, Aberdeen Proving Ground, Maryland, May 1984.
36. Kriebel, A.R., Air Blast in Tunnels and Chambers, Final Report DASA 1200-11, Supplement 1, Prepared for Defense Civil Preparedness Agency, URS Research Company, San Mateo, California, September 1972.

37. Makino, R. C., The Kirkwood-Brinkley Theory of the Propagation of Spherical Shock Waves and Its Comparison With Experiment, BRL Report 750, Aberdeen Proving Ground, Maryland, April 1951.
38. McIntyre, F. L., TNT Equivalency Test Results of Selected High Explosives, Propellants, and Pyrotechnics in Surface Burst Configurations, Contractor Report, Prepared by Technical Services Laboratory, National Space Technology Laboratories, NSTL MS 39529, for U.S. Army Research and Development Engineering Center, Dover, New Jersey, Sponsored by U.S. Army - AMCCOM, July 1986.
39. Melichar, J. F., The Propagation of Blast Waves Into Chambers, BRL Memorandum Report 1920, Aberdeen Proving Ground, Maryland, March 1966.
40. Olson, W. C., Patterson, J. D. II, and Williams, J. S., The Effect of Atmospheric Pressure on the Reflected Impulse From Blast Waves, BRL Memorandum Report 1241, Aberdeen Proving Ground, Maryland, January 1960.
41. Reeves H., and Robinson W. T., Hastings Igloo Hazards Tests for Small Explosive Charges, Memorandum Report AKBL-MR-03356, prepared by U. S. Army Armament Research and Development Center, Ballistic Research Laboratory, Aberdeen Proving Ground, Maryland, May 1984.
42. Reisler, R. E., Kennedy, L. W., and Keofon, J. H., High Explosive Multi-Burst Air Blast Phenomena (Simultaneous and Non Simultaneous Detonations), BRL Technical Report AKBL-TR-02142, Aberdeen Proving Ground, Maryland, February 1979.
43. Sachs, R. G., The Dependence of Blast on Ambient Pressure and Temperature, BRL Report 466, Aberdeen Proving Ground, Maryland, 1964.
44. Shear, R. E., Incident and Reflected Blast Pressures for Pentolite, BRL Report 1262, Aberdeen Proving Ground, Maryland, September 1964.
45. Shear, R. E. and McCane, P., Normally Reflected Shock Front Parameters, BRL Memorandum Report 1273, Aberdeen Proving Ground, Maryland, May 1965.
46. Swisdak, M.M., Jr., Explosion Effects and Properties: Part I - Explosion Effects in Air, NSWC/WOL/TR 75-116, Naval Surface Warfare Center, White Oak, Silver Spring, Maryland, October 1975.
47. The Effects of Nuclear Weapons, S. Glasstone, Editor, U. S. Atomic Energy Commission, Washington, D. C., (Revised Edition), 1964.
48. Voltz, R. D., and Kiger, S. A., An Evaluation of the Separated Bay Concept for a Munition Assembly Complex; An Experimental Investigation of the Department of Energy Building 12-64 Complex, Technical Report SL-84-6, prepared by Structures Laboratory, U.S. Army Engineer Waterways Experiment Station, Vicksburg, Mississippi, for Department of Energy, Albuquerque Operations, Amarillo, Texas, September 1983.
49. Ward, J. M. (DOD Explosives Safety Board), Swisdak, M. M., Jr., Lorcham I. J., and Soper W. G. (NSWC), Lorenz R. A. (Boeing Military Aircraft Company), Modeling of Debris and Airblast Effects from Explosion Inside

Sealed Hardened Aircraft Shelters, Final Report NSWC TR 85-470, prepared by Naval Surface Weapons Center, Silver Spring, Maryland, May 1985.

50. Warnecke, C. H., Data Report: Support Test Evaluation of a Pre-Engineered Building, TECOM Project No. 2-CO-PIC-004, U.S. Army Dugway Proving Ground, Dugway, Utah, June 1977.
51. Wenzel, A. B. and Esparza, E. D., Measurements of Pressures and Impulses at Close Distances From Explosive Charges Buried and in Air, Final Report on Contract No. DAAK02-71-C-0393 with U.S. Army MERDC, Fort Belvoir, Virginia, 1972.
52. Wilton, C. and Gabrielsen, B. L., Shock Tunnel Tests of Preloaded and Arched Wall Panels, Final Report URS 7030-10, prepared for Defense Civil Preparedness Agency, URS Research Company, San Mateo, California, June 1973.
53. Wilton, C. and Gabrielsen, B. L., Shock Tunnel Tests of Wall Panels, Technical Report, Volume I, Test Information and Analysis, URS 7030-7, prepared for Defense Civil Preparedness Agency, URS Research Company, San Mateo, California, January 1972.
54. Wilton, C., Kaplan, K., and Gabrielsen, B.L., The Shock Tunnel: History and Results, Volume II - Loading Studies, Final Report SSI 7618-1, prepared for Defense Civil Preparedness Agency, Scientific Service, Inc., Redwood City, California, March 1978.
55. Zaker, T. A., Blast Pressures From Sequential Explosions, Phase Report II, Project J6166, IIT Research Institute, Chicago, Illinois, March 25, 1969.

Primary and Secondary Fragments

56. Amos, C. W., Fragment Resistance of Martensitic Steel Sheets (U), AMRA TR-64-01, (CONFIDENTIAL), U.S. Army Materials Research Agency, Watertown, Massachusetts, January 1964.
57. Apgar, J. W., Reaction of Mild Steel Targets to Exploding Munitions (U), U.S. Army Ballistic Research Laboratories, Aberdeen Proving Ground, Maryland (CONFIDENTIAL), October 1967.
58. Baker, W. E., Non-Nuclear Weapons Effects on Protective Structures (U), AFWL-TR-67-133 (SECRET), Mechanics Research, Inc., Houston, Texas, for U.S. Air Force Weapons Laboratory, January 1969.
59. Beth, R. A., Final Report on Concrete Penetration, Report No A-388, National Defense Research Committee, Office of Scientific Research and Development, March 1946.
60. Bulmash, G., Kingery C.N., and Coulter, G.A., Velocity Measurements of Acceptor Wall Fragments From the Mass Detonation of Neighboring Above-Ground Barricaded Munition Storage Magazine Model, Technical Report BRL-TR-2719, prepared by U.S. Army Ballistic Research Laboratory, Aberdeen Proving Ground, Maryland, March 1986.

61. Cohen, E. and Dobbs N., Design Procedures and Details for Reinforced Concrete Structures Utilized in Explosive Storage and Manufacturing Facilities, Ammann & Whitney, Consulting Engineers, New York, New York, Annals of the New York Academy of Sciences, Conference on Prevention of and Protection Against Accidental Explosion of Munitions, Fuels and Other Hazardous Mixtures, Vol. 152, Art. 1, 1968.
62. Doyle, J.M., Klein, M.J. and Shah, H., Design of Missile Resistant Concrete Panels, Preprints of the 2nd International Conference on Structural Mechanics in Reactor Technology, Vol. 4, Commission of the European Communities, Brussels, 1973, Paper No. J 3/3.
63. Effects of Impact and Explosion, Volume 1, Office of Scientific Research and Development, National Defense Research Committee, Washington, D.C., 1946.
64. Fundamentals of Protective Design for Conventional Weapons, prepared by U.S. Army Engineer Waterways Experiment Station, Vicksburg, Mississippi, for Office, Chief of Engineers, U.S. Army, Washington, D.C., July 1984.
65. Gewaltney, R. C., Missile Generation and Protection in Light-Water-Cooled Power Reactor Plants, Nuclear Safety, 10(4): July-August 1969.
66. Giere, A. C., Calculating Fragment Penetration and Velocity Data for Use in Vulnerability Studies, NAVORD Report 6621, U.S. Naval Nuclear Evaluation Unit, Albuquerque, New Mexico, October 1959.
67. Gurney, R. W., The Initial Velocities of Fragments from Bombs, Shells and Grenades, Report No. 405, Ballistic Research Laboratories, Aberdeen Proving Ground, Maryland, September 1943.
68. Gurney, R. W., The Mass Distribution of Fragments from Bombs, Shells and Grenades, Report No. 448, Ballistic Research Laboratories, Aberdeen Proving Ground, Maryland, February 1944.
69. Healey, J. J., and Weissman, S., Principles of Fragment Characteristics and Impact Effects in Protective Design, Materials of the Sixteenth Explosive Safety Seminar, September 1974.
70. Hoffman, P. R., McMath, R.R., and Migotsky, E., Projectile Penetration Studies, AFWL Technical Report No. WL-TR-64-102, Avco Corporation for the Air Force Weapons Laboratory, Kirtland Air Force Base, December 1964.
71. Industrial Engineering Study to Establish Safety Design Criteria for Use in Engineering of Explosive Facilities and Operations, Ammann & Whitney, Consulting Engineers, New York, New York, Report for Picatinny Arsenal, Dover, New Jersey, April 1963.
72. Johnson, C. and Moseley, J.W., Preliminary Warhead Terminal Ballistic Handbook. Part 1: Terminal Ballistic Effects, NAVWEPS Report No. 7673, U.S. Naval Weapons Laboratory, Dahlgren, Virginia, March 1964.

73. Kolsky, H., Stress Waves in Solids, Dover Publications, New York, New York, 1963.
74. Kymer, J.R., Penetration Performance of Arrow Type Projectiles, Report R-1814, U.S. Army Frankford Arsenal, Philadelphia, Pennsylvania, May 1966.
75. Mott, R.I., A Theoretical Formula for the Distribution of Weights of Fragments, AC-3642 (British), March 1943.
76. Mott, R.I., A Theory of Fragmentation, Army Operational Research Group Memorandum, 113-AC-6427, Great Britian, 1943.
77. Non-Nuclear Weapons Effects on Protective Structures (U), Technical Report No. AFWL-TR-69-57, Air Force Weapons Laboratory, Kirtland Air Force Base, December 1964.
78. Non-Nuclear Weapons Effects on Protective Structures (U), Technical Report No. AFWL-TR-69-57, (SECRET), Mechanics Research, Inc., for the Air Force Weapons Laboratory, Kirtland Air Force Base, September 1969.
79. Recht, R., et al., Application of Ballistic Perforation Mechanics to Target Vulnerability and Weapons Effectiveness Analysis (U), NWC TR 4333 (CONFIDENTIAL), Denver Research Institute for the Naval Weapons Center, China Lake, California, October 1967.
80. Reeves H., and Robinson W. T., Hastings Igloo Hazards Tests for Small Explosive Charges, Memorandum Report ARBL-MR-03356, prepared by U.S. Army Armament Research and Development Center, Ballistic Research Laboratory, Aberdeen Proving Ground, Maryland, May 1984.
81. Rinehart, J. S. and Pearson, J., Behavior of Metals Under Impulsive Loads, The American Society of Metals, Cleveland, Ohio, 1954.
82. Robertson, H. P., Terminal Ballistics, Preliminary Report, Committee on Passive Protection Against Bombing, National Research Council, January 1941.
83. Sterne, T. E., A Note on the Initial Velocities of Fragments from Warheads, Report No. 648, Ballistic Research Laboratories, Aberdeen Proving Ground, Maryland, September 1947.
84. Thomas, L. H., Computing the Effect of Distance on Damage by Fragments, Report No. 468, Ballistic Research Laboratories, Aberdeen Proving Ground, Maryland, May 1944.
85. Voltz, R.D., and Kiger, S. A., An Evaluation of the Separated Bay Concept for a Munition Assembly Complex; an Experimental Investigation of the Department of Energy Building 12-64 Complex, Technical Report SL-83-6, prepared by Structures Laboratory, U. S. Army Engineer Waterways Experiment Station, Vicksburg, Mississippi, for Department of Energy, Albuquerque Operations, Amarillo, Texas.
86. Ward, J. M. (DOD Explosives Safety Board), Swisdak, M. M., Jr., Peckham, P. J., and Soper, W. G. (NSWC), Lorenz, R. A. (Boeing Military Aircraft

Company), Modeling of Debris and Airblast Effects from Explosions Inside Scaled Hardened Aircraft Shelters, Final Report NSWC TR 85-470, prepared by Naval Surface Weapons Center, Silver Spring, Maryland, May 1985.

Shock Loads

87. American Society of Civil Engineers (ASCE), A Comparative Study of Structural Response to Explosion-Induced Ground Motions, ASCE, New York, New York, 1975.
88. Auld, H. E., A Study of Air-Blast-Induced Ground Motions, Ph.D. Thesis, University of Illinois, May 1967.
89. Baladi, G. Y., and P. F. Hadala, Ground Shock Calculation Parameter Study Report I Effect of Various Nonlinear Elastic Plastic Model Formulations, Waterways Experiment Station Technical Report S-71-4, April 1971.
90. Ballard, R. F., R. E. Leach, Middle North Series, Mixed Company Event, Strong Motion Seismic Measurements, Defense Nuclear Agency Report POR-6746, July 25, 1973.
91. Barkan, D. D., Dynamics of Bases and Foundations, McGraw Hill Book Co., New York, New York 1962.
92. Baron, M. L., A Summary of Some Analytical Studies on Air Blast Induced Ground Motions, Defense Atomic Support Agency Report 2634, March 1971.
93. Baron, M. L., I. Nelson, and I. Sandler, Investigation of Air Induced Ground Shock Effect Resulting from Various Explosive Sources, Report 2 Influence of Constitutive Models on Ground Motion Predictions, Waterways Experiments Station Contract Report S-71-10, November 1971.
94. Batchelder, F. E., et al., Hardness Program - Non-EMP, Hardness Program Plan for Safeguard Ground Facilities, Vol. 1, Management and Technical Plan, U. S. Army Corps of Engineers, Huntsville Division, HNDDSP-73-153-ED-R, August 16, 1974.
95. Carder, D. S., and W. K. Cloud. Surface Motion from Large Underground Explosions, J. Geophys. Res., 64, 1471-1487, 1959.
96. Carnes, B. L., and J. A. Conway. Mine Throw I: Cratering Effects of a Multiton Near Surface Detonation in Desert Alluvium, Waterways Experiment Station Technical Report N-73-3, May 1973.
97. Christensen, W. J., Air Blast Induced Ground Shock, Navy Bureau of Yards and Decks Technical Study 27, September 1959.
98. Cooper, H. F., Jr., and J. L. Bratton, Calculation of Vertical Airblast-Induced Ground Motions from Nuclear Explosions in Frenchman Flat, Air Force Weapons Laboratory Report AFWL-TR-73-111, October 1973.
99. Cooper, H. F., Jr., Empirical Studies of Ground Shock and Strong Motions in Rock, Defense Nuclear Agency Report 3245F, October 1973.

100. Crandell, F. J., Ground Vibrations Due to Blasting and Its Effect Upon Structures, Journal Boston Soc., Civil Engineers, Vol. 36, p. 245, 1949.
101. Crandell, F. J., Transmission Coefficient for Ground Vibrations Due to Explosions, J. Boston Soc. Civil Engineering, 47, 152-168, 1960.
102. Crawford, R. E., C. J. Higgins, and E. H. Bultmann. Air Force Manual for Design and Analysis of Hardened Structures, Air Force Weapons Laboratory Report AFWL-TR-74-102, October 1974.
103. Day, J. D., H. J. Stout, and D. W. Murrell, Middle Gust Calibration Shots: Ground Motion Measurements, Waterways Experiment Station Technical Report N-75-1, February 1975.
104. Duvall, Wilbur I. and D. E. Fogelson, Review of Criteria for Estimating Damage to Residences from Blasting Vibrations, Bureau of Mines Report of Investigation 5968, 1962.
105. Dvorak, A., Seismic Effects of Blasting on Brick Houses, Proce Geofyrikeniha Ustance Ceskoslavenski Akademie, Vol. No. 169, Geofysikalni Sbornik, pp. 189-202, 1962.
106. Edwards, A. T. and T. D. Northwood, Experimental Studies of the Effects of Blasting on Structures, The Engineer, V. 210, pp. 538-546, September 30, 1960.
107. Eubanks, R. A. and B. R. Juskie Shock Hardening of Equipment, Shock and Vibrations Bulletin, No. 32, P. December 1963.
108. Galbraith, F. W., Operation Distal Plain Final Report Proj. 3.02b Shock Spectrum Measurements, TRW Systems Group Report 05318-6001-R000, January 1968.
109. Galbraith, F. W., Operation Prairie Flat, Proj. LN-306 Shock Spectrum Measurements, Defense Atomic Support Agency Report POR-2107, February 1970.
110. Grubaugh, R. E., and L. E. Elliot, Scaling of Ground Shock Spectra, Defense Atomic Support Agency Report DASA-1921, February 1967.
111. Habberjam, G. M. and J. T. Whetton. On the Relationship Between Seismic and Amplitude and Charge of Explosive Fired in Routine Blasting Operations, Geophysics 17, 116-128, January 1952.
112. Hendron, A. J. Jr., Correlation of Operation Snowball Ground Motions with Dynamic Properties of Test Site Soils, Waterways Experiment Station Miscellaneous Paper I-745, October 1965.
113. Hoffman, H. V., F. M. Sauer, and B. Barclay, Operation Prairie Flat, Proj. LN-308 Strong Ground Shock Measurements, Defense Atomic Support Agency Report POR-2108, April 1971.
114. Hudson, D. E., J. L. Alford, and W. D. Iwan, Ground Accelerations Caused by Large Quarry Blasts, Bull. Seismic Soc., A, 51, 191-202, 1961.

115. Ichiro, I., On the Relationship Between Seismic Ground Amplitude and the Quantity of Explosives in Blasting, Reprint from Memoirs of the Faculty of Engineering, Kyoto University, 15, 579-587, 1953.
116. Ingram, J. K., Project Officer's Final Report Operation Distant Plain Events 1, 2A, 3, 4, and 5, Proj. 3.02A Earth Motion and Stress Measurements, Waterways Experiment Station Technical Report N-71-3, May 1971.
117. Ingram, L. F., Ground Motions from High Explosive Experiments, Waterways Experiment Station Miscellaneous Paper N-72-10, December 1972.
118. Jaramillo, E. E., and R. E. Pozega, Middle Gust Free-Field Data Analysis, Air Force Weapons Laboratory Report AFWL-TR-73-251, April 1974.
119. Joachim, C. E., Mine Shaft Series, Events Mine Under and Mine Ore; Ground Motion and Stress Measurements, Waterways Experiment Station Technical Report N-72-1, January 1972.
120. Kennedy, T. E., In-Structure Motion Measurements, Proj. LN-315 Operation Prairie Flat, Waterways Experiment Station Technical Report N-70-11, July 1970.
121. Kochly, J. A., and T. F. Stubbs, Mine Shaft Series, Mineral Rock Particle Velocity Measurements from a 100-ton TNT Detonation on Granite, Defense Nuclear Agency Report POR-2162, May 24, 1971.
122. Lamb, H., On the Propagation of Tremors Over the Surface of an Elastic Solid, Philosophical Transactions of Royal Society London, Series A, Volume 203, September 1904.
123. Langefors, Ulf, B. Kihlstron, and H. Westerberg, Ground Vibrations in Blasting, Water Power, pp. 335-338, 390-395, 421-424, February 1958.
124. Lockard, D. M., Crater Parameters and Material Properties, Air Force Weapons Laboratory Report AFWL-TR-74-200, October 1974.
125. Meirels, E. C. and A. R. Wright, Hardness Program - Non-EMP, Hardness Program Plan for Safeguard Ground Facilities, Vol. 2, Safeguard Structures and TSE Description, U.S. Army Corps of Engineers, Huntsville Division, HNDDSP-73-153-ED-R, November 1973.
126. Morris, G., The Reduction of Ground Vibrations from Blasting Operations, Engineering, pp. 460-465, April 1957.
127. Morris, W. E., and others, Operation Jangle Blast and Shock Measurements I, Armed Forces Special Weapons Project Report WT 366, June 1952.
128. Murphey, B. F., Particle Motions Near Explosions in Halite, Journal of Geophysical Research, Vo. 66, No. 3, March 1961, pp. 947-958.

129. Murrell, D. W., Operation Mine Shaft, Mineral Rock Event, Far-out Ground Motions From a 100-ton Detonation on Granite, Waterways Experiment Station Technical Report N-72-6, April 1972.
130. Murrell, D. W., Operation SNOWBALL, Project 3.6 - Earth Motion Measurements, Waterways Experiment Station Technical Report TR 1-759, March 1967.
131. Newmark, N. M., and others, Air Force Design Manual Principles and Practices for Design of Hardened Structures, Air Force Special Weapons Center Report AFSWC-TDR-62-138, December 1962.
132. Nicholls, H. R., C. F. Johnson, and W. I. Duvall, Blasting Vibrations and Their Effects on Structures, Bureau of Mines Bulletin 656, 1971.
133. Odello, R. and P. Price, Ground Shock Effects from Accidental Explosions, Picatinny Arsenal Technical Report 4995, November 1976.
134. Palaniswamy, K., and J. L. Merritt, Evaluation of Middle Gust Data: Acoustic Path Length Scaling of Peak Velocities, Space and Missile Systems Organization Report 72-006-T4, November 1973.
135. Parsons, R. M., and others, Guide for the Design of Shock Isolation Systems for Underground Protective Structures, Air Force Special Weapons Center Report AFSWC-TDR-62-64, October 1962.
136. Phillips, B. R., and G. Y. Baladi, Results of Two Free-Field Code Calculations Versus Field Measurements for the Distant Plain 1A Event, Waterways Experiment Station Miscellaneous Paper S-73-21, April 1973.
137. Proceedings of the Mixed Company/Middle Gust Results Meeting 13-15 March 1973, Vol. II. Edited by General Electric-Tempo, Defense Nuclear Agency Report 3151-P2, May 1973.
138. Rausch, E., Maschinenfundamente Und Andere Dynamische Bauaufgaben, Vertrieb VDE Verlag G.M.B.H. (Berlin), 1943.
139. Reiher, H. and F. J. Meister, Die Empfindlichkeit der Menschen gegen Erschutterungen, Forsch. Gebiete Ingenieurwesen, Vol. 2, No. 11, pp. 381-386, 1931.
140. Richart, F. E. Jr., J. R. Hall, and R. D. Woods, Vibration of Soils and Foundations, Prentice-Hall, Inc., Englewood Cliffs, New Jersey, 1970.
141. Ricker, N., The Form and Nature of Seismic Waves and the Structure of Seismograms, Geophysics, 5, 348-366, 1940.
142. Sachs, D. C., and C. M. Swift, Small Explosion Tests, Project Mole, Armed Forces Special Weapons Project Report 291, Vols. I & II, December 1955.
143. Sager, R. A., Concrete Arch Studies, Proj. 3.2, Operation Snowball, Waterways Experiment Station Miscellaneous Paper I-736, August 1965.

144. Sandler, I.S., J. P. Wright, and M. L. Baron, Ground Motion Calculations for Events II and III of the Middle Gust Series, Defense Nuclear Agency Report DNA 3290T, April 1974.
145. Steffens, R. J., The Assessment of Vibration Intensity and its Application to the Study of Building Vibrations, National Building Studies Special Report No. 19, Department of Scientific and Industrial Research, Building Research Station, London, England, 1952.
146. Sauer, F. M., and C. T. Vincent, Ferris Wheel Series - Flat Top Event Earth Motion and Pressure Histories, Defense Atomic Support Agency Report Ferris Wheel POR-3002, April 1967.
147. Sauer, F. M., editor, Nuclear Geoplosics, A Sourcebook of Underground Phenomena and Effects of Nuclear Explosions, in 5 parts, Defense Atomic Support Agency Report DASA-1285, May 1964.
148. Sauer, F. M., Summary Report on Distant Plain Events 6 and 1a Ground Motion Experiments, Defense Atomic Support Agency Report DASA-2587, October 1970.
149. Teichmann, G. A. and R. Westwater, Blasting and Associated Vibrations, Engineering, pp. 460-465, April 1957.
150. Thoenen, J. R., and S. L. Windes, Seismic Effects of Quarry Blasting, Bureau of Mines Bulletin, 442, 83, 1942.
151. URS/John A. Blume & Associates, Seismic Hazard and Building Structure Behavior at the Pantex Facility, April 1976.
152. Vincent, C. T., Operation Prairie Flat, Proj. LN-304 Earth Pressure and Ground Shock Profile Measurements, Defense Atomic Support Agency Report POR-2113, May 1969.
153. Weidlinger, P., and A. Matthews, A Method for the Prediction of Ground Shock Phenomena in Soils, Air Force Special Weapons Center Report AFSWC-TDR-61-66, March 1962.
154. Westline, P. S., Esparza, E. D., and Wenzel, A. B., Analysis and Testing of Pipe Response to Buried Explosive Detonations, SwRI Final Report for American Gas Association, July 1978.
155. Willis, D. E. and J. T. Wilson, Maximum Vertical Ground Displacement of Seismic Waves Generated by Explosive Blasts, Bulletin Seismic Safety of America, 50, 455-459, 1960.
156. Zaccor, J. V., Procedures for Prediction of Ground Shock Phenomena Based on One-Dimensional Shock Propagation Considerations: Procedures and Applications, Waterways Experiment Station Contract Report 3-171, April 1967.
157. Zolasko, J. S., and G. Y. Baladi, Free-Field Code Predictions Versus Field Measurements: A Comparative Analysis for the Prairie Flat Event, Waterways Experiment Station Miscellaneous Paper S-71-6, March 1971.

DISTRIBUTION LIST

Commander
Armament Research, Development, and
Engineering Center
U.S. Army Armament, Munitions, and
Chemical Command
ATTN: SMCAR-MSI (5)
SMCAR-AES
SMCAR-AES-M (10)
SMCAR-SF
Dover, NJ 07801-5001

Commander
U.S. Army Armament, Munitions, and
Chemical Command
ATTN: AMSMC-GCL(D)
Dover, NJ 07801-5001

Administrator
Defense Technical Information Center
ATTN: Accessions Division (12)
Cameron Station
Alexandria, VA 22304-6145

Director
Ballistic Research Laboratory
ATTN: AMXBR-OD-ST
Aberdeen Proving Ground, MD 21005-5066

Commander
U.S. Army Armament Munitions and
Chemical Command
ATTN: SMCAR-ESP-L
AMSMC-SF(R) (2)
AMSMC-IR(R)
AMSMC-EN(R)
Rock Island, IL 61299-6000

Commander
Chemical Research and Development Center
U.S. Army Armament, Munitions and
Chemical Command
ATTN: SMCCR-SPS-IL
SMCCR-RSP-A
Aberdeen Proving Ground, MD 21010-5423

Commander
U.S. Army Materiel Command
ATTN: AMCSF
5001 Eisenhower Avenue
Alexandria, VA 22333

Director
AMC Field Safety Activity
ATTN: AMCOS
Charleston, IN 47111

Chief
Benet Weapons Laboratory, CCAC
Armament Research, Development, and
Engineering Center
U.S. Army Armament, Munitions and
Chemical Command
ATTN: SMCAR-CCB-TL
Watervliet, NY 12189-5000

Director
U.S. Army Materiel Systems
Analysis Activity
ATTN: AMXSY-MP
Aberdeen Proving Ground, MD 21005-5066

CRDC Resident Operations Office
ATTN: SMCCR-TSE-OA
National Space Technology Laboratories
NSTL, MS 39529

Chairman
Department of Defense Explosives
Safety Board
ATTN: J. Ward
P. Price (2)
Hoffman Bldg 1, Room 856C
2461 Eisenhower Avenue
Alexandria, VA 22331

HQUSACE
ATTN: DAEN-ECE-T (10)
DAEN-RDM
Washington, DC 20314

Commander
U.S. Army Engineering Division
ATTN: HNDED-CS (R. Lein) (10)
P.O. Box 1600
Huntsville, AL 35807

Commander
U.S. Army Construction Engineering
Research Laboratory
P.O. Box 4005 (2)
Champaign, IL 61820

Commander
U.S. Army Cold Regions Research
and Engineering Laboratory
P.O. Box 282 (2)
Hanover, NH 03755

Commander
U.S. Army Engineer Waterways
Experiment Station
ATTN: Library, Helen Ingram (2)
P.O. Box 631
Vicksburg, MS 39180-0631

Commander
Naval Facilities Engineering Command
ATTN: Code FPO-3A, Room 12N57 (20)
200 Stovall Street
Alexandria, VA 22332

Commanding Officer
Naval Civil Engineering Laboratory
ATTN: Code L51, W. Keenan (15)
Port Hueneme, CA 93043

Chief of Naval Operations
Department of the Navy
ATTN: NOP-411F
Washington, DC 20350

Commander
Naval Sea Systems Command
ATTN: SEA-06H1
Naval Sea Systems Command Headquarters
Washington, DC 20362

Commander
David W. Taylor Naval Ship Research
and Development Center
Bethesda, MD 20084

Commander
Naval Surface Weapons Center
ATTN: G10 (J. Proctor)
R12 (W. Filler)
R15 (J. Connor)
R15 (M. Swisdak)
White Oak Laboratory
Silver Spring, MD 20910

Facilities and Maintenance Branch
Department of Energy
Albuquerque Operations
Amarillo Area Office
ATTN: Mr. L.M. Paradee, Chief (5)
P.O. Box 30030
Amarillo, TX 79120

Department of Energy
Facilities and Construction
Maintenance Division
Albuquerque Operations
ATTN: Mr. Manuel G. Martinez (5)
P.O. Box 5400
Albuquerque, NM 87115

AFESC/RDC
ATTN: W.C. Buchholtz (5)
Tyndall AFB, FL 30403

Ammann & Whitney Consulting Engineers
ATTN: N. Dobbs
96 Morton Street
New York, NY 10014

Southwest Research Institute
ATTN: Mark G. Whitney (5)
P.O. Drawer 28510
6220 Culebra Road
San Antonio, TX 78284

Wilfred Baker Engineering
218 E. Edgewood Place (5)
San Antonio, TX 78209

Illinois Institute of Technology
Research Institute
ATTN: H.S. Napadensky
10 West 35th Street
Chicago, IL 60616

Defense Contract Administration Service
Management Area, Dayton (DCASR-CLE-GDQ)
c/o Defense Electronics Supply Center
ATTN: Bill Loser
Dayton, OH 45444

AFATL/DLYV
ATTN: Mr. Ralph McGuire
Eglin AFB, FL 32542

USAED, Europe
EUUDAD-TA
ATTN: Roger Crowson (2)
APO New York 09757

DCSAR, Cleveland
ATTN: DCSAR-CLE-OS (4)
1240 East 9th Street
Cleveland, OH 44135

Officer in Charge
White Oak Lab
Naval Surface Weapons Center Detachment
ATTN: Robert Hutcheson, Code 12
10901 New Hampshire Avenue
Silver Springs, MD 20903-5000

HQ USAF/LEEE
ATTN: Satish Abrol (5)
Bldg 516
Bolling AFB
Washington, DC 20332-5000

Department of the Navy
Atlantic Division
Naval Facilities Engineering Command
Code 402, Owen Hewitt
Norfolk, VA 23511-6287

DCSAR N-1-QSS
ATTN: Richard Castell
201 Varick Street
New York, NY 10014-4811